JSCSEN 86(11)1013–1130(2021)

ISSN 1820-7421(Online)

Journal of the Serbian Chemical Society

Electronic version

VOLUME 86

No 11

BELGRADE 2021

Available on line at

www.shd.org.rs/JSCS/

The full search of JSCS is available through

DOAJ DIRECTORY OF OPEN ACCESS JOURNALS

www.doaj.org

The **Journal of the Serbian Chemical Society** (formerly Glasnik Hemijskog društva Beograd), one volume (12 issues) per year, publishes articles from the fields of chemistry. The **Journal** is financially supported by the **Ministry of Education, Science and Technological Development of the Republic of Serbia.**

Articles published in the **Journal** are indexed in **Clarivate Analytics products: Science Citation Index-Expanded™** – accessed *via* **Web of Science®** and **Journal Citation Reports®**.

Impact Factor announced 2020: **1.097; 5-year Impact Factor**: **1.023**.

Articles appearing in the **Journal** are also abstracted by: **Scopus, Chemical Abstracts Plus (CAplus℠), Directory of Open Access Journals, Referativnii Zhurnal (VINITI), RSC Analytical Abstracts, EuroPub, Pro Quest** and **Asian Digital Library.**

Publisher:	**Serbian Chemical Society**, Karnegijeva 4/III, P. O. Box 36, 1120 Belgrade 35, Serbia tel./fax: +381–11–3370–467, E-mails: **Society** – shd@shd.org.rs; **Journal** – jscs@shd.org.rs Home Pages: **Society** – http://www.shd.org.rs/, **Journal** – http://www.shd.org.rs/JSCS/
Internet Service:	Contents, Abstracts and full papers (from Vol 64, No. 1, 1999) are available in the electronic form at the Web Site of the **Journal** (http://www.shd.org.rs/JSCS/).
Former Editors:	**Nikola A. Pušin** (1930–1947), **Aleksandar M. Leko** (1948–1954), **Panta S. Tutundžić** (1955**–**1961), **Miloš K. Mladenović** (1962–1964), **Đorđe M. Dimitrijević** (1965–1969), **Aleksandar R. Despić** (1969–1975), **Slobodan V. Ribnikar** (1975–1985), **Dragutin M. Dražić** (1986–2006).
Editor-in-Chief:	BRANISLAV Ž. **NIKOLIĆ**, Serbian Chemical Society (E-mail: jscs-ed@shd.org.rs)
Deputy Editor:	DUŠAN **SLADIĆ**, Faculty of Chemistry, University of Belgrade
Sub editors:	
Organic Chemistry	DEJAN **OPSENICA**, Institute of Chemistry, Technology and Metallurgy, University of Belgrade JÁNOS **CSANÁDI**, Faculty of Science, University of Novi Sad
Biochemistry and Biotechnology	OLGICA **NEDIĆ**, INEP – Institute for the Application of Nuclear Energy, University of Belgrade
Inorganic Chemistry	MILOŠ **ĐURAN**, Serbian Chemical Society
Theoretical Chemistry	IVAN **JURANIĆ**, Serbian Chemical Society
Physical Chemistry	LJILJANA **DAMJANOVIĆ-VASILIĆ**, Faculty of Physical Chemistry, University of Belgrade
Electrochemistry	SNEŽANA **GOJKOVIĆ**, Faculty of Technology and Metallurgy, University of Belgrade
Analytical Chemistry	SLAVICA **RAŽIĆ**, Faculty of Pharmacy, University of Belgrade
Polymers	BRANKO **DUNJIĆ**, Faculty of Technology and Metallurgy, University of Belgrade
Thermodynamics	MIRJANA **KIJEVČANIN**, Faculty of Technology and Metallurgy, University of Belgrade
Chemical Engineering	TATJANA **KALUĐEROVIĆ RADOIČIĆ**, Faculty of Technology and Metallurgy, University of Belgrade
Materials	RADA **PETROVIĆ**, Faculty of Technology and Metallurgy, University of Belgrade
Metallic Materials and Metallurgy	NENAD **RADOVIĆ**, Faculty of Technology and Metallurgy, University of Belgrade
Environmental and Geochemistry	VESNA **ANTIĆ**, Faculty of Agriculture, University of Belgrade
History of and Education in Chemistry	DRAGICA **TRIVIĆ**, Faculty of Chemistry, University of Belgrade
English Language Editors:	LYNNE **KATSIKAS**, Serbian Chemical Society VLATKA **VAJS**, Serbian Chemical Society JASMINA **NIKOLIĆ**, Faculty of Technology and Metallurgy, University of Belgrade
Technical Editors:	VLADIMIR **PANIĆ**, ALEKSANDAR **DEKANSKI**, VUK **FILIPOVIĆ**, Institute of Chemistry, Technology and Metallurgy, University of Belgrade
Journal Manager & Web Master:	ALEKSANDAR **DEKANSKI,** Institute of Chemistry, Technology and Metallurgy, University of Belgrade
Office:	VERA **ĆUŠIĆ**, Serbian Chemical Society

Editorial Board

From abroad: **R. Adžić**, Brookhaven National Laboratory (USA); **A. Casini**, University of Groningen (The Netherlands); **G. Cobb**, Baylor University (USA); **D. Douglas**, University of British Columbia (Canada); **G. Inzelt**, Etvos Lorand University (Hungary); **N. Katsaros**, NCSR "Demokritos", Institute of Physical Chemistry (Greece); **J. Kenny**, University of Perugia (Italy); **Ya. I. Korenman**, Voronezh Academy of Technology (Russian Federation); **M. D. Lechner**, University of Osnabrueck (Germany); **S. Macura**, Mayo Clinic (USA); **M. Spiteller**, INFU, Technical University Dortmund (Germany); **M. Stratakis**, University of Crete (Grecce); **M. Swart**, University de Girona (Cataluna, Spain); **G. Vunjak-Novaković**, Columbia University (USA); **P. Worsfold**, University of Plymouth (UK); **J. Zagal**, Universidad de Santiago de Chile (Chile).

From Serbia: **B. Abramović**, **V. Antić, V. Beškoski**, **J. Csanadi**, **Lj. Damjanović-Vasilić**, **A. Dekanski**, **V. Dondur**, **B. Dunjić**, **M. Đuran, S. Gojković**, **I. Gutman**, **B. Jovančićević**, **I. Juranić**, **L. Katsikas**, **M. Kijevčanin**, **V. Leovac**, **S. Milonjić**, **V.B. Mišković-Stanković, O. Nedić**, **B. Nikolić**, **J. Nikolić, D. Opsenica**, **V. Panić**, **M. Petkovska**, **R. Petrović**, **I. Popović**, **B. Radak**, T. **Kaluđerović Radiočić, N. Radović**, **S. Ražić**, **D. Sladić**, **S. Sovilj**, **S. Šerbanović**, **B. Šolaja**, **Ž. Tešić**, **D. Trivić, V. Vajs**.

Subscription: The annual subscription rate is **150.00 €** including postage (surface mail) and handling. For Society members from abroad rate is **50.00 €**. For the proforma invoice with the instruction for bank payment contact the Society Office (E-mail: shd@shd.org.rs) or see JSCS Web Site: http://www.shd.org.rs/JSCS/, option Subscription.

Godišnja pretplata: Za članove SHD: **2.500,00 RSD**, za penzionere i studente: **1000,00 RSD**, a za ostale: **3.500,00 RSD**:za organizacije i ustanove: **16.000,00 RSD**. Uplate se vrše na tekući račun Društva: **205-13815-62**, poziv na broj **320**, sa naznakom "pretplata za JSCS".

Nota: Radovi čiji su svi autori članovi SHD prioritetno se publikuju.

Odlukom Odbora za hemiju Republičkog fonda za nauku Srbije, br. 66788/1 od 22.11.1990. godine, koja je kasnije potvrđena odlukom Saveta Fonda, časopis je uvršten u kategoriju međunarodnih časopisa (**M-23**). Takođe, aktom Ministarstva za nauku i tehnologiju Republike Srbije, 413-00-247/2000-01 od 15.06.2000. godine, ovaj časopis je proglašen za publikaciju od posebnog interesa za nauku. **Impact Factor** časopisa objavljen 2020. godine iznosi **1,097**, a petogodišnji **Impact Factor 1,023**.

INSTRUCTIONS FOR AUTHORS (2021)

GENERAL

The *Journal of the Serbian Chemical Society* (the *Journal* in further text) is an international journal publishing papers from all fields of chemistry and related disciplines. Twelve issues are published annually. The Editorial Board expects the editors, reviewers, and authors to respect the well-known standard of professional ethics.

Types of Contributions

Original scientific papers	(up to 15 typewritten pages, including Figures, Tables and References) report original research which must not have been previously published.
Short communications	(up to 8 pages) report unpublished preliminary results of sufficient importance to merit rapid publication.
Notes	(up to 5 pages) report unpublished results of short, but complete, original research
Authors' reviews	(up to 40 pages) present an overview of the author's current research with comparison to data of other scientists working in the field
Reviews[a]	(up to 40 pages) present a concise and critical survey of a specific research area. Generally, these are prepared at the invitation of the Editor
Surveys	(about 25 pages) communicate a short review of a specific research area.
Book and Web site reviews	(1 - 2 pages)
Extended abstracts	(about 4 pages) of Lectures given at meetings of the Serbian Chemical Society Divisions
Letters to the Editor	report miscellaneous topics directed directly to the Editor

[a]Generally, Authors' reviews, Reviews and Surveys are prepared at the invitation of the Editor.

Submission of manuscripts

Manuscripts should be submitted using the **OnLine Submission Form**, available on the JSCS Web Site (**http://www.shd-pub.org.rs/index.php/JSCS**). The manuscript must be uploaded as a Word.doc or .rtf file, with tables and figures (including the corresponding captions – above Tables and below Figures), placed within the text to follow the paragraph in which they were mentioned for the first time.

Please note that **Full Names (**First Name, Last Name), **Full Affiliation** and **Country** (from drop down menu) of **ALL OF AUTHORS** (written in accordance with English spelling rules - the first letter capitalized) must be entered in the manuscript Submission Form (Step 3). Manuscript Title, authors' names and affiliations, as well as the Abstract, **WILL APPEAR** in the article listing, as well as in **BIBLIOGRAPHIC DATABASES (WoS, SCOPUS...)**, in the form and in the order entered in the author details

Graphical abstract

Graphical abstract is a one-image file containing the main depiction of the authors work and/or conclusion and must be supplied along with the manuscript. It must enable readers to quickly gain the main message of the paper and to encourage browsing, help readers identify which papers are most relevant to their research interests. Authors must provide an image that clearly represents the research described in the paper. The most relevant figure from the work, which summarizes the content, can also be submitted. The image should be submitted as a separate file in **Online Submission Form - Step 2**.

Specifications: The graphical abstract should have a clear start and end, reading from top to bottom or left to right. Please omit unnecessary distractions as much as possible.

- **Image size:** minimum of 500×800 pixels (W×H) and a minimum resolution of 300 dpi. If a larger image is sent, then please use the same ratio: 16 wide × 9 high. Please note that your image will be scaled proportionally to fit in the available window in TOC; a 150x240 pixel rectangle. Please be sure that the quality of an image cannot be increased by changing the resolution from lower to higher, but only by rescanning or exporting the image with a higher resolution, which can be set in usual "settings" option.
- **Font:** Please use Calibri and Symbol font with a large enough font size, so it is readable even from the image of a smaller size (150 × 240 px) in TOC.
- **File type:** JPG and PNG only.

No additional text, outline or synopsis should be included. Please do not use white space or any heading within the image.

Cover Letter

Manuscripts must be accompanied by a cover letter (strictly uploaded in **Online Submission Step 2**) in which the type of the submitted manuscript and a warranty as given below are given. The Author(s) has(have) to warranty that the manuscript submitted to the *Journal* for review is original, has been written by the stated author(s) and has not been published elsewhere; is currently not being considered for publication by any other journal and will not be submitted for such a review while under review by the *Journal*; the manuscript contains no libellous or other unlawful statements and does not contain any materials that violate any personal or proprietary rights of any other person or entity. All manuscripts will be acknowledged on receipt (by e-mail).

Illustrations

Illustrations (Figs, schemes, photos…) in TIF or EPS format (JPG format is acceptable for colour and greyscale photos, only), must be additionally uploaded (Online Submission Step 2) as a separate file or one archived (.zip, .rar or .arj) file. Figures and/or Schemes should be prepared according to the **Artwork Instructions -** http://www.shd.org.rs/JSCS/jscs-pdf/Artwork_Instructions.pdf!

For any difficulties and questions related to **OnLine Submission Form -** https://www.shd-pub.org.rs/index.php/JSCS/submission/wizard, please refer to **User Guide -** https://openjournal-systems.com/ojs-3-user-guide/ , Chapter **Submitting an Article -** https://openjournalsystems.com/ojs-3-user-guide/submitting-an-article/. If difficulties still persist, please contact JSCS Editorial Office at **JSCS@shd.org.rs**

A manuscript not prepared according to these instructions will be returned for resubmission without being assigned a reference number.

Conflict-of-Interest Statement*: Public trust in the peer review process and the credibility of published articles depend in part on how well a conflict of interest is handled during writing, peer review, and editorial decision making. A conflict of interest exists when an author (or the author's institution), reviewer, or editor has financial or personal relationships that inappropriately influence (bias) his or her actions (such relationships are also known as dual commitments, competing interests, or competing loyalties). These relationships vary from those with negligible potential to those with great potential to influence judgment, and not all relationships represent true conflict of interest. The potential for a conflict of interest can exist whether or not an individual believes that the relationship affects his or her scientific judgment. Financial relationships (such as employment, consultancies, stock ownership, honoraria, paid expert testimony) are the most easily identifiable conflicts of interest and the most likely to undermine the credibility of the journal, the authors, and of science itself. However, conflicts can occur for other reasons, such as personal relationships, academic competition, and intellectual passion.

Informed Consent Statement*: Patients have a right to privacy that should not be infringed without informed consent. Identifying information, including patients' names, initials, or hospital numbers, should not be published in written descriptions, photographs, and pedigrees unless the information is essential for scientific purposes and the patient (or parent or guardian) gives written informed consent for publication. Informed consent for this purpose requires that a patient who is identifiable be shown the manuscript to be published. Authors should identify Individuals who provide writing assistance and disclose the funding source for this assistance. Identifying details should be omitted if they are not essential. Complete anonymity is difficult to achieve, however, and informed consent should be obtained if there is any doubt. For example, masking the eye region in photographs of patients is inadequate protection of anonymity. If identifying characteristics are altered to protect anonymity, such as in genetic pedigrees, authors should provide assurance that alterations do not distort scientific meaning and editors should so note. The requirement for informed consent should be included in the journal's instructions for authors. When informed consent has been obtained it should be indicated in the published article.

Human and Animal Rights Statement* When reporting experiments on human subjects, authors should indicate whether the procedures followed were in accordance with the ethical standards of the responsible committee on human experimentation (institutional and national) and with the Helsinki Declaration of 1975, as revised in 2000 (5). If doubt exists whether the research was conducted in accordance with the Helsinki Declaration, the authors must explain the rationale for their approach, and demonstrate that the institutional review body explicitly approved the doubtful aspects of the study. When reporting experiments on animals, authors should be asked to indicate whether the institutional and national guide for the care and use of laboratory animals was followed.

---

*International Committee of Medical Journal Editors ("Uniform Requirements for Manuscripts Submitted to Biomedical Journals"), February 2006

PROCEDURE

All contributions will be peer reviewed and only those deemed worthy and suitable will be accepted for publication. The Editor has the final decision. To facilitate the reviewing process, authors are encouraged to suggest up to three persons competent to review their manuscript. Such suggestions will be taken into consideration but not always accepted. If authors would prefer a specific person not be a reviewer, this should be announced. The Cover Letter must be accompanied by these suggestions. Manuscripts requiring revision should be returned according to the requirement of the Editor, within 60 days upon reception of the reviewing comments by e-mail.

The *Journal* maintains its policy and takes the liberty of correcting the English as well as false content of manuscripts **provisionally accepted** for publication in the first stage of reviewing process. In this second stage of manuscript preparation by JSCS Editorial Office, the author(s) may be required to supply some **additional clarifications and corrections**. This procedure will be executed during copyediting actions, with a demand to author(s) to perform corrections of unclear parts before the manuscript would be published OnLine as **finally accepted manuscript (OLF Section of the JSCS website)**. Please note that the manuscript can receive the status of **final rejection** if the author's corrections would not be satisfactory.

When finally accepted manuscript is ready for printing, the corresponding author will receive a request for proof reading, which should be performed within 2 days. Failure to do so will be taken as the authors agree with any alteration which may have occurred during the preparation of the manuscript for printing.

Accepted manuscripts of active members of the Serbian Chemical Society (all authors) have publishing priority.

MANUSCRIPT PRESENTATION

Manuscripts should be typed in English (either standard British or American English, but consistent throughout) with 1.5 spacing (12 points Times New Roman; Greek letters in the character font Symbol) in A4 format leaving 2.5 cm for margins. For Regional specific, non-standard characters that may appear in the text, save documents with Embed fonts Word option: *Save as -> (Tools) -> Save Options… -> Embed fonts in the text.*

The authors are requested to seek the assistance of competent English language expert, if necessary, to ensure their English is of a reasonable standard. The Serbian Chemical Society can provide this service in advance of submission of the manuscript. If this service is required, please contact the office of the Society by e-mail (jscs-info@shd.org.rs).

Tables, figures and/or schemes must be embedded in the main text of the manuscript and should follow the paragraph in which they are mentioned for the first time. **Tables** must be prepared with the aid of the **WORD table function**, without vertical lines. The minimum size of the font in the tables should be **10 pt**. Table columns must not be formatted using multiple spaces. Table rows must not be formatted using any returns (enter key; ↵ key) and are **limited to 12 cm width**. Tables should not be incorporated as graphical objects. **Footnotes to Tables** should follow them and are to be indicated consequently (in a single line) in superscript letters and separated by semi-column.

Table caption must be placed above corresponding Table, while **Captions of the Illustrations** (Figs. Schemes...) must follow the corresponding item. **The captions, either for Tables or Illustrations**, should make the items comprehensible without reading of the main text (but clearly referenced in), must follow numerical order (Roman for Tables, Arabic for Illustrations), and should not be provided on separate sheets or as separate files.

High resolution Illustrations (named as Fig. 1, Fig. 2… and/or Scheme 1, Scheme 2…) in **TIF or EPS format** (JPG format is acceptable for photos, only) **must be additionally uploaded as a separate files or one archived (.zip, .rar) file.**

Illustrations should be prepared according to the ARTWORK INSTRUCTIONS - http://www.shd.org.rs/JSCS/jscs-pdf/Artwork_Instructions.pdf. **!**

All pages of the manuscript must be numbered continuously.

DESIGNATION OF PHYSICAL QUANTITIES AND UNITS

IUPAC recommendations for the naming of compounds should be followed. SI units, or other permissible units, should be employed. The designation of physical quantities must be in italic throughout the text (including figures, tables and equations), whereas the units and indexes (except for indexes having the meaning of physical quantities) are in upright letters. They should be in Times New Roman font. In graphs and tables, a slash should be used to separate the designation of a physical quantity from the unit

(example: p / kPa, j / mA cm^{-2}, t / °C, T_0 / K, τ / h, ln (j / mA cm^{-2})…). Designations such as: p (kPa), t [min]…, are not acceptable. However, if the full name of a physical quantity is unavoidable, it should be given in upright letters and separated from the unit by a comma (example: Pressure, kPa; Temperature, K; Current density, mA cm^{-2}…). Please do not use the axes of graphs for additional explanations; these should be mentioned in the figure captions and/or the manuscript (example: "pressure at the inlet of the system, kPa" should be avoided). The axis name should follow the direction of the axis (the name of y-axis should be rotated by 90°). Top and right axes should be avoided in diagrams, unless they are absolutely necessary.

Latin words, as well as the names of species, should be in *italic*, as for example: *i.e.*, *e.g.*, *in vivo*, *ibid*, *Calendula officinalis* L., *etc*. The branching of organic compound should also be indicated in *italic*, for example, *n*-butanol, *tert*-butanol, *etc*.

Decimal numbers must have decimal points and not commas in the text (except in the Serbian abstract), tables and axis labels in graphical presentations of results. Thousands are separated, if at all, by a comma and not a point.

Mathematical and chemical equations should be given in separate lines and must be numbered, Arabic numbers, consecutively in parenthesis at the end of the line. All equations should be embedded in the text Complex equations (fractions, integrals, matrix…) should be prepared with the aid of the **Microsoft Equation 3.0** (or higher) or **MathType** (Do not use them to create simple equations and labels). **Using the Insert -> Equation option, integrated in MS Office 2010 and MS Office 2013, as well as insertion of equation objects within paragraph text IS NOT ALLOWED.**

ARTICLE STRUCTURE

- TITLE PAGE;
- MAIN TEXT – including Tables and Illustrations with corresponding captions;
- SUPPLEMENTARY MATERIAL (optional**)**

Title page

- **Title** in bold letters, should be clear and concise, preferably 12 words or less. The use of non-standard abbreviations, symbols and formulae is discouraged.
- AUTHORS' NAMES in capital letters with the full first name, initials of further names separated by a space and surname. Commas should separate the author's names except for the last two names when 'and' is to be used. In multi-affiliation manuscripts, the author's affiliation should be indicated by an Arabic number placed in superscript after the name and before the affiliation. Use * to denote the corresponding author(s).
- *Affiliations* should be written in italic. The e-mail address of the corresponding author should be given after the affiliation(s).
- *Abstract:* A one-paragraph abstract written of 150 – 200 words in an impersonal form indicating the aims of the work, the main results and conclusions should be given and clearly set off from the text. Domestic authors should also submit, on a separate page, an Abstract - Izvod, the author's name(s) and affiliation(s) in Serbian (Cyrillic letters). (Домаћи аутори морају доставити Извод (укључујући имена аутора и афилијацију) на српском језику, исписане ћирилицом, иза Захвалнице, а пре списка референци.) For authors outside Serbia, the Editorial Board will provide a Serbian translation of their English abstract.
- *Keywords:* Up to 6 keywords should be given. Do not use words appearing in the manuscript title
- RUNNING TITLE: A one line (maximum five words) short title in capital letters should be provided.

Main text – should have the form:

- **INTRODUCTION,**
- **EXPERIMENTAL (RESULTS AND DISCUSSION),**
- **RESULTS AND DISCUSSION (EXPERIMENTAL),**
- **CONCLUSIONS,**
- **NOMENCLATURE (optional) and**
- ***Acknowledgements*: If any.**
- REFERENCES (Citation of recent papers published in chemistry journals that highlight the significance of work to the general readership is encouraged.)

The sections should be arranged in a sequence generally accepted for publication in the respective fields. They subtitles should be in capital letters, centred and NOT numbered.

- The INTRODUCTION should include the aim of the research and a concise description of background information and related studies directly connected to the paper.
- The EXPERIMENTAL section should give the purity and source of all employed materials, as well as details of the instruments used. The employed methods should be described in sufficient detail to enable experienced persons to repeat them. Standard procedures should be referenced and only modifications described in detail. On no account should results be included in the experimental section.

Chemistry

Detailed information about instruments and general experimental techniques should be given in all necessary details. If special treatment for solvents or chemical purification were applied that must be emphasized.

Example: Melting points were determined on a Boetius PMHK or a Mel-Temp apparatus and were not corrected. Optical rotations were measured on a Rudolph Research Analytical automatic polarimeter, Autopol IV in dichloromethane (DCM) or methanol (MeOH) as solvent. IR spectra were recorded on a Perkin-Elmer spectrophotometer FT-IR 1725X. ^{1}H and ^{13}C NMR spectra were recorded on a Varian Gemini-200 spectrometer (at 200 and 50 MHz, respectively), and on a Bruker Ultrashield Advance III spectrometer (at 500 and 125 MHz, respectively) employing indicated solvents (*vide infra*) using TMS as the internal standard. Chemical shifts are expressed in ppm (δ / ppm) values and coupling constants in Hz (J / Hz). ESI-MS spectra were recorded on Agilent Technologies 6210 Time-Of-Flight LC-MS instrument in positive ion mode with CH_3CN/H_2O 1/1 with 0.2 % HCOOH as the carrying solvent solution. Samples were dissolved in CH_3CN or MeOH (HPLC grade purity). The selected values were as follows: capillary voltage = 4 kV, gas temperature = 350 °C, drying gas flow 12 L min^{-1}, nebulizer pressure = 310 kPa, fragmentator voltage = 70 V.The elemental analysis was performed on the Vario EL III- C,H,N,S/O Elemental Analyzer (Elementar Analysensysteme GmbH, Hanau-Germany). Thin-layer chromatography (TLC) was performed on precoated Merck silica gel 60 F254 and RP-18 F254 plates. Column chromatography was performed on Lobar LichroPrep Si 60 (40-63 μm), RP-18 (40-63 μm) columns coupled to a Waters RI 401 detector, and on Biotage SP1 system with UV detector and FLASH 12+, FLASH 25+ or FLASH 40+ columns pre packed with KP-SIL [40-63 μm, pore diameter 6 nm (60 Å)], KP-C18-HS (40-63 μm, pore diameter 9 nm (90 Å) or KP-NH [40-63 μm, pore diameter 10 nm (100 Å)] as adsorbent. Compounds were analyzed for purity (HPLC) using a Waters 1525 HPLC dual pump system equipped with an Alltech, Select degasser system, and dual λ 2487 UV-VIS detector. For data processing, Empower software was used (methods A and B). Methods C and D: Agylent Technologies 1260 Liquid Chromatograph equipped with Quat Pump (G1311B), Injector (G1329B) 1260 ALS, TCC 1260 (G1316A) and Detector 1260 DAD VL+ (G1315C). For data processing, LC OpenLab CDS ChemStation software was used. For details, see Supporting Information.

1. Synthesis experiments

Each paragraph describing a synthesis experiment should begin with the name of the product and any structure number assigned to the compound in the Results and Discussions section. Thereafter, the compound should be identified by its structure number. Use of standard abbreviations or unambiguous molecular formulas for reagents and solvents, and of structure numbers rather than chemical names to identify starting materials and intermediates, is encouraged.

When a new or improved synthetic method is described, the yields reported in key experimental examples, and yields used for comparison with existing methods, should represent amounts of isolated and purified products, rather than chromategraphically or spectroscopically determined yields. Reactant quantities should be reported in weight and molar units and for product yields should be reported in weight units; percentage yields should only be reported for materials of demonstrated purity. When chromatography is used for product purification, both the support and solvent should be identified.

2. Microwave experiments

Reports of syntheses conducted in microwave reactors must clearly indicate whether sealed or open reaction vessels were used and must document the manufacturer and model of the reactor, the method of monitoring the reaction mixture temperature, and the temperature-time profile. Reporting a wattage rating or power setting is not an acceptable alternative to providing temperature data. Manuscripts describing work done with domestic (kitchen) microwave ovens will not be accepted except for studies where the unit is used for heating reaction mixtures at atmospheric pressure.

3. Compound characterization

The Journal upholds a high standard for compound characterization to ensure that substances being added to the chemical literature have been correctly identified and can be synthesized in known yield and purity by the reported preparation and isolation methods. For **all new** compounds, evidence adequate to establish both **identity** and **degree of purity** (homogeneity) must be provided.

Identity *- Melting point.* All homogeneous solid products (*e.g.* not mixtures of isomers) should be characterized by melting or decomposition points. The colors and morphologies of the products should also be noted.

Specific rotations. Specific rotations based on the equation $[\alpha]^t; D = (100\ \alpha) / (l\ c)$ should be reported as unitless numbers as in the following example: $[\alpha]^{20}$; D = -25.4 (c 1.93, $CHCl_3$), where c / g mL^{-1} is concentration and l / dm is path length. The units of the specific rotation, (deg mL) / (g dm), are implicit and are not included with the reported value.

Spectra/*Spectral Data.* Important IR adsorptions should be given.

For all new diamagnetic substances, NMR data should be reported (^1H, ^{13}C, and relevant heteronuclei). ^1H NMR chemical shifts should be given with two digits after the decimal point. Include the number of protons represented by the signal, signal multiplicity, and coupling constants as needed (*J* italicized, reported with up to one digit after the decimal). The number of bonds through which the coupling is operative, ^xJ, may be specified by the author if known with a high degree of certainty. ^{13}C NMR signal shifts should be rounded to the nearest 0.01 ppm unless greater precision is needed to distinguish closely spaced signals. Field strength should be noted for each spectrum, not as a comment in the general experimental section. Hydrogen multiplicity (C, CH, CH_2, CH_3) information obtained from routine DEPT spectra should be included. If detailed signal assignments are made, the type of NOESY or COSY methods used to establish atom connectivity and spatial relationships should be identified in the Supporting Information. Copies of spectra should also be included where structure assignments of complex molecules depend heavily on NMR interpretation. Numbering system used for assignments of signals should be given in the Supporting Information with corresponding general structural formula of named derivative.

HPLC/LCMS can be substituted for biochemistry papers where the main focus is not on compound synthesis.

HRMS/*elemental analysis.* To support the molecular formula assignment, HRMS data accurate within 5 ppm, or combustion elemental analysis [carbon and hydrogen (and nitrogen, if present)] data accurate within 0.5 %, should be reported for new compounds. HRMS data should be given in format as is usually given for combustion analysis: calculated mass for given formula following with observed mass: (+)ESI-HRMS *m*/*z*: [molecular formula + H]$^+$ calculated mass, observed mass. Example: (+)ESI-HRMS *m*/*z*: calculated for [$C_{13}H_8BrCl_2N + H^+$] 327.92899, observed 327.92792.

NOTE: in certain cases, a crystal structure may be an acceptable substitute for HRMS/elemental analysis.

Biomacromolecules. The structures of biomacromolecules may be established by providing evidence about sequence and mass. Sequences may be inferred from the experimental order of amino acid, saccharide, or nucleotide coupling, from known sequences of templates in enzyme-mediated syntheses, or through standard sequencing techniques. Typically, a sequence will be accompanied by MS data that establish the molecular weight.

Example: Product was isolated upon column chromatography [dry flash (SiO_2, eluent EA, EA/MeOH gradient 95/5 → 9/1, EA/MeOH/NH_3 gradient 18/0.5/0.5 → 9/1/1, and flash chromatography (Biotage SP1, RP column, eluent MeOH/H_2O gradient 75/25 → 95/5, N-H column, eluent EA/Hex gradient 6/3 → EA). was obtained after flash column chromatography (Biotage SP NH column, eluent hexane/EA 4:6 → 2:6). Yield 968.4 mg (95 %). Colorless foam softens at 96-101 °C. $[\alpha]^{20}$; D = +0,163 (c =2.0×10^{-3} g/mL, CH_2Cl_2). IR (ATR): 3376w, 2949m, 2868w, 2802w, 1731s, 1611w, 1581s, 1528m, 1452m, 1374s, 1331w, 1246s, 1171m, 1063w, 1023m, 965w, 940w, 881w, 850w, 807w, cm^{-1}. ^1H NMR (500 MHz, $CDCl_3$, δ): 8.46 (*d*, 1H, J = 5.4, H-2'), 7.89 (*s*, 1H, J = 2.0, H-8'), 7.71 (*d*, 1H, J = 8.9, H-5'), 7.30 (*dd*, 1H, J_1 = 8.8, J_2 = 2.1, H-6'), 6.33 (*d*, 1H, J = 5.4, H-3'), 6.07 (*s*, HN-Boc, exchangeable with D_2O), 5.06 (*s*, 1H, H-12), 4.92-4.88 (*m*, 1H, H-7), 4.42 (*bs*, H-3), 3.45 (*s*,CH_3-N), 3.33 (*bs*, H-9'), 3.05-2.95 (*m*, 2H, H-11'), 2.70-2.43 (*m*, 2H, H-24) and HN, exchangeable with D_2O), 2.07 (*s*, CH_3COO), 2.04 (*s*, CH_3COO), 1.42 (*s*, 9H, $(CH_3)_3$C-N(Boc)), 0.88 (*s*, 3H, CH_3-10), 0.79 (*d*, 3H,J = 6.6, CH_3-20), 0.68 (*s*, 3H, CH_3-13). ^{13}C NMR (125 MHz, $CDCl_3$, δ): 170.34, 170.27, 151.80, 149.92, 148.87, 134.77, 128.36, 125.11, 121.43, 117.29, 99.98, 75.41, 70.82, 50.43, 49.66, 47.60, 47.33, 44.97, 43.30, 41.83, 41.48, 37.65, 36.35, 35.44, 34.89,

34.19, 33.23, 31.24, 28.79, 28.35, 27.25, 26.45, 25.45, 22.74, 22.63, 21.57, 21.31, 17.85, 12.15. (+)ESI-HRMS (*m/z*): calculated for $[C_{45}H_{67}ClN_4O_6 + H]^+$ 795.48219, observed 795.48185. Combustion analysis for $C_{45}H_{67}ClN_4O_6$: Calculated. C 67.94, H 8.49, N 7.04; found C 67.72, H 8.63, N 6.75. HPLC purity: method A: RT 1.994, area 99.12 %; method C: RT 9.936, area 98.20 %.

Purity **-** Evidence for documenting compound purity should include one or more of the following:

a) Well-resolved high field 1D ^{1}H NMR spectrum showing at most only trace peaks not attributable to the assigned structure and a standard 1D proton-decoupled ^{13}C NMR spectrum. Copies of the spectra should be included as figures in the Supporting Information.
b) Quantitative gas chromatographic analytical data for distilled or vacuum-transferred samples, or quantitative HPLC analytical data for materials isolated by column chromatography or separation from a solid support. HPLC analyses should be performed in two diverse systems. The stationary phase, solvents (HPLC), detector type, and percentage of total chromatogram integration should be reported; a copy of the chromatograms may be included as a figure in the Supporting Information.
c) Electrophoretic analytical data obtained under conditions that permit observing impurities present at the 5 % level.

HRMS data may be used to support a molecular formula assignment **but cannot be used as a criterion of purity**.

4. Biological Data

Quantitative biological data are required for all tested compounds. Biological test methods must be referenced or described in sufficient detail to permit the experiments to be repeated by others. Detailed descriptions of biological methods should be placed in the experimental section. Standard compounds or established drugs should be tested in the same system for comparison. Data may be presented as numerical expressions or in graphical form; biological data for extensive series of compounds should be presented in tabular form. Tables consisting primarily of negative data will not usually be accepted; however, for purposes of documentation they may be submitted as supporting information. Active compounds obtained from combinatorial syntheses should be resynthesized and retested to verify that the biology conforms to the initial observation.

Statistical limits (statistical significance) for the biological data are usually required. If statistical limits cannot be provided, the number of determinations and some indication of the variability and reliability of the results should be given. References to statistical methods of calculation should be included. Doses and concentrations should be expressed as molar quantities (*e.g.*, mol/kg, μmol/kg, M, mM). The routes of administration of test compounds and vehicles used should be indicated, and any salt forms used (hydrochlorides, sulfates, *etc.*) should be noted. The physical state of the compound dosed (crystalline, amorphous; solution, suspension) and the formulation for dosing (micronized, jet-milled, nanoparticles) should be indicated. For those compounds found to be inactive, the highest concentration (*in vitro*) or dose level (*in vivo*) tested should be indicated.

- The RESULTS AND DISCUSSION should include concisely presented results and there significance discussed and compared to relevant literature data. The results and discussion may be combined or kept separate.
- The inclusion of a CONCLUSION section, which briefly summarizes the principal conclusions, is recommended.
- NOMENCLATURE is optional but, if the authors wish, a list of employed symbols may be included.
- REFERENCES should be numbered sequentially as they appear in the text. Please note that any reference numbers appearing in the Illustrations and/or Tables and corresponding captions must follow the numbering sequence of the paragraph in which they appear for the first time. When cited, the reference number should be superscripted in Font 12, following any punctuation mark. In the reference list, they should be in normal position followed by a full stop. Reference entry must not be formatted using Carriage returns (enter key; ↵ key) or multiple space key. The formatting of references to published work should follow the *Journal'*s style as follows:

Journals[a]:	A. B. Surname1, C. D. Surname2, *J. Serb. Chem. Soc.* **Vol** (Year) first page Number (https://doi.org/doi)[b]
Books:	A. B. Surname1, C. D. Surname2, *Name of Book*, Publisher, City, Year, pp. 100-101 (https://doi.org/doi)[b]
Compilations:	A. B. Surname1, C. D. Surname2, in *Name of Compilation*, A. Editor1, C. Editor2, Ed(s)., Publisher, City, Year, p. 100 (https://doi.org/doi)[b]
Proceedings:	A. B. Surname1, C. D. Surname2, in *Proceedings of Name of the Conference or Symposium*, (Year), Place of the Conference, Country, *Title of the Proceeding*, Publisher, City, Year, p. or Abstract No. 100
Patents:	A. B. Inventor1, C. D. Inventor2, (Holder), Country Code and patent number (registration year)
Chemical Abstracts:	A. B. Surname1, C. D. Surname2, *Chem. Abstr*. CA 234 567a; For non-readily available literature, the Chemical Abstracts reference should be given in square brackets: [C.A. 139/2003 357348t] after the reference
Standards:	EN ISO 250: *Name of the Standard* (Year)
Websites:	Title of the website, URL in full (date accessed)

[a] When citing Journals, the International Library Journal abbreviation is required. Please consult, *e.g.*, https://images.webofknowledge.com/WOK46/help/WOS/A_abrvjt.html

[b] doi should be replaced by doi number of the Article, for example: http://dx.doi.org/10.2298/JSC161212085B (as active link). If doi do not exist, provide the link to the online version of the publication.

Only the last entry in the reference list should end with a full stop.

The names of all authors should be given in the list of references; the abbreviation *et al.* may only be used in the text. The original journal title is to be retained in the case of publications published in any language other than English (please denote the language in parenthesis after the reference). Titles of publications in non-Latin alphabets should be transliterated. Russian references are to be transliterated using the following transcriptions:

ж→zh, х→kh, ц→ts, ч→ch, ш→sh, щ→shch, ы→y, ю→yu, я→ya, э→e, й→i, ь→’.

Supplementary material

Authors are encouraged to presentthe information and results non-essential to the understanding of their paper as SUPPLEMENTARY MATERIAL (can be uploaded inStep 4 of Online Submission). This material may include as a rule, but is not limited to, the presentation of analytical and spectral data demonstrating the identity and purity of synthesized compounds, tables containing raw data on which calculations were based, series of figures where one example would remain in the main text, etc. The Editorial Board retain the right to assign such information and results to the Supplementary material when deemed fit. Supplementary material does not appear in printed form but can be downloaded from the web site of the JSCS.

Mathematical and chemical equations should be given in separate lines and must be numbered, Arabic numbers, consecutively in parenthesis at the end of the line. All equations should be embedded in the text Complex equations (fractions, integrals, matrix…) should be prepared with the aid of the Microsoft Equation 3.0 (or higher) or MathType (Do not use them to create simple equations and labels). Using the Insert -> Equation option, integrated in MS Office 2010 and MS Office 2013, as well as insertion of equation objects within paragraph text IS NOT ALLOWED.

Deposition of crystallographic data

Prior to submission, the crystallographic data included in a manuscript presenting such data should be deposited at the appropriate database. Crystallographic data associated with organic and metal-organic structures should be deposited at the Cambridge Crystallographic Data Centre (CCDC) by e-mail to **deposit@ccdc.cam.ac.uk**

Crystallographic data associated with inorganic structures should be deposited with the Fachinformationszentrum Karlsruhe (FIZ) by e-mail to **crysdata@fiz-karlsruhe.de**. A deposition number will then be provided, which should be added to the reference section of the manuscript.

For detailed instructions please visit the JSCS website:
https://www.shd-pub.org.rs/index.php/JSCS/Instructions

ARTWORK INSTRUCTIONS

JSCS accepts only **TIFF** or **EPS** formats, as well as **JPEG** format (only for colour and greyscale photographs) for electronic artwork and graphic files. **MS files** (Word, PowerPoint, Excel, Visio) **NOT acceptable**. Generally, scanned instrument data sheets should be avoided. Authors are responsible for the quality of their submitted artwork. Every single Figure or Scheme, as well as any part of the Figure (A, B, C…) should be prepared according to following instructions (every part of the figure, A, B, C…, must be submitted as an independent single graphic file):

TIFF

Virtually all common artwork and graphic creation software is capable of saving files in TIFF format. This 'option' can normally be found under 'the 'Save As...' or 'Export...' commands in the 'File' menu.

TIFF (Tagged Image File Format) is the recommended file format for bitmap, greyscale and colour images.

- Colour images should be in the RGB mode
- When supplying TIFF files, please ensure that the files are supplied at the correct resolution:
    1. Line artwork: minimum of 1000 dpi
    2. RGB image: minimum of 300 dpi
    3. Greyscale image: minimum of 300 dpi
    4. Combination artwork (line/greyscale/RGB): minimum of 500 dpi
- Images should be tightly cropped, without frame and any caption.
- If applicable please re-label artwork with a font supported by JSCS (Arial, Helvetica, Times, Symbol) and ensure it is of an appropriate font size.
- Save an image in TIFF format with LZW compression applied.
- It is recommended to remove Alpha channels before submitting TIFF files.
- It is recommended to flatten layers before submitting TIFF files.

Please be sure that quality of an image cannot be increased by changing the resolution from lower to higher, but only by rescanning or exporting the image with higher resolution, which can be set in usual "settings" facilities.

EPS

Virtually all common artwork creation software, such as Canvas, ChemDraw, CorelDraw, SigmaPlot, Origin Lab…, are capable of saving files in EPS format. This 'option' can normally be found under the 'Save As...' or 'Export...' commands in the 'File' menu.

For vector graphics, EPS (Encapsulated PostScript) files are the preferred format as long as they are provided in accordance with the following conditions:

- when they contain bitmap images, the bitmaps should be of good resolution (see instructions for TIFF files)
- when colour is involved, it should be encoded as RGB
- an 8-bit preview/header at a resolution of 72 dpi should always be included
- embed fonts should always included and only the following fonts should be used in artwork: Arial, Helvetica, Times, Symbol
- the vertical space between the parts of an illustration should be limited to the bare necessity for visual clarity
- no data should be present outside the actual illustration area
- line weights should range from 0.35 pt to 1.5 pt
- when using layers, they should be reduced to one layer before saving the image (Flatten Artwork)

JPEG

Virtually all common artwork and graphic creation software is capable of saving files in JPEG format. This 'option' can normally be found under 'the 'Save As...' or 'Export...' commands in the 'File' menu.

JPEG (Joint Photographic Experts Group) is the acceptable file format **only for colour and greyscale photographs**. JPEG can be created with respect to photo quality (low, medium, high; from 1 to 10), ensuring file sizes are kept to a minimum to aid easy file transfer. Images should have a minimum resolution of 300 dpi. Image width: minimum 3.0 cm; maximum 12.0 cm.

Please be sure that quality of an image cannot be increased by changing the resolution from lower to higher, but only by rescanning or exporting the image with higher resolution, which can be set in usual "settings" facilities.

SIZING OF ARTWORK

- JSCS aspires to have a uniform look for all artwork contained in a single article. Hence, it is important to be aware of the style of the journal.
- Figures should be submitted in black and white or, if required, colour (charged). If coloured figures or photographs are required, this must be stated in the cover letter and arrangements made for payment through the office of the Serbian Chemical Society.
- As a general rule, the lettering on an artwork should have a finished, printed size of 11 pt for normal text and no smaller than 7 pt for subscript and superscript characters. Smaller lettering will yield a text that is barely legible. This is a rule-of-thumb rather than a strict rule. There are instances where other factors in the artwork, (for example, tints and shadings) dictate a finished size of perhaps 10 pt. Lines should be of at least 1 pt thickness.
- When deciding on the size of a line art graphic, in addition to the lettering, there are several other factors to address. These all have a bearing on the reproducibility/readability of the final artwork. Tints and shadings have to be printable at the finished size. All relevant detail in the illustration, the graph symbols (squares, triangles, circles, *etc*.) and a key to the diagram (to explain the explanation of the graph symbols used) must be discernible.
- The sizing of halftones (photographs, micrographs,...) normally causes more problems than line art. It is sometimes difficult to know what an author is trying to emphasize on a photograph, so you can help us by identifying the important parts of the image, perhaps by highlighting the relevant areas on a photocopy. The best advice that can be given to graphics suppliers is not to over-reduce halftones. Attention should also be paid to magnification factors or scale bars on the artwork and they should be compared with the details inside. If a set of artwork contains more than one halftone, again please ensure that there is consistency in size between similar diagrams.

General sizing of illustrations which can be used for the Journal of the Serbian Chemical Society:

- Minimum fig. size: 30 mm width
- Small fig. size - 60 mm width
- Large fig. size - 90 mm width
- Maximum fig. size - 120 mm width

Pixel requirements (width) per print size and resolution for bitmap images:

	Image width	A	B	C
Minimal size	30 mm	**354**	**591**	**1181**
Small size	60 mm	**709**	**1181**	**2362**
Large size	90 mm	**1063**	**1772**	**3543**
Maximal size	120 mm	**1417**	**2362**	**4724**

A: 300 dpi > RGB or Greyscale image
B: 500 dpi > Combination artwork (line/greyscale/RGB)
C: 1000 dpi> Line artwork

The designation of physical quantities and graphs formatting

The designation of physical quantities on figures must be in italic, whereas the units are in upright letters. They should be in Times New Roman font. In graphs a slash should be used to separate the designation of a physical quantity from the unit (example: p / kPa, t °C, T_0 / K, τ / h, ln (j / mA cm^{-2})…). Designations such as: p (kPa), t [min]…, are not acceptable. However, if the full name of a physical quantity is unavoiable, it should be given in upright letters and separated from the unit by a comma (example: Pressure, kPa, Temperature, K…). Please do not use the axes of graphs for additional explanations; these should be mentioned in the figure captions and/or the manuscript (example: "pressure at the inlet of the system, kPa" should be avoided). The axis name should follow the direction of the axis (the name of y-axis should be rotated by 90°). Top and right axes should be avoided in diagrams, unless they are absolutely necessary. Decimal numbers must have decimal points and not commas in the axis labels in graphical presentations of results. Thousands are separated, if at all, by a comma and not a point.

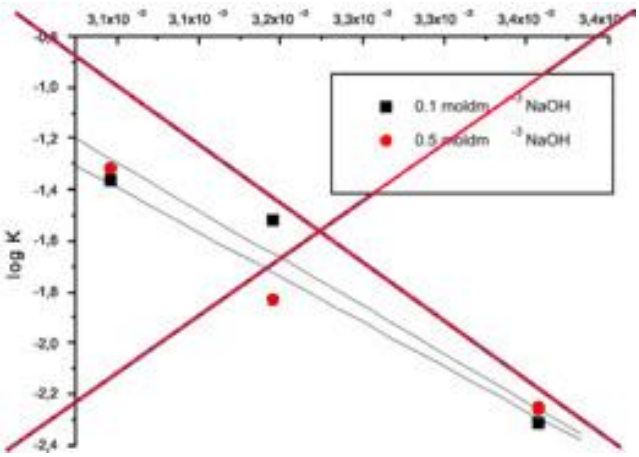

INCORRECT

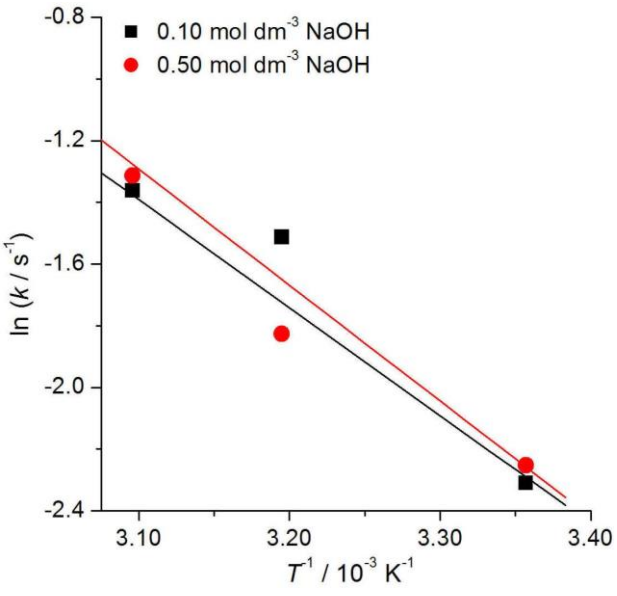

CORRECT

The **Journal of the Serbian Chemical Society** (formerly Glasnik Hemijskog društva Beograd), one volume (12 issues) per year, publishes articles from the fields of chemistry. The **Journal** is financially supported by the **Ministry of Education, Science and Technological Development of the Republic of Serbia.**

Articles published in the **Journal** are indexed in **Clarivate Analytics products: Science Citation Index-Expanded™** – accessed *via* **Web of Science®** and **Journal Citation Reports®**.

Impact Factor announced 2021: **1.240; 5-year Impact Factor**: **1.144**.

Articles appearing in the **Journal** are also abstracted by: **Scopus, Chemical Abstracts Plus (CAplus℠), Directory of Open Access Journals, Referativnii Zhurnal (VINITI), RSC Analytical Abstracts, EuroPub, Pro Quest** and **Asian Digital Library.**

Publisher:	**Serbian Chemical Society**, Karnegijeva 4/III, P. O. Box 36, 1120 Belgrade 35, Serbia tel./fax: +381–11–3370–467, E-mails: **Society** – shd@shd.org.rs; **Journal** – jscs@shd.org.rs Home Pages: **Society** – http://www.shd.org.rs/, **Journal** – http://www.shd.org.rs/JSCS/
Internet Service:	Contents, Abstracts and full papers (from Vol 64, No. 1, 1999) are available in the electronic form at the Web Site of the **Journal** (http://www.shd.org.rs/JSCS/).
Former Editors:	**Nikola A. Pušin** (1930–1947), **Aleksandar M. Leko** (1948–1954), **Panta S. Tutundžić** (1955–1961), **Miloš K. Mladenović** (1962–1964), **Đorđe M. Dimitrijević** (1965–1969), **Aleksandar R. Despić** (1969–1975), **Slobodan V. Ribnikar** (1975–1985), **Dragutin M. Dražić** (1986–2006).
Editor-in-Chief:	BRANISLAV Ž. **NIKOLIĆ**, Serbian Chemical Society (E-mail: jscs-ed@shd.org.rs)
Deputy Editor:	DUŠAN **SLADIĆ**, Faculty of Chemistry, University of Belgrade
Sub editors:	
Organic Chemistry	DEJAN **OPSENICA**, Institute of Chemistry, Technology and Metallurgy, University of Belgrade JÁNOS **CSANÁDI**, Faculty of Science, University of Novi Sad
Biochemistry and Biotechnology	OLGICA **NEDIĆ**, INEP – Institute for the Application of Nuclear Energy, University of Belgrade
Inorganic Chemistry	MILOŠ **ĐURAN**, Serbian Chemical Society
Theoretical Chemistry	IVAN **JURANIĆ**, Serbian Chemical Society
Physical Chemistry	LJILJANA **DAMJANOVIĆ-VASILIĆ**, Faculty of Physical Chemistry, University of Belgrade
Electrochemistry	SNEŽANA **GOJKOVIĆ**, Faculty of Technology and Metallurgy, University of Belgrade
Analytical Chemistry	SLAVICA **RAŽIĆ**, Faculty of Pharmacy, University of Belgrade
Polymers	BRANKO **DUNJIĆ**, Faculty of Technology and Metallurgy, University of Belgrade
Thermodynamics	MIRJANA **KIJEVČANIN**, Faculty of Technology and Metallurgy, University of Belgrade
Chemical Engineering	TATJANA **KALUĐEROVIĆ RADOIČIĆ**, Faculty of Technology and Metallurgy, University of Belgrade
Materials	RADA **PETROVIĆ**, Faculty of Technology and Metallurgy, University of Belgrade
Metallic Materials and Metallurgy	NENAD **RADOVIĆ**, Faculty of Technology and Metallurgy, University of Belgrade
Environmental and Geochemistry	VESNA **ANTIĆ**, Faculty of Agriculture, University of Belgrade
History of and Education in Chemistry	DRAGICA **TRIVIĆ**, Faculty of Chemistry, University of Belgrade
English Language Editors:	LYNNE **KATSIKAS**, Serbian Chemical Society VLATKA **VAJS**, Serbian Chemical Society JASMINA **NIKOLIĆ**, Faculty of Technology and Metallurgy, University of Belgrade
Technical Editors:	VLADIMIR **PANIĆ**, ALEKSANDAR **DEKANSKI**, VUK **FILIPOVIĆ**, Institute of Chemistry, Technology and Metallurgy, University of Belgrade
Journal Manager & Web Master:	ALEKSANDAR **DEKANSKI,** Institute of Chemistry, Technology and Metallurgy, University of Belgrade
Office:	VERA **ĆUŠIĆ**, Serbian Chemical Society

Editorial Board

From abroad: **R. Adžić**, Brookhaven National Laboratory (USA); **A. Casini**, University of Groningen (The Netherlands); **G. Cobb**, Baylor University (USA); **D. Douglas**, University of British Columbia (Canada); **G. Inzelt**, Etvos Lorand University (Hungary); **N. Katsaros**, NCSR "Demokritos", Institute of Physical Chemistry (Greece); **J. Kenny**, University of Perugia (Italy); **Ya. I. Korenman**, Voronezh Academy of Technology (Russian Federation); **M. D. Lechner**, University of Osnabrueck (Germany); **S. Macura**, Mayo Clinic (USA); **M. Spiteller**, INFU, Technical University Dortmund (Germany); **M. Stratakis**, University of Crete (Grecce); **M. Swart**, University de Girona (Cataluna, Spain); **G. Vunjak-Novaković**, Columbia University (USA); **P. Worsfold**, University of Plymouth (UK); **J. Zagal**, Universidad de Santiago de Chile (Chile).

From Serbia: **B. Abramović**, **V. Antić, V. Beškoski**, **J. Csanadi**, **Lj. Damjanović-Vasilić**, **A. Dekanski**, **V. Dondur**, **B. Dunjić**, **M. Đuran, S. Gojković**, **I. Gutman**, **B. Jovančićević**, **I. Juranić**, **L. Katsikas**, **M. Kijevčanin**, **V. Leovac**, **S. Milonjić**, **V.B. Mišković-Stanković, O. Nedić**, **B. Nikolić**, **J. Nikolić, D. Opsenica**, **V. Panić**, **M. Petkovska**, **R. Petrović**, **I. Popović**, **B. Radak**, T. **Kaluđerović Radiočić, N. Radović**, **S. Ražić**, **D. Sladić**, **S. Sovilj**, **S. Šerbanović**, **B. Šolaja**, **Ž. Tešić**, **D. Trivić, V. Vajs**.

Subscription: The annual subscription rate is **150.00 €** including postage (surface mail) and handling. For Society members from abroad rate is **50.00 €**. For the proforma invoice with the instruction for bank payment contact the Society Office (E-mail: shd@shd.org.rs) or see JSCS Web Site: http://www.shd.org.rs/JSCS/, option Subscription.

Godišnja pretplata: Za članove SHD: **2.500,00 RSD**, za penzionere i studente: **1000,00 RSD**, a za ostale: **3.500,00 RSD**:za organizacije i ustanove: **16.000,00 RSD**. Uplate se vrše na tekući račun Društva: **205-13815-62**, poziv na broj **320**, sa naznakom "pretplata za JSCS".

Nota: Radovi čiji su svi autori članovi SHD prioritetno se publikuju.

Odlukom Odbora za hemiju Republičkog fonda za nauku Srbije, br. 66788/1 od 22.11.1990. godine, koja je kasnije potvrđena odlukom Saveta Fonda, časopis je uvršten u kategoriju međunarodnih časopisa (**M-23**). Takođe, aktom Ministarstva za nauku i tehnologiju Republike Srbije, 413-00-247/2000-01 od 15.06.2000. godine, ovaj časopis je proglašen za publikaciju od posebnog interesa za nauku. **Impact Factor** časopisa objavljen 2021. godine iznosi **1,240**, a petogodišnji **Impact Factor 1,144**.

Journal of the Serbian Chemical Society
JSCS-info@shd.org.rs • www.shd.org.rs/JSCS

J. Serb. Chem. Soc. Vol. 86, No. 11 (2021)

CONTENTS*

Published by the Serbian Chemical Society
Karnegijeva 4/III, P.O. Box 36, 11120 Belgrade, Serbia
Printed by the Faculty of Technology and Metallurgy
Karnegijeva 4, P.O. Box 35-03, 11120 Belgrade, Serbia

* For colored figures in this issue please see electronic version at the Journal Home Page: http://www.shd.org.rs/JSCS/

Journal of the Serbian Chemical Society
JSCS@tmf.bg.ac.rs • www.shd.org.rs/JSCS
J. Serb. Chem. Soc. *86* (11) 1013–1021 (2021)
JSCS–5479
Original scientific paper
Published 1 October 2021

Synthesis and assessment of the cytotoxic effect of some of 1,4-dihydropyridine derivatives which contain azole moiety

SAEED GHORBANNEJAD[1], KARIM AKBARI DILMAGHANI[1]* and ABBAS NIKOO[2]

[1]*Department of Chemistry, Faculty of Science, Urmia University, Urmia, Iran and* [2]*Shahid Bakeri High Education Center, Urmia University, Urmia, Iran*

(Received 18 August 2020, revised 5 August, accepted 10 August 2021)

Abstract: A number of 1,4-dihydropyridine derivatives (**9a**–**d**, **10a**–**d** and **11a**–**d**) were designed and synthesized by the reaction of 1,3,4-oxadiazole-5-thiones and 1,2,4-triazole-5-thiones to 2,6-dibromomethyl-3,5-diethoxycarbonyl-4-(3--nitrophenyl)-1,4-dihydropyridine. The synthesized compounds were characterized using FT-IR, ^{1}H-NMR, ^{13}C-NMR spectral data, ESI-MS and elemental analysis. The cytotoxicity of the synthesized compounds was evaluated in human breast cancer (MCF-7) cells based on the results of MTT assay. The results indicated that compound diethyl 4-(3-nitrophenyl)-2,6-bis[((5-(3-nitrophenyl)-1,3,4-oxadiazol-2-yl)thio)methyl]-1,4-dihydro pyridine-3,5-dicarboxylate (**9b**) with (IC_{50} = 23±2.32 μM) was the most potent derivative against MCF-7 cells. Based on the results, the use of oxadiazole moiety in the C2 and C6 positions of 1,4-dihydropyridine ring system enhanced the cytotoxic potential of these derivatives. Therefore, some of the oxadiazole-substituted 1,4-DHPs may facilitate further modifications which result in the discovery of potent cytotoxic agents.

Keywords: dimethylformamide; 3-nitrobenzaldehyde; 1,3,4-oxadiazole; 1,2,4-triazole.

INTRODUCTION

1,4-Dihydropyridines (DHPs) have assumed considerable importance in the field of organic and medicinal chemistry due to their interesting pharmacological activities. The results of different studies have highlighted the fact that the DHPs are highly effective calcium antagonists and are used for treating various cardiovascular system (CVS) activities.[1–3] In addition to the CVS activities of DHPs, they possess a variety of biological activities including, cytotoxic activities,[4–6] anti-proliferative activities,[7] multidrug resistance activities[8,9] and anti-tumour activities.[10–13] However, synthesizing DHPs derivatives is an active and ongoing

* Corresponding author. E-mail: k.adilmaghani@urmia.ac.ir
https://doi.org/10.2298/JSC200818064G

research area. Chemotherapy is still one of the most effective methods for treating cancer. The potential uses of the DHPs scaffolds in the chemotherapy are well-documented and stem from their suitability for reversing the drug resistance in the treatment of cancer.[14,15] Calcium channel blockers like verapamil[16] and nicardipine,[17] among others have been reported to successfully overcome drug resistance.

Notwithstanding, the introduction of calcium channel blockers to clinical use might pose a therapeutic problem which results from their strong vasodilator function.[18] Consequently, a substance which has a strong capability to overcome anticancer drug resistance and does not lead to calcium antagonistic activity can be of great value in chemotherapy. Research has shown that, generally, DHPs display more cytotoxicity towards cancer cells in comparison with the non-cancer cells.[19] The discovery of new DHP derivatives can encourage the development of novel and effective therapies for diverse pathologies, including cancer.

The efficiency of oxadiazole and triazole derivatives has been assessed and proved for a wide range of pharmacological uses. The connection of 1,3,4-oxadiazoles or 1,2,4-triazoles to the 1,4-DHPs core has produced a combination scaffold. The DHPs can be selectively functionalized in several positions. The synthesis and anticancer activities of bis(1,3,4-oxadiazole-2-thiol) and bis(4-amino-1,2,4-triazole-3-thiole) derivatives of DHPs in the C3 and C5 have been reported.[20] Moreover, research has shown the synthesis and biological activities of 1,3,4-oxadiazole derivatives which are linked to N1 of DHP ring system.[21] In spite of the highly developed chemistry of the DHPs, there is not adequate information about the synthesis of 1,4-DHPs bearing-substituents other than hydrogen atoms or alkyl groups in the C2 and C6. In our previous study, we reported the synthesis and antimicrobial assessment of 1,4-dihydropyridines with azole derivatives in the C2 and C6 positions of DHP ring.[22] Based on the above-mentioned gap in the related literature, the present study focuses on synthesizing the novel 1,4-dihydropyridine derivative, which are linked to triazole and oxadiazole moieties, and evaluating their cytotoxic activities.

EXPERIMENTAL

The chemicals of Sigma–Aldrich and Merck were used to produce the chemicals of this study. The solvents were purified based on the standard procedures before their use in the study. The thin-layer chromatography (TLC) analysis was performed in the case of the recoated silica gel (E-Merck kieselgel 60 F_{254} Aluminium sheets) plates. *N*-bromosuccinimide (NBS) and tetramethylsilane (TMS) were purchased from Merck. The melting points were determined on open capillaries using a digital melting point apparatus. The FT-IR spectra were recorded as KBr pellets on a thermo Nicolet Nexus 670 FT-IR. The ^{1}H- and ^{13}C-NMR spectra were recorded on the Bruker Avance AQS 300 MHz spectrometer at 300 and 100 MHz, respectively. The chemical shifts were measured in dimethyl sulfoxide (DMSO-d_6) as solvent relative to TMS as the internal standard. These abbreviations were used to describe the multiplicities of signals in NMR spectra (s = singlet, d = doublet, t = triplet, q = quartet, dd =

doublet of doublets and br = broad signal). The mass spectra were recorded on a JEOL-JMS 600 (FAB MS) instrument and the ESI-MS spectra were recorded on an Agilent Technologies 5975C VL MSD mass spectrometer which operated at an ionization potential of 70 eV. The CHNS analysis was performed using CHNS-932 Leco analyser. The **3a**–**d**[23,24], **4a**–**d**[25], **5a**–**d**[26] and **6a**–**d**[27] compounds were produced according to the reviewed literature.

Analytical and spectral data of the synthesized compound are given in Supplementary material to this paper.

Procedure for preparing diethyl 2,6-dimethyl-4-(3-nitrophenyl)-1,4-dihydropyridine-3,5-dicarboxylate (7)

A mixture of ethylacetoacetate (0.02 mol, 2.60 g), ammonium acetate (0.015 mol, 1.16 g) and 3-nitrobenzaldehyde (0.01 mol, 1.51 g) in 50 % ethanol (50 mL) was mixed well under reflux for 12 h. The contests were cooled after the reaction (which was monitored by TLC *via* *n*-hexane/EtOAc (4:1) as eluent. The precipitate was filtered, washed with water and crystallized from ethanol.[28,29]

*Procedure for synthesizing diethyl 2,6-bis(bromomethyl)-4-(3-itrophenyl)-1,4-dihydropyridine-3,5-dicarboxylate (**8**)*

NBS (0.02 mol, 3.56 g) was added to a solution of the diethyl 2,6-dimethyl-4-(3-nitrophenyl)-1,4-dihydropyridine-3,5-dicarboxylate (**7**, 0.01 mol, 3.74 g) in methanol (100 mL) portion-wise at ambient temperature. The reaction mixture was stirred at room temperature for 24 h. The pale yellow precipitate was filtered and washed with water. The precipitate was crystallized from ethanol.[29]

*General procedure for synthesizing the **9a**–**d**, **10a**–**d** and **11a**–**d** compounds*

A mixture of **3a**–**d, 4a**–**d** or **6a**–**d** (0.02 mol), NaOH (0.02 mol, 0.8 g) and DMF/H_2O (50/50, 50 mL) was stirred at room temperature for 1 h. Moreover, diethyl 2,6-bis(bromomethyl)-4-(3-nitrophenyl)-1,4-dihydropyridine-3, and 5-dicarboxylate (**8**, 0.01 mol, 5.32 g) were added to it and it was stirred at room temperature for 8–12 h. The reaction mixture was poured into water (100 mL) and the residue was extracted with CH_2Cl_2. The organic layer was washed with water, dried over Na_2SO_4 and evaporated and recrystallized from ethanol.

Biological assessment

Reagent and chemical. (RPMI-1640) and fetal bovine serum (FBS) were purchased from (Gibco, USA). 3-(4,5-Dimethylthiazole-2-yl)-2,5-diphenyltetrazolium bromide (MTT) was obtained from Sigma. Penicillin/streptomycin was purchased from Invitrogen (San Diego, CA, USA). Dimethyl sulphoxide (DMSO) were obtained from Merck.

Cell culture. The human breast cancer cells (MCF-7) were purchased from National Cell Bank of Iran (Pasteur, Tehran, Iran). These cells were cultured in Roswell Park Memorial Institute 1640 (RPMI-1640) (Gibco, USA) medium which was enriched with 10 % fetal bovine serum (FBS, Gibco, USA), 100 unit/mL penicillin and 100 mg/mL streptomycin and was maintained under 37 °C and 5 % CO_2 conditions. The cells, which reached the 70 % confluence, were sub cultured and were used for conducting the experiments.

Cell viability assay (MTT). In order to determine the cytotoxic effect of various compounds on the viability of MCF-7 cells, the MTT reduction assay was performed as described previously.[30-32] First MCF-7 cells were plated in 96-well microplates at a density of 1×10^4 cells per well and were maintained overnight at 37 °C to allow them to attach to the bottom of the wells. After cell attachment, the medium was removed and cells were treated with various compounds (**9a**–**d**, **10a**–**d** and **11a**–**d**) at the concentrations which ranged from 10 to 100 μM.

All of the compounds were dissolved in DMSO and were diluted in medium in a way that the maximum concentration of DMSO in the wells did not exceed 0.5 %. Cells were further incubated for 48 h. Thirdly, the fresh medium, which contained 500 µg/mL MTT powder, was added to each well and plates were incubated for another 4 h time at 37 °C. Then MTT and media mixtures were removed and formazan crystals which formed by the mitochondrial dehydrogenase activity of vital cell were solubilized in 200 µl DMSO and was put on an orbital shaker for 20 min. Finally, the absorbance of each plate was measured at 570 nm with the background correction at 620 nm using an Elisa plate reader (Statefax, USA). Effects of the drug cell viability were calculated using cells treated with DMSO as control. Cell survival was calculated using the formula: Survival, % = [(absorbance of treated cells – absorbance of culture medium)/(absorbance of untreated cells – absorbance of culture medium)]×100. The experiment was done in triplicate and the inhibitory concentration (*IC*) values were calculated from a dose-response curve. Graph Pad Prism software 6.01 was used to calculate IC_{50} values. IC_{50} is the concentration in µM required for 50 % inhibition of cell growth as compared to that of the untreated control. IC_{50} values were determined from the linear portion of the curve by calculating the concentration of agent that reduced absorbance in treated cells, compared to control cells, by 50 %. Evaluation is based on mean values from three independent experiments, each comprising at least six micro cultures per concentration level. IC_{50} Values represent the mean of triplicate determination (n = 3) ± *SD* with (95 %) confidence interval. The cytotoxicity of the synthesized derivatives was not compared to standard drugs.[33]

RESULTS AND DISCUSSION

The **3a**–**d**, **4a**–**d**, **5a**–**d** and **6a**–**d** derivatives were prepared according to the method which was described in the relevant literature.[23–27] It is well-known that the thiol–thione tautomeric equilibrium exists in **3a**–**d**, **4a**–**d** and **6a**–**d** compounds. On the basis of ^{1}H-NMR and FT-IR experimental findings, it is argued that the thione tautomer is more stable than thiol in the solution. ^{1}H-NMR spectra of these compounds exhibited the NH signal as a broad peak in the δ 12–14 ppm range which supports the proposed thione structure. The appearance of a C=S absorption peak in the 1248–1278 cm^{-1} region indicated that the oxadiazoles and triazoles were in their thione form.[34]

Diethyl 2,6-dimethyl-4-(3-nitrophenyl)-1,4-dihydropyridine-3,5-dicarboxylate (**7**) was synthesized using the classical Hantzsch three-component reaction method. This method includes the cyclocondensation of 3-nitrobenzaldehyde with two equivalents of ethyl acetoacetate in the presence of a nitrogen donor such as ammonia or ammonium acetate (based on the procedure reported in the literature).[33] We needed a quick entry into 1,4-dihydropyridine-3,5-dicarboxylic acid diesters in which the 2,6-methyl groups were altered by a range of different groups. Allylic bromination is the replacement of a hydrogen on a carbon adjacent to a double bond. Allylic bromination in dihydropyridines was performed by NBS.

The synthesis of 2,6-dibromomethyl-3,5-diethoxycarbonyl-1,4-dihydropyridine (**8**) was achieved as a result of the bromination of the corresponding 2,6-dimethyl-4-(3-nitrophenyl)-1,4-dihydropyridine-3,5-dicarboxylate (**7**) by NBS in methanol according to the procedure which was described in the literature.[29] The

bromine atoms in compound **8** can be replaced with the other substituents (Scheme 1).

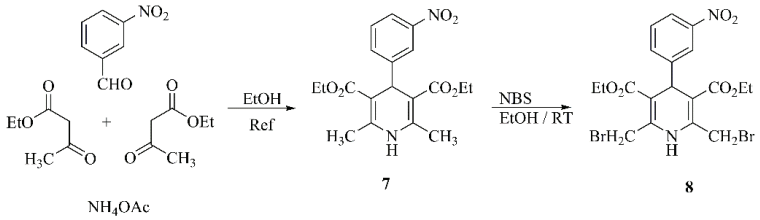

Scheme 1. Synthesis of compound **8**.

The replacement of the bromines of compound **8** with 1,2,4-triazole-5-thiones **3a**–**d**, 1,3,4-oxadiazole-5-thiones **4a**–**d** and 4-amino-3-mercapto-1,2,4-triazoles **6a**–**d** was carried out in the presence of sodium hydroxide as a base in DMF in order to afford the corresponding coupled 1,4- DHP_S (**9a**–**d**, **10a**–**d** and **11a**–**d**) (Scheme 2).

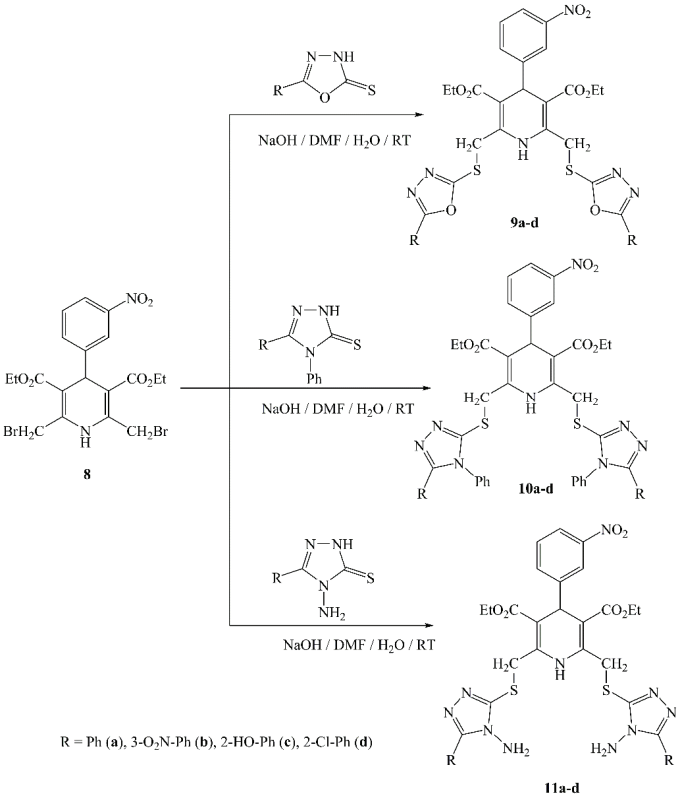

Scheme 2. The synthesis of compounds **9a**–**d**, **10a**–**d** and **11a**–**d**.

The structures of **9a**–**d**, 10**a**–**d** and **11a**–**d** compounds were identified using spectroscopic methods. In the IR spectra the disappearance of the C=S absorption peak in the 1248–1278 cm^{-1} region and the absence of NH peak at δ 12–14 ppm supported the connection of oxadiazole and triazoles to 1,4-DHP ring. The CH_2X protons in the C2 and C6 positions of symmetrically substituted 1,4-dihydropyridine ring became diastereotopic and provided an AB system in the corresponding ^{1}H-NMR spectra. The extent of the observed anisotropy of the methylene protons must have been influenced by the spatial conformation between the ester groups and the formation of a CH···O=C intramolecular hydrogen bonding.[35]

The increase in concentration resulted in a decrease in the viability of cells for all of the compounds and indicated that the cytotoxicity of all of the compounds depended on the concentration. Some of the compounds including **10a** and **c** did not display a high level of cytotoxicity towards MCF-7 cells. Nonetheless, a number of the other compounds including **9b** and **d** displayed a high level of cytotoxicity towards these cells at a concentration which was confirmed by their IC_{50} values. According to the in vitro MTT assay, the IC_{50} represents the concentration of the newly synthesized compounds that is required for 50 % inhibition of the human breast cancer cell (MCF-7) viability. The IC_{50} value for each compound was calculated and summarized in Table I. As shown in Table I, based on the IC_{50} value, the most cytotoxic compound was **9b**. Therefore, it can be suggested that, this compound is a potent cytotoxic agent.

TABLE I. Cytotoxic activity of the synthesized 1,4-DHP derivatives assessed by the MTT assay

Compound	R	Molecular weight	IC_{50} / μM MCF-7	IC_{50} / μg mL^{-1} MCF-7
9a	C_6H_5–	726	45±2.72	32.67
9b	3-NO_2–C_6H_4–	816	23±2.32	18.76
9c	2-HO–C_6H_4–	758	40±4.65	30.32
9d	2-Cl–C_6H_4–	794	33±1.55	26.20
10a	C_6H_5–	876	63±3.10	55.12
10b	3-NO_2–C_6H_4–	966	57±4.27	55.06
10c	2-OH–C_6H_4–	908	>100	
10d	2-Cl–C_6H_4–	944	49±3.10	46.25
11a	C_6H_5–	754	54±3.10	40.71
11b	3-NO_2–C_6H_4–	844	44±1.8	36.16
11c	2-HO–C_6H_4–	786	51±4.6	39.16
11d	2-Cl–C_6H_4–	822	47±4.65	38.63

CONCLUSION

In the present study, diethyl-2,6-dimethyl-4-(3-nitrophenyl)-1,4-dihydropyridine-3 and 5-dicarboxylate derivatives were coupled with 1,3,4-oxadiazole-5-thiones and 1,2,4-triazole-5-thiones in the C2, C6 positions of 1,4-dihydropyridine ring system in order to produce compounds with greater cytotoxicity. The synthesized compounds were characterized using FT-IR, ^{1}H-NMR, ^{13}C-NMR spec-

tral data, ESI mass and elemental analysis. The cytotoxic effects of the new compounds on human breast cancer (MCF-7) cells were investigated using MTT assay. The results of the MTT assay showed that a number of compounds including **9b** and **d** displayed good cytotoxicity at a certain concentration. This finding was confirmed by their IC_{50} values. The highest potency was observed in the case of MCF-7 cells (**9b**: IC_{50} = 23±2.32 μM). Based on the results, the **10c** compound did not have a cytotoxic effect on the tested cancer cell line due to its bulky scaffold and the steric hindrance in its site of action. These preliminary encouraging results of the biological screening of the tested compounds may offer an excellent framework for the discovery of potent cytotoxic agents in this field.

SUPPLEMENTARY MATERIAL

Additional data and information are available electronically at the pages of journal website: https://www.shd-pub.org.rs/index.php/JSCS/article/view/9811, or from the corresponding author on request.

Acknowledgements. The authors are grateful to Urmia University which provided them with a fellowship for the present study. Our grateful thanks go to Dr. Vahid Shafiei-Irannejad and Morteza Molaparast (from Cellular and Molecular Medicine Institute, Urmia University of Medical Sciences) who investigated the cytotoxicity of the compounds and to Prof. Dr. Joachim Thiem (from Hamburg University) and Prof. Dr. Abdolali Alizadeh (from Tarbiat Modares University) for the ESI-MS.

ИЗВОД

СИНТЕЗА И ОДРЕЂИВАЊЕ ЦИТОТОКСИЧНОГ ЕФЕКТА ДЕРИВАТА 1,4-ДИХИДРОПИРИДИНА КОЈИ САДРЖЕ АЗОЛСКУ СТРУКТУРУ

SAEED GHORBANNEJAD[1], KARIM AKBARI DILMAGHANI[1] и ABBAS NIKOO[2]

[1]*Department of Chemistry, Faculty of Science, Urmia University, Urmia, Iran и* [2]*Shahid Bakeri High Education Center, Urmia University, Urmia, Iran*

Синтетисана је серија деривата 1,4-дихидропиридина (**9a**–**d**, **10a**–**d** и **11a**–**d**) реакцијом 1,3,4-оксадиазол-5-тиона или 1,2,4-триазол-5-тиона са 2,6-дибромметил-3,5-диетоксикарбонил-4-(3-нитрофенил)-1,4-дихидропиридином. Синтетисана једињења су окарактерисана помоћу FT-IR, ^{1}H-NMR, ^{13}C-NMR и ESI-MS спектара и елементалном анализом. Испитана је цитотоксичност добијених деривата према ћелијама хуманог канцера дојке (MCF-7) MTT есејом. Резултати указују да једињење диетил 4-(3-нитрофенил)-2,6-бис[((5-(3-нитрофенил)-1,3,4-оксадиазол-2-ил)тио)метил]-1,4-дихидропиридин-3,5-дикарбоксилат (**9b**) са (IC_{50} = 23 ± 2,32 μM) има највећу активност према MCF-7 ћелијама. На основу добијених резултата оксадиазолски део структуре на C2 и C6 положајима 1,4-дихидропиридинског система повећава цитотоксични потенцијал ових деривата. Из тога произилази да би неки 1,4-DHP деривати који садрже оксадиазолске супституенте омогућили припрему нових активнијих једињења.

(Примљено 18. августа 2020, ревидирано 5. августа, прихваћено 10. августа 2021)

REFERENCES

1. D. J. Triggle, *Biochem. Pharmacol.* **74** (2007) 1 (http://dx.doi.org/10.1016/j.bcp.2007.01.016)

2. C. Bladen, M. G. Gündüz, R. Şimşek, C. Şafak, G. W. Zamponi, *Pflugers Arch – Eur. J. Physiol*. **466** (2014) 1355 (http://dx.doi.org /10.1007/s00424-013-1376-z)
3. R. Bansal, G. Narang, C. Calle, R. Carron, K. Pemberton, A. L. Harvey, *Drug Dev. Res.* **74** (2013) 50 (http://dx.doi.org/10.1002/ddr.21056)
4. N. Razzaghi-Asl, R. Miri, O. Firuzi, *Iran. J. Pharm. Sci.* **15** (2016) 413 (http://dx.doi.org/10.22037/IJPR.2016.1870)
5. A. Ahamed, I. A. Arif, M. Mateen, R. S. Kumar, A. Idhayadhull, *Saudi J. Biol. Sci.* **25** (2018) 1227 (http://dx.doi.org/10.1016/j.sjbs.2018.03.001)
6. J. Marín-Prida, G. L. P. Andreu, C. P. Rossignoli, M. G. Durruthy, E. O. Rodríguez, Y. V. Reyes, R. F. Acosta, S. A. Uyemura, L. C. Alberici, *Toxicol.* In Vitro **42** (2017) 21 (http://dx.doi.org/10.1016/j.tiv.2017.03.011)
7. D. Viradiya, S. Mirza, F. Shaikh, R. Kakadiya, A. Rathod, N. Jain, R. Rawal, A. Shah, *Anticancer Agents Med. Chem.* **17** (2017) 1003 (http://dx.doi.org/10.2174/1871520616666161206143251)
8. F. Shekari, H. Sadeghpour, K. Javidnia, L. Saso, F. Nazari, O. Firuzi, R. Miri, *Eur. J. Pharmacol.* **746** (2015) 233 (http://dx.doi.org/10.1016/j.ejphar.2014.10.058)
9. S. Tasaka, H. Ohmori, N. Gomi, M. Iino, T. Machida, A. Kiue, S. Naito, M. Kuwano, *Bioorganic Med. Chem. Lett.* **11** (2001) 275 (http://dx.doi.org/10.1016/S0960-894X(00)00651-X)
10. H. Engi, H. Sakagami, M. Kawase, A. Parecha, D. Manvar, H. Kothari, P. Adlakha, A. Shah, N. Motohashi, I. Ocsovszki, J. Molnar, In Vivo **20** (2006) 637 (https://www.researchgate.net/publication/6705056)
11. M. F. Mohamed, A. F. Darweesh, A. H. M. Elwahy, I. A. Abdelhamid, *RSC Adv*. **6** (2016) 40900 (http://dx.doi.org/10.1039/c6ra04974e)
12. O. Firuzi, K. Javidnia, E. Mansourabadi, L. Saso, A.R. Mehdipour, R. Miri, *Arch. Pharm. Sci. Res.* **36** (2013) 1392 (http://dx.doi.org/10.1007/s12272-013-0149-8)
13. M. G. Pavani, M. Nunez, P. Brigidi, B. Vitali, R. Gambari, *Bioorg. Med. Chem.* **10** (2002) 449 (http://dx.doi.org/10.1016/S0968-0896(01)00294-2)
14. R. Miri, A. Mehdipour, *Bioorg. Med. Chem.* **16** (2008) 8329 (http://dx.doi.org/10.1016/j.bmc.2008.07.025)
15. A. Zarrin, A. R. Mehdipour, R. Miri, *Chem. Biol. Drug. Des.* **76** (2010) 369 (http://dx.doi.org/10.1111/j.1747-0285.2010.01025.x)
16. J. R. Warr, F. Brewer, M. Anderson, J. Fergusson, *Cell Biol. Int. Rep.* **10** (1986) 389 (http://dx.doi.org/10.1016/0309-1651(86)90011-1)
17. T. Tsuruo, H. Kawabata, N. Nagumo, H. lida, Y. Kitatani, S. Tsukagoshi, Y. Sakurai, *Cancer Chemother. Pharmacol.* **15** (1985) 16 (http://dx.doi.org/10.1007/BF00257287)
18. T. Godfraind, *J. Cardiovasc. Pharmacol. Ther.* **19** (2014) 501 (http://dx.doi.org/10.1177/1074248414530508)
19. B. Laupeze, L. Amiot, N. Bertho, J. M. Grosset, G. Lehne, R. Fauchet, O. Fardel, *Hum. Immunol.* **62** (2001) 1073 (http://dx.doi.org/10.1016/S0198-8859(01)00307-X)
20. R. Surendrakumar, A. Manilal, A. J. Abdul Nasser, B. Merdekios, X. Chen, A. Idhayadhulla, *J. Pharmacol. Toxicol.* **9** (2014) 119 (https://dx.doi.org/10.3923/jpt.2014.119.128)
21. A. B. Archana, D. R. Dinesh, S. G. Paraag, Y. S. Prabhakar, *Int. J. Pharm. Chem*. **4** (2014) 62 (http://dx.doi.org/10.7439/ijpc.v4i2.75)
22. M. Ziaie, K. Akbari Dilmaghani, A. Tukmechi, *Acta Chim. Slov*. **64** (2017) 895 (http://dx.doi.org/10.17344/acsi.2017.3506)

23. R. M. Shaker, *ARKIVOC* **IX** (2006) 59 (https://dx.doi.org/10.3998/ark.5550190.0007.904)
24. A. A. Aly, A. A. Hassan, M. M. Makhlouf, S. Brase, *Molecules* **25** (2020) 3036 (http://dx.doi.org/10.3390/molecules25133036)
25. A. A. Othman, M. Kihel, S. Amara, *Arab. J. Chem*. **12** (2019) 1660 (http://dx.doi.org/10.1016/j.arabjc.2014.09.003)
26. K. M. Dawood, A. M. Farag, H. A. Abdel-Aziz, *Heteroat. Chem.* **16** (2005) 621 (http://dx.doi.org/10.1002/hc.20162)
27. J. Shneine, Y. H. Alaraji, *IJSR* **5** (2016) 1411 (https://www.ijsr.net/get_abstract.php?paper_id=NOV161902)
28. S. D. Bajaj, O. A. Mahodaya, P. V. Tekade, V. B. Patil, S. D. Kukade, *Russ. J. Gen. Chem*. **87** (2017) 546 (http://dx.doi.org/10.1134/S1070363217030264)
29. V. Palermo, A. G. Sathicq, T. Constantieux, J. Rodriguez, P. G. Vazquez, G. P. Romanelli, *Catal. Lett*. **146** (2016) 1634 (http://dx.doi.org/10.1007/s10562-016-1784-8)
30. D. Viradiya, S. Mirza, F. Shaikh, R. Kakadiya, A. Rathod, N. Jain, R. Rawal, A. Shah, *Anti-Cancer Agents Med. Chem.* **17** (2017) 1003 (http://dx.doi.org/10.2174/1871520616666161206143251)
31. N. Razzaghi-Asl, R. Miri, O. Firuzi, *Iran. J. Pharm. Res*. **15** (2016) 413 (http://dx.doi.org/10.22037/ijpr.2016.1870)
32. R. Surendra kumar, A. Idhayadhulla, A. Jamal Abdul Nasser, K. Murali, *Indian J. Chem., B* **50** (2011) 1140 (http://nopr.niscair.res.in/handle/123456789/12520)
33. R. Sarkhosh Inanlou, M. Molaparast, A. Mohammadzadeh, V. Shafiei Irannejad, *Chem. Biol. Drug. Des.* **95** (2019) 215 (http://dx.doi.org/10.1111/cbdd.13621)
34. K. H. Chikhalia, D. B. Vashi, M. J. Patel, *J. Enzyme Inhib. Med. Chem.* **24** (2009) 617 (http://dx.doi.org/10.1080/14756360802318936)
35. M. Petrova, R. Muhamadejev, B. Vigante, B. Cekavicus, A. Plotniece, G. Duburs, E. Liepinsh, *Molecules* **16** (2011) 8041 (http://dx.doi.org/10.3390/molecules16098041).

Journal of the Serbian Chemical Society
JSCS@tmf.bg.ac.rs • www.shd.org.rs/JSCS
J. Serb. Chem. Soc. 86 (11) S252–S283 (2021) *Supplementary material*

SUPPLEMENTARY MATERIAL TO

Synthesis and assessment of the cytotoxic effect of some of 1,4-dihydropyridine derivatives which contain azole moiety

SAEED GHORBANNEJAD[1], KARIM AKBARI DILMAGHANI[1]* and ABBAS NIKOO[2]

[1]*Department of Chemistry, Faculty of Science, Urmia University, Urmia, Iran and* [2]*Shahid Bakeri High Education Center, Urmia University, Urmia, Iran*

J. Serb. Chem. Soc. 86 (11) (2021) 1013–1021

Diethyl 2,6-bis(bromomethyl)-4-(3-itrophenyl)-1,4-dihydropyridine-3,5-dicarboxylate ***(8)***

Yield 3830 mg (72 %). Yellow solid; m.p.: 252-254 °C. IR (KBr): 3297m, 3111w, 2979w, 1693s, 1641m, 1514s, 1437w, 1352s, 1292s, 1220s, 1139s, 1095s, 760w, 711w, cm^{-1}. ^1H NMR (300 MHz, DMSO-d_6, δ): 8.16 (*s*, 1H, ArH), 8.07 (*d*, 1H, *J* = 7.8, ArH), 7.64 (*d*, 1H, *J* = 7.5, ArH), 7.44 (*t*, 1H, *J* = 8.1, ArH), 6.63 (*s*, 1H, NH), 5.15 (*s*, 1H, CH), 4.88 (*d*, 2H, *J* = 11.71, CH_2Br), 4.69 (*d*, 2H, *J* = 11.4, CH_2Br), 4.10-4.25 (*m*, 4H, 2×OCH_2), 1.27 (*t*, 6H, *J* = 7.2, 2CH_3). ^{13}C NMR (100 MHz, DMSO-d_6, *δ*): 165.40, 165.15, 149.03, 148.35, 148.86, 147.60, 145.31, 134.23, 129.88, 129.78, 122.09, 121.98, 121.74, 121.53, 102.36, 102.34, 60.17, 60.09, 27.18, 26.66, 14.07, 13.92. (+)ESI-HRMS (*m/z*): calculated for $[C_{19}H_{20}Br_2N_2O_6 + H]^+$ 529.97, observed 529.1. Combustion analysis of $C_{19}H_{20}Br_2N_2O_6$: Calculated. C 42.88, H 3.79, N 5.26; found C 42.52, H 3.81, N 5.11.

Diethyl 4-(3-nitrophenyl)-2,6-bis[((5-phenyl-1,3,4-oxadiazol-2-yl)thio)methyl]-1,4-dihydro-pyridine-3,5-di carboxylate ***(9a)***

Yield 6030 mg (83 %).Yellow solid; m.p.: 120-122 °C. IR (KBr): 3223w, 3098w, 2981w, 1690s, 1521s, 1470s, 1344m, 1288m, 1205s, 1091s, 1044m, 783w, 696m, cm^{-1}. ^1H NMR (300 MHz, DMSO-d_6, *δ*): 9.65 (*s*, 1H, NH), 7.99 (*s*, 1H, ArH), 7.92 (*d*, 1H, *J* = 9, ArH), 7.77 (*d*, 4H, *J* = 8.1, ArH), 7.40-7.65 (*m*, 8H, ArH), 5.03 (*s*, 1H, CH), 4.68 (*d*, 2H, *J* = 13.5, CH_2S), 4.40 (*d*, 2H, *J* = 13.5, CH_2S), 3.92 (*q*, 4H, *J* =7.2, 2×OCH_2), 1.06 (*t*, 6H, *J* = 6.9, 2×CH_3). ^{13}C NMR (100 MHz, DMSO-d_6, δ): 165.80, 165.60, 162.42, 148.61, 147.48, 145.27, 134.12, 132.08, 129.71, 129.26, 126.30, 122.90, 123.04, 121.60, 102.92, 60.11, 32.17, 13.75. (+)ESI-HRMS (*m/z*): calculated for $[C_{35}H_{30}N_6O_8S_2 + H]^+$

* Corresponding author. E-mail: k.adilmaghani@urmia.ac.ir

726.1567, observed 726.4. Combustion analysis for $C_{35}H_{30}N_6O_8S_2$: Calculated. C 57.84, H 4.16, N 11.56, S 8.82; found C 57.79, H 4.24, N 11.68, S 8.72.

Diethyl 4-(3-nitrophenyl)-2,6-bis[((5-(3-nitrophenyl)-1,3,4-oxadiazol-2-yl)thio)methyl]-1,4-dihydro pyridine-3,5-dicarboxylate ***(9b)***

Yield 6450 mg (79 %). Yellow solid; m.p.: 114-116 °C. IR (KBr): 3286w, 3244w, 3104w, 2979w, 1690s, 1630m, 1486s, 1401m, 1351s, 1282s, 1218s, 1157s, 1101s, 1055s, 917w, 744m, 712m, 625m, 560m, cm^{-1}. ^1H NMR (300 MHz, DMSO-d_6, δ): 9.63 (*s*, 1H, NH), 8.49 (*m*, 2H, ArH), 8.37 (*m*, 2H, ArH), 8.19 (*m*, 2H, ArH), 7.75-7.95 (*m*, 4H, ArH), 7.35-7.60 (*m*, 2H, ArH), 5.02 (*s*, 1H, CH), 4.65 (*d*, 2H, J = 13.8, CH_2S), 4.44 (*d*, 2H, J = 12.9, CH_2S), 3.95 (*q*, 4H, J = 6.9, 2×OCH_2), 1.07 (*t*, 6H, J=7.2, 2×CH_3). ^{13}C NMR (100 MHz, DMSO-d_6, δ): 165.53, 164.07, 163.54, 148.47, 148.05, 147.46, 145.01, 134.03, 132.24, 131.19, 129.59, 126.35, 124.32, 121.93, 121.49, 120.76, 103.01, 60.13, 32.11, 13.76. (+)ESI-HRMS (*m/z*): calculated for $[C_{35}H_{28}N_8O_{12}S_2 + H]^+$ 816.1268, observed 816.2. Combustion analysis for $C_{35}H_{28}N_8O_{12}S_2$: Calculated. C 51.47, H 3.46, N 13.72, S 7.85; found C 51.13, H 3.58, N 13.91, S 7.71.

Diethyl 2,6-bis[((5-(2-hydroxyphenyl)-1,3,4-oxadiazol-2-yl)thio)methyl]-4-(3-nitrophenyl)--1,4-dihydropyridine-3,5-dicarboxylate ***(9c)***

Yield 5690 mg (75 %). Yellow solid; m.p.: 150-152 °C. IR (KBr): 3288w, 3237w, 3107w, 2980w, 1690s, 1626m, 1590w, 1527m, 1484s, 1407w, 1349m, 1286s, 1248m, 1216m, 1161m, 1100s, 1053m, 963w, 864w, 830w, 749m, 708m, 673w, 631w, 541w, cm^{-1}. ^1H NMR (300 MHz, DMSO-d_6, δ): 10.14 (*bs*, 2H, 2×OH), 9.64 (*s*, 1H, NH), 8.00 (*s*, 1H, ArH), 7.93 (*d*, 1H, J = 7.8, ArH), 7.63 (*d*, 1H, J = 7.8, ArH), 7.30-7.60 (*m*, 5H, ArH), 7.05 (*d*, 2H, J = 8.4, ArH), 6.89 (*t*, 2H, J = 7.2, ArH), 5.02 (*s*, 1H, CH), 4.64 (*d*, 2H, J = 12.61, CH_2S), 4.42 (*d*, 2H, J = 13.21, CH_2S), 3.95 (*q*, 4H, J =7.2, 2×OCH_2), 1.08 (*t*, 6H, J = 6.9, 2×CH_3). ^{13}C NMR (100 MHz, DMSO-d_6, δ): 165.53, 165.14, 161.85, 156.20, 148.56, 147.39, 145.03, 134.14, 133.46, 129.67, 128.46, 122.02, 122.52, 119.49, 117.02, 109.16, 102.88, 60.05, 32.24, 13.75. (+)ESI-HRMS (*m/z*): calculated for $[C_{35}H_{30}N_6O_{10}S_2 + H]^+$ 758.15, observed 758.45. Combustion analysis for $C_{35}H_{30}N_6O_{10}S_2$: Calculated. C 55.40, H 3.99, N 11.08, S 8.45; found C 55.13, H 4.08, N 11.23, S 8.34.

Diethyl 2,6-bis[((5-(2-chlorophenyl)-1,3,4-oxadiazol-2-yl)thio)methyl]-4-(3-nitrophenyl)-1,4--dihydropyridine-3,5-dicarboxylate ***(9d)***

Yield 6440 mg (81 %). Yellow solid; m.p.: 92-94 °C. IR (KBr): 3276w, 3206w, 3067w, 2976w, 1687s, 1505s, 1439m, 1346m, 1283m, 1218m, 1162m, 1093s, 1042m, 759m, 695w, 602w, cm^{-1}. ^1H NMR (300 MHz, DMSO-d_6, δ): 9.63 (*s*, 1H, NH), 7.90-8.00 (*m*, 2H, ArH), 7.78 (*t*, 2H, J = 7.8, ArH), 7.55-7.70 (*m*, 5H, ArH), 7.40-7.50 (*m*, 3H, ArH), 5.01 (*s*, 1H, CH), 4.62 (*d*, 2H, J = 13.5, CH_2S), 4.48 (*d*, 2H, J = 13.5, CH_2S), 3.95 (*q*, 4H, J = 6.9, 2×OCH_2), 1.08 (*t*, 6H, J = 7.2, 2×CH_3). ^{13}C NMR (100 MHz, DMSO-d_6, δ): 165.52, 163.76, 163.10,

148.42, 147.40, 144.88, 134.07, 133.22, 131.73, 131.09, 130.91, 129.62, 127.65, 122.02, 122.52, 121.94, 121.55, 102.98, 60.06, 32.16, 13.75. HRMS-FAB (*m/z*): calculated for $[C_{35}H_{28}Cl_2N_6O_8S_2 + H]^+$ 795.6630, observed 795.071. Combustion analysis for $C_{35}H_{28}Cl_2N_6O_8S_2$: Calculated. C 52.83, H 3.55, N 10.56, S 8.06; found C 52.66, H 3.71, N 10.63, S 8.01.

Diethyl 4-(3-nitrophenyl)-2,6-bis[(4,5-diphenyl-4H-1,2,4-triazol-3-ylthio)methyl]-1,4-dihydropyridine-3,5-di carboxylate ***(10a)***

Yield 7450 mg (85 %). Yellow solid; m.p.: 134-136 °C. IR (KBr): 3331w, 3293w, 3120w, 2979w, 1690s, 1629m, 1513s, 1409m, 1353m, 1289s, 1224s, 1161m, 1097s, 1054w, 752m, 601w, cm^{-1}. ^1H NMR (300 MHz, DMSO-d_6, δ): 9.63 (*s*, 1H, NH), 7.95-8.05 (*m*, 2H, ArH), 7.62 (*d*, 2H, *J* = 7.5, ArH), 7.40-7.55 (*m*, 7H, ArH), 7.25-7.40 (*m*, 13H, ArH), 5.02 (*s*, 1H, CH), 4.44 (*s*, 4H, 2×CH_2S), 3.96 (*q*, 4H, *J* = 6.6, 2×OCH_2), 1.08 (*t*, 6H, *J* = 7.5, 2CH_3). ^{13}C NMR (100 MHz, DMSO-d_6, δ): 165.63, 154.55, 151.35, 148.62, 147.39, 145.34, 134.33, 133.83, 129.96, 129.79, 128.51, 127.83, 127.62, 126.55, 122.09, 121.45, 102.36, 59.88, 32.33, 13.84. (+)ESI-HRMS (*m/z*): calculated for $[C_{47}H_{40}N_8O_6S_2 + H]^+$ 876.2512, observed 876.4. Combustion analysis for $C_{47}H_{40}N_8O_6S_2$: Calculated. C 64.37, H 4.60, N 12.78, S 7.31; found C 64.21, H 4.77, N 12.83, S 7.14.

Diethyl 4-(3-nitrophenyl)-2,6-bis[(5-(3-nitrophenyl)-4-phenyl-4H-1,2,4-triazol-3-ylthio) methyl]-1,4-dihydro pyridine-3,5-dicarboxylate ***(10b)***

Yield 7160 mg (74 %). Yellow solid; m.p.: 155-157 °C. IR (KBr): 3076w, 2979w, 1689s, 1642w, 1527s, 1499s, 1349s, 1284m, 1216m, 1165m, 1094s, 1040m, 905w, 807w, 772w, 742w, 698m, 606w, cm^{-1}. ^1H NMR (300 MHz, DMSO-d_6, δ): 9.56 (*s*, 1H, NH), 8.16 (*d*, 2H, *J* = 8.1, ArH), 7.99 (*d*, 4H, *J* = 8.1, ArH), 7.04-7.75 (*m*, 16H, ArH), 4.99 (*s*, 1H, CH), 4.44 (*s*, 4H, 2×CH_2S), 3.97 (*q*, 4H, *J* = 6.9, 2×OCH_2), 1.09 (*t*, 6H, *J* = 6.9, 2×CH_3). ^{13}C NMR (100 MHz, DMSO-d_6, δ): 165.76, 152.74, 152.43, 148.71, 147.50, 145.45, 134.46, 133.73, 133.39, 130.51, 130.39, 130.19, 129.77, 127.94, 127.63, 124.39, 124.39, 122.19, 122.11, 121.57, 102.40, 60.01, 32.32, 13.92. HRMS-FAB (*m/z*): calculated for $[C_{47}H_{38}N_{10}O_{10}S_2 + H]^+$ 967.0010, observed 967.209. Combustion analysis for $C_{47}H_{38}N_{10}O_{10}S_2$: Calculated. C 58.38, H 3.96, N 14.48, S 6.63; found C 58.11, H 4.03, N 14.53, S, 6.49.

Diethyl 2,6-bis[(5-(2-hydroxyphenyl)-4-phenyl-4H-1,2,4-triazol-3-ylthio)methyl]-4-(3-nitrophenyl)-1,4-dihydropyridine-3,5-dicarboxylate ***(10c)***

Yield 7090 mg (78 %). Yellow solid; m.p.: 185-187 °C. IR (KBr): 3272w, 3202w, 3065m, 2977m, 1686s, 1505s, 1345m, 1284m, 1218m, 1164m, 1094s, 1039m, 915w, 767m, 696m, 602w, cm^{-1}. ^1H NMR (300 MHz, DMSO-d_6, δ): 10.21 (*s*, 2H, 2×OH), 7.95-8.05 (*m*, 2H, ArH), 9.63 (*s*, 1H, NH), 7.59 (*d*, 1H, *J* = 7.2, ArH), 7.51 (*t*, 1H, *J* = 7.5, ArH), 7.35-7.45 (*m*, 6H, ArH), 7.02-7.35 (*m*, 6H, ArH), 7.13 (*d*, 2H, *J* = 7.2, ArH), 6.70-6.85 (*m*, 4H, ArH), 4.98 (*s*, 1H, CH), 4.44 (*s*, 4H, 2×CH_2S), 3.98 (*q*, 4H, *J* = 6.9, 2×OCH_2), 1.10 (*t*, 6H, *J* = 6.9, 2×CH_3).

^{13}C NMR (100 MHz, DMSO-d_6, δ): 165.60, 155.90, 153.67, 150.50, 148.61, 147.41, 145.17, 134.31, 133.87, 131.60, 130.16, 129.74, 129.45, 129.30, 127.85, 126.89, 122.08, 121.47, 118.74, 115.97, 113.31, 102.48, 59.91, 32.24, 13.85. (+)ESI-HRMS (*m/z*): calculated for $[C_{47}H_{40}N_8O_8S_2 + H]^+$ 908.2411, observed 908.6. Combustion analysis for $C_{47}H_{40}N_8O_8S_2$: Calculated. C 62.10, H 4.44, N 12.33, S 7.06; found C 61.92, H 4.63, N 12.45, S 6.95.

Diethyl 2,6-bis[(5-(2-chlorophenyl)-4-phenyl-4H-1,2,4-triazol-3-ylthio)methyl]-4-(3-nitrophenyl)-1,4-dihydropyridine-3,5-dicarboxylate ***(10d)***

Yield 7570 mg (80 %). Yellow solid; m.p.: 140-142 °C. IR (KBr): 3279w, 3204w, 3066w, 2978w, 1689s, 1642w, 1599w, 1525s, 1497s, 1435m, 1385w, 1348m, 1312w, 1283m, 1252m, 1216m, 1164m, 1093s, 1039m, 764m, 734w, 694m, 602w, cm^{-1}. ^{1}H NMR (300 MHz, DMSO-d_6, *δ*): 9.63 (*s*, 1H, NH), 7.95-8.05 (*m*, 2H, ArH), 7.20-7.65 (*m*, 20H, ArH), 5.00 (*s*, 1H, CH), 4.47 (*s*, 4H, 2×CH_2S), 3.99 (*q*, 4H, *J* = 7.2, 2×OCH_2), 1.10 (*t*, 6H, *J* = 7.2, 2×CH_3). ^{13}C NMR (100 MHz, DMSO-d_6, δ): 165.64, 153.03, 150.74, 148.62, 147.49, 145.14, 134.34, 133.12, 132.63, 132.25, 129.78, 129.70, 129.49, 129.40, 127.23, 126.92, 126.35, 122.11, 121.56, 102.62, 59.99, 32.35, 13.88. (+)ESI-HRMS (*m/z*): calculated for $[C_{47}H_{38}Cl_2N_8O_6S_2 + H]^+$ 944.1733, observed 944.35. Combustion analysis for $C_{47}H_{38}Cl_2N_8O_6S_2$: Calculated. C 59.68, H 4.05, N 11.85, S 6.78; found C 59.41, H 4.33, N 11.94, S 6.58.

Diethyl 2,6-bis[(4-amino-5-phenyl-4H-1,2,4-triazol-3-ylthio)methyl]-4-(3-nitrophenyl)-1,4-dihydropyridine-3,5-dicarboxylate ***(11a)***

Yield 5660 mg (75 %). Yellow solid; m.p.: 189-191 °C. IR (KBr): 3351w, 3276w, 3172w, 3071w, 2978w, 2937w, 1691s, 1636m, 1526s, 1499s, 1348m, 1285m, 1260w, 1212m, 1162m, 1092s, 1043m, 770w, 691m, cm^{-1}. ^{1}H NMR (300 MHz, DMSO-d_6, *δ*): 9.68 (*s*, 1H, NH), 7.90-8.10 (*m*, 6H, ArH), 7.40-7.60 (*m*, 8H, ArH), 6.19 (*s*, 4H, 2×NH_2), 5.04 (*s*, 1H, CH), 4.51 (*d*, 2H, *J* = 13.5, CH_2S), 4.36 (*d*, 2H, *J* = 13.2, CH_2S), 4.02 (*q*, 4H, *J* = 6, 2×OCH_2), 1.14 (*t*, 6H, *J* = 6.9, 2×CH_3). ^{13}C NMR (100 MHz, DMSO-d_6, δ): 165.82, 154.34, 153.00, 148.79, 147.48, 145.89, 134.44, 129.88, 129.81, 129.31, 128.51, 127.86, 126.72, 126.34, 122.16, 121.55, 102.34, 60.03, 31.27, 13.96. HRMS-FAB (*m/z*): calculated for $[C_{35}H_{34}N_{10}O_6S_2 + H]^+$ 754.8410, observed 755.217. Combustion analysis for $C_{35}H_{34}N_{10}O_6S_2$: Calculated. C 55.69, H 4.54, N 18.58, S 8.50; found C 55.41, H 4.73, N 18.68, S 8.38.

Diethyl 2,6-bis[(4-amino-5-(3-nitrophenyl)-4H-1,2,4-triazol-3-ylthio)methyl]-4-(3-nitrophenyl)-1,4-dihydropyridine-3,5-dicarboxylate ***(11b)***

Yield 5740 mg (68 %). Yellow solid; m.p.: 202-204 °C. IR (KBr): 3356w, 3272w, 3167m, 3065w, 2975m, 1690s, 1634m, 1506s, 1345m, 1272m, 1210m, 1156m, 1091s, 773m, 689m, 588w, cm^{-1}. ^{1}H NMR (300 MHz, DMSO-d_6, *δ*): 9.65 (*s*, 1H, NH), 8.81 (*s*, 1H, ArH), 8.37 (*d*, 2H, *J* = 9.3, ArH), 8.27 (*d*, 2H, *J* = 8.1, ArH), 7.95-8.05 (*m*, 2H, ArH), 7.65-7.80 (*m*, 3H, ArH), 7.45-7.60 (*m*,

2H, ArH), 6.28 (*s*, 4H, 2×NH_2), 6.28 (*s*, 1H, CH), 4.37 (*d*, 2H, *J* = 13.2, CH_2S), 4.53 (*d*, 2H, *J* = 13.2, CH_2S), 4.03 (*q*, 4H, *J* = 7.2, 2×OCH_2), 1.13 (*t*, 6H, *J* = 7.2, 2×CH_3). ^{13}C NMR (100 MHz, DMSO-d_6, δ): 165.71, 153.65, 152.21, 148.70, 147.67, 154.68, 134.31, 133.69, 130.12, 129.67, 128.11, 124.20, 122.18, 121.92, 121.44, 102.34, 59.93, 31.38, 13.88. (+)ESI-HRMS (*m/z*): calculated for $[C_{35}H_{32}N_{12}O_{10}S_2 + H]^+$ 844.1806, observed 844.2. Combustion analysis for $C_{35}H_{32}N_{12}O_{10}S_2$: Calculated. C 49.76, H 3.82, N 19.90, S 7.59; found C 49.61, H 3.93, N 20.11, S 7.42.

Diethyl 2,6-bis[(4-amino-5-(2-hydroxyphenyl)-4H-1,2,4-triazol-3-ylthio)methyl]-4-(3-nitrophenyl)-1,4-dihydropyridine-3,5-dicarboxylate ***(11c)***

Yield 5510 mg (70 %). Yellow solid; m.p.: 204.5-206.5 °C. IR (KBr): 3194m, 3075s, 2978s, 1690s, 1632m, 1593m, 1494s, 1403m, 1361m, 1285s, 1248s, 1157s, 1091s, 750s, 698s, 612w, cm^{-1}. ^{1}H NMR (300 MHz, DMSO-d_6, *δ*): 11.01 (*s*, 2H, 2×OH), 9.69 (*s*, 1H, NH), 8.00-8.02 (*m*, 1H, ArH), 7.98 (*d*, 1H, *J* = 8.7, ArH), 7.82 (*d*, 2H, *J* = 7.5, ArH), 7.66 (*d*, 1H, *J* = 7.8, ArH), 7.52 (*t*, 1H, *J* = 7.5, ArH), 7.36 (*t*, 2H, *J* = 7.5, ArH), 7.11 (*d*, 2H, *J* = 7.8, ArH), 6.93 (*t*, 2H, *J* = 7.8, ArH), 6.06 (*s*, 4H, 2NH_2), 5.04 (*s*, 1H, CH), 4.54 (*d*, 2H, *J* = 13.8, CH_2S), 4.38 (*d*, 2H, *J* = 13.2, CH_2S), 4.02 (*q*, 4H, *J* = 5.7, 2×OCH_2), 1.13 (*t*, 6H, *J* = 7.2, 2×CH_3). ^{13}C NMR (100 MHz, DMSO-d_6, δ): 165.71, 155.68, 153.96, 152.49, 148.74, 145.72, 134.34, 131.59, 129.81, 129.48, 122.09, 121.48, 119.15, 116.38, 112.69, 102.33, 59.95, 30.91, 13.90. HRMS-FAB (*m/z*): calculated for $[C_{35}H_{34}N_{10}O_8S_2 + H]^+$ 786.8390, observed 787.206. Combustion analysis for $C_{35}H_{34}N_{10}O_8S_2$: Calculated. C 53.43, H 4.36, N 17.80, S 8.15; found C 53.09, H 4.52, N 18.20, S 8.03.

Diethyl 2,6-bis[(4-amino-5-(2-chlorophenyl)-4H-1,2,4-triazol-3-ylthio)methyl]-4-(3-nitrophenyl)-1,4-dihydropyridine-3,5-dicarboxylate ***(11d).***

Yield 6260 mg (76 %). Yellow solid; m.p.: 174-176 °C. IR (KBr, cm^{-1}): 3330m, 3208w, 3071w, 2977m, 1684s, 1636m, 1523s, 1456m, 1345m, 1287m, 1215m, 1164m, 1098s, 1043m, 757m, cm^{-1}. ^{1}H NMR (300 MHz, DMSO-d_6, *δ*): 9.76 (*s*, 1H, NH), 7.95-8.05 (*m*, 2H, ArH), 7.40-7.70 (*m*, 10H, ArH), 5.93 (*s*, 4H, 2×NH_2), 5.05 (*s*, 1H, CH), 4.57 (*d*, 2H, *J* = 13.5, CH_2S), 4.42 (*d*, 2H, *J* = 13.2, CH_2S), 4.04 (*q*, 4H, *J* = 4.5, 2×OCH_2), 1.15 (*t*, 6H, *J* = 6.6, 2×CH_3). ^{13}C NMR (100 MHz, DMSO-d_6, δ): 165.67, 152.11, 148.70, 147.40, 145.69, 134.37, 133.35, 132.41, 131.77, 131.10, 130.93, 129.85, 129.64, 127.65, 127.01, 126.11, 122.09, 121.48, 102.42, 59.96, 31.11, 13.89. (+)ESI-HRMS (*m/z*): calculated for $[C_{35}H_{32}Cl_2N_{10}O_6S_2 + H]^+$ 822.1325, observed 822.2. Combustion analysis for $C_{35}H_{32}Cl_2N_{10}O_6S_2$: Calculated. C 51.03, H 3.92, N 17.00, S 7.79; found C 50.94, H 3.98, N 17.13, S 7.61.

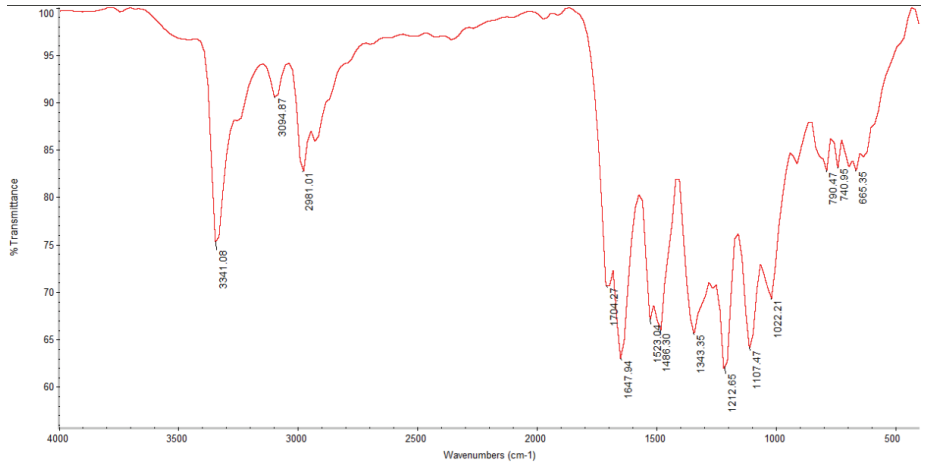

Fig. S-1. FT-IR spectra of compound (**7**)

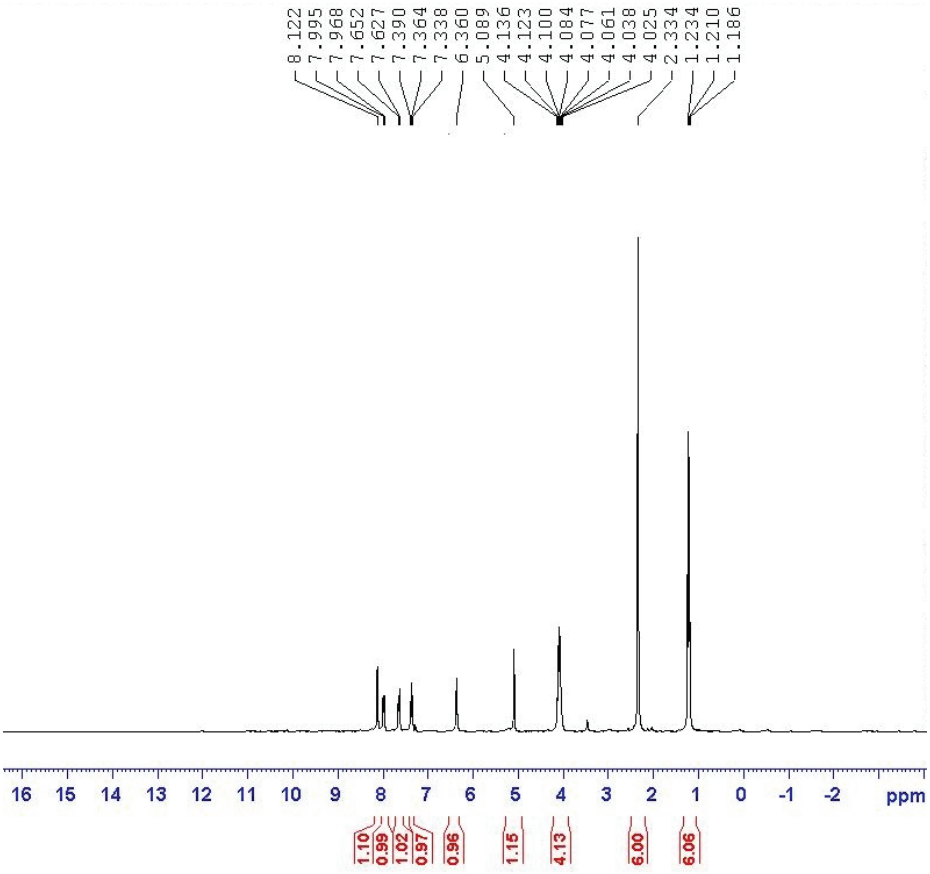

Fig. S-2. ^{1}H-NMR spectra of compound (**7**)

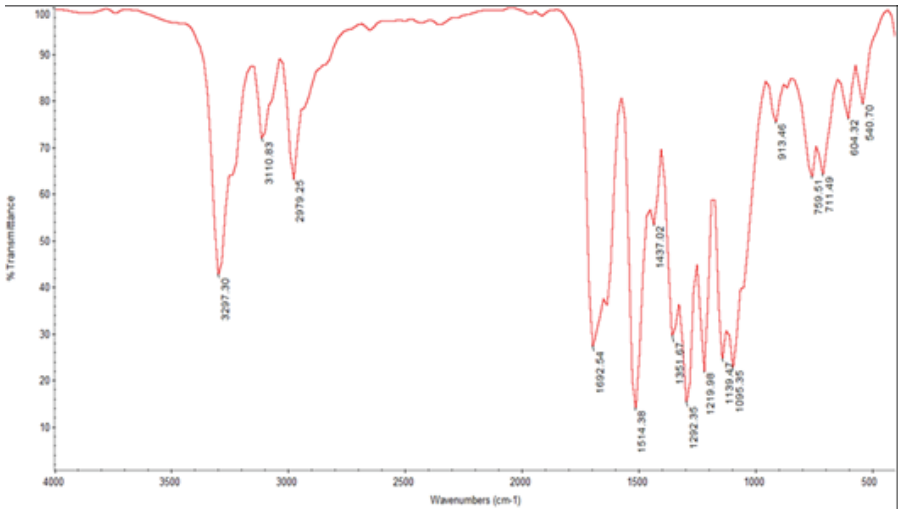

Fig. S-3. FT-IR spectra of compound (**8**)

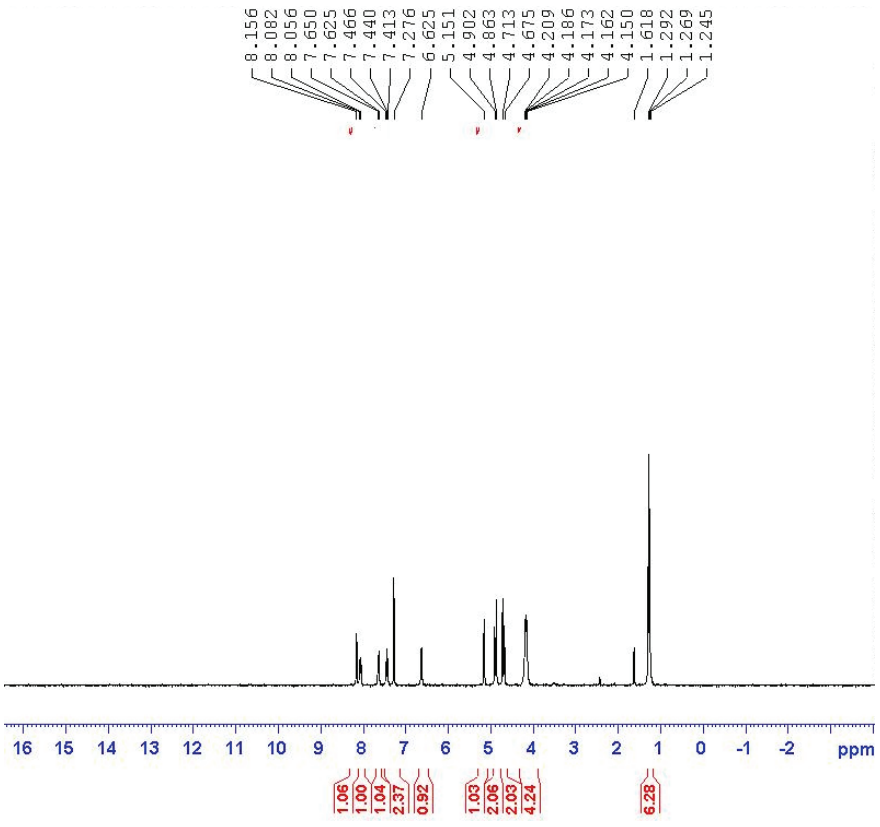

Fig. S-4. ^{1}H-NMR spectra of compound (**8**)

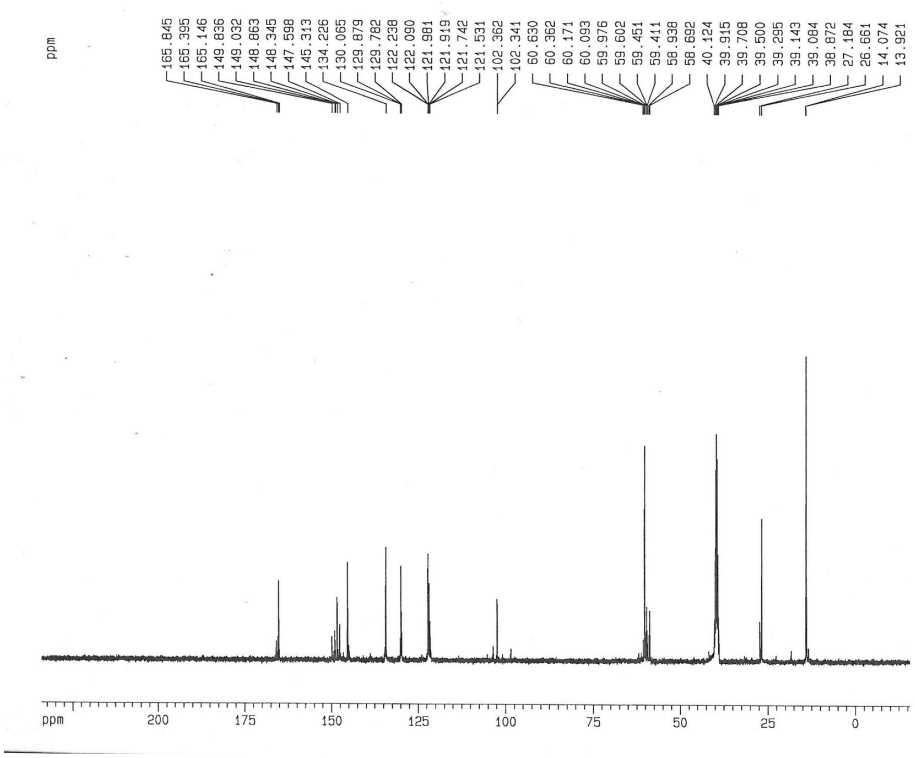

Fig. S-5. ^{13}C-NMR spectra of compound (**8**)

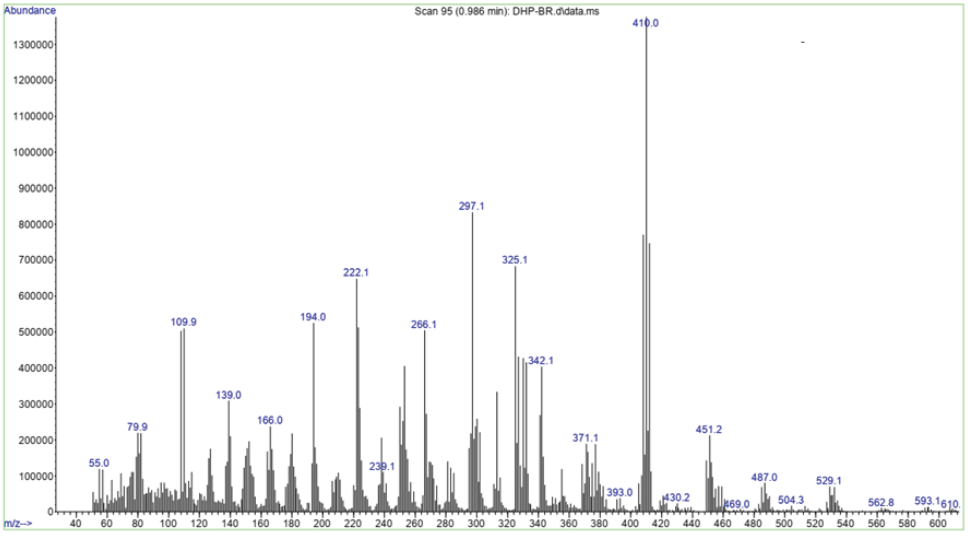

Fig. S-6. ESI-HRMS spectra of compound (**8**)

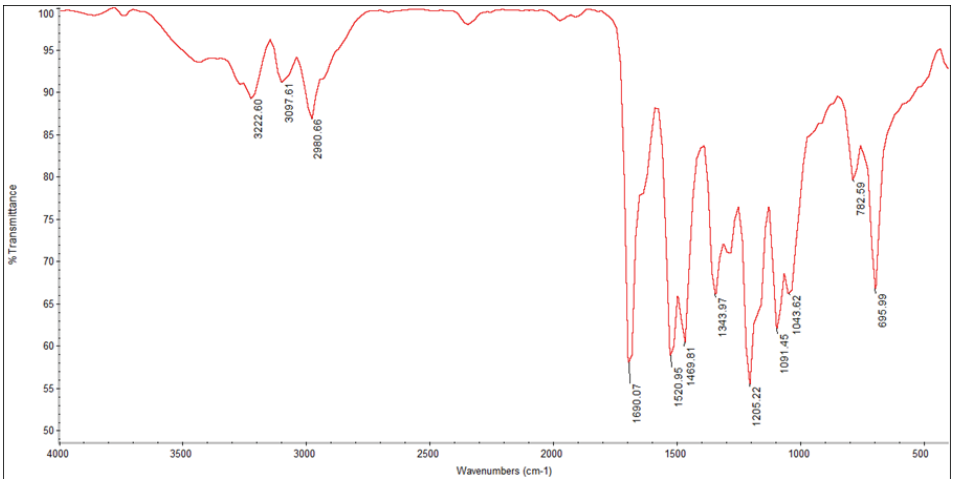

Fig. S-7. FT-IR spectra of compound (**9a**)

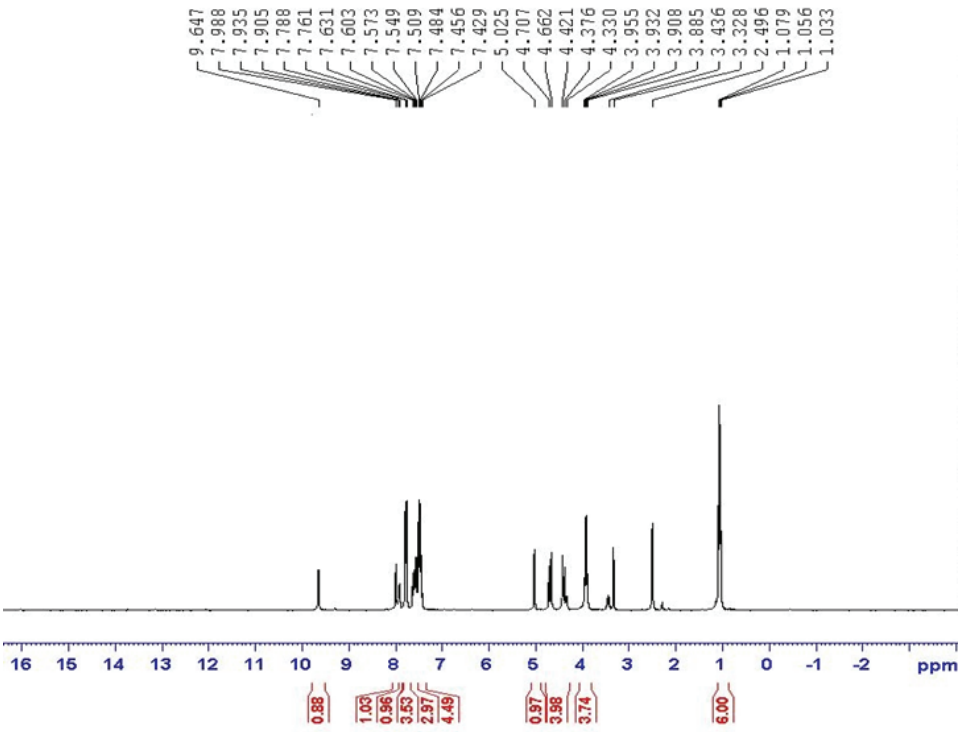

Fig. S-8. ^{1}H-NMR spectra of compound (**9a**)

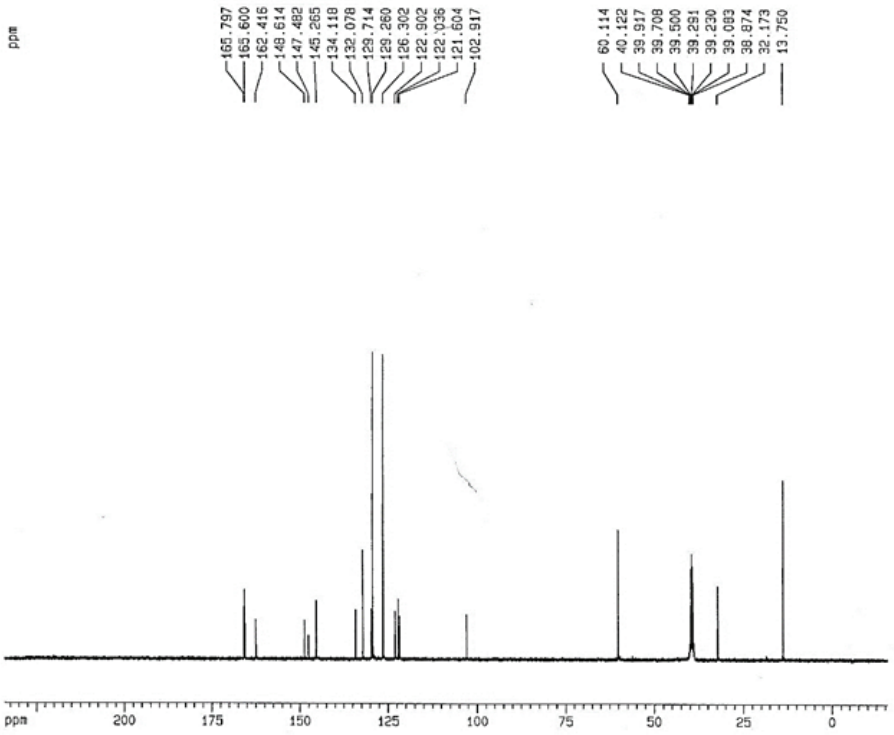

Fig. S-9. ^{13}C-NMR spectra of compound (**9a**)

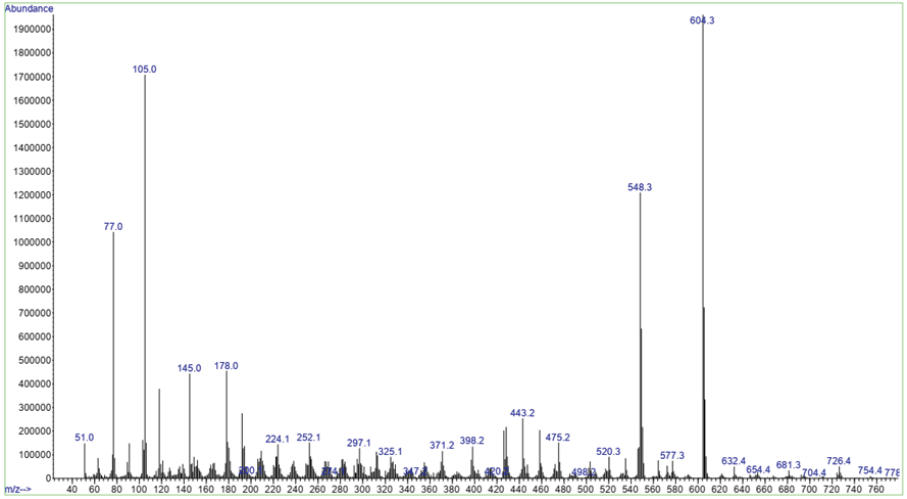

Fig. S-10. ESI-HRMS spectra of compound (**9a**)

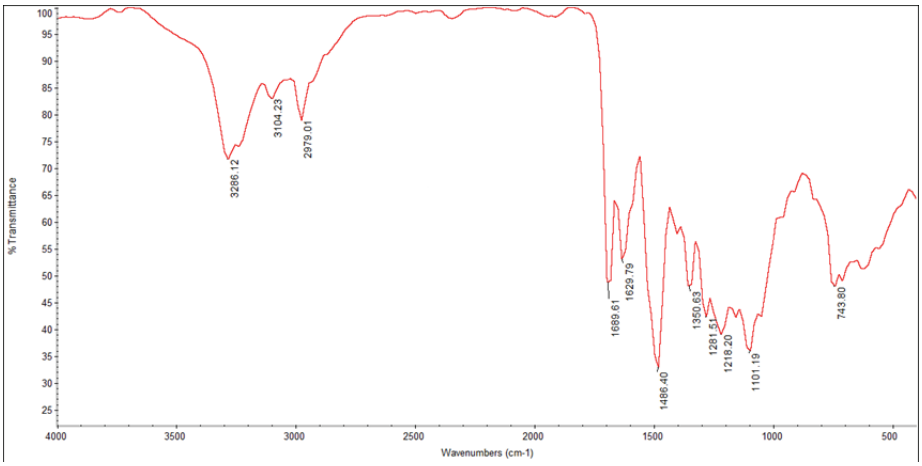

Fig. S-11. FT-IR spectra of compound (**9b**)

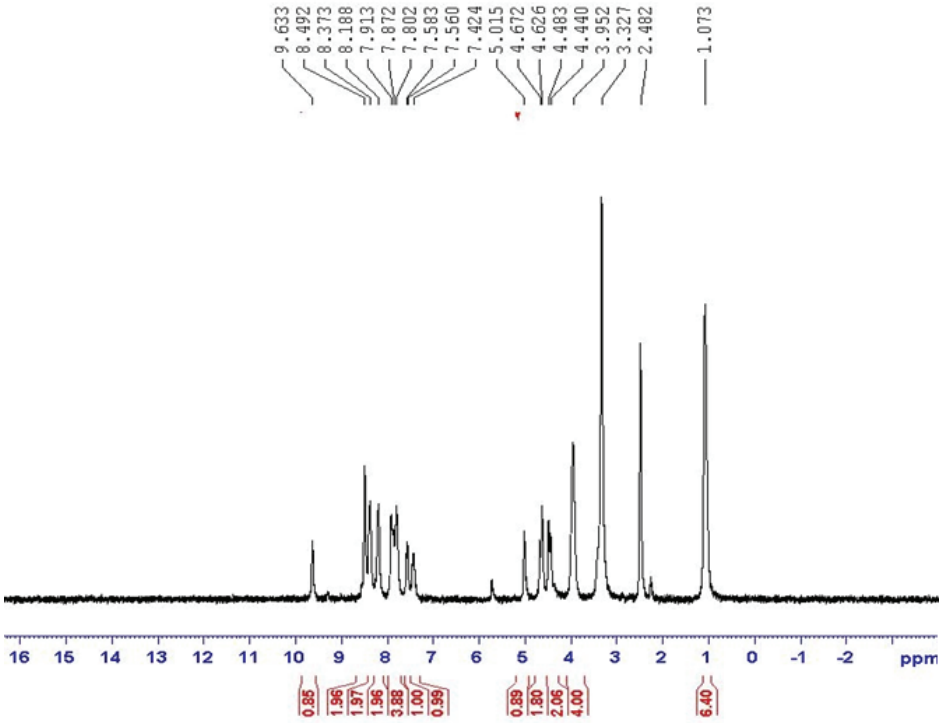

Fig. S-12. ^{1}H-NMR spectra of compound (**9b**)

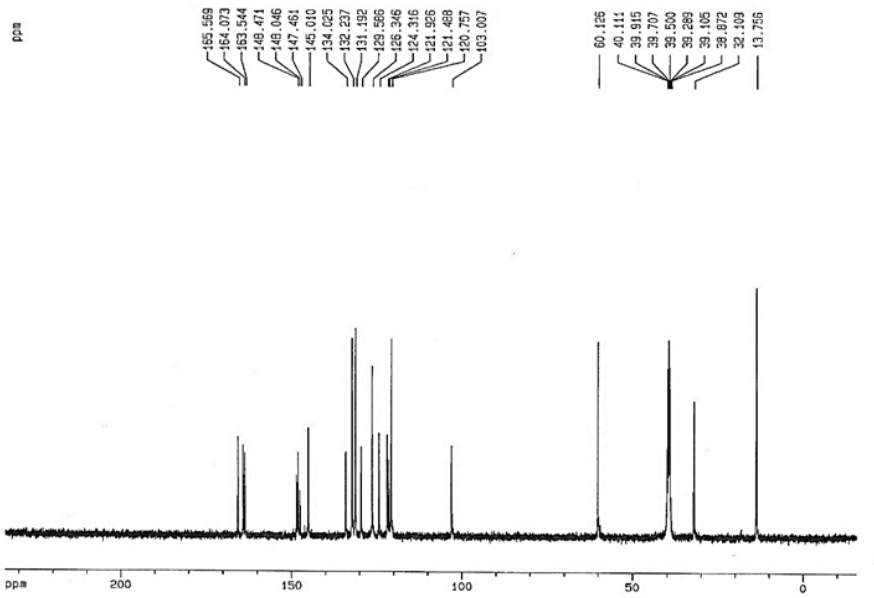

Fig. S-13. ^{13}C-NMR spectra of compound (**9b**)

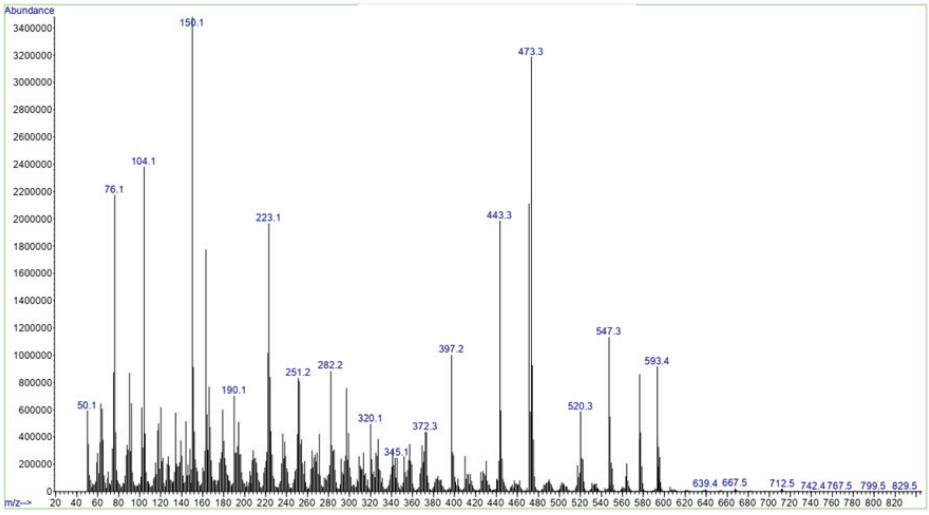

Fig. S-14. ESI-HRMS spectra of compound (**9b**)

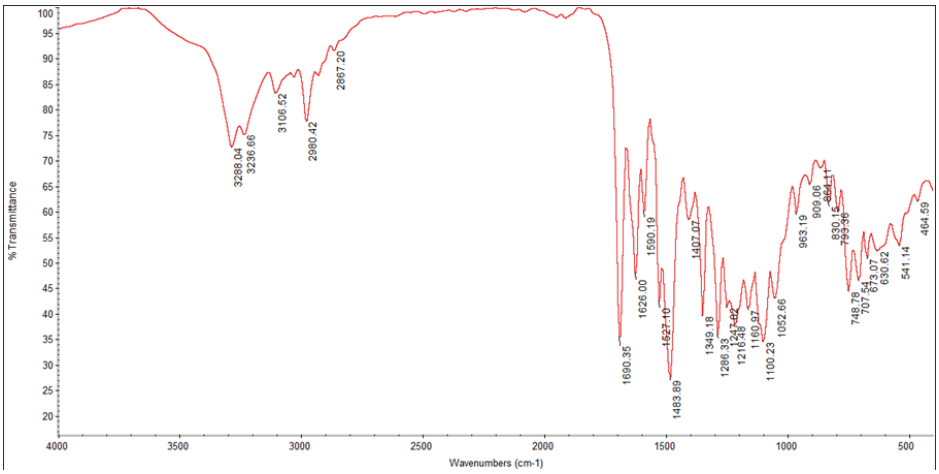

Fig. S-15. FT-IR spectra of compound (**9c**)

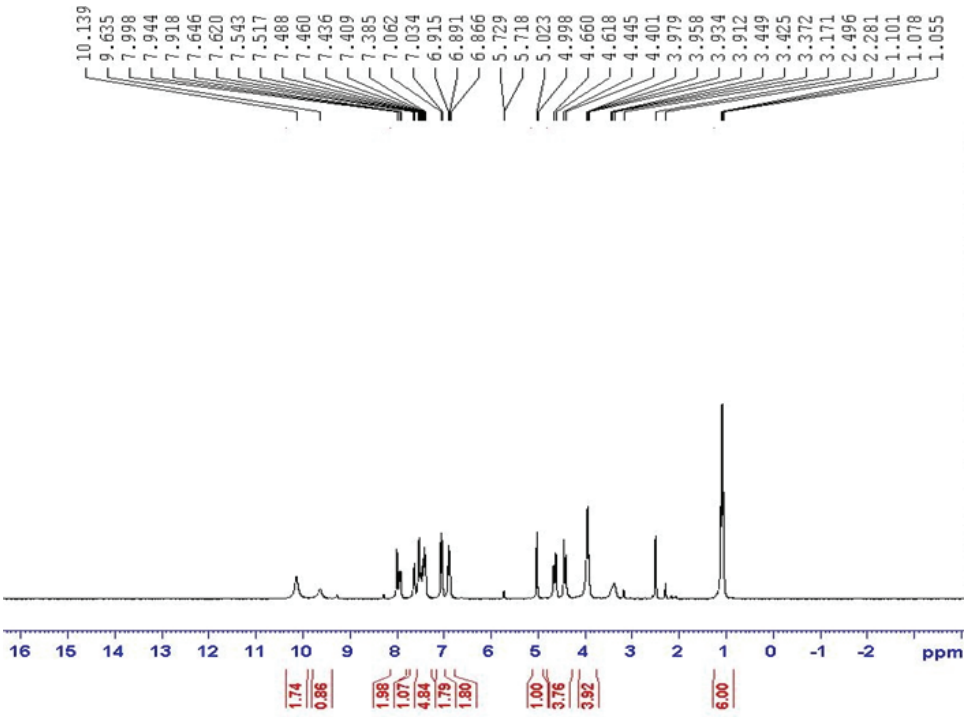

Fig. S-16. ^{1}H-NMR spectra of compound (**9c**)

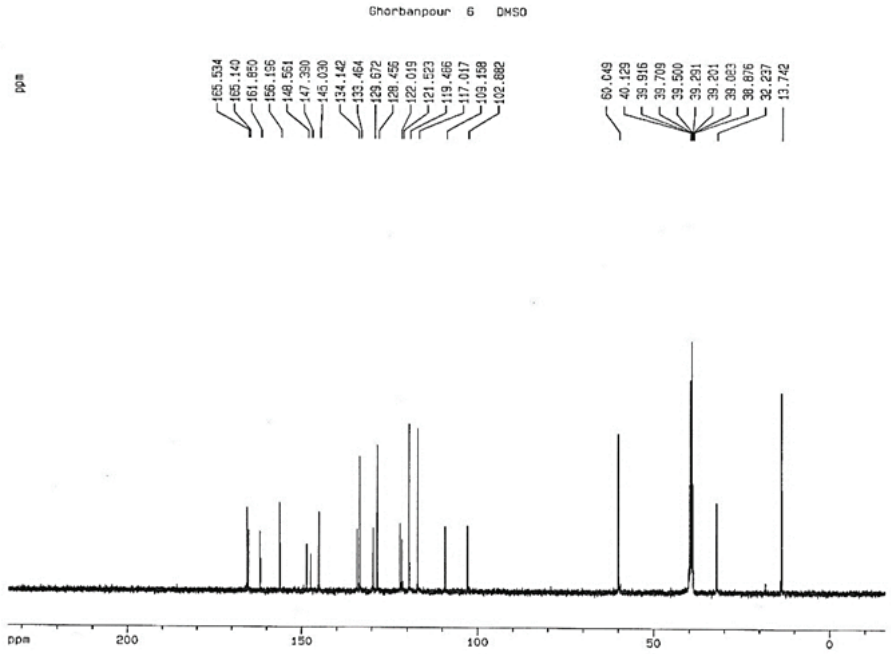

Fig. S-17. ^{13}C-NMR spectra of compound (**9c**)

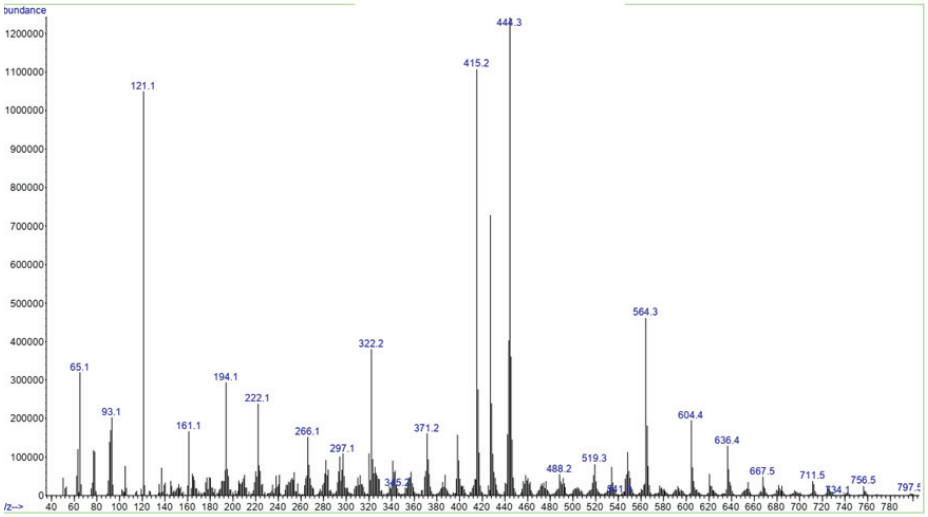

Fig. S-18. ESI-HRMS spectra of compound (**9c**)

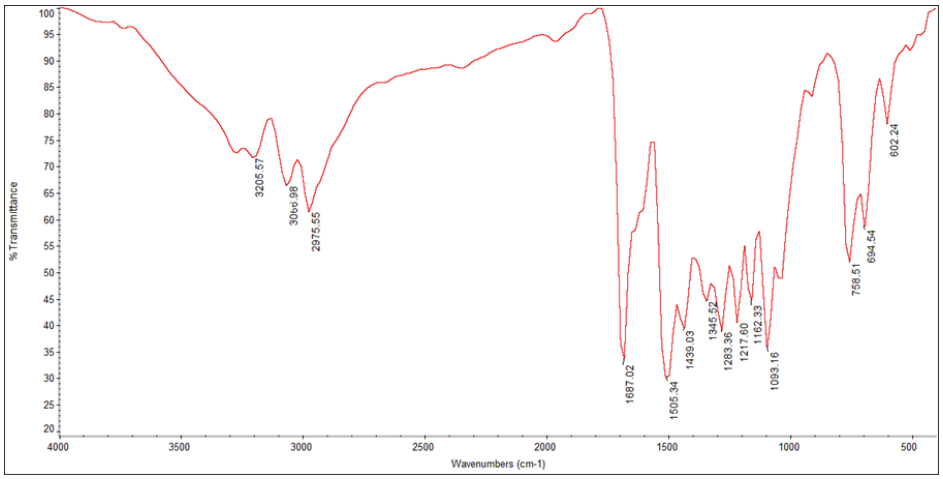

Fig. S-19. FT-IR spectra of compound (**9d**)

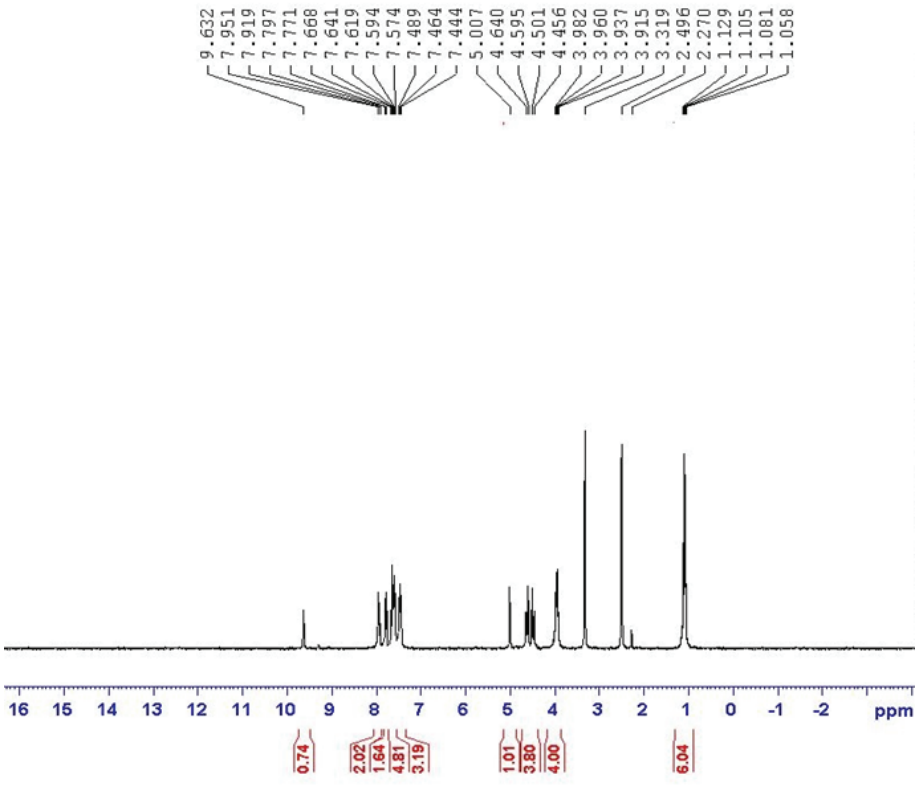

Fig. S-20. ^{1}H-NMR spectra of compound (**9d**)

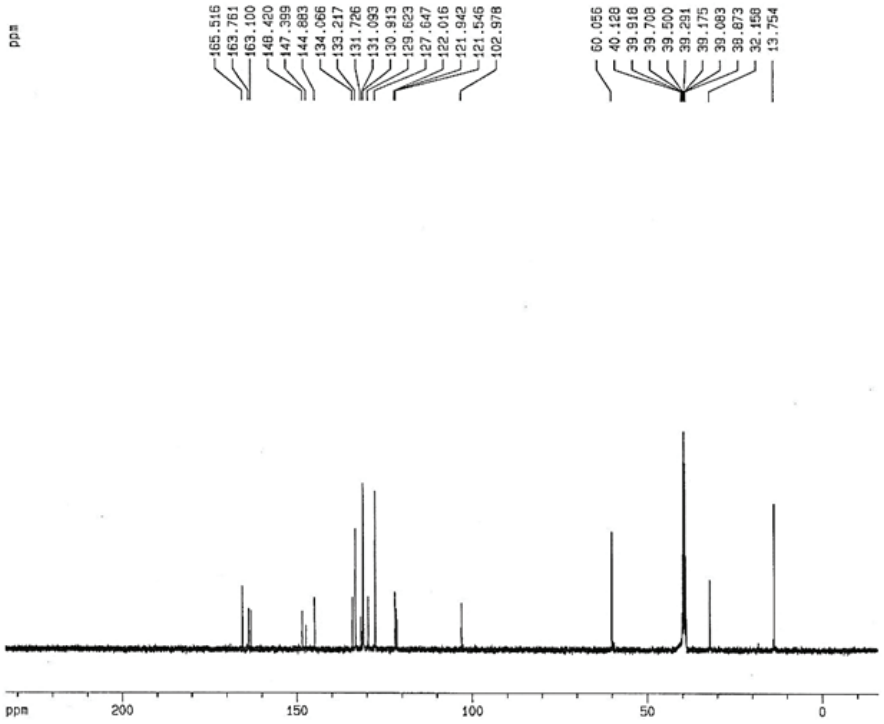

Fig. S-21. ^{13}C-NMR spectra of compound (**9d**)

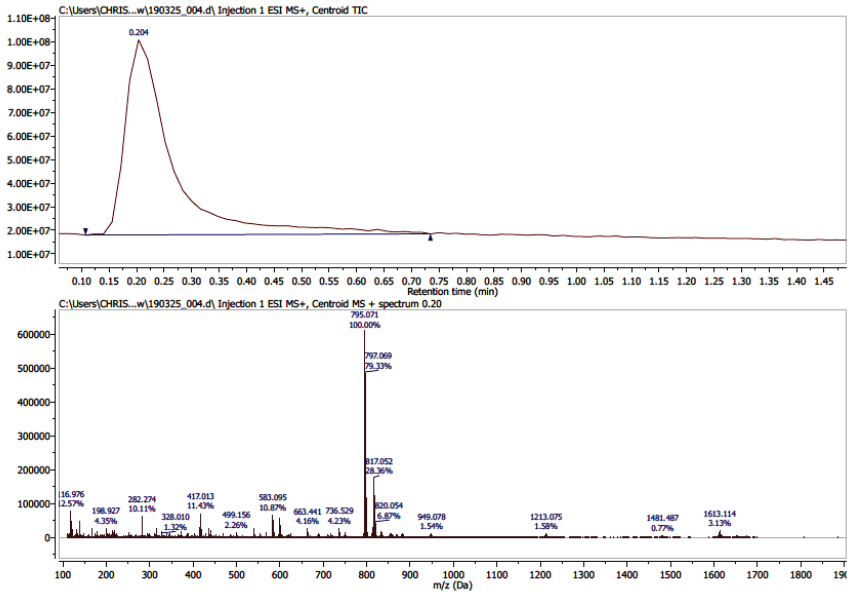

Fig. S-22. HRMS-FAB spectra of compound (**9d**)

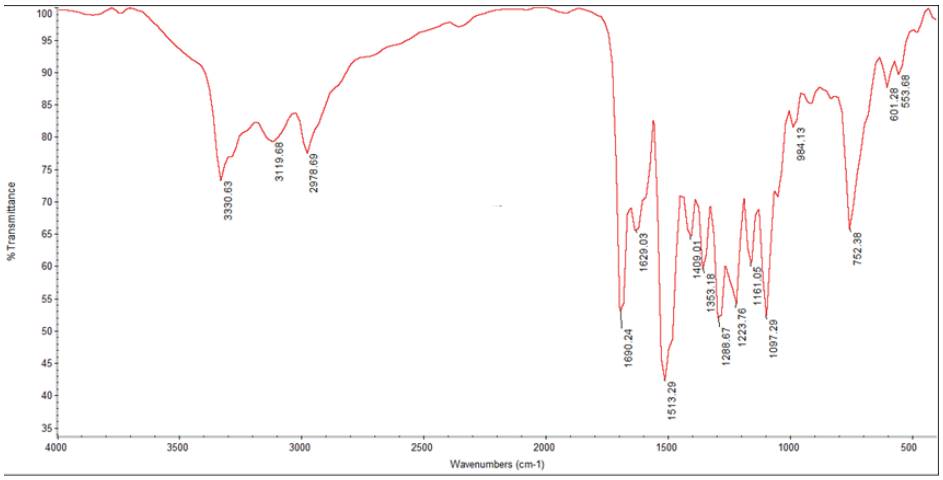

Fig. S-23. FT-IR spectra of compound (**10a**)

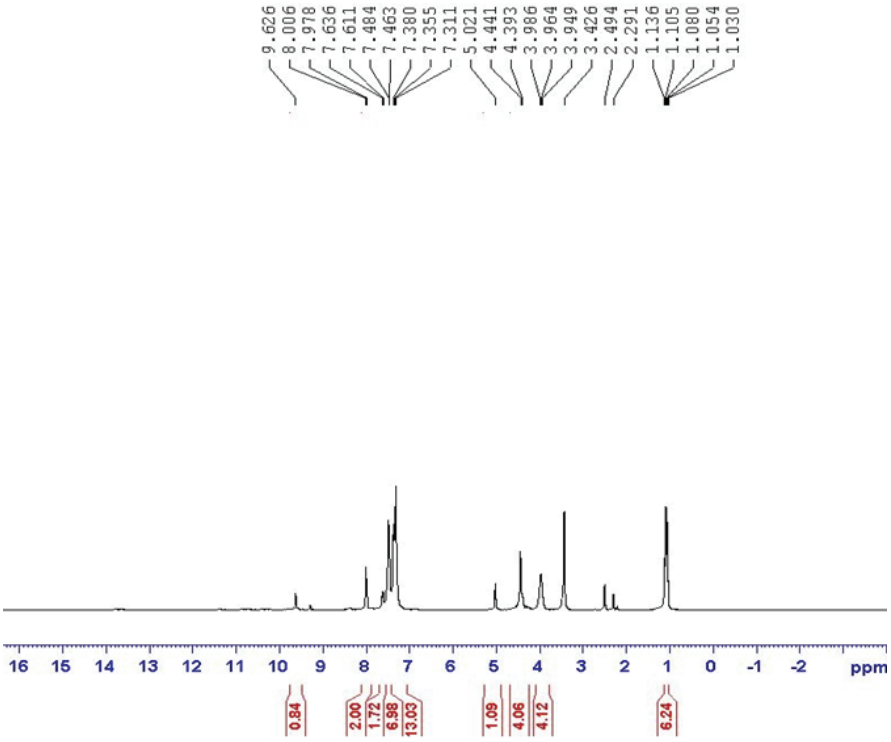

Fig. S-24. ^{1}H-NMR spectra of compound (**10a**)

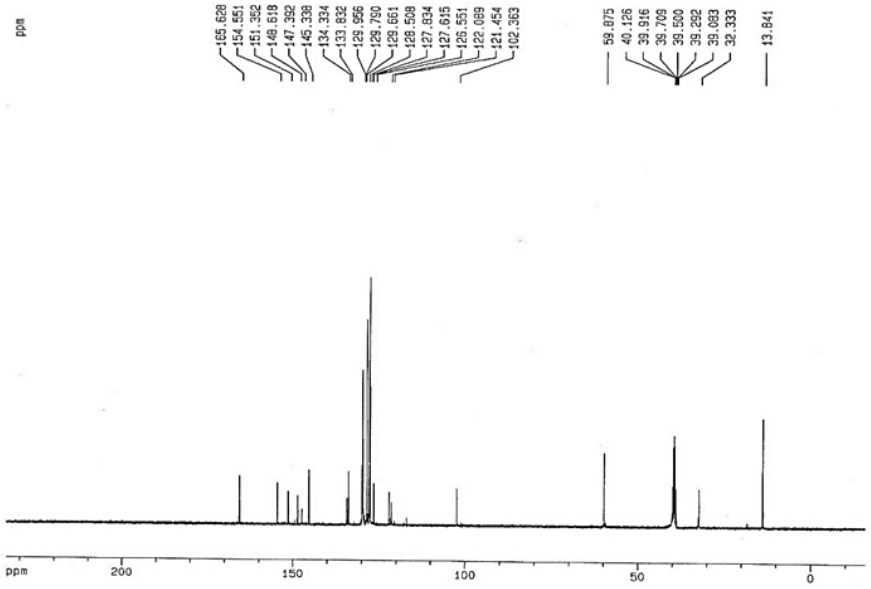

Fig. S-25. ^{13}C-NMR spectra of compound (**10a**)

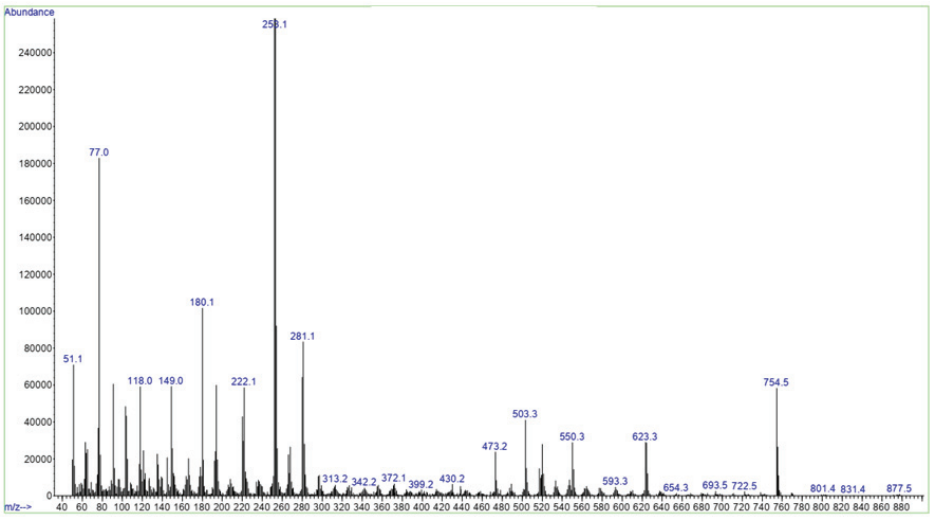

Fig. S-26. ESI-HRMS spectra of compound (**10a**)

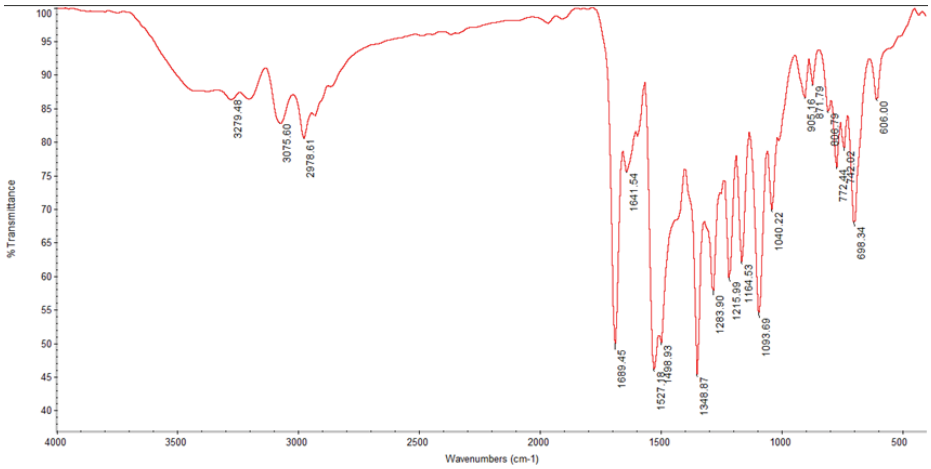

Fig. S-27. FT-IR spectra of compound (**10b**)

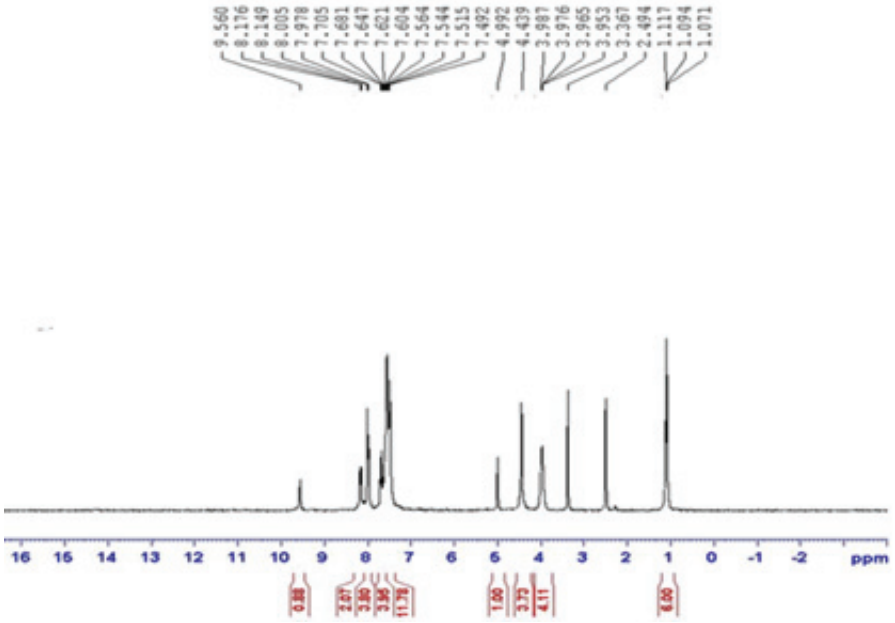

Fig. S-28. ^{1}H-NMR spectra of compound (**10b**)

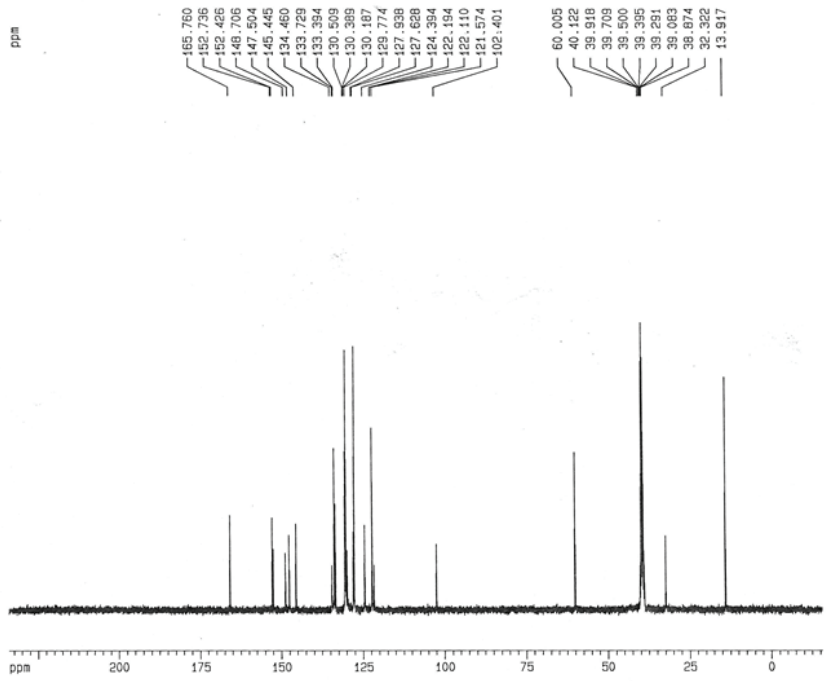

Fig. S-29. ^{13}C-NMR spectra of compound (**10b**)

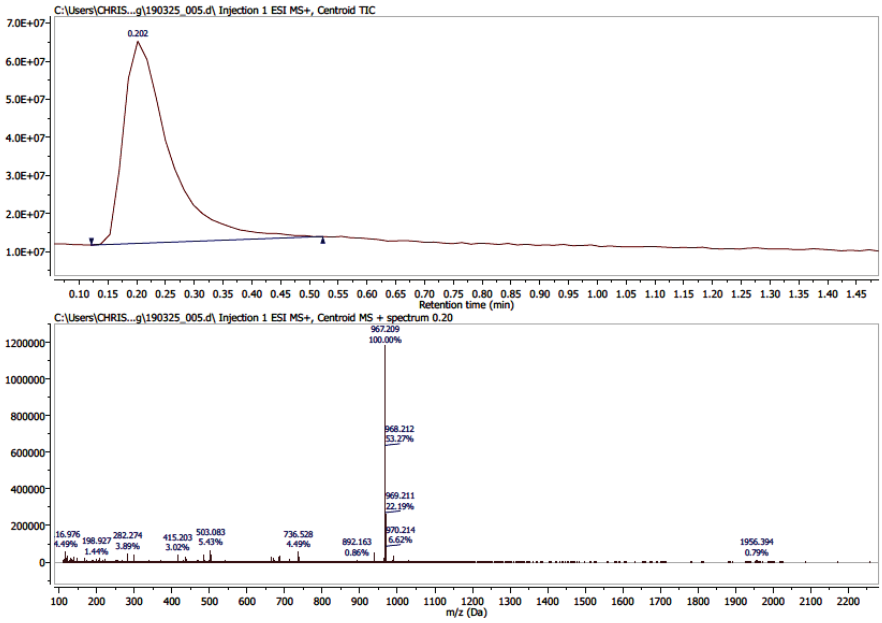

Fig. S-30. HRMS-FAB spectra of compound (**10b**)

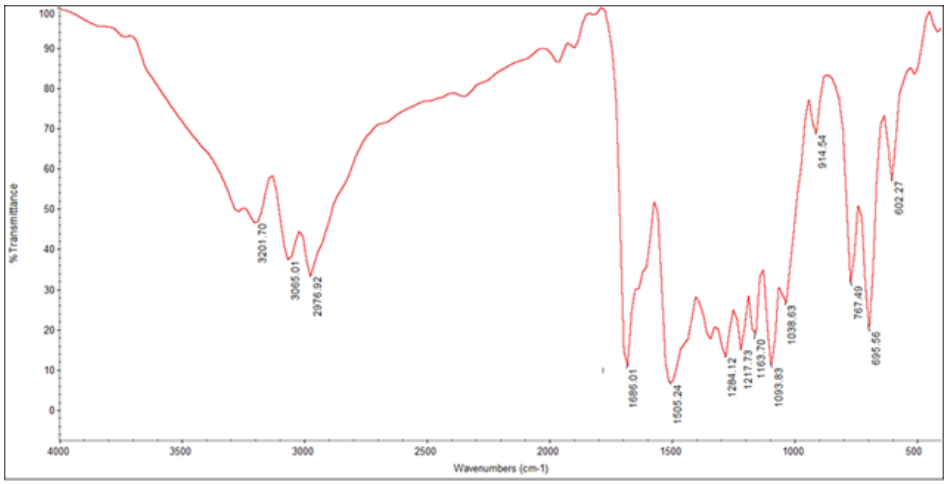

Fig. S-31. FT-IR spectra of compound (**10c**)

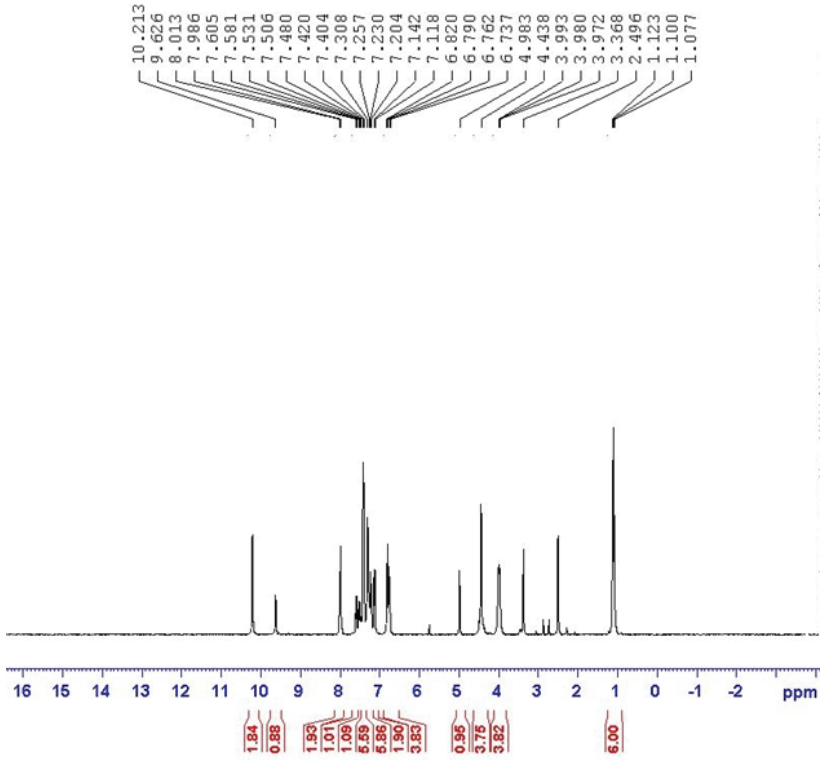

Fig. S-32. ^{1}H-NMR spectra of compound (**10c**)

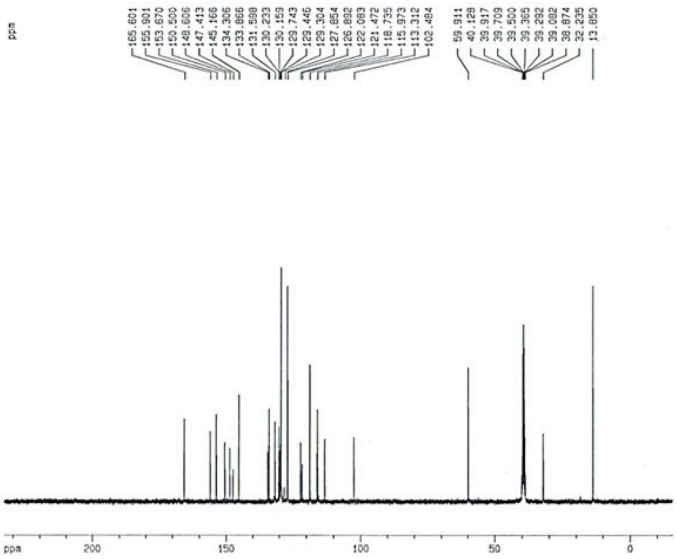

Fig. S-33. ^{13}C-NMR spectra of compound (**10c**)

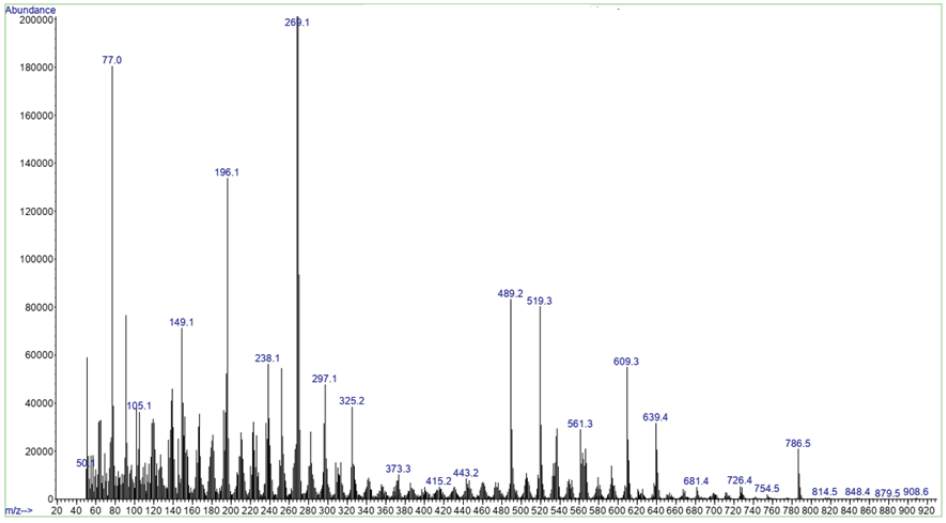

Fig. S-34. ESI-HRMS spectra of compound (**10c**)

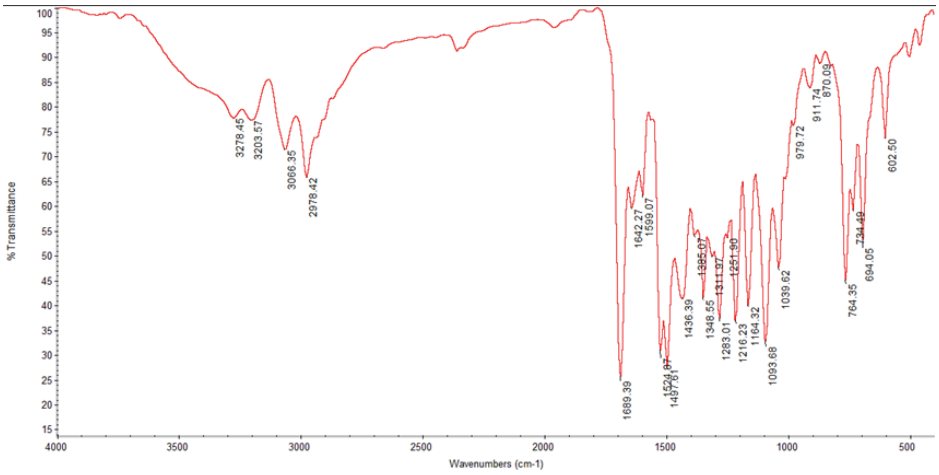

Fig. S-35. FT-IR spectra of compound (**10d**)

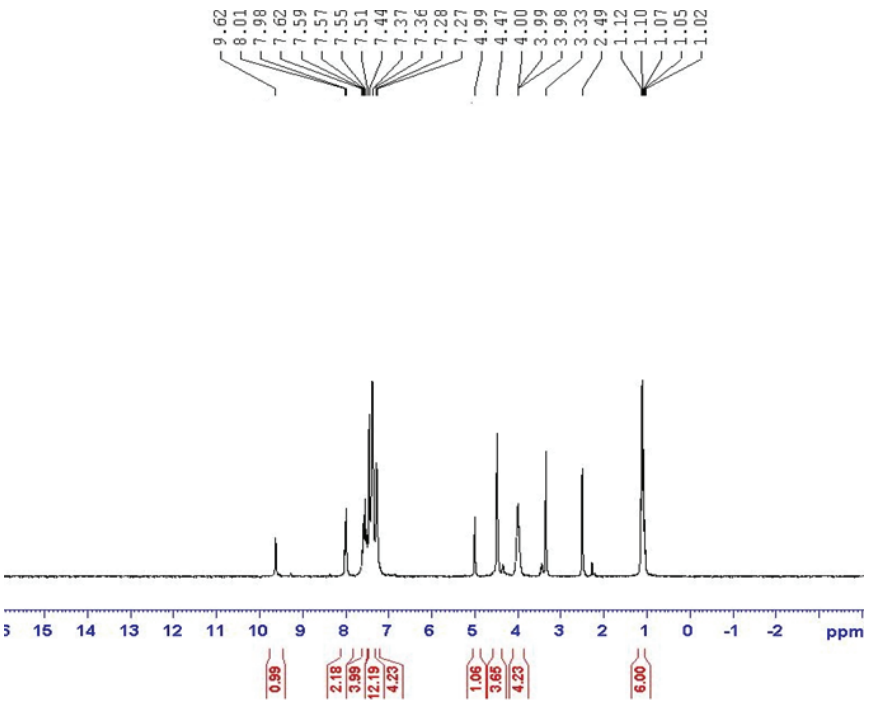

Fig. S-36. ^{1}H-NMR spectra of compound (**10d**)

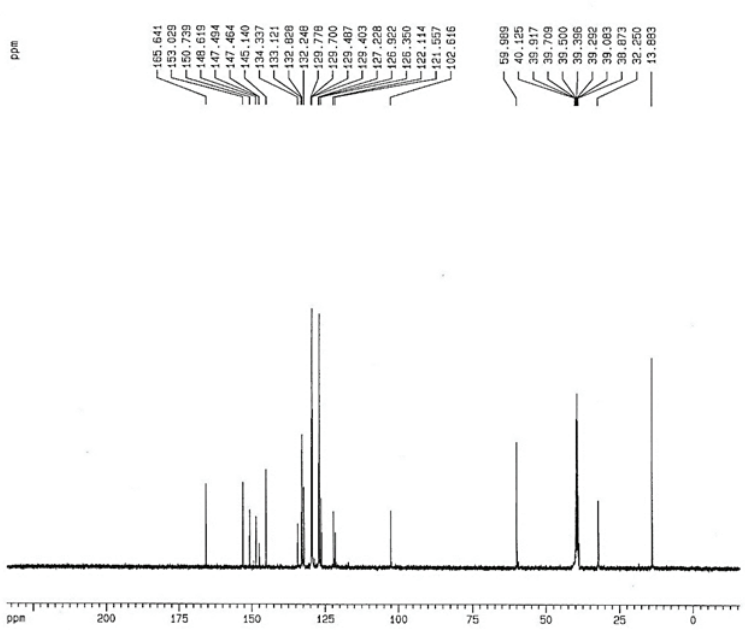

Fig. S-37. ^{13}C-NMR spectra of compound (**10d**)

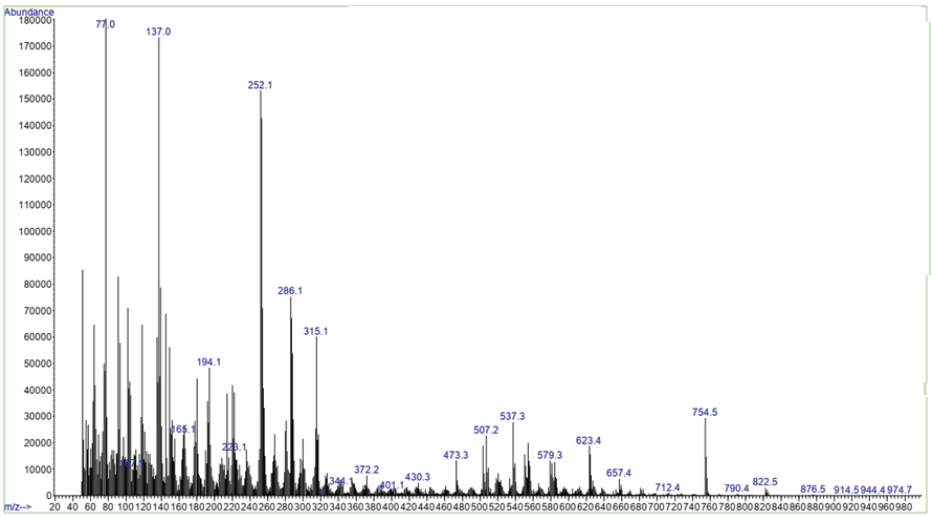

Fig. S-38. ESI-HRMS spectra of compound (**10d**)

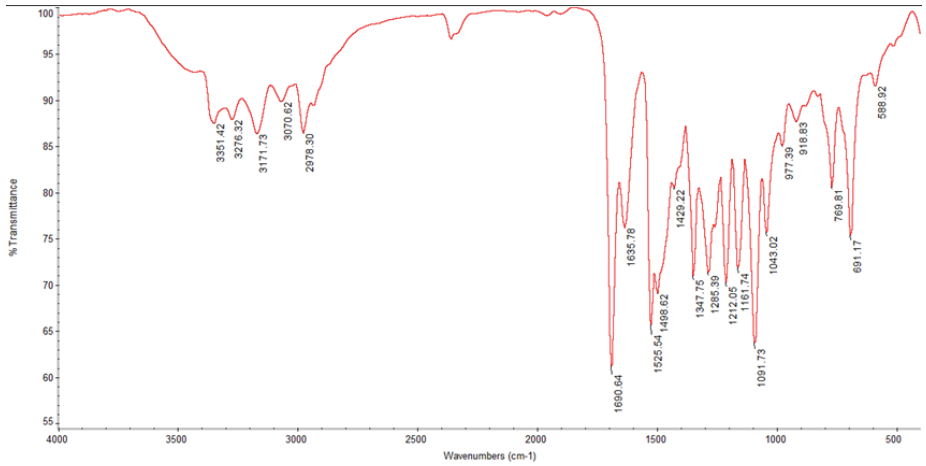

Fig. S-39. FT-IR spectra of compound (**11a**)

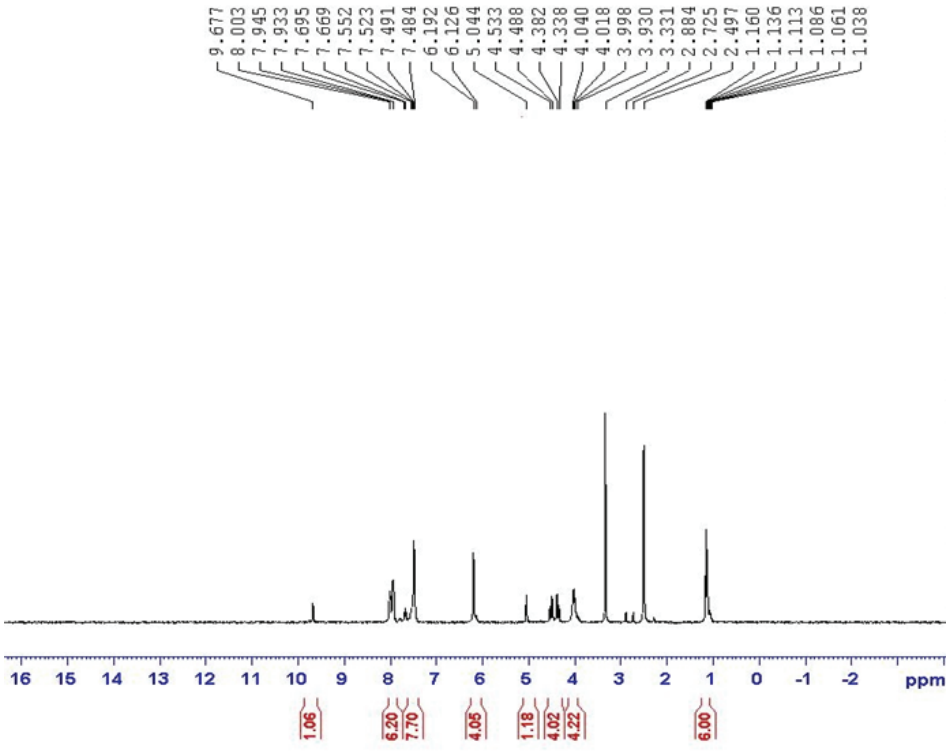

Fig. S-40. ^{1}H-NMR spectra of compound (**11a**)

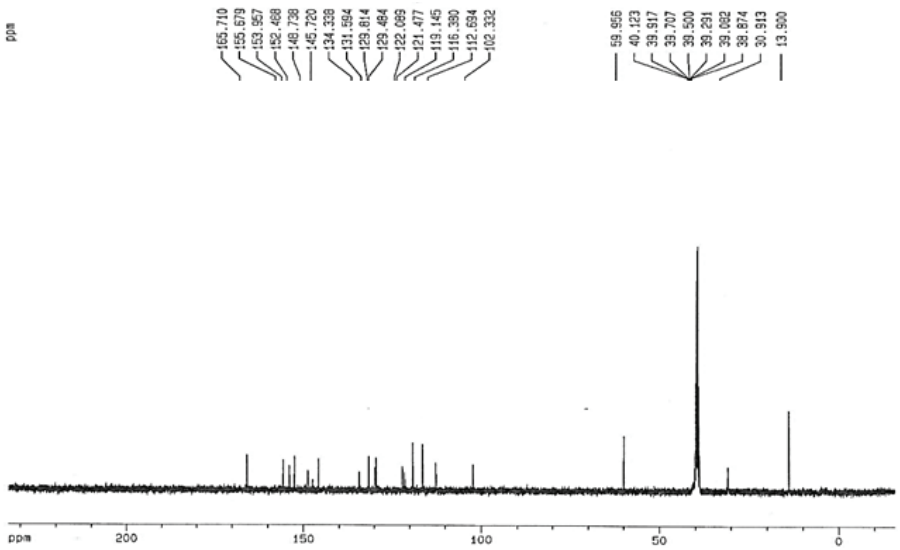

Fig. S-41. ^{13}C-NMR spectra of compound (**11a**)

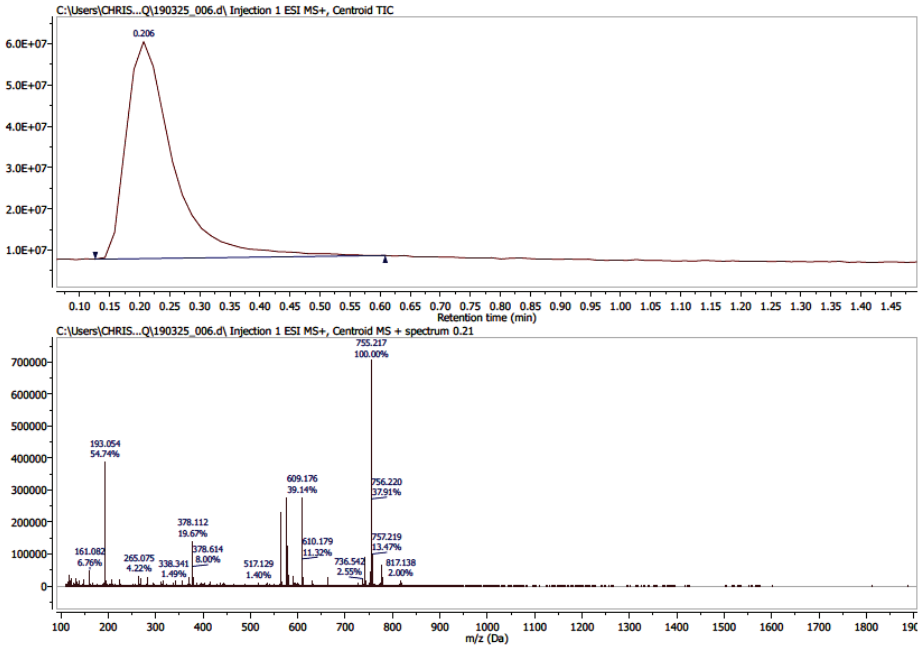

Fig. S-42. HRMS-FAB spectra of compound (**11a**)

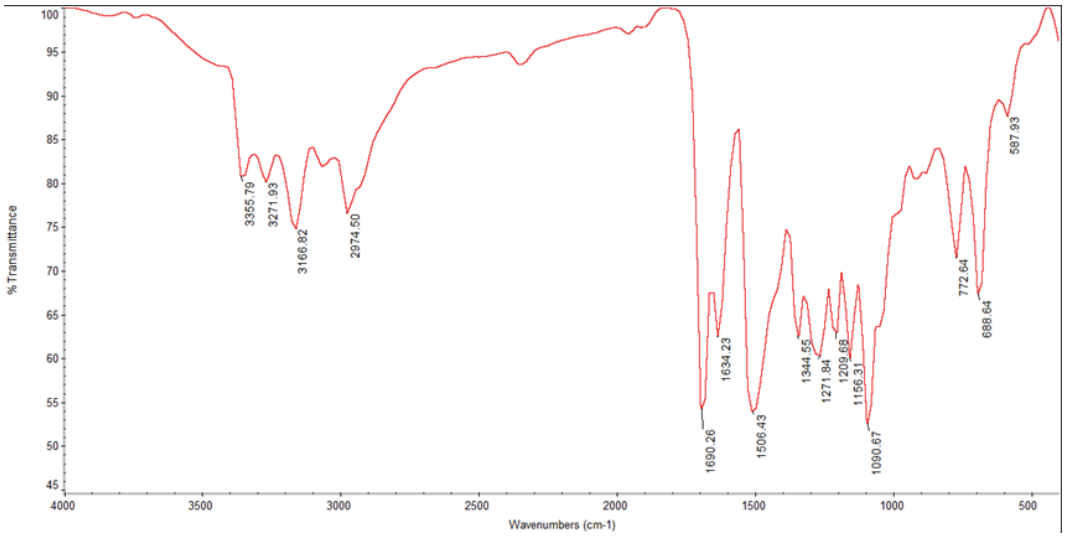

Fig. S-43. FT-IR spectra of compound (**11b**)

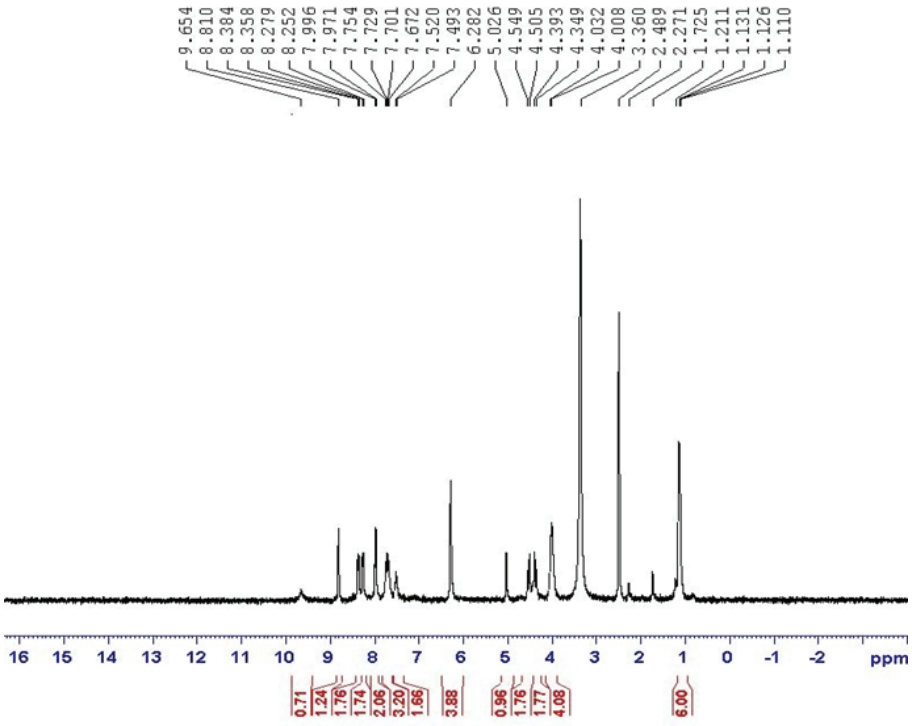

Fig. S-44. ^{1}H-NMR spectra of compound (**11b**)

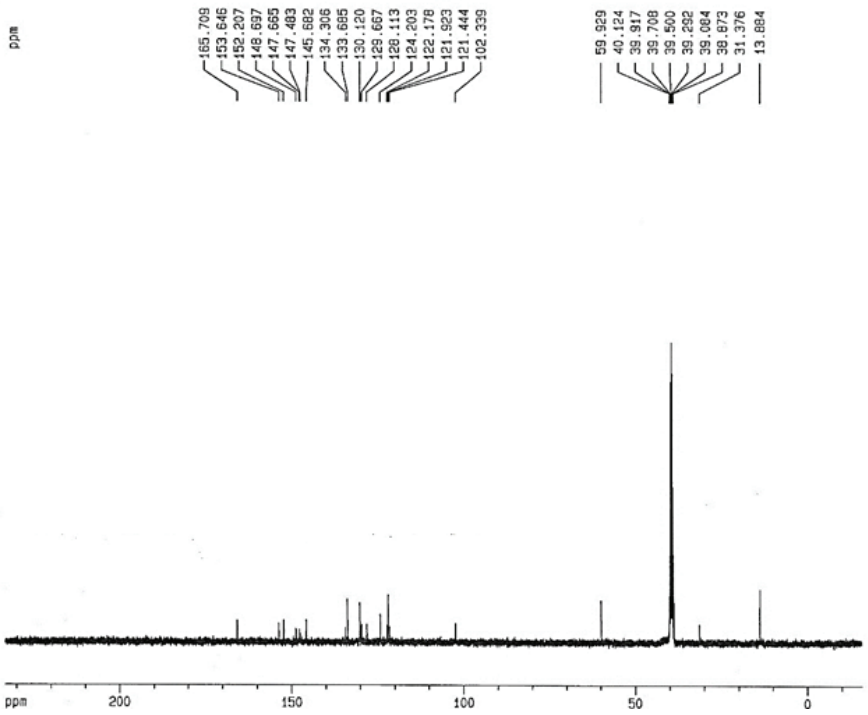

Fig. S-45. ^{13}C-NMR spectra of compound (**11b**)

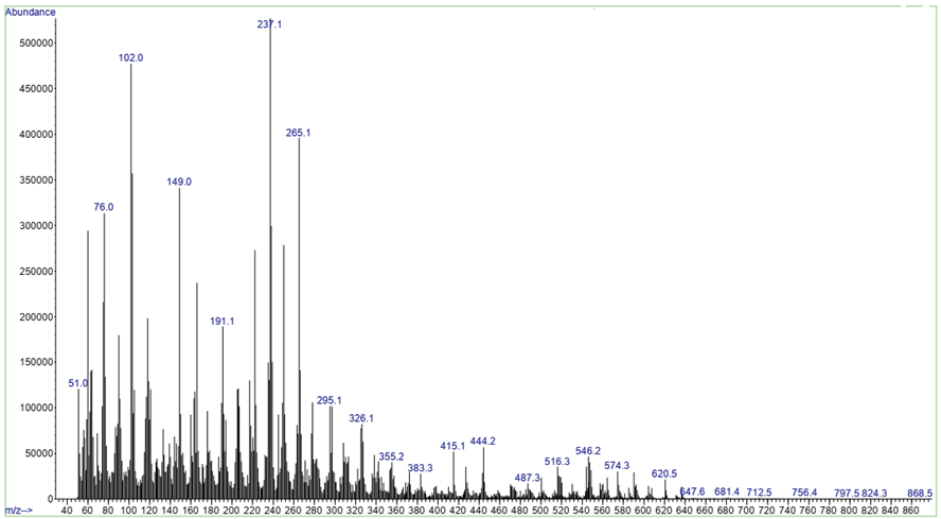

Fig. S-46. ESI-HRMS spectra of compound (**11b**)

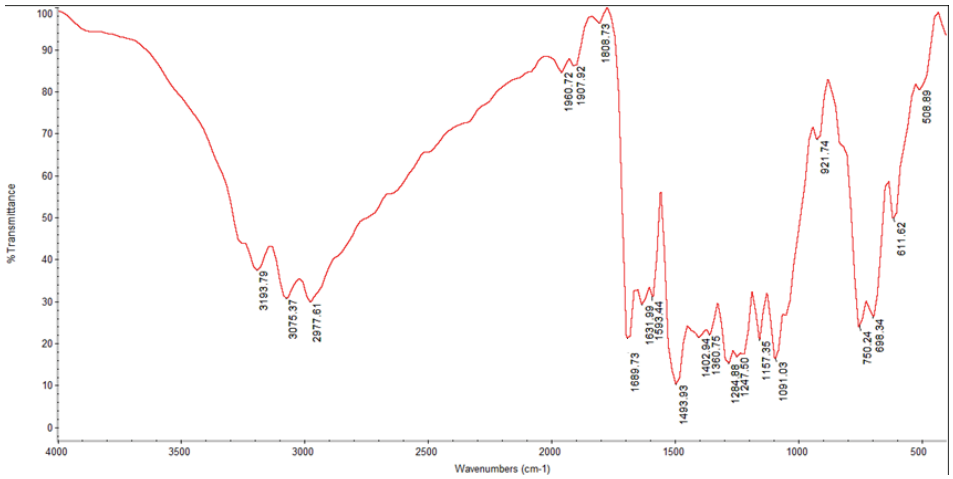

Fig. S-47. FT-IR spectra of compound (**11c**)

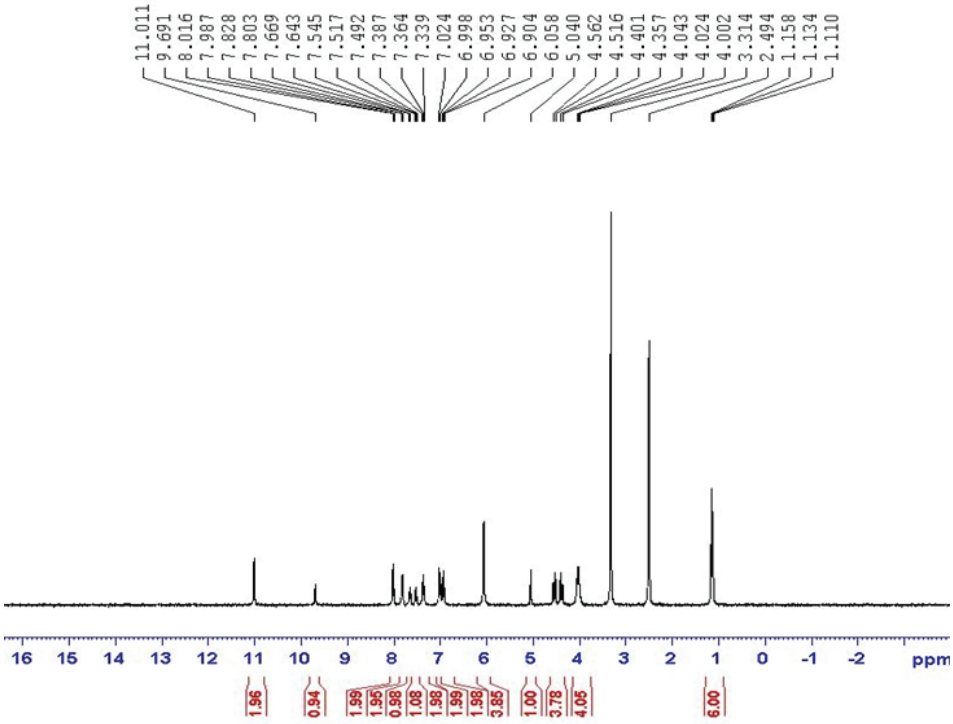

Fig. S-48. ^{1}H-NMR spectra of compound (**11c**)

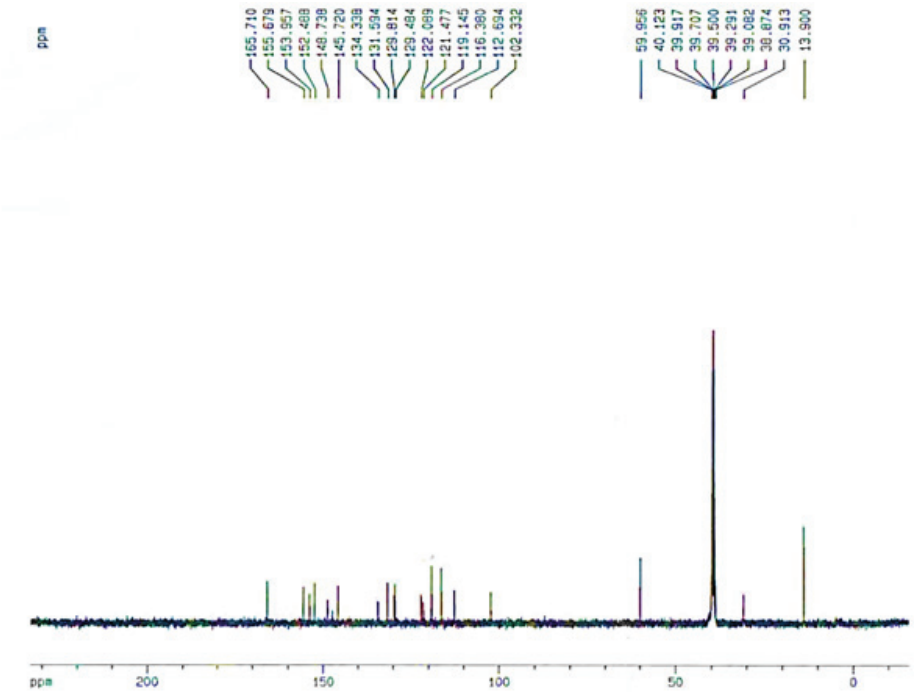

Fig. S-49. ^{13}C-NMR spectra of compound (**11c**)

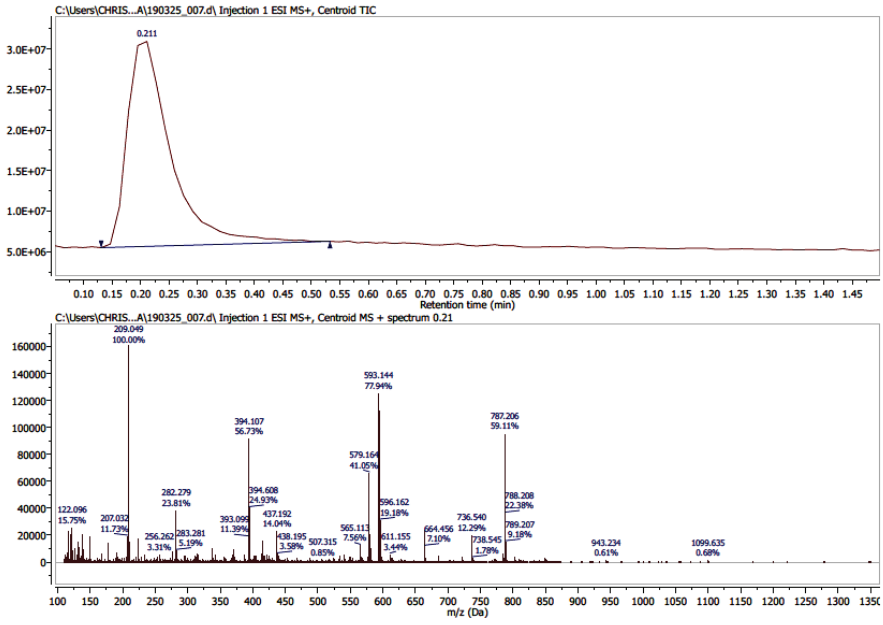

Fig. S-50. HRMS-FAB spectra of compound (**11c**)

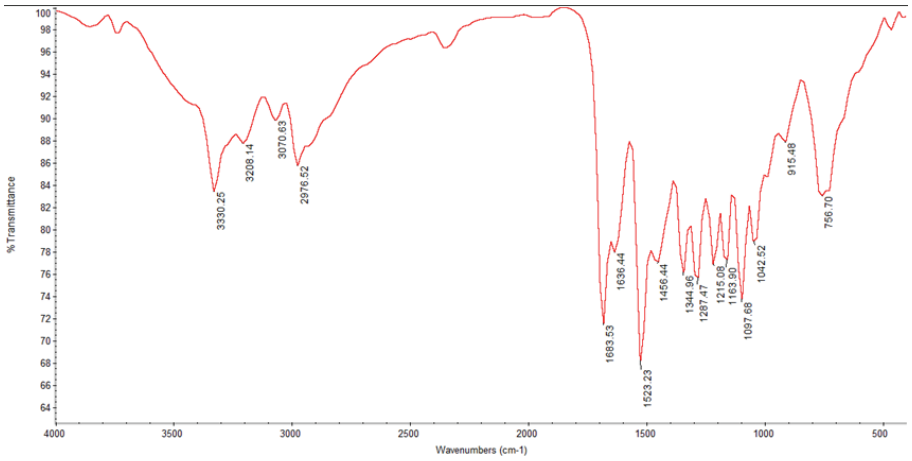

Fig. S-51. FT-IR spectra of compound (**11d**)

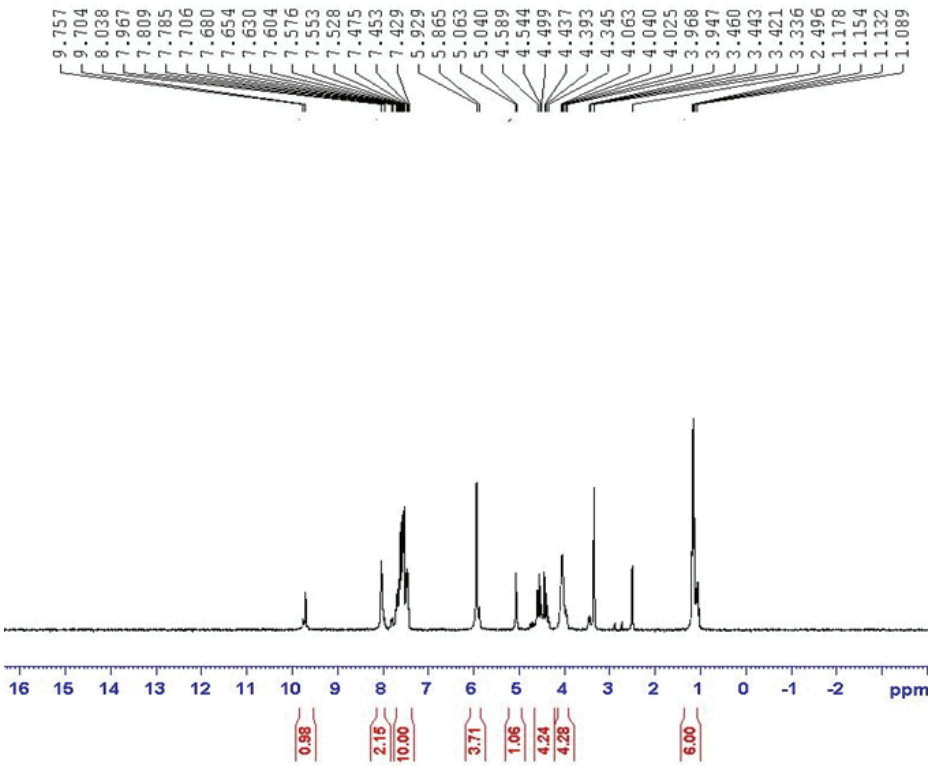

Fig. S-52. ^{1}H-NMR spectra of compound (**11d**)

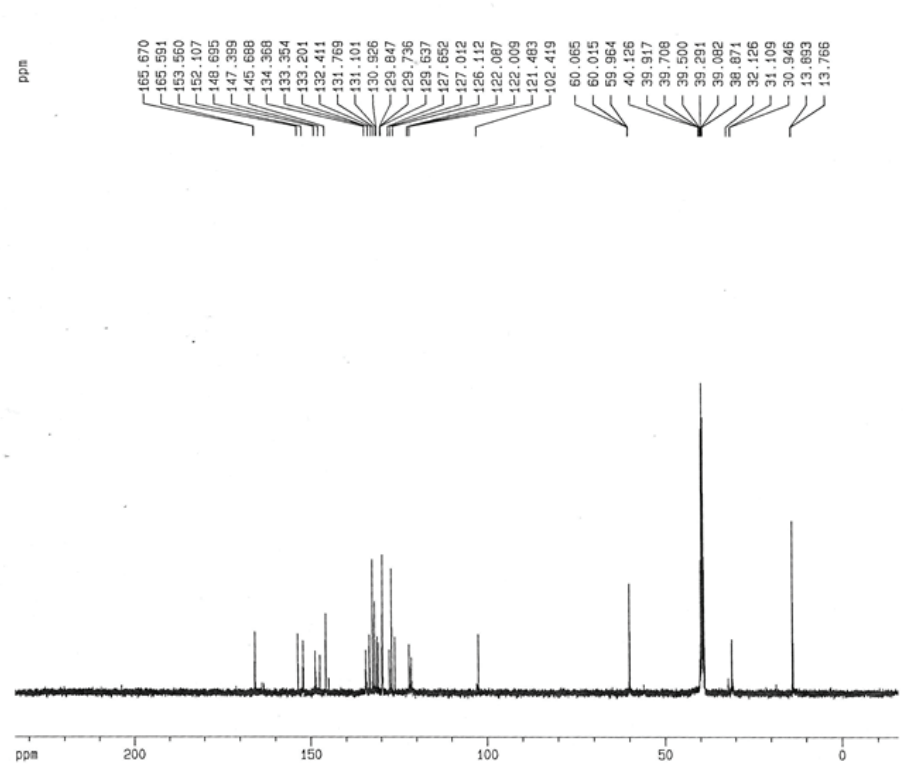

Fig. S-53. ^{13}C-NMR spectra of compound (**11d**)

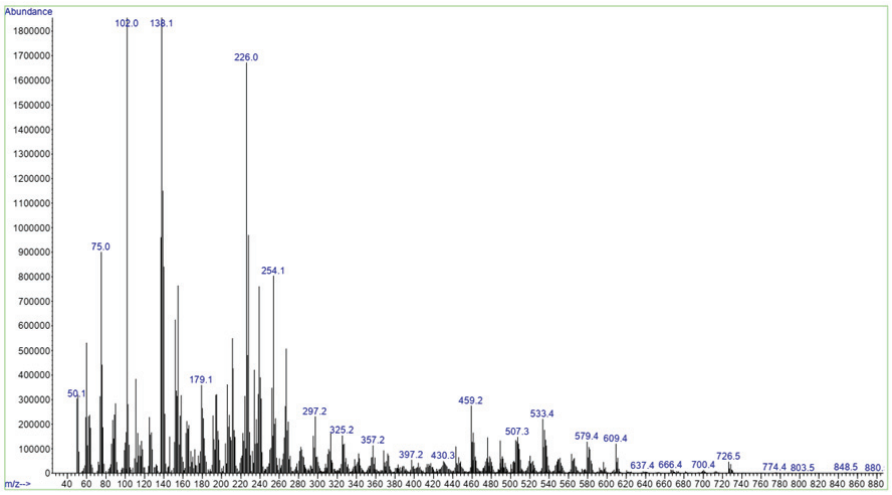

Fig. S-54. ESI-HRMS spectra of compound (**11d**).

Journal of the Serbian Chemical Society
JSCS@tmf.bg.ac.rs • www.shd.org.rs/JSCS
J. Serb. Chem. Soc. *86* (11) 1023–1037 (2021)
JSCS–5480
Original scientific paper
Published 24 September 2021

Fulleropyrrolidines with orthogonally flexible substituents – Synthesis and electrochemical properties

DRAGANA JOVANOVIĆ[1], JOVANA STANOJKOVIĆ[1], DŽENETA HALILOVIĆ[1], REJHANA KOLAŠINAC[1], TATJANA J. KOP[2], MIRA S. BJELAKOVIĆ[2] and DRAGANA R. MILIĆ[1]*

[1]*University of Belgrade – Faculty of Chemistry, Studentski trg 12–16, 11158, Belgrade, Serbia and* [2]*University of Belgrade – Institute of Chemistry, Technology and Metallurgy, Department of Chemistry, Njegoševa 12, 11000, Belgrade, Republic of Serbia*

(Received 8 July, revised 23 August, accepted 24 August 2021)

Abstract: A large series of disubstituted fulleropyrrolidines was synthesized and analyzed by cyclic voltammetry. The three main groups of target compounds differ by a flexible *N*-chain, while their further diversity was achieved by the introduction of various rigid, aryl substituents at the pyrrolidine carbon. Some dialkyl analogues were also designed for comparison, A standard [3+2]-cycloaddition of *in situ* generated azomethine ylides to C_{60} afforded a variety of disubstituted fulleropyrrolidines. Furthermore, a set of dumbbell-shaped di(fulleropyrrolidine) derivatives containing rigid fumaryl or isophthaloyl diamide platform was prepared with the aim of investigating a long-range effect of the second fulleropyrrolidine moiety on their electrochemical properties. All compounds were fully characterized by comparative analysis of spectral data, while examination of electrochemical properties was performed on representative samples, distinguished by main structural subunits. All compounds expressed quite similar electron-accepting ability, lower than C_{60}, but higher in comparison to structurally similar *N*-methylfulleropyrrolidine.

Keywords: fullerene; cyclic voltammetry; substituents' flexibility.

INTRODUCTION

Fulleropyrrolidines are a class of fullerene derivatives with a pyrrolidine ring fused to the (6:6) junction of the C_{60}. Due to a variety of easily available synthetic precursors, simple preparation, stability under atmospheric conditions,[1–5] as well as suitable physical and chemical properties, they are extensively used in biomedical and materials sciences.[1–5] To the present day, various synthetic protocols for the synthesis of fulleropyrrolidines containing different substituents on the pyrrolidine ring have been developed. One of the most frequent and widely

* Corresponding author. E-mail: dmilic@chem.bg.ac.rs
https://doi.org/10.2298/JSC210708069J

accepted method for the synthesis of fulleropyrrolidines is 1,3-dipolar cycloaddition of azomethine ylides to electron deficient fullerene C_{60} (Prato reaction).[6,7] Such highly reactive intermediates are usually produced *in situ* by the condensation of *α*-amino acids with carbonyl compounds and further decarboxylation of obtained iminium salts.[6,7] Furthermore, other approaches for the preparation of azomethine ylides have been designed, including acid-catalyzed,[8] photochemical[9] or thermal[10] desilylation of trimethylsilyl amino derivatives, tautomerization of imines,[11,12] as well as photochemically-induced reactions of tertiary amines.[13,14] At the same time, variously substituted fulleropyrrolidines have also been prepared utilizing many other methods, such as thermal reactions of aromatic aldehydes and various primary amines,[15,16] thermal and photochemical reactions of *α*-amino acids and amino acid esters without an aldehyde,[17,18] reaction of amino acids and quaternary ammonium salts[19] or reaction of halides and α-amino acids[20] with C_{60}. As the first efficient approach for a controlled chiral functionalization of fullerene, Martin and coworkers reported stereo- and enantioselective cycloaddition of *α*-iminoesters to C_{60}, catalyzed by metal/ligand chiral complexes.[21,22] Thereafter, a stereo controlled, ferric perchlorate-mediated reaction of C_{60} with arylmethanamines provided *N*-unsubstituted-2,5-diarylfulleropyrrolidines, easily transformable to trisubstituted analogues.[23]

Great interest in fulleropyrrolidines as promising electron acceptor materials in organic photovoltaic cells (OPCs) has arisen in the recent decade.[5] It was found that the solubility, optical, electrochemical and morphological properties of fulleropyrrolidines played an essential role in achieving the optimal donor-acceptor compatibility and constructing OPCs with upgraded performances.[5] Comprehensive investigations in the field of alternative electron acceptor materials include the study of fulleropyrrolidine analogues of [6,6]-phenyl C_{61} butyric acid methyl ester ($PC_{61}BM$), the well-known reference for all kinds of fullerene acceptors in OPCs. Several research groups have synthesized and examined fulleropyrrolidine derivatives containing various aryl, alkyl or polyether groups at the pyrrolidine ring, with similar or better electrochemical and photovoltaic properties compared to those of $PC_{61}BM$ under the same conditions.[24–28] All of them have demonstrated that the nature and position of the substituent, electrochemical properties (reflected in the LUMO energy level), and particularly its interactions with the donor polymer had an impact on the solar cell output. Hence, the structural modifications of the substitution pattern, as a method for fine tuning the photovoltaic properties, appeared to be the way for enhancing performances and application of fulleropyrrolidines. Extended research related to fulleropyrolidines as well as $PC_{61}BM$ has been achieved by exploring the influence of *N*-substitution on the optoelectronic, photovoltaic, and morphological properties of the photoactive layer of P3HT/fulleropyrrolidine. It was found that *N*-phenylfulleropyrrolidines expressed a similar reduction pot-

ential, but better miscibility with the polymer donor and higher power conversion efficiency in comparison to *N*-alkyl analogues.[26,29]

These observations complemented with our experience on the chemistry of fulleropyrolidines inspired us to investigate systematically the influence of the type and position of substituents at the pyrrolidine ring on electrochemical properties of the novel fullerene derivatives. The design of the presented research includes structural variation at two positions of the fulleropyrolidine core – the pyrrolidine nitrogen and the carbon adjacent to it (C-2) – by moieties of orthogonal flexibility. Beside the spatial orientation at the right angle, the term orthogonally is frequently used to describe independency or quite different properties, as was done here, and can also be found in chromatography, chemistry of protecting groups, or in a new discipline – bio-orthogonal chemistry. Thus, two different aminoalkyl chains (C6 and C10), as well as more soluble long amino-trioxa-alkyl moieties were chosen as flexible *N*-substituents, while rigid aromatic fragments containing both electron-accepting and electron-donating groups were introduced at the C-2 position. Furthermore, one compound with only flexible substituents (C6 and C9 at the pyrrolidine *N* and C-2, respectively) was selected for comparison and introduction in more complex structures in which the rigid segment was located far from fulleropyrrolidine. Finally, constructing dumbbell-like architectures by connecting designed monoadducts *via* two different rigid diamide platforms (fumaryl and isophthaloyl) gave the possibility to investigate a long-range influence of the second fulleropyrrolidine on the electrochemical properties of the compounds. In addition, such well-defined complex structure with subunits suitable to induce self-assembly by different non-covalent interactions (π–π of the fullerene core and diamide H-bonds) could be a valuable substrate in the field of supramolecular chemistry.

In aim to broaden the cluster of fulleropyrrolidine based candidates for OPCs, herein the synthesis and electrochemical properties of new sets of mono- and di-fulleropyrrolidines functionalized by alkyl, polyether, aromatic and diamide structural segments are reported. Furthermore, to evaluate preliminary their applicability in OPCs, corresponding LUMO energy levels are also calculated.

EXPERIMENTAL

General

1,6-Diaminohexane, 1,10-diaminodecane, 1,13-diamino-4,7,10-trioxatridecane, di-*tert*-butyl dicarbonate, benzyl bromoacetate, paraformaldehyde, decanal, benzaldehyde, methoxy- and nitrobenzaldehyde isomers, fumaryl chloride, and isophthaloyl chloride were purchased from Sigma Aldrich and used without further purification. Flash column chromatography (FCC) and dry-column flash chromatography (DCFC) were performed with Merck silica gel 0.04–0.063 and 0.015–0.04 mm, respectively. Thin layer chromatography (TLC) was carried out on precoated silica gel 60 F_{254} plates. The IR spectra were recorded with a Perkin-Elmer FTIR 1725X spectrophotometer. The UV spectra were recorded with a GBC Cintra 40 UV–Vis spectrophotometer. ^{1}H- and ^{13}C-NMR spectra were recorded with Varian Gemini 200

(^{1}H at 200 MHz, ^{13}C at 50 MHz) and Bruker Avance spectrometers (^{1}H at 500 MHz, ^{13}C at 125 MHz). Chemical shifts (δ) are expressed in ppm and coupling constants (J) in Hz. TMS was used as an internal reference. The sample wer dissolved in the indicated solvent system. The homonuclear 2D (DQF-COSY) and the heteronuclear 2D ^{1}H–^{13}C spectra (HSQC, HMBC) were recorded with the usual settings. High-resolution mass spectra (HRMS) were obtained using positive electrospray ionization techniques (ESI) recorded on Bruker-ESI TOF, Agilent Technologies 6210 TOF LC–MS, and LTQ Orbitrap XL instruments. Pyrrolidinic H and C were labeled as HC_{pyrr}. Atoms belonging to the fullerene moiety were written without any label. The H and C atoms of the $R^1$and R^2 moieties are numbered starting from the pyrrolidine ring. The C atoms of nonyl-group, presented as C', are numbered starting from the pyrrolidine ring.

Analytical and spectral data are given in the Supplementary material to this paper.

Electrochemical measurements

The electrochemical behavior of C_{60} derivatives was investigated using 1 mM solutions of the tested compounds in a dry and degassed mixture ODCB/DMF 2:1 containing 0.1 M TBAP as a supporting electrolyte. To remove oxygen from the electrolyte, the system was bubbled with argon prior to each experiment and an argon atmosphere above the liquid surface was maintained during the scans. The electrochemical measurements were carried out on CH1760b Electrochemical workstation potentiostat (CH Instruments, Austin, TX, USA) using a conventional three-electrode cell (5 mL) equipped with a GCE (glassy carbon electrode) as the working, Ag/Ag^+ (a silver wire in contact with 0.01 M $AgNO_3$ and 0.10 M TBAP in acetonitrile) as the reference, and a platinum wire as the auxiliary electrode, calibrated with a ferrocene/ferrocenyl couple (Fc/Fc^+) as an internal standard. All experiments were performed at room temperature in the potential range of –2.5 to 0.5 V *vs.* Ag/Ag^+ (*i.e.* –2.9 to 0.1 V *vs.* Fc/Fc^+), at sweep rates between 0.01 and 0.1 V/s. All half-wave reduction potentials are presented in V *vs.* Fc/Fc^+ (measured $E_{1/2}$ of Fc/Fc^+: 0.411 V *vs.* Ag/Ag^+ in ODCB/DMF 2:1).

Mono-protection of diamines **1** was accomplished by a published methodology.[30] Compounds **2a**,[31] **2b**,[31] **2c**,[32] **3a**,[31] **3b**,[31] **3c**,[33] **4a**,[31] **4b**,[31] **4c**[33] and **5a**[31] were prepared according to published procedures.

*General procedure for the synthesis of fulleropyrrolodine monoadducts **6**–**18***

A suspension of C_{60} (0.1 mmol), the corresponding amino acid **4a**–**c** (0.1 mmol) and an appropriate aldehyde (≈0.5 mmol) in PhMe (70–80 mL) was heated at reflux and the solvent was then evaporated to dryness. The residue was purified by dry column flash chromatography (DCFC) on SiO_2 using listed gradients of solvents as eluents. The first fraction was unconsumed C_{60} and the second one afforded the monoadduct. Subsequent precipitation from a concentrated CH_2Cl_2 solution with MeOH gave the pure fulleropyrrolidine derivatives (**6**–**–18**, with the exception of 2-nitrophenyl derivative **16c**), as brown powders.

*General procedure for the synthesis of di(fulleropyrrolodine)diamides **19–26***

a) N-*Boc-deprotection.* A solution of *N*-Boc protected derivative (**5a**, **7a** or **11c-15c**, 0.1 mmol) in TFA/DCM mixture (1:1, 10–12 mL) was stirred at room temperature for 24 h and evaporated to dryness. The excess of TFA was removed by coevaporation with PhMe (3×10 mL), giving the corresponding TFA salt in quantitative yield, which was used without purification for further coupling;

b) Coupling of fullerene monoadduct with fumaryl chloride or isophtaloyl chloride. To a solution of the corresponding TFA salt (0.1 mmol) in 30 mL of CH_2Cl_2 was added 2 mL of pyridine, the mixture was stirred for 20 min at room temperature, and then DMAP (0.3 mmol)

was introduced and the mixture was stirred for an additional 15 min at room temperature. After addition of fumaryl chloride or isophthaloyl chloride (0.05 mmol), the mixture was left to stir for 48 h at room temperature. The solvent was evaporated, and the residue was purified by flash column chromatography (FCC) on SiO_2, with use of the eluents listed below. Subsequent precipitation from $CHCl_3$ solution with MeOH gave the pure fulleropyrrolidine diamides (**19**–**26**), as brown powders.

RESULTS AND DISCUSSION

Synthesis

Three principal series of target fulleropyrrolidines differing by long, flexible pyrrolidine *N*-substituents were designed. To this purpose, alkylamino and polyoxaalkylamino side chains containing hexamethylene, decamethylene and trioxatridecane units were chosen (**a**, **b** and **c**-series of compounds, respectively, Scheme 1). Furthermore, rigid aromatic subunits with variously positioned electron-donating (OMe) and electron-accepting (NO_2) groups, and more soluble alkyl-segment (C9) were employed as pyrrolidine C-2 substituents. In addition, corresponding 2-phenyl and 2-unsubstituted analogues were designed as referent compounds. Finally, two rigid platforms, built of isophtaloyl- and fumaryl-diamide moieties were used for the construction of dumbbell-like difulleropyrrolidines.

Following the described strategy, target compounds were synthesized according to Scheme 1. A standard three-step procedure, consisting of the Boc--monoprotection of commercially available diamines **1**, mono-alkylation of their non-protected amino group by benzyl bromoacetate (BBA) and Pd/C catalyzed hydrogenolysis of obtained benzyl esters **3**, provided *N*-derivatized glycines **4** in satisfactory yields (overall 11–42 %). Utilizing the well-known Prato method[1,2,6] based on the 1,3-dipolar cyclo-addition of azomethine ylides to C_{60}, the obtained acids **4** were treated with fullerene and nine commercially available aldehydes (formaldehyde, decanal, benzaldehyde, nitro- and methoxy benzaldehydes) in refluxing toluene. Easily accomplished purification by dry column flash chromatography on SiO_2 afforded a series of fulleropyrrolidines **5**–**18** in expected yields (23–44 %), except for the lack of the expected 2-nitrophenyl derivative **16c**. Unusually, the reaction with *o*-nitrobenzaldehyde afforded 2-unsubstituted fulleropyrrolidine **11c** (11 %) as the only product (Supplementary material, Fig. S--61). Since Zhang *et al.*[34,35] have reported the successful preparation and characterization of all three isomeric 2-(nitrophenyl)fulleropyrrolidine derivatives by the Prato cycloaddition reaction with sarcosine, an atempt was made to synthesize derivative **16c** under their reaction conditions, but again only product **11c** was obtained. At the same time, the finding was in accordance with the published degradation of 2-nitrobenzaldehyde to formaldehyde *via* 1,7-electrocyclization of the corresponding ylide to the adjacent nitro-group, observed in reactions with non-fullerene dipolarophiles.[36]

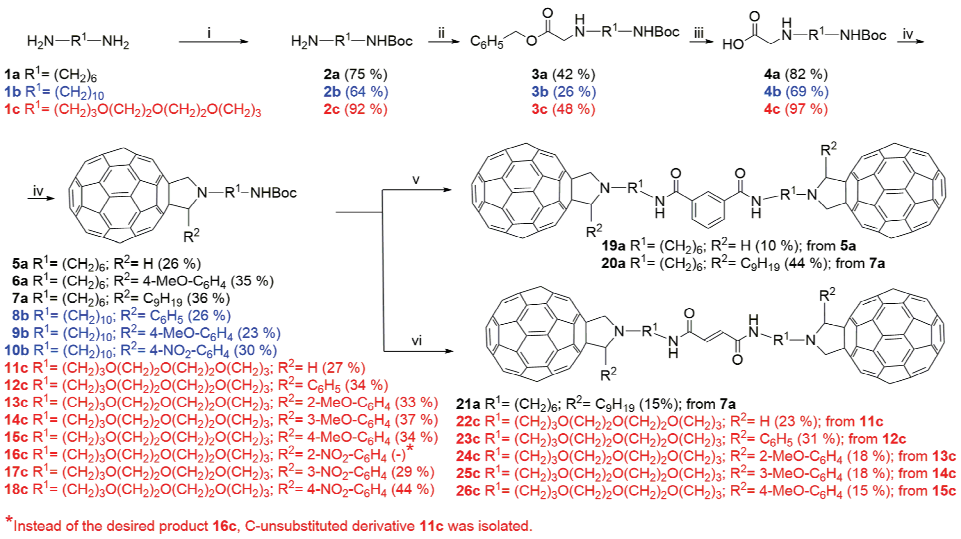

Scheme 1. Synthetic route towards C_{60} fulleropyrrolidine derivatives **5-26** starting from diamines **1a**–**c**: *i*) Boc_2O, $CHCl_3$, 0 °C → r.t., 24 h; *ii*) BBA, CH_2Cl_2, 0 °C → r.t., 24 h; *iii*) H_2, Pd/C, MeOH, r.t., 2 h; *iv*) C_{60}, R^2-CHO, PhMe, reflux; *v*) (a) **5a** or **7a**, TFA/CH_2Cl_2, r.t., 24 h; (b) isophthaloyl-chloride, DMAP, CH_2Cl_2, Py/ODCB, r.t., 48 h; *vi*) (a) **7a** or **11c–15c**, TFA/CH_2Cl_2, r.t., 24 h; (b) fumaryl-chloride, DMAP, CH_2Cl_2, Py, r.t., 48 h.

To prepare more complex derivatives – di(fulleropyrrolidines), some of synthesized compounds were used as precursors, since *N*-Boc protected fulleropyrrolidine amines represent good precursors for amide coupling with appropriate diacids (platforms). The TFA-mediated deprotection in dichloromethane provided almost quantitatively corresponding TFA-salts, which were further transformed to difullerene derivatives by coupling with isophthaloyl or fumaryl dichloride in the presence of DMAP and pyridine. To examine the influence of changes in the platform flexibility on the properties of the compound, the monoadduct **7a** was coupled to both the rigid isophthaloyl and slightly more flexible fumaryl-platform, providing di(fulleropyrrolidines) **20a** and **21a**, respectively. In addition, monoadduct **5a**, with unsubstituted C-2 position, was also transformed to difulerene derivative **19a**, but extremely low solubility disabled its full characterization. Consequently, compound **19a,** characterized only by the ^{1}H-NMR and IR spectra, was not used for further studies. In the other cases, the structure of the platform was chosen by complementarity with the C-2 substituent, *i.e.*, more flexible fumaric acid served to link fulleropyrolidines with rigid, aromatic segment at pyrrolidine C-2. So, utilizing monoadducts **11c** and **12c** (with H and Ph moieties at C-2) as model compounds, as well as **13c**–**15c** (2-, 3-, and 4-methoxyphenyl moieties at C-2), difullerenes **22c**–**26c** were obtained in yields varying from 15 to 31 % (Scheme 1).

Structure determination

The structures of the known compounds **2**–**5** were confirmed by comparison with literature data (see Supplementary material). As was mentioned before, the poorly soluble compound **19a** was characterized only by its ^{1}H-NMR and IR spectra. In addition, compounds **20a** and **21a** expressed extremely low ionizability/solubility under the applied conditions, so neither ESI-TOF, nor HESI Orbitrap provided satisfactory mass spectra. The structures of all other synthesized fullerene compounds were characterized in detail by high-resolution mass spectrometry (HRMS), FT-IR, UV–Vis, 1D (^{1}H-NMR and ^{13}C-NMR) and 2D NMR spectra (COSY, HSQC and HMBC, Supplementary material). The correct positive ionization peak was observed in ESI-TOF and HESI Orbitrap mass spectra for all ionizable fulleropyrrolidines, while the UV−Vis spectra showed a characteristic peak in the range of 431–433 nm, typical for [6,6]-monoadducts of C_{60}.

All peaks belonging to substituted fulleropyrrolidine moieties were observed in the corresponding NMR spectra. The characteristic ^{1}H/^{13}C-NMR signals of all the new synthesized fullerene derivatives are given in Tables S-I–S-III). As representative examples, the ^{1}H-NMR spectra of the monosubstituted fulleropyrrolidine **11c**, the disubstituted 2-phenyl- (**12c**) and the isomeric 2-(methoxyphenyl)-3,4-fulleropyrrolidines (**13c**–**15c**), as well as the corresponding difullerene diamides **22c–26c** synthesized from them are presented in Figs. 1 and 2, respectively. Unlike the characteristic fulleropyrrolidine ^{1}H singlet at δ 4.4 ppm for C-unsubstituted fulleropyrrolidine **11c**, the ^{1}H-NMR spectra of the newly synthesized disubstituted C_{60} derivatives contained the expected multiplication of the signals. Thus, the pyrrolidine proton attached to the chiral C-2, gave a singlet in a narrow δ range of 5.0–5.7 ppm (R^2- aryl) or a triplet at δ = 4.13 ppm (R^2-nonyl). At the same time, two diastereotopic protons at pyrrolidine C-5 responded as two doublets in a wide δ range of 4.10–5.14 ppm, with a coupling constant of 10 Hz.

Except for the 2-(2-methoxyphenyl)-substituted derivatives **13c** and **24c**, the other 2-arylfulleropyrolidines displayed a broadening of the *ortho*-H (HC_{ar}(2',6') singlet in the δ range of 7.3–8.7 ppm, indicating the restricted rotation of the phenyl group on the pyrrolidine ring in the case of *ortho*-substituted derivatives, as well as the fast exchange between *ortho*-H in the others.[37,38] In addition, the remaining aromatic protons gave the usual phenyl signal pattern, located in the δ zone of 6.8–8.7 ppm (Figs. 1 and 2, and Tables S-I–S-III). Due to distinct chemical environments, the methylene protons adjacent to pyrrolidine nitrogen (CH_2(1)) appeared as two sets of quite distant multiplets ($\Delta\delta$ = 0.5–1 ppm, Figs. 1 and 2), which is in good agreement with other reported *N*-(alky)pyrrolidino-fullerenes.[39] The presence of the *N*-*tert*-butoxycarbonyl protecting group (NH-COOC(CH_3)$_3$)

was confirmed by two singlets – a broad one in the δ range of 4.5–5.0 ppm attributable to the carbamate proton, and one at $\delta \approx 1.5$ ppm assigned to the CH_3 group.

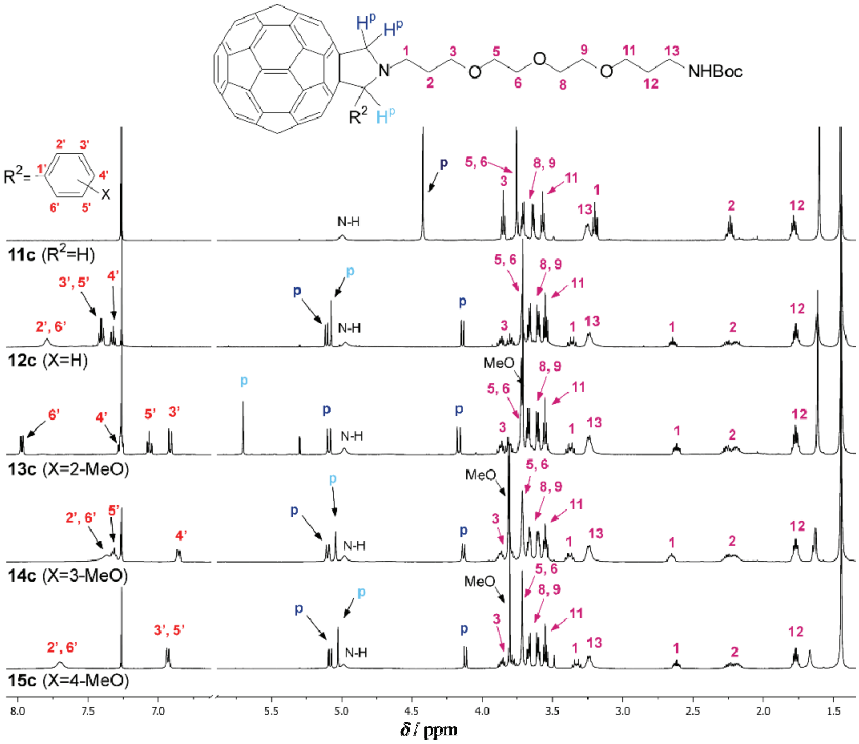

Fig. 1. Comparison of the ^{1}H-NMR spectra of monosubstituted fulleropyrrolidine **11c** and disubstituted fulleropyrrolidines **12c**–**15c**.

In accordance with the C_1 symmetry of mono- fulleropyrrolidines, the 58 sp^2 carbons of the fullerene moiety resonated in all cases in the same region (δ 135––157 ppm) giving a similar number of signals (at least 43). Two peaks in narrow δ ranges of 77.1−76.1 and 70.8−68.8 ppm, attributable to two sp^3 C of the fullerene subunit confirmed the 6,6-ring junction of the C_{60} to the pyrrolidine ring. In addition, the pyrrolidine methine carbon bearing an aromatic or the nonyl group resonates at $\delta \approx 82$ and 77 ppm, respectively, except for 2-MeO-C_6H_4-derivatives **13c** and **24c** ($\delta \approx 74$ ppm), whereas the pyrrolidine methylene carbon in all cases appeared at $\delta \approx 67$ ppm. Moreover, the *N*-Boc segment resonated at δ 156 (C=O), 79 (C) and 28.5 ppm (CH_3). Besides the disappearance of the ^{1}H- and ^{13}C--signals belonging to the *N*-Boc group, the NMR spectra of difullerene compounds **21a**, **22c**–**26c** showed the expected signals corresponding to the fumaramide CO bond at $\delta \approx 165$ ppm, the fumaramide double bond signals at about δ 6.8 ppm/133 ppm, as well as an exchangeable amide NH proton in the δ range of

6.9–8.0 ppm (Fig. 2, Table S-III). In addition, the characteristic peaks of the isophthaloyl diamide moiety in difullerenes **19a** and **20a** were located in their ^{1}H-NMR spectra at δ 6.3 (amide NH), 8.2 (H(2)), 7.9 (H(4,6)) and 7.5 ppm (H(5)), as well as in the ^{13}C-NMR spectrum of **20a** at δ 166.6, 135.1, 125.3, 129.7 and 129.0 ppm for amide CO, aryl C(1,3), C(2), C(4,6) and C(5), respectively (Table S-III). Additionally, the ^{1}H-NMR and ^{13}C-NMR spectra of all the prepared derivatives revealed the presence of the signals of aliphatic protons and carbons belonging to the R^1 and R^2 methylene and methyl groups on the pyrrolidine ring (Figs. 1 and 2, Tables S-I–S-III).

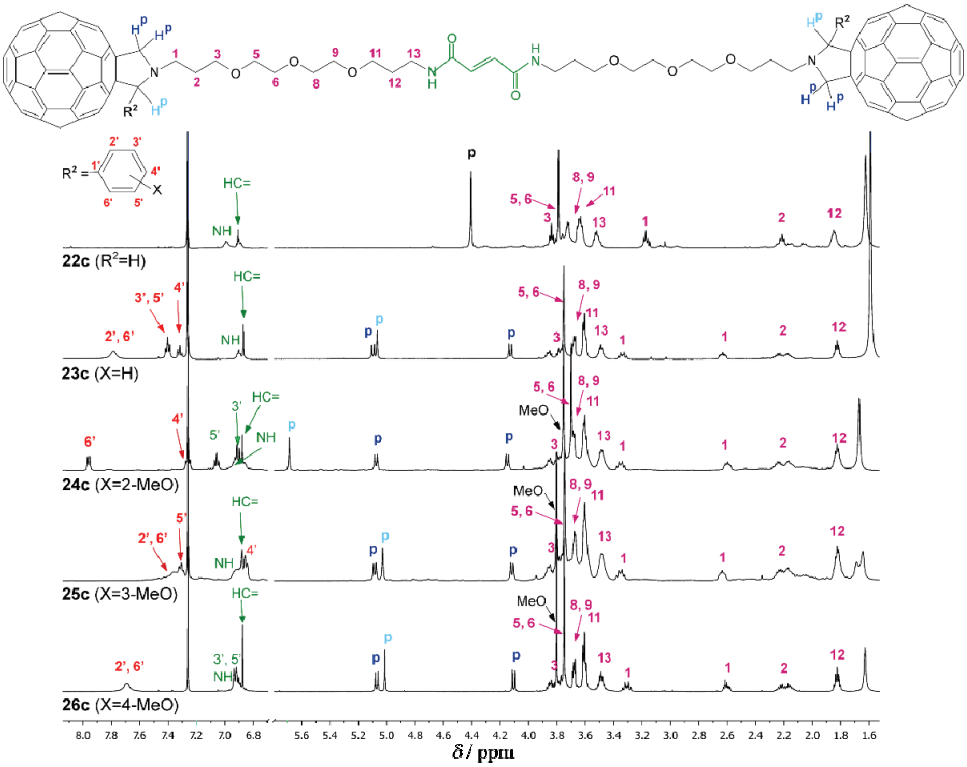

Fig. 2. Comparison of the ^{1}H-NMR spectra of difulleropyrrolidine diamides **22c**–**26c**.

Electrochemical properties

The redox properties of fullerene derivatives, as well as the possibility of intermolecular electronic communication between their segments were studied by the cyclic voltammetry (CV). To these purposes, a set of 12 representative compounds, differing in the number of the fullerene subunits, structure of the central rigid platform in diffulerene compounds, and *N*- and C-pyrrolidine substituents was selected. In addition, the C_{60} and *N*-methylfulleropyrrolidine (NMFP) were

used as referent compounds. The CV curves of tested samples were recorded in an ODCB / DMF (2:1) mixture at different scan rates, varying from 50 to 200 mV s^{-1}. At higher scan rates, voltammograms with broad end, low separated peaks were obtained, while better electrochemical response was achieved only at the lowest scan rate of 50 mV s^{-1}. Under such conditions, all tested samples gave a uniform electrochemical response consisting of three redox waves attributable to three successive reversible redox processes on the fullerene cage (Fig. 3). Their half-potentials were in a quite narrow interspace of 40 mV. Thus, the first reduction occurred in the range from –1.02 to –1.06 V *vs.* Fc/Fc^+, the second from –1.44 to –1.48 V *vs.* Fc/Fc^+, and the third one at $E_{1/2}$ = –2.06 – –2.10 V *vs.* Fc/Fc^+ (Table I). As can be seen from Table I and Fig. 4, the number of fullerene subunits had no influence on electrochemical behavior of derivatives (**7a** *vs.* **20a** or **21a**, **12c** *vs.* **23c** and **13c** *vs.* **24c**). The same effect was observed by varying the structure of the central rigid platform in difullerene compounds (**20a** *vs.* **21a**). Further, an almost identical electron accepting ability was observed in monofullerenes regardless of the presence *N*-alkyl or trioxa tether (**6a** *vs.* **9b** *vs.* **15c**, **8b** *vs.* **12c**), as well as C-alkyl, phenyl or isomeric methoxyphenyl substituted pyrrolidine subunits (**12c** *vs.* **13c** *vs.* **14c** *vs.* **15c**, **6a** *vs.* **7a** and **8b** *vs.* **9b**). In addition, no electronic communications between fullerene subunits in diffulerene compounds were observed, since redox processes proceeded simultaneously, affording the same half-potential values for both carbon spheres. The absence of interfullerene interactions in the ground state was also found in other dumbbell-derivatives,[40,41] with the exception of diffullerenes connected directly *via* oxygen[42] or a metal.[43–45]

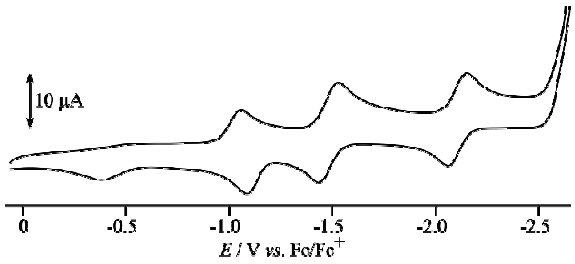

Fig. 3. A representative CV voltammogram (compound **6a**).

All tested compounds expressed the expected, slightly aggravated electron affinity of the fullerene subunit upon functionalization, reflected in the negatively shifted potentials in comparison to pristine C_{60} (Fig. 4). However, less disruption of the π-electronic system than in the referent NMFP was observed. Consequently, the corresponding LUMO energy levels were also negatively shifted by 140–180 eV in comparison to pristine C_{60}, but in the same range, more positive relative to NMFP (120–160 eV, Fig. 4).

TABLE I. Half-wave reduction potentials and the LUMO energy levels of selected compounds in ODCB/DMF (2:1) at a scan rate of 50 mV

Run	Compound	$E_{1/2}$ / V			E_{LUMO}[a] / eV
		I	II	III	
1	C_{60}[a]	–0.88	–1.34	–1.88	–5.68
2	**6a**	–1.04	–1.46	–2.08	–5.84
3	**7a**	–1.02	–1.46	–2.10	–5.82
4	**8b**	–1.04	–1.45	–2.09	–5.84
5	**9b**	–1.04	–1.46	–2.08	–5.84
6	**12c**	–1.04	–1.46	–2.08	–5.84
7	**13c**	–1.06	–1.46	–2.10	–5.86
8	**14c**	–1.04	–1.48	–2.08	–5.84
9	**15c**	–1.04	–1.46	–2.08	–5.84
10	**20a**	–1.04	–1.44	–2.10	–5.84
11	**21a**	–1.06	–1.46	–2.08	–5.86
12	**23c**	–1.06	–1.45	–2.06	–5.86
13	**24c**	–1.05	–1.48	–2.10	–5.85
14	NMFP	–1.14	–1.54	–2.16	–5.94

[a]$E_{LUMO} = -4.80 + E_{1/2}$; [b]the only compound that showed four reduction waves, with $E_{1/2}$ (IV) = –2.42 V

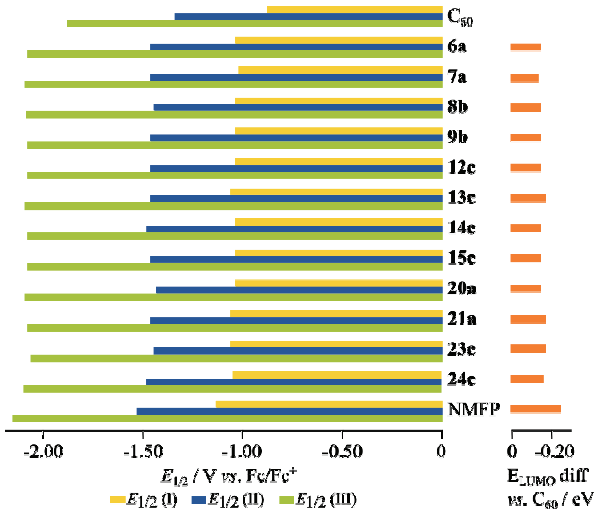

Fig. 4. Distribution of half-wave potentials of tested compounds and their LUMO energy levels relative to those of C_{60}.

Furthermore, analysis of obtained voltammograms pointed to a strong adsorption on the electrode surface, since almost negligible separation of anodic and cathodic peaks of the first reduction/reoxidation in majority of compounds (9 out of 12) was found.[46] Additionally, the multiplication of signals in some samples (4 out of 12) varying from small shoulders to a clearly doubled waves indicated the presence of both adsorbed and dissolved species.[46]

Finally, no linear correlation between the peak current and the scan rate, nor its square root value was found in any compound, implying a mutual contribution of diffusion and absorption controlled redox processes.

CONCLUSIONS

To understand more in detail the effect of the pyrrolidine substitution on the electrochemical properties of fulleropyrrolidines, as well as to expand the spectrum of fulleropyrrolidine OPCs candidates, a group of new compounds was designed, synthesized and studied by cyclic voltammetry. The impact of alteration of the structural segments at the pyrrolidine carbon and nitrogen was investigated by the introduction of linear and different aromatic substituents at pyrrolidine C-2, as well as various flexible side chains at nitrogen. In addition, to study the long-range effect of the second fullerene moiety on the electrochemical properties of the compounds, a corresponding dumbbell-like framework was designed by bridging two fulleropyrrolidine units *via* different rigid, diamide platforms. Following a simple synthetic pathway, a variety of new compounds was obtained and fully characterized by means of spectral data. In almost all cases, the expected compounds were formed in satisfactory yields. The only deviation was observed in the reaction with 2-nitrobenzaldehyde, which afforded exclusively C-unfunctionalized fulleropyrrolidine despite a published preparation of such a product. Nevertheless, an indirect formation of formaldehyde as reactive species agreed with the published degradation of 2-nitrobenzaldehyde to formaldehyde in the presence of non-fullerene dipolarophiles. Cyclic voltammetry experiments, performed on selected compounds differing in main structural subunits, revealed their highly uniform electrochemical behavior, regardless of the nature of the substituents. All samples expressed lower electron-accepting ability, and consequently lower LUMO energy level than the unfunctionalized C_{60}. On the other hand, they showed more favorable electrochemical properties in comparison to the structurally more similar referent compound *N*-methylfulleropyrolidine. In addition, a strong adsorption of majority of compounds on the electrode surface made them suitable for further research oriented towards the design of electrodes with upgraded sensitivity.

SUPPLEMENTARY MATERIAL

Additional data and information, containing experimental details, tabular representation of the NMR data of compounds **6**–**26**, copies of their HRMS, ^{1}H-NMR, ^{13}C-NMR, COSY and HMBC spectra, and the CV curves of all tested compounds, are available electronically at the pages of journal website: https://www.shd-pub.org.rs/index.php/JSCS/article/view/10935, or from the corresponding author on request.

Acknowledgement. This research was supported by the Ministry of Education, Science and Technological Development of the Republic of Serbia (Contracts 451-03-9/2021-14/ /200168 and 451-03-9/2021-14/200026).

ИЗВОД

ФУЛЕРОПИРОЛИДИНИ СА ОРТОГОНАЛНО ФЛЕКСИБИЛНИМ СУПСТИТУЕНТИМА – СИНТЕЗА И ЕЛЕКТРОХЕМИЈСКЕ ОСОБИНЕ

ДРАГАНА ЈОВАНОВИЋ[1], ЈОВАНА СТАНОЈКОВИЋ[1], ЦЕНЕТА ХАЛИЛОВИЋ[1], РЕЈХАНА КОЛАШИНАЦ[1], ТАТЈАНА Ј. КОП[2], МИРА С. БЈЕЛАКОВИЋ[2] и ДРАГАНА Р. МИЛИЋ[1]

[1]Универзитет у Београду – Хемијски факултет, Студентски трг 12-16, 11158 Београд и [2]Универзитет у Београду – Институт за хемију, технологију и металургију, Центар за хемију, Његошева 12, 11000 Београд

Велика серија дисупституисаних фулеропиролидина је синтетисана и анализирана цикличном волтаметријом. Три главне групе циљних једињења разликују се по флексибилном бочном низу на атому азота, а додатна диверсификација постигнута је увођењем различитих крутих, арил-супституената на пиролидинском атому угљеника. За поређење су синтетисани и одређени диалкил-аналози. Сет дисупституисаних фулеропиролидина добијен је стандардном [3+2]-циклоадицијом ин ситу генерисаних азометинских илида на C_{60}. Осим тога, у циљу испитивања даљинског утицаја фулеропиролидинске структуре на електрохемијске особине, синтетисани су и дифулеренски деривати код којих су терминално позициониране фулеренске подјединице премошћене фумарилном или изофталоилном крутом платформом. Сва једињења су у потпуности окарактерисана упоредном анализом спектралних података, док је сет одабраних једињења, са разликама у главним структурним подјединицама, искоришћен за испитивање електрохемијских особина. Сва испитивана једињења показала су врло сличну способност прихватања електрона, нижу у односу на C_{60}, а вишу од структурно сличног *N*-метилфулеропиролидина.

(Примљено 8. јула, ревидирано 23. августа, прихваћено 24. августа 2021)

REFERENCES

1. M. Prato, Michele Maggini, *Acc. Chem. Res.* **31** (1998) 519 (https://doi.org/10.1021/ar970210p)
2. N. Tagmatarchis, M. Prato, *Synlett* **6** (2003) 768 (http://dx.doi.org/10.1002/chin.200329261)
3. A. Mateo-Alonso, C. Sooambar, M. Prato, *Org. Biomol. Chem.* **4** (2006) 1629 (http://dx.doi.org/10.1039/b516948h)
4. B. I. Kharisov, O. V. Kharissova, M. Jimenez Gomez, U. Ortiz Mendez, *Ind. Eng. Chem. Res.* **48** (2009) 545 (http://dx.doi.org/10.1021/ie800602j)
5. R. Ganesamoorthy, G. Sathiyan, P. Sakthivel, *Sol. Energy Mat. Sol., C* **161** (2017) 102 (http://dx.doi.org/10.1016/j.solmat.2016.11.024)
6. M. Maggini, G. Scorrano, M. Prato, *J. Am. Chem. Soc.* **115** (1993) 9798 (https://doi.org/10.1021/ja00074a056)
7. M. Prato, M. Maggini, G. Scorrano, *Synth. Met.* **77** (1996) 89 (https://doi.org/10.1016/0379-6779(96)80065-8)
8. X. Zhang, M. Willems, C. S. Foote, *Tetrahedron Lett.* **34** (1993) 8187 (https://doi.org/10.1016/S0040-4039(00)61386-2)
9. S. H. Lim, D. W. Cho, P. S. Mariano, *Heterocycles* **93** (2016) 202 (https://doi.org/10.3987/COM-15-S(T)19)
10. M. Iyoda, F. Sultana, M. Komatsu, *Chem. Lett.* **24** (1995) 1133 (https://doi.org/10.1246/cl.1995.1133)

11. S-H. Wu, W-Q. Sun, D-W. Zhang, L-H. Shu, H-M. Wu, J-F. Xu, X-F. Lao, *J. Chem. Soc., Perkin Trans. 1* (1998) 1733 (https://doi.org/10.1039/A705962K)
12. P. A. Troshin, A. S. Peregudov, D. Mühlbacher, R. N. Lyubovskaya, *Eur. J. Org. Chem*. (2005) 3064 (https://doi.org/10.1002/ejoc.200500048)
13. K-F. Liou, C-H. Cheng, *Chem. Commun.* (1996) 1423 (https://doi.org/10.1039/CC9960001423)
14. G. E. Lawson, A. Kitaygorodskiy, B. Ma, C. E. Bunker, Y-P. Sun, *J. Chem. Soc., Chem. Commun.* (1995) 2225 (https://doi.org/10.1039/C39950002225)
15. J-L. Shi, X-F. Zhang, H-J. Wang, F-B. Li, X-X. Zhong, C-X. Liu, L. Liu, C-Y. Liu, H-M. Qin, Y-S. Huang, *J. Org. Chem*. **81** (2016) 7662 (https://doi.org/10.1021/acs.joc.6b01389)
16. M. Zhang, H-J. Wang, F-B. Li, X-X. Zhong, Y-S. Huang, L. Liu, C-Y. Liu, A. M. Asiri, K. A. Alamry, *J. Org. Chem.* **82** (2017) 8617 (https://doi.org/10.1021/acs.joc.7b01507)
17. L. Gan, D. Zhou, C. Luo, H. Tan, C. Huang, M. Lü, J. Pan, Y. Wu, *J. Org. Chem.* **61** (1996) 1954 (https://doi.org/10.1021/jo951933u)
18. S-E. Zhu, X. Cheng, Y-J. Li, C-K. Mai, Y-S. Huang, G-W. Wang, R-F. Peng, B. Jin, S-J. Chu, *Org. Biomol. Chem.* **10** (2012) 8720 (https://doi.org/10.1039/c2ob26066b)
19. B. Jin, R-F. Peng, J. Shen, S-J. Chu, *Tetrahedron Lett.* **50** (2009) 5640 (https://doi.org/10.1016/j.tetlet.2009.07.097)
20. B. Jin, J. Shen, R. Peng, C. Chen, S. Chu, *Eur. J. Org. Chem.* (2014) 6252 (http://dx.doi.org/10.1002/ejoc.201402655)
21. S. Filippone, E. E. Maroto, Á. Martín-Domenech, M. Suarez, N. Martín, *Nat. Chem*. **1** (2009) 578 (http://dx.doi.org/10.1038/NCHEM.361)
22. E. E. Maroto, M. Izquierdo, S. Reboredo, J. Marco-Martínez, S. Filippone, N. Martín, *Acc. Chem. Res.* **47** (2014) 2660 (https://doi.org/10.1021/ar500201b)
23. J-L. Shi, F-B. Li, X-F. Zhang, J. Wu, H-Y. Zhang, J. Peng, C-X. Liu, L. Liu, P. Wu, J-X. Li, *J. Org. Chem.* **81** (2016) 1769 (https://doi.org/10.1021/acs.joc.5b02412)
24. K. Yoshimura, K. Sugawara, S. Sakumichi, K. Matsumoto, Y. Uetani, S. Hayase, T. Nokami, T. Itoh, *Chem. Lett.* **42** (2013) 1209 (https://doi.org/10.1246/cl.130506)
25. K. Matsumoto, K. Hashimoto, M. Kamo, Y. Uetani, S. Hayase, M. Kawatsura, T. Itoh, *J. Mater. Chem.* **20** (2010) 9226 (https://doi.org/10.1039/C0JM01565B)
26. M. Karakawa, T. Nagai, K. Adachi, Y. Ie, Y. Aso, *J. Mater. Chem., A* **2** (2014) 20889 (https://doi.org/10.1039/c4ta04857a)
27. M. Karakawa, T. Nagai, T. Irita, K. Adachi, Y. Ie, Y. Aso, *J. Fluor. Chem.* **144** (2012) 51 (https://doi.org/10.1016/j.jfluchem.2012.09.009)
28. M. Karakawa, T. Nagai, K. Adachi, Y. Ie, Y. Aso, *RSC Adv*. **7** (2017) 7122 (https://doi.org/10.1039/c6ra27661j)
29. Y. Liang, Y. Hao, X. Liu, L. Feng, M. Chen, Q. Tang, N. Chen, M. Tang, B. Sun, Y. Zhou, B. Song, *Carbon* **92** (2015) 185 (https://doi.org/10.1016/j.carbon.2015.04.011)
30. C. Dardonville, C. Fernandez-Fernandez, S-L. Gibbons, G. J. Ryan, N. Jagerovic, A. M. Gabilondo, J. J. Meana, L. F. Callado, *Bioorg. Med. Chem.* **14** (2006) 6570 (https://doi.org/10.1016/j.bmc.2006.06.007)
31. A. Mitrović, N.Todorović, A. Žekić, D. Stanković, Dragana Milić, Veselin Maslak, *Eur. J. Org. Chem.* (2013) 2188 (https://doi.org/10.1002/ejoc.201201631)
32. Erkang Fan, Zhongsheng Zhang, Wendy E. Minke, Zheng Hou, Christophe L. M. J. Verlinde, Wim G. J. Hol, *J. Am. Chem. Soc.* **122** (2000) 2663 (https://doi.org/10.1021/ja993388a)

33. K. Kordatos, T. Da Ros, S. Bosi, E. Vazquez, M. Bergamin, C. Cusan, F. Pellarini, V. Tomberli, B. Baiti, D. Pantarotto, V. Georgakilas, G. Spalluto, M. Prato, *J. Org. Chem.* **66** (2001) 4915 (https://doi.org/10.1021/jo015608k)
34. X. Zhang, X-D. Li, *Chin. Chem. Lett.* **25** (2014) 501 (http://dx.doi.org/10.1016/j.cclet.2013.11.050)
35. R-F. Peng, B. Jin, K. Cao, Y-J. Shu, S-J. Chu, *Chin. J. Org. Chem.* **27** (2007) 276 (http://sioc-journal.cn/Jwk_yjhx/EN/Y2007/V27/I02/276)
36. M. Nyerges, A. Virányi, W. Zhang, P. W. Groundwater, G. Blaskó, L. Tóke, *Tetrahedron* **60** (2004) 9937 (http://dx.doi.org/10.1016/j.tet.2004.08.026)
37. F. Ajamaa, T. M. F. Duarte, C. Bourgogne, M. Holler, P. W. Fowler, J-F. Nierengarten, *Eur. J. Org. Chem.* (2005) 3766 (http://dx.doi.org/10.1002/ejoc.200500315)
38. K. H. Le Ho, S. Campidelli, *Adv. Nat. Sci.: Nanosci. Nanotechnol.* **5** (2014) 025008 (6pp) (http://dx.doi.org/10.1088/2043-6262/5/2/025008)
39. E. Busseron, J-J. Cid, A. Wolf, G. Du, E. Moulin, G. Fuks, M. Maaloum, P. Polavarapu, A. Ruff, A-K. Saur, S. Ludwigs, N. Giuseppone, *ACS Nano* **9** (2015) 2760 (http://dx.doi.org/10.1021/nn506646m)
40. C-H. Andersson, L. Nyholm, H. Grennberg, *Dalton Trans.* **41** (2012) 2374 (https://doi.org/10.1039/C2DT12097F)
41. M. A. Lebedeva, T. W. Chamberlain, E. S. Davies, B. E. Thomas, M. Schröder, A. N. Khlobystov, *Beilstein J. Org. Chem.* **10** (2014) 332 (https://doi.org/10.3762/bjoc.10.31)
42. A. L. Balch, D. A. Costa, W. R. Fawcett, K. Winkler, *J. Phys. Chem.* **100** (1996) 4823 (https://doi.org/10.1021/jp953144m)
43. K. Fujiwara, K. Komatsu, *Org. Lett.* **4** (2002) 1039 (https://doi.org/10.1021/ol025630f)
44. Y. Murata, A. Han, K. Komatsu, *Tetrahedron Lett.* **44** (2003) 8199 (https://doi.org/10.1016/j.tetlet.2003.09.077)
45. K. Lee, H. Song, B. Kim, J. T. Park, S. Park, M-G. Choi, *J. Am. Chem. Soc.* **124** (2002) 2872 (https://doi.org/10.1021/ja017496k)
46. A. J. Bard, L. R. Faulkner, *Electrochemical Methods – Fundamentals and Applications*, 2nd ed., John Wiley & Sons, Inc, New York, 2001, p. 589 (ISBN: 978-0-471-04372-0).

Journal of the Serbian Chemical Society
JSCS@tmf.bg.ac.rs • www.shd.org.rs/JSCS
J. Serb. Chem. Soc. 86 (11) S284–S358 (2021) *Supplementary material*

SUPPLEMENTARY MATERIAL TO

Fulleropyrrolidines with orthogonally flexible substituents – Synthesis and electrochemical properties

DRAGANA JOVANOVIĆ[1], JOVANA STANOJKOVIĆ[1], DŽENETA HALILOVIĆ[1], REJHANA KOLAŠINAC[1], TATJANA J. KOP[2], MIRA S. BJELAKOVIĆ[2] and DRAGANA R. MILIĆ[1]*

[1]*University of Belgrade – Faculty of Chemistry, Studentski trg 12–16, 11158, Belgrade, Serbia and* [2]*University of Belgrade – Institute of Chemistry, Technology and Metallurgy, Department of Chemistry, Njegoševa 12, 11000, Belgrade, Republic of Serbia*

J. Serb. Chem. Soc. 86 (11) (2021) 1023–1037

ANALYTICAL AND SPECTRAL DATA

Monoadduct ***6a***. A suspension of C_{60} (100 mg, 0.139 mmol), amino acid **4a** (38 mg, 0.139 mmol) and 4-methoxybenzaldehyde (94.5 mg, 84.4 μL, 0.694 mmol, 5 mol-equiv.) in PhMe (100 mL) was heated at reflux for 0.5 h. DCFC: PhMe gave unreacted C_{60} (39.9 mg, 40 %); PhMe/EtOAc 9:1 gave monoadduct **6a** (51.5 mg, 35 %). IR (ATR, cm^{-1}): 3446, 3366, 1713, 1513, 1250, 1175; ^{1}H-NMR (500 MHz, $CDCl_3$, δ / ppm): 7.70 (2H, *brs*, $HC(2,6)_{ar}$), 6.94 (2H, *d*, *J* = 8.5 Hz, $HC(3,5)_{ar}$), 5.07 (1H, *d*, *J* = 9.5 Hz, H_2C_{pyrr}), 5.00 (1H, *s*, HC_{pyrr}), 4.55 (1H, brs, NHBoc), 4.10 (1H, *d*, *J* = 9.5 Hz, H_2C_{pyrr}), 3.81 (3H, s, OCH_3), 3.24-3.12 (3H, *m*, HC(1) + $H_2C(6)$), 2.57-2.49 (1H, *m*, HC(1)), 2.01-1.92 (1H, *m*, HC(2)), 1.92-1.82 (1H, *m*, HC(2)), 1.73-1.63 (1H, *m*, HC(3)), 1.63-1.42 (5H, *m*, HC(3), $H_2C(4)$, $H_2C(5)$), 1.46 (9H, *s*, H_3C); ^{13}C-NMR (125 MHz, $CDCl_3$, δ / ppm): 159.70 ($C_{ar}(4)$), 156.88, 156.16 (**C**OO^{t}Bu), 154.51, 153.95, 147.46, 147.01, 146.70, 146.55, 146.45, 146.41, 146.36, 146.30, 146.25, 146.09, 145.93, 145.73, 145.71, 145.68, 145.61, 145.47, 145.42, 145.38, 145.36, 145.28, 144.87, 144.80, 144.56, 143.30, 143.14, 142.82, 142.72, 142.70, 142.50, 142.44, 142.27, 142.16, 142.13, 141.97, 141.82, 141.67, 140.31, 140.27, 140.04, 139.67, 136.94, 136.73, 135.91, 135.88, 130.73 ($C_{ar}(2,6)$), 129.45 ($C_{ar}(1)$), 114.11 ($C_{ar}(3,5)$), 82.25 (CH_{pyrr}), 79.23 (C(^{t}Bu)), 77.09 (sp^3-C_{60}), 69.01 (sp^3-C_{60}), 67.01 (H_2C_{pyrr}), 55.36 (OCH_3), 53.06 (C(1)), 40.82 (C(6)), 30.32 (C(5)), 28.62 (CH_3), 28.44 (C(2)), 27.42 (C(3)), 27.04 (C(4)); UV/Vis (CH_2Cl_2, λ_{max} / nm, (ε / $mol^{-1}dm^3cm^{-1}$)): 267 (120630), 308 (48720), 430 nm (4250); HRMS(HESI-Orbitrap) (*m/z*): Calcd. for $C_{80}H_{32}N_2O_3$ +H^+: 1069.2491. Found: 1069.2496.

Monoadduct ***7a***. A suspension of C_{60} (100 mg, 0.139 mmol), amino acid **4a** (38 mg, 0.139 mmol) and decanal (108 mg, 130 μL, 0.694 mmol, 5 mol-equiv) in PhMe (100 mL) was heated at reflux for 0.5 h. DCFC: PhMe gave unreacted C_{60} (39.0 mg, 39 %); PhMe/EtOAc 9:1 gave monoadduct **7a** (53.8 mg, 36 %). IR (ATR / cm^{-1}): 3363, 1713, 1459, 1169; ^{1}H-NMR (500 MHz, $CDCl_3$, δ/ ppm): 4.90 (1H, *d*, *J* = 10.0 Hz, H_2C_{pyrr}), 4.57 (1H, *brs*, NHBoc), 4.13 (1H, *t*, *J* = 4.5 Hz, HC_{pyrr}), 4.12 (1H, *d*, *J* = 10 Hz, H_2C_{pyrr}), 3.56-3.49 (1H, *m*, HC(1)),

* Corresponding author. E-mail: dmilic@chem.bg.ac.rs

3.20 (2H, *brq*, *J* = 6 Hz, $H_2C(6)$), 2.87-2.80 (1H, *m*, HC(1)), 2.52-2.43 (1H, *m*, HC(1')), 2.43-2.34 (1H, *m*, HC(1')), 2.01-1.79 (4H, *m*, $H_2C(2)$, $H_2C(2')$), 1.72-1.25 (33H, *m*), 1.56 (9H, *s*, CH_3), 0.87 (3H, *t*, *J* = 5 Hz, $H_3C(9')$; ^{13}C-NMR (125 MHz, $CDCl_3$, δ / ppm): 156.75, 156.01 (**C**OO^{t}Bu), 155.12, 155.04, 154.98, 153.74, 147.19, 147.17, 146.73, 146.61, 146.34, 146.25, 146.23, 146.14, 146.05, 146.01, 145.96, 145.93, 145.78, 145.69, 145.59, 145.34, 145.27, 145.23, 145.22, 145.17, 144.72, 144.58, 144.40, 143.19, 143.05, 142.66, 142.63, 142.59, 142.25, 142.22, 142.15, 142.11, 142.05, 141.82, 141.75, 141.69, 140.23, 140.17, 139.81, 139.59, 137.09, 136.23, 135.64, 135.47, 79.13 (C(^{t}Bu)), 77.41 (CH_{pyrr}), 76.34 (sp^3-C_{60}), 70.80 (sp^3-C_{60}), 66.88 (H_2C_{pyrr}), 52.46 (C(1)), 40.61 (C(6)), 31.91 (C7'), 31.14 (C(1')), 30.21 (C(5)), 29.53 (C(3')), 29.48 (C(8')), 29.29, 28.66 (C(2)), 28.46 (CH_3(^{t}Bu)), 27.48 (C(2')), 27.41 (C(3)), 26.91 (C(4)), 22.69 (C(8'), 14.14 (C(9'); UV/Vis (CH_2Cl_2, λ_{max} / nm (ε / mol^{-1}dm^{3}cm^{-1})): 256 (31200), 309 (10200), 430 (1300); HRMS(ESI/TOF): (*m/z*) calcd. for $C_{82}H_{44}N_2O_2$+H)$^+$: 1089.3476. Found: 1089.3454.

*Monoadduct **8b***. A suspension of C_{60} (50.5 mg, 0.070 mmol), amino acid **4b** (23.0 mg, 0.070 mmol) and PhCHO (37.1 mg, 35.58 µl, 0.350 mmol) in PhMe (50 mL) was heated at reflux for 4 h. DCFC: PhMe gave unreacted C_{60} (16.7 mg, 33 %) and monoadduct **8b** (19.6 mg, 26 %). IR (ATR, cm^{-1}): 3338, 1710, 1243, 1165; ^{1}H-NMR (500 MHz, $CDCl_3$, δ / ppm): 7.81 (2H, *brs*, $HC(2,6)_{ar}$), 7.41 (2H, *t*, *J* = 7.5 Hz, $HC(3,5)_{ar}$), 7.32 (1H, *tt*, *J* = 7.5 Hz & 1.0 Hz, $HC(4)_{ar}$), 5.10 (1H, *d*, *J* = 9 Hz, H_2C_{pyrr}), 5.06 (1H, *s*, HC_{pyrr}), 4.50 (1H, *brs*, NHBoc), 4.12 (1H, *d*, *J* = 9 Hz, H_2C_{pyrr}), 3.27-3.19 (1H, *m*, HC(1)), 3.12 (2H, brq, *J* = 6.5 Hz, $H_2C(10)$, 2.58-2.52 (1H, *m*, HC(1)), 2.00-1.93 (1H, *m*, HC(2)), 1.91-1.83 (1H, *m*, HC(2)), 1.67-1.60 (1H, *m*, HC(3)), 1.45 (9H, *s*, CH_3), 1.60-1.28 (*m*); ^{13}C-NMR (125 MHz, $CDCl_3$, δ / ppm): 156.63, 155.97 (**C**OO^{t}Bu), 154.35, 153.62, 147.29, 146.84, 146.51, 146.29, 146.24, 146.20, 146.18, 146.14, 146.11, 146.08, 145.91, 145.75, 145.57, 145.55, 145.51, 145.47, 145.30, 145.25, 145.21, 145.19, 145.12, 144.71, 144.61, 144.39, 143.14, 142.98, 142.66, 142.54, 142.33, 142.27, 142.12, 142.10, 142.01, 141.92, 141.81, 141.66, 141.49, 140.16, 140.11, 139.82, 139.37, 137.40 (C_{ar}(1)), 136.80, 136.57, 135.81, 135.70, 129.48 (C_{ar}(2,6)), 128.57 (C_{ar}(3,5)), 128.39 (C_{ar}(4)), 82.59 (CH_{pyrr}), 79.00 (C(^{t}Bu)), 77.00 (sp^3-C_{60}), 68.95 (sp^3-C_{60}), 66.89 (H_2C_{pyrr}), 53.12 (C(1)), 40.65 (C(10)), 30.09 (C(9)), (29.66, 29.61, 29.58, 29.33 C(4-7)), 28.44 (CH_3), 28.35 (C(2)), 27.53 (C(3)), 26.85 (C(8)); UV/Vis ($CHCl_3$, λ_{max} / nm (ε / mol^{-1}dm^{3}cm^{-1}): 325 (13129), 431 (3107), 692 (2089). HRMS(ESI/TOF): (*m/z*): calcd for $C_{83}H_{38}N_2O_2$+H)$^+$: 1095.3006. Found: 1095.3002.

*Monoadduct **9b***. A suspension of C_{60} (50.5 mg, 0.070 mmol), amino acid **4b** (23 mg, 0.070 mmol) and 4-methoxybenzaldehyde (47.6 mg, 42.58 µL, 0.350 mmol) in PhMe (50 mL) was heated at reflux for 4 h. DCFC: PhMe gave unreacted C_{60} (17.2 mg, 34 %) and monoadduct **9b** (17.9 mg, 23 %). IR (ATR, cm^{-1}): 3354, 1705, 1246, 1170; ^{1}H-NMR (500 MHz, $CDCl_3$, δ / ppm): 7.72 (2H, brs, $HC(2,6)_{ar}$), 6.94 (2H, *d*, *J* = 8.5 Hz, $HC(3,5)_{ar}$), 5.08 (1H, *d*, *J* = 9.0 Hz, H_2C_{pyrr}), 5.01 (1H, *s*, HC_{pyrr}), 4.50 (1H, *brs*, NHBoc), 4.10 (1H, *d*, *J* = 9.5 Hz, H_2C_{pyrr}), 3.81 (3H, *s*, OCH_3), 3.24-3.17 (1H, *m*, HC(1)), 3.12 (2H, *brq*, *J* = 6 Hz, $H_2C(10)$), 2.56-2.49 (1H, *m*, HC(1)), 2.00-1.92 (1H, *m*, HC(2)), 1.90-1.81 (1H, *m*, HC(2)), 1.45 (9H, *s*, CH_3), 1.69-1.28 (25H, *m*); ^{13}C-NMR (125 MHz, $CDCl_3$, δ / ppm): 159.50 (C_{ar}(4)), 156.76, 155.98 (**C**OO^{t}Bu), 154.40, 153.83, 147.29, 146.87, 146.55, 146.40, 146.29, 146.24, 146.20, 146.12, 146.08, 145.92, 145.91, 145.76, 145.58, 145.55, 145.51, 145.44, 145.30, 145.26, 145.21, 145.20, 145.12, 144.71, 144.64, 144.40, 143.15, 142.97, 142.66, 142.56, 142.54, 142.34, 142.29, 142.11, 142.00, 141.96, 141.81, 141.66, 141.51, 140.15, 140.09, 139.88, 139.50, 136.79, 136.58, 135.75, 130.58 (C_{ar}(2,6)), 129.36 (C_{ar}(1)), 113.92 (C_{ar}(3,5)), 82.10 (CH_{pyrr}), 79.01 (C(^{t}Bu)), 77.13 (sp^3-C_{60},from HMBC), 68.87 (sp^3-C_{60}),

66.86 (H_2C_{pyrr}), 55.20 (CH_3O), 53.02 (C(1)), 40.47 (C(10)), 30.10 (C(9)), 29.66, 29.62, 29.59, 29.34 (C(4-7)), 28.45 (CH_3), 28.33 (C(2)), 27.55 (C(3), 26.85 (C(8); UV/Vis (CH_2Cl_2, λ_{max} / nm (ε / $mol^{-1}dm^3cm^{-1}$): 324 (17977), 431 (2112), 702 (168); HTMS (ESI/TOF): *m/z* calcd for $(C_{84}H_{40}N_2O_3+H)^+$ 1125.3112. Found: 1125.3112.

*Monoadduct **10b***. A suspension of C_{60} (50.5 mg, 0.070 mmol), amino acid **4b** (22.9 mg, 0.069 mmol) and 4-nitrobenzaldehyde (52.4 mg, 0.347 mmol, 5 mol-equiv) in PhMe (50 mL) was heated at reflux for 4 h. DCFC: PhMe gave unreacted C_{60} (15.6 mg, 31 %) and monoadduct **10b** (24.2 mg, 30 %). IR (ATR, cm^{-1}): 3452, 1712, 1522, 1245, 1168; ^{1}H-NMR (500 MHz, $CDCl_3$, δ / ppm): 8.29 (2H, *d*, *J* = 9 Hz, $HC(3,5)_{ar}$), 8.03 (2H, brs, $HC(2,6)_{ar}$), 5.18 (1H, *s*, HC_{pyrr}), 5.14 (1H, *d*, *J* = 9.5 Hz, H_2C_{pyrr}), 4.51 (1H, *brs*, NHBoc), 4.17 (1H, *d*, *J* = 9.0 Hz, H_2C_{pyrr}), 3.15-3.03 (3H, *m*, HC(1) & $H_2C(10)$), 2.64-2.56 (m, 1H, HC(1)), 2.03-1.95 (m, 1H, HC(2)), 1.93-1.86 (m, 1H, HC(2)), 1.69-1.62 (1H, *m*, HC(3)), 1.59-1.28 (*m*), 1.45 (9H, *s*, CH_3); ^{13}C-NMR (125 MHz, $CDCl_3$, δ / ppm): 156.00 (C_{full} and **C**OO^{t}Bu), 153.79, 152.50 ($C_{ar}(4)$), 152.07, 147.97, 147.38, 147.34, 146.34, 146.25, 146.20, 146.16, 145.99, 145.65, 145.63, 145.57, 145.48, 145.43 ($C(1)_{ar}$), 145.38, 145.30, 145.23, 144.75, 144.54, 144.45, 144.34, 143.21, 143.06, 142.76, 142.64, 142.58, 142.28, 142.24, 142.18, 142.15, 142.08, 142.05, 142.00, 141.96, 141.83, 141.81, 141.72, 141.59, 140.28, 140.00, 139.54, 137.14, 136.29, 136.08, 135.53, 130.21 ($C_{ar}(2,6)$), 123.85 ($C_{ar}(3,5)$), 81.66 (CH_{pyrr}), 79.02 (C(^{t}Bu)), 76.18 (sp^3-C_{60}), 68.95 (sp^3-C_{60}), 66.87 (H_2C_{pyrr}), 53.38 (C(1)), 40.64 (C(10)), 30.10 (C(9)), (29.64, 29.61, 29.57, 29.32, C(4-7), 28.44 (CH_3), 28.33 (C(2)), 27.54 (C(3)), 26.83 (C(8)); UV/Vis (CH_2Cl_2): λ_{max} (ε) = 323 (41002), 431 (4123), 700 nm (296 $mol^{-1}dm^3cm^{-1}$); HRMS (ESI/TOF): *m/z* calcd for $(C_{83}H_{37}N_3O_4+H)^+$: 1140.2857. Found: 1140.2846.

*Monoadduct **11c***.[1] A suspension of C_{60} (285 mg, 0.395 mmol), amino acid **4c** (150 mg, 0.395 mmol) and formaldehyde (59.3 mg, 1.977 mmol, 5 mol-equiv) in PhMe (250 mL) was heated at reflux for 10 min. DCFC: PhMe gave unreacted C_{60} (145 mg, 51 %); PhMe/EtOAc 8:2 gave monoadduct **11c** (112.7 mg, 27 %). IR (ATR, cm^{-1}): 3359, 2927, 2866, 1710, 1515, 1363, 1346, 1248, 1171, 1119; ^{1}H-NMR ($CDCl_3$, 500 MHz, δ / ppm): 5.00 (1H, *brs*, NHBoc), 4.42 (4H, *s*, H_2C_{pyrr}), 3.85 (2H, *t*, *J* = 6.0 Hz, $H_2C(3)$), 3.77-3.73 (4H, *m*, $H_2C(5,6)$), 3.73-3.61 (4H, *m*, $H_2C(8,9)$), 3.57 (2H, *t*, *J* = 6.0 Hz, $H_2C(11)$), 3.28-3.22 (2H, *m*, $H_2C(13)$), 3.20 (2H, *t*, *J* = 7.5 Hz, $H_2C(1)$), 2.24 (2H, *quint*, *J* = 7.0 Hz, $H_2C(2)$), 1.78 (2H, *quint*, *J* = 6.0 Hz, $H_2C(12)$), 1.45 (9H, *s*, H_3C); ^{13}C-NMR (125 MHz, $CDCl_3$, 125 MHz, δ / ppm): 156.20 (**C**OO^{t}Bu), 155.25, 147.47, 146.41, 146.25, 146.23, 145.56 145.45, 144.73, 143.26, 142.79, 142.41, 142.23, 142.05, 140.31, 136.38, 79.11 (**C**(^{t}Bu)), 70.89 (sp^3-C_{60}), 70.88 & 70.82 (C(6,8)), 70.58 & 70.46 (C(5,9)), 69.82 (C(11)), 69.64 (C(3)), 68.13 (H_2C_{pyrr}),51.89 (C(1)), 38.77 (C(13)), 29.83 (C(12)), 29.14 (C(2)), 28.65 (CH_3); UV-Vis (CH_2Cl_2, λ_{max} / nm (ε / $mol^{-1}dm^3cm^{-1}$)): 254 (169400), 429 (5800), 700 (800); HRMS (ESI/TOF): *m/z* calcd for $(C_{77}H_{34}N_2O_5+H)^+$: 1067.2552. Found: 1067.2530.

*Monoadduct **12c***. A suspension of C_{60} (250 mg, 0.346 mmol), amino acid **4c** (131.2 mg, 0.346 mmol) and C_6H_5CHO (183.7 mg, 176 μL, 1.72 mmol) in PhMe (250 mL) was heated at reflux for 4 h. DCFC: PhMe gave unreacted C_{60} (134.9 mg, 54 %); PhMe/EtOAc 85:15 gave monoadduct **12c** (135.6 mg, 34 %). IR (ATR, cm^{-1}): 3455, 3427, 3348, 2920, 2854, 2802, 1709, 1247, 1170, 1120; ^{1}H-NMR (500 MHz, $CDCl_3$, δ / ppm): 7.79 (2H, *brs*, $HC(2,6)_{ar}$), 7.41 (2H, *t*, *J* = 7.5 Hz, $HC(3,5)_{ar}$), 7.32 (1H, *tt*, *J* = 7.5 Hz & 1.5 Hz, $HC(4)_{ar}$), 5.11 (1H, *d*, *J* = 9.5 Hz, H_2C_{pyrr}), 5.08 (1H, *s*, HC_{pyrr}), 4.97 (1H, *brs*, NHBoc), 4.14 (1H, *d*, *J* = 9 Hz, H_2C_{pyrr}), 3.89-3.77 (2H, *m*, $H_2C(3)$), 3.74-3.68 (4H, *m*, $H_2C(5,6)$), 3.68-3.58 (4H, *m*, $H_2C(8,9)$), 3.55 (2H, *t*, *J* = 6 Hz, $H_2C(11)$), 3.36 (1H, *dt*, *J* = 12.0 Hz & 8.0 Hz, HC(1)), 3.27-3.20 (2H, *m*, $H_2C(13)$), 2.68-2.61 (1H, *m*, HC(1)), 2.30-2.15 (2H, *m*, $H_2C(2)$), 1.77 (2H, *quint*,

J = 6 Hz, $H_2C(12)$), 1.45 (9H, *s*, CH_3); ^{13}C-NMR (125 MHz, $CDCl_3$, δ / ppm): = 156.53, 156.03 (**C**OO^{t}Bu), 154.19, 153.52, 153.46, 147.30, 146.81, 146.47, 146.30, 146.25, 146.22, 146.15, 146.13, 146.09, 145.93, 145.73, 145.53, 145.48, 145.31, 145.27, 145.22, 145.20, 145.13, 144.71, 144.61, 144.40, 144.38, 143.15, 142.98, 142.68, 142.55, 142.29, 142.27, 142.15, 142.13, 142.10, 142.01, 141.97, 141.91, 141.80, 141.68, 141.51, 140.18, 140.14, 139.83, 139.38, 137.20, 136.74, 136.51, 135.84, 135.72, 129.48 6)), 128.57 128.45)), 82.52 (CH_{pyrr}), 78.92 (C(^{t}Bu)), 76.72 (sp^3-C_{60}, from HMBC), 70.72 & 70.65 (C(6,8)), 70.36 & 70.27 (C(5,9)), 69.65 (C(11)), 69.41 (C(3)), 68.90 (sp^3-C_{60}), 66.82 (H_2C_{pyrr}), 49.79 (C(1)), 38.61 (C(13)), 29.64 (C(12)), 28.48 (CH_3), 28.40 (C(2)); UV/Vis (CH_2Cl_2, λ_{max} / nm, (ε / mol^{-1}dm^{3}cm^{-1})): 324 (38839), 431 (4318), 702 (320); HRMS(ESI/TOF): *m/z* calcd for ($C_{83}H_{38}N_2O_5$ +H)$^+$ 1143.2854. Found: 1143.2857.

Monoadduct ***13c***. A suspension of C_{60} (100 mg, 0.139 mmol), amino acid **4c** (52.5 mg, 0.139 mmol) and 2-methoxybenzaldehyde (47.25 mg, 0.347 mmol, 2.5 equiv) in PhMe (100 mL) was heated at reflux for 10 min. DCFC: PhMe gave unreacted C_{60} (37.6 mg, 38 %); PhMe/EtOAc 80:20 gave monoadduct **13c** (53.7 mg, 33 %). IR (ATR, cm^{-1}): 3361, 3048, 2929, 2868, 1711, 1493, 1247, 1172, 1118; ^{1}H-NMR (500 MHz, $CDCl_3$, δ / ppm): 7.97 (1H, *dd*, *J* = 7.5 Hz & 1.5 Hz, $HC(6)_{ar}$), 7.27 (1H, *td*, *J* = 7.5 Hz & 2.0 Hz, $HC(4)_{ar}$), 7.06 (1H, *t*, *J* = 7.5 Hz, $HC(5)_{ar}$), 6.91 (1H, *d*, *J* = 8.5 Hz, $HC(3)_{ar}$), 5.70 (H, *s*, $1HC_{pyrr}$), 5.09 (1H, *d*, *J* = 9.0 Hz, H_2C_{pyrr}), 4.98 (1H, brs, NHBoc), 4.17 (1H, *d*, *J* = 9 Hz, H_2C_{pyrr}), 3.90-3.84 (1H, *m*, HC(3)), 3.84-3.77 (1H, *m*, HC(3)), 3.75-3.69 (4H, *m*, $H_2C(5,6)$), 3.71 (3H, *s*, OCH_3), 3.69-3.58 (4H, *m*, $H_2C(8,9)$), 3.55 (2H, *t*, *J* = 6 Hz, $H_2C(11)$), 3.37 (1H, *dt*, *J* = 12.0 Hz & 8.0 Hz, HC(1)), 3.24 (2H, *brq*, *J* = 5.5 Hz, $H_2C(13)$), 2.65-2.58 (1H, *m*, HC(1)), 2.31-2.15 (2H, *m*, $H_2C(2)$), 1.77 (2H, *quint*, *J* = 6.5 Hz, $H_2C(12)$), 1.45 (9H, s, CH_3); ^{13}C-NMR (125 MHz, $CDCl_3$, δ / ppm): 158.34 ($C_{ar}(2)$), 157.24, 156.19 (**C**OO^{t}Bu), 155.28, 154.47, 154.26, 147.44, 146.93, 146.72, 146.38, 146.35, 146.32, 146.25, 146.20, 146.09, 146.06, 145.85, 145.73, 145.72, 145.69, 145.44, 145.40, 145.37, 145.24, 145.21, 145.16, 144.73, 144.58, 144.52, 143.20, 143.14, 142.78, 142.71, 142.68, 142.48, 142.43, 142.33, 142.24, 142.11, 141.96, 141.86, 141.69, 140.35, 140.28, 139.54, 139.52, 136.69, 136.53, 136.31, 134.67, 130.14 ($C_{ar}(6)$), 129.11 ($C_{ar}(4)$), 125.92 ($C_{ar}(1)$), 121.20 ($C_{ar}(5)$), 111.17 ($C_{ar}(3)$), 79.07 (C(^{t}Bu)), 76.16 (sp^3-C_{60}), 74.45 (CH_{pyrr}), 70.88 and 70.82 (C(6,8)), 70.50 and 70.43 (C(5,9)), 69.81 (C(11)), 69.63 (C(3)), 69.32 (sp^3-C_{60}), 66.85 (H_2C_{pyrr}), 55.33 (OCH_3), 50.00 (C(1)), 38.78 (C(13)), 29.79 (C(12)), 28.64 (CH_3), 28.61 (C(2)); UV/Vis (CH_2Cl_2, λ_{max} / ppm, (ε / mol^{-1} dm^3 cm^{-1})): 256 (104400), 307 (38700), 431 (4700), 704 (900); HRMS (ESI/TOF): *m/z* calcd. for ($C_{84}H_{40}N_2O_6$+Na)$^+$: 1195.2790. Found: 1195.2776.

Monoadduct ***14c***. A suspension of C_{60} (200 mg, 0.277 mmol), amino acid **4c** (105 mg, 0.277 mmol) and 3-methoxybenzaldehyde (187.8 mg, 169 μL, 1.38 mmol) in PhMe (100 mL) was heated at reflux for 20 min. DCFC: PhMe gave unreacted C_{60} (73.8 mg, 37 %); PhMe/EtOAc 80:20 gave monoadduct **14c** (120.1 mg, 37 %). IR (ATR / cm^{-1}): 3366, 3050, 2952, 1711, 1266, 1173, 1122; ^{1}H-NMR (500 MHz, $CDCl_3$, δ / ppm): 7.36 (2H, brs, $HC(2)_{ar}$ &, $HC(6)_{ar}$), 7.31 (1H, *t*, *J* = 8 Hz, $HC(5)_{ar}$), 6.86 (1H, *brd*, *J* = 8 Hz, $HC(4)_{ar}$), 5.10 (1H, *d*, *J* = 9.5 Hz, H_2C_{pyrr}), 5.04 (1H, *s*, HC_{pyrr}), 4.98 (1H, *brs*, NHBoc), 4.13 (1H, *d*, *J* = 9.5 Hz, H_2C_{pyrr}), 3.90-3.83 (1H, *m*, HC(3)), 3.83-3.75 (1H, *m*, HC(3)), 3.81 (3H, *s*, OCH_3), 3.75-3.69 (4H, *m*, $H_2C(5,6)$), 3.69-3.58 (4H, *m*, $H_2C(8,9)$), 3.55 (2H, *t*, *J* = 6 Hz, $H_2C(11)$), 3.38 (1H, *dt*, *J* = 12.0 Hz & 8.5 Hz, HC(1)), 3.24 (2H, *brq*, *J* = 5.5 Hz, $H_2C(13)$), 2.69-2.61 (1H, *m*, HC(1)), 2.32-2.13 (2H, *m*, $H_2C(2)$), 1.77 (2H, *quint*, *J* = 6.5 Hz, $H_2C(12)$), 1.45 (9H, *s*, CH_3); ^{13}C-NMR (125 MHz, $CDCl_3$, δ / ppm): 159.94 ($C(3)_{ar}$), 156.60, 156.18 (**C**OO^{t}Bu), 154.36, 153.78, 153.60, 147.46, 147.07, 146.60, 146.46, 146.41, 146.37, 146.31, 146.26, 146.24,

146.09, 145.89, 145.68, 145.48, 145.45, 145.42, 145.39, 145.36, 145.28, 144.86, 144.78, 144.55, 143.31, 143.13, 142.83, 142.72, 142.41, 142.30, 142.27, 142.22, 142.16, 142.07, 141.95, 141.83, 141.70, 140.34, 140.28, 139.96, 139.61, 138.99 (C_{ar}(1)), 136.72, 136.69, 135.96, 135.86, 129.71 (C_{ar}(5)), 122.15 (C_{ar}(6)), 114.94 (C_{ar}(2)), 114.00 (C_{ar}(4), 82.56 (CH_{pyrr}), 79.07 (C(^{t}Bu)), 76.72 (sp^3-C_{60}), 70.86 and 70.80 (C(6,8)), 70.50 and 70.42 (C(5,9)), 69.79 (C(11)), 69.60 (C(3)), 69.04 (sp^3-C_{60}), 66.95 (H_2C_{pyrr}), 55.51 (OCH_3), 50.01 (C(1)), 38.77 (C(13)), 29.80 (C(12)), 28.63 (CH_3), 28.54 (C(2)); UV/Vis (CH_2Cl_2, λ_{max} / nm, (ε / mol^{-1}dm^{3}cm^{-1})): = 256 (173200), 305 (60000), 431 (6900), 702 (1100); HRMS (ESI/TOF): *m/z* calcd for ($C_{84}H_{40}N_2O_6$+Na)$^+$: 1195.2790. Found 1195.2781.

*Monoadduct **15c***. A suspension of C_{60} (97.8 mg, 0.136 mmol), amino acid **4c** (51.4 mg, 0.136 mmol) and 4-methoxybenzaldehyde (92.6 mg, 82.7 μL, 0.680 mmol) in PhMe (100 mL) was heated at reflux for 10 min. DCFC: PhMe gave unreacted C_{60} (25.7 mg, 26 %); PhMe/EtOAc 80:20 gave monoadduct **15c** (54.0 mg, 34 %). IR (ATR, cm^{-1}): 3343, 2923, 2862, 1709, 1299, 1168, 1104; ^{1}H-NMR (500 MHz, $CDCl_3$, δ / ppm): 7.70 (2H, *brs*, $HC(2,6)_{ar}$), 6.93 (2H, *d*, *J* = 9 Hz, $HC(3,5)_{ar}$), 5.08 (1H, *d*, *J* = 9 Hz, H_2C_{pyrr}), 5.02 (1H, *s*, HC_{pyrr}), 4.99 (1H, *brs*, NHBoc), 4.12 (1H, *d*, *J* = 9 Hz, H_2C_{pyrr}), 3.88-3.83 (1H, *m*, HC(3)), 3.80 (3H, *s*, OCH_3), 3.82-3.76 (1H, *m*, HC(3)), 3.73-3.69 (4H, *m*, H_2C(5,6)), 3.69-3.58 (4H, *m*, H_2C(8,9)), 3.55 (2H, *t*, *J* = 6 Hz, H_2C(11)), 3.33 (1H, *dt*, *J* = 12.0 Hz & 8.5 Hz, HC(1)), 3.24 (2H, *brq*, *J* = 5 Hz, H_2C(13)), 2.65-2.58 (1H, *m*, HC(1)), 2.29-2.15 (2H, *m*, H_2C(2)), 1.77 (2H, *quint*, *J* = 6 Hz, H_2C(12)), 1.44 (9H, *s*, CH_3); ^{13}C-NMR (125 MHz, $CDCl_3$, δ / ppm): = 159.53 (C_{ar}(4)), 156.64, 156.02 (**C**OO^{t}Bu), 154.22, 153.72, 147.29, 146.82, 146.50, 146.34, 146.24, 146.20, 146.13, 146.11, 146.08, 145.92, 145.73, 145.52, 145.44, 145.32, 145.30, 145.26, 145.19, 145.11, 144.70, 144.62, 144.39, 143.13, 142.97, 142.66, 142.53, 142.29, 142.26, 142.14, 142.10, 141.98, 141.93, 141.79, 141.66, 141.50, 140.15, 140.10, 139.87, 139.50, 136.72, 136.51, 135.77, 135.73, 130.57 (C_{ar}(2,6)), 129.15 (C_{ar}(1)), 113.88 (C_{ar}(3,5)), 82.01 (CH_{pyrr}), 78.90 (C(^{t}Bu)), 76.90 (sp^3-C_{60}), 70.70 and 70.64 (C(6,8)), 70.34 and 70.25 (C(5,9)), 69.62 (C(11)), 69.46 (C(3)), 68.80 (sp^3-C_{60}), 66.77 (H_2C_{pyrr}), 55.19 (OCH_3), 49.68 (C(1)), 38.59 (C(13)), 29.63 (C(12)), 28.47 (CH_3), 28.37 (C(2)); UV/Vis (CH_2Cl_2, λ_{max} / nm (ε / mol^{-1}dm^{3}cm^{-1})): 324 (41735), 431 (4760), 702 (375); HRMS(ESI/TOF): *m/z*: calcd for ($C_{84}H_{40}N_2O_6$ +H]$^+$: 1173.2959. Found: 1173.2971.

*Unsuccessful attempts (a, b) to synthesize 2-(2-nitrophenyl)fulleropyrrolidine monoadduct **16c***. (a - according to the general procedure, SI-Fig. S-1) - A suspension of C_{60} (100 mg, 0.138 mmol, 1 mol-equiv), amino acid **4c** (52.5 mg, 0.138 mmol, 1 mol-equiv) and 2-nitrobenzaldehyde (104.8 mg, 0.694 mmol, 5 mol-equiv) in PhMe (100 mL) was heated at reflux for 1.5 h. DCFC: PhMe gave unreacted C_{60} (35.0 mg, 35 %); PhMe/EtOAc 75:25 gave monoadduct **11c** (17.8 mg, 11 %).

(b - according to the procedure for the synthesis of 2-(2-nitrophenyl)fulleropyrrolidine derivative reported by Chinese authors, molar ratio of C_{60}/2-nitrobenzaldehyde/amino acid are 1:1:2, at 100 °C, SI-Fig' S-1)[2] - A suspension of C_{60} (10.7 mg, 0.0148 mmol, 1 mol-equiv), amino acid **4c** (10.8 mg, 0.0286 mmol, 2 mol-equiv) and 2-nitrobenzaldehyde (2.2 mg, 0.0145 mmol, 1 mol-equiv) in PhMe (100 mL) was heated at 100 °C for 24 h. DCFC: PhMe gave unreacted C_{60} (5.4 mg, 50 %); PhMe/EtOAc 75:25 gave monoadduct **11c** (4.75 mg, 28 %). In both cases (a, b), the expected 2-(2-nitrophenyl)fulleropyrrolidine was not obtained.

*Monoadduct **17c***. A suspension of C_{60} (100 mg, 0.138 mmol), amino acid **4c** (52.5 mg, 0.138 mmol) and 3-nitrobenzaldehyde (104.8 mg, 0.694 mmol) in PhMe (100 mL) was heated at reflux for 10 min. DCFC: PhMe gave unreacted C_{60} (35.0 mg, 35 %); PhMe/EtOAc 85:15 gave monoadduct **17c** (48 mg, 29 %). IR (ATR / cm^{-1}): 3360, 3063, 2926, 2867, 1709, 1530,

1348, 1248, 1171, 1121; ^{1}H-NMR (500 MHz, $CDCl_3$, δ / ppm): 8.67 (1H, *brs*, $HC(2)_{ar}$), 8.21 (2H, *brdd*, J = 8.5 Hz & 2.0 Hz, $HC(4,6)_{ar}$), 7.62 (1H, *t*, J = 7.5 Hz, $HC(5)_{ar}$), 5.20 (1H, *s*, HC_{pyrr}), 5.14 (d, J = 9.5 Hz, 1H, H_2C_{pyrr}), 4.96 (br s, 1H, NHBoc), 4.19 (d, J = 9.5 Hz, 1H, H_2C_{pyrr}), 3.84 (t, J = 6.5 Hz, 2H, $H_2C(3)$), 3.75-3.67 (m, 4H, $H_2C(5,6)$), 3.67-3.57 (m, 4H, $H_2C(8,9)$), 3.54 (t, J = 6 Hz, 2H, $H_2C(11)$), 3.29 (dt, J = 12.0, 8.0 Hz,1H, HC(1)), 3.24 (br q, J = 6.0 Hz, 2H, $H_2C(13)$), 2.72-2.66 (1H, *m*, HC(1)), 2.31-2.16 (2H, *m*, $H_2C(2)$), 1.77 (2H, *quint*, J = 6.0 Hz, $H_2C(12)$), 1.44 (9H, *s*, H_3C); ^{13}C-NMR (125 MHz, $CDCl_3$, δ / ppm): 156.16, 156.11 (**C**OO^{t}Bu), 153.75, 152.58, 152.08, 148.57 $(C(3)_{ar}$, from HMBC), 147.52, 147.48, 146.47, 146.39, 146.36, 146.31, 146.23, 146.13, 145.79, 145.72, 145.62, 145.56, 145.53, 145.46, 145.37, 144.89, 144.63, 144.60, 144.48, 143.32, 143.19, 142.89, 142.78, 142.70, 142.40, 142.33, 142.29, 142.22, 142.20, 142.16, 141.96, 141.93, 140.44, 140.42, 140.26, 140.04 $(C(1)_{ar}$, 139.62, 137.35, 136.44, 136.26, 135.74, 135.56 $(C(6)_{ar})$, 129.79 $(C(5)_{ar})$, 124.34 $(C(2)_{ar})$, 123.77 $(C(4)_{ar})$, 81.63 (CH_{pyrr}), 79.06 (C(^{t}Bu)), 76.29 (sp^3-C_{60})), 70.82 & 70.75 (C(6,8)), 70.51 & 70.38 (C(5,9)), 69.73 (C(11)), 69.18 (C(3)), 68.93 (sp^3-C_{60}), 66.86 (H_2C_{pyrr}), 50.09 (C(1)), 38.72 (C(13)), 29.81 (C(12)), 28.62 (CH_3), 28.45 (C(2)); UV/Vis (CH_2Cl_2, λ_{max} / nm (ε / mol^{-1}dm^{3}cm^{-1})): 256 (156900), 311 (51800), 431 (5500), 702 (800); HRMS (ESI/TOF): *m/z* calcd for $(C_{83}H_{37}N_3O_7$+Na)$^+$: 1210.2535. Found: 1210.2506.

*Monoadduct **18c***. A suspension of C_{60} (101 mg, 0.140 mmol), amino acid **4c** (53.1 mg, 0.140 mmol) and 4-nitrobenzaldehyde (110 mg, 0.728 mmol) in PhMe (100 mL) was heated at reflux for 15 min. DCFC: PhMe gave unreacted C_{60} (35.0 mg, 35 %); PhMe/EtOAc 80:20 gave monoadduct **18c** (73.8 mg, 44 %). IR (ATR / cm^{-1}): 3341, 2925, 2865, 1703, 1520, 1343, 1249, 1168, 1103; ^{1}H-NMR (500 MHz, $CDCl_3$, δ / ppm): 8.29 (2H, *d*, J = 9.0 Hz, $HC(3,5)_{ar}$), 8.03 (2H, *brs*, $HC(2,6)_{ar}$), 5.20 (1H, *s*, HC_{pyrr}), 5.14 (1H, *d*, J = 9.5 Hz, H_2C_{pyrr}), 4.96 (1H, *brs*, NHBoc), 4.18 (1H, *d*, J = 9.5 Hz, H_2C_{pyrr}), 3.88-3.80 (2H, *m*, $H_2C(3)$), 3.75-3.69 (4H, *m*, $H_2C(5,6)$), 3.69-3.58 (4H, *m*, $H_2C(8,9)$), 3.55 (2H, *t*, J = 6 Hz, $H_2C(11)$), 3.30 (1H, *dt*, 8.5 Hz, J = 12.0, HC(1)), 3.24 (2H, *brq*, J = 5.5 Hz, $H_2C(13)$), 2.71-2.64 (1H, *m*, HC(1)), 2.29-2.17 (2H, *m*, $H_2C(2)$), 1.77 (2H, *quint*, J = 6 Hz, $H_2C(12)$), 1.44 (9H, *s*, H_3C); ^{13}C-NMR (125 MHz, $CDCl_3$, δ / ppm): 156.01, 155.90 (**C**OO^{t}Bu), 153.63, 152.36, 151.99, 147.96 $(C_{ar}(4))$, 147.37, 147.34, 146.33, 146.22, 146.18, 145.99, 145.63, 145.57, 145.40, 145.34, 145.32, 145.23, 145.00 $(C(1)_{ar})$, 144.73, 144.52, 144.44, 144.33, 143.20, 143.05, 142.76, 142.64, 142.58, 142.23, 142.17, 142.14, 142.08, 142.04, 141.98, 141.94, 141.82, 141.78, 141.72, 141.59, 140.29, 139.99, 139.53, 137.07, 136.23, 136.10, 135.56, 130.24 $(C_{ar}(2,6))$, 123.82 $(C_{ar}(3,5))$, 81.55 (CH_{pyrr}), 78.91 (C(^{t}Bu)), 76.13 (sp^3-C_{60})), 70.72 & 70.65 (C(6,8)), 70.37 & 70.25 (C(5,9)), 69.59 (C(11)), 68.96 (C(3)), 68.89 (sp^3-C_{60}), 66.74 (H_2C_{pyrr}), 49.88 (C(1)), 38.56 (C(13)), 29.66 (C(12)), 28.47 (CH_3), 28.30 (C(2)); UV/Vis (CH_2Cl_2, λ_{max} / nm (ε mol^{-1} dm^3 cm^{-1})): = 323 (37996), 421 (3443), 700 nm (356); HRMS(ESI/TOF): *m/z* calcd for $(C_{83}H_{37}N_3O_7$ +H)$^+$: 1188.2704. Found: 1188.2689.

*Difullerene diamide **19a***. a) Starting from the protected amine derivative **5a** (20.0 mg, 0.021 mmol), the TFA salt (20.0 mg) was obtained; b) TFA salt (20.0 mg), pyridine (160 μL), DMAP (7.9 mg, 0.065 mmol), isophthaloyl chloride (8.45 mg, 0.042 mmol) in dry CH_2Cl_2 (4 mL) and ODCB (5 mL) were used. Due to extreme insolubility of the reaction product, elution with mixtures of different solvents was carried out. FCC: Elution with PhMe/$CHCl_3$/ODCB/MeOH 5:5:0.5:0.5 gave diamide **19a** (2.0 mg, 10 %). FTIR (ATR, cm^{-1}): 3344, 2926, 1651, 1540, 1431, 1159; ^{1}H-NMR (500 MHz, $CDCl_3$, δ / ppm): 8.21 (1H, *s*, $H_{ar}C(2)$), 7.91 (2H, *dd*, J = 9.2, 1.5 Hz, $H_{ar}C(4,6)$), 7.53 (1H, *t*, J = 7.5 Hz, $H_{ar}C(5)$, 6.30 (2H, brs, NHCO), 4.41 (8H, *s*, H_2C_{pyrr}), 3.56 (4H, *q*, J = 7.0 Hz, $H_2C(6)$), 3.10 (4H, *t*, J = 7.5 Hz,

$H_2C(1)$), 1.97 (4H, *quint*, *J* = 7.0 Hz,), 1.77 (*4H*, quint, *J* = 7.0 Hz), 1.73-1.67 (4H, *m*), 1.65-1.58 (4H, *m*).

Difullerene diamide ***20a***, a) Starting from the protected amine derivative **7a** (20.0 mg, 0.018 mmol), TFA salt (20.0 mg) was obtained; b) TFA salt (20.0 mg, 0.028 mmol), pyridine (1 mL), DMAP (6.6 mg, 0.054 mmol), isophthaloyl chloride (1.83 mg, 0.009 mmol) in dry CH_2Cl_2 (20 mL) were used. Due to extreme insolubility of the reaction product, elution with mixtures of different solvents was carried out. FCC: Elution with PhMe/$CHCl_3$/MeOH 5:5:0.024 gave diamide **20a** (8.5 mg, 44 %). FTIR (ATR / cm^{-1}): 3300, 2921, 1652, 1525, 1459, 1182; ^{1}H-NMR (500 MHz, $CDCl_3$, δ / ppm): 8.22 (1H, *s*, $HC(2)_{ar}$), 7.92 (2H, *dd*, *J* = 9.2 & 2.0 Hz, $HC(4,6)_{ar}$), 7.53 (1H, *t*, *J* = 8.0 Hz, $HC(5)_{ar}$), 6.30 (2H, *brt*, *J* = 5.5 Hz, NHCO), 4.91 (2H, *d*, *J* = 10.0 Hz, H_2C_{pyrr}), 4.13 (2H, *t*, *J* = 5.0 Hz, HC_{pyrr}), 4.12 (2H, *d*, *J* = 10.0 Hz, H_2C_{pyrr}), 3.60-3.51 (4H, *q* at 3.56 ppm, *J* = 7.0 Hz, $H_2C(6)$ overlapped with *m* (2H), HC(1)), 2.90-2.82 (2H, *m*, HC(1)), 2.53-2.43 (2H, *m*, HC(1')), 2.43-2.33 (2H, *m*, HC(1')), 2.03-1.90 (4H, *m*, $H_2C(2)$), 1.90-1.82 (4H, *m*, $H_2C(2')$), 1.78 (4H, *quint*, *J* = 7.0 Hz, $H_2C(5)$), 1.74-1.64 (4H, *m*, $H_2C(3)$), 1.64-1.57 (4H, *m*, $H_2C(4)$), 1.46 (4H, *quint*, *J* = 7.0 Hz, $H_2C(3')$), 1.35 (4H, *brquint*, *J* = 7.5 Hz, $H_2C(4')$), 1.32-1.19 (16H, *m*, $H_2C(5'-8')$), 0.87 (6H, *t*, *J* = 7.0 Hz, $H_3C(9')$). ^{13}C-NMR (125 MHz, $CDCl_3$, δ / ppm): 166.56 (CO), 156.75, 155.09, 155.01, 153.75, 147.20, 147.18, 146.74, 146.61, 146.35, 146.26, 146.24, 146.15, 146.07, 146.02, 145.98, 145.94, 145.77, 145.71, 145.60, 145.36, 145.34, 145.28, 145.26, 145.24, 145.21, 145.18, 144.71, 144.59, 144.42, 143.19, 143.07, 142.68, 142.65, 142.61, 142.27, 142.24, 142.23, 142.17, 142.15, 142.12, 142.05, 142.04, 141.82, 141.75, 141.71, 137.08, 136.22, 135.65, 135.50, 135.09 ($C_{ar}(1,3)$), 129.70 ($C(4,6)_{ar}$), 129.00 ($C(5)_{ar}$), 125.33 ($C(2)_{ar}$), 77.34 (CH_{pyrr}, from HSQC), 76.39 (sp^3-C_{60}), 70.79 (sp^3-C_{60}), 66.85 (H_2C_{pyrr}), 52.38 (C(1)), 40.25 (C(6)), 31.92 (C(7')), 31.14 (C(1'), 30.22 (C(3'), 29.72 (C(5)), 29.55 (C(4')), 29.50, 29.30, 28.60 (C(2)), 27.53 (C(2'), 27.38 C(3)), 27.04 (C(4)), 22.70 (C(8')), 14.16 (C(9')). UV/Vis (CH_2Cl_2, λ_{max}/ nm, (ε / $mol^{-1}dm^3cm^{-1}$)): 256 (31200), 309 (10200), 431 (1300).

Difullerene diamide ***21a***. a) Starting from the protected amine derivative **7a** (124 mg, 0.114 mmol), TFA salt (126 mg) was obtained; b) TFA salt (126 mg), pyridine (3 mL), DMAP (40 mg, 0.327 mmol), fumaryl chloride (8.72 mg, 6.2 µL, 0.057 mmol) in dry CH_2Cl_2 (30 mL) were used. FCC: Elution with PhMe/$CHCl_3$/MeOH 4:4:0.2 and subsequent precipitation gave diamide **21a** (17.9 mg, 15 %). IR (ATR, cm^{-1}): 3430, 3305, 2924, 2854, 1730, 1643, 1461; ^{1}H-NMR (500 MHz, $CDCl_3$/CS_2/CD_3OH), δ / ppm: 7.98 (1H, *brt*, *J* = 5.5 Hz, NHCO), 6.82 (1H, *s*, HC=), 4.90 (1H, *d*, *J* = 10 Hz, H_2C_{pyrr}), 4.13 (1H, *t*, *J* = 5.0 Hz, HC_{pyrr}; overlapped at 4.12, with 1H, *d*, *J* = 10.0 Hz, H_2C_{pyrr}), 3.57-3.48 (1H, *m*, HC(1)), 3.38 (2H, *brq*, *J* = 6.5 Hz, $H_2C(6)$), 2.88-2.80 (1H, *m*, HC(1)), 2.53-2.43 (1H, *m*, HC(1')), 2.43-2.32 (1H, *m*, HC(1')), 2.00-1.89 (2H, *m*, $H_2C(2)$), 1.89-1.80 (2H, *m*, $H_2C(2')$), 1.75-1.65 (2H, *m*, $H_2C(5)$), 1.65-1.60 (2H, *m*, $H_2C(3)$), 1.60-1.51 (2H, *m*, $H_2C(4)$), 1.46 (2H, *quin*t, *J* = 7.5 Hz, $H_2C(3')$), 1.39-1.32 (2H, *m*, $H_2C(4')$), 1.32-1.18 (8H, *m*, $H_2C(5'+6'+7'+8')$), 0.87 (3H, *t*, *J* = 7.5 Hz, $H_3C(9')$); ^{13}C-NMR (125 MHz, $CDCl_3$/CS_2/CD_3OH, δ / ppm): = 165.07 (C=O), 156.44, 154.80, 154.73, 153.43, 146.99, 146.97, 146.50, 146.38, 146.11, 146.07, 146.05, 145.95, 145.87, 145.82, 145.77, 145.75, 145.57, 145.46, 145.38, 145.18, 145.08, 145.04, 144.97, 144.52, 144.39, 144.23, 144.21, 143.00, 142.87, 142.48, 142.45, 142.41, 142.06, 142.02, 141.97, 141.92, 141.89, 141.86, 141.63, 141.57, 141.52, 140.06, 140.01, 139.65, 139.42, 136.92, 136.06, 135.47, 135.29, 132.41 (CH=)), 77.20 (CH_{pyrr}), 76.13 (sp^3-C_{60}), 70.51 (sp^3-C_{60}), 66.69 (H_2C_{pyrr}), 52.39 (C(1)), 39.81 (C(6)), 31.81 (C(7')), 30.99 (C(1')), 30.12 (C(3'), 29.46 (C(4')), 29.40 (C(5')), 29.20 and 29.13 (C(5), C(6')), 28.54 (C(2)), 27.43 (C(2')), 27.37

(C(3)), 26.97 (C(4)), 22.62 (C(8')), 14.00 (C(9')); UV/Vis (CH_2Cl_2, λ_{max} nm / (ε / mol^{-1}dm^{3}cm^{-1})): 256 (51700), 319 (16800), 431 (1600).

*Difullerene diamide **22c**.* a) Starting from the protected amine derivative **11c** (112.7 mg, 0.106 mmol), TFA salt was obtained; b) TFA salt, pyridine (3.3 mL), DMAP (38.1 mg, 0.312 mmol), fumaryl chloride (7.97 mg, 5.63 μL, 0.052 mmol) in dry CH_2Cl_2 (60 mL) were used. FCC: Elution with $CHCl_3$/MeOH 100:1 and subsequent precipitation gave diamide **22c** (24.5 mg, 23 %). IR (ATR, cm^{-1}): 3370, 2921, 2855, 1732, 1640, 1541, 1370, 1336, 1093; ^{1}H-NMR ($CDCl_3$, 500 MHz, δ / ppm): 6.99 (2H, *brs*, NHCO), 6.91 (2H, *s*, HC=CH), 4.41 (8H, *s*, H_2C_{pyrr}), 3.84 (4H, *brt*, *J* = 6.5 Hz, $H_2C(3)$), 3.81-3.76 (8H, *m*, $H_2C(5,6)$), 3.75-3.60 (12H, *m*, $H_2C(8,9,11)$), 3.56-3.48 (4H, *m*, $H_2C(13)$), 3.17 (4H, *t*, *J* = 7.0 Hz, $H_2C(1)$), 2.21 (4H, *quint*, *J* = 7.0 Hz, $H_2C(2)$), 1.90-1.80 (4H, *m*, $H_2C(12)$); ^{13}C-NMR ($CDCl_3$, 125 MHz, δ / ppm): 164.43 (CO), 155.25, 147.46, 146.40, 146.26, 146.22, 145.86 145.56, 145.45, 144.73, 143.26, 142.79, 142.41, 142.23, 142.04, 140.31, 136.39, 133.27 (CH=), 70.87 (sp^3-C_{60}), 70.81 and 70.68 (C(6,8)), 70.58 & 70.46 (C(5,9)), 70.21 (C(11)), 69.59 (C(3)), 68.11 (H_2C_{pyrr}),51.91 (C(1)), 38.82 (C(13)), 29.12 (C(2)), 28.71 (C(12)); UV-Vis (CH_2Cl_2, λ_{max} / nm (ε / mol^{-1}dm^{3}cm^{-1})): 256 (134100), 322 (42600), 431 (6600), 702 (1500); HRMS (ESI/TOF): *m/z* calcd for $(C_{148}H_{52}N_4O_8+H)^+$: 2013.3869. Found: 2013.3870.

*Difullerene diamide **23c**.* a) Starting from the protected amine derivative **12c** (135.6 mg, 0.119 mmol), TFA salt was obtained; b) TFA salt, pyridine (3.84 mL), DMAP (43.4 mg, 0.355 mmol), fumaryl chloride (9.06 mg, 6.4 μL, 0.059 mmol) in dry CH_2Cl_2 (80 mL) were used. FCC: Elution with $CHCl_3$/MeOH 100:1.2 and subsequent precipitation gave diamide **23c** (39.3 mg, 31 %). IR (ATR, cm^{-1}): 3291, 3077, 3003, 2925, 2868, 1634, 1550, 1461, 1246, 1116; ^{1}H-NMR (500 MHz, $CDCl_3$, δ / ppm): = 7.79 (4H, *brs*, $HC(2,6)_{ar}$), 7.40 (4H, *t*, *J* = 7.5 Hz, $HC(3,5)_{ar}$), 7.32 (2H, *t*, *J* = 7.5, $HC(4)_{ar}$), 6.90 (2H, *t*, *J* = 5.5, NH), 6.87 (2H, *s*, HC=), 5.10 (2H, *d*, *J* = 9.5 Hz, H_2C_{pyrr}), 5.07 (2H, *s*, HC_{pyrr}), 4.13 (2H, *d*, *J* = 9.5 Hz, H_2C_{pyrr}), 3.89-3.75 (4H, *m*, $H_2C(3)$), 3.75 (8H, *s*, $H_2C(5,6)$), 3.70-3.65 (8H, *m*, $H_2C(8,9)$), 3.60 (4H, *t*, *J* = 6 Hz, $H_2C(11)$), 3.53-3.46 (4H, *m*, $H_2C(13)$), 3.34 (2H, *dt*, *J* = 12.0 Hz & 8.5 Hz, HC(1)), 2.67-2.60 (2H, *m*, HC(1)), 2.28-2.12 (4H, *m*, $H_2C(2)$), 1.82 (4H, *quint*, *J* = 5.5 Hz, $H_2C(12)$); ^{13}C-NMR (125 MHz, $CDCl_3$, δ / ppm): 164.38 (CO), 156.70, 153.65, 153.62, 147.47, 146.46, 146.38, 146.29, 146.09, 145.91, 145.65, 145.48, 145.44, 145.37, 145.30, 144.57, 144.55, 143.15, 142.72, 142.44, 142.32, 142.26, 142.18, 142.14, 141.97, 141.84, 140.34, 140.30, 139.99, 139.54, 139.39, 138.88, 137.39 ($C_{ar}(1)$), 136.91, 136.68, 136.01, 135.89, 133.24 (HC=), 129.65 ($C_{ar}(2,6)$), 128.75 ($C_{ar}(3,5)$), 128.62 (*p*-$C_{ar}(4)$), 82.67 (CH_{pyrr}), 76.86 (sp^3-C_{60}, from HMBC), 70.81, 70.70, 70.57 and 70.46 (C(5,6,8,9)), 70.26 (C(11)), 69.57 (C(3)), 69.06 (sp^3-C_{60}), 66.98 (H_2C_{pyrr}), 49.96 (C(1)), 38.85 (C(13)), 28.68 (C(12)), 28.55 (C(2)); UV/Vis (CH_2Cl_2, λ_{max} / nm (ε / mol^{-1}dm^{3}cm^{-1})): =256 (124500), 307 (41900), 431 (5200), 702 (900); HRMS (ESI/TOF): *m/z* calcd for $(C_{160}H_{60}N_4O_8+Na)^+$: 2187.4314. Found: 2187.4258.

*Difullerene diamide **24c**.* a) Starting from the protected amine derivative **13c** (120 mg, 0.102 mmol), TFA salt was obtained; b) TFA salt, pyridine (3.2 mL), DMAP (36.9 mg, 0.302 mmol), fumaryl chloride (7.72 mg, 5.46 μL, 0.050 mmol) in dry CH_2Cl_2 (32 mL) were used. FCC: Elution with $CHCl_3$/MeOH 100:0.25 and subsequent precipitation gave diamide **24c** (20 mg, 18 %). IR (ATR, cm^{-1}): 3286, 3071, 3003, 2920, 2863, 2803, 1631, 1549, 1456, 1428, 1333, 1178, 1118, 979; ^{1}H-NMR (500 MHz, $CDCl_3$, δ / ppm): 7.96 (2H, *brd*, *J* = 7.5 Hz, $HC(6)_{ar}$), 7.26 (2H, *brt*, *J* = 7.0 Hz, $HC(4)_{ar}$), 7.06 (2H, *t*, *J* = 7.5 Hz, $HC(5)_{ar}$), 6.92 (2H, *brd*, *J* = 7.0 Hz, $HC(3)_{ar}$), 6.88 (2H, *s*, CH=), 6.87 (1H, *brs*, NHCO), 5.69 (2H, *s*, HC_{pyrr}), 5.08 (2H, *d*, *J* = 9.5 Hz, H_2C_{pyrr}), 4.15 (2H, *d*, *J* = 9.0 Hz, H_2C_{pyrr}), 3.89-3.74 (4H, *m*, $H_2C(3)$), 3.70 (6H, *s*, OCH_3), 3.78-3.72 (8H, *m*, $H_2C(5,6)$), 3.70-3.53 (8H, *m*, $H_2C(8,9)$), 3.60 (4H, *brt*

(overlapped with *m*), *J* = 5.0 Hz , $H_2C(11)$), 3.54-3.43 (4H, *m*, $H_2C(13)$), 3.39-3.31 (2H, *m*, H-C(1)), 2.64-2.56 (2H, *m*, H-C(1)), 2.28-2.12 (4H, *m*, $H_2C(2)$), 1.87-1.77 (4H, *m*, $H_2C(12)$); ^{13}C-NMR (125 MHz, $CDCl_3$, δ / ppm): 164.40 (C=O), 158.34 $(C(2)_{ar})$, 157.24, 155.28, 154.47, 154.25, 147.43, 146.95, 146.72, 146.38, 146.36, 146.31, 146.25, 146.20, 146.09, 146.05, 145.74, 145.69, 145.43, 145.39, 145.36, 145.23, 145.21, 145.16, 144.73, 144.58, 144.5, 143.19, 143.14, 142.77, 142.70, 142.68, 142.47, 142.44, 142.32, 142.24, 142.23, 142.12, 141.97, 141.86, 141.69, 140.34, 140.28, 139.54, 139.51, 136.70, 136.54, 136.32, 134.69, 133.22 (CH=), 130.13 $(C(6)_{ar})$, 129.12 $(C(4)_{ar})$, 125.93 $(C(1)_{ar})$, 121.22 $(C(5)_{ar})$, 111.19 ($C(3_{ar})$, 76.16 (sp^3-C_{60}), 74.45 (CH_{pyrr}), 70.82, 70.71, 70.44 and 70.27 (C(5,6,8,9)), 70.55 (C(11)), 69.61 (C(3)), 69.32 (sp^3-C_{60}), 66.84 (H_2C_{pyrr}), 55.34 (OCH_3), 50.03 (C(1)), 38.77 (C(13)), 28.72 (C(12)), 28.60 (C(2)); UV/Vis (CH_2Cl_2, λ_{max} / nm (ε / $mol^{-1}dm^3cm^{-1}$)): 254 (204500), 431 (8000), 702 (600); HRMS (ESI/TOF): *m/z* calcd for $(C_{162}H_{64}N_4O_{10}+Na)^+$: 2247.4526. Found: 2247.4523.

Difullerene diamide ***25c***. a) Starting from the protected amine derivative **14c** (120 mg, 0.102 mmol), TFA salt was obtained; b) TFA salt, pyridine (3.2 mL), DMAP (36.9 mg, 0.302 mmol), fumaryl chloride (7.72 mg, 5.46 μL, 0.050 mmol) in dry CH_2Cl_2 (32 mL) were used. FCC: Elution with $CHCl_3$/MeOH 100:0.25 and subsequent precipitation gave diamide **25c** (20.6 mg, 18 %). IR (ATR, cm^{-1}): 3366, 2952, 1711, 1603, 1512, 1458, 1363, 1173, 1122, 1045; ^{1}H-NMR (500 MHz, $CDCl_3$, δ / ppm): 7.36 (4H, *brs*, $HC(2,6)_{ar}$), 7.31 (2H, *t*, *J* = 7.5 Hz, $HC(5)_{ar}$), 6.92 (1H, *brs*, NHCO), 6.88 (2H, *s*, CH=), 6.85 (2H, *brd*, *J* = 8.5 Hz, $HC(4)_{ar}$), 5.08 (2H, *d*, *J* = 9.5 Hz, H_2C_{pyrr}), 5.03 (2H, s, HC_{pyrr}), 4.16 (2H, *d*, *J* = 9.5 Hz, H_2C_{pyrr}), 3.90-3.72 (4H, *m*, $H_2C(3)$), 3.80 (3H, *s*, OCH_3), 3.78-3.72 (8H, *m*, $H_2C(5,6)$), 3.70-3.53 (8H, *m*, $H_2C(8,9)$), 3.60 (4H, *brt* (overlapped with *m*), *J* = 4.5 Hz , $H_2C(11)$), 3.53-3.43 (4H, *m*, $H_2C(13)$), 3.38-3.31 (2H, *m*, H-C(1)), 2.68-2.59 (2H, *m*, H-C(1)), 2.28-2.08 (4H, *m*, $H_2C(2)$), 1.87-1.75 (4H, *m*, $H_2C(12)$); ^{13}C-NMR (125 MHz, $CDCl_3$, δ /ppm): 164.38 (C=O), 159.90 $(C(3)_{ar})$, 156.60, 154.36, 153.79, 153.60, 147.46, 147.07, 146.62, 146.46, 146.41, 146.37, 146.31, 146.26, 146.24, 146.09, 145.91, 145.69, 145.48, 145.45, 145.42, 145.39, 145.36, 145.29, 144.87, 144.78, 144.55, 143.31, 143.14, 142.84, 142.72, 142.43, 142.41, 142.29, 142.27, 142.22, 142.17, 142.15, 142.08, 141.95, 141.83, 141.70, 140.34, 140.28, 139.96 $(C(1)_{ar})$, 139.61, 139.01, 136.74, 136.71, 135.98, 135.88, 133.24 (CH=), 129.73 $(C(5)_{ar})$, 121.90 $(C(6)_{ar})$, 115.37 ($C(2)_{ar}$, from HMBC), 114.03 $(C(4)_{ar})$, 82.54 (CH_{pyrr}), 76.72 (sp^3-C_{60}), 70.80, 70.69, 70.42 and 70.26 (C(5,6,8,9)), 70.55 (C(11)), 69.60 (C(3)), 69.05 (sp^3-C_{60}), 66.94 (H_2C_{pyrr}), 55.54 (OCH_3), 50.06 (C(1)), 38.77 (C(13)), 28.71 (C(12)), 28.54 (C(2)); UV/Vis (CH_2Cl_2, λ_{max} / nm (ε / $mol^{-1}dm^3cm^{-1}$)): 254 (101900), 431 (3900), 702 (200); HRMS (ESI/TOF): *m/z* calcd for $(C_{162}H_{64}N_4O_{10}+Na)^+$: 2247.4526. Found: 2247.4572.

Difullerene diamide ***26c***. a) Starting from the protected amine derivative **15c** (64.2 mg, 0.055 mmol), TFA salt (74.7 mg) was obtained; b) TFA salt (74.7 mg, 0.063 mmol), pyridine (2 mL), DMAP (23.1 mg, 0.189 mmol), fumaryl chloride (4.81 mg, 3.4 μL, 0.031 mmol) in dry CH_2Cl_2 (30 mL) were used. FCC: Elution with PhMe/$CHCl_3$/MeOH 2:6:0.2 and subsequent precipitation gave diamide **26c** (8.9 mg, 15 %). IR (ATR, cm^{-1}): 3309, 3078, 2954, 2923, 2868, 1724, 1649, 1341, 1099; ^{1}H-NMR (500 MHz, $CDCl_3$, δ ppm): 7.69 (2H, brs, $HC(2,6)_{ar}$), 6.93 (2H, *d*, *J* = 8.5 Hz, $HC(3,5)_{ar}$), 6.90 (1H, brs, NHCO), 6.88 (1H, *s*, CH=), 5.07 (1H, *d*, *J* = 9 Hz, H_2C_{pyrr}), 5.01 (1H, *s*, HC_{pyrr}), 4.10 (1H, *d*, *J* = 9 Hz, H_2C_{pyrr}), 3.88-3.81 (2H, *m*, $H_2C(3)$), 3.80 (3H, *s*, OCH_3), 3.78-3.72 (4H, *m*, $H_2C(5,6)$), 3.70-3.57 (4H, *m*, $H_2C(8,9)$), 3.61 2H, (t (overlapped with *m*), *J* = 5.5 Hz , $H_2C(11)$), 3.49 (2H, *quint*, *J* = 5 Hz, $H_2C(13)$), 3.34-3.27 (1H, *m*, H-C(1)), 2.64-2.57 (1H, *m*, H-C(1)), 2.26-2.11 (2H, *m*, $H_2C(2)$), 1.82 (2H, *quint*, *J* = 6 Hz, $H_2C(12)$); ^{13}C-NMR (125 MHz, $CDCl_3$, δ / ppm): 164.22 (C=O),

159.53 (*p*-C_{ar}), 156.65, 154.24, 153.73, 153.68, 147.30, 146.83, 146.53, 146.35, 146.29, 146.25, 146.21, 146.14, 146.12, 146.09, 145.92, 145.75, 145.54, 145.45, 145.31, 145.26, 145.21, 145.12, 144.71, 144.63, 144.40, 143.14, 142.98, 142.67, 142.54, 142.32, 142.28, 142.11, 142.00, 141.80, 141.67, 141.51, 140.15, 140.11, 139.88, 139.51, 136.74, 136.53, 135.78, 135.75, 133.08 (CH=), 130.58 (C_{ar}(2,6), 129.18 (C_{ar}(1)), 113.94 (C_{ar}(3,5)), 82.00 (CH_{pyrr}), 76.90 (sp^3-C_{60}, from HMBC), 70.65, 70.54, 70.41, 70.27 (C(5, 6, 8, 9)), 70.09 (C(11)), 69.46 (C(3)), 68.81 (sp^3-C_{60}), 66.77 (H_2C_{pyrr}), 55.21 (OCH_3), 49.73 (C(1)), 38.62 (C(13)), 28.55 (C(12)), 28.37 (C(2)); UV/Vis (CH_2Cl_2, λ_{max} / nm (ε / $mol^{-1}dm^3cm^{-1}$)): 318 (30630), 327 (29350), 431 (4020); HRMS (ESI/TOF): *m/z* calcd for $(C_{162}H_{64}N_4O_{10}+Na)^+$: 2247.4526. Found: 2247.4492.

TABLE S-I. ^{1}H- and ^{13}C-NMR chemical shifts of characteristic signals of fullerene monoadducts **6**–**10**

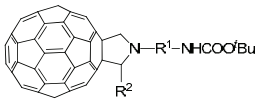

^{1}H/^{13}C		**6a**	**7a**	**8b**	**9b**	**10b**
		Chemical shifts, ppm				
	R^1	$(CH_2)_6$[1]			$(CH_2)_{10}$[1]	
	R^2	4-MeO-C_6H_4	C_9H_{19}[2]	C_6H_5	4-MeO-C_6H_4	4-NO_2-C_6H_4
HC(2)$_{pyrr}$		5.00s, 82.25	4.13t, 77.41	5.06s, 82.59	5.01s, 82.10	5.18s, 81.66
H_2C(5)$_{pyrr}$	**pyrr.**	5.07d/4.10d 67.01	4.90d/4.12d 66.88	5.10d/4.12d 66.89	5.08d/4.10d 66.86	5.14d/4.17d 66.87
H_2C(1)		3.24-3.12m 2.57-2.49m 53.06	3.56-3.49m 2.87-2.80m 52.46	3.27-3.19m 2.58-2.52m 53.12	3.24-3.17m 2.56-2.49m 53.02	3.15-3.03m 2.64-2.56m 53.38
H_2C(6)		3.24-3.12m 40.82	3.20brq, 40.61	-	-	-
H_2C(10)	**R^1**			3.20br q, 40.65	3.12br q, 40.47	3.15-3.03m, 40.64
NH		4.55br s	4.57br s	4.50br s	4.50br s	4.51br s
CO		156.16	156.01	155.97	155.98	156.00
^{t}Bu		1.46s 28.62 79.23	1.56s 28.46 79.13	1.45s 28.44 79.00	1.45s 28.45 79.01	1.45s 28.44 79.02
H_2C(1')		-	2.52-2.43m 2.43-2.34m 31.14	-	-	-
H_3C(9')		-	0.87t, 14.14	-	-	-
C_{ar}(1)		-	-	137.40	129.36	145.43
HC$_{ar}$(2,6)	**R^2**	7.70br s 130.73	-	7.81br s 129.48	7.72br s 130.58	8.03br s 130.21
HC$_{ar}$(3,5)		6.94d 114.11	-	7.41t 128.57	6.94d 113.92	8.29d 123.85
HC$_{ar}$(4)		- 159.70	-	7.32tt 128.39	- 159.50	- 145.43
MeO		3.81s 55.36	-	-	3.81s 55.20	-

[1]C atoms of R^1 substituent (hexamethylene and decamethylene) are numbered starting from the *N*-pyrrolidine ring; [2]C atoms of the nonyl-group, presented as C', are numbered starting from the pyrrolidine C(2) atom

TABLE S-II. ^{1}H- and ^{13}C-NMR chemical shifts of characteristic signals of the fullerene monoadducts **11c-18c**

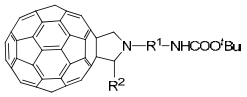

^{1}H/^{13}C		**11c**	**12c**	**13c**	**14c**	**15c**	**17c**	**18c**
		Chemical shifts, ppm						
	R[1]	$(CH_2)_3O(CH_2)_2O(CH_2)_2O(CH_2)_3$						
	R[2]	H	C_6H_5	2-MeO-C_6H_4	3-MeO-C_6H_4	4-MeO-C_6H_4	3-NO_2-C_6H_4	4-NO_2-C_6H_4
$HC(2)_{pyrr}$	**pyr r.**	4.42s	5.08s 82.52	5.70s 74.45	5.04s 82.56	5.02s 82.01	5.20s 81.63	5.20s 81.55
$H_2C(5)_{pyrr}$			5.11d/4.14d 66.82	5.09d/4.17d 66.85	5.10d/4.13d 66.95	5.08d/4.12d 66.77	5.14d/4.19d 66.86	5.14d/4.18d 66.74
$H_2C(1)$		3.20t 51.89	3.36dt 2.68-2.61m 49.79	3.37dt 2.65-2.58m 50.00	3.38dt 2.69-2.61m 50.01	3.33dt 2.65-2.58m 49.68	3.29dt 2.72-2.66 50.09	3.30dt 2.71-2.64m 49.88
$H_2C(13)$		3.28-3.22m 38.77	3.27-3.20m 38.61	3.24br q 38.78	3.24br q 38.77	3.24br q 38.59	3.24br q 38.72	3.24br q 38.56
H_2C-O (6C-O)	**R[1]**	3.88-3.53 68-71	3.90-3.50 69-71	3.75-3.53 70-71	3.90-3.50 69-71	3.90-3.50 69-71	3.90-3.50 68-71	3.90-3.50 68-71
NH		5.00br s	4.97br s	4.98br s	4.98br s	4.99br s	4.96br s	4.96br s
CO		156.20	156.03	156.19	156.18	156.02	156.11	155.90
^{t}Bu		1.45 28.65	1.45s 28.48 78.92	1.45s 28.64 79.07	1.45s 28.63 79.07	1.44s 28.47 78.90	1.44s 28.62 79.06	1.44s 28.47 78.91
$C_{ar}(1)$		-	137.20	125.92	138.99	129.15	140.04	145.00
$HC_{ar}(2)$		-	7.79br s 129.48	- 158.34	7.36 br s 114.94	7.70br s 130.57	8.67br s 124.34	8.03br s 130.24
$HC_{ar}(3)$		-	7.41t 128.57	6.91d 111.17	- 159.94	6.93d 113.88	- 148.57	8.29d 123.82
$HC_{ar}(4)$	**R[2]**	-	7.32tt 128.45	7.27td 129.11	6.86br d 114.00	- 159.53	8.21br dd 123.77	- 145.00
$HC_{ar}(5)$		-		7.06t 121.20	7.31t 129.71		7.62t 129.79	
$HC_{ar}(6)$		-		7.97dd 130.14	7.36br s 122.15		8.21br dd 135.56	
MeO		-	-	3.71 55.33	3.81s 55.51	3.80s 55.19	-	-

C atoms of R^1 substituent (4,7,10-trioxatridecamethylene) are numbered starting from the *N*-pyrrolidine ring.

TABLE S-III. ^{1}H- and ^{13}C-NMR chemical shifts of characteristic signals of difullerene diamides **19-26**

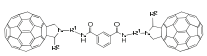
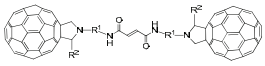

$^{1}H/^{13}C$		**19a***	**20a**	**21a**	**22c**	**23c**	**24c**	**25c**	**26c**
		Chemical shifts, ppm							
	R^1	$(CH_2)_6$	$(CH_2)_6$		$(CH_2)_3O(CH_2)_2O(CH_2)_2O(CH_2)_3$				
	R^2	H	C_9H_{19}	C_9H_{19}	H	C_6H_5	2-MeO-$-C_6H_4$	3-MeO-$-C_6H_4$	4-MeO-$-C_6H_4$
$HC(2)_{pyrr}$	**pyrr.**	4.41s -	4.13t 77.34	4.13t 77.20	4.41s 68.11	5.07s 82.67	5.69s 74.45	5.03s 82.54	5.01s 82.00
$H_2C(5)_{pyrr}$			4.91d/4.12d 66.85	4.90d/4.13d 66.69		5.10d/4.13d 66.98	5.08d/4.15d 66.84	5.08d/4.16d 66.94	5.07d/4.10d 66.77
$H_2C(1)$		3.10t -	2.90-2.82m 52.38	3.57-3.48m 2.88-2.80m 52.39	3.17t 51.91	3.38-3.30m 2.67-2.60m 50.00	3.38-3.31m 2.64-2.56m 50.03	3.38-3.31m 2.68-2.59m 50.06	3.34-3.27m 2.64-2.57m 49.73
$H_2C(6)$		3.56q -	3.60-3.51m 40.25	3.38br q 39.81	-	-	-	-	-
$H_2C(13)$	**R^1**	-	-	-	3.56-3.48m 38.82	3.53-3.46m 38.81	3.54-3.43m 38.77	3.53-3.43m 38.77	3.49quint 38.62
H_2C-O (6C)		-	-	-	3.90-3.55 69-71	3.90-3.55 69-71	3.90-3.55 69-71	3.90-3.55 69-71	3.90-3.55m 69-71
NH		6.30br s-	6.30br t	7.98br t	6.99br s	6.90br t	6.87br s	6.92br s	6.90br s
CO			166.56	165.07	164.43		164.40	164.38	164.22
$H_2C(1')$		- - -	2.53-2.43m 2.43-2.33m 31.14	2.53-2.43m 2.43-2.32m 30.99	-	-	-	-	-
$H_3C(9')$		- -	0.87t 14.16	0.87t 14.00	-	-	-	-	-
$C_{ar}(1)$		-	-	-	-	137.39	125.93	139.96	129.18
$HC_{ar}(2)$		-	-	-	-	7.79br s 129.65	- 158.34	7.36br s 115.37	7.69br s 130.58
$HC_{ar}(3)$	**R^2**	-	-	-	-	7.40t 128.75	6.92br d 111.19	- 159.90	6.93d 113.94
$HC_{ar}(4)$		-	-	-	-	7.32t 128.62	7.26br d 129.12	6.85br d 113.89	- 159.53
$HC_{ar}(5)$		-	-	-	-		7.06t 121.22	7.31t 129.73	
$HC_{ar}(6)$		-	-	-	-		7.96br d 130.13	7.36brs 121.90	
MeO		-	-	-	-		3.70s 55.34	3.80s 55.54	3.80s 55.21
HC=CH	**fumaryl or iso-phthaloyl uuus**	-	-	6.82s 132.41	6.91 133.27	6.87s 133.24	6.88 133.22	6.88s 133.24	6.88s 133.08
$C_{ar}(1,3)$		-	- /135.1	-			-	-	-
$HC_{ar}(2)$		8.21s	8.22s/125.3	-			-	-	-
$HC_{ar}(4,6)$		7.91dd	7.92dd/129.7	-			-	-	-
$HC_{ar}(5)$		7.53t	7.53t/129.0	-			-	-	-

* Only the ^{1}H NMR spectrum was recorded due to its low solubility.
C atoms of R^1 substituent ($(CH_2)_6$and 4,7,10-trioxatridecamethylene) are numbered starting from the *N*-pyrrolidine ring.
C atoms of C_9H_{19}-group, presented as C', are numbered starting from the pyrrolidine C(2) atom.

2-Methoxyphenyl-substituted fulleropyrrolidine derivative ***6a***

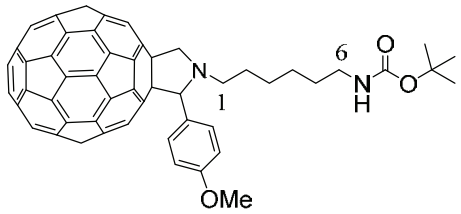

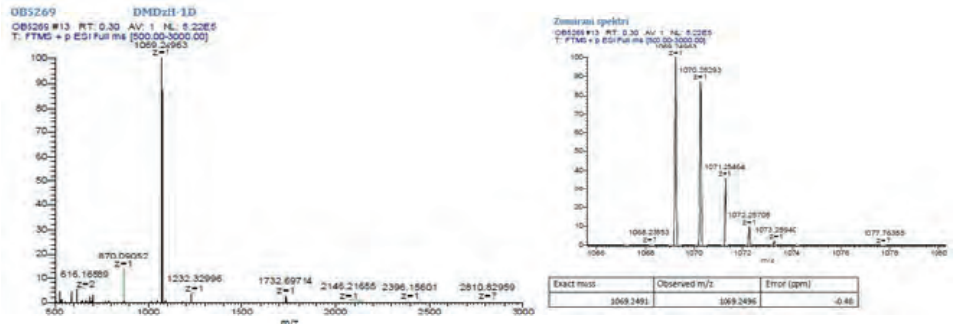

Fig. S-1. Mass spectrum of **6a**.

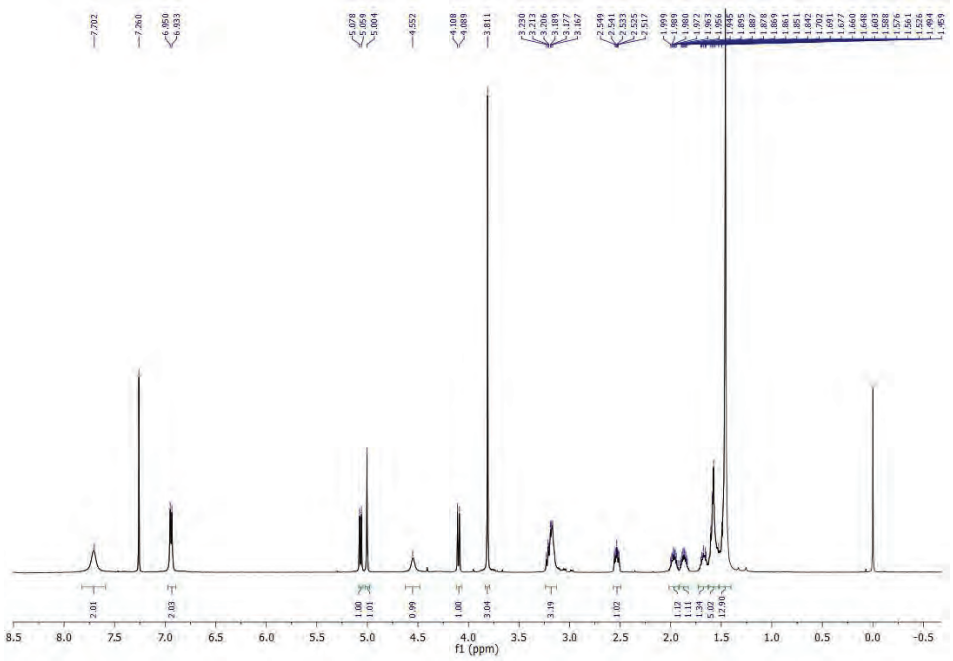

Fig. S-2. ^{1}H-NMR spectrum of **6a**.

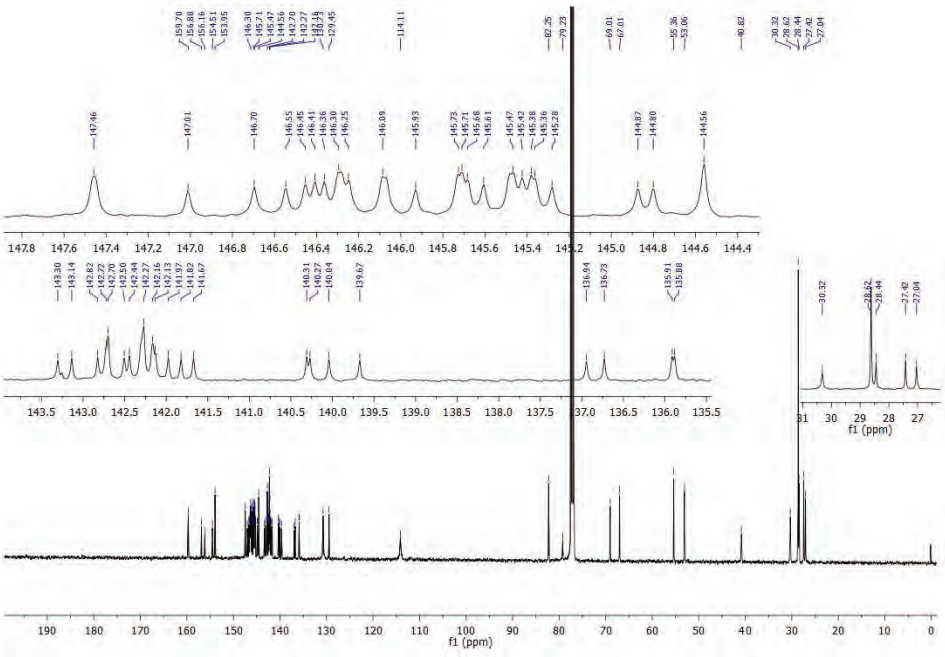

Fig. S-3. ^{13}C-NMR spectrum of **6a**.

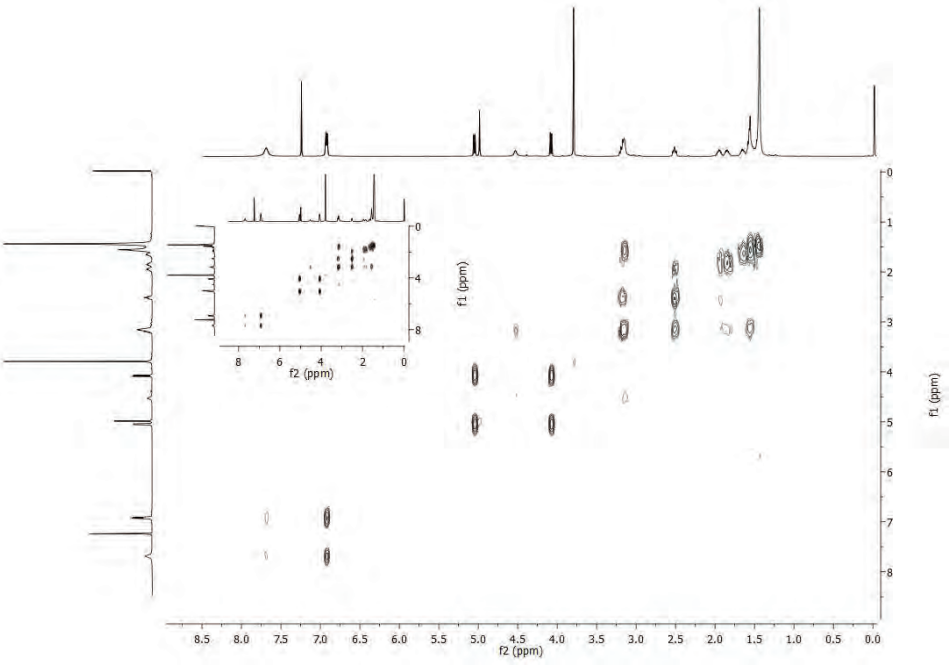

Fig. S-4. COSY spectrum of **6a**.

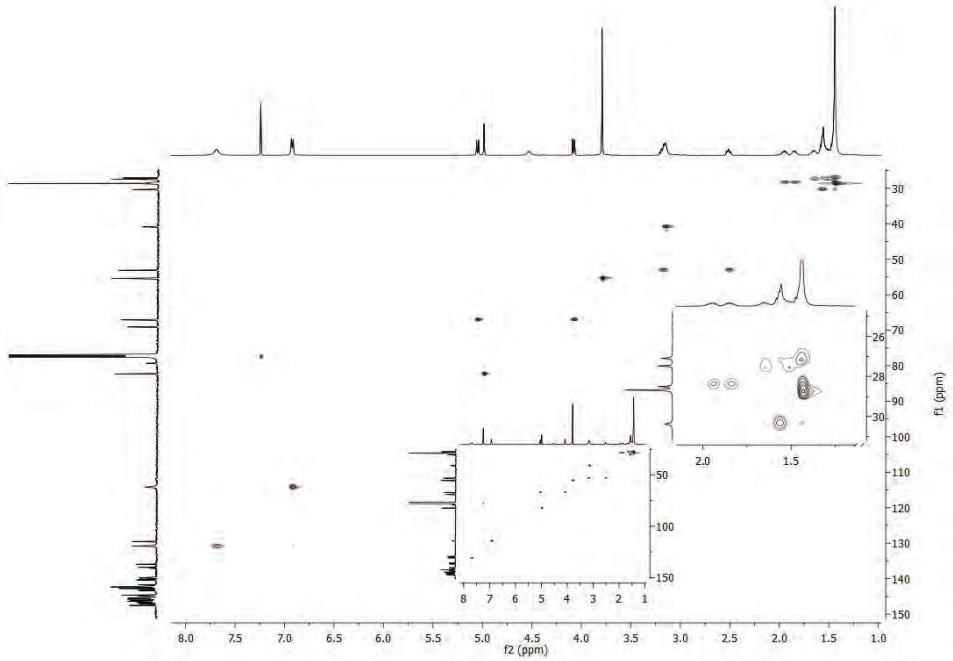

Fig. S-5. HSQC spectrum of **6a**.

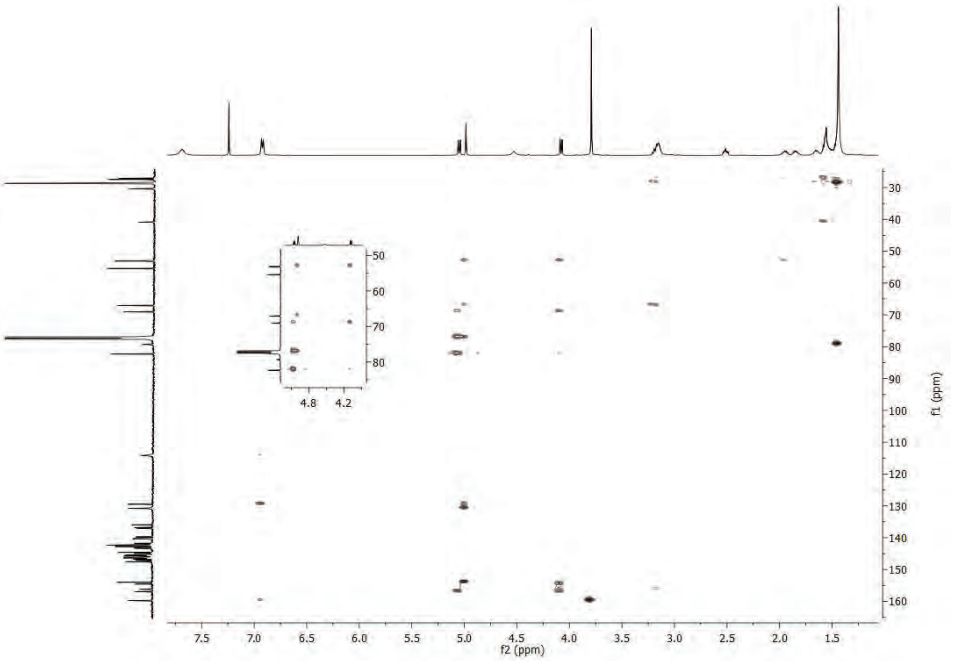

Fig. S-6. HMBC spectrum of **6a**.

Nonyl-substituted fulleropyrrolidine derivative ***7a***

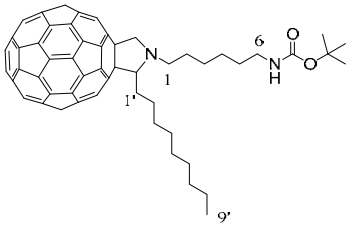

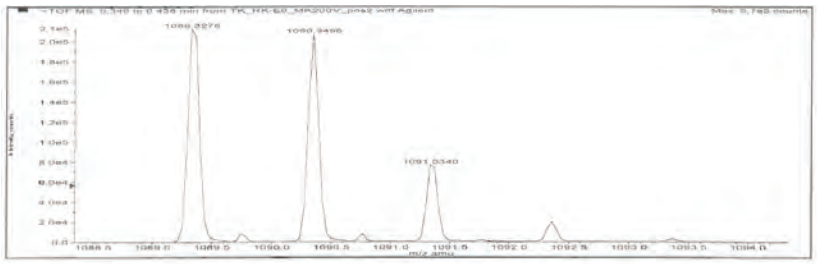

Formula	Compound name	Mass	Peak RT (min)	Peak area	Description
C82H44N2O2	–	1088.34028	0.38	1.39537 E6	–

Species	Abundance (counts)	Ion Mass	Measured Mass	Error (mDa)	Error (ppm)	Ret. Time Error (min)
(M+H)+	225149.68	1089.34756	1089.34545	-2.10045	-1.94	–

Fig. S-7. Mass spectrum of **7a**.

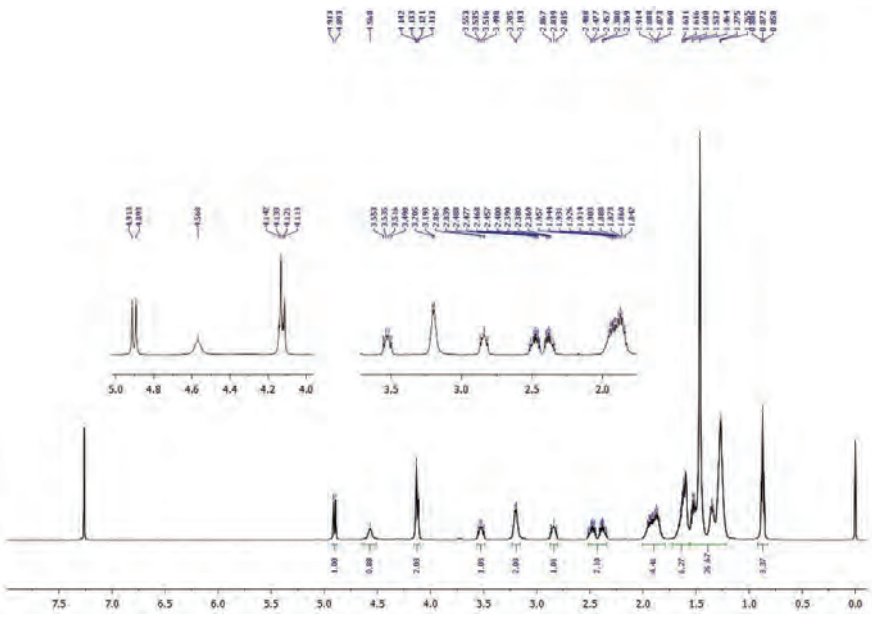

Fig. S-8. ^{1}H-NMR spectrum of **7a**.

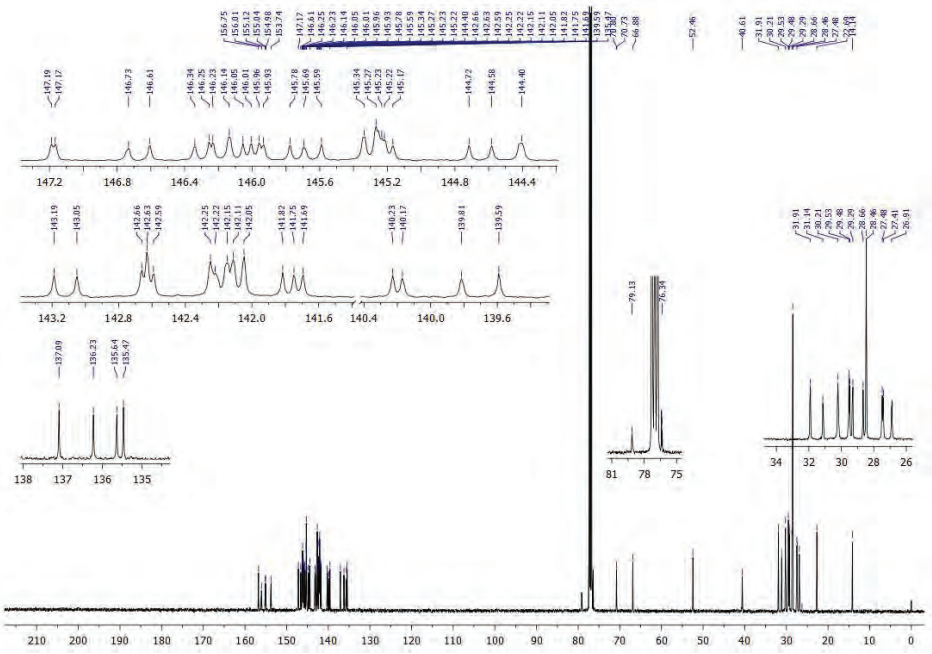

Fig. S-9. ^{13}C-NMR spectrum of **7a**.

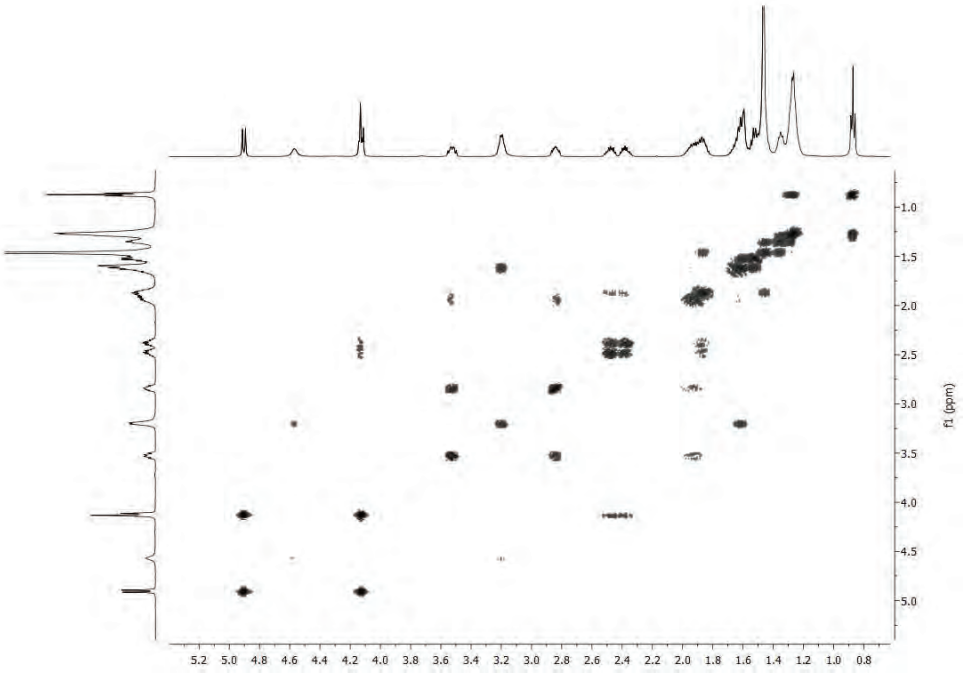

Fig. S-10. COSY spectrum of **7a**.

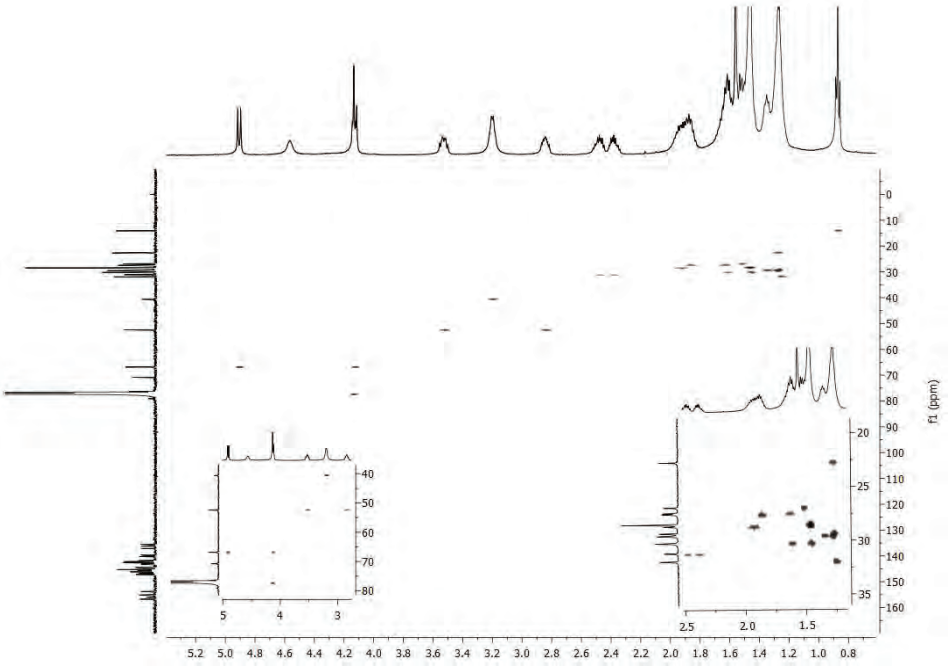

Fig. S-11. HSQC spectrum of **7a**.

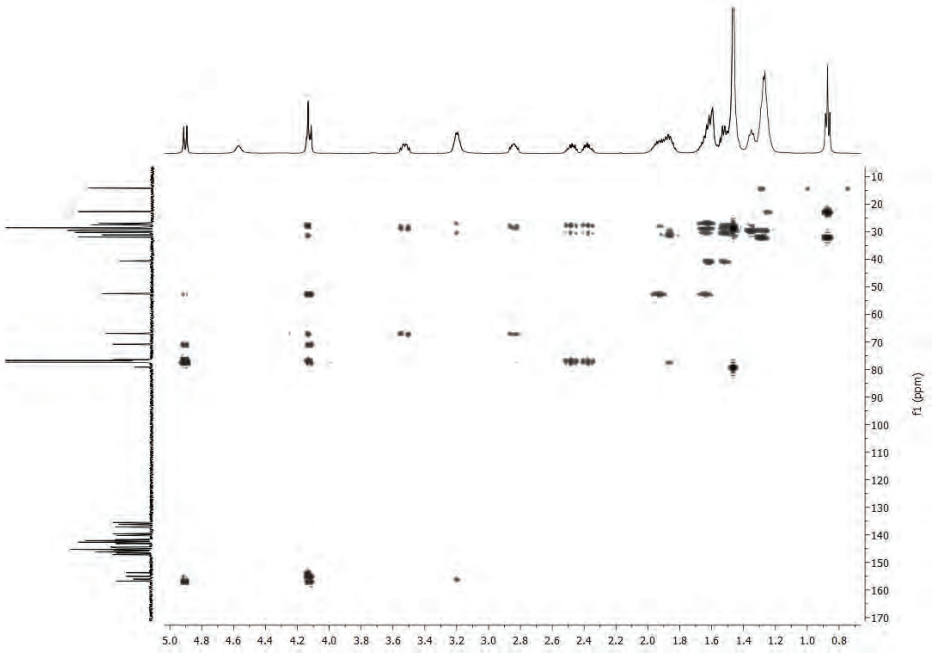

Fig. S-12. HMBC spectrum of **7a**.

Phenyl-substituted fulleropyrolidine derivative ***8b***

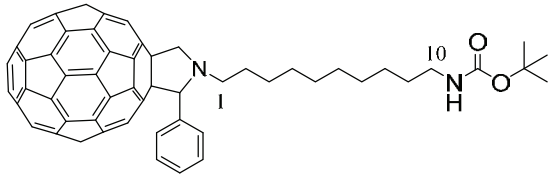

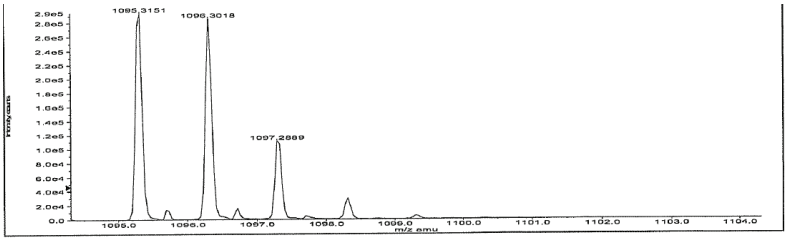

Formula	Compound name	Mass	Peak RT (min)	Peak area	Description
C83H38N2O2	–	1094.29333	0.38	2.45318 E6	--

Species	Abundance (counts)	Ion Mass	Measured Mass	Error (mDa)	Error (ppm)	Ret. Time Error (min)
[M+H]+	306739.07	1095.30060	1095.30025	-0.35594	-0.32	

Fig. S-13. Mass spectrum of **8b**.

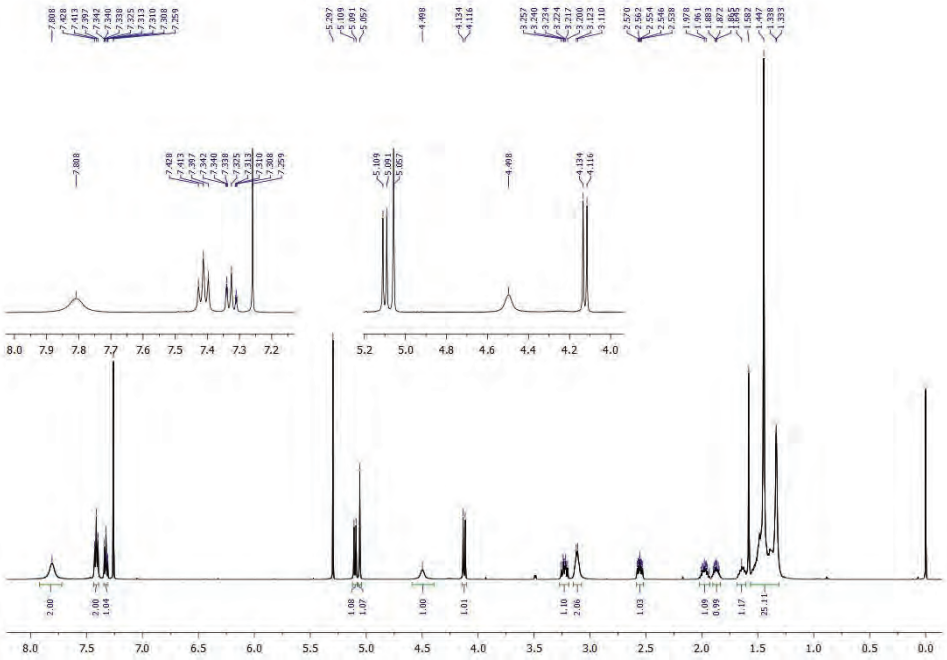

Fig. S-14. ^{1}H-NMR spectrum of **8b**.

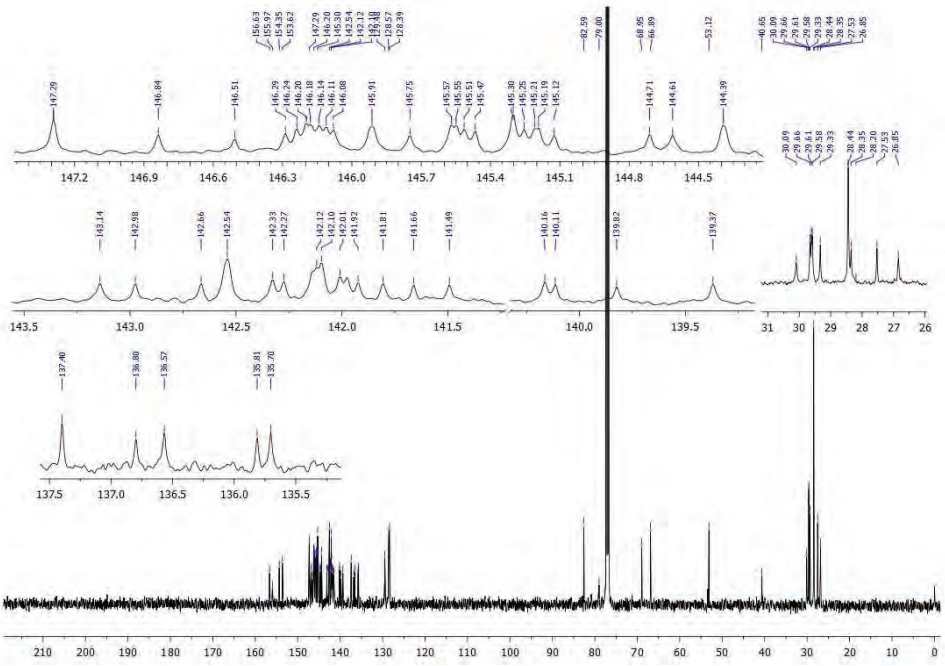

Fig. S-15. ^{13}C-NMR spectrum of **8b**.

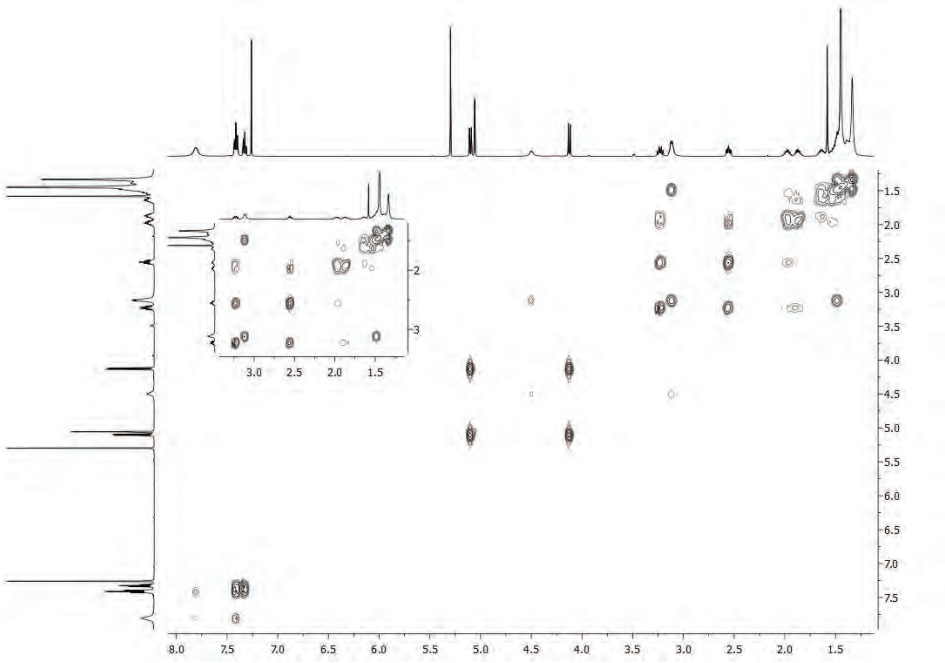

Fig. S-16. COSY spectrum of **8b**.

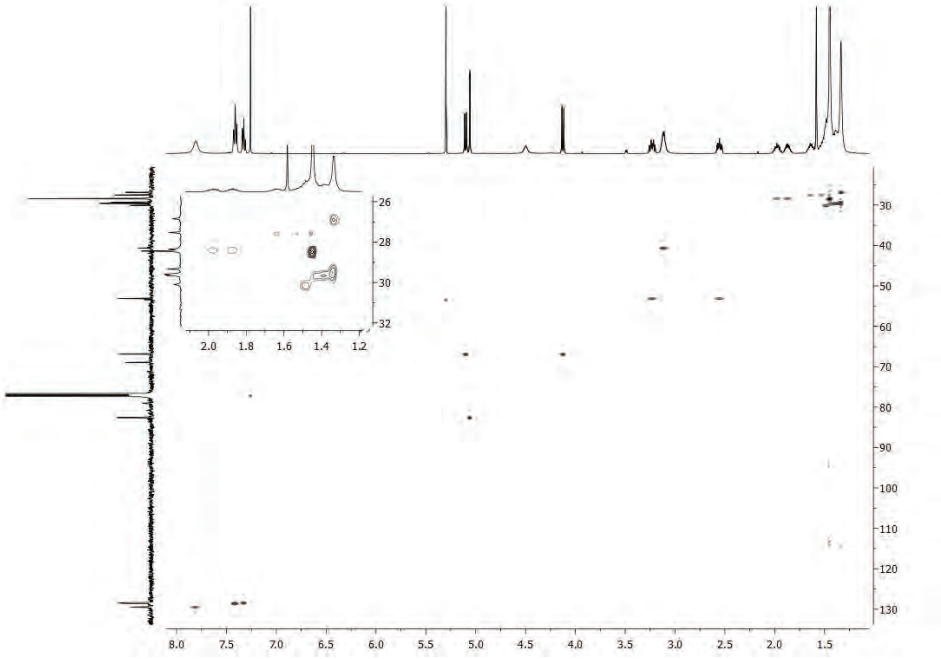

Fig. S-17. HSQC spectrum of **8b**.

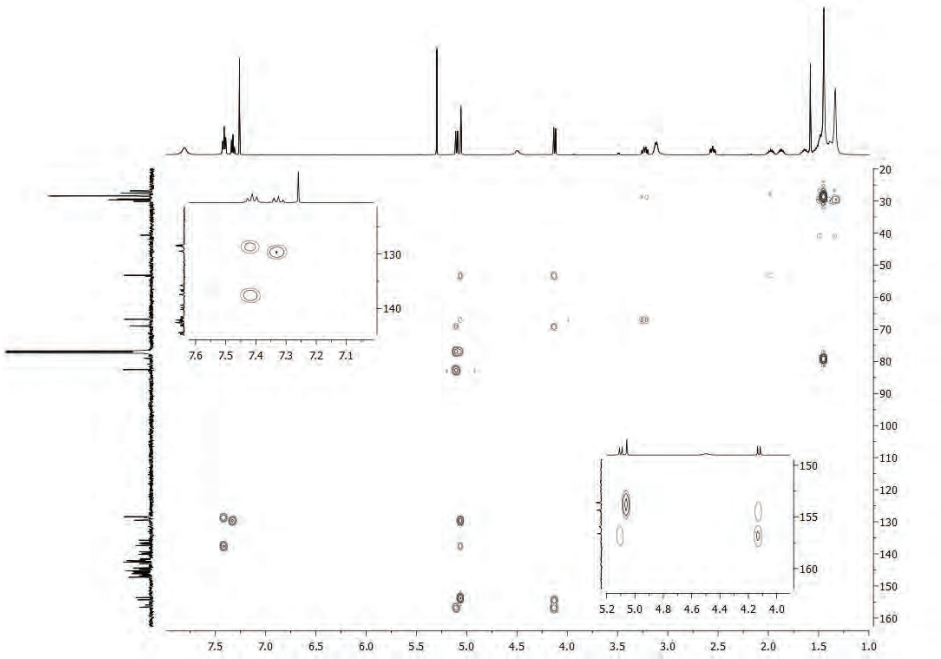

Fig. S-18. HMBC spectrum of **8b**.

4-Methoxyphenyl-substituted fulleropyrolidine derivative ***9b***

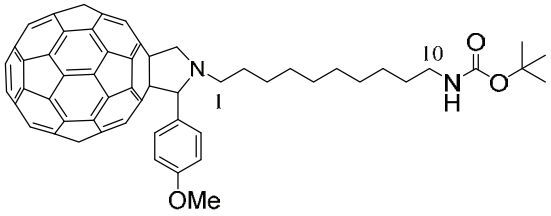

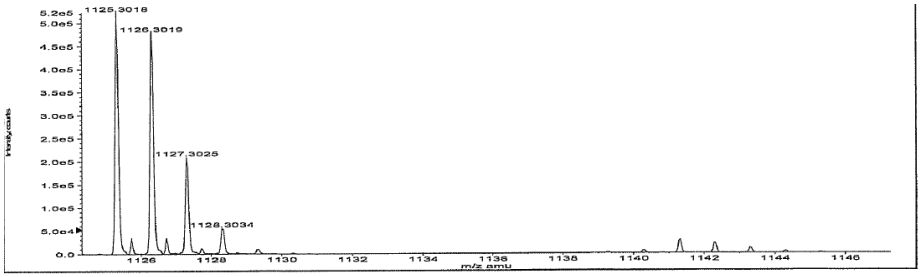

Formula	Compound name	Mass	Peak RT (min)	Peak area	Description
C84H40N2O3	--	1124.30389	0.38	4.77221 E6	--

Species	Abundance (counts)	Ion Mass	Measured Mass	Error (mDa)	Error (ppm)	Ret. Time Error (min)
[M+H]+	529296.69	1125.31117	1125.31122	0.05235	0.05	--

Fig. S-19. Mass spectrum of **9b**.

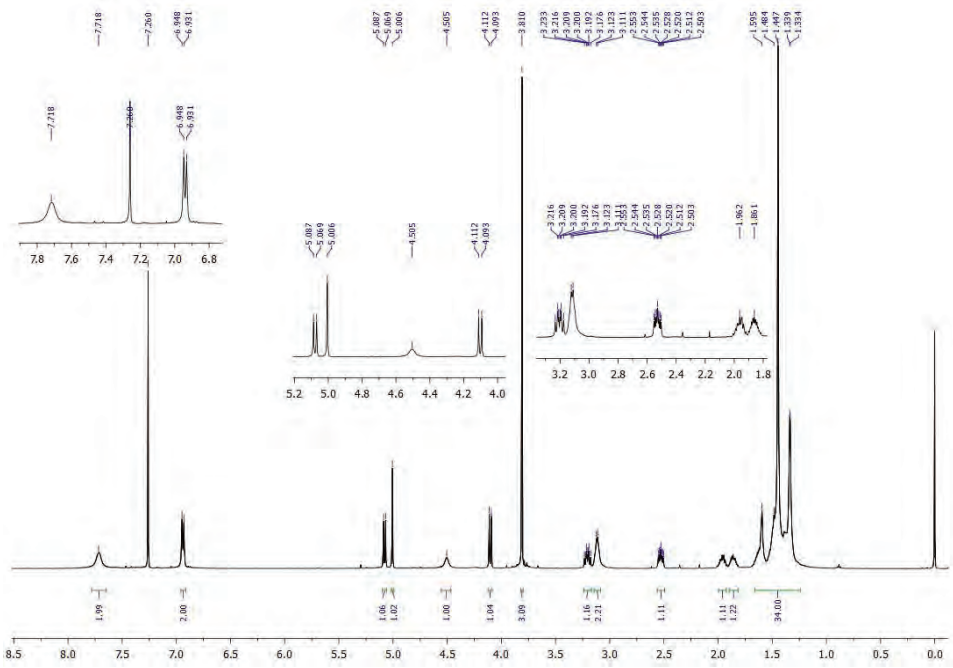

Fig. S-20. ^{1}H-NMR spectrum of **9b**.

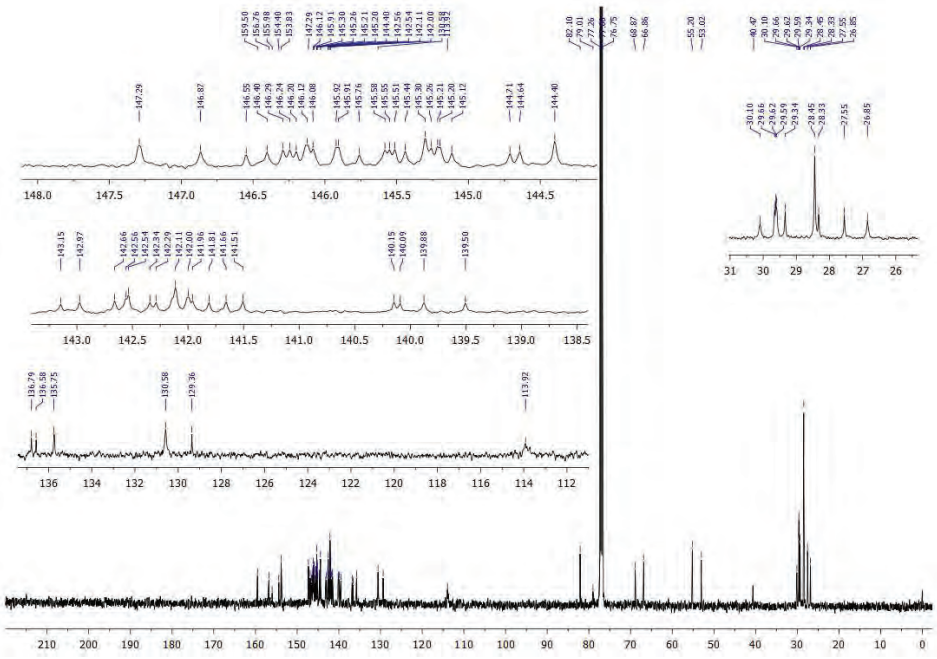

Fig. S-21. ^{13}C-NMR spectrum of **9b**.

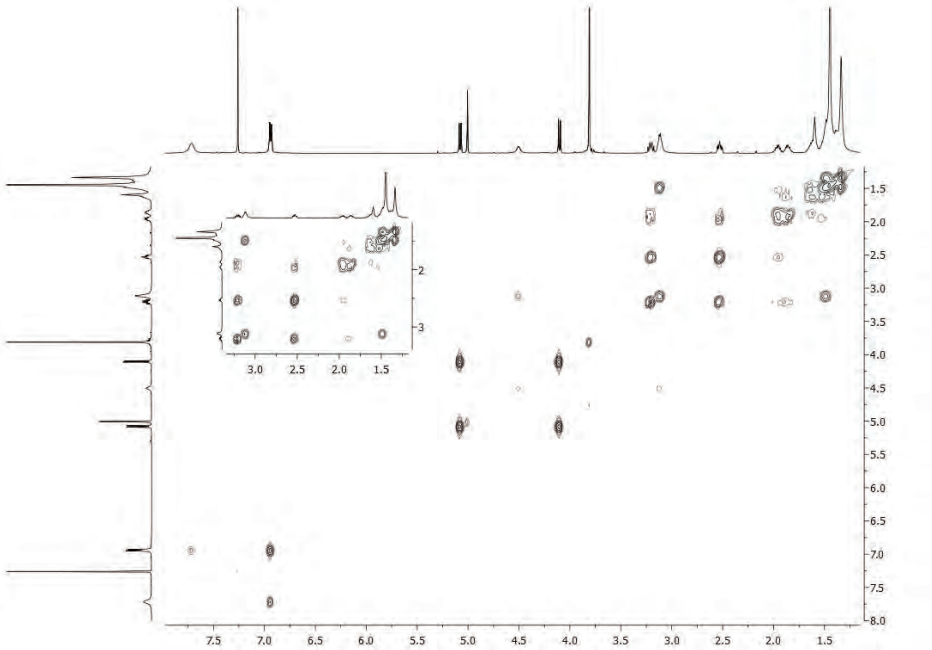

Fig. S-22. COSY spectrum of **9b**.

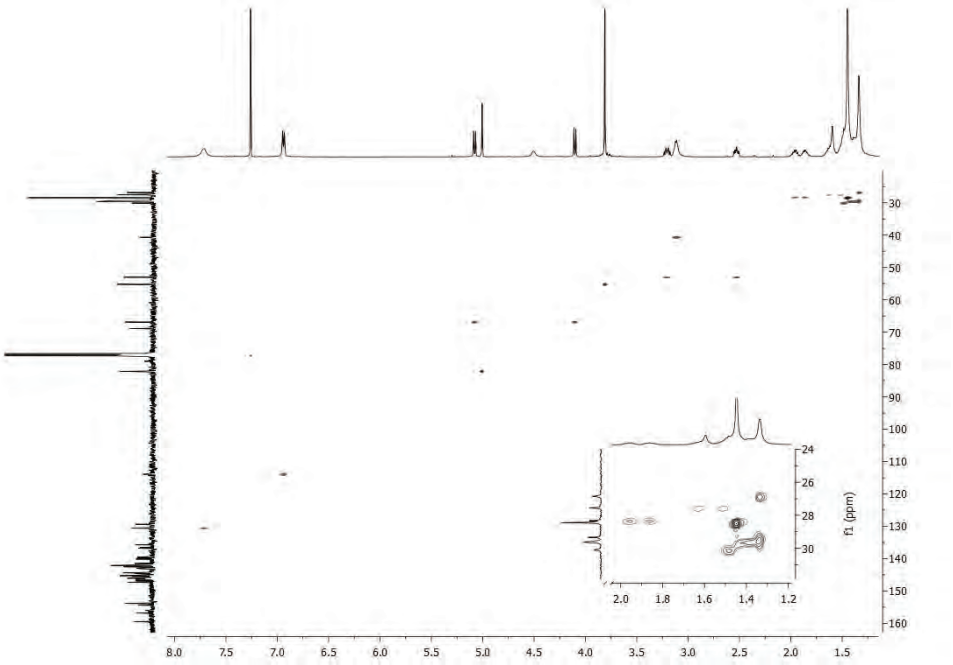

Fig. S-23. HSQC spectrum of **9b**.

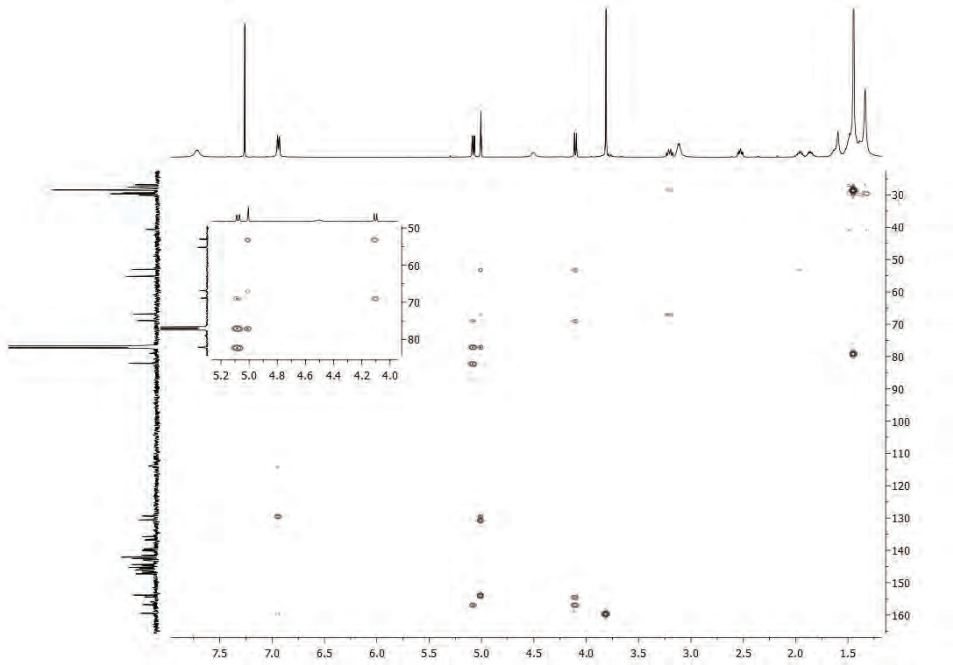

Fig. S-24. HMBC spectrum of **9b**.

4-Nitrophenyl-substituted fulleropyrrolidine derivative ***10b***

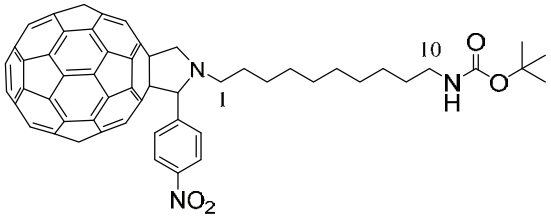

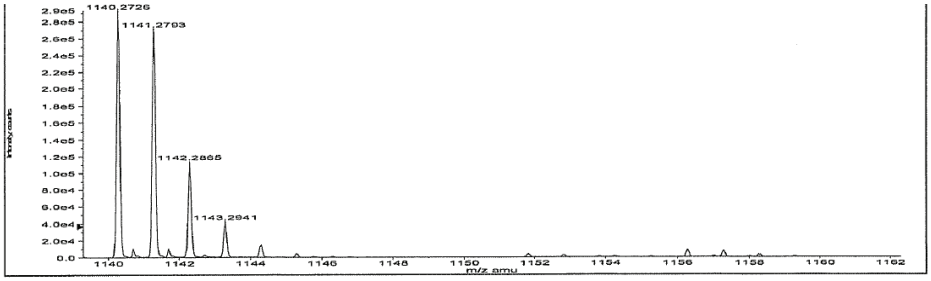

Formula	Compound name	Mass	Peak RT (min)	Peak area	Description
C83H37N3O4	–	1139.27841	0.37	1.71257 E6	–

Species	Abundance (counts)	Ion Mass	Measured Mass	Error (mDa)	Error (ppm)	Ret. Time Error (min)
[M+H]+	299830.20	1140.28568	1140.28465	-1.02968	-0.90	–

Fig. S-25. Mass spectrum of **10b**.

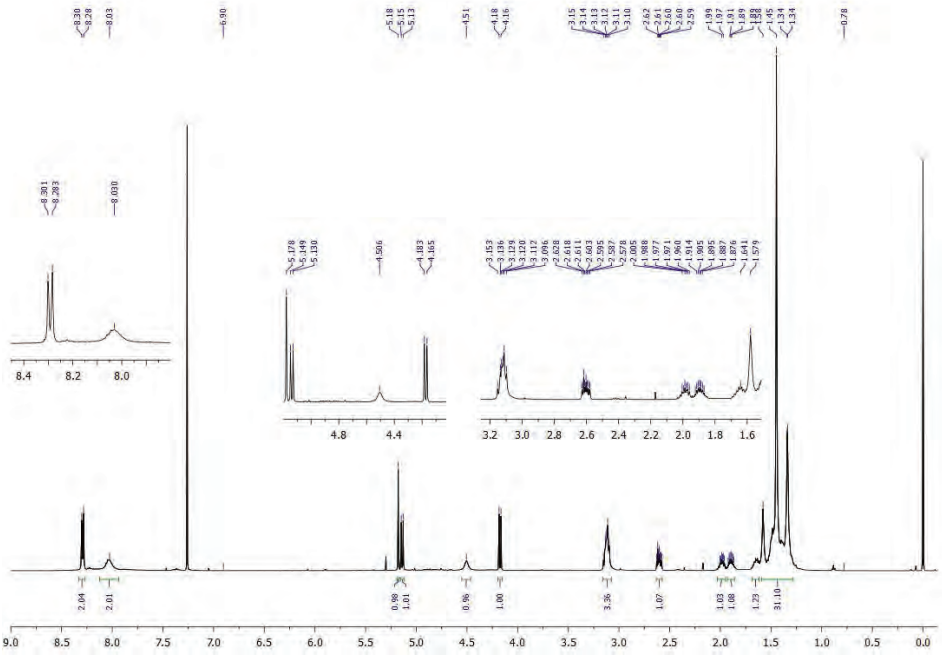

Fig. S-26. ^{1}H-NMR spectrum of **10b**.

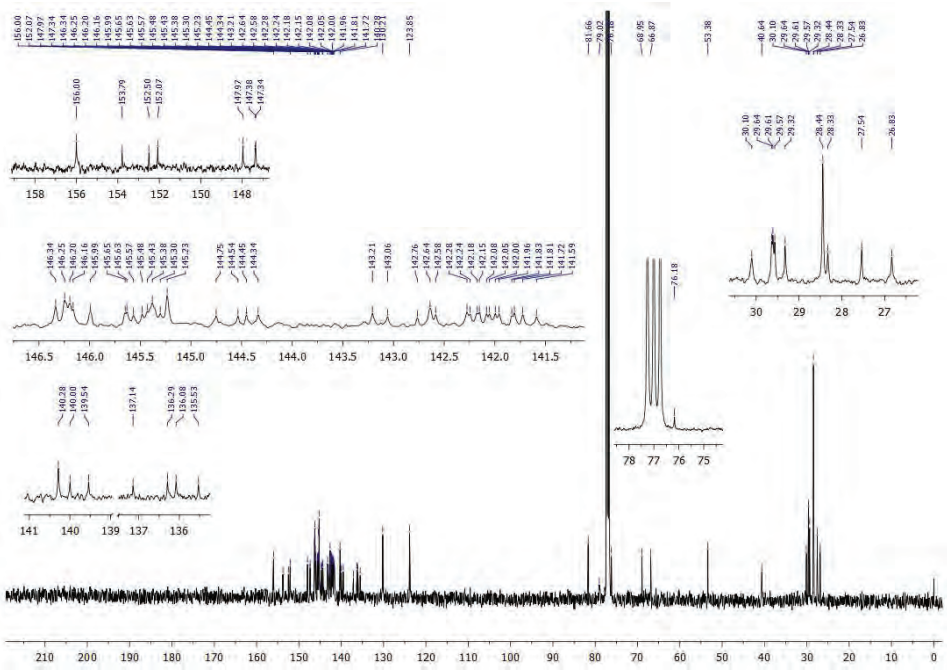

Fig. S-27. ^{13}C-NMR spectrum of **10b**.

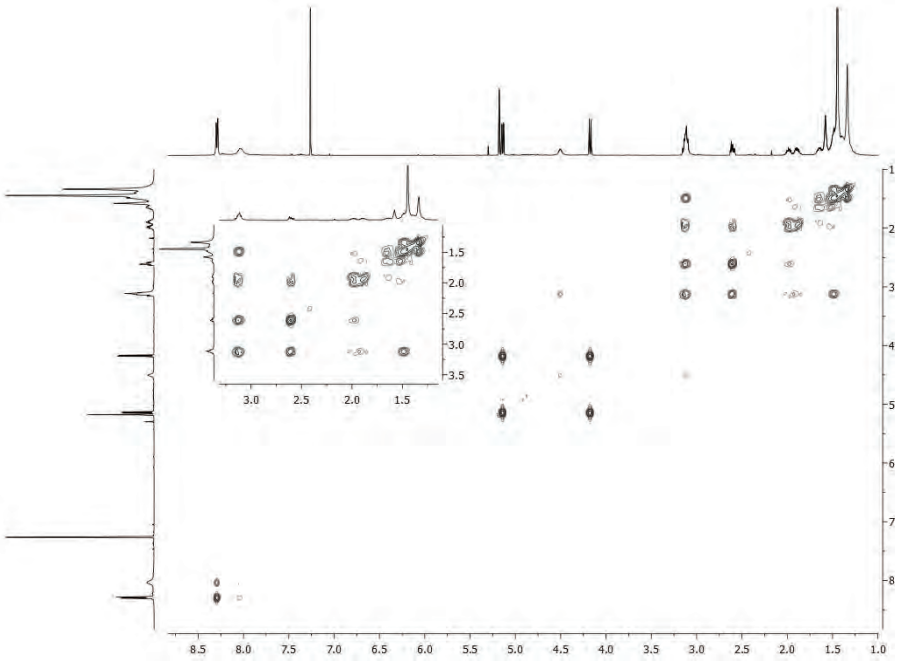

Fig. S-28. COSY spectrum of **10b**.

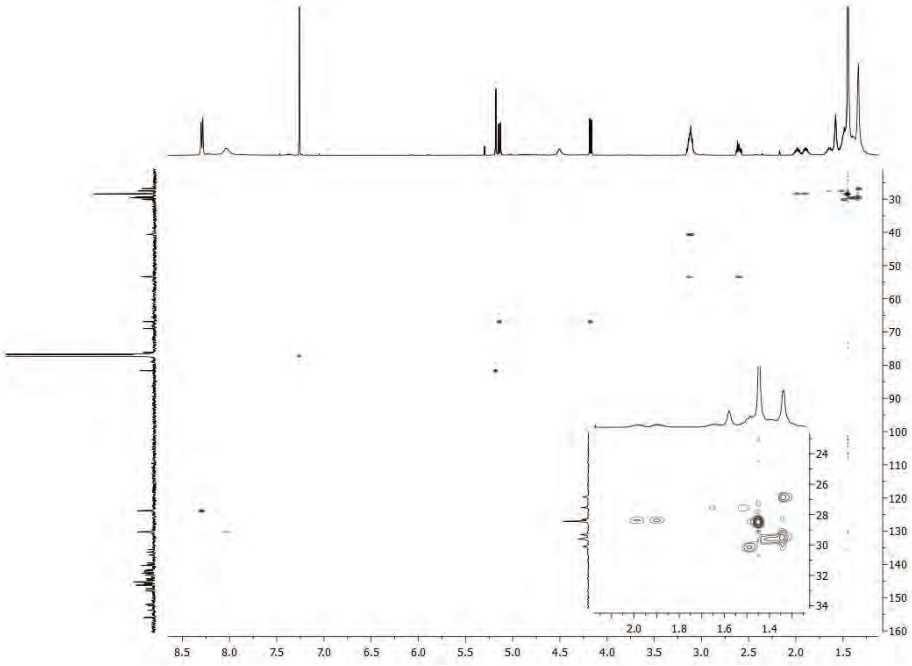

Fig. S-29. HSQC spectrum of **10b**.

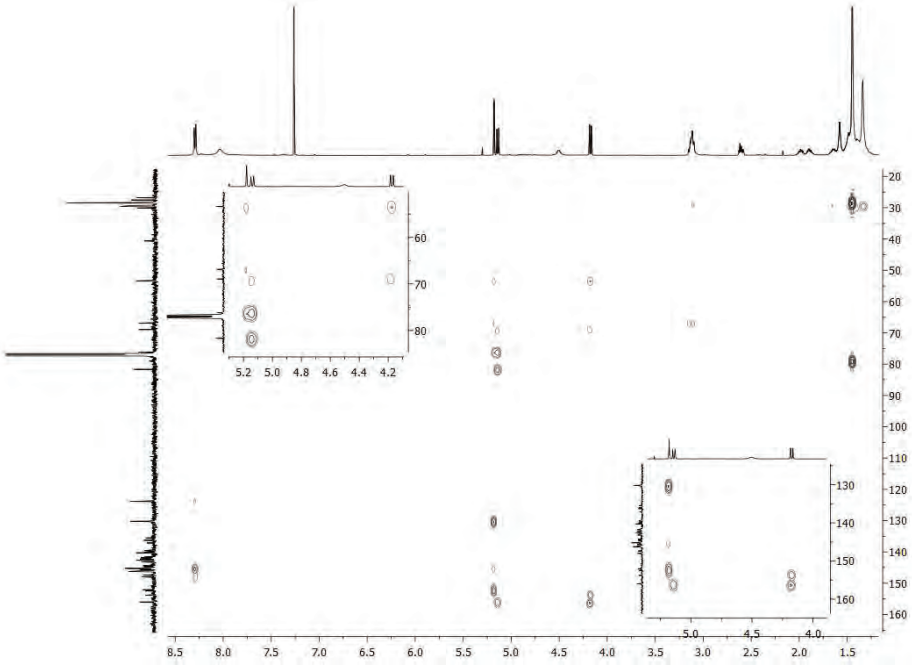

Fig. S-30. HMBC spectrum of **10b**.

Fulleropyrrolidine derivative ***11c***

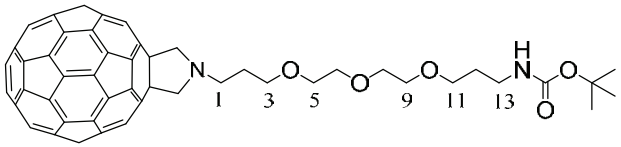

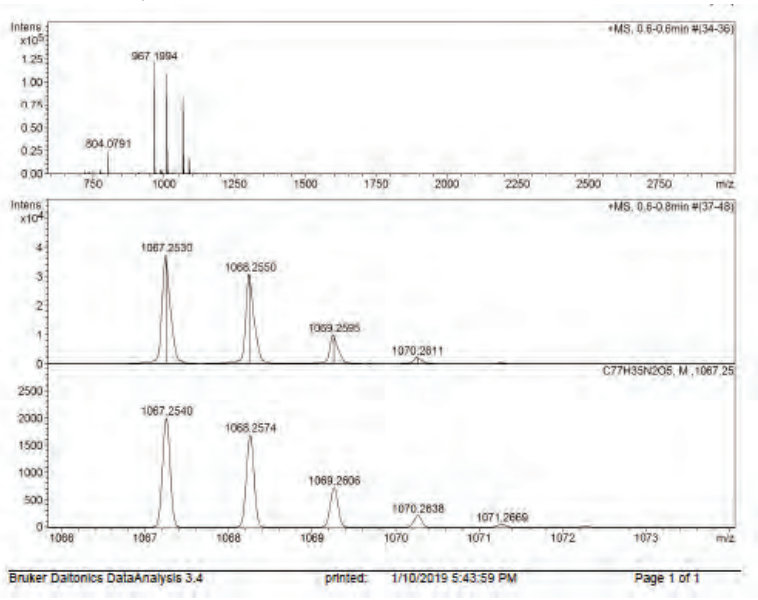

Fig. S-31. Mass spectrum of **11c**.

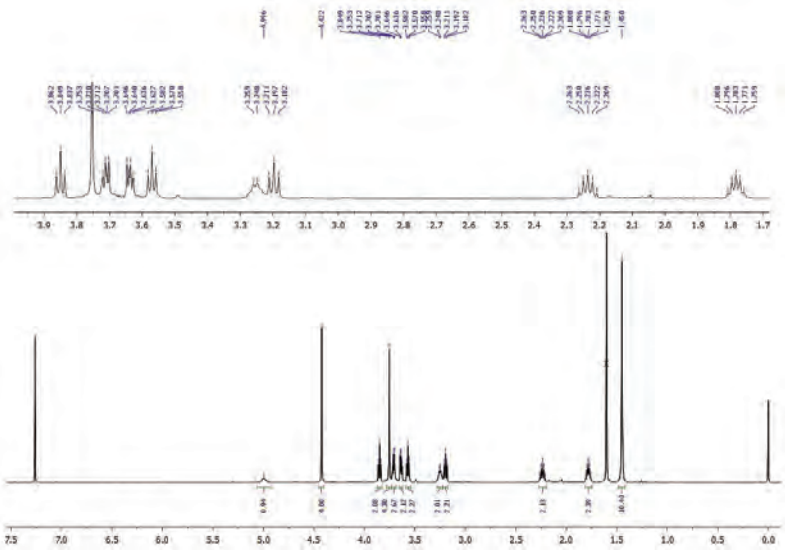

Fig. S-32. ^{1}H-NMR spectrum of **11c**.

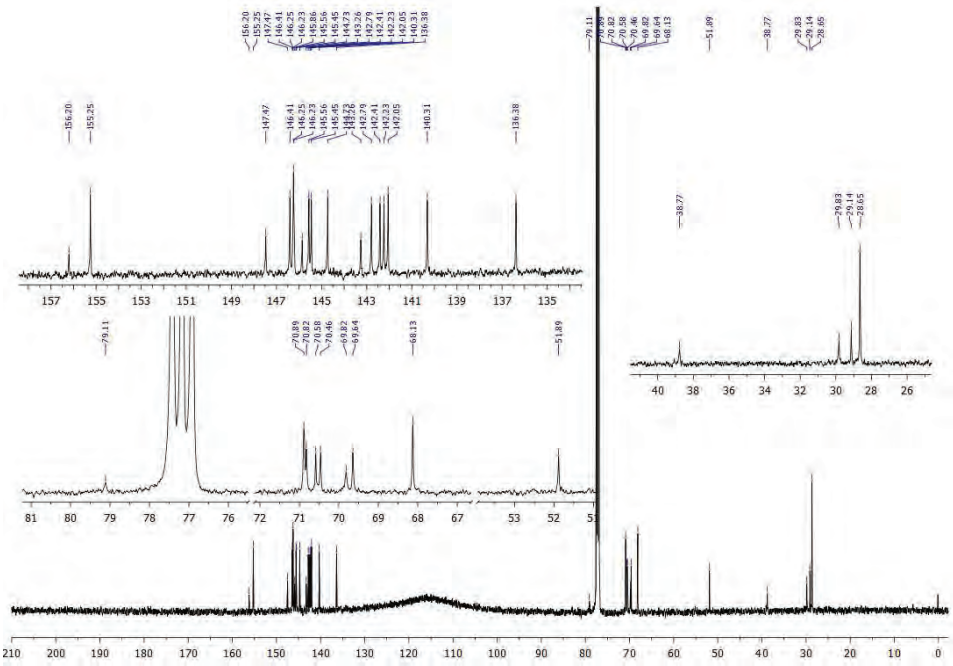

Fig. S-33. ^{13}C-NMR spectrum of **11c**.

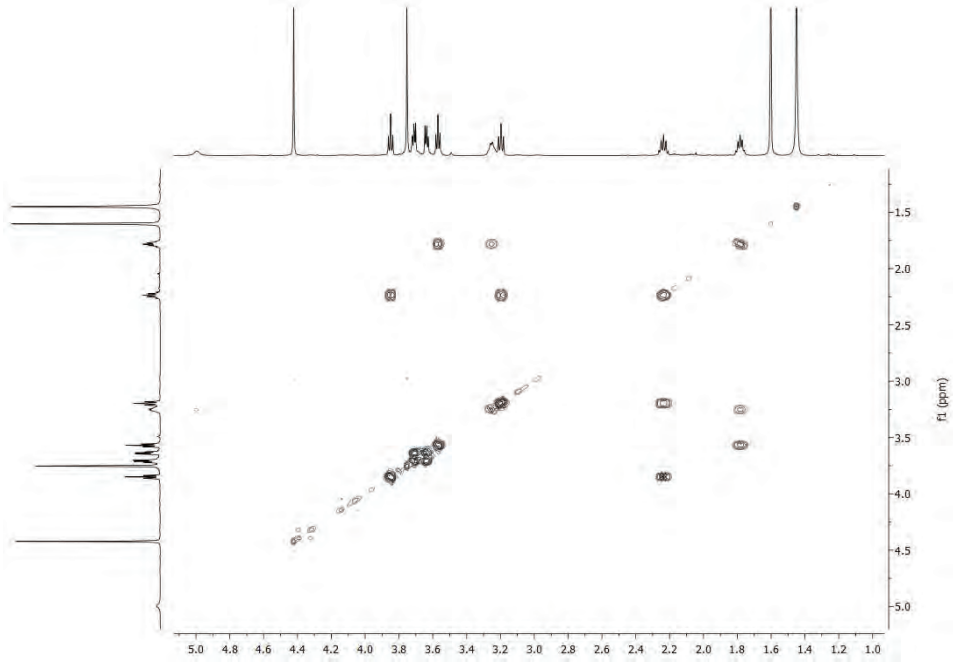

Fig. S-34. COSY spectrum of **11c**.

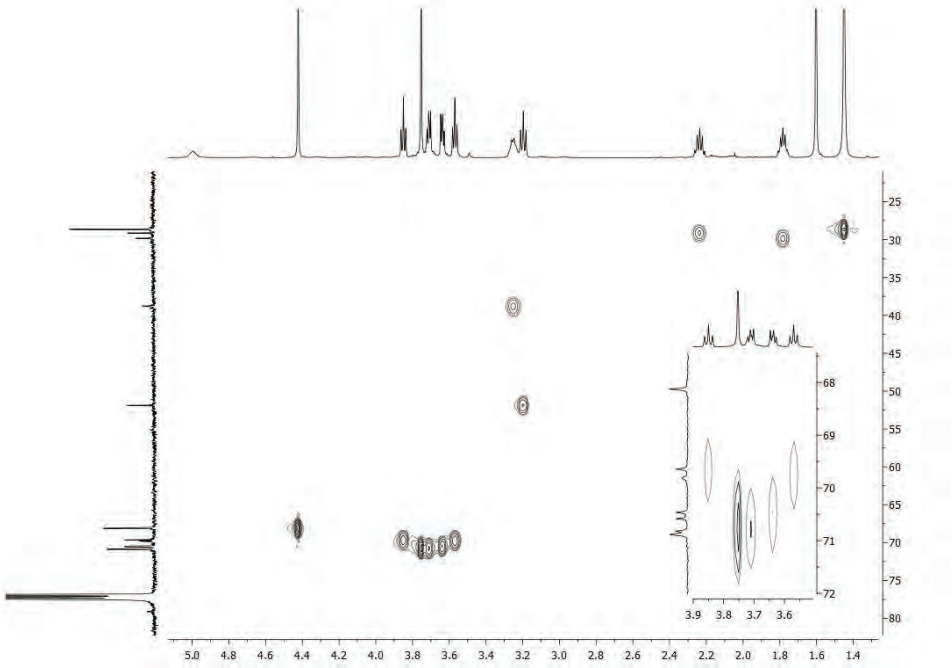

Fig. S-35. HSQC spectrum of **11c**.

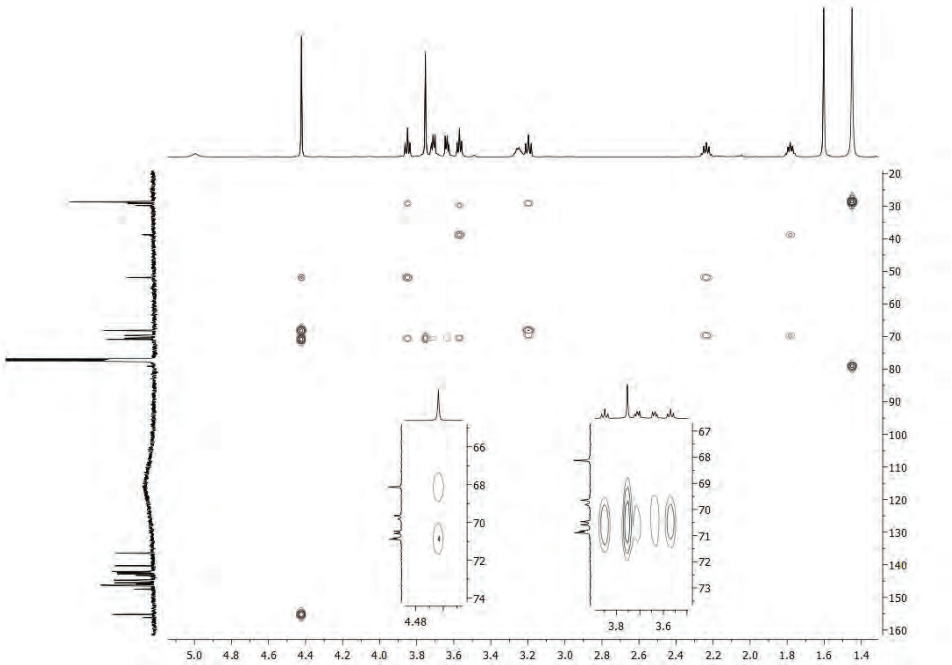

Fig. S-36. HMBC spectrum of **11c**.

Phenyl-substituted fulleropyrrolidine derivative ***12c***

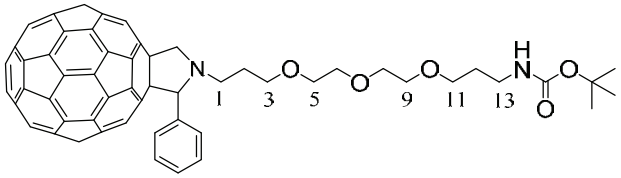

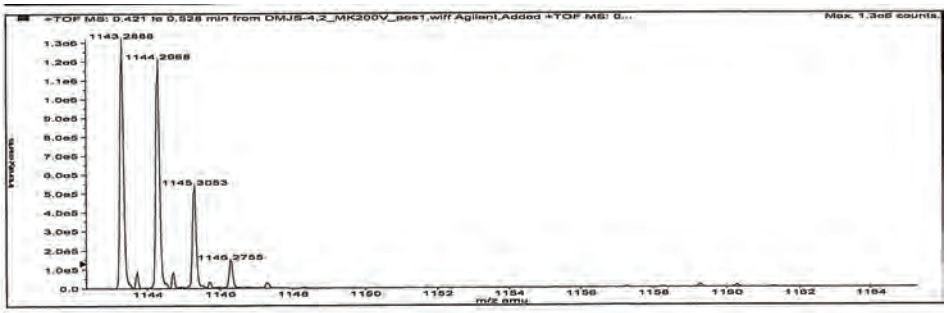

Formula	Compound name	Mass	Peak RT (min)	Peak area	Description
C83H38N2O5	–	1142.27807	0.40	8.52645 E6	–

Species	Abundance (counts)	Ion Mass	Measured Mass	Error (mDa)	Error (ppm)	Ret. Time Error (min)
[M+H]+	1319795.11	1143.28535	1143.28570	0.34878	0.31	–

Fig. S-37. Mass spectrum of **12c**.

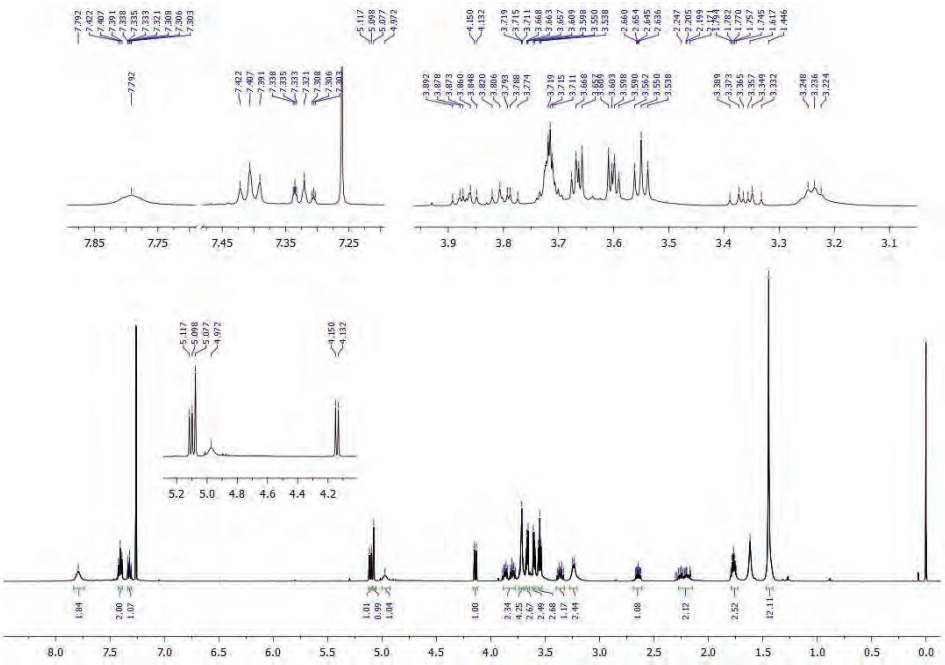

Fig. S-38. ^{1}H-NMR spectrum of **12c**.

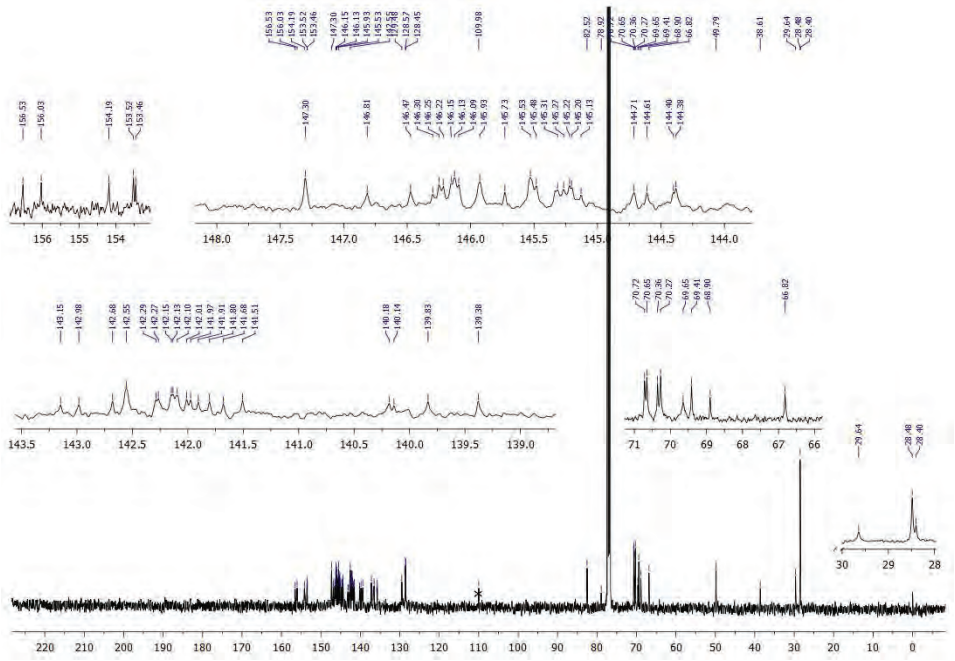

Fig. S-39. ^{13}C-NMR spectrum of **12c**.

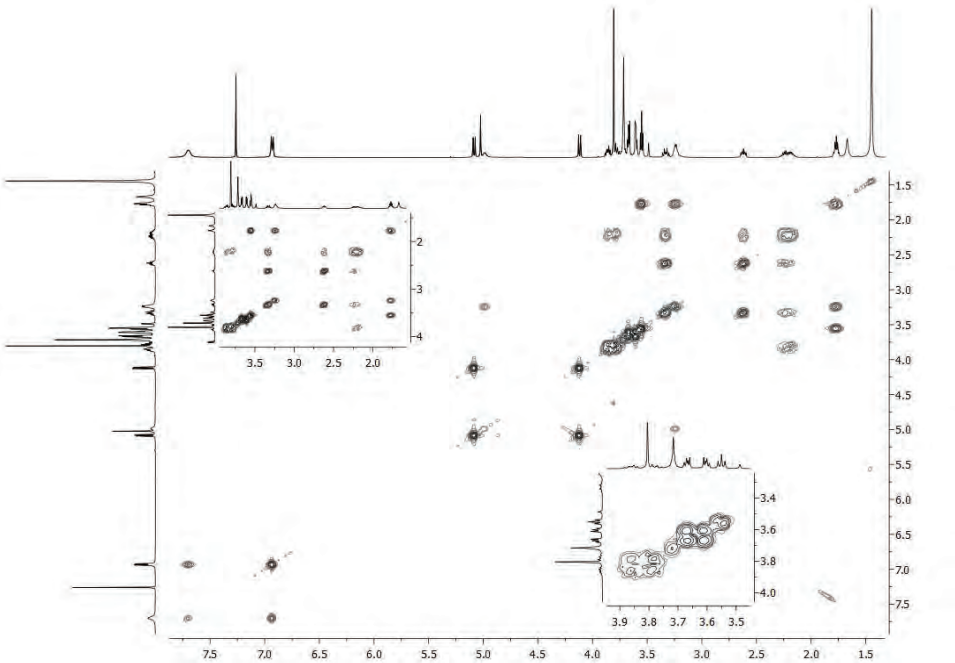

Fig. S-40. COSY spectrum of **12c**.

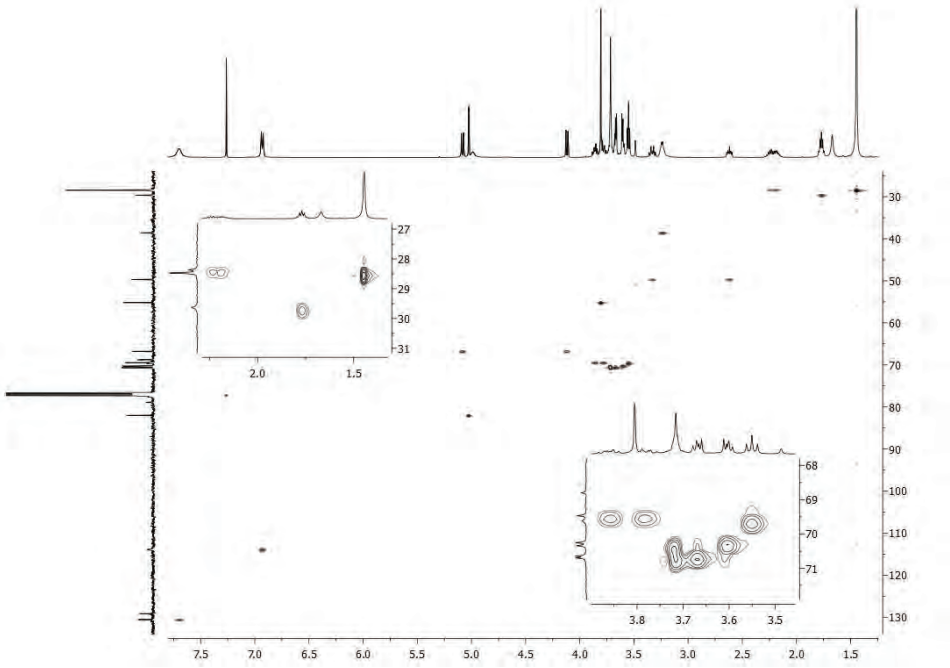

Fig. S-41. HSQC spectrum of **12c**.

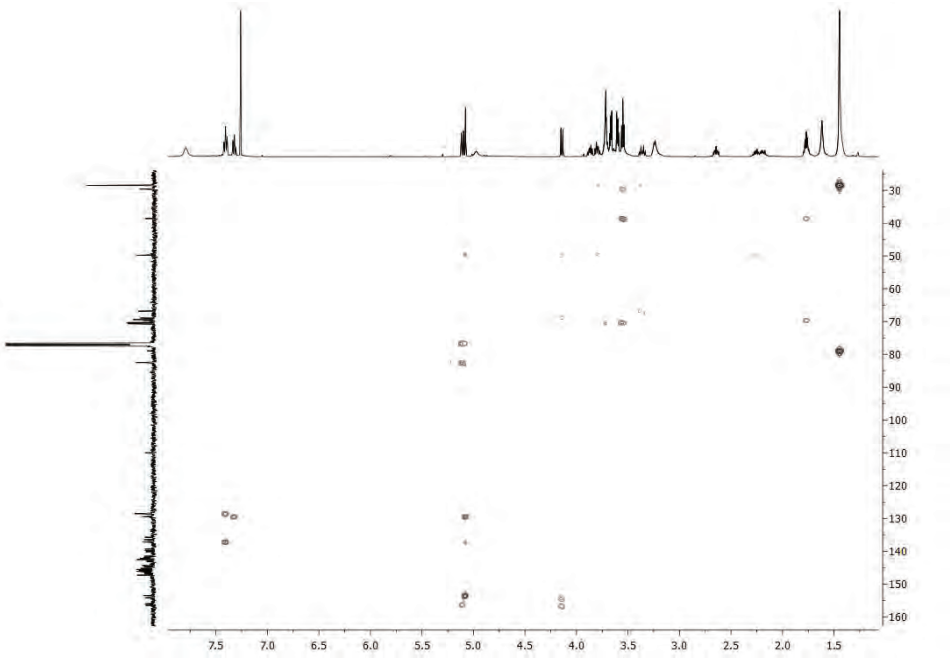

Fig. S-42. HMBC spectrum of **12c**.

*2-Methoxyphenyl-substituted fulleropyrrolidine derivative **13c***

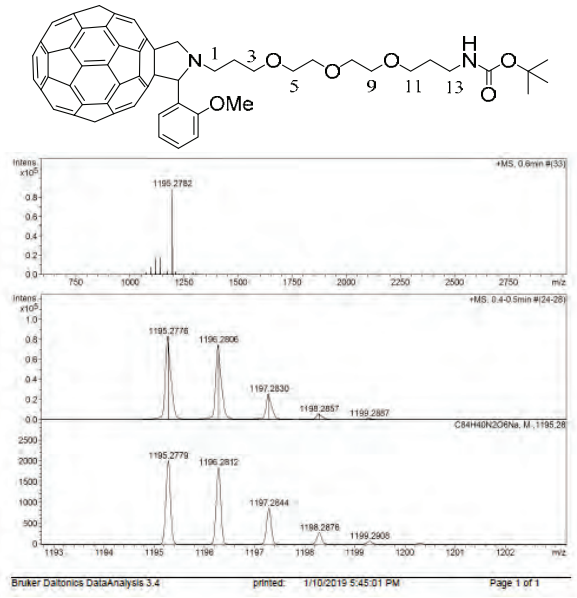

Fig. S-43. Mass spectrum of **13c**.

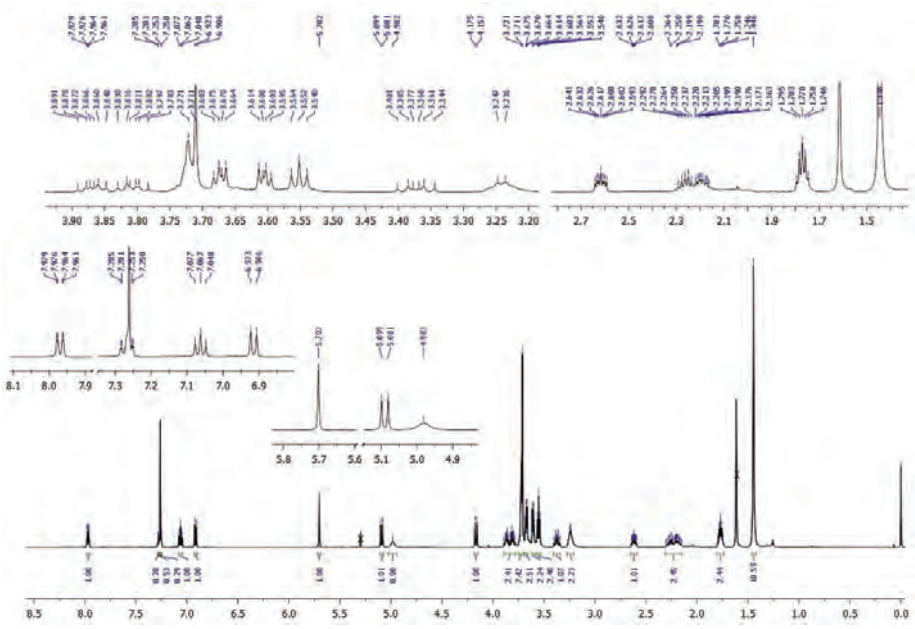

Fig. S-44. ^{1}H-NMR spectrum of **13c**.

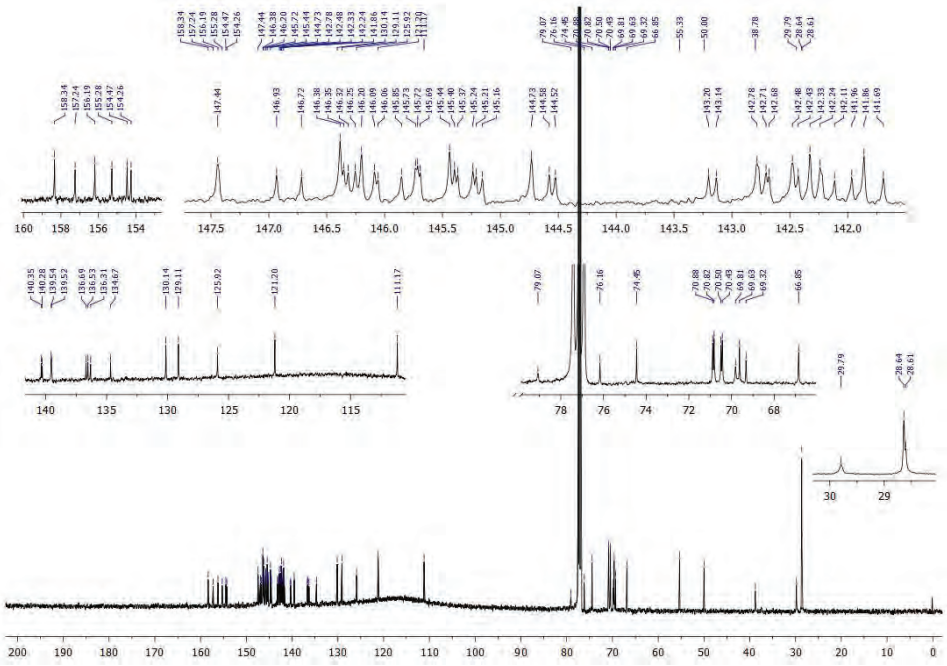

Fig. S-45. ^{13}C-NMR spectrum of **13c**.

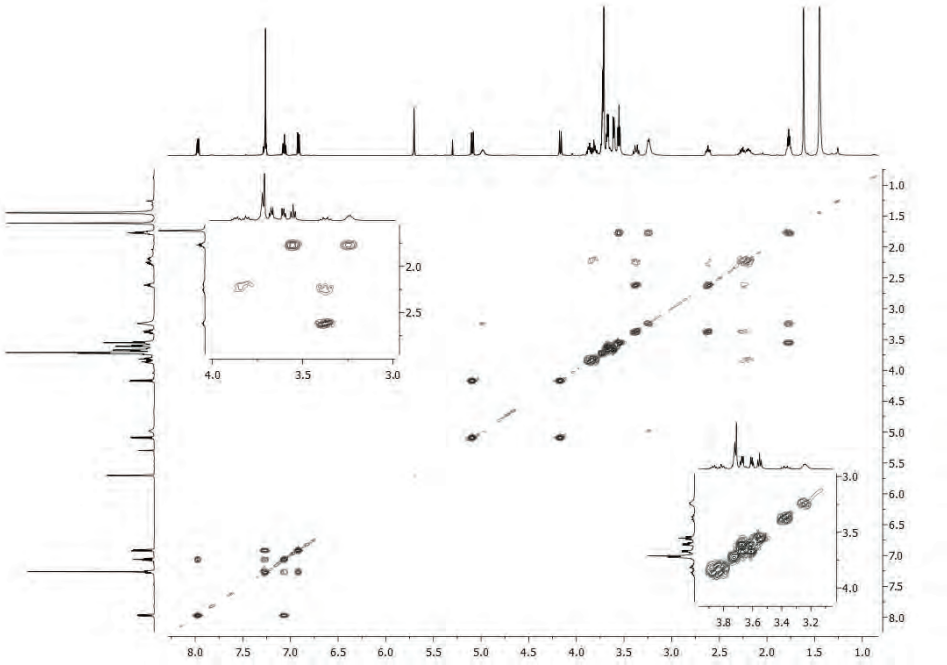

Fig. S-46. COSY spectrum of **13c**.

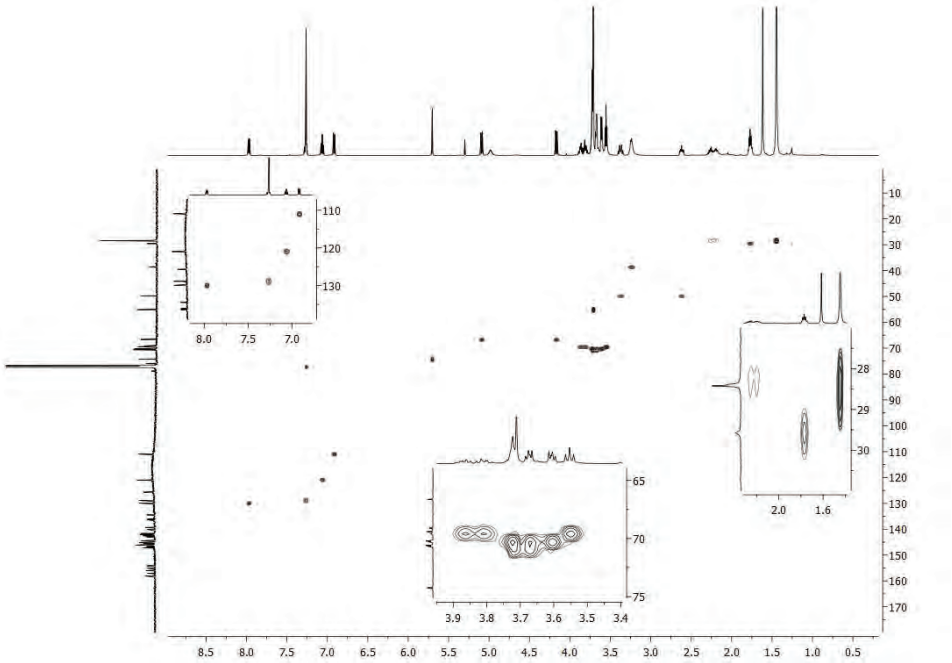

Fig. S-47. HSQC spectrum of **13c**.

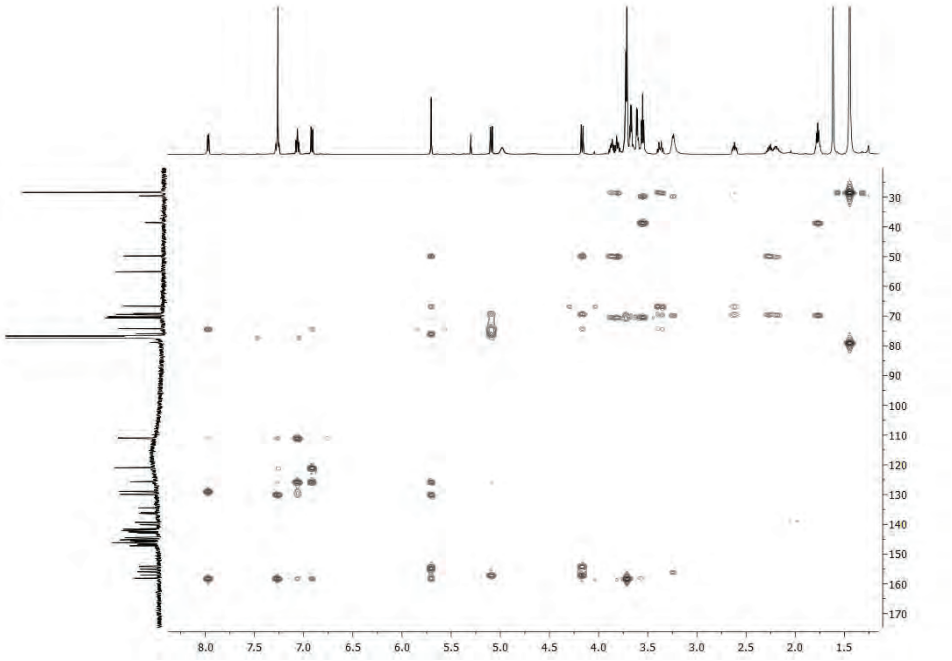

Fig. S-48. HMBC spectrum of **13c**.

3-Methoxyphenyl-substituted fulleropyrrolidine derivative ***14c***

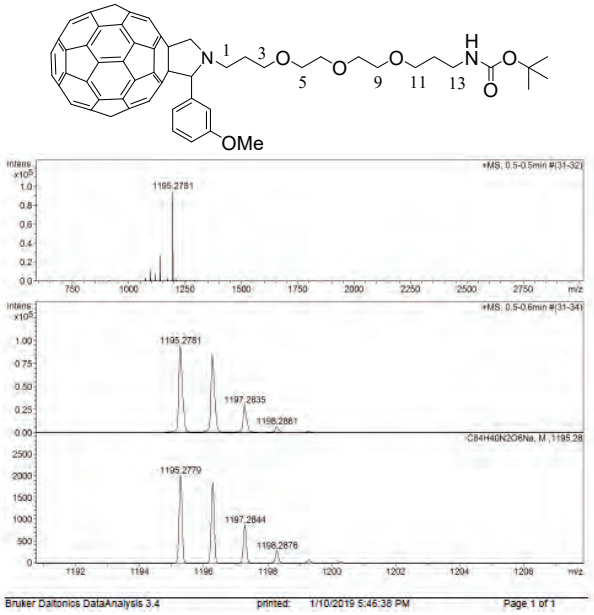

Fig. S-49. Mass spectrum of **14c**.

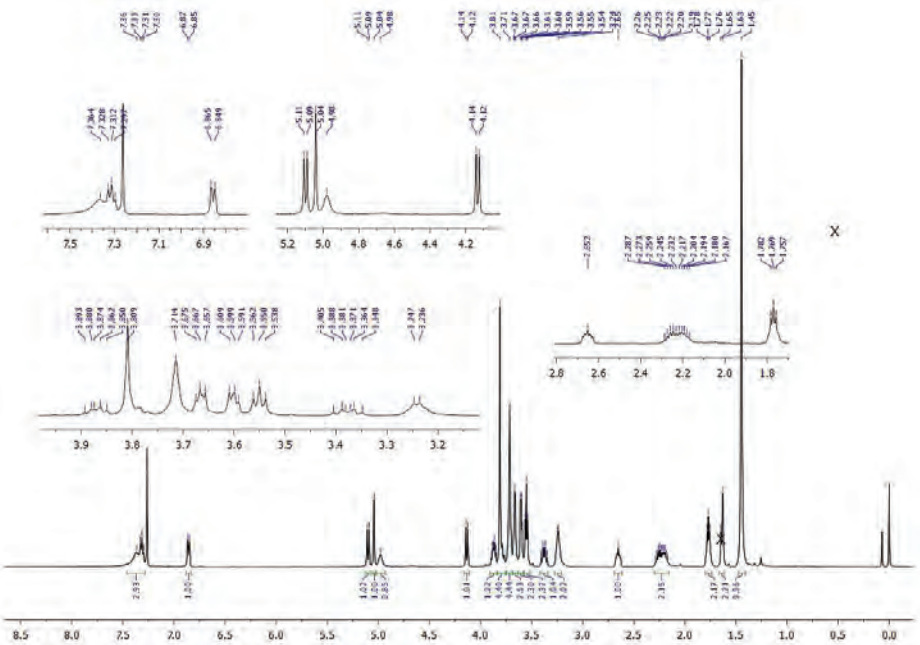

Fig. S-50. ^{1}H-NMR spectrum of **14c**.

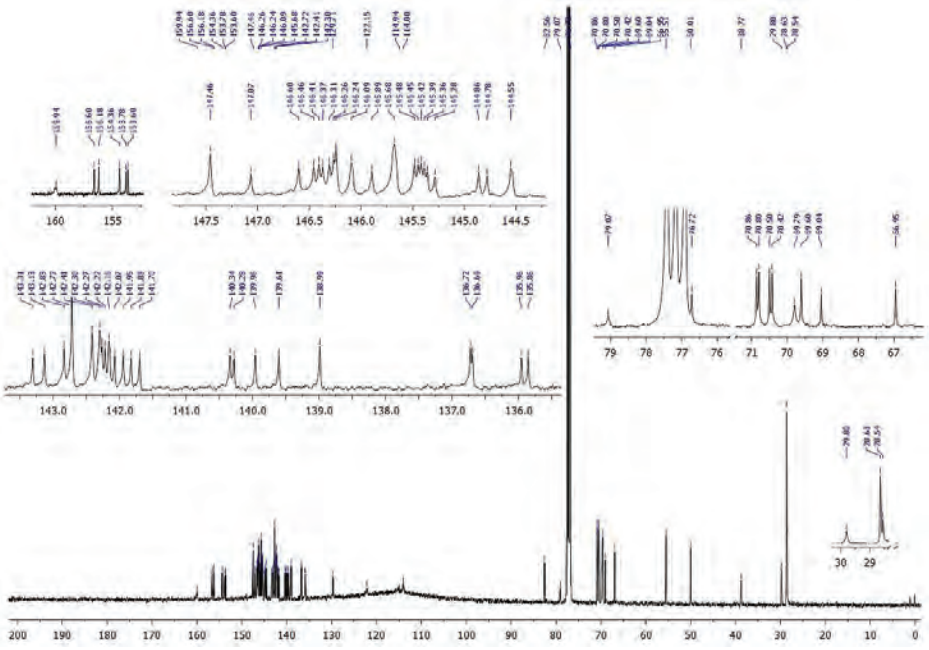

Fig. S-51. ^{13}C-NMR spectrum of **14c**.

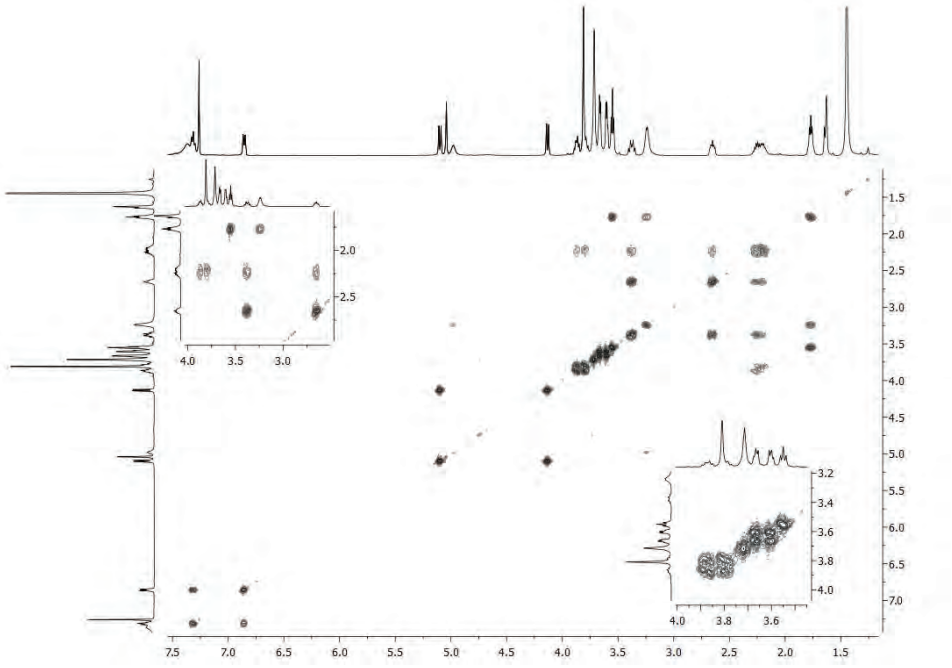

Fig. S-52. COSY spectrum of **14c**.

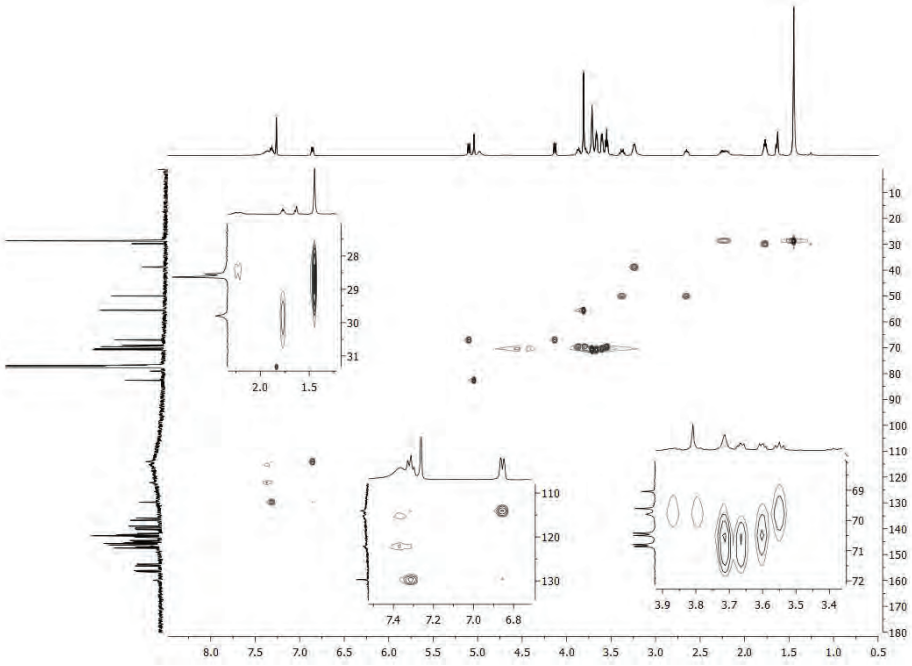

Fig. S-53. HSQC spectrum of **14c**.

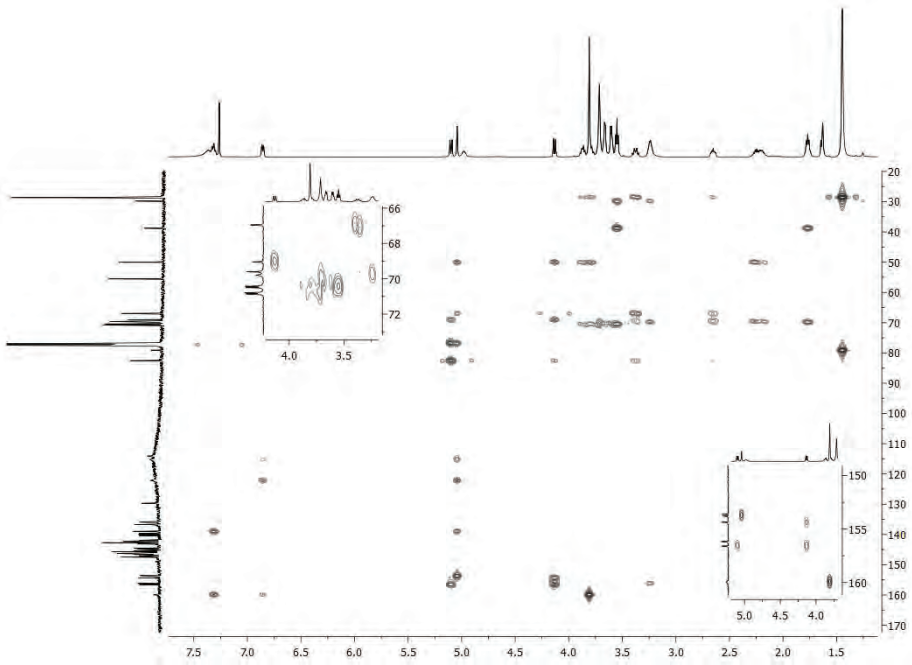

Fig. S-54. HMBC spectrum of **14c**.

4-Methoxyphenyl-substituted fulleropyrrolidine derivative ***15c***

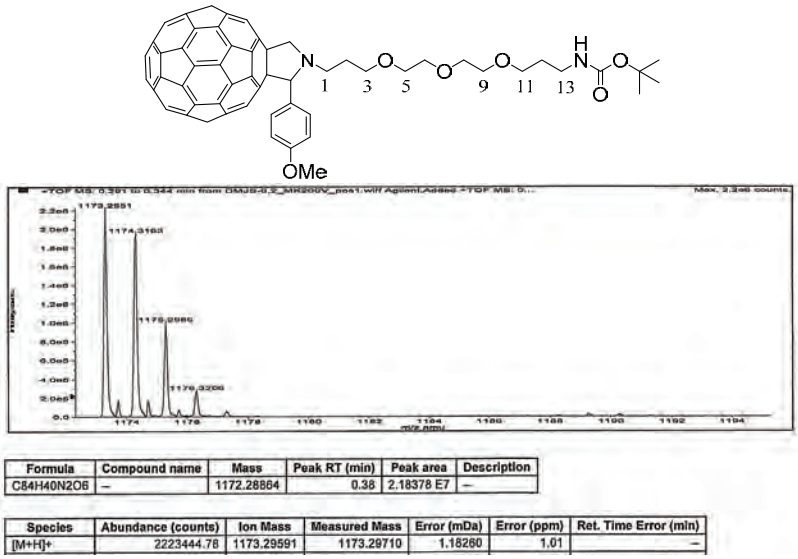

Formula	Compound name	Mass	Peak RT (min)	Peak area	Description
C84H40N2O6	–	1172.28864	0.38	2.18378 E7	–

Species	Abundance (counts)	Ion Mass	Measured Mass	Error (mDa)	Error (ppm)	Ret. Time Error (min)
[M+H]+	2223444.78	1173.29591	1173.29710	1.18260	1.01	–

Fig. S-55. Mass spectrum of **15c**.

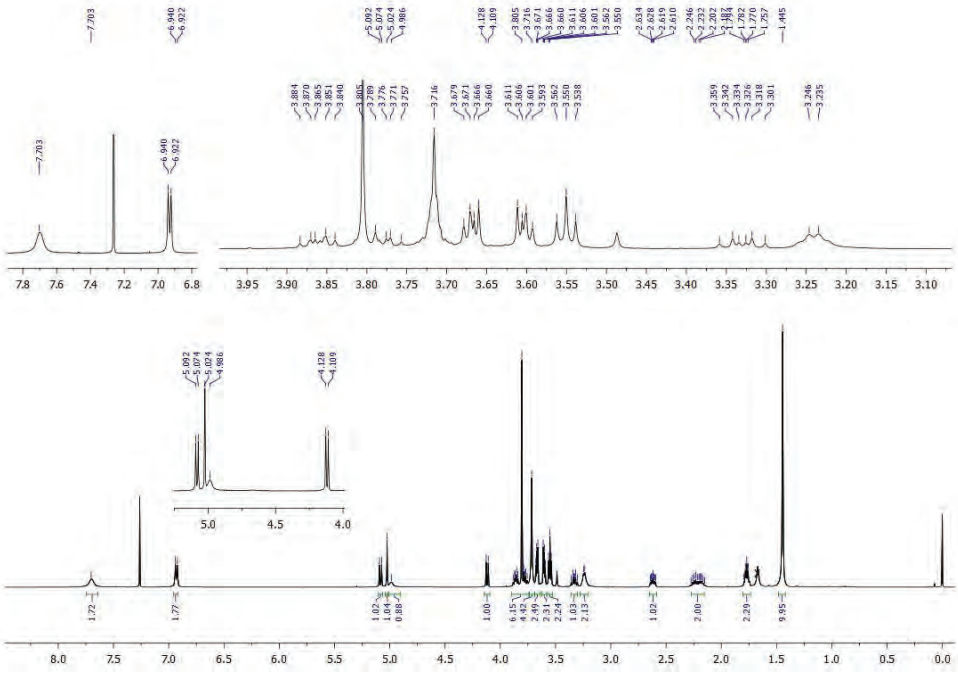

Fig. S-56. ^{1}H-NMR spectrum of **15c**.

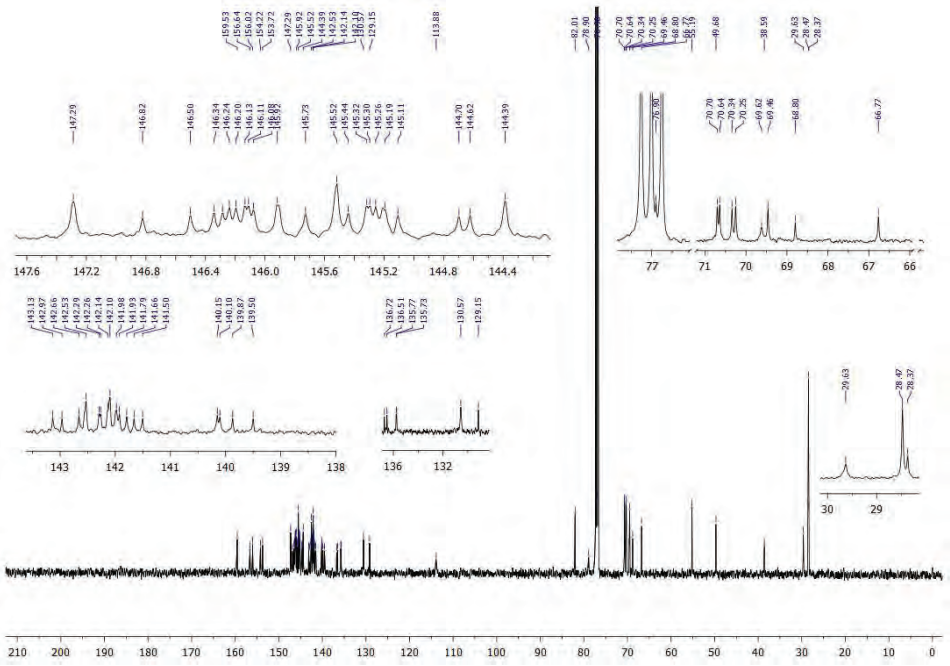

Fig. S-57. ^{13}C-NMR spectrum of **15c**.

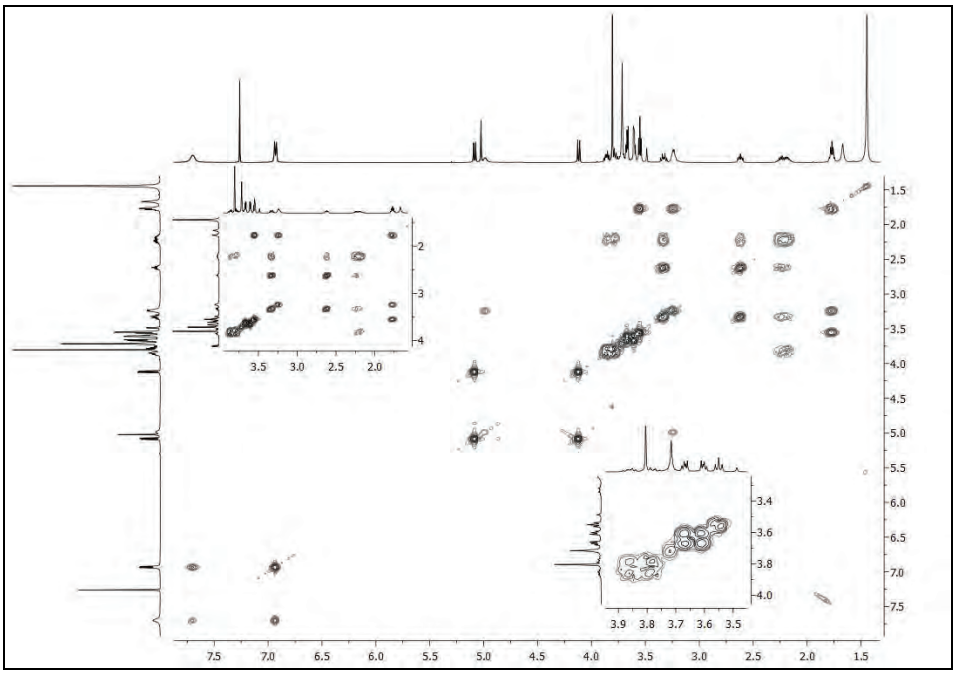

Fig. S-58. COSY spectrum of **15c**.

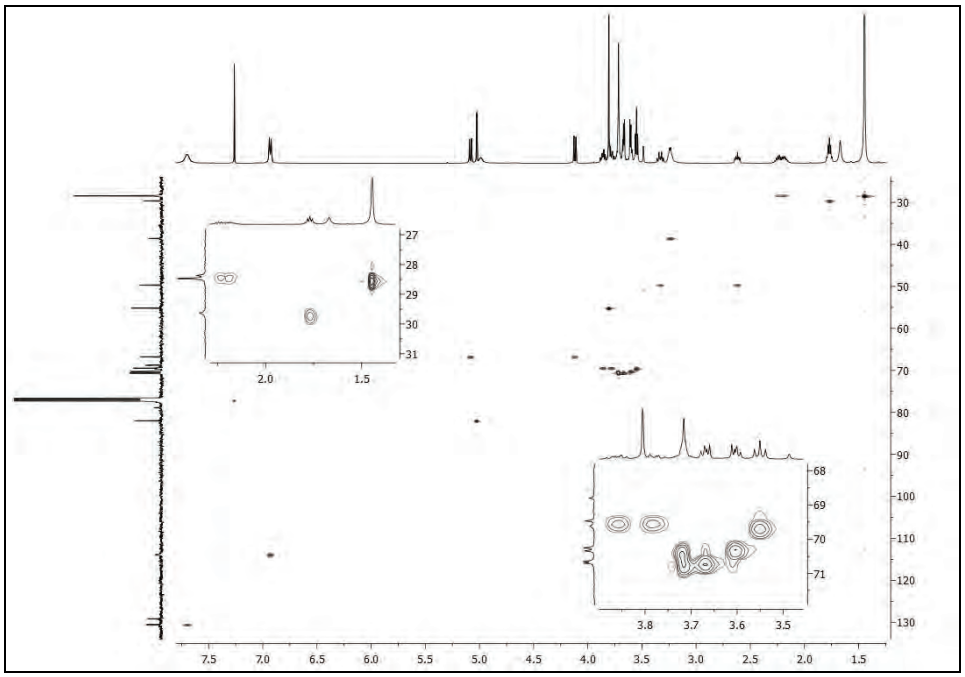

Fig. S-59. HSQC spectrum of **15c**.

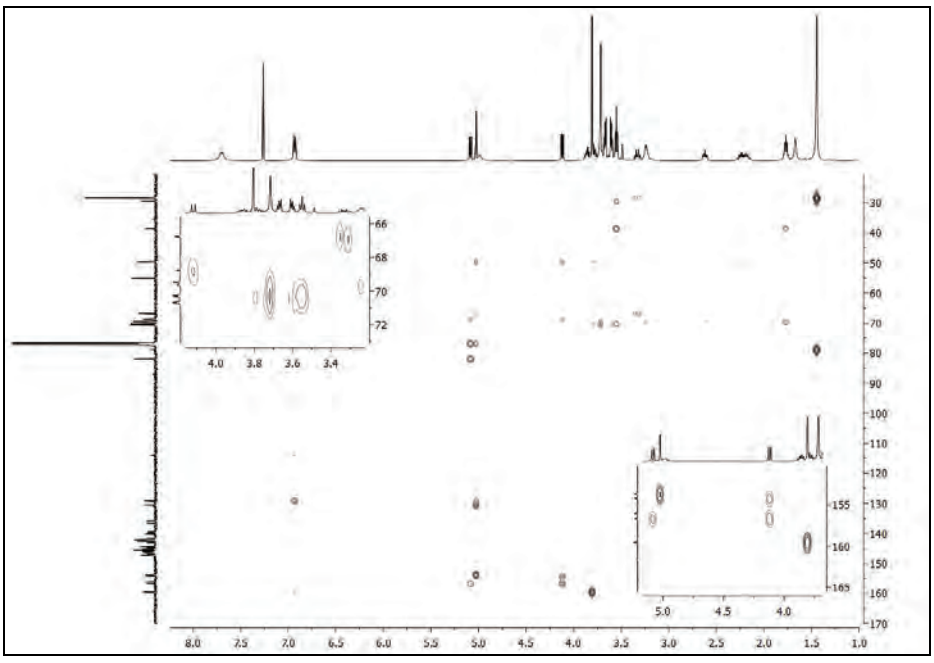

Fig. S-60. HMBC spectrum of **15c**.

Attempts to prepare 2-nitrophenyl-substituted fulleropyrrolidine derivative ***16c*** *(see Experimental part)*

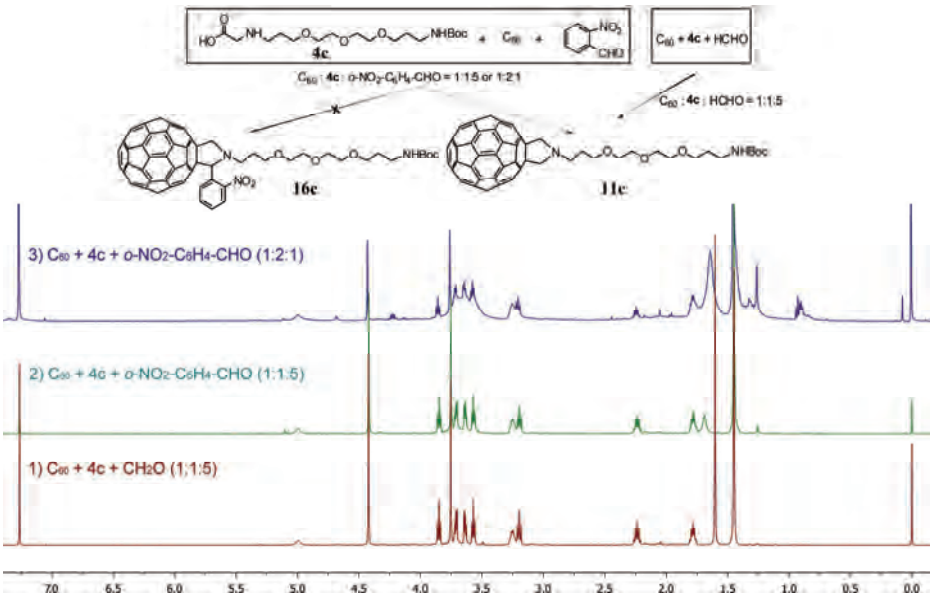

Fig. S-61. Comparison of the ^{1}H-NMR spectra of a same product (**11c**) obtained in the Prato reaction of C_{60} with amino acid **4c** and 2-nitrobenzaldehyde in different relative ratios [2) molar ratio of C_{60}:**4c**:2-nitrobenzaldehyde 1:1:5, reflux; 3) molar ratio of C_{60}:**4c**:2-nitrobenzaldehyde 1:2:1, 100 °C], and with paraformaldehyde [1) molar ratio of C_{60}:**4c**:paraformaldehyde 1:1:5, reflux].

3-Nitrophenyl-substituted fulleropyrrolidine derivative ***17c***

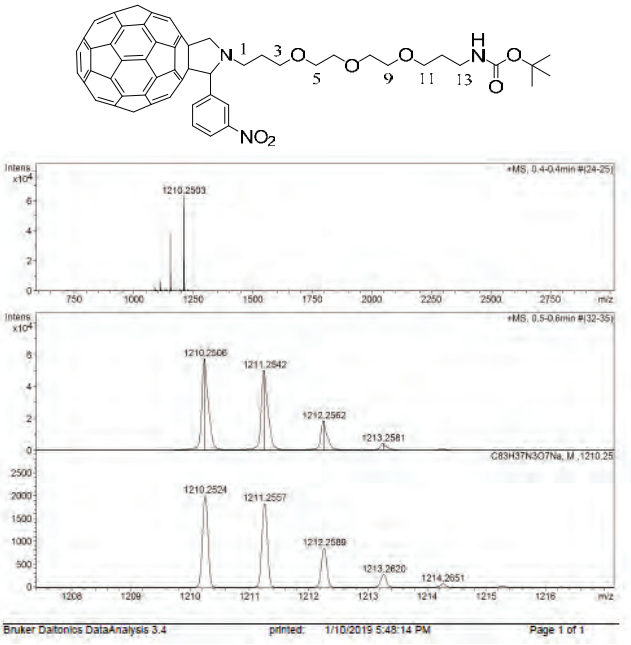

Fig. S-62. Mass spectrum of **17c**.

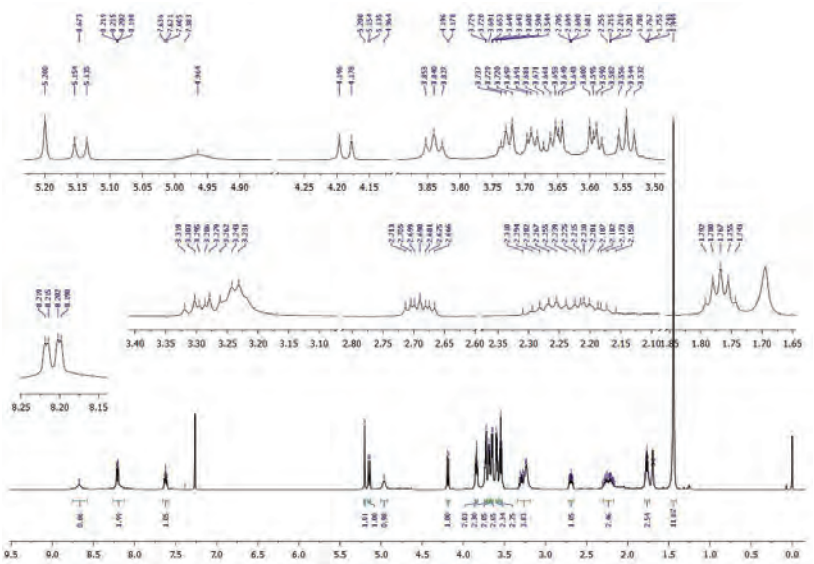

Fig. S-63. ^{1}H-NMR spectrum of **17c**.

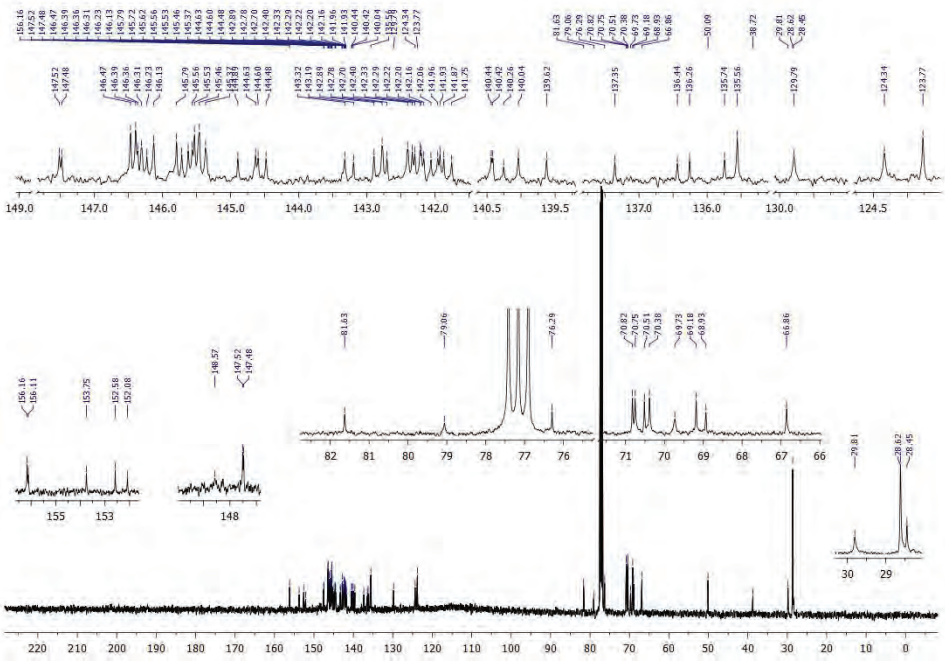

Fig. S-64. ^{13}C-NMR spectrum of **17c**.

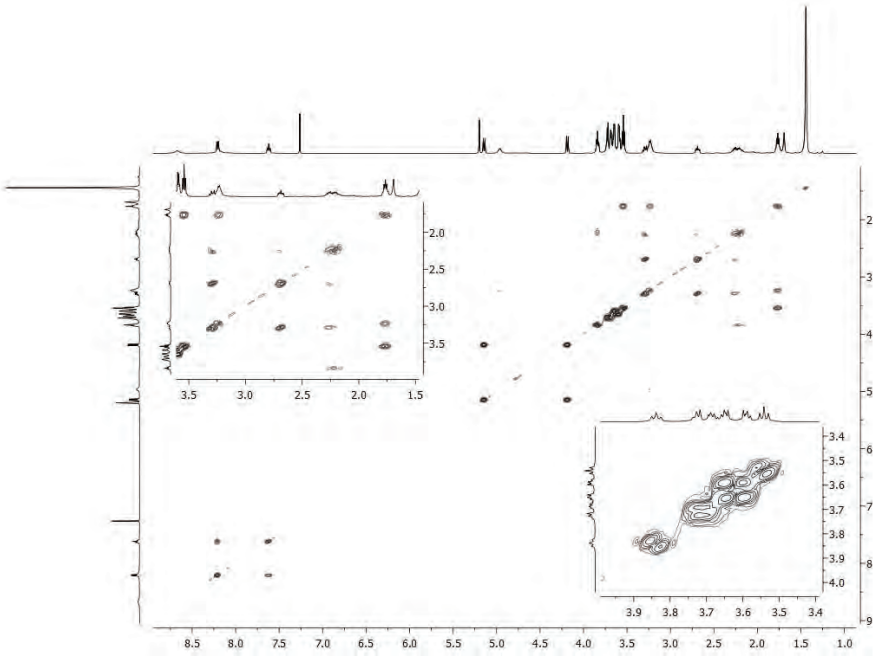

Fig. S-65. COSY spectrum of **17c**.

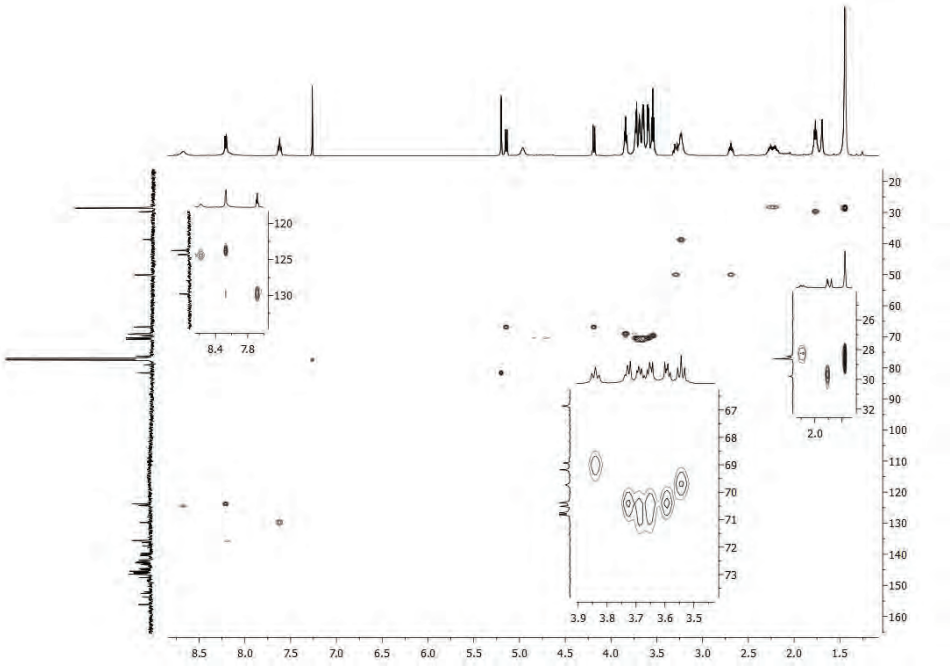

Fig. S-66. HSQC spectrum of **17c**.

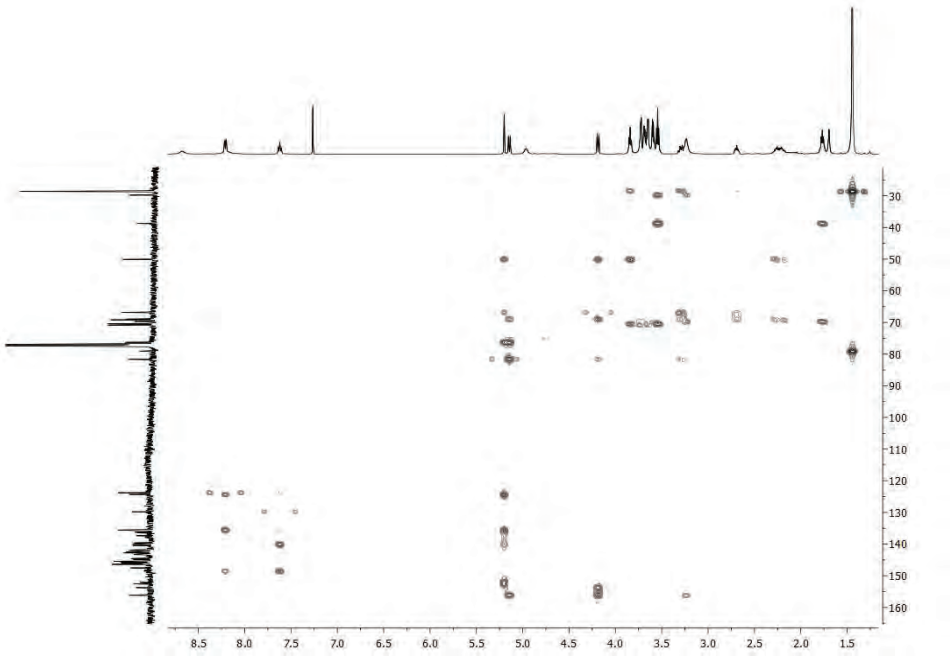

Fig. S-67. HMBC spectrum of **17c**.

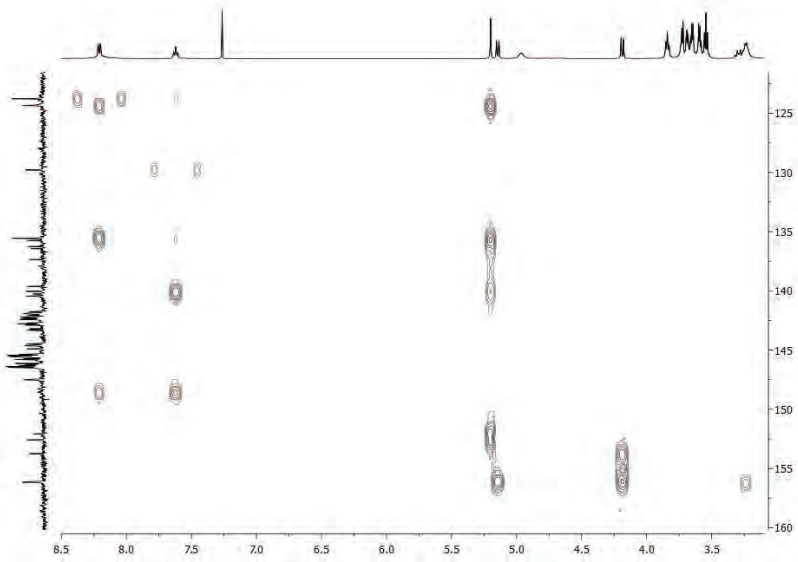

Fig. S-68. Part of the HMBC spectrum of **17c**.

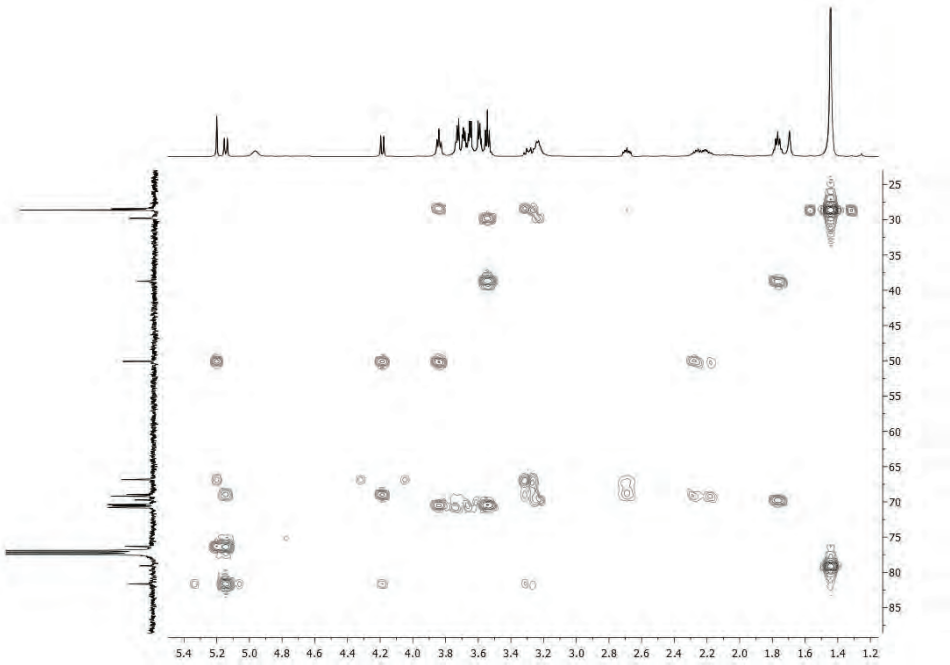

Fig. S-69. Part of the HMBC spectrum of **17c**.

4-Nitrophenyl-substituted fulleropyrrolidine derivative ***18c***

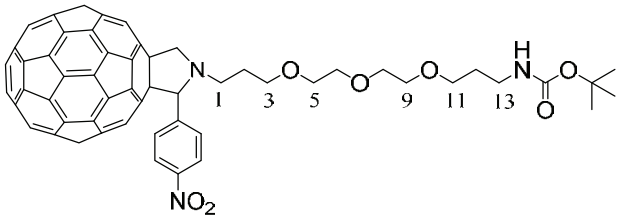

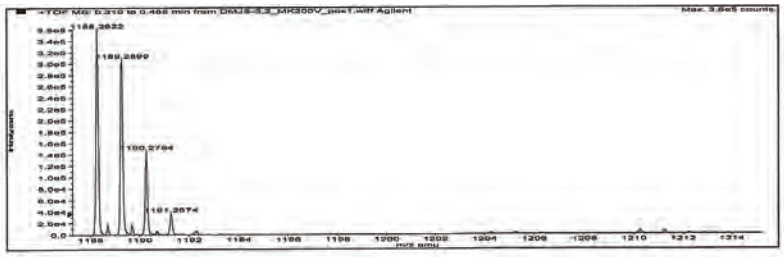

Formula	Compound name	Mass	Peak RT (min)	Peak area	Description
C83H37N3O7	–	1187.26315	0.39	4.46294 E6	–

Species	Abundance (counts)	Ion Mass	Measured Mass	Error (mDa)	Error (ppm)	Ret. Time Error (min)
[M+H]+	363811.92	1188.27043	1188.26888	-1.54909	-1.30	–

Fig. S-70. Mass spectrum of **18c**

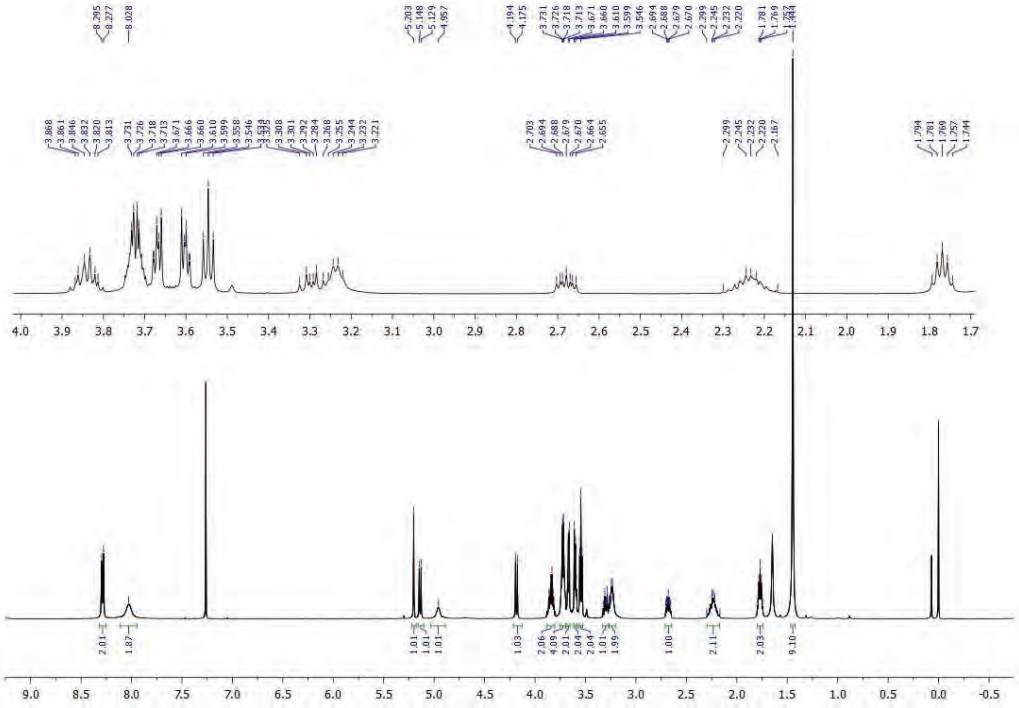

Fig. S-71. ^{1}H-NMR spectrum of **18c**.

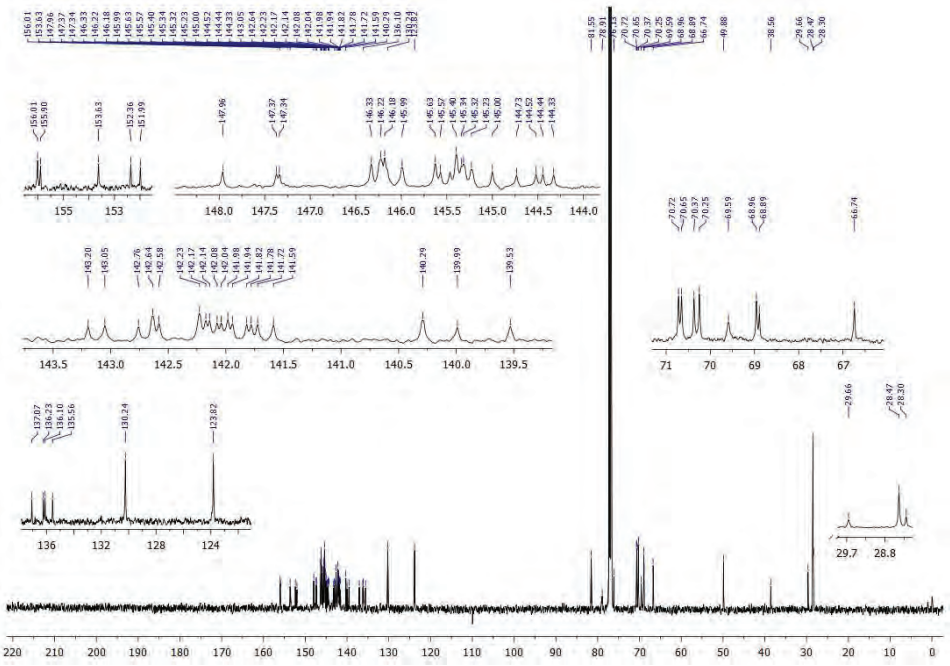

Fig. S-72. ^{13}C-NMR spectrum of **18c**.

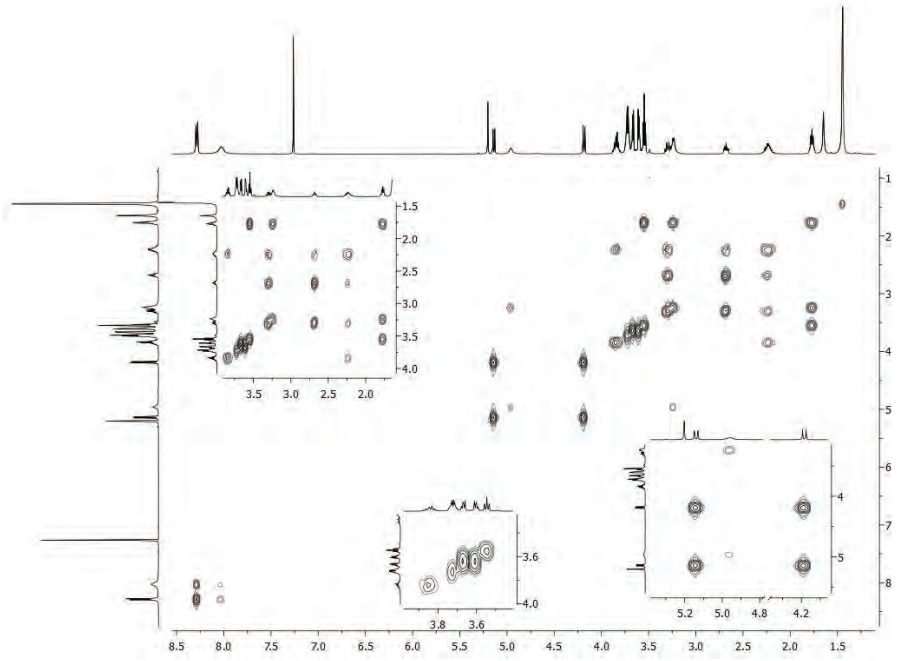

Fig. S-73. COSY spectrum of **18c**.

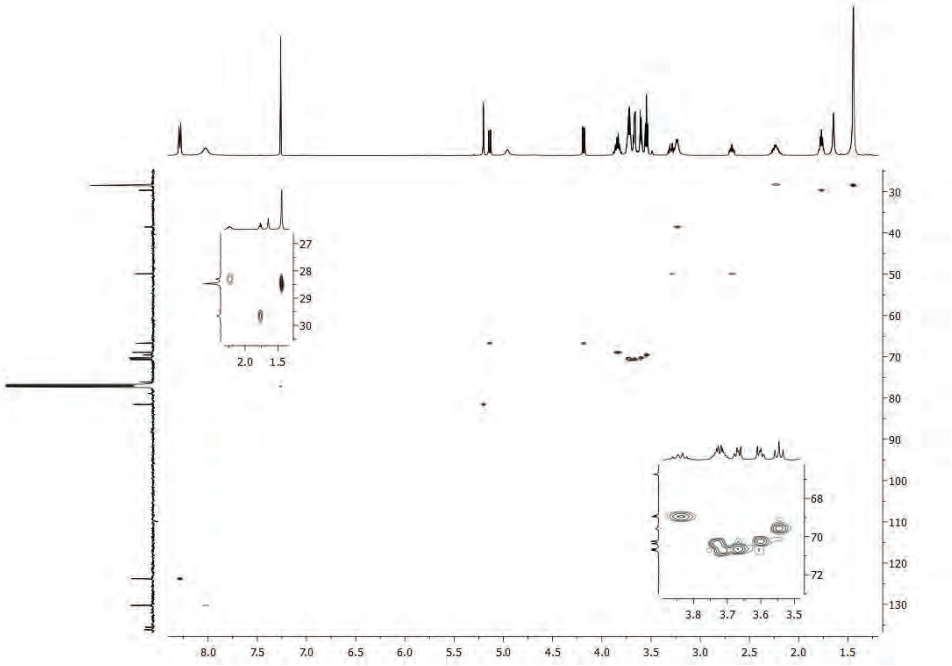

Fig. S-74. HSQC spectrum of **18c**.

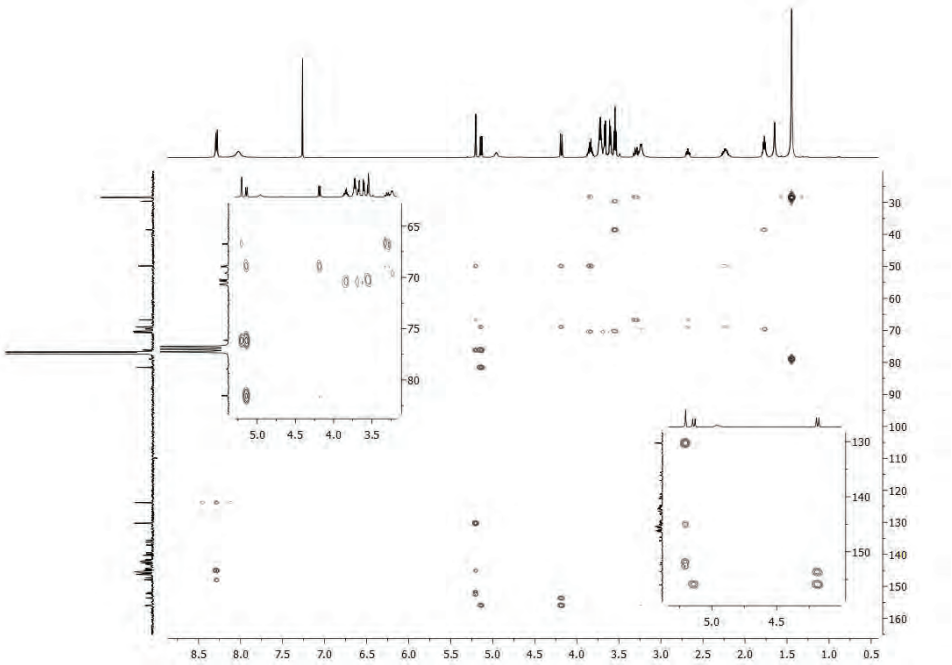

Fig. S-75. HMBC spectrum of **18c**.

Diamide ***19a***

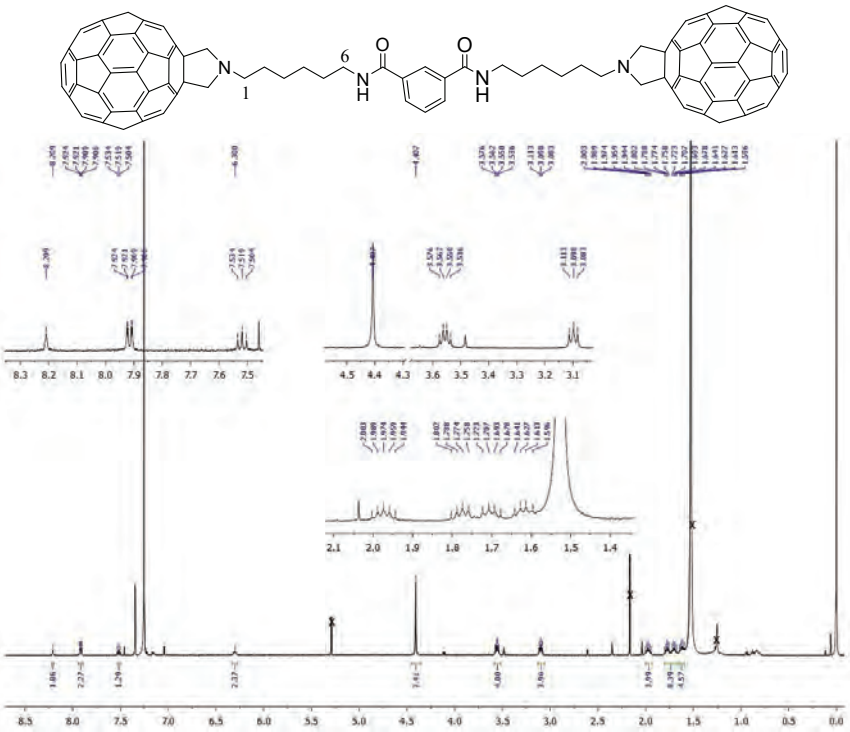

Fig. S-76. ^{1}H-NMR spectrum of **19a**.

*Diamide **20a***

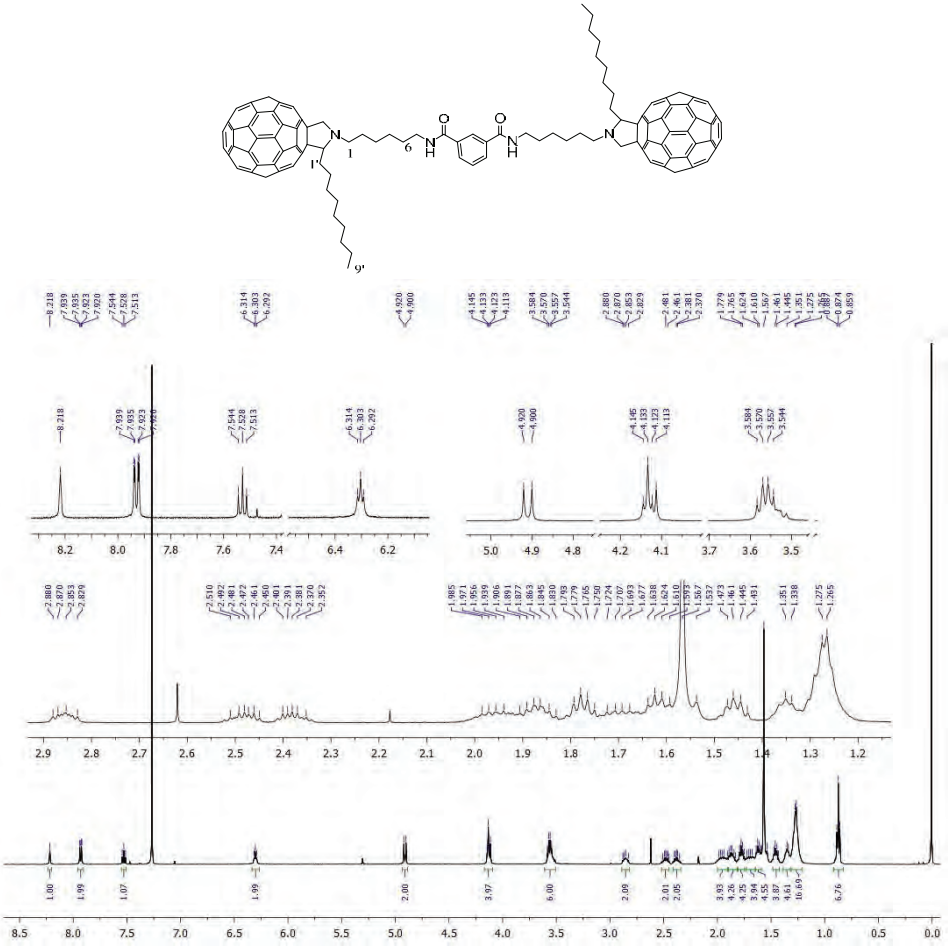

Fig. S-77. ^{1}H-NMR spectrum of **20a**.

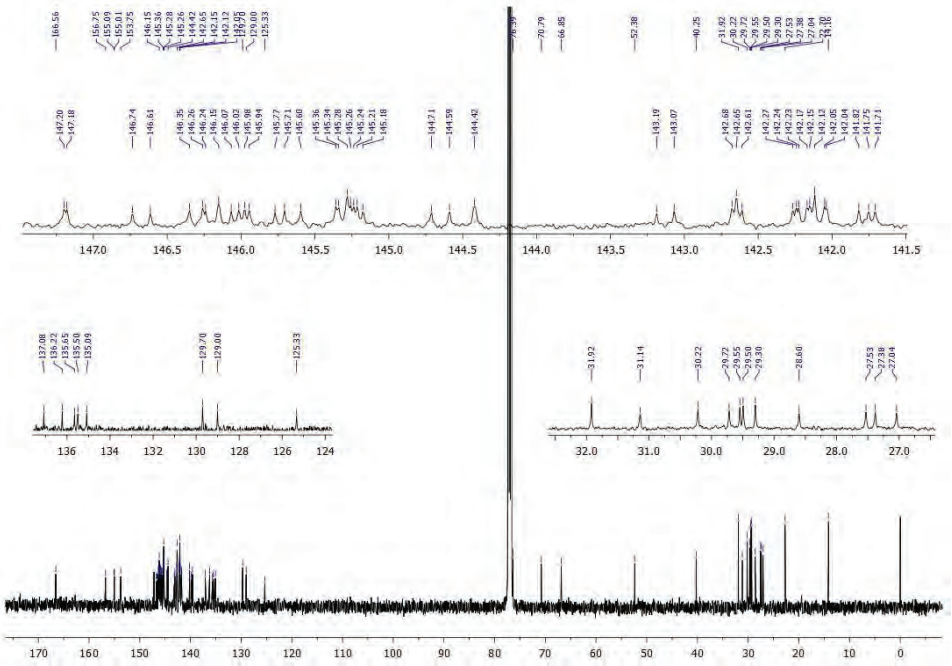

Fig. S-78. ^{13}C-NMR spectrum of **20a**.

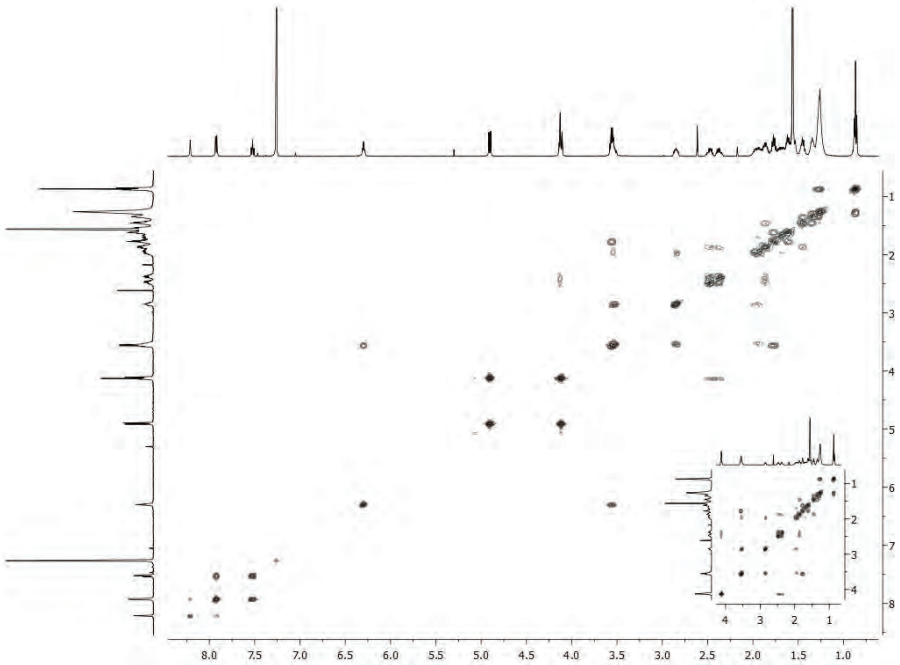

Fig. S-79. COSY spectrum of **20a**.

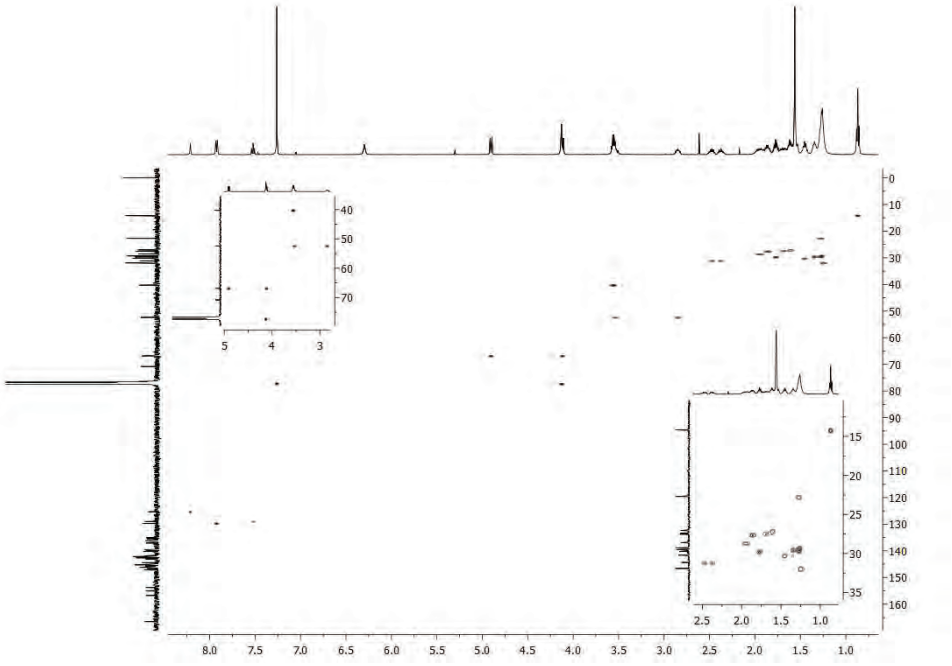

Fig. S-80. HSQC spectrum of **20a**.

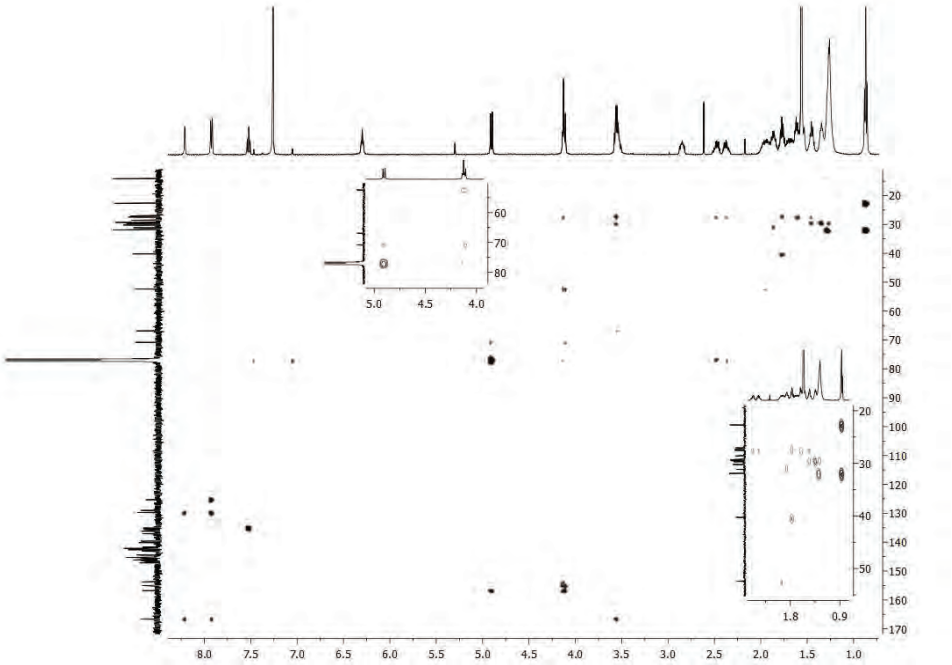

Fig. S-81. HMBC spectrum of **20a**.

*Diamide **21a***

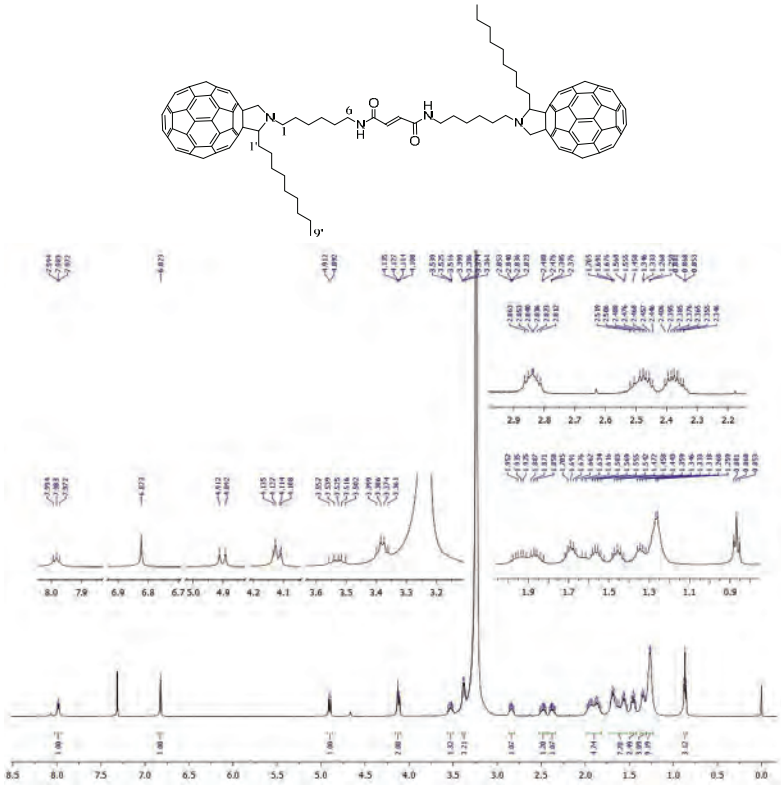

Fig. S-82. ^{1}H-NMR spectrum of **21a**.

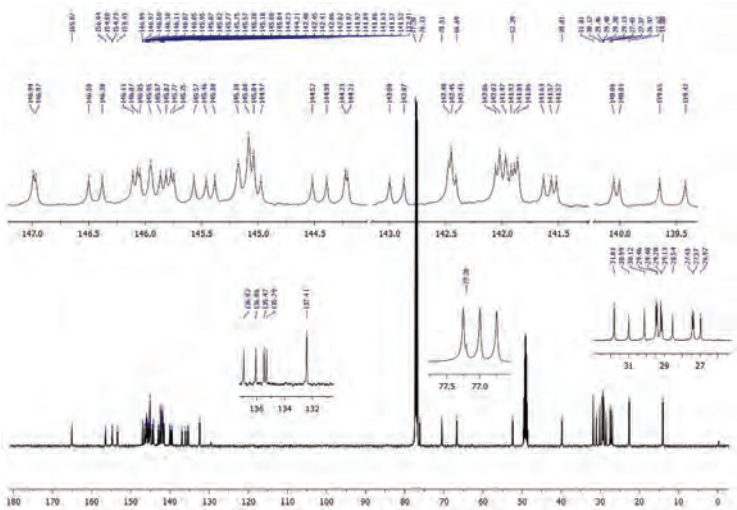

Fig. S-83. ^{13}C-NMR spectrum of **21a**.

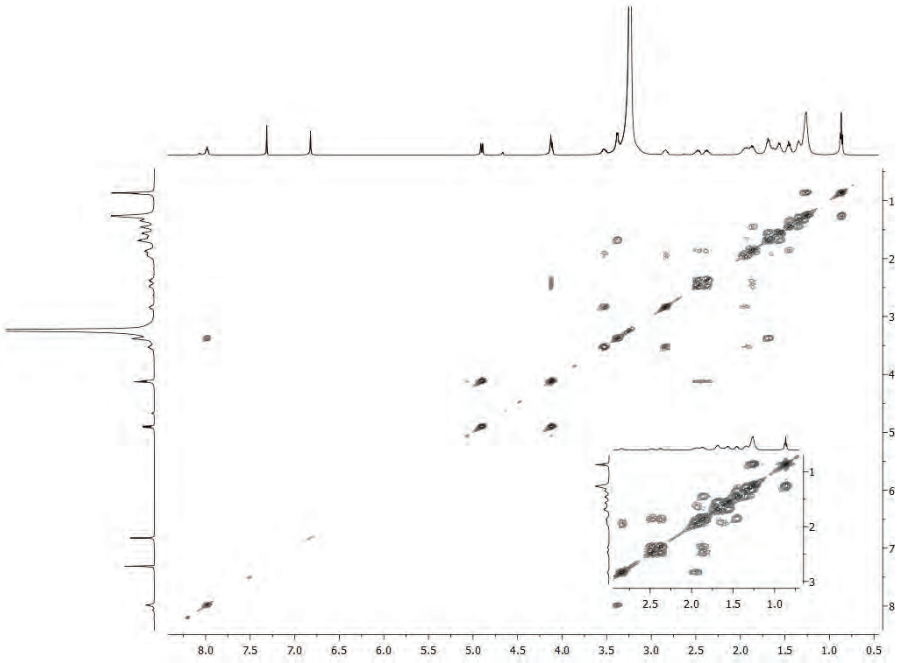

Fig. S-84. COSY spectrum of **21a**.

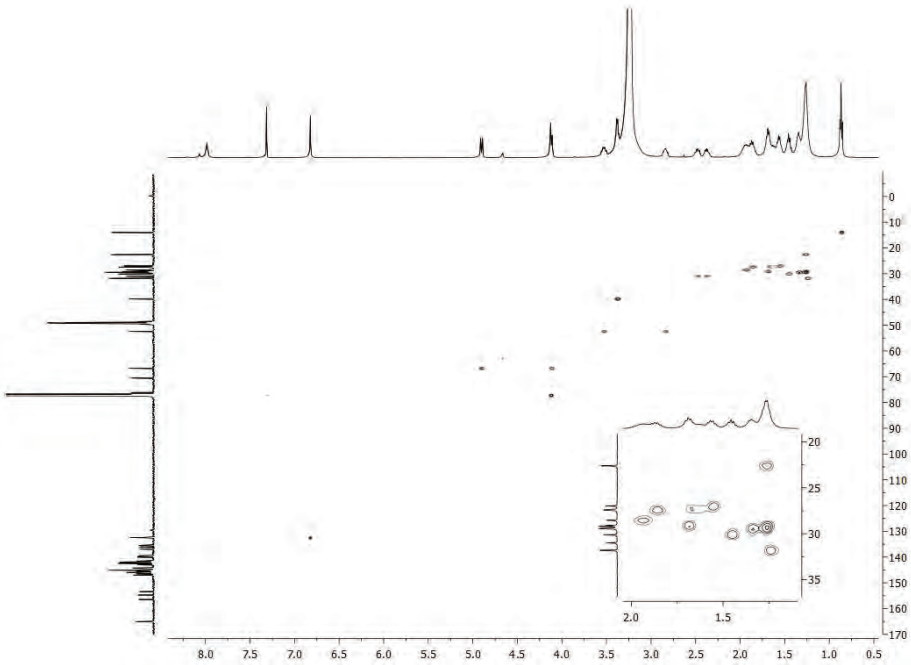

Fig. S-85. HSQC spectrum of **21a**.

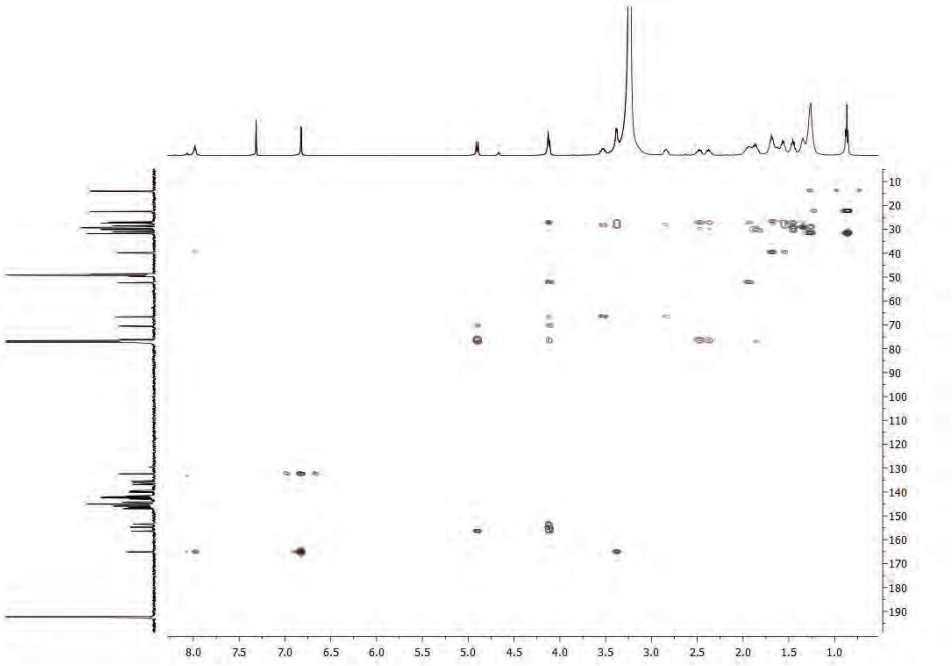

Fig. S-86. HMBC spectrum of **21a**.

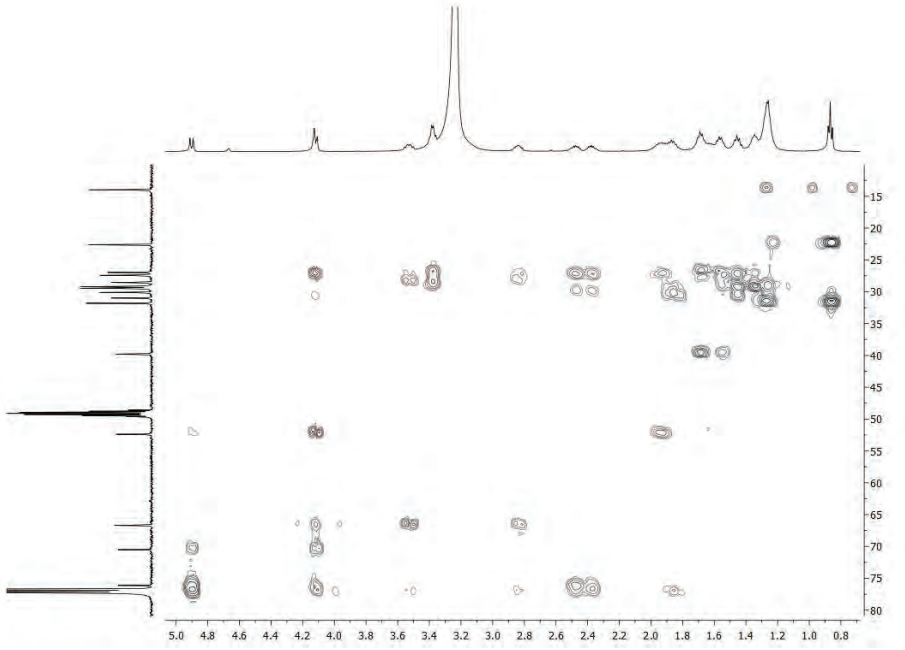

Fig. S-87. Part of the HMBC spectrum of **21a**.

Diamide ***22c***

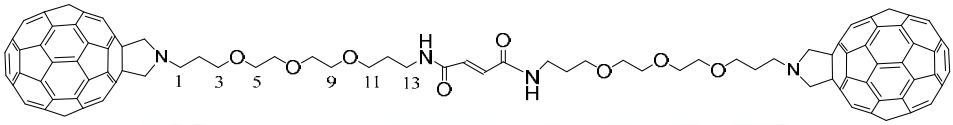

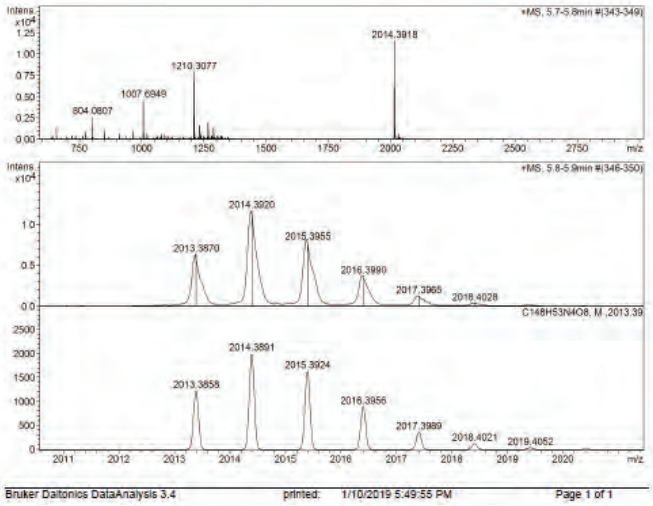

Fig. S-88. Mass spectrum of **22c**.

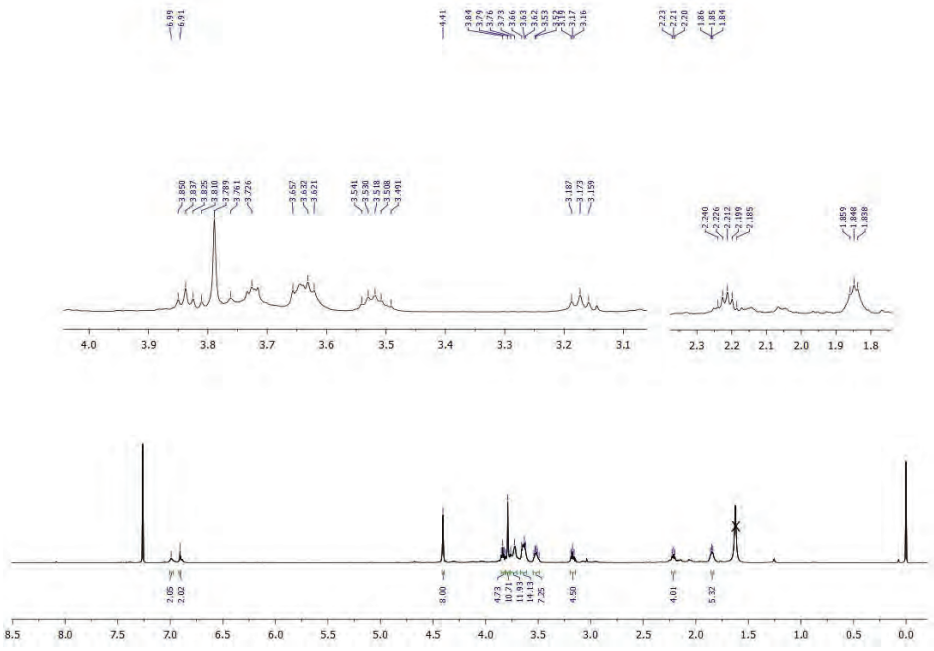

Fig. S-89. ^{1}H-NMR spectrum of **22c**.

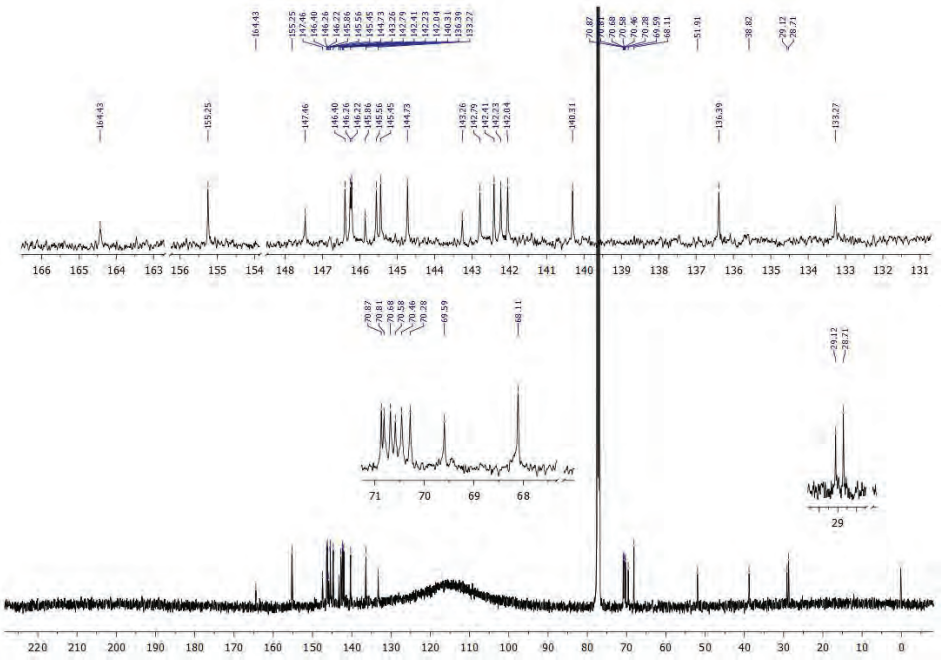

Fig. S-90. ^{13}C-NMR spectrum of **22c**.

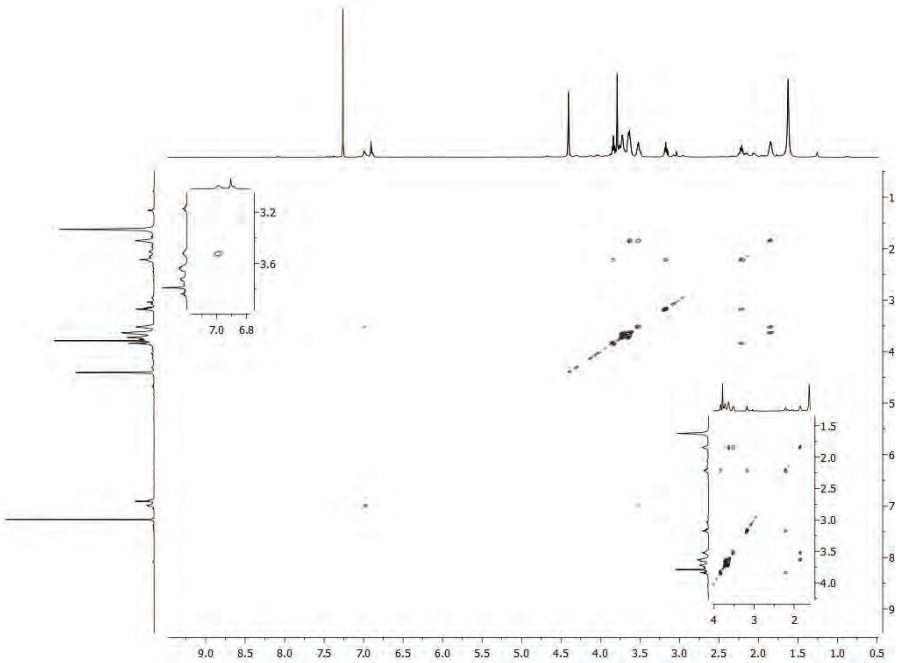

Fig. S-91. COSY spectrum of **22c**.

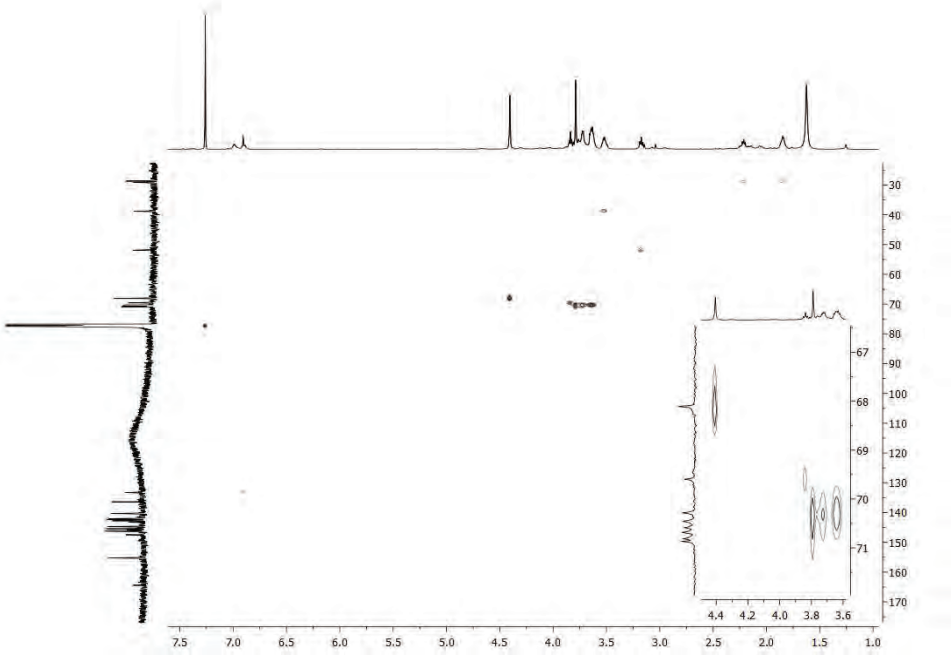

Fig. S-92. HSQC spectrum of **22c**.

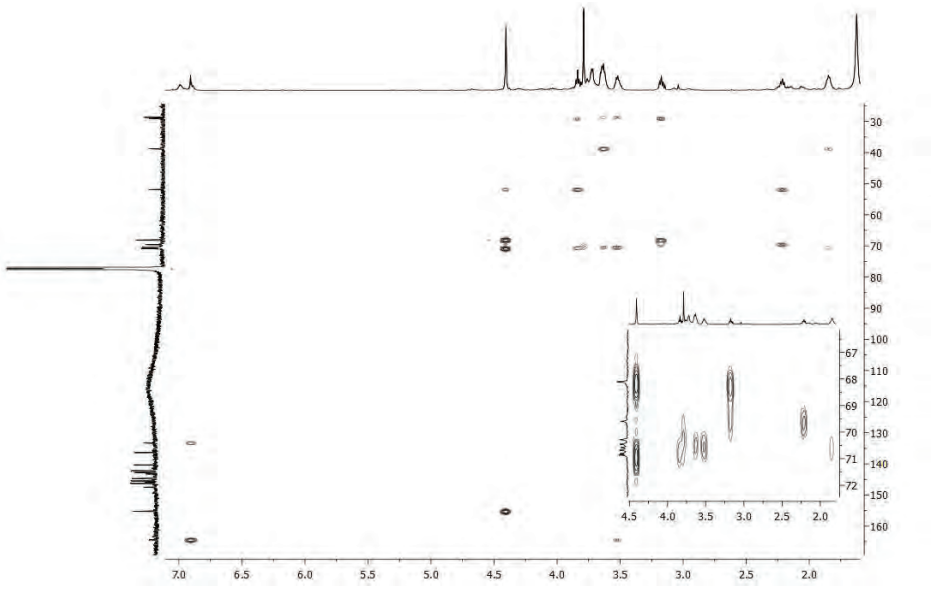

Fig. S-93. HMBC spectrum of **22c**.

Diamide ***23c***

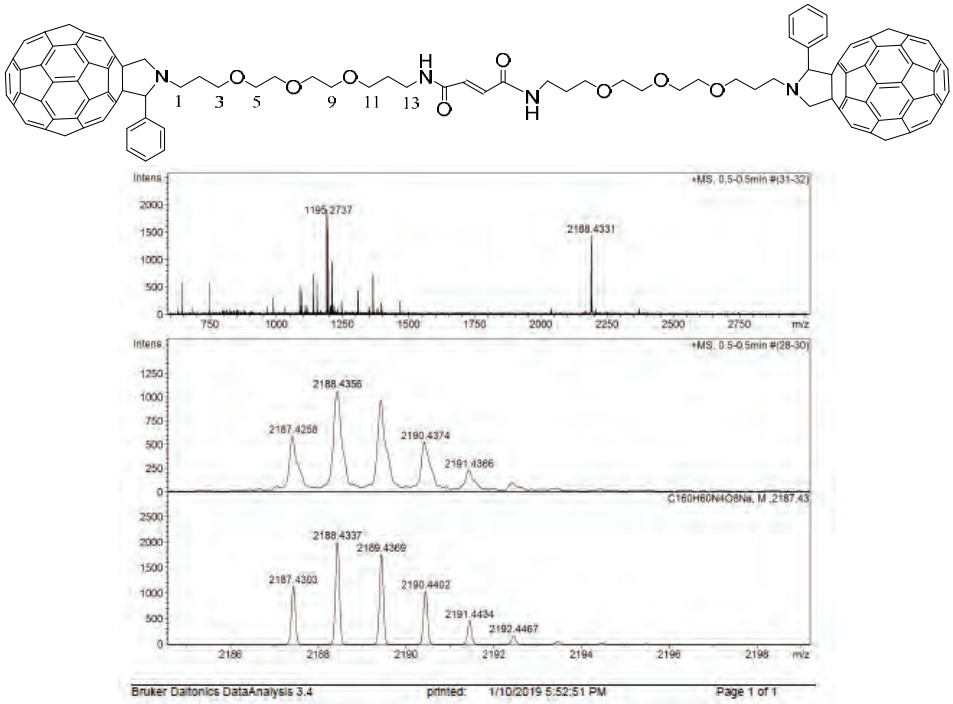

Fig. S-94. Mass spectrum of **23c**.

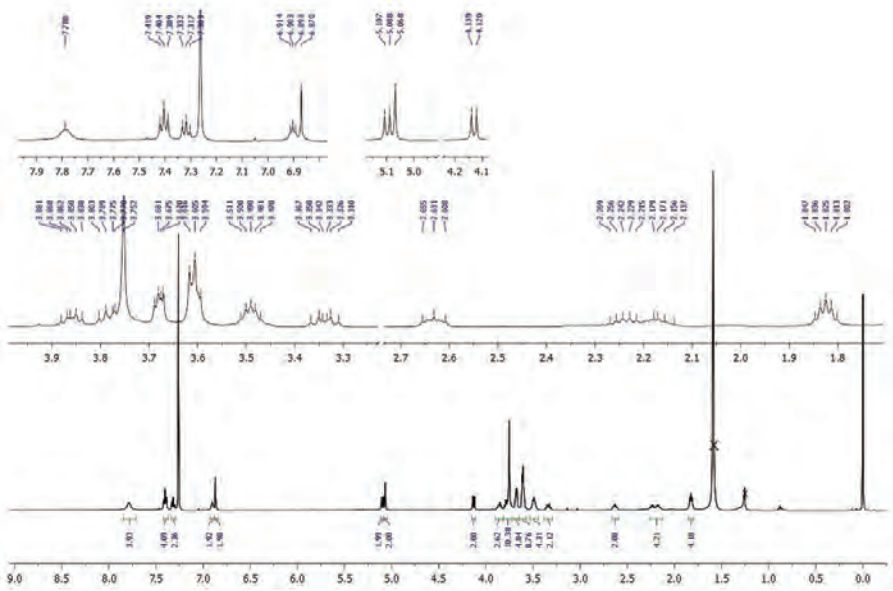

Fig. S-95. ^{1}H-NMR spectrum of **23c**.

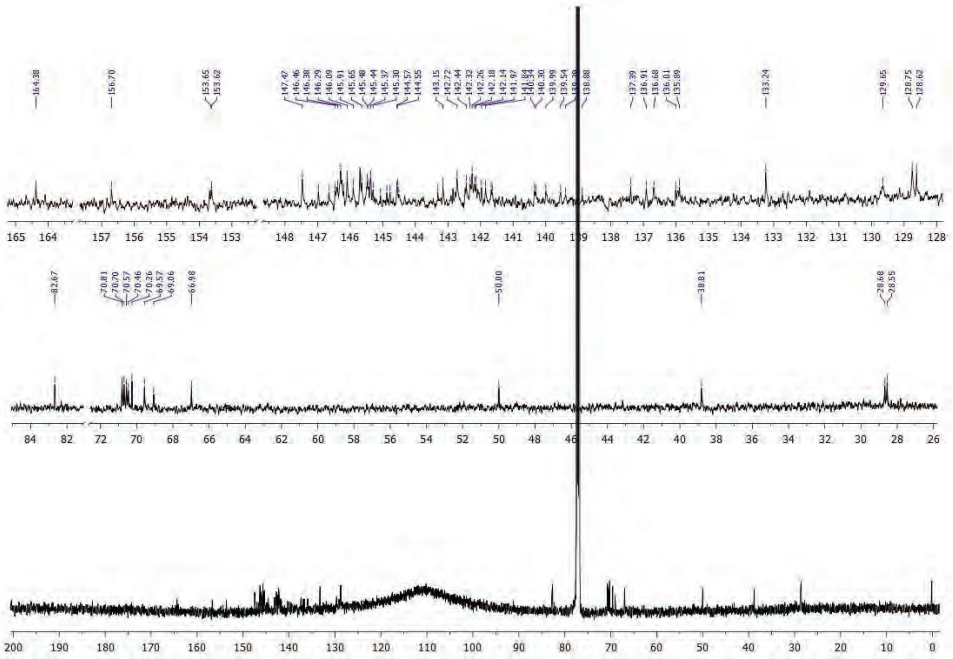

Fig. S-96. ^{13}C-NMR spectrum of **23c**.

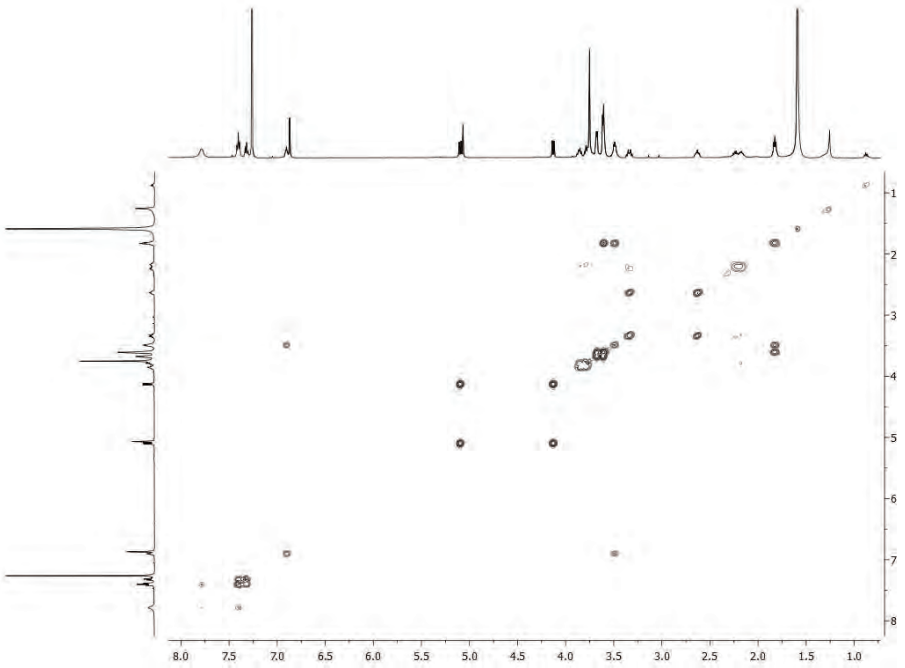

Fig. S-97. COSY spectrum of 23.c

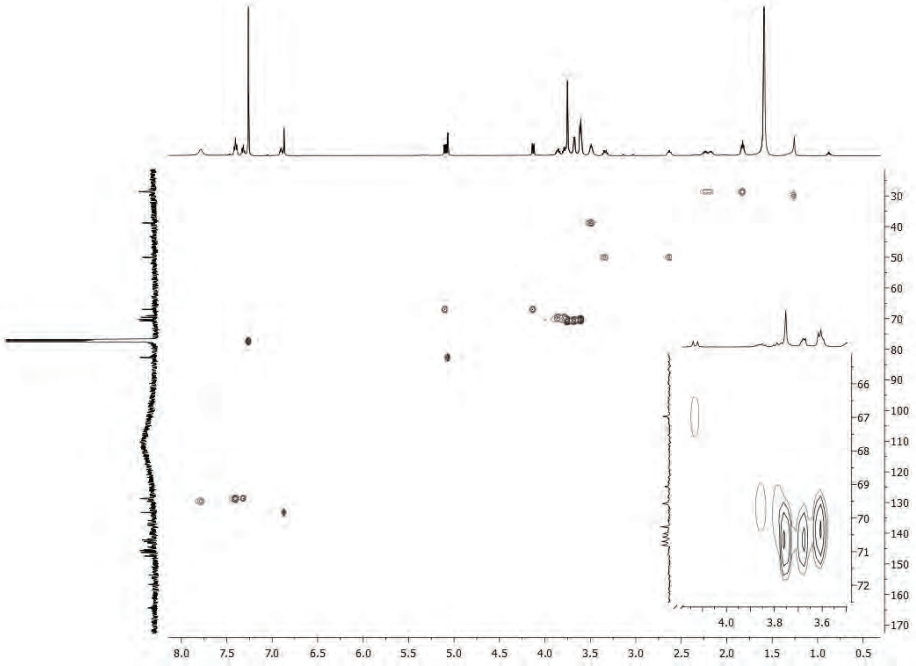

Fig. S-98. HSQC spectrum of **23c**.

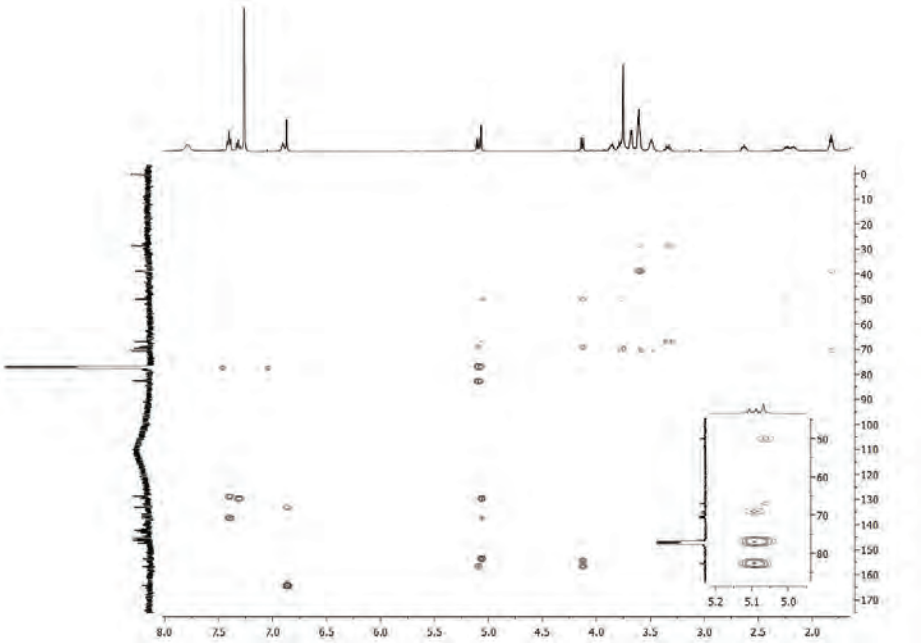

Fig. S-99. HMBC spectrum of **23c**.

*Diamide **24c***

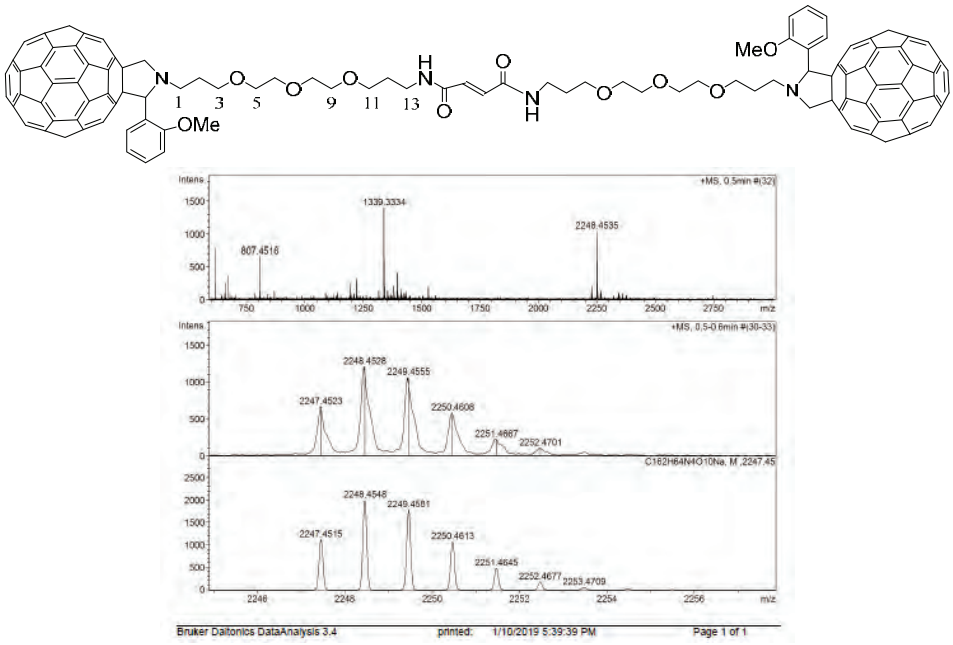

Fig. S-100. Mass spectrum of **24c**.

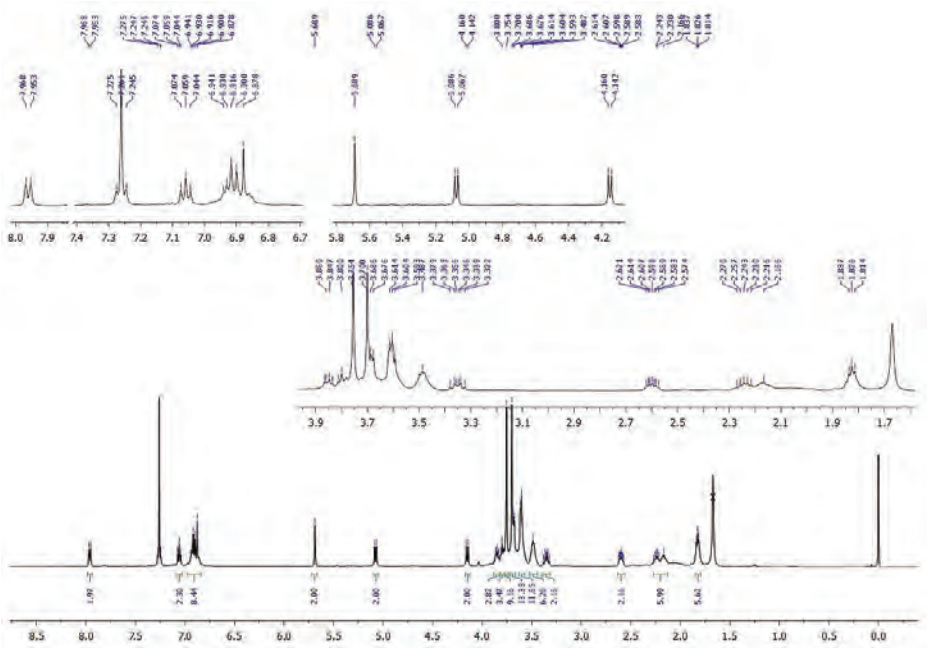

Fig. S-101. ^{1}H-NMR spectrum of **24c**.

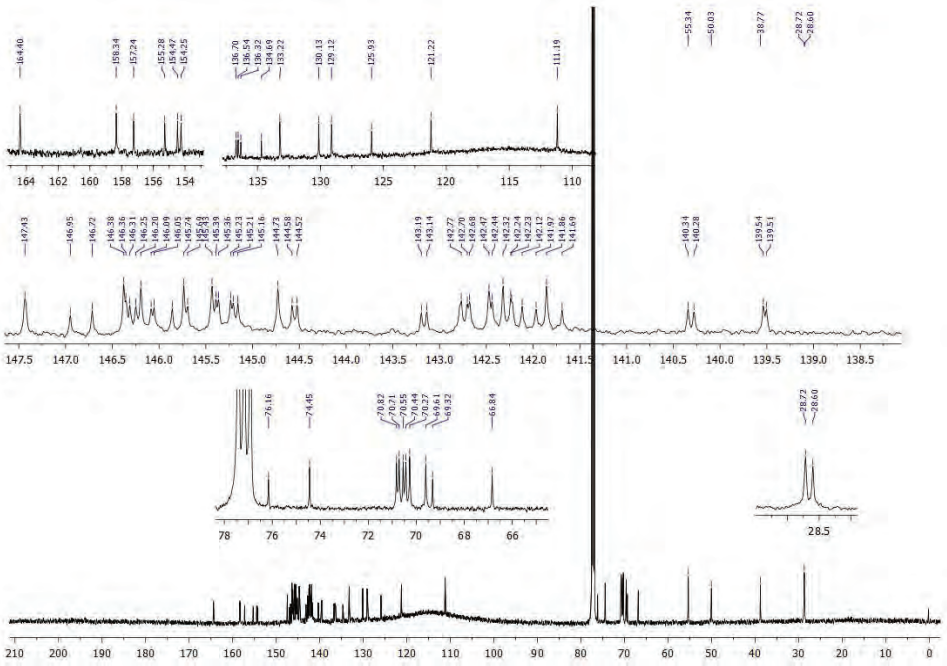

Fig. S-102. ^{13}C-NMR spectrum of **24c**

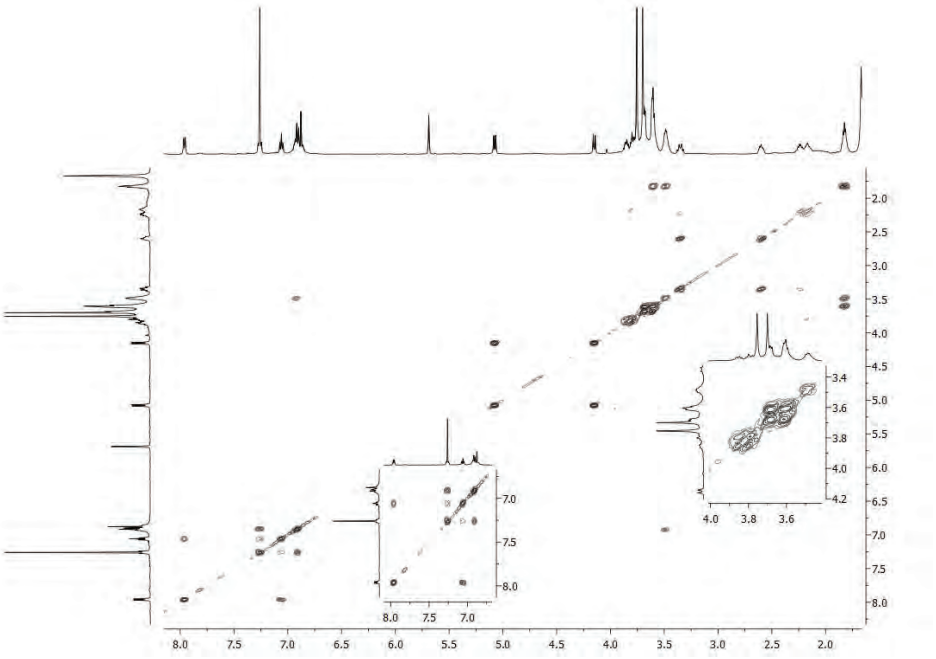

Fig. S-103. COSY spectrum of **24c**.

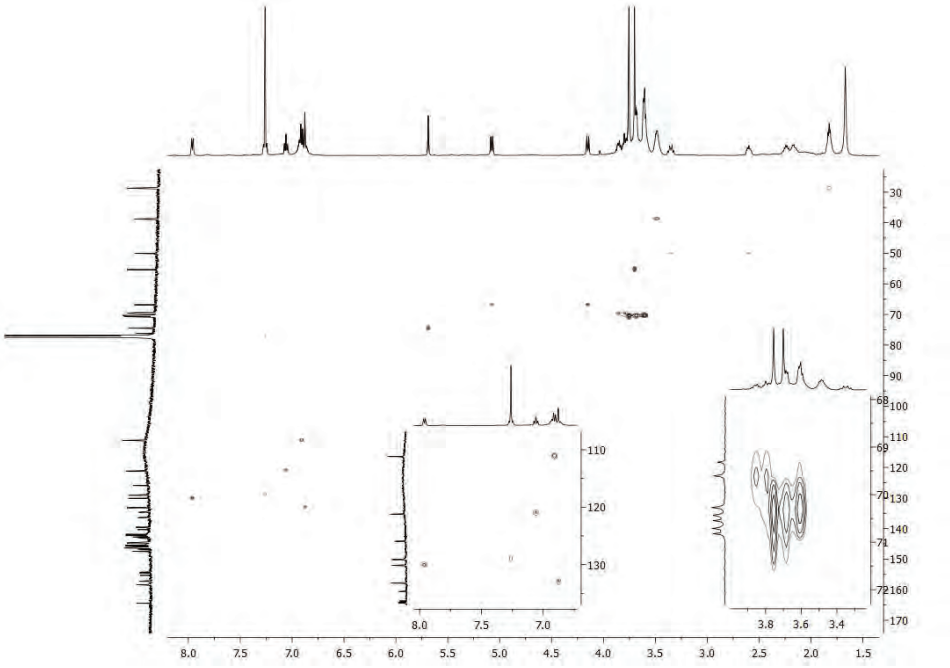

Fig. S-104. HSQC spectrum of **24c**.

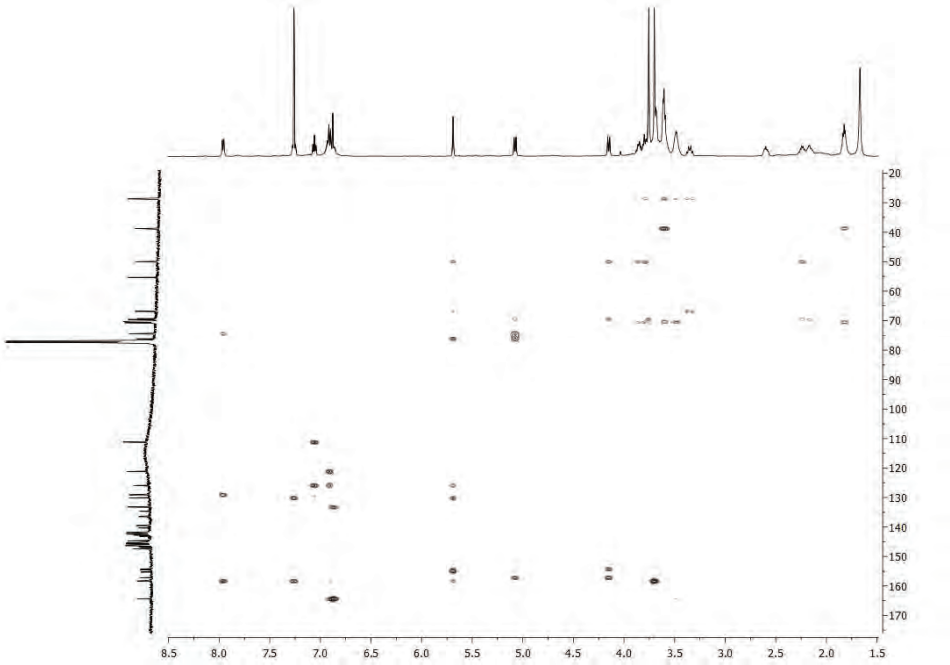

Fig. S-105. HMBC spectrum of **24c**.

Diamide ***25c***

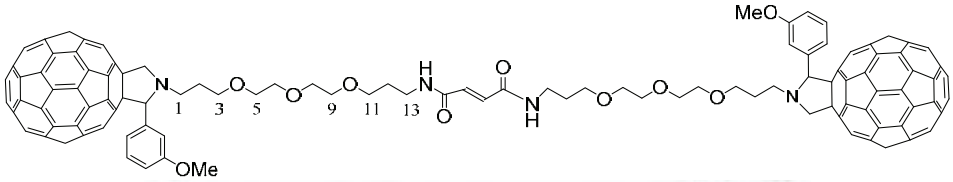

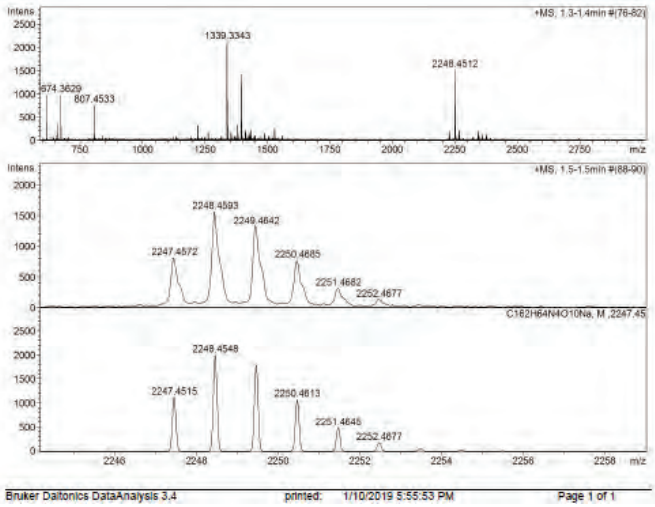

Fig. S-106. Mass spectrum of **25c**.

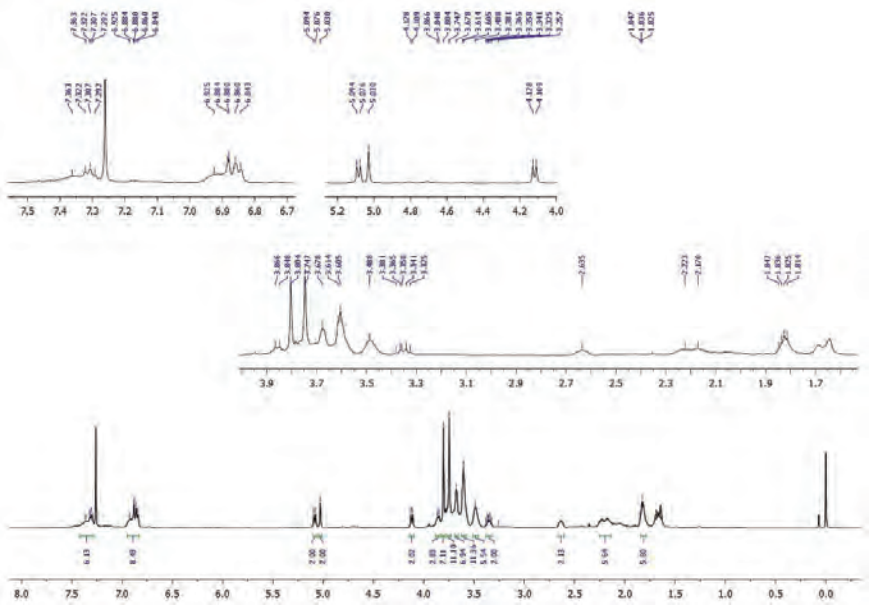

Fig. S-107. ^{1}H-NMR spectrum of **25c**.

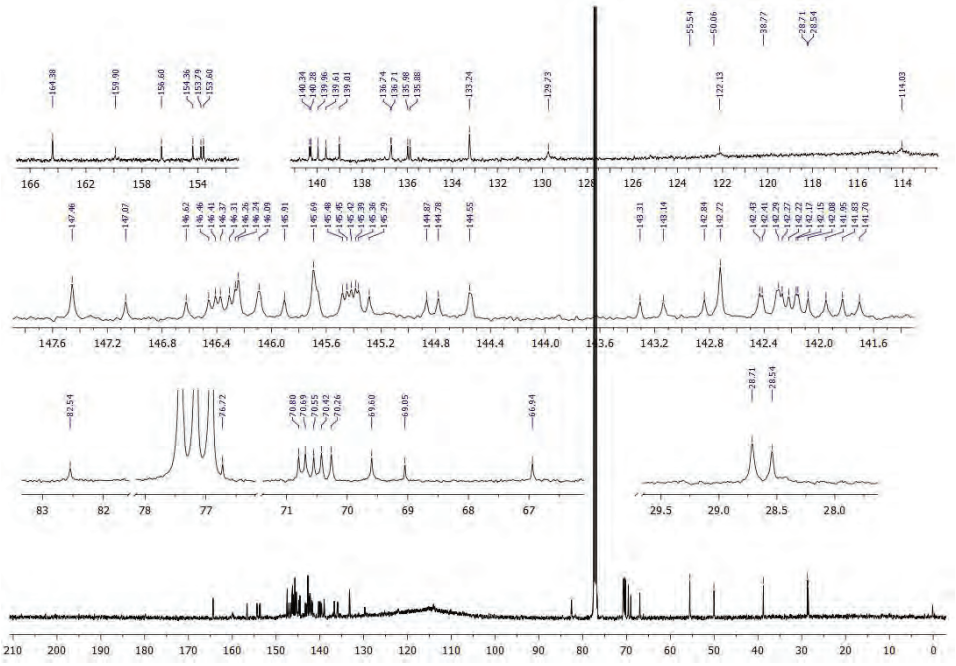

Fig. S-108. ^{13}C-NMR spectrum of **25c**.

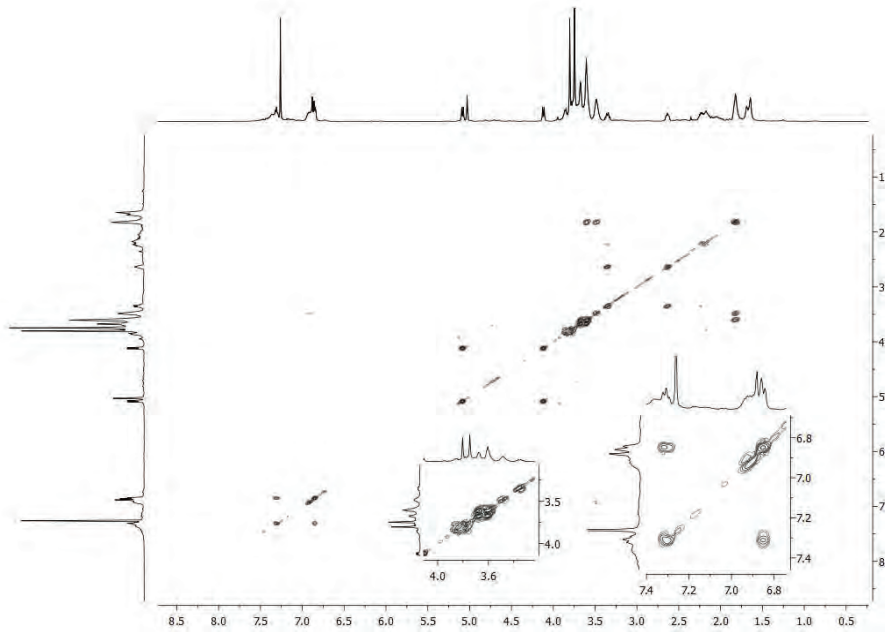

Fig. S-109. COSY spectrum of **25c**.

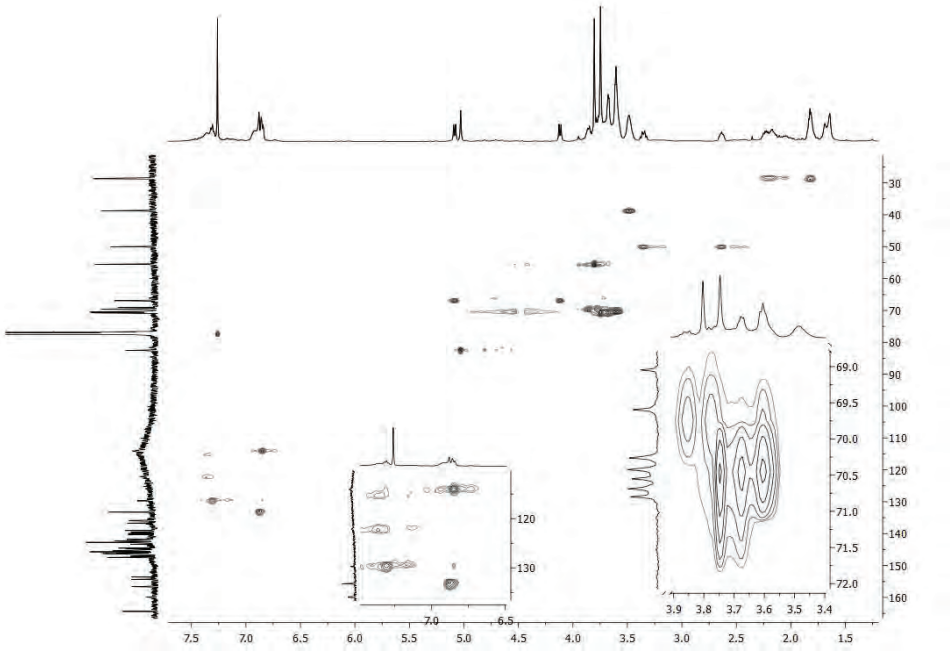

Fig. S-110. HSQC spectrum of **25c**.

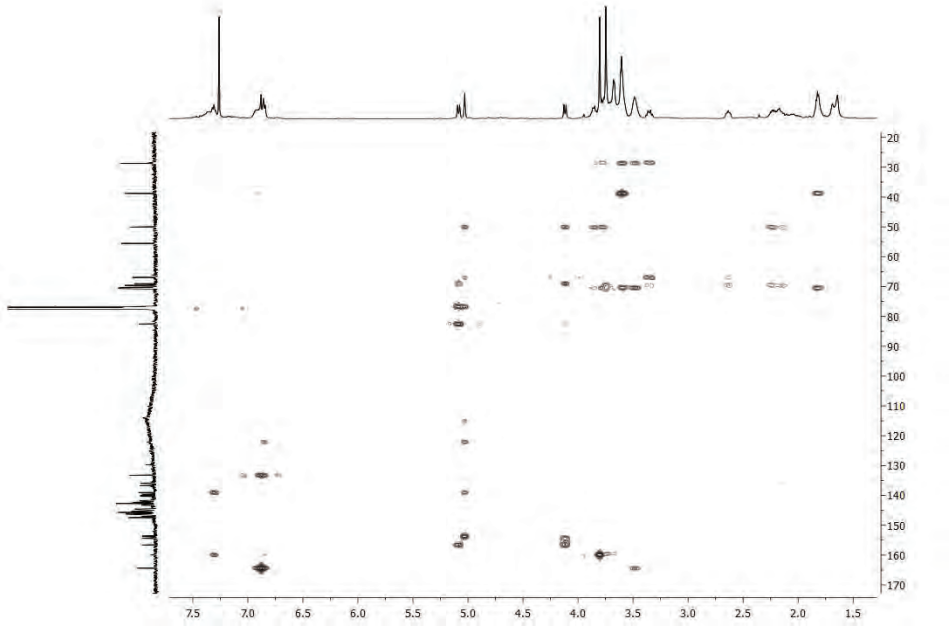

Fig. S-111. HMBC spectrum of **25c**.

Diamide ***26c***

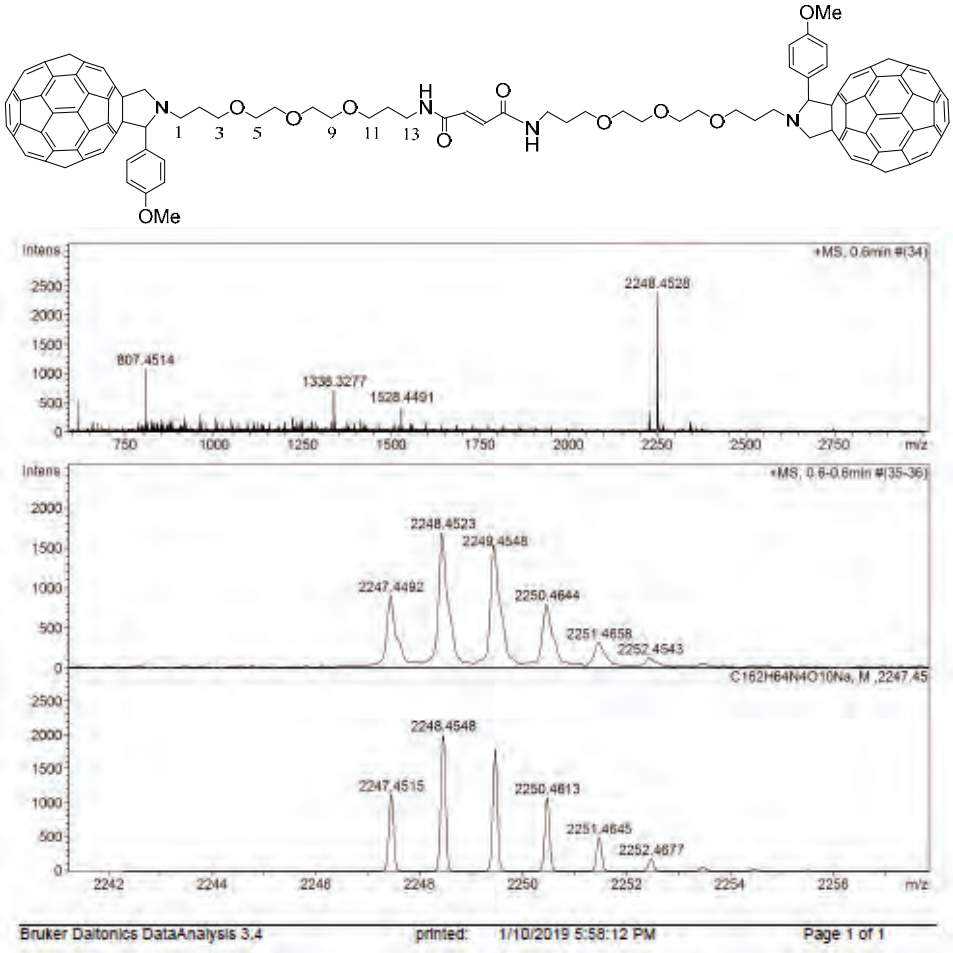

Fig. S-112. Mass spectrum of **26c**.

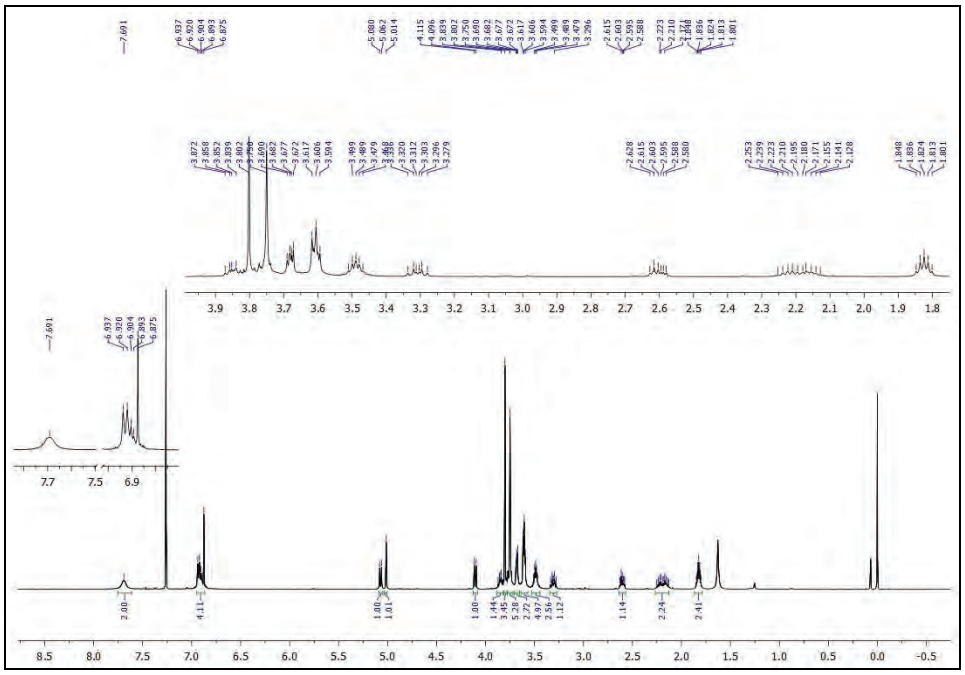

Fig. S-113. ^{1}H-NMR spectrum of **26c**.

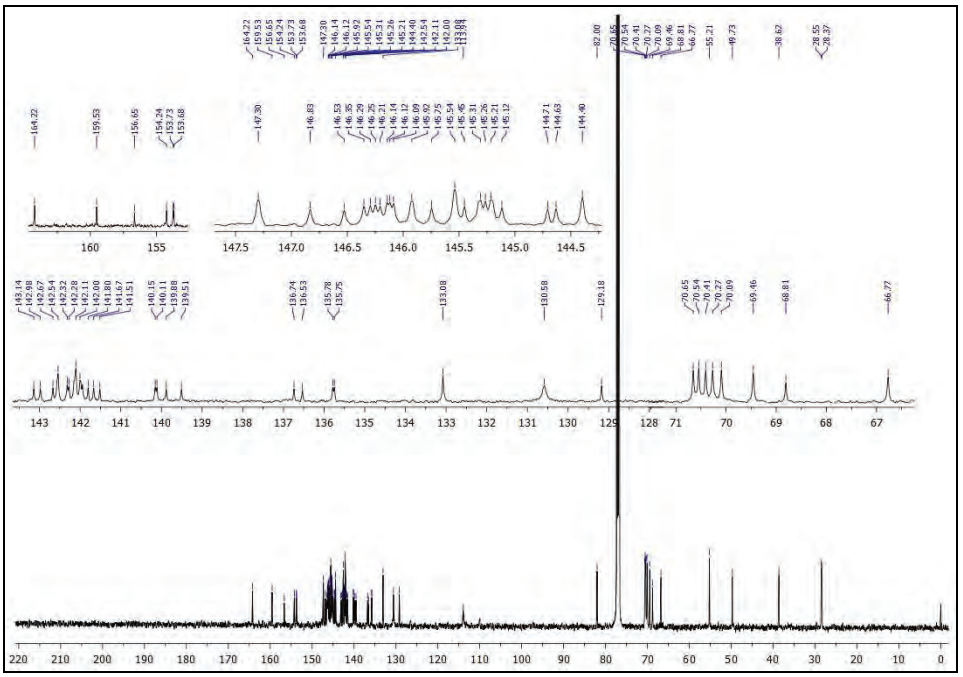

Fig. S-114. ^{13}C-NMR spectrum of **26c**.

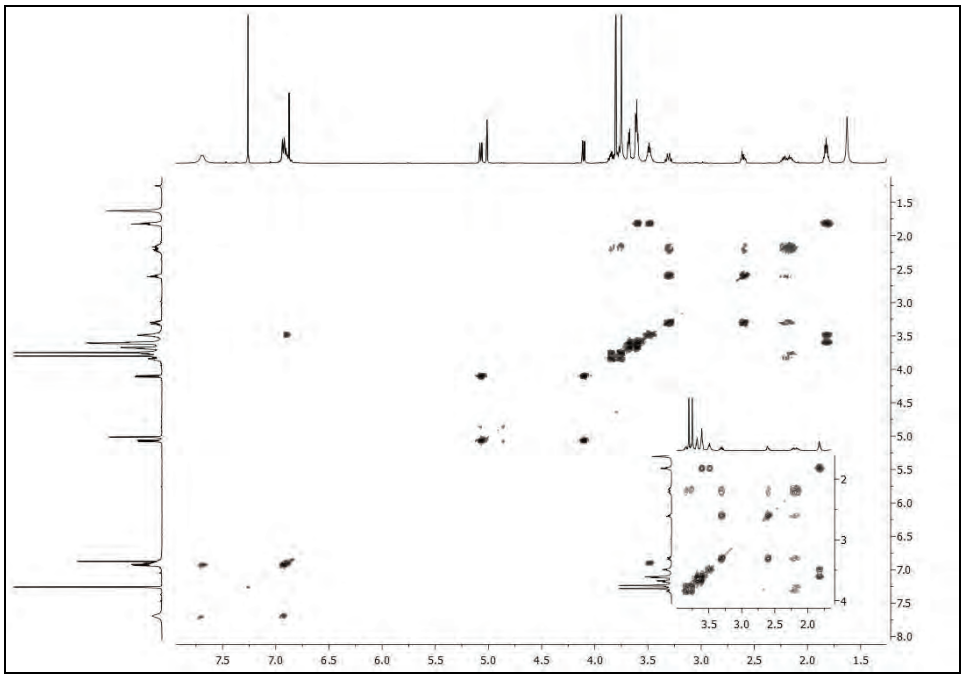

Fig. S-115. COSY spectrum of **26c**.

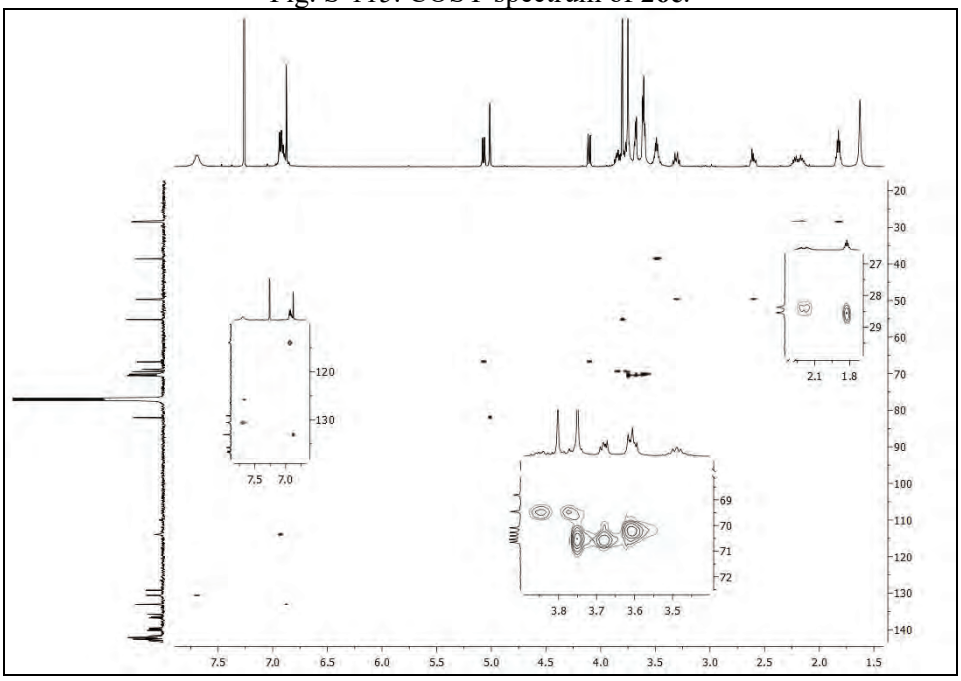

Fig. S-116. HSQC spectrum of **26c**.

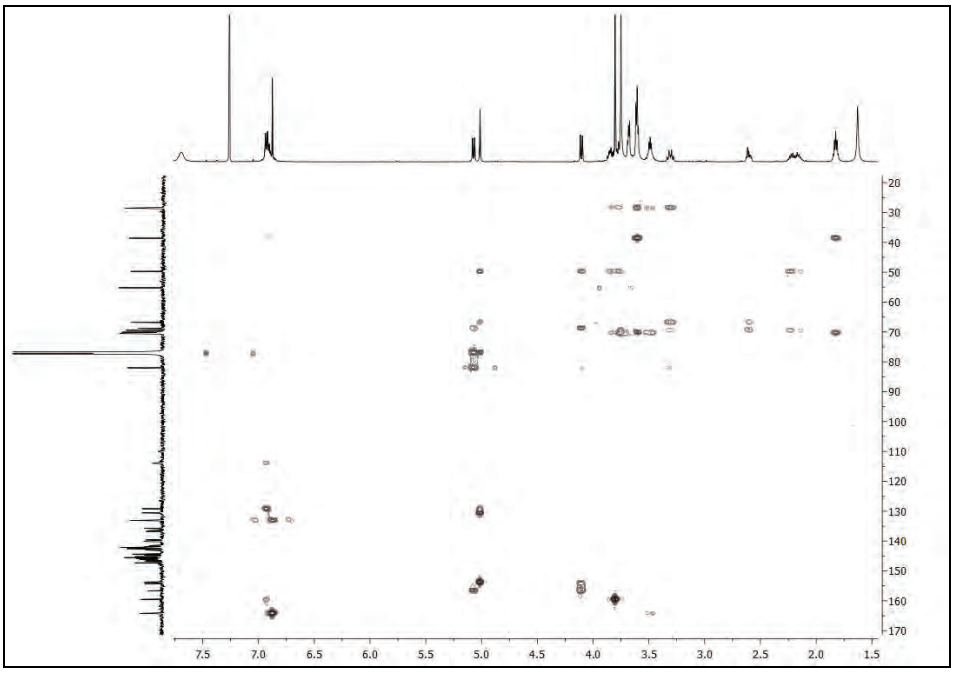

Fig. S-117. HMBC spectrum of **26c**.

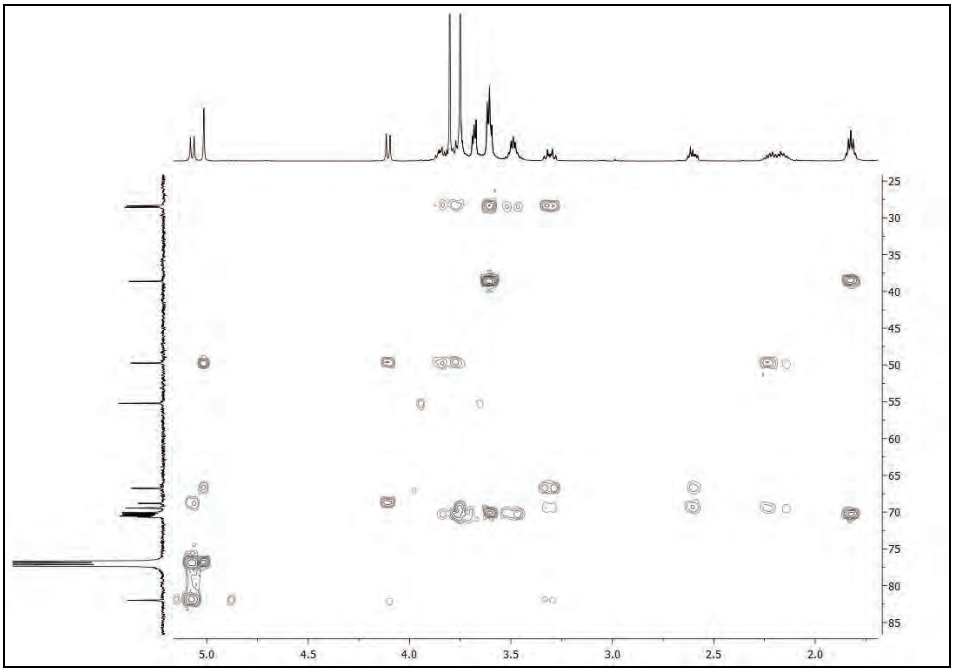

Fig. S-118. Part of the HMBC spectrum of **26c**.

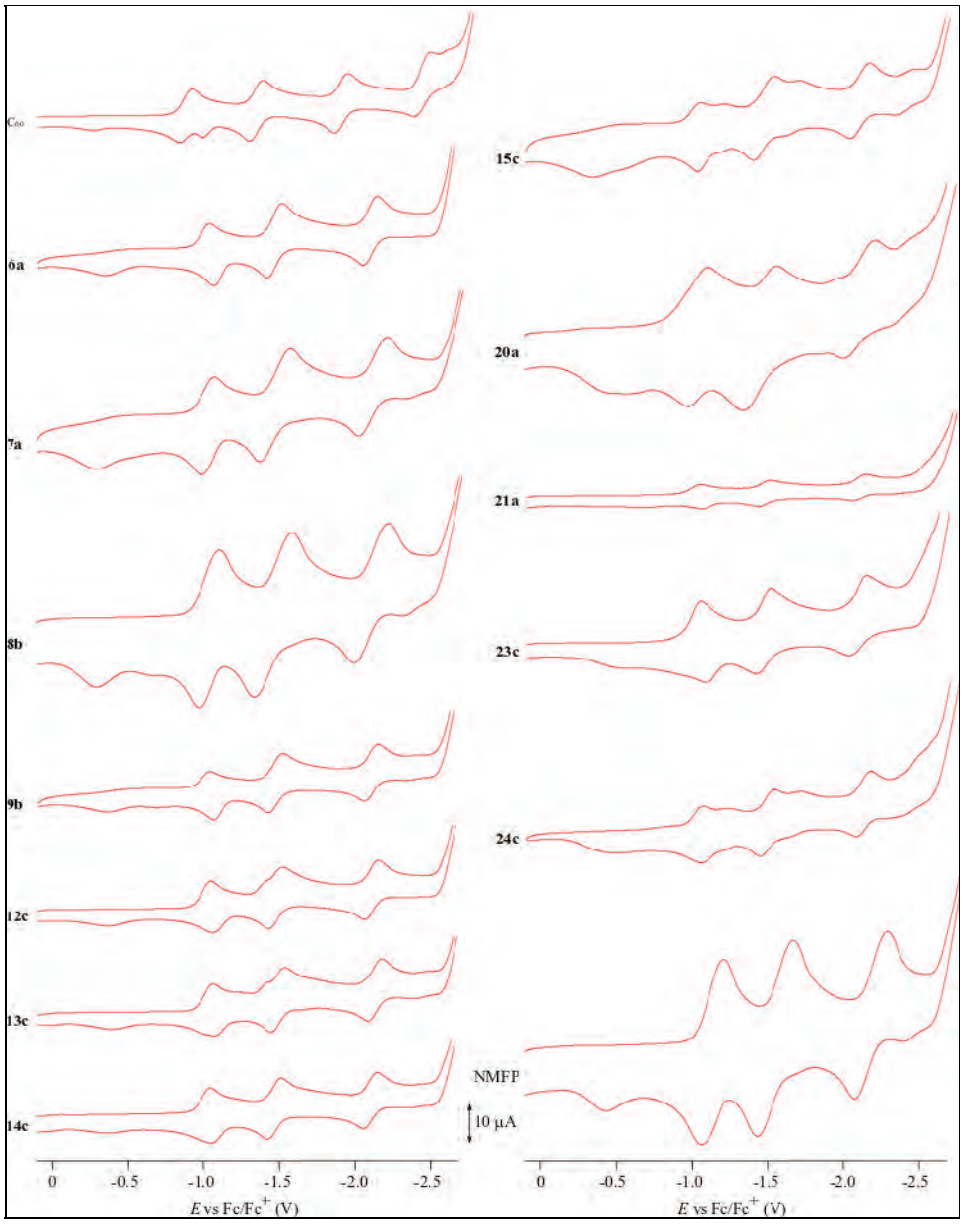

Fig. S-119. CV curves of 1 mM solution in ODCB/DMF mixture (2:1) containing 0.1 M TBAP, recorded with GCE–Ag/Ag$^+$–Pt system at 50 mV.

REFERENCES

1. K. Kordatos, T. Da Ros, S. Bosi, E. Vazquez, M. Bergamin, C. Cusan, F. Pellarini, V. Tomberli, B. Baiti, D. Pantarotto, V. Georgakilas, G. Spalluto, M. Prato, *J. Org. Chem.* **66** (2001) 4915 (https://doi.org/10.1021/jo015608k)

2. R-F. Peng, B. Jin, K. Cao, Y-J, Shu, S-J. Chu, *Chinese J. Org. Chem.*, **27** (2007) 276 (in Chinese) (http://sioc-journal.cn/Jwk_yjhx/EN/Y2007/V26/I02/276).

Journal of the Serbian Chemical Society
JSCS@tmf.bg.ac.rs • www.shd.org.rs/JSCS
J. Serb. Chem. Soc. *86* (11) 1039–1052 (2021)
JSCS–5481
Original scientific paper
Published 10 September 2021

Synthesis and characterization of Fe_3O_4/PEG-400/oxalic acid magnetic nanoparticles as a heterogeneous catalyst for the synthesis of pyrrolin-2-ones derivatives

SEYRAN ESMAEILZADEH and DAVOOD SETAMDIDEH*

Department of Chemistry, Mahabad Branch, Islamic Azad University, Mahabad, Iran

(Received 21 May, revised 5 August, accepted 10 August 2021)

Abstract: In this study, oxalic acid was successfully loaded onto Fe_3O_4/PEG-400 under ultrasonic irradiation and Fe_3O_4/PEG/oxalic acid as a new nanomagnetic catalyst was synthesized. The chemical structure of the catalyst was investigated by the FT-IR, XRD, EDX and SEM methods. The catalyst was used for the synthesis of 3-acyl-5-hydroxy-3-pyrrolin-2-one derivatives from the corresponding aldehydes, anilines and dimethyl acetylenedicarboxylate (DMAD) by a one-pot and three-component MCR reaction in the excellent yields (90–95 %) of products within 24 h at room temperature. Fourteen samples are available. The recovered catalyst could be satisfactorily used for a second and third run without regeneration. This method has a green and eco-friendly profile. In addition, this research introduces an improved mechanism for these types of reaction. The chemical structures of new compounds was characterized by their FT-IR, ^{1}H-NMR, ^{13}C--NMR and mass spectra.

Keywords: iron(II),iron(III) oxide; nano-composite catalyst; 2-pyrrolidinone; green chemistry; MCR.

INTRODUCTION

In many catalytic methods, recyclability, recovery, non-toxicity and economical affordability are four valuable characteristics. Magnetic nanoparticle (MNPs) catalysts due to their simple synthesis, easy application, great efficient reusability by magnetic force, low toxicity and economics, are attractive.[1] Such acceptable qualities have caused MNPs to become desirable substitutes for some catalysts.[2–4] Surface functionalized magnetic Fe_3O_4 nanoparticles have been used in biotechnology and catalysis as a functional substance. There are a variety of different magnetic nanoparticles for the core magnetic support, but Fe_3O_4 nanoparticles have been widely investigated due to their low toxicity, super paramagnetic behavior, large surface areas and especially presenting a great number of OH

* Corresponding author. E-mail: d.setamdideh@iau-mahabad.ac.ir
https://doi.org/10.2298/JSC210521059E

groups on the exterior of their particles.[5,6] Therefore, specific shells of different substances can be built to enclose the Fe_3O_4 core, for example: forming proper functional groups for specified different actuators, ligands, and catalysts.[7] On the other hands, interest in magnetic nanoparticles (MNPs) have been increasing for applications in organic synthesis.[8,9] The surface of magnetic nanoparticles can be functionalized by surface modifications for performing of a variety of organic reactions.[10]

Multicomponent reactions (MCRs) have been of interest in one-pot synthesis of heterocyclic compounds,[11] such as pyrrolidinones.[12] The pyrrolin-2-one moiety is important in organic compounds because of its biological activity in some drugs and natural products, for example: cotinine (the predominant metabolite of nicotine in tobacco),[13] doxapram hydrochloride (a respiratory stimulant),[14] ethosuximide (a succinimide anticonvulsant),[15] lactacystin (synthesized by bacteria of the genus Streptomyces),[16] salinosporamide A (produced by the bacteria *Salinispora tropica*,[17] (−)-azaspirene (an angiogenesis inhibitor that is extracted from the fungus Neosartorya sp).[18] In view of the importance of these compounds, some synthetic methods have been reported.[19–24] Moreover, the synthesis of pyrrolin-2-one derivatives, involving the coupling of aromatic aldehydes, arylamines with acetylenedicarboxylate derivatives, has been studied, and the development of this procedure under a green profile is attractive and desired, such as: a) using of admicellar catalysis such nano-TiO_2,[25] b) in water for non-bulky products,[26] c) in the presence of *p*-toluensulfonic acid,[12] d) using unconventional energy sources such as ultrasound irradiation[27] or microwaves,[28] e) with application of ionic liquids[29] and f) nano magnetic particles Fe_3O_4@SiO_2@Propyl-ANDSA as a reusable catalyst.[30] The study of these methods clarified the development of this procedure under green profile is more attractive and desired. Furthermore, for the extension of green chemistry, several eco-friendly procedures for the synthesis of heterocyclic compounds have been reported.[11,31] On the other hand, for a synthetic project a series of pyrrolin-2--ones were needed. Encouraged by these results, attention was directed to a new methodology for the room temperature synthesis of 3-acyl-5-hydroxy-3-pyrrolin--2-one derivatives from aldehydes, anilines and dimethyl acetylenedicarboxylate (DMAD) catalyzed by Fe_3O_4/PEG-400/oxalic acid as a novel reusable magnetic nano-catalyst, as shown in Scheme 1.

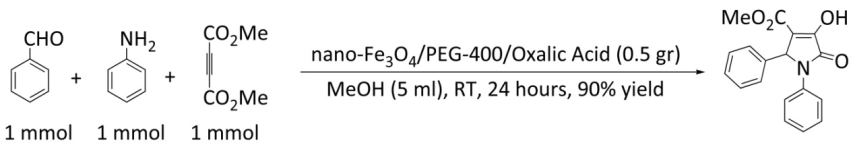

Scheme 1. The synthesis of 1,5-diphenyl-3-hydroxy-4-methoxycarbonyl-3-pyrrolin-2-one.

EXPERIMENTAL

Materials

All solvents and reagents were obtained from the Sigma–Aldrich Company. FT-IR, ^{1}H- and ^{13}C-NMR spectra were recorded on a PerkinElmer FT-IR RXI and (250 or 500) MHz Bruker spectrometers, respectively. The products were characterized by their FT-IR, ^{1}H-NMR, and ^{13}C-NMR spectra and comparison with authentic samples for known products. The new compounds characterization has been supported by mass spectrum obtained using Agilent Technology (HP), MS model: 5973 network mass selective detector (ion source: electron impact (*EI*) 70 eV, ion source and analyzer temperature 230 °C, analyzer: quadrupole). The nanostructures were characterized using a Holland Philips (model: PW1730) Xpert X-ray powder diffraction (XRD) diffractometer (CuK, radiation, λ = 0.154056 nm), Step size 0.05°, time per step, 1 s (2θ 5–80°). Scanning electron microscopy (SEM) of the nanoparticles was performed on a model FESEM: Tescan company (model: Mira III), Czech Republic. Energy dispersive X-ray analysis (EDX) was performed by FESEM: Tescan company (model: Mira II, detector: SAMX, France). Elma (S60H, Germany) with high-performance transducer system with 37 kHz was used.

Preparation of Fe_3O_4 magnetic nanoparticles

The magnetic Fe_3O_4 nanoparticles were prepared by the chemical co-precipitation method.[8,32] $FeCl_2{\cdot}4H_2O$ (2.25 g) and $FeCl_3{\cdot}6H_2O$ (6.11 g) were dissolved into 400 mL deoxygenated water. The reaction was followed by the dropwise addition of 20 mL of concentrated liquid NH_3 under vigorous stirring and N_2 protection at 80 °C. The obtained magnetic nanoparticles were separated from solution by a powerful magnet and were washed with 200 mL deionized water three times. Finally the products were dried at 40 °C overnight to give Fe_3O_4 nanoparticles.

Preparation of Fe_3O_4/PEG-400 magnetic nanoparticles

The magnetic Fe_3O_4/PEG-400 nanoparticles were synthesized by modification of a method known in the literature.[8,32] The detailed procedure is described as following: Fe_3O_4 nanoparticles (1 g) were dispersed in 60 mL deionized water in an ultrasonic bath for 30 min under nitrogen gas. Then PEG-400 (5 ml) was added, and the mixed solution was irradiated in an ultrasonic bath for 1 h under nitrogen gas at 80–90 °C. After the reaction, the Fe_3O_4/PEG-400 nanoparticles were isolated with a strong magnet and washed with deionized water and dried at 40 °C overnight to give Fe_3O_4/PEG-400.

Preparation of Fe_3O_4/PEG-400/oxalic acid magnetic nanoparticles

The Fe_3O_4/PEG400 nano composite (5 g) was dispersed in ethanol (20 mL) in an ultrasonic bath for 30 min. Subsequently, oxalic acid (0.75 g) was added to the reaction mixture. The mixture was irradiated in an ultrasonic bath for 1 h under nitrogen gas at 80–90 °C. The resulting magnetic nanocomposite was separated from the suspension by a strong external magnet. They were washed with ethanol (2×10 ml) and acetone (2×5 ml), and then dried at 40 °C overnight to give magnetic Fe_3O_4/PEG-400/oxalic acid nano particles.

The synthesis of 1,5-diphenyl-3-hydroxy-4-methoxycarbonyl-3-pyrrolin-2-one by Fe_3O_4/PEG-400/oxalic acid: A typical procedure

In a round-bottomed flask (25 mL) equipped with a magnetic stirrer, a mixture of benzaldehyde (0.106 g, 1 mmol), aniline (0.093 g, 1 mmol) and Fe_3O_4/PEG-400/oxalic acid (0.5 g) in 5 mL of methanol was prepared and strongly stirred at ambient temperature for 30 min. Then dimethyl acetylenedicarboxylate (DMAD, 0.14 g, 1 mmol) was added to the mixture.

The reaction was completed within 24 h. The reaction was monitored over silica gel 60 F_{254} aluminum sheet (eluent: ethyl acetate/*n*-hexane: 1/1).The catalyst was separated using a strong magnet. The separated catalyst was washed with acetone two times and then dried in oven for reuse in further reactions. The solvent was evaporated under reduced pressure and further purification was achieved by recrystallization from methanol. The white solid was achieved in excellent yield 0.28 g (90 %) with a melting point 173–175 °C. The product was characterized by their ^{1}H-NMR, ^{13}C-NMR and FT-IR spectra.

Analytical and spectral data are given in the Supplementary material to this paper.

RESULTS AND DISCUSSION

Oxalic acid is a stronger than acetic acid (pk_{a1} = 1.27). It was assumed that by addition of oxalic acid to the mixture of benzaldehyde and aniline, the condensation reaction between them would proceed easily for the preparation of imine as an intermediate. However, the results showed that oxalic acid reacts with aniline and produces oxalate precipitation in many cases. Therefore, many aniline derivatives cannot efficiently react with benzaldehydes derivatives. To avoid the preparation of oxalate precipitation, it was decided to use oxalic acid on Fe_3O_4/PEG-400 magnetic nanoparticles. According to method presented in the literature,[8,32] Fe_3O_4/PEG-400 magnetic nanoparticles were synthesized by the modified preparation approach. After the synthesis nano-Fe_3O_4/PEG-400, oxalic acid was loaded using ultrasonic irradiation onto this magnetic core. Therefore, the magnetic nanoparticles of Fe_3O_4/PEG-400/oxalic acid were successfully prepared, as shown in Scheme 2. The chemical structure of this catalyst was characterized by different methods, *i.e.*, FT-IR, XRD, EDX and SEM. Furthermore, attempts were made to load other organic acids, such as acetic acid, citric acid, succinic acid, phthalic acid and tartaric acid, onto Fe_3O_4/PEG-400, but these attempts were unsuccessful. It seems Fe_3O_4/PEG-400 has a selectivity for loading oxalic acid, which is because of the chemical structure and the molecular size of oxalic acid. Oxalic acid has two carboxyl groups that make strong hydrogen bonds with the hydroxyl groups of PEG-400 loaded on the Fe_3O_4 magnetic core. In addition, the molecular structure of oxalic has an appropriate size for trapping by PEG-400. On the contrary, although succinic acid, phthalic acid and tartaric acid have two carboxyl groups, the size of the molecular structure of these compounds is greater than that of oxalic acid and they cannot be trapped by Fe_3O_4/PEG-400. Moreover, acetic acid has one carboxylic group which cannot make a strong hydrogen bond with Fe_3O_4/PEG-400. Some interaction for the stabilization of oxalic acid on Fe_3O_4/PEG-400 magnetic nanoparticles are shown in Scheme 2.

The FT-IR spectra of nano-Fe_3O_4, nano-Fe_3O_4/PEG-400 and nano-Fe_3O_4/PEG-400/oxalic acid are shown in Fig. 1 (A, B and C, respectively). The FT-IR spectrum of nano-Fe_3O_4 shows bands at 3367 (assigned to O–H stretching vibrations of absorbed water),[33] 1625 (assigned to O–H bending vibration of water

molecules),[34] 1399 (assigned to Fe–O stretching vibration),[35] 631 (attributed to some amount of maghemite)[36] and 581 cm^{-1} (assigned to the Fe–O bending vibration).[37]

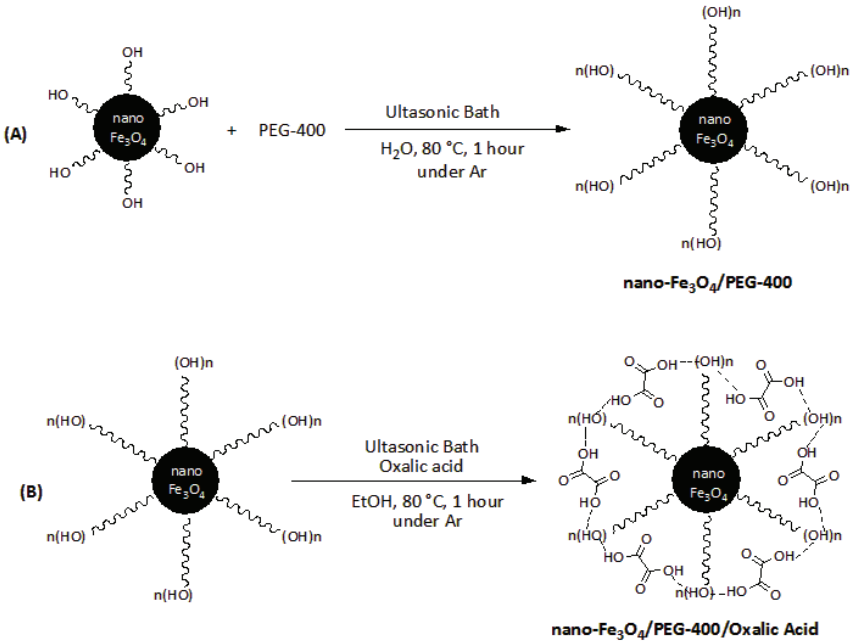

Scheme 2. The steps for synthesis of nano magnetic Fe_3O_4/PEG-400 and nano magnetic Fe_3O_4/PEG-400/oxalic acid.

The FT-IR spectrum of Fe_3O_4/PEG-400 shows bands at 3366 (assigned to O–H stretching vibrations of PEG-400), 2867 (assigned to C–H stretching vibrations of PEG-400), 1637 (assigned to O–H bending vibration of the absorbed water), 1449 (assigned to C–H bending vibration of PEG-400), 1349 (assigned to O–H bending of vibrations of PEG-400), 1248 (assigned to C–O stretch of PEG-400), 1097 (assigned to C–C–O stretching vibrations of PEG--400), 947 (assigned to O–H bending vibration of PEG-400), 631 (attributed to some amount of maghemite) and 579 cm^{-1} (assigned to the Fe–O bending vibration). The FT-IR spectrum of Fe_3O_4/PEG-400/oxalic acid shows bands at 3367 (assigned to O–H stretching vibrations of PEG-400 and COOH stretching vibrations of oxalic acid), 2870 (assigned to C–H stretching vibrations of PEG-400), 1712 (assigned to C=O bond stretching of the COOH group), 1624 (assigned to O–H bending vibration of the absorbed water), 1384 (assigned to C–H bending vibration of PEG-400), 1304 (assigned to C–O stretch vibrations of PEG-400), 1087 (assigned to C–C–O stretching vibrations of PEG-400), 1036 (assigned to C–C–O stretching vibrations of COOH group), 940 (assigned to O–H bending

vibration of PEG-400), 805 (assigned to O–H bending vibration of COOH group), 631 (attributed to some amount of maghemite) and 553 cm^{-1} (assigned to the Fe–O bending vibration). The spectrum of nano-Fe_3O_4 (Fig. 1A) shows an absorption at 1399 cm^{-1}, which is assigned to Fe–O stretching bond. This absorption does not appear in the spectrum of Fe_3O_4/PEG-400 (Fig. 1B). This could be explained by the covering of PEG-400 layer. The existence of PEG-400 layer in the spectrum of Fe_3O_4/PEG-400 can be seen by the C–H stretching vibration at 2867 cm^{-1} as well as the 1449 cm^{-1} C–H bending vibration and 1087 cm^{-1} C–C–O stretching vibrations with strong intensity. The data strongly suggest that the Fe_3O_4 nanoparticles were successfully coated with PEG-400 layer. On the other hands, the spectrum of nano-Fe_3O_4/PEG-400/oxalic acid (Fig. 1C) in comparison of the spectrum of Fe_3O_4/PEG-400 (Fig. 1B) shows a peak at 1712 cm^{-1} for C=O bond stretching, as well as the 1036 cm^{-1} C–C–O stretching vibration, and the 805 cm^{-1} O–H bending vibration of the COOH group. These peaks indicate the existence of oxalic acid in Fe_3O_4/PEG-400 nanoparticles. Therefore, the data shows that oxalic acid was successfully loaded on Fe_3O_4/PEG-400 nanoparticles for preparation of nano-Fe_3O_4/PEG-400/oxalic acid catalyst. The Fe–O bending vibration was shifted from 579 to 553 cm^{-1} after addition of oxalic acid to Fe_3O_4/PEG-400. This red shift would not have happened after addition of oxalic acid, unless the coverage of the Fe particle with PEG molecules was not completed or oxalic acid causes hydrolysis of some Fe–O–C bonds on Fe_3O_4/PEG--400 or other unknown reactions.

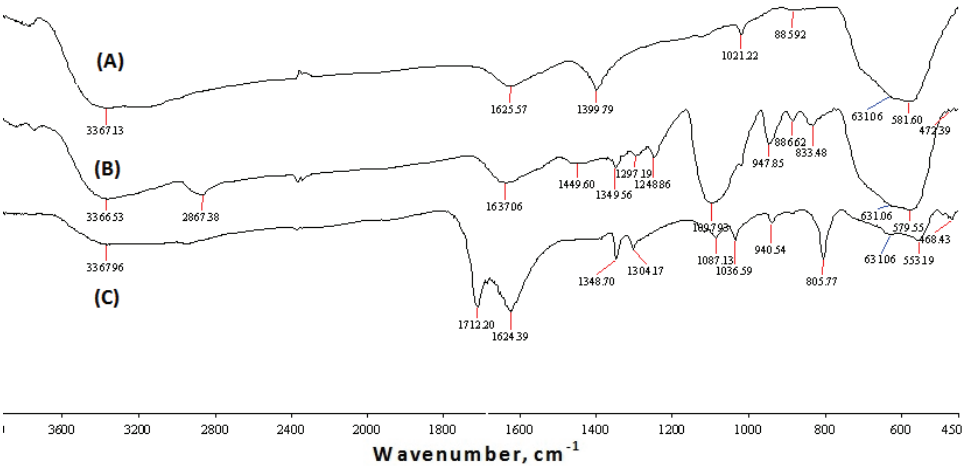

Fig. 1. The FT-IR spectra of the magnetic nano-Fe_3O_4 nanoparticles (A), the magnetic nano-Fe_3O_4/PEG-400 nanoparticles (B) and the magnetic nano-Fe_3O_4/PEG-400/oxalic acid nanoparticles (C).

The XRD patterns of the magnetic nano-Fe_3O_4/PEG/oxalic acid are presented in Fig. 2. In the 2θ range of 20–70°, the peak positions are indexed as (220), (31 1), (222), (400), (422), (511) and (440). The diffraction peaks suggest the particles are indexed to nano-Fe_3O_4, which is in good agreement with the literature[38] and reveals the existence of a magnetic nano-Fe_3O_4 core in the magnetic nano-Fe_3O_4/PEG/oxalic acid.

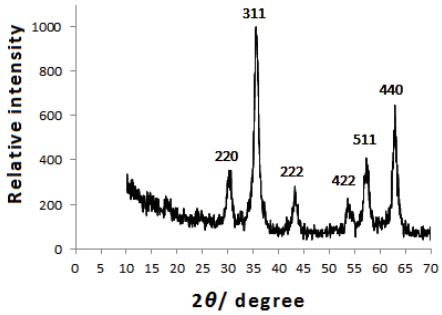

Fig. 2. The XRD patterns of the magnetic Fe_3O_4/PEG-400/oxalic acid nanoparticles.

The SEM images of the nano-magnetic Fe_3O_4/PEG-400 particles Fig. 3A and the nano-magnetic Fe_3O_4/PEG-400/oxalic acid Fig. 3B present particles of size and morphology of nanoparticles. The results show nanoparticles in the range of nanometers of uniform size and spherical shape.

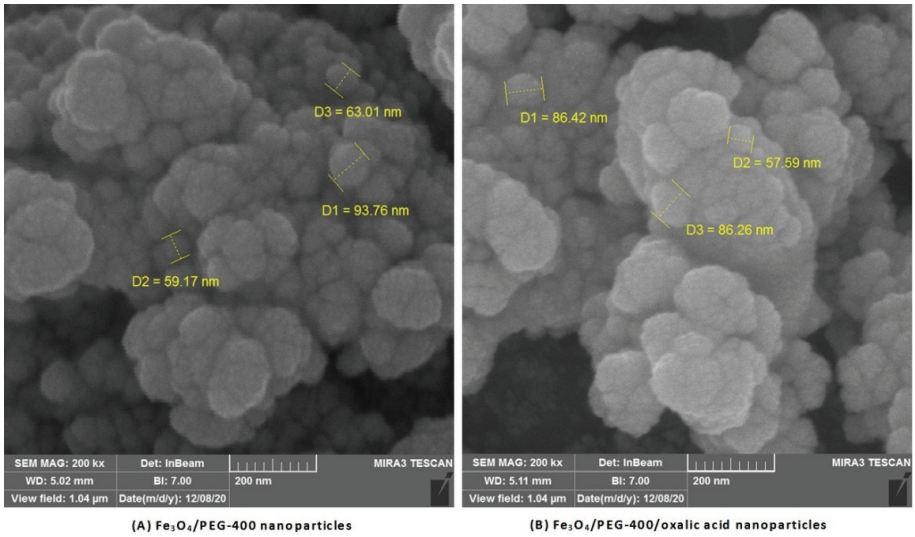

(A) Fe_3O_4/PEG-400 nanoparticles (B) Fe_3O_4/PEG-400/oxalic acid nanoparticles

Fig. 3. A) An SEM image of the magnetic Fe_3O_4/PEG-400 nanoparticles and B) an SEM image of magnetic Fe_3O_4/PEG-400/oxalic acid nanoparticles.

The surface chemical composition of magnetic nano-Fe_3O_4/PEG (Fig. 4A) and magnetic nano-Fe_3O_4/PEG/oxalic acid (Fig. 4B) were analyzed by EDX.

The EDX spectrum for nano-Fe_3O_4/PEG shows iron (67.17 wt. %), oxygen (25.71 wt. %) and carbon (7.12 wt. %). It reveals that the iron was from magnetic Fe_3O_4, carbon from PEG-400 and oxygen from Fe_3O_4 and PEG-400. According to these results PEG-400 loaded more than 7 wt.% on the surface of the magnetic Fe_3O_4 nano-particles. Additionally, the EDX spectrum for the magnetic nano-Fe_3O_4/PEG/oxalic acid shows iron (27.04 wt. %) (from Fe_2O_3), oxygen (55.92 wt. %, from Fe_3O_4, PEG-400 and oxalic acid) and carbon (17.03 wt. %, from PEG-400 and oxalic acid). A comparison of the results of the EDX spectra shows that oxalic acid loaded more than 10 wt. % on the surface of the magnetic nano-Fe_3O_4//PEG-400 particles.

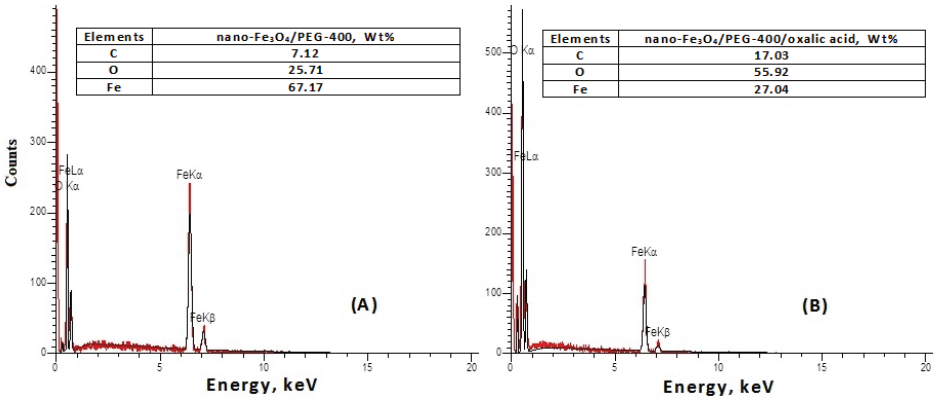

Fig. 4. A) The EDX analysis of the magnetic Fe_3O_4/PEG-400 nanoparticles. B) The EDX analysis of the magnetic Fe_3O_4/PEG-400/oxalic acid nanoparticles.

After characterization of the chemical structure of magnetic nano-Fe_3O_4/ /PEG/oxalic acid, several reactions for optimum reaction conditions were performed, as shown in Table I. The reaction conditions were carefully examined. It was the best to combine benzaldehyde (1 mmol), aniline (1 mmol), and 0.5 g magnetic Fe_3O_4/PEG/Oxalic acid nano particles as the catalyst in methanol, and the mixture was stirred at room temperature for 30 min. The order of addition components is important to avoid by-products. Then, methyl acetylenedicarboxylate (DMAD) was added, and the reaction was completed after 24 h to give the corresponding pyrrolin-2-ones in 90 % yields as shown in Table I, entry 7–8 and Scheme 1.

The all the new products were characterized by their FT-IR, ^{1}H-NMR, ^{13}C--NMR and mass spectra. The C=O stretching frequency in the FT-IR spectrum of the products appears around 1675–1691 cm^{-1} (Table II, column 5). The chemical shifts of the CH group in heterocyclic ring (Table II, column 4), which appears at around 5.29 to 6.47 ppm, as a singlet signal. Melting points of the products

(Table II, column 6) were measured and compared with literature data for the known compounds.[25–30]

TABLE I. Optimization of the reaction conditions for the reaction of benzaldehye (1 mmol), aniline (1 mmol), DAMD (1 mmol) in the presence of magnetic Fe_3O_4/PEG-400/oxalic acid nano-particles as catalyst at room temperature for the synthesis of 1,5-diphenyl-3-hydroxy-4--methoxycarbonyl-3-pyrrolin-2-one, as shown in Scheme 1

Entry	Catalyst	Amount	Solvent	*t* / h	Conversion, %[a]
1	Oxalic acid	1–10 mmol	EtOH	72	30>
2	Oxalic acid	1–10 mmol	MeOH	72	30>
3	Fe_3O_4/PEG-400	1 g	EtOH	72	0
4	Fe_3O_4/PEG-400	1 g	MeOH	72	0
5	Fe_3O_4/PEG-400/Oxalic acid	0.25 g	EtOH	72	50>
6	Fe_3O_4/PEG-400/Oxalic acid	0.25 g	MeOH	72	50>
7	Fe_3O_4/PEG-400/Oxalic acid	0.5 g	EtOH	24	90>
8	Fe_3O_4/PEG-400/Oxalic acid	0.5 g	MeOH	24	100
9	Fe_3O_4/PEG-400/Oxalic acid	1 g	MeOH	24	100

[a]The conversions were monitored by TLC, eluent: (EtOAc/*n*-hexane:1/1)

The efficiency of this protocol was examined by the reaction of a variety of aromatic aldehydes and arylamines. All the reactions were completed in appropriate times within 24 h in the excellent yields of pure products (90–96 %) as shown in Table II.

TABLE II. The synthesis of 3-acyl-5-hydroxy-3-pyrrolin-2-one derivatives from aldehydes (Ar), anilines (Ar') and DMAD under the optimized reaction condition (Table 1, entry 2)

Entry	Ar	Ar'	δ_{CH} / ppm	$\nu_{C=O}$ / cm^{-1}	m.p., °C	Yield, %
1[27]	Phenyl	phenyl	5.71	1681	173–175	90
2[25]	3-Nitrophenyl	phenyl	5.65	1686	204–206	90
3[27]	2-Cholorophenyl	phenyl	6.47	1686	200–202	92
4[26]	2-Methoxyphenyl	phenyl	5.73	1691	167–169	90
5[26]	2-Boromophentyl	phenyl	6.41	1686	203–205	90
6[25]	4-Bromophenyl	4-bromophenyl	5.29	1684	218–220	95
7[12]	Phenyl	4-methoxyphenyl	5.63	1675	170–171	90
8	3-Bromophenyl	4-bromophenyl	5.64	1689	230–231	95
9	4-Methoxyphenyl	4-bromophenyl	5.64	1683	165–167	92
10	2-Methoxyphenyl	4-methoxyphenyl	6.23	1687	210–212	94
11	2-Chlorophenyl	4-bromophenyl	6.38	1683	193–194	95
12	2-Methoxyphenyl	4-methylphenyl	6.25	1686	173–175	90
13	3-Bromophenyl	4-methylphenyl	6.08	1686	184–186	91
14	3-Nitrophenyl	4-bromophenyl	5.69	1679	176–178	91

The magnetic Fe_3O_4/PEG-400/oxalic acid nanoparticles provide a catalyst system that can release hydronium ion smoothly *in situ* to the reaction in the best concentration for the reaction to proceed. The participation of oxalate by this catalyst was not observed during of the reactions. In addition, according to the

chemical structure of Fe_3O_4/PEG-400/oxalic acid, the OH and CO_2H groups can provide a good polarity on the catalyst surface. On the other hand, all moieties in this reaction are polar. Therefore, they can condense easily on Fe_3O_4/PEG--400/oxalic acid surface by dipolar–dipolar interactions.

The proposed mechanism is shown in Schemes 3 and 4. The magnetic Fe_3O_4/ /PEG-400/oxalic acid nanoparticles catalyst activates aldehyde to produce imine (A) as an intermediate by reaction with aniline (Scheme 3, step 1). Then, the obtained H_2O molecules react with the activated DMAD and the imine moiety to produce the corresponding pyrrolin-2-one (B, Scheme 3, step 2).

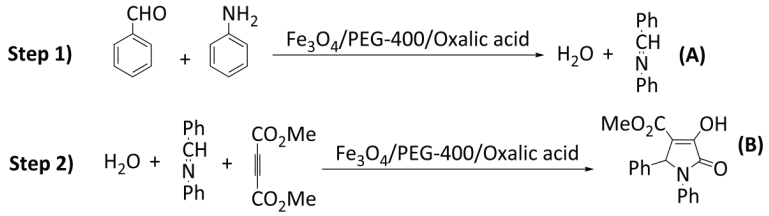

Scheme 3. The proposed steps for the synthesis of 1,5-diphenyl-3-hydroxy-4-methoxy-carbonyl-3-pyrrolin-2-one by the magnetic Fe_3O_4/PEG-400/oxalic acid nanoparticles.

The mechanism for step (1) in Scheme 3 is known. The mechanism for step 2 is shown in Scheme 4. The DMAD is activated by the protonation of the carboxylate group by the catalyst (Scheme 4, A). This process provides the required activation energy for further progress of the reaction. Then, the imine moiety Scheme 4B attacks the protonated carboxylate group of DMAD (Scheme 4, pathway I). Simultaneously, H_2O attacks to β-carbon of the protonated carboxylic acid on DMAD (Scheme 4, pathway II) which produces a stabilized intermediate *via* the intermolecular addition and cyclization (Scheme 4, C). Thereby, the corresponding five-membered heterocyclic compounds (Scheme 4, D) were synthesized by the condensation concerted reaction.

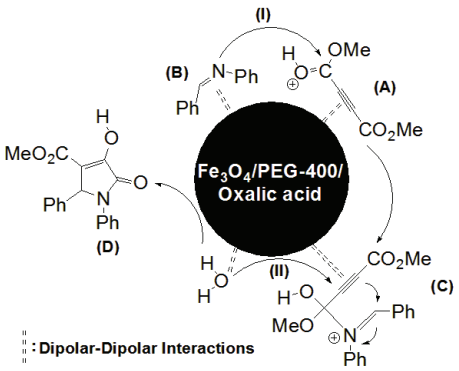

Scheme 4. The modified mechanism of step (2) for the synthesis of pyrrolin-2-ones.

The reusability of nano-Fe_3O_4/PEG-400/oxalic acid catalyst was examined. Recycling of the catalyst is an important characteristic because of environmental and economic concerns. After completion of the reaction, the magnetic nano-catalyst was easily and efficiently separated from the product by an external magnetic field. The nano-Fe_3O_4/PEG/oxalic acid was washed two or three times with acetone and dried at room temperature. It is notable that the recycled catalyst could be used two more times again. For example, in the second and third rounds, the yields of the product (Table II, entry 1) were 87 and 85 %, respectively. However, oxalic acid should be loaded on Fe_3O_4/PEG-400 according to the instruction for the further rounds. Thus the recovered and regenerated catalyst could be useful for reaction with loss of activity.

The efficiency of Fe_3O_4/PEG-400/oxalic acid nonmagnetic catalyst for the synthesis of pyrrolin-2-one derivatives was compared with other reported protocols as shown in Table III. In all cases Fe_3O_4/PEG-400/oxalic acid catalyst has a good potential for the synthesis of this class of compounds.

TABLE III. Comparison of synthesis of 1,5-diphenyl-3-hydroxy-4-methoxycarbonyl-3-pyrrolin-2-one by different reported protocols. All synthesis are green

Entry	Protocol	Yield,%	Time	Reusable cat.	Reference
1	Fe_3O_4/PEG-400/OA	94	24 h	Yes	This work
2	*p*-TsOH/EtOH	62	24 h	Non	12
3	TiO_2 admicelle/H_2O	75	18 h	Non	25
4	EtOH/H_2O	87	15 h	Non	26
5	Citric acid/US/EtOH	90	20 min	Non	27
6	*p*-TsOH/MW/EtOH	96	6 min	No	28
7	[bmim]BF_4/PEG-400	89	1 h	Yes	29a
8	MW/[BBSI]Cl/Glycol	90	5 min	Yes	29b
9	[BBSI]Cl/ball milling	90	25 min	Yes	29c
10	Fe_3O_4@SiO_2@Propyl–ANDSA/EtOH	87	8 h	Yes	30

CONCLUSIONS

Oxalic acid was have loaded on magnetic Fe_3O_4/PEG-400 for the synthesis of magnetic Fe_3O_4/PEG-400/oxalic acid nanoparticles as a catalyst. The chemical structure of this compound was characterized and approved by different methods (FT-IR, XRD, EDX and SEM). Then, the magnetic Fe_3O_4/PEG-400/ /oxalic acid nanoparticles were applied for the preparation of a variety of pyrrolin-2-ones, using aromatic aldehydes, anilines and dimethyl acetylenedicarboxylate (DMAD) precursors in one-pot, three-component condensation reaction at room temperature with excellent yields of products (90–95 %). Easy work-up, mild reaction conditions, appropriate catalyst (reusable, economic and eco--friendly), high efficiency and green profile make to this new protocol more attractive for the synthesis of these classes of compounds. Therefore, this new convenient protocol can be added to the list of the currently used methodologies.

SUPPLEMENTARY MATERIAL

Additional data and information are available electronically at the pages of journal website: https://www.shd-pub.org.rs/index.php/JSCS/article/view/10785, or from the corresponding author on request.

Acknowledgement. The authors gratefully appreciated the financial support of this work by the research council of Islamic Azad University branch of Mahabad.

ИЗВОД

СИНТЕЗА И КАРАКТЕРИЗАЦИЈА Fe_3O_4/PEG-400/ОКСАЛНА КИСЕЛИНА МАГНЕТНИХ НАНОЧЕСТИЦА КАО ХЕТЕРОГЕНОГ КАТАЛИЗАТОРА ЗА СИНТЕЗУ ПИРОЛИН-2-ОН ДЕРИВАТА

SEYRAN ESMAEILZADEH и DAVOOD SETAMDIDEH

Department of Chemistry, Mahabad Branch, Islamic Azad University, Mahabad, Iran

Наношењем оксалне киселине на Fe_3O_4/PEG-400 уз ултразвучно озрачивање успешно је синтетисан нови Fe_3O_4/PEG/оксална киселина наномагнетни катализатор. Применом FT-IR спектроскопије, XRD, EDX и SEM метода испитивана је структура добијеног катализатора. Катализатор је коришћен за синтезу 3-ацил-5-хидрокси-3-пиролин-2-она деривата из одговарајућих алдехида, анилина и диметил ацетилендикарбоксилата (DMAD) у једном реакционом суду и трокомпонентном MCR реакцијом, са високим приносима (90–95 %) током 24 h на собној температури. Добијено је 14 узорака. Једном употребљени катализатор може се са успехом употребити још два пута без регенерације. Описани метод има добар еколошки профил. Поред тога, описана истраживања представљају побољшање механизма за реакције овог типа. Хемијска структура добијених једињења одређена је на бази FT-IR, ^{1}H-NMR, ^{13}C-NMR и масених спектара.

(Примљено 21. маја, ревидирано 5. августа, прихваћено 10. августа 2021)

REFERENCES

1. S. Shylesh, V. Schunemann, W. R. Thiel, *Angew. Chem. Int. Ed*. **49** (2010) 3428 (https://doi.org/10.1002/ange.200905684)
2. Y. Zhu, L. P. Stubbs, F. Ho, R. Liu, C. P. Ship, J. A. Maguire, N. S. Hosmane, *ChemCatChem* **2** (2010) 365 (https://doi.org/10.1002/cctc.200900314)
3. H. Veisi, J. Gholami, H. Ueda, P. Mohammadi, M. Noroozi, *J. Mol. Catal., A* **365** (2015) 216 (https://doi.org/10.1016/j.molcata.2014.10.012)
4. R. B. Nasir-Baigand, R. S. Varma, *Chem. Commun*. **49** (2013) 752 (https://doi.org/10.1039/c2cc35663e)
5. B. Abbas Khakiani, K. Pourshamsian, H. Veisi, *J. Appl. Organometal. Chem.* **29** (2015) 259 (https://doi.org/10.1002/aoc.3282)
6. E. McCafferty, J. P. Wightman, *Surf. Interface Anal*. **26** (1998) 549 (https://doi.org/10.1002/(sici)1096-9918(199807)26:8<549::aid-sia396>3.0.co;2-q)
7. P. Riente, C. Mendozaa, M. A. Peric, *J. Mater. Chem*. **21** (2011) 7350 (https://doi.org/10.1039/c1jm10535c)
8. a) F. A. Tameh, J. Safaei-Ghomi, M. Mahmoudi-Hashemi, H. Shahbazi-Alavi, *RSC Adv.* **6** (2016) 74802 (https://doi.org/10.1039/c6ra08458c) b) J. Safaei-Ghomi, F. Eshteghal, *Ultra Sonochem.* **38** (2017) 488 (https://doi.org/10.1016/j.ultsonch.2017.03.047) c) R. Ghorbani-Vaghei, N. Sarmast, J. Mahmoodi, *J. Appl. Organometal. Chem.* **31** (2017) e3681 (https://doi.org/10.1002/aoc.3681)

9. H. Zeng, J. Li, Z. L. Wang, J. P. Liu, S. Sun, *Nano Lett*. **4** (2004) 187 (https://doi.org/10.1021/nl035004r)
10. R. Ghosh, L. Pradhan, Y. Priyabala, D. Meena, R. Tewari, A. Kumar, S. Sharma, G. Vatsa, B. Pandey, R. S. Ningthoujam, *J. Mater. Chem.* **21** (2011) 13388 (https://doi.org/10.1039/c1jm10092k)
11. D. Setamdideh, *J. Serb. Chem. Soc.* **81** (2016) 971 (https://doi.org/10.2298/jsc160202050s)
12. J. Sun, Q. Wu, E. Y. Xia, C. G. Yan, *Eur. J. Org. Chem*. (2011) 2981. (https://doi.org/10.1002/ejoc.201100008)
13. L. P. Dwoskin, L. Teng, S. T. Buxton, P. A. Crooks, *J. Pharmacol. Exp. Ther*. **288** (1999) 905 (https://jpet.aspetjournals.org/content/288/3/905.short)
14. P. Singh, V. Dimitriou, R. P. Mahajan, A. W. Crossley, *Br. J. Anaesth.* **71** (1993) 685 (https://doi.org/10.1093/bja/71.5.685)
15. P. N. Patsalos, *Epilepsia* **46** (2005) 140 (https://doi.org/10.1111/j.1528-1167.2005.00326.x)
16. S. Omura, T. Fujimoto, K. Otoguro, K. Matsuzaki, R. Moriguchi, H. Tanaka, Y. Sasaki, *J. Antibiot*. **44** (1991) 113 (https://doi.org/10.7164/antibiotics.44.113)
17. R. H. Feling, G. O. Buchanan, T. J. Mincer, C. A. Kauffman, P. R. Jensen, W. Fenical, *Angew. Chem. Int. Ed*. **42** (2003) 355 (https://doi.org/10.1002/anie.200390115)
18. Y. Asami, H. Kakeya, R. Onose, A. Yoshida, H. Matsuzaki, H. Osada, *Org. Lett.* **4** (2002) 2845 (https://doi.org/10.1021/ol020104+)
19. M. S. F. Franco, G. A. Casagrande, C. Raminelli, S. Moura, M. Rossatto, F. H. Quina, C. M. P. Pereira, A. F. C. Flores, L. Pizzuti, *Synth. Commun*. **45** (2015) 692 (https://doi.org/10.1080/00397911.2014.978504)
20. M. Andana, S. I. Hashimoto, *Tetrahedron Lett*. **39** (1998) 79 (https://doi.org/10.1016/S0040-4039(97)10493-2)
21. D. R. Choi, K. Y. Lee, Y. S. Chung, J. E. Joo, Y. H. Kim, Ch. Y. Oh, Y. S. Lee, W. H. Ham, *Arch. Pharm. Res*. **28** (2005) 151 (https://doi.org/10.1007/bf02977706)
22. L. E. Burgess, A. I. Meyers, *J. Org. Chem.* **57** (1992) 1656 (https://doi.org/10.1021/jo00032a012)
23. L. E. Overman, T. P. Remarchuk, *J. Am. Chem. Soc*. **124** (2002) 12 (https://doi.org/10.1021/ja017198n)
24. V. Singh, R. Saxena, S. Batra, *J. Org. Chem*. **70** (2005) 353 (https://doi.org/10.1021/jo048411b)
25. R. Sarkar, C. Mukhopadhyay, *Tetrahedron Lett*. **54** (2013) 3706 (https://doi.org/10.1016/j.tetlet.2013.05.017)
26. A. M. Zonouz, I. Eskandari, B. Notash, *Synth. Commun*. **45** (2015) 2115 (https://doi.org/10.1080/00397911.2015.1065506)
27. H. Ahankar, A. Ramazani, K. Slepokura, T. Lis, S. W. Joo, *Green Chem*. **18** (2016) 3582 (https://doi.org/10.1039/c6gc00157b)
28. K. S. Marapala, N. Venkatesh, M. Swapna, P. R. Venkateswar, *Int. J. ChemTech Res.* **13** (2020) 227 (https://doi.org/10.20902/ijctr.2019.130128)
29. a) S. Pervaram, D. Ashok, C. Venkata Ramana Reddy, M. Sarasija, A. Ganesh, *Chem. Data Coll.* **29** (2020) 100508 (https://doi.org/10.1016/j.cdc.2020.100508) b) N. Ghaffari Khaligh, T. Mihankhah, M. Rafie Johan, S. J. J. Titinchi, *Green Process Synth.* **8** (2019) 373 (https://doi.org/10.1515/gps-2019-0004) c) N. Ghaffari Khaligh, T. Mihankhah, M. Rafie Johan, *Synth. Commun*. **49** (2019) 1334 (https://doi.org/10.1080/00397911.2019.1601225)

30. R. Ghorbani-Vaghei, N. Sarmast, J. Mahmoodi, *J. Appl. Organomet. Chem.* **31** (2017) e3681 (https://doi.org/10.1002/aoc.3681)
31. D. Setamdideh, *J. Mex. Chem. Soc*. **59** (2015) 191 (https://doi.org/10.29356/jmcs.v59i3.34)
32. Z. Zhang, J. Kong, *J. Haz. Mater.* **193** (2011) 325 (https://doi.org/10.1016/j.jhazmat.2011.07.033)
33. G. Nabiyouni, M. Julaee, D. Ghanbari, P. C. Aliabadi, and N. Safaie, *J. Ind. Eng. Chem.* **21** (2015) 599 (https://doi.org/10.1016/j.jiec.2014.03.025)
34. A. B. Savić, D. Cokesa, S. Lazarević, B. Jokić, D. Janaćković, R. Petrović, L. S. Živković, *Powder Technol*. **301**(2016) 511 (https://doi.org/10.1016/j.powtec.2016.06.028)
35. D. V. Quy, N. M. Hieu, P. T. Tra, N. H. Nam, N. H. Hai, N. T. Son, P. T. Nghia, N. T. V. Anh, T. T. Hong, N. H. Luong, *J. Nanomaterials*, 2013, Article ID 603940 (http://doi.org/10.1155/2013/603940)
36. T. Koutzarova, S. Kolev, C. Ghelev, D. Paneva, I. Nedkov, *Phys. Status Solidi, C* **3** (2006) 1302 (https://doi.org/10.1002/pssc.200563115)
37. M. F. Tai, C. W. Lai, S. B. Abdul Hamid, *J. Nanomater*, 2016, Article ID 8612505 (https://doi.org/10.1155/2016/8612505)
38. K. S. Loh, Y. H. Lee, A. Musa, A. A. Salmah, I. Zamri, *Sensors* **8** (2008) 5775 (https://doi.org/10.3390/s8095775).

Journal of the Serbian Chemical Society
JSCS@tmf.bg.ac.rs • www.shd.org.rs/JSCS
J. Serb. Chem. Soc. 86 (11) S359–S379 (2021)
Supplementary material

SUPPLEMENTARY MATERIAL TO

Synthesis and characterization of Fe_3O_4/PEG-400/oxalic acid magnetic nanoparticles as a heterogeneous catalyst for the synthesis of pyrrolin-2-ones derivatives

SEYRAN ESMAEILZADEH and DAVOOD SETAMDIDEH*

Department of Chemistry, Mahabad Branch, Islamic Azad University, Mahabad, Iran

J. Serb. Chem. Soc. 86 (11) (2021) 1039–1052

*1-(4-Boromophenyl)-5-(3-boromophenyl)-3-hydroxy-4-methoxycarbonyl-3-pyrrolin-2-one (Table II, entry **8**)*

Limon solid; yield: 0.44 g (95 %); m.p. 230–231 °C; FT-IR (KBr, ν_{max} / cm^{-1}): 3309 (OH), 2952, 1717 (C=O), 1689 (C=O), 1490, 1374, 1212, 1011; ^{1}H-NMR (250.13 MHz, $CDCl_3$, δ / ppm): 3.70 (3H, *s*, OCH_3), 5.64 (1H, *s*, CH), 6.14–7.39 (8H, *m*, Ar), 8.93 (1H, *brs*, OH); ^{13}C-NMR (62.90 MHz, $CDCl_3$, δ / ppm) 52.27, 60.66, 102.92, 112.69, 123.42, 126.05, 130.33, 132.05, 132.23, 135.02, 137.06, 152.39, 156.23, 160.93 (C=O); Mass (*m*/*z*): 469 (M^++4), 467.1 (M^++2), 465.1 (M^+), 267.0, 208 (100%), 157.1, 129.1, 101.1.

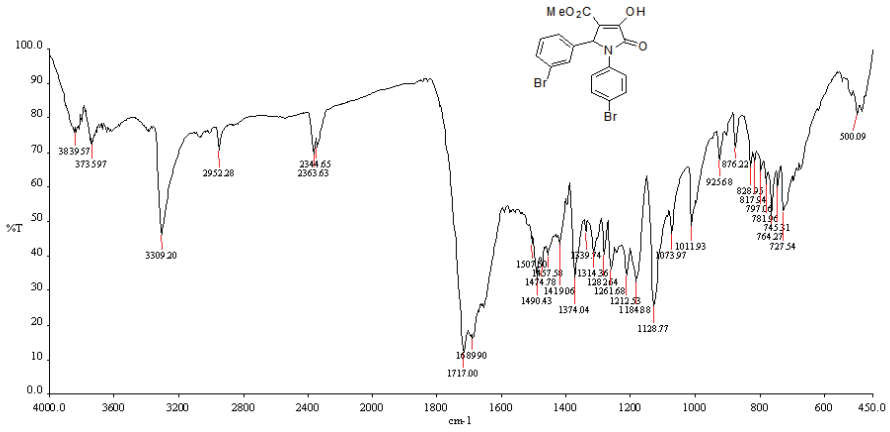

Fig. S-1. FT-IR (KBr, cm^{-1}) spectrum of compound **8**.

* Corresponding author. E-mail: d.setamdideh@iau-mahabad.ac.ir

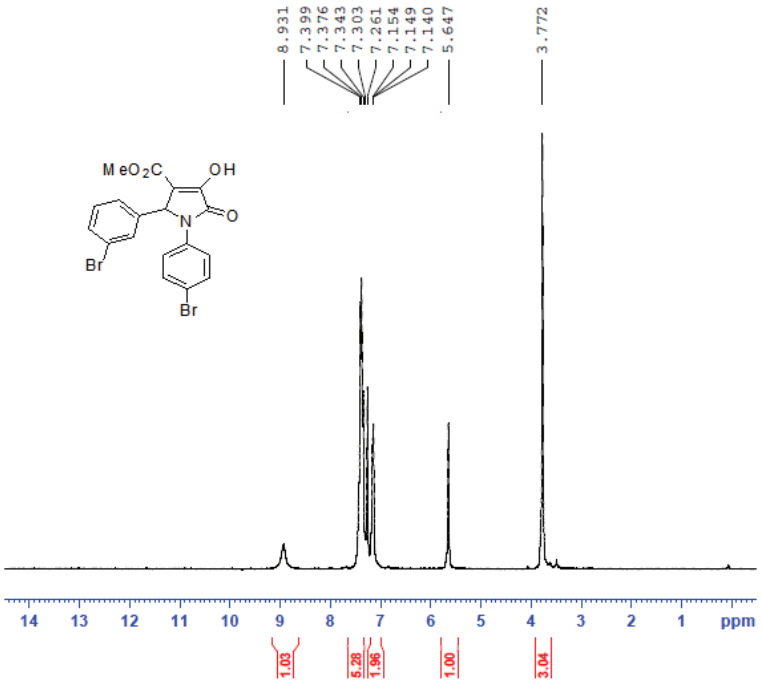

Fig. S-2. ^{1}H-NMR spectrum of compound **8** (250 MHz, $CDCl_3$, δ / ppm).

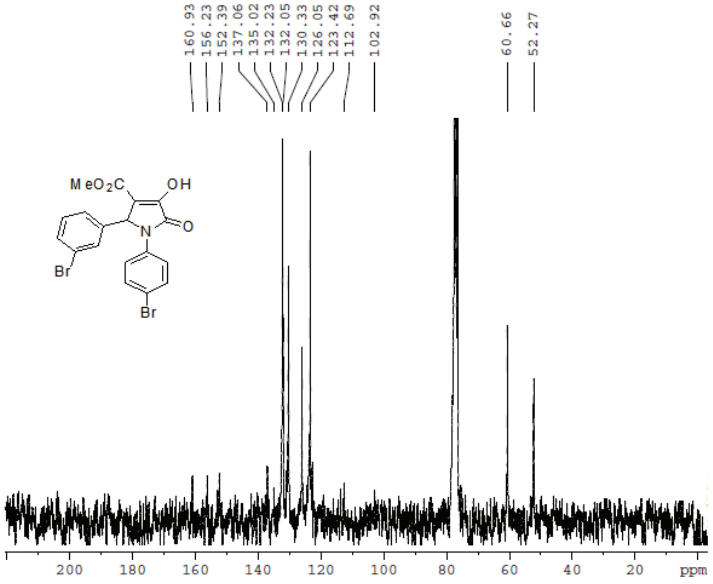

Fig. S-3. ^{13}C-NMR spectrum of compound **8** (63 MHz, $CDCl_3$, δ / ppm).

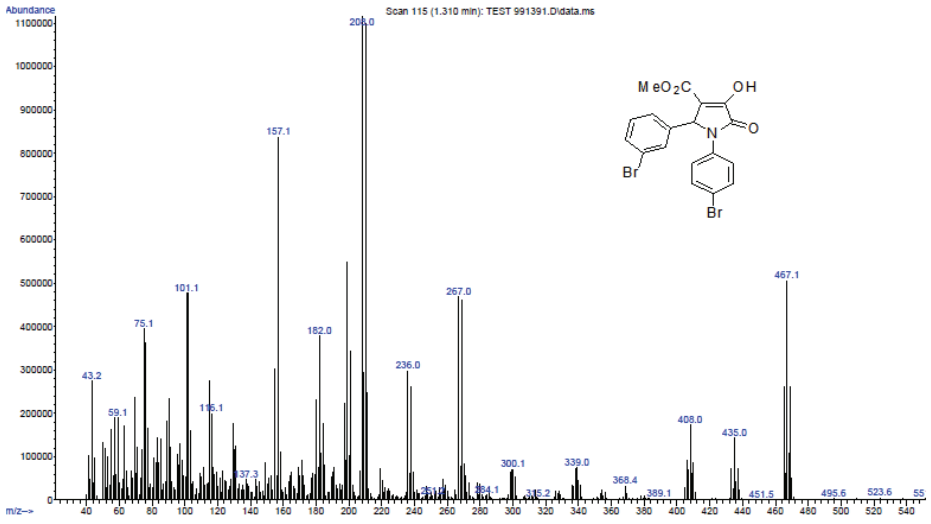

Fig. S-4. Mass spectrum of compound **8**.

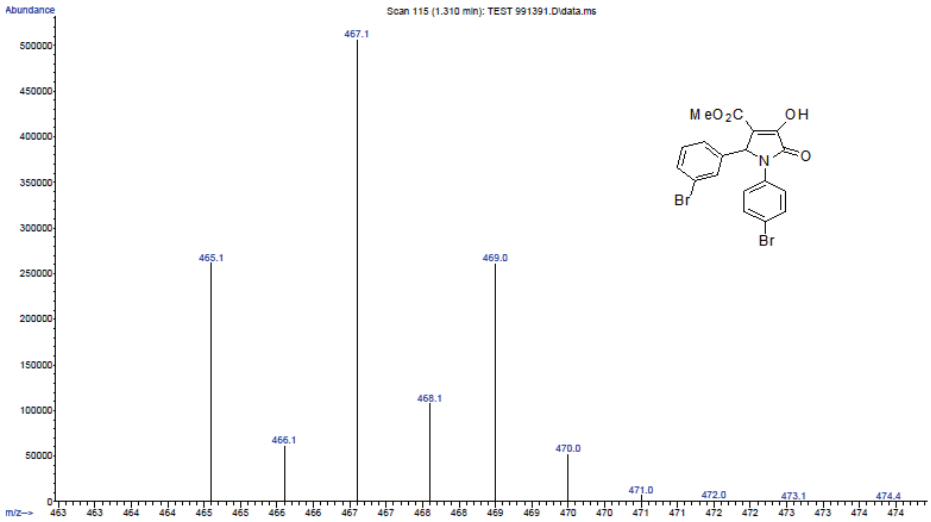

Fig. S-5. Mass spectrum of compound **8**.

*1-(4-Boromophenyl)-5-(4-methoxyphenyl)-3-hydroxy-4-methoxycarbonyl-3-pyrrolin-2-one (Table II, entry **9**)*

White yellow solid; Yield: 0.38 g (92 %); m.p.: 165–167 °C; FT-IR (KBr, ν_{max} / cm^{-1})): 3214 (OH), 2952, 1710 (C=O), 1683(C=O), 1495, 1374, 1229, 1031; ^{1}H-NMR (MHz: 250.13, $CDCl_3$, δ / ppm): 3.74 (6H, *s*, 2×OCH_3), 5.64 (1H, *s*, CH), 6.76–7.87 (8H, *m*, Ar), 8.9 (1H, *brs*, OH); ^{13}C-NMR (MHz: 62.90, $CDCl_3$, δ / ppm): 52.10, 55.16, 60.99, 113.06, 114.22, 118.99, 123.62, 126.21, 128.53, 132.00, 135.30, 155.69, 159.70, 162.77 (C=O), 165.16 (C=O); Mass (*m*/*z*): 419.1 (M^++2), 417.2 (M^+), 289.1, 219.2 (100 %), 151.1, 134.2, 97.2.

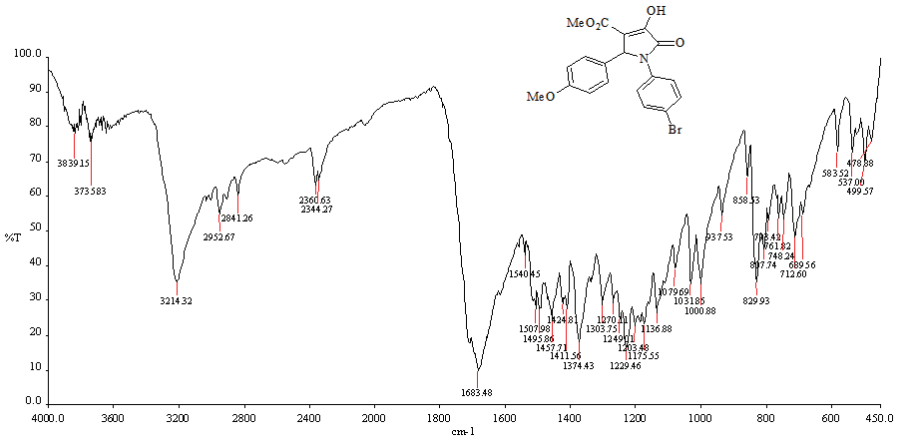

Fig. S-6. FT-IR (KBr, cm^{-1}) spectrum of compound **9**.

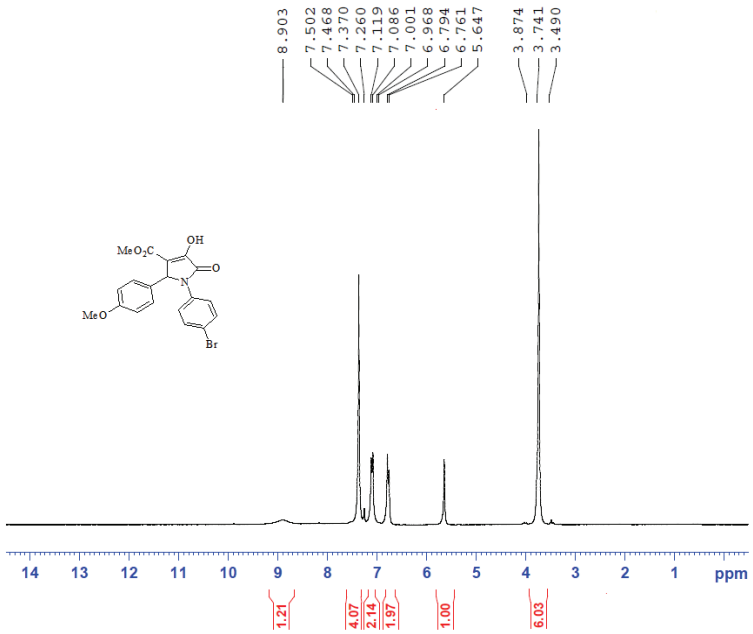

Fig. S-7. ^{1}H-NMR spectrum of compound **9** (250 MHz, $CDCl_3$, δ / ppm).

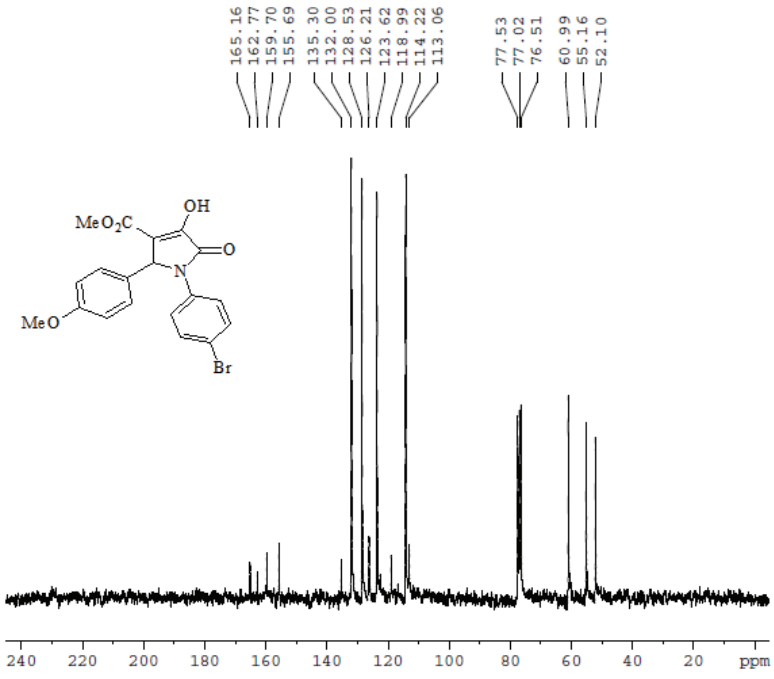

Fig. S-8. ^{13}C-NMR spectrum of compound **9** (63 MHz, $CDCl_3$, δ / ppm).

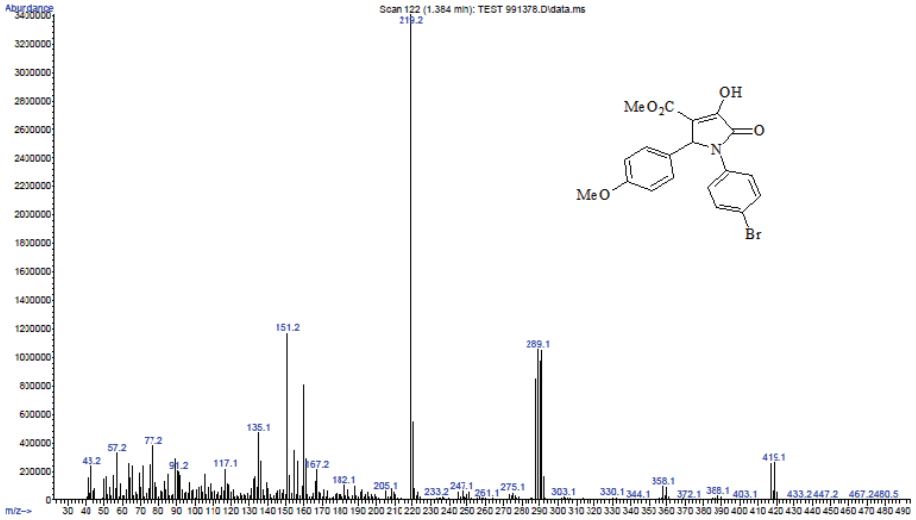

Fig. S-9. Mass spectrum of compound **9**.

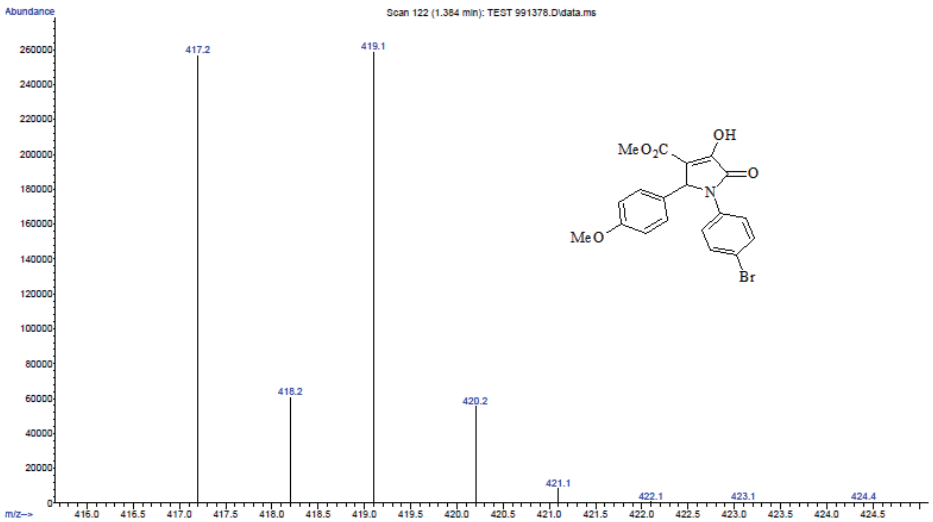

Fig. S-10. Mass spectrum of compound **9**.

*1-(4-Methoxyphenyl)-5-(2-methoxyphenyl)-3-hydroxy-4-methoxycarbonyl-3-pyrrolin-2-one (Table II, entry **10**)*

White solid, Yield: 0.34 g (94 %); m.p.: 210–212 °C; FT-IR (KBr, ν_{max} / cm^{-1})): 3273 (OH), 2954, 1723 (C=O), 1687 (C=O), 1495, 1372, 1247, 1131; ^{1}H-NMR (250.13 MHz, $CDCl_3$, δ / ppm): 3.70 (3H, *s*, OCH_3), 3.88 (3H, *s*, OCH_3), 6.23 (1H, *s*, CH), 6.79–7.46 (m, 8H, Ar), 8.93 (brs, 1H, OH). The ^{13}C-NMR (62.90 MHz, $CDCl_3$, δ / ppm): 30.89, 52.03, 55.87, 111.48, 118.60, 121.08, 122.99, 127.52, 129.91, 131.82, 135.58, 156.58, 162.50 (C=O); Mass (*m*/*z*): 369.2 (M^+), 337.2, 219.1 (100 %), 151.2, 131.1, 83.2, 57.2.

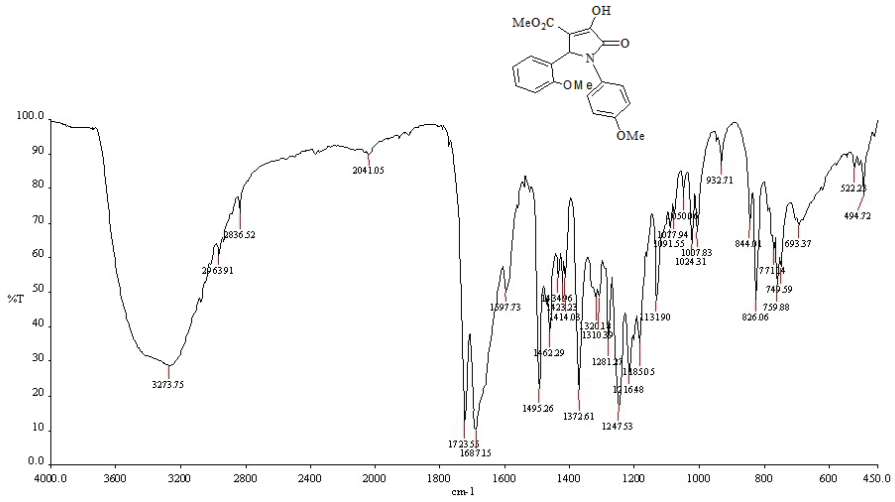

Fig. S-11. FT-IR (KBr / cm^{-1}) spectrum of compound **10**.

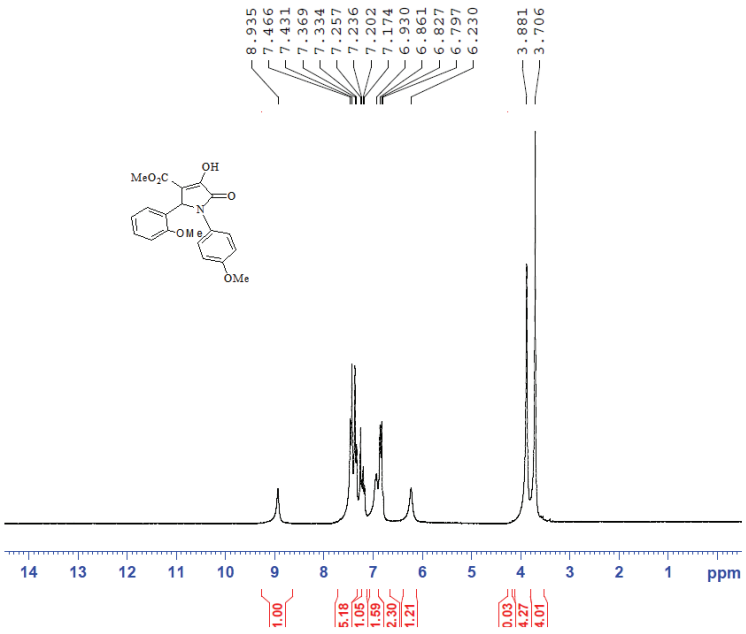

Fig. S-12. ^{1}H-NMR spectrum of compound **10** (250 MHz, $CDCl_3$, δ / ppm).

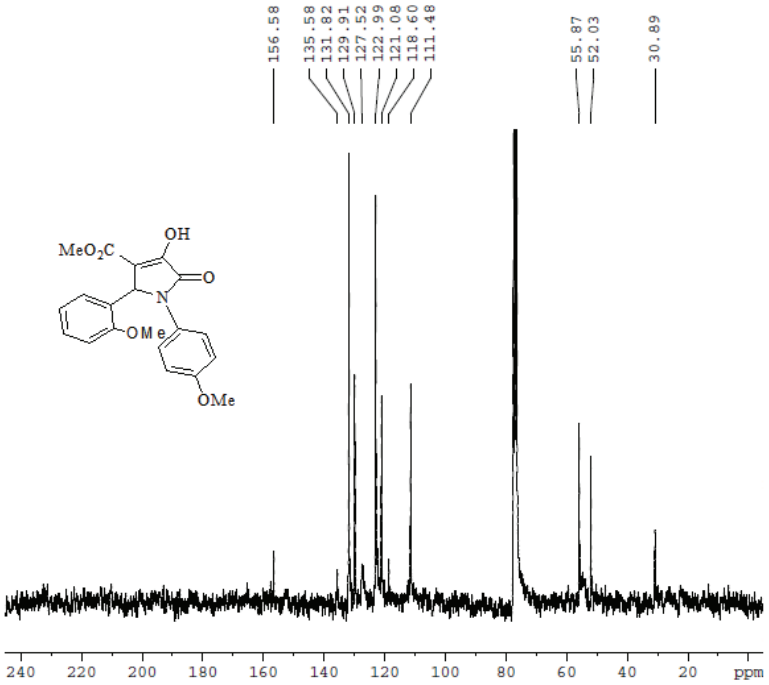

Fig. S-13. ^{13}C-NMR spectrum of compound **10** (63 MHz, $CDCl_3$, δ / ppm).

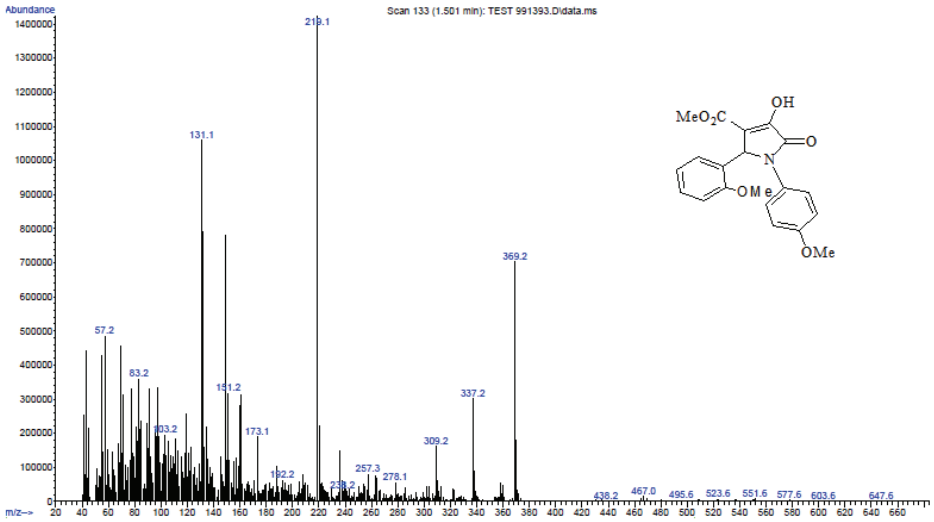

Fig. S-14. Mass spectrum of compound **10**.

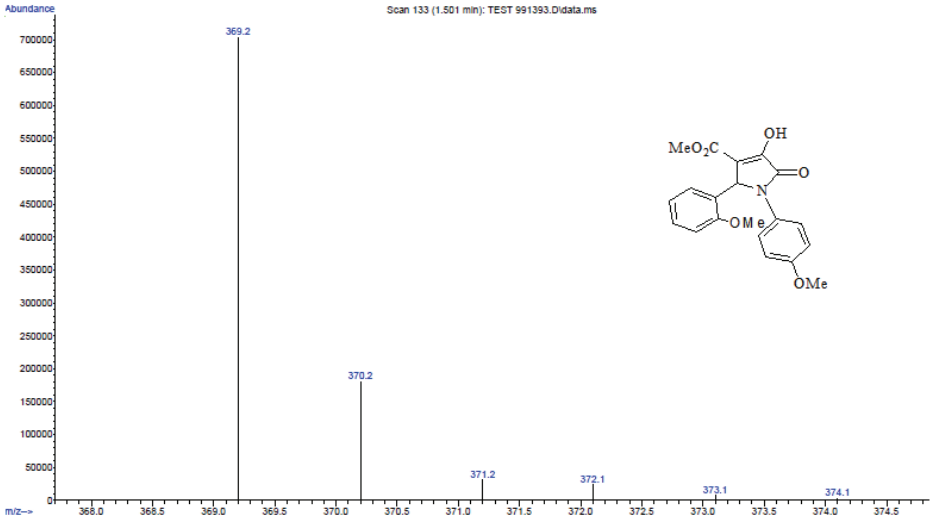

Fig. S-15. Mass spectrum of compound **10**.

*1-(4-Boromophenyl)-5-(2-cholorophenyl)-3-hydroxy-4-methoxycarbonyl-3-pyrrolin-2-one (Table II, entry **11**)*

White solid, Yield: 0.40 g (95%). m.p.: 193–194 °C. FT-IR (KBr, ν_{max} /cm^{-1}): 3309 (OH), 2954, 1714 (C=O), 1683 (C=O), 1490, 1363, 1234, 1009; ^{1}H-NMR (250.13 MHz, CDC_{l3}, δ / ppm): 3.72 (3H, *s*, OCH_3), 6.38 (1H, *s*, CH), 6.70–7.40 (8H, *m*, Ar); ^{13}C-NMR (62.90 MHz, $CDCl_3$ δ / ppm): 52.18, 56.38, 112.79, 119.06, 122.94, 126.73, 127.65, 129.92, 132.13, 135.07, 156.69, 162.64 (C=O), 165.15 (C=O), Mass (*m*/*z*): 425.1 (M^++4), 423.1 (M^++2), 421.1 (M^+), 391.0, 223.1, 164.1 (100%), 136.1, 101.1, 75.1.

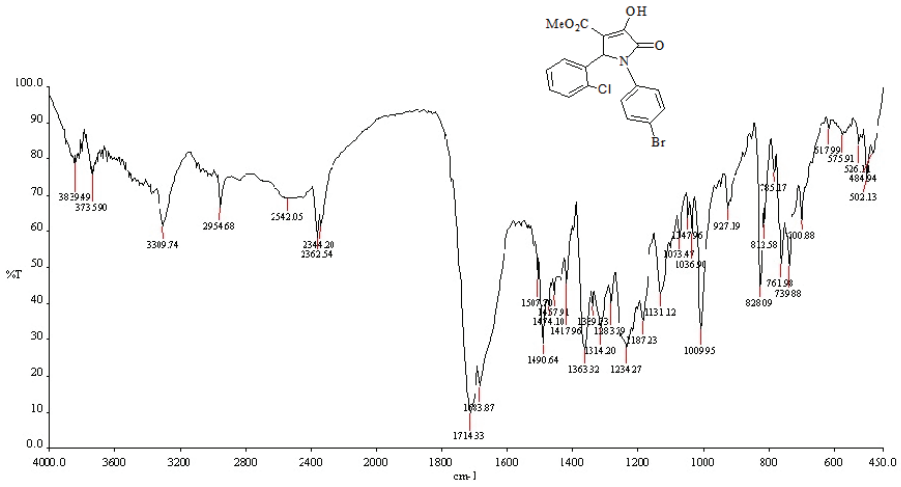

Fig. S-16. FT-IR (KBr, cm^{-1}) spectrum of compound **11**.

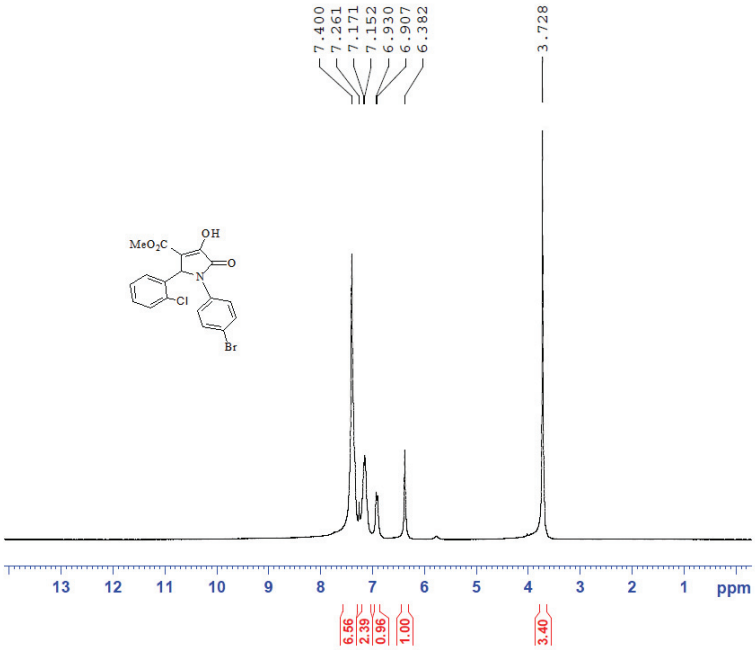

Fig. S-17. ^{1}H-NMR spectrum of compound **11** (250 MHz, $CDCl_3$, δ / ppm).

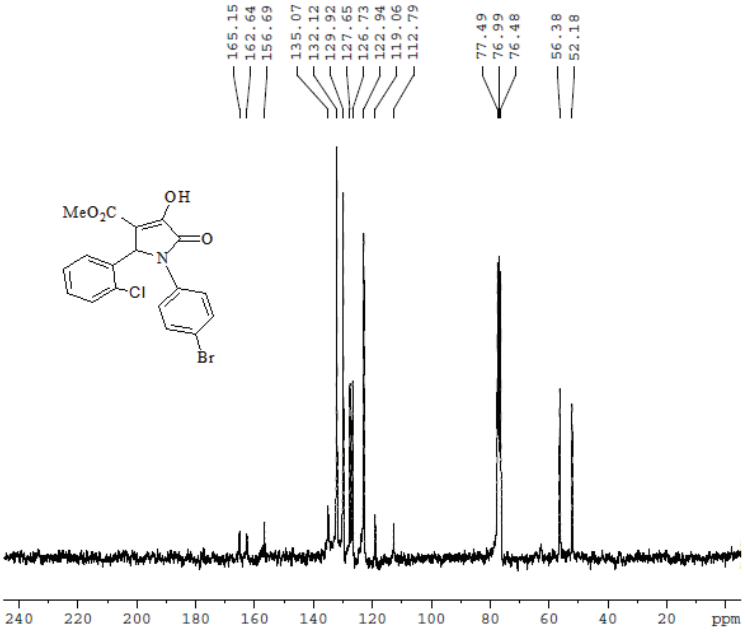

Fig. S-18. ^{13}C-NMR spectrum of compound **11** (63 MHz, $CDCl_3$, δ / ppm).

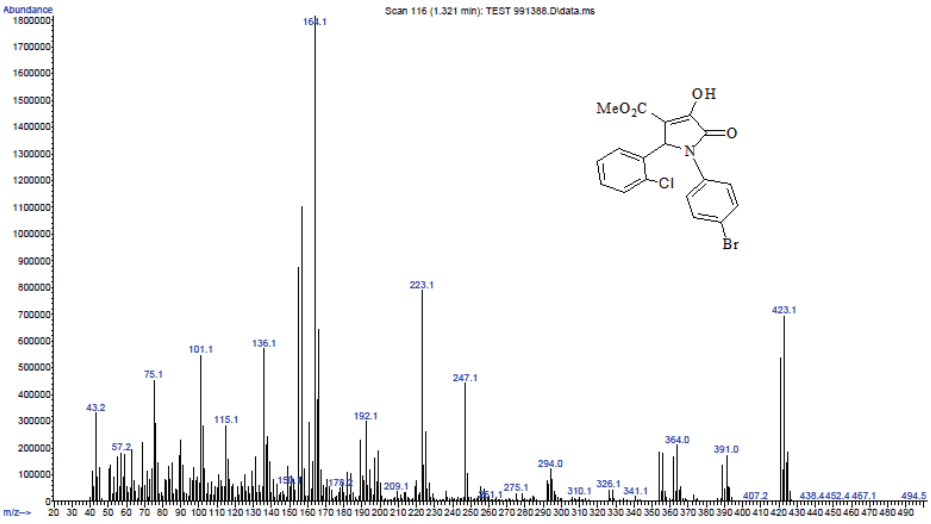

Fig. S-19. Mass spectrum of compound **11**.

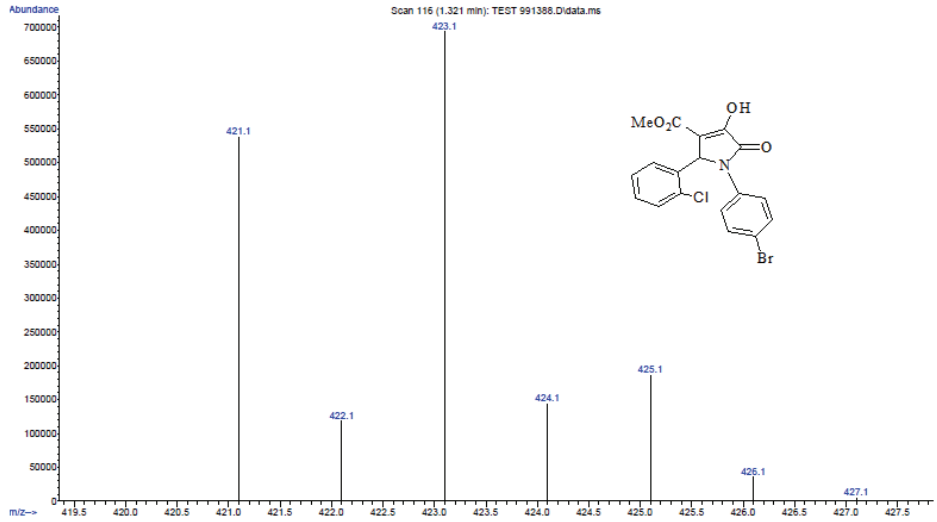

Fig. S-20. Mass spectrum of compound **11**.

*1-(4-Methylphenyl)-5-(2-methoxyphenyl)-3-hydroxy-4-methoxycarbonyl-3-pyrrolin-2-one (Table 2, entry **12**)*

White solid; Yield: 0.31 g (90 %); m.p.: 173–175 °C; FT-IR (KBr, ν_{max} / cm^{-1}): 3220 (OH), 2963, 1720 (C=O), 1686 (C=O), 1513, 1379, 1245, 1131; ^{1}H-NMR ($CDCl_3$, 250.13 MHz, δ / ppm): 2.22 (3H, *s*, CH_3), 3.70 (3H, *s*, OCH_3), 3.86 (3H, *s*, OCH_3), 6.25 (1H, *s*, CH), 6.78–7.40 (8H, *m*, Ar), 9.10 (1H, brs, OH); ^{13}C-NMR (62.90 MHz, $CDCl_3$, δ / ppm): 20.88, 51.96, 55.70, 55.86, 111.40, 120.91, 121.84, 122.93, 127.52, 129.35, 129.65, 133.81, 135.34, 156.67, 157.81, 162.96 (C=O), 165.42 (C=O). Mass (m/z): 353.2 (M^+), 321.2, 294.1, 278.1, 238.2, 219.1 (100%), 188.0, 160.1 133.1, 91.2, 65.2.

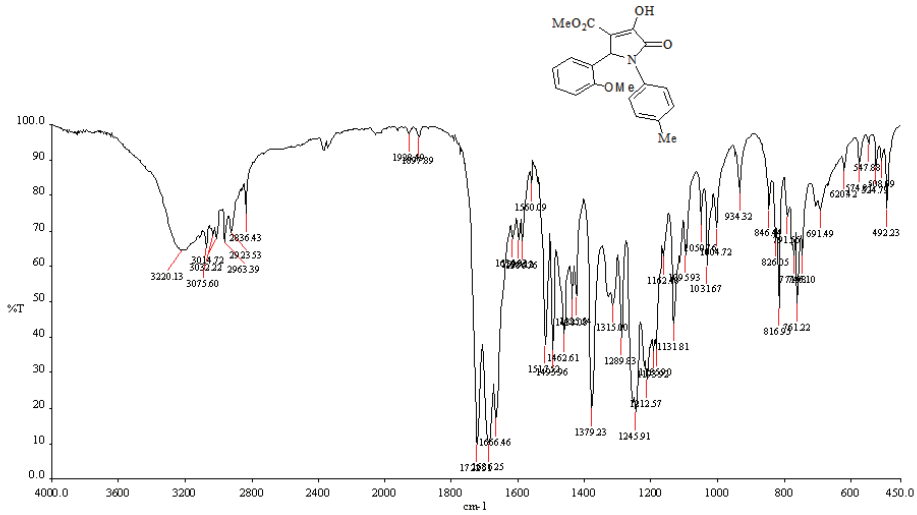

Fig. S-21. FT-IR (KBr, cm^{-1}) spectrum of compound **12**.

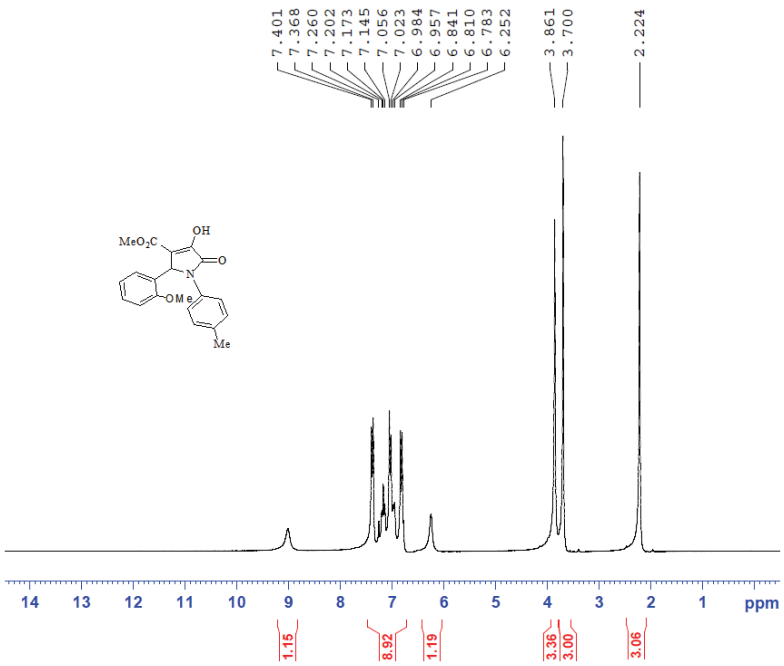

Fig. S-22. ^{1}H-NMR spectrum of compound **12** (250 MHz, $CDCl_3$, δ / ppm).

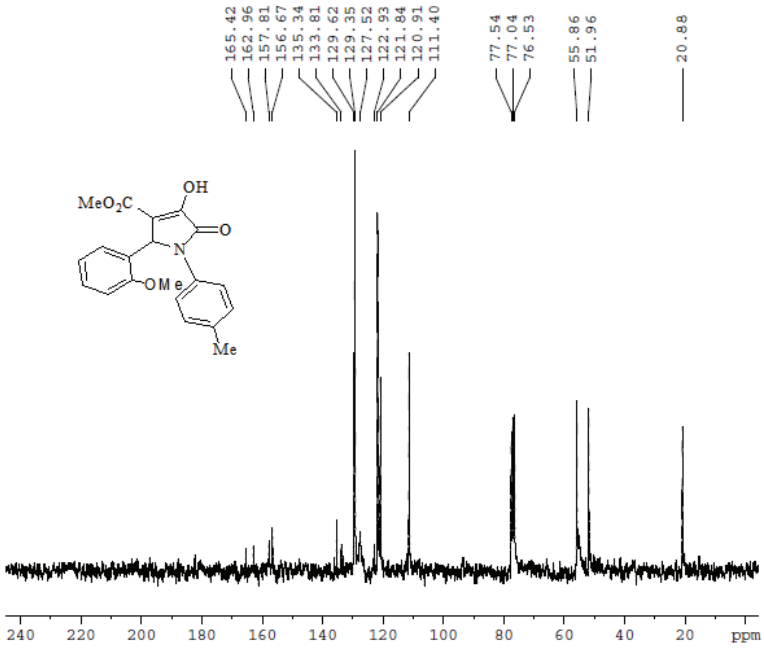

Fig. S-23. ^{13}C-NMR spectrum of compound **12** (63 MHz, $CDCl_3$, δ / ppm).

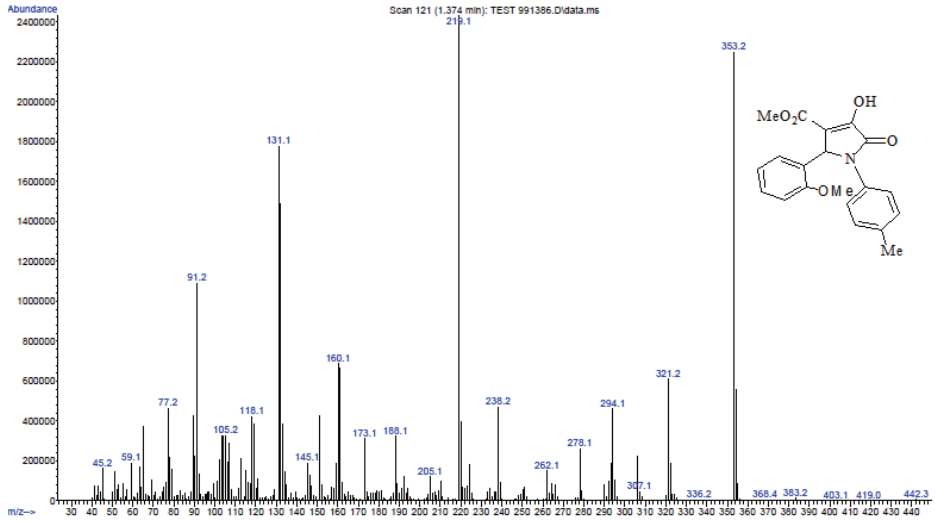

Fig. S-24. Mass spectrum of compound **12**.

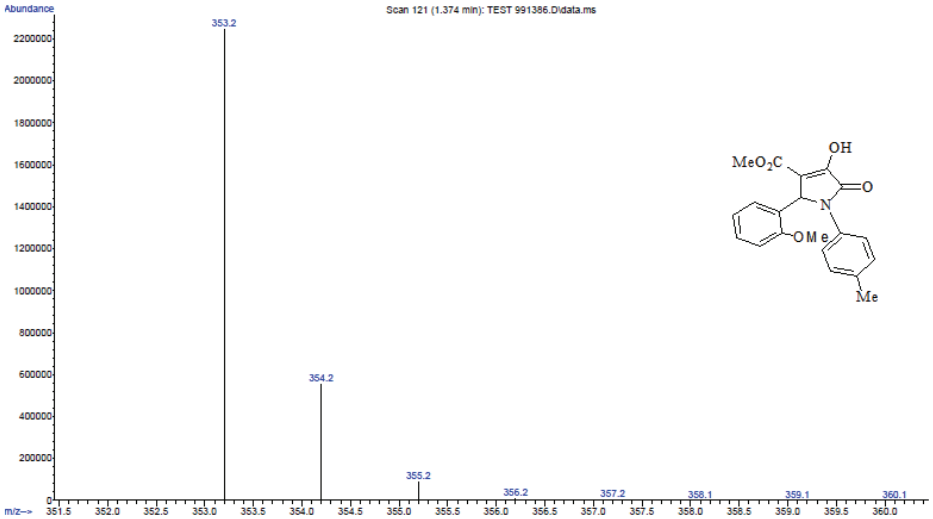

Fig. S-25. Mass spectrum of compound **12**.

*1-(4-Methylphenyl)-5-(3-boromophenyl)-3-hydroxy-4-methoxycarbonyl-3-pyrrolin-2-one (Table II, entry **13**)*

Yellow solid; Yield: 0.36 g (91 %); m.p.: 184–186 °C; FT-IR (KBr, ν_{max} / cm^{-1}): 3322 (OH), 2953, 1720 (C=O), 1686 (C=O), 1513, 1351, 1262, 1127; ^{1}H-NMR (500 MHz, DMSO-d_6, δ / ppm): 2.21 (3H, *s*, CH_3), 3.62 (3H, *s*, OCH_3), 6.08 (1H, *s*, CH), 7.05–7.53 (8H, *m*, Ar), 11.92 (1H, *brs*, OH); ^{13}C-NMR (MHz, 100.51, DMSO-d_6, δ / ppm): 20.90, 51.64, 60.34, 111.62, 122.95, 127.01, 129.71, 130.94, 131.17, 131.35, 133.96, 135.33, 140.01, 153.47, 162.91 (C=O), 164.19 (C=O); Mass (*m*/*z*): 403.1 (M^++2), 401.2 (M^+), 369.1, 342.1, 269.0, 236.0, 208.0, 180.0, 157.1, 138.1 (100%), 115.2, 91.2, 65.2.

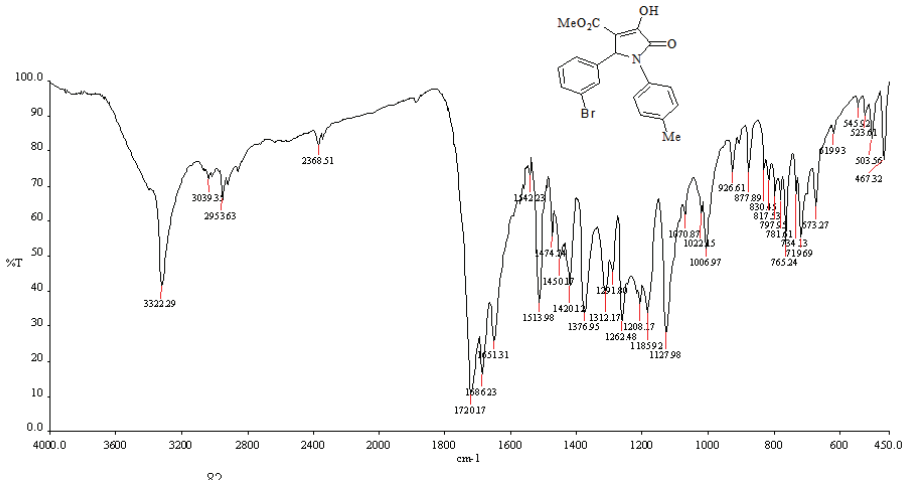

Fig. S-26. FT-IR (KBr, cm^{-1}) spectrum of compound **13**.

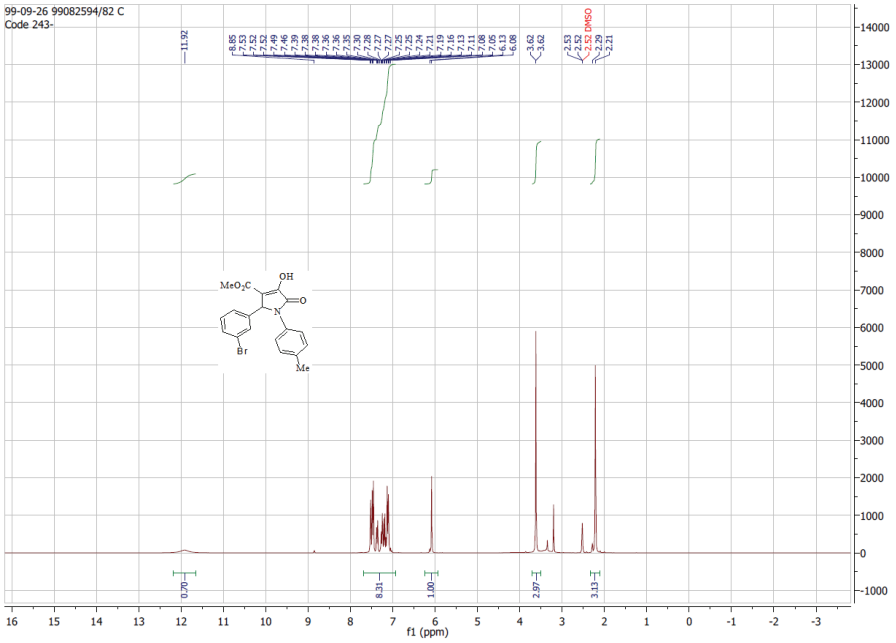

Fig. S-27. ^{1}H-NMR spectrum of compound **13** (500 MHz, DMSO-d_6, δ / ppm).

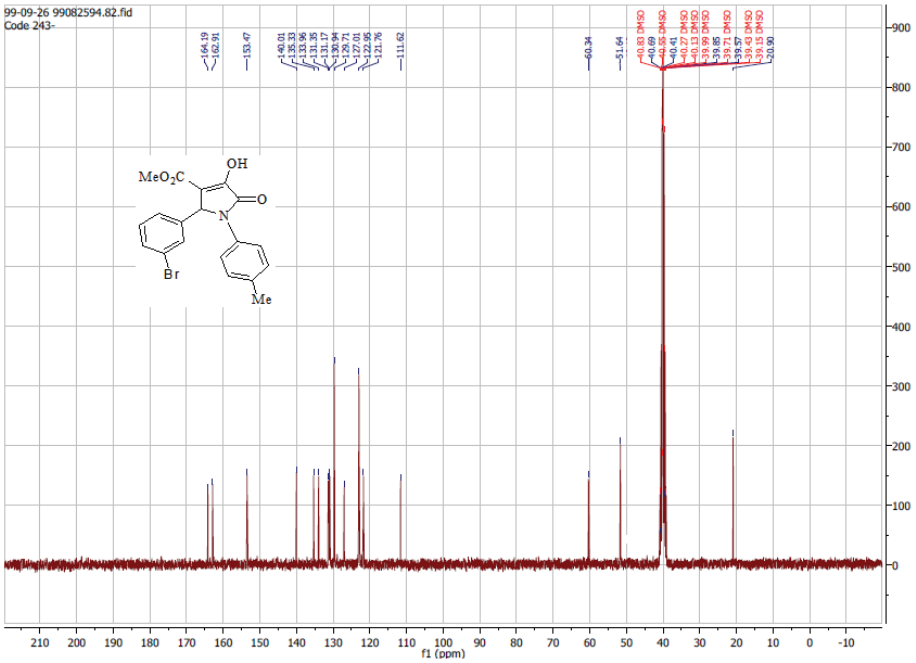

Fig. S-28. ^{13}C-NMR spectrum of compound **13** (100 MHz, DMSO-d_6, δ / ppm).

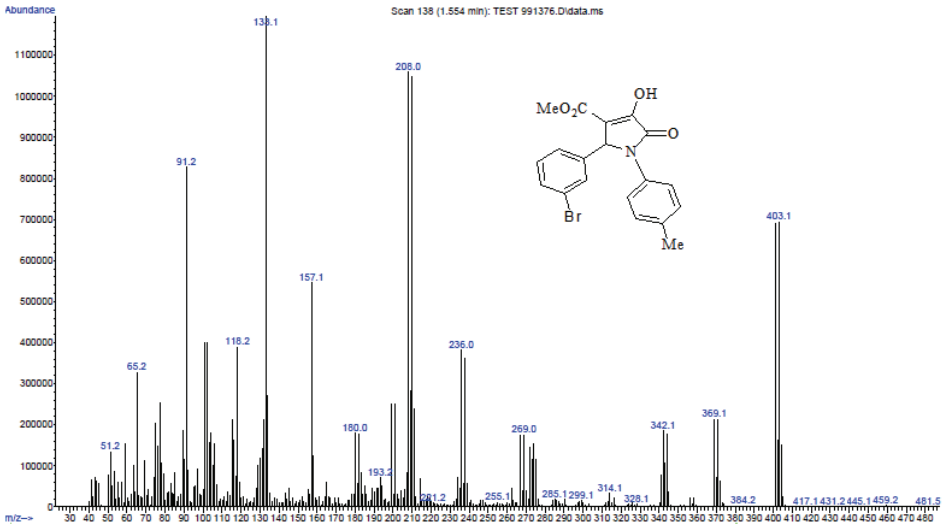

Fig. S-29. Mass spectrum of compound **13**.

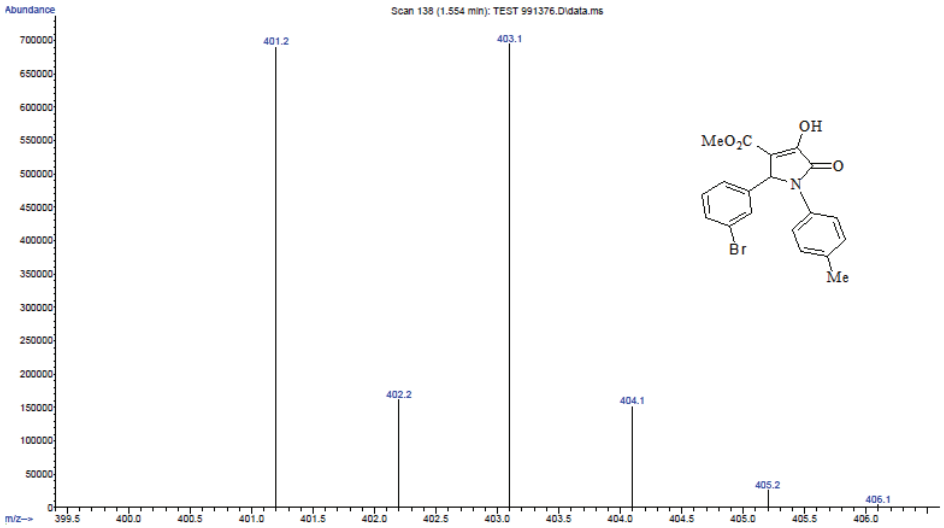

Fig. S-30. Mass spectrum of compound **13**.

*1-(4- Bromophenyl)-5-(3-nitrophenyl)-3-hydroxy-4-methoxycarbonyl-3-pyrrolin--2-one (Table II, entry **14**)*

White solid; Yield: 0.39 g (90 %); m.p.: 220–222 °C. FT-IR (KBr, ν_{max} / cm^{-1}): 3290 (OH), 2952, 1716 (C=O), 1693 (C=O), 1529 (NO_2), 1493, 1358 (NO_2), 1213, 1190; ^{1}H-NMR (250.13 MHz, $CDCl_3$, δ / ppm): 3.76 (3H, *s*, OCH_3), 5.82 (1H, *s*, CH), 7.21–8.1 (8H, *m*, Ar), 8.90 (1H, *s*, OH); ^{13}C-NMR (MHz 100.51, DMSO-d_6, δ / ppm): 51.73, 59.76, 111.63, 118.45, 123.58, 124.75, 130.46, 132.20, 134.43, 135.67, 139.44, 148.08, 153.48, 162.82 (C=O), 164.45 (C=O); Mass (*m*/*z*): 434.1 (M^++2), 432.1 (M^+), 402.1, 373.1, 306.1, 234.1, 218.1, 197, 175.1 (100%), 157.1, 129.1, 101.1, 76.1.

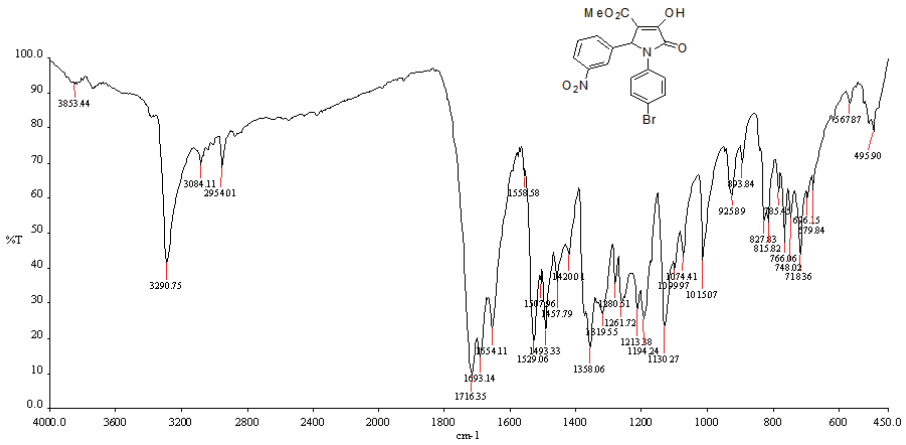

Fig. S-31. FT-IR (KBr, cm^{-1}) spectrum of compound **14**.

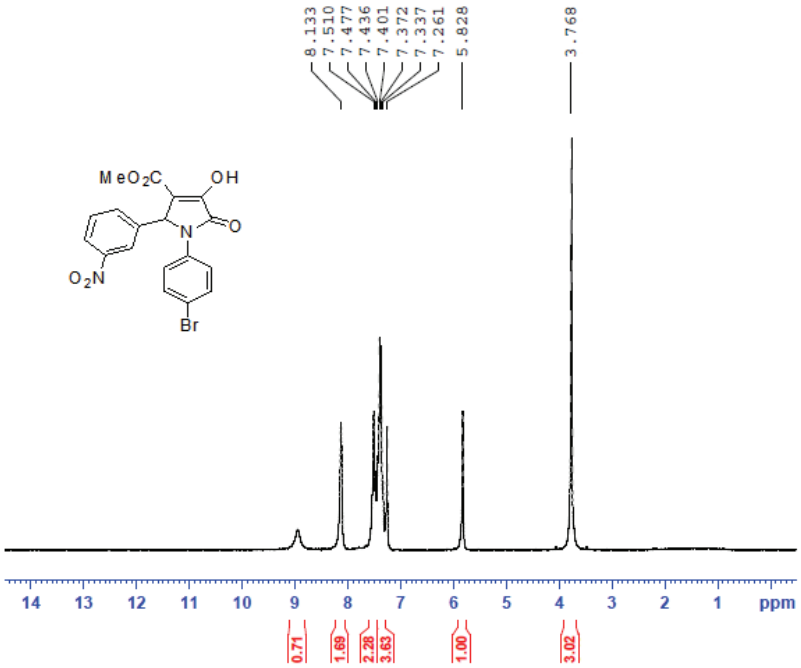

Fig. S-32. ^{1}H-NMR spectrum of compound **14** (250 MHz, $CDCl_3$, δ / ppm).

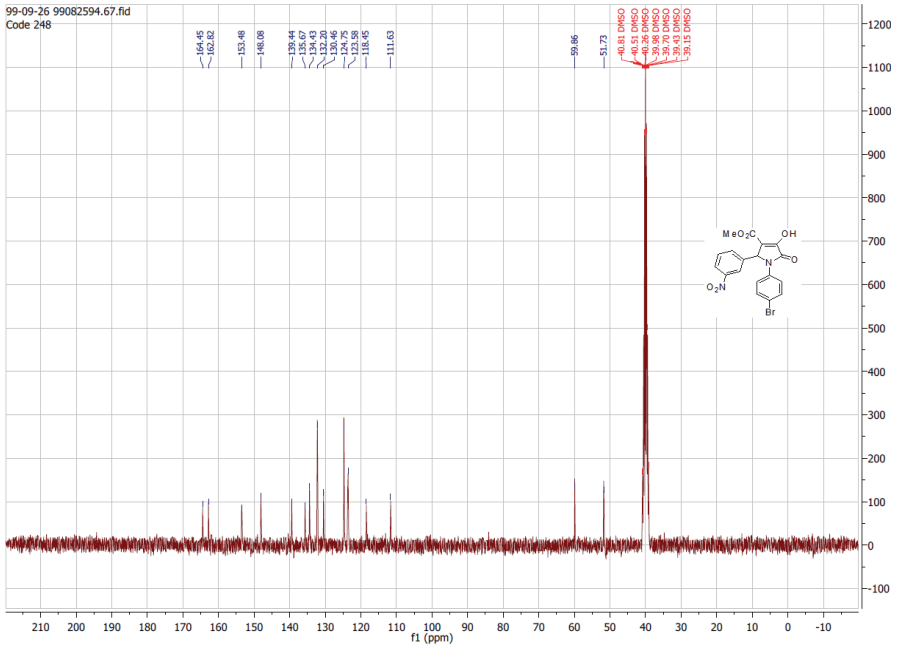

Fig. S-33. ^{13}C-NMR spectrum of compound **14** (100 MHz, DMSO-d_6, δ / ppm).

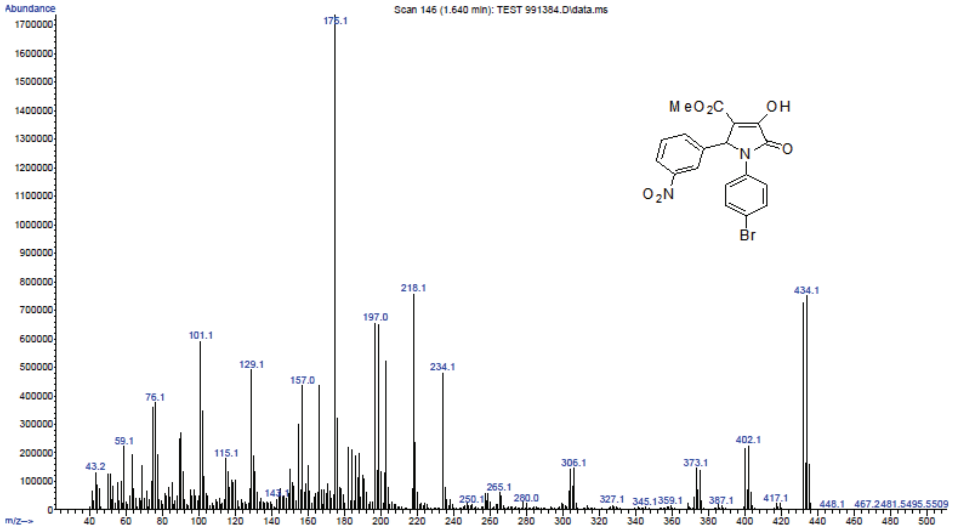

Fig. S-39. Mass spectrum of compound **14**.

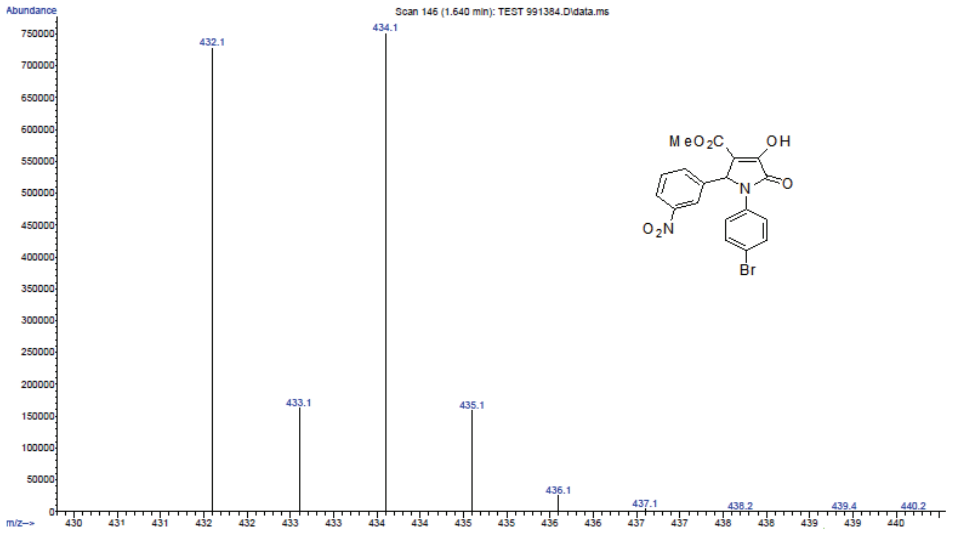

Fig. S-40. Mass spectrum of compound **14**.

Journal of the Serbian Chemical Society
JSCS@tmf.bg.ac.rs • www.shd.org.rs/JSCS
J. Serb. Chem. Soc. *86* (11) 1053–1065 (2021)
JSCS–5482
Original scientific paper
Published 14 September 2021

The evaluation of chemoselectivity in multicomponent domino Knoevenagel/Diels–Alder reaction: A DFT study

MINA ATTARBASHI, NADER ZABARJAD SHIRAZ* and MARJANEH SAMADIZADEH

Department of Chemistry, Central Tehran Branch, Islamic Azad University, Tehran, Iran

(Received 29 January, revised 16 June, accepted 13 July 2021)

Abstract: Herein, the chemoselectivity of the multicomponent domino Knoevenagel/Diels–Alder reaction is investigated in terms of theoretical calculations. The structures of reagents, transition states, intermediates and products are optimized at the M062X/6-31+G(d,p) level of theory. The reaction mechanism involves processes of bond rotation, isomerization, asymmetric cycloaddition, acid–base and nucleophile–electrophile competitions, which are studied for the purpose of delivering a clear information of the mechanism in terms of chemoselectivity considerations. Accordingly, the chemoselectivity of the reaction is controlled by the releasing acetone during the decomposition of Meldrum acid in the presence of methanol and L-proline ($\Delta G^{\#}$ = 61.45 kcal** mol^{-1}). Comparing calculated results (gas and solvent phase) with the experimental ones showed that using these reagents are the kinetical favourite path for the chemoselective multicomponent cascade Knoevenagel/Diels–Alder reaction to produce the predominant product (>95 %). The results suggest that the creation of cis-spiro cyclohexanone is the predominant chemoselective product under kinetic control of the desired enone.

Keywords: theoretical study; cycloaddition; condensation reaction; cascade reaction.

INTRODUCTION

Due to the expedient access to complex polycyclic products in a single highly atom-economical step, multi-component coupling reactions (MCRS) mainly include simultaneous reactions of three or more reagents. MCRS make an easily achieved substituent diversity into the core structure by varying each component.[1,2]

The improvement of the reaction efficiency, the avoidance of toxic reagents, the reduction of waste, and the responsible use of our resources are critical con-

* Corresponding author. E-mail: zabarjad_sh@yahoo.com
https://doi.org/10.2298/JSC210119066A
** 1 kcal = 4184 J

cerns in modern synthetic organic chemistry.[3] Consisting of several bond-forming reactions, the domino or tandem reactions can solve many of these concerns. Domino reactions take place under the established common reaction conditions and are also involved with two or more bond-forming transformations.[4] Homo-domino reactions are classified as a combination of reactions involving the same mechanism, whereas heterodomino reactions are classified as a sequence of reactions with different mechanisms.[5]

As an ultimate goal in organic chemistry, the catalytic asymmetric assembly of simple and readily available precursor molecules, into stereochemically complex products, the name of domino reactions has become known.[6] Furthermore, the development of domino and other multicomponent reaction methodologies can provide a convenient admission to produce more complex compounds from simple starting materials.[2,7,8] The incorporation of a Diels–Alder reaction sequence is the fundamental key to many interesting variants of these reactions.[9–11]

Recently, organocatalysis has emerged as a promising synthetic tool for the constructing of C–C and C–N bonds in aldol,[12] Michael,[13] Mannich,[14] Diels––Alder[15] and other reactions[16] with very good chemoelectivity and stereoselectivity. In these recently described reactions, structurally simple and steady state of chiral organoamines enable iminium and enamine-based transformations with compounds containing carbonyl group. They could be used as catalysts in operationally simple and sometimes ecologically approachable experimental procedures.

Thus far, the extensive research have described the asymmetric assembly reactions involving aldol-aldol,[17–19] Michael-aldol,[20–22] Mannich-allylation,[23] Mannich-cyanation,[24,25] amination-aldol[26] and Knoevanagel–Michael[27] reactions. Recently, two motivating domino reactions were founded on Knoevenagel/Diels–Alder reaction sequences. The first was the direct organocatalytic asymmetric domino Knoevenagel/Diels–Alder reaction sequence, in order to accomplish the diastereo- and enantio-selective construction of highly substituted spiro [5.5]undecane-1,5,9-triones.[28] The second was the direct organocatalytic, hetero-domino, Knoevenagel/Diels–Alder/epimerization sequence with the intention to prepare symmetric prochiral and highly substituted spiro[cyclohexane--1,2′-indan]-1′,3′,4-triones in diastereospecific mode from the commercially existing 4-substituted 3-buten-2-ones, aldehydes and 1,3-indandione.[29]

In the synthesis of natural products and in materials chemistry, spirocyclic ketones are attractive intermediates[30,31] which are ideal starting materials for the synthesis of fenestranes, which could attend as uncommon designs for engineering of liquid crystal and chemistry science of dendrimers as well as for the building of the graphite cuttings in a saddle-like, 3D distorted core.[32,33] Additionally, the biphenyl moiety is an example of advantaged structure and this meets the priority of research in selecting biologically relevant chemical fragments, in

order to enhance the value of the resulting library as a source of bioactive compounds.[34]

The preliminary results (Scheme 1) indicated that the three-component reaction between benzylideneacetone **1**, aromatic aldehydes **2** and Meldrum acid **3** catalyzed by L-proline **4** resulted in some biologically active compounds of chiral spirocyclic ketone scaffolds **5** with excellent chemoselectivity (>95 %).[35]

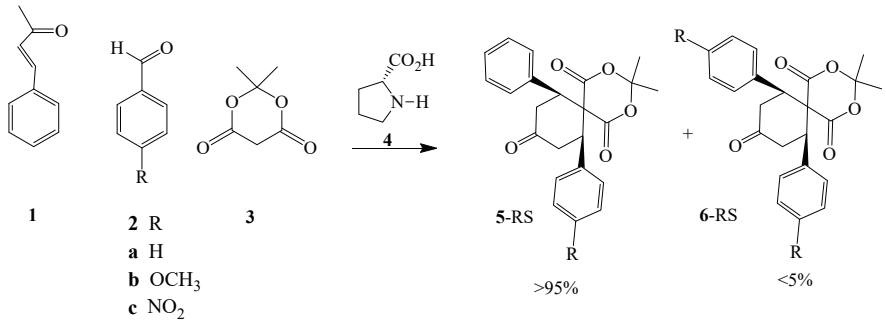

Scheme 1. Diastereoselective three-component reaction between benzylideneacetone **1**, aromatic aldehydes **2** and Meldrum acid **3** catalyzed by L-proline **4**.

The literature survey indicated that Knoevenagel/Diels–Alder has several distinct steps including Knoevenagel condensation and Diels–Alder cycloaddition, in which **5**-*RS* has been identified as a major product (Scheme S-1 in the Supplementary material to this paper). In the most reliable representation, Knoevenagel condensation occurs by reacting aldehyde **2** with Meldrum acid **3** in the presence of L-proline **4** as a catalyst to form alkylidene **8**. Simultaneously, diene **7** is formed through benzylideneacetone **1** and L-proline **4** condensation.[35]

Although there is much data about Knoevenagel condensation and Diels–Alder reaction individually, based on our survey of the literature, there are not sufficient theoretical studies concerning interpretation of chemoselectivity of Knoevenagel/Diels–Alder reaction. Recent increasing interest in domino Knoevenagel/Diels–Alder reaction, coupled with insufficient information concerning the clarification of the chemoselectivity of this reaction, was intended to study the chemoselectivity of domino Knoevenagel/Diels–Alder reaction. To extend the chemeoselectivity of Knoevenagel/Diels–Alder reaction, this research was initiated with the idea of selecting a suitable multi-component reaction that allows the efficient generation of structurally and stereochemically complex skeletons, bearing functionalities, which enable the attachment of the biasing elements. In the arena of multi-component reactions, we focused on the domino processes performance. We develop this theoretical study based on DFT calculations on how to interpret and predict the outcome of chemoselectivity, kinetic and

thermodynamic control of the Knoevenagel/Diels–Alder reaction in the presence of L-proline **4,** as a common chiral secondary amine catalyst.

THEORETICAL METHOD

Geometries of the structures were fully optimized with the internal 6-31+G(d,p) basis set, and DFT (M062X) method procedures implemented in Gamess software.[36] To choose the method and basis set, many factors need to be considered. Among several available methods/ /basis sets we use M06-2X/6-311+G(d,p) for following reasons. M06-2X/6-311+G(d,p) level of theory has been recommended for thermochemical data estimations including calculations that predict the ΔG values for the equilibria between enamines and ketones with the acceptable accuracy. The effect of solvent was studied by the polarizable continuum model (PCM) approaches and using M06-2X method with energy differences below 1 kcal mol^{-1}. Usually ordinary DFT methods (such as B3LYP) do not recognize the weak attraction between pairs of non-polar atoms and between pairs of molecules arising from the interaction of instantaneous multi-poles, but modern DFT methods, such as M06-2X are known to perform much better in the samw field.[37-40]

The frequency analysis were used in order to obtain the zero-point energies (ZPE), and confirmed the transition states with only one imaginary frequency and the reagents, intermediates, and products with zero imaginary frequency.[41] The starting materials and products were re-localized from the transition states by IRC calculations. Gibbs energy changes in a.u. (Hartree) were considered to compare relative stabilities (kcal mol^{-1}). The relative energy of transition states (**8**-TS, **7**-TS), intermediates (**8** and **7**) and products (**5** and **6**) were calculated by comparing their Gibbs energy change to the energy changes of relevant starting materials (Tables I–IV). The experimental findings showed that the reaction was facilitated by using methanol as a protic solvent. To survey the outcome of the reaction in a protic solvent, single--point calculations were accomplished at the same level of theory in PCM for methanol as a solvent. Gibbs energy changes in gas phase and solvent are presented in the Supplementary material file along with the Cartesian coordinates of optimized geometry of each structures.

RESULTS AND DISCUSSION

According to the experimental data, the domino Knoevenagel/Diels–Alder reaction progressed with an excellent chemoselectivity mode (>95 %) (Scheme 1).[35] To evaluate the results and the mechanism of the chemoselectivity, we reported the energy profile of this reaction by the quantum calculation on reagents, intermediates, transition states and all possible products involved in this reaction. Among various possibilities which are available for reagents (benzylideneacetone **1**, aldehyde **2**, Meldrum acid **3** and L-proline **4**) in order to to be in the reaction mixture, the reaction chooses the pathway that yields chemoselective Spirocyclic ketone **5**-*RS* in the presence of L-proline **4**. As shown in Scheme 1, the final product could have two isomers **5**-*RS* and **6**-*RS*. Although, *cis*-spiro-cyclohexanone **5**-*RS* was the main product of this reaction based on the experimental results. The chemoselectivity could happen through two possible steps.[35,42]

In this Diels–Alder reaction step *cis*-spiro **5**-*RS* and **6**-*RS* were produced through cyclization of diene **7** and dienophile **8**. Based on the obtained results, endo-Y orientation in **9**-*SR*-TS was a transition state, which passed through to

produce **9**-*RS*, and finally **5**-*RS* and/or **6**-*RS*. Based on the calculations, there were not considerable differences between $\Delta G^{\#}$ (kcal mol^{-1}) of these transition states that result in **6**-*RS* and **5**-*RS* as products (Table S-I, Supplemantary material).[42] Thus, according to the Diels–Alder reaction, both chemoselective products (**5** and **6**) were potentially capable to be produced in the reaction. Consequently, the Diels–Alder step could not control the observed experimental chemoselectivity of the reaction. In other word, it seems that this step may not be appropriate to explain the chemoselectivity of the reaction.

Knoevenagel condensation reaction step. In this reasonable step, diene **7** and dieneophile **8** were formed (Scheme S-1 in the Supplementary material). To study the chemoselectivity of the reaction, the ground states of reagents and components involved in the Knoevenagel step of domino Knoevenagel/Diels–Alder reaction were optimized at M062X/6-31+G(d,p) level of theory in gas, the Gibbs energy changes, and relative stabilities ($\Delta G^{\#}$) for components involved in the mechanism are summarized in Table I. The selected optimized geometries of the most stable structure of transition states were represented in Fig. S-1.

TABLE I. Energy of the relevant optimized transition states, intermediates, and dienophile **8** compared to Gibbs free energy of reagents in the gas phase for knoevenagel condensation

Formation of aldol **11**				Formation of dienophile **8**							
Addition step 4				E2 mechanism				E1 mechanism			
No.	ΔG / kcal mol^{-1}			No.	ΔG^4 / kcal mol^{-1}			No.	ΔG / kcal mol^{-1}		
R=	H	OCH_3	NO_2	R=	H	OCH_3	NO_2	R=	H	OCH_3	NO_2
10	0.00	0.00	0.00	**11**	3.37	6.74	-12.53	**11**	3.37	6.74	-12.53
3-TS	44.57	44.57	44.57	**12**-TS	62.22	59.76	57.39	**14**-TS1	56.05	44.43	60.00
3-enol	9.95	9.95	9.95	**13**-TS	56.44	67.27	53.94	**14**-Int	27.19	28.13	33.03
10-TS	46.82	49.18	38.29	**8**	0.76	17.79	26.41	**14**-TS2	79.76	75.77	77.16
11-Int	16.46	7.68	34.78					**8**	0.76	17.79	26.41
11-TS	29.64	17.21	68.30								
11	3.37	6.74	-12.53								

To prepare diene **7** and dienophile **8,** the reaction occured in several steps which are discussed in details.

1. Condensation of Meldrum acid **3** with aldehyde **2** to form dienophile **8**.
2. Degradation of dienophile **8** and releasing acetone **21** as a byproduct.
3. Aldol condensation of acetone **21** with aldehyde **2** to produce enone **29**.
4. Condensation of enone **29** with L-proline **4** to produce diene **7**.

*1. Condensation of Meldrum acid **3** with aldehyde **2** to form dienophile **8***

In this step, dienophile **8** was produced through the condensation reation between Meldrum acid **3** and aldehyde **2**. There was an alternative mechanism to explain this reaction in which Meldrum acid **3** was condensed with L-proline **4** to produce corresponding enamine in order to facilitate a condensation reaction to aldehyde **2**.[43] In this study the role of L-proline **4** role was ignored in the enol-

ization step in order to simplify the calculations, so the Scheme 2 was designed as Knoevenagel condensation reaction, in which Meldrum acid **3** enolized to **3**-enol ($\Delta G^{\#}$ = 9.95 kcal mol^{-1}) *via* **3**-TS ($\Delta G^{\#}$ = 44.57 kcal mol^{-1}). Intermediate **11** ($\Delta G^{\#}$ = 16.46 kcal mol^{-1}) was formed through **10**-TS ($\Delta G^{\#}$ = 46.82 kcal mol^{-1}) as a result of **3**-enol and aldehyde **2** addition reaction. The intermediate transferred an intermolecular proton (**11**-TS, $\Delta G^{\#}$ = 29.64 kcal mol^{-1}) to produce **11,** which was 3.37 kcal mol^{-1} more stable than the starting materials. In the next step, E1 or E2 mechanism was executed during the dehydration reaction to produce compound. E2 mechanism was performed by anti ($\Delta G^{\#}$ = 58.85 kcal mol^{-1}) or syn ($\Delta G^{\#}$ = 53.07 kcal mol^{-1}) mechanism. Comparison of the $\Delta G^{\#}$ of these reactions showed that the syn pathway had less activation energy compared to the anti-mechanism. The optimized structures of **12**-TS and **13**-TS demonstrated that the hydrogen bonding in **13**-TS could explain more stability of the transition state (Scheme S-2, Supplementary material, and Table I).

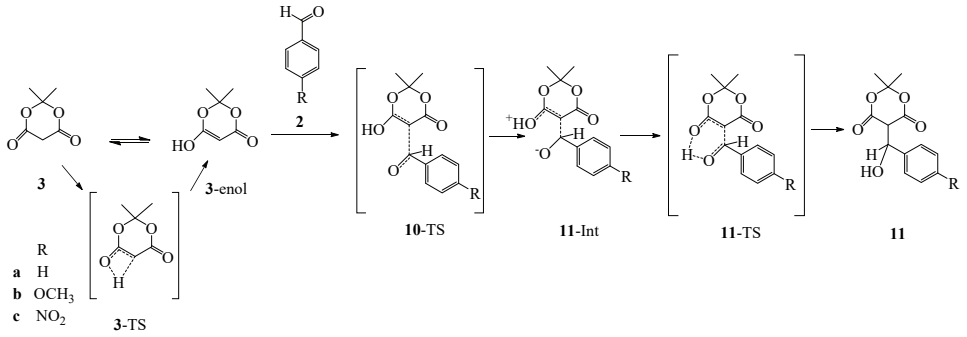

Scheme 2. Mechanism of Knoevenagel reaction to produce dienophile **8**.

Considering the E1 mechanism, **14-**Int carbocation ($\Delta G^{\#}$ = 27.19 kcal mol^{-1}) was formed through **14**-TS1 ($\Delta G^{\#}$ = 52.68 kcal mol^{-1}), and then it was converted to dienophile **8** by losing proton from **14**-TS2 ($\Delta G^{\#}$ = 52.57 kcal mol^{-1}). Consequently, E2 elimination with the syn orientation, passing through the least activation energy (53.07 kcal mol^{-1}), was preferred for the reaction. The electron withdrawing group (NO_2) stabilized aldol **11c**, while destabilized dienophile **8c** in comparison with corresponding starting materials.

*2. Degradation of dienophile **8** and releasing acetone **21** as a byproduct*

Enone **29**, which is considered as one of the compounds to produce isomer **6**, was formed during the condensation of acetone molecule **21** and aldehyde **2**. The required acetone could be released by a reaction between dienophile **8** and methanol (the solvent in the reaction). The released acetone was made by of methanol attacked to one of the carbonyl groups of compound **8** in order to produce intermediates **15** and **16** (Scheme 3), which were 54.23 and 46.63 kcal mol^{-1} less

stable than dienophile **8**, respectively. Hemi-orthoesters **17** and **18** were yielded through the proton transfer reaction of these intermediates (**15** and **16**). Next, the last intermediates were degraded in the presence of L-proline **4** through transition states **19** ($\Delta G^{\#}$ = 63.86 kcal mol^{-1}) and **20** ($\Delta G^{\#}$ = 61.45 kcal mol^{-1}) to produce acetone **21** and corresponding salt **22** (Table II, Fig. S-1).

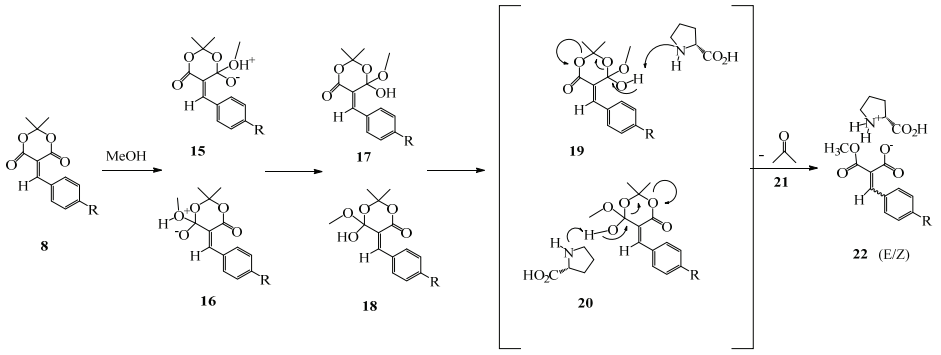

Scheme 3. Mechanism of acetone **21** production.

The comparison of relative energies showed that the departing of acetone **21** was the rate determining step of the degradation reaction (RDS, **20**, $\Delta G^{\#}$ = = 61.45 kcal mol^{-1}). The electron withdrawing NO_2 substituent increased $\Delta G^{\#}$ relatively (**19**c-TS and **20**c-TS) for about 8 kcal mol^{-1} when compared to the relevant substituted free derivatives (Table II).

TABLE II. $\Delta G^{\#}$ / kcal mol^{-1} of the relevant optimized transition states, intermediates and products compared to Gibbs energy changes of starting materials (**3**+**2**) in the gas phase for the formation of acetone

No.	R=			No.	R=		
	H	OCH_3	NO_2		H	OCH_3	NO_2
8	0.76	17.79	26.41	**8**	0.76	17.79	26.41
15	54.99	58.30	52.31	**16**	47.39	50.70	44.72
17	7.68	10.99	5.00	**18**	11.46	14.77	8.78
19-TS	71.54	74.09	79.27	**20**-TS	72.91	73.60	80.79
22-Z	–4.76	–1.45	–7.44	**22**-E	–9.09	–5.78	–11.77

*3. Aldol condensation of acetone **21** with aldehyde **2** to produce enone **29***

In this step, additional reaction of the produced acetone and aldehyde **2** conducted a reaction to form enone **29**. This reaction was similar to the knoevenagel condensation. The aldol condensation could be considered by the participating of L-proline **4** through enamine mechanism.[43] In this survey, an intermolecular enolization process was designed. According to our proposed mechanism, acetone **21** converted to **21**-enol ($\Delta G^{\#}$ = 12.05 kcal mol^{-1}) passing through **21**-TS

($\Delta G^{\#}$ = 56.11 kcal mol^{-1}, Scheme 4). **24**-Int ($\Delta G^{\#}$ = 19.67 kcal mol^{-1}) was formed through **23**-TS ($\Delta G^{\#}$ = 36.71 kcal mol^{-1}) by adding **21**-enol and aldehyde **2**, a proton transfer ($\Delta G^{\#}$ = 14.30 kcal mol^{-1}) of this zwitter-ion intermediate (**24**--TS) which led to *β*-hydroxy ketone **24** ($\Delta G^{\#}$ = 1.65 kcal mol^{-1}). In the final step, enon **29** was produced by a dehydration reaction, which could occurred by E2 and/or E1 mechanism (Scheme S-3, Supplementary material). Based on this assumption, there were four possible TS structures (**25**-TS, **26**-TS, **27**-TS and **28**--TS). For the E2 dehydration mechanism, it was necessary to consider the Pro-R and Pro-S hydrogens to perform either syn or anti-eliminations (Scheme 4, Table III). The lowest $\Delta G^{\#}$ of 48.98 kcal mol^{-1} belonged to **26**-TS in which Pro-S hydrogen was eliminated by the syn mechanism. Also, **26**-TS was in eclipsed conformation so that the aryl and the carbonyl groups were far from each other and hydrogen bonding in syn orientation provided a favoured TS for E2 elimination mechanism (Fig. S-1).

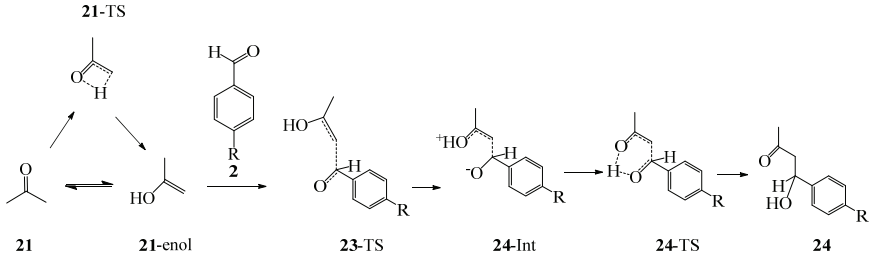

Scheme 4. Mechanism of aldol reaction to produce compound **22**.

TABLE III. $\Delta G^{\#}$ / kcal mol^{-1} of the relevant optimized transition states and product **29** compared to Gibbs energy changes of starting materials (**2**+**21**) in the gas phase for aldol condensation

Formation of aldol **24** Addition mechanism				Formation of enone **29**							
No.	R			No.	E2 Mechanism R			No.	E1 Mechanism R		
	H	OCH_3	NO_2		H	OCH_3	NO_2		H	OCH_3	NO_2
2+21	0	0	0	**24**	1.65	4.96	-1.18	**24**	1.65	4.96	-1.18
2+21-TS	56.11	56.11	56.11	**25**-TS	61.92	59.77	71.53	**30**-TS1	53.80	35.77	80.13
2+21-enol	12.05	12.05	12.05	**26**-TS	48.98	48.86	59.87	**31**-TS1	51.58	34.11	77.20
23-TS	48.76	55.23	29.16	**27**-TS	67.27	64.59	77.62	**32**-Int	19.67	8.54	22.69
24-Int	19.67	8.54	22.69	**28**-TS	64.96	64.23	76.14	**30**-TS2	57.33	45.74	27.03
24-TS	33.97	19.89	49.85	**29**-E	3.39	10.21	-11.38	**31**-TS2	54.67	44.32	22.95
24	1.65	4.96	-1.18	**29**-Z	16.37	15.15	-6.94	**29**-E	3.39	10.21	-11.38
								29-Z	16.37	15.15	-6.94

29-*E* was considered as a main product of this reaction, because it was 12.98 kcal mol^{-1} more stable than **29**-*Z* isomer. There were two possible transition state

structures (**30**-TS1, **31**-TS1), in E1 mechanism with $\Delta G^{\#}$ of 53.80 and 51.58 kcal mol^{-1}, respectively. So, the reaction chose the kinetically favourite pathway (**30**--TS1) to produce **32**-Int ($\Delta G^{\#}$ = 19.67 kcal mol^{-1}). In the next step, the proton could be removed by two transition states (**30**-TS2, $\Delta G^{\#}$ = 57.33 kcal mol^{-1}) and (**31**-TS2, $\Delta G^{\#}$ = 54.67 kcal mol^{-1}, Fig. S-1).

In this case, the reaction went through **30**-TS2 to produce enone **29**-*E*. By comparing $\Delta G^{\#}$ of the E1 and E2 mechanisms, the E2 mechanism *via* syn orientation ($\Delta G^{\#}$ = 48.98 kcal mol^{-1}) was accepted as the best pathway for dehydration reaction. The resulted enone **29**-*E* as the product of this step, proceeded a condensation reaction with L-proline **4** in the next step.

The results of calculations on the substituted reagents showed that $\Delta G^{\#}$ of **23**-TS was declined using an electron withdrawing group (NO_2) on aldehyde **2**. In the first step of the E1 mechanism, the electron releasing group (OCH_3) facilitated the OH^- departure and stabilized the cationic intermediate **32**-int, whereas the NO_2 group showed a contradictory effect on kinetic ($\Delta G^{\#}$) of this step. In the second step of the E1 mechanism the NO_2 group decreased $\Delta G^{\#}$ of deprotonation of transition states.

*4. Condensation of enone **29** with L-proline **4** to produce diene **7***

The intermediate **33** ($\Delta G^{\#}$ = 41.24 kcal mol^{-1}) was produced through the addition reaction between L-proline **4** and enone **1** and/or **29** (which was produced in previous step), this intermediate transferred a proton *via* **34**-TS ($\Delta G^{\#}$ = = 13.11 kcal mol^{-1}) to yield hemiaminal **35** ($\Delta G^{\#}$ = 37.79 kcal mol^{-1}) and was dehydrated by passing through an anti-oriented transition state **36**-TS ($\Delta G^{\#}$ = = 17.77 kcal mol^{-1}) to produce diene **7**. Among the different geometrical isomers and rotamers of **7**, the *trans*-s-*cis* **7** was the most stable isomer ($\Delta G^{\#}$ = 6.62 kcal mol^{-1}) and performed the Diels–Alder reaction with dienophile **8**. In terms of the effects of substitutes, the calculations demonstrated that all components bearing of NO_2 group, as an electron withdrawing group involved in this step, became more stable in comparison with the unsubstituted isomers (Scheme 5, Table IV).

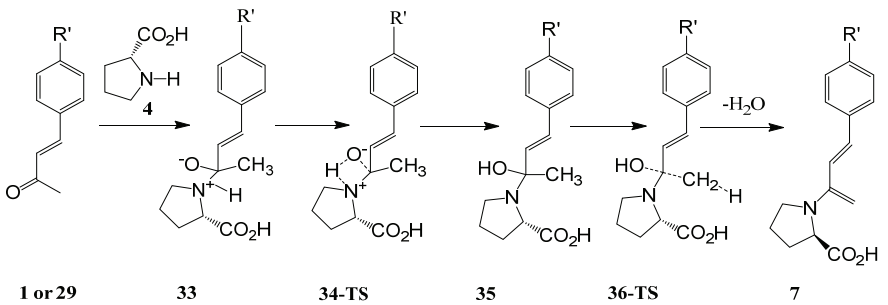

Scheme 5. Mechanism of producing diene **7**.

TABLE IV. $\Delta G^{\#}$ / kcal mol^{-1} of the relevant optimized transition states, intermediates and diene **7** compared to Gibbs energy changes of starting materials (**29**+**4**) in the gas phase

R	No.					
	29+**4**	**33**	**34**-TS	**35**	**36**-TS	**7**
H	0	41.24	54.35	37.79	55.56	6.62
OCH_3	0	43.81	58.54	41.65	59.99	1.75
NO_2	0	28.13	39.6	25.96	41.10	3.00

The optimized structure of **13**-TS showed that, leaving H^+ and OH^- groups were co-planar, and this dehydration step could be considered as a concerted reaction, but breaking of the C–H bond was more progressive (2.18 Å) than that of the C–O departing bond (1.65 Å). In **30**-TS2, the departing proton was located at 2.41 Å from the carbon atom and the conjugated system was almost planar, which made this transition state more stable. In **36**-TS, the C–H and C–O bonds were broken almost at the same extend, so the TS could be considered as a normal E2 transition state. On the other hand, of the formation of the O–H bond (2.32 Å) facilitated the dehydration of the molecule (Fig. S-1). Comparison of the calculations showed that the formation of product **6** required extra steps to complete the reaction. These steps, which led to diene **7,** included the acetone releasing step which could be considered as the rate determining step of the Knoevenagel reaction ($\Delta G^{\#}$ = 61.45 kcal mol^{-1}). In other words, this step caused a delay in the reaction to produce isomer **6**. To conclude, compound **5** as a chemoselective product was a product of the direct Diels–Alder reaction of ready to go available enone **1** with dienophile **8**.

Experimental findings showed that the reaction was promoted by the use of methanol as a protic solvent. Methanol as a protic solvent enhanced the reaction.[35] To survey the effect of protic solvent on kinetics of the reaction, the single-point calculations were conducted at the same level of theory in the polarizable continuum model (PCM) solvent utilizing methanol. The trend of the results in methanol was in agreement with the gas phase, all components involved in the mechanism were more stable in methanol in comparison to the gas phase. According to the calculations, Gibbs energies changes were decreased for 4–6 kcal mol^{-1} for the reagents and the products, 6–10 and 6–11 kcal mol^{-1} for the transition states and the intermediates, respectively, in the presence of methanol. Considering the polar solvent and polar character of transition states especially for the E1 mechanism, the product **8** proceeds *via* a polar transition state. The protic polar solvent (methanol) stabilized ionic intermediates **14**-Int and **32**-Int more than other reagents and transition states, and consequently declined the activation energy of the elimination step. As a consequence, activation energy of **14**-Int and **32**-Int have been decreased to 50.24 and 35.93 kcal mol^{-1}, respectively. The solvent effect is more considerable for reagents, transition states and

intermediates in Knoevenagel part of reaction, in comparison to Diels–Alder step for all substituents.

CONCLUSION

In summary, DFT calculations, especially in terms of chemoselectivity, provided a geometrical image of components involved in the Knoevanagel step in the multicomponent domino Knoevenagel/Diels–Alder reaction. The comparison of the calculated results with the experimental ones showed that using the active reagents has been kinetically the favourite pathway for the chemoselective multicomponent domino Knoevenagel/Diels–Alder reaction to produce **5**-RS as the predominant product (>95 %). Conversely, the reaction needed extra steps to produce the isomer **6**. These extra steps included the acetone releasing process, which was the rate determining step of the Knoevenagel reaction ($\Delta G^{\#}$ = 61.45 kcal mol^{-1}). Consequently, this difficult step caused a delay in the reaction to produce the product **6**. The solvent effect studies showed that methanol, as a polar protic solvent, declined the activation energy ($\Delta G^{\#}$), and promoted the reaction. In addition, the electron withdrawing group (NO_2) could accelerate the reaction to occur more convenient. It is worth noting that using the substituted enone **1** and adding acetone to the mixture of the reaction could affect the chemoselectivity of the reaction and still be a subject for future to research. This theoretical prediction may provide insights for researchers who are interested to design novel chemoselective products for the multicomponent domino Knoevenagel/Diels–Alder reactions considering desired substituents.

SUPPLEMENTARY MATERIAL

Additional data and information are available electronically at the pages of journal website: https://www.shd-pub.org.rs/index.php/JSCS/article/view/10333, or from the corresponding author on request.

ИЗВОД

ПРОЦЕНА ХЕМОСЕЛЕКТИВНОСТИ КОД МУЛТИКОМПОНЕТНЕ ДОМИНО KNOEVENAGEL/DIELS–ALDER РЕАКЦИЈЕ. DFT СТУДИЈА

MINA ATTARBASHI, NADER ZABARJAD SHIRAZ И MARJANEH SAMADIZADEH

Department of Chemistry, Central Tehran Branch, Islamic Azad University, Tehran, Iran

Овде је путем теоријских процена истраживана мултикомпонентна домино Knoevenagel/Diels–Alder реакција. Структуре реагенаса, прелазних стања и производа оптимизоване су на M062X/6-31+G(d,p) нивоу теорије. Механизам реакције укључује процесе ротације везе, изомерирацију, асиметричну циклоадицију, те киселинско–базна и нуклеофилно–електрофилна надметања, која су проучавана да би се добила јасна слика механизма у погледу разматрања хемоселективности. На основу тога, хемоселективност реакције је контролисана отпуштањем ацетона при разлагању Meldrum киселине у присуству метанола и l-пролина ($\Delta G^{\#}$ = 61,45 kcal/mol). Поређење израчунатих резултата са експерименталним показује да је коришћење ових реагенаса кинетички фаворизован пут за хемоселективну мултикомпонентну каскадну Knoevenagel/Diels–Alder реакцију

којом се добија главни производ (>95 %). Резултати показују да је *cis*-спиро-циклохексанона предоминантан хемоселективни производ под кинетичком контролом жељеног енона.

(Примљено 29. јануара, ревидирано 16. јуна, прихваћено 13. јула 2021)

REFERENCES

1. L. Reguera, D. G. Rivera, *Chem. Rev*. **119** (2019) 9836 (https://doi.org/10.1021/acs.chemrev.8b00744)
2. U. K. Sharma, P. Ranjan, E. V. Van der Eycken, S.-L. You, *Chem. Soc. Rev.* **49** (2020) 8721 (https://doi.org/10.1039/D0CS00128G)
3. R. C. Cioc, E. Ruijter, R. V. Orru, *Green Chem*. **16** (2014) 2958 (https://doi.org/10.1039/C4GC00013G)
4. H. Pellissier, *Adv. Synth. Catal.* **358** (2016) 2194 (https://doi.org/10.1002/adsc.201600462)
5. M. Ashe, *Master Thesis*, University of Southampton, Faculty of Natural and Environmental Sciences, Southampton, 2016 (http://eprints.soton.ac.uk/id/eprint/397980)
6. S. M. Xu, L. Wei, C. Shen, L. Xiao, H. Y. Tao, C. J. Wang, *Nat. Commun.* **10** (2019) 5553 (https://doi.org/10.1038/s41467-019-13529-z)
7. M. Wang, Z. Shi, *Chem. Rev.* **120** (2020) 7348 (https://doi.org/10.1021/acs.chemrev.9b00384)
8. H. A. Younus, M. Al. Rashida, A. Hameed, M. Uroos, U. Salar, S. Rana, K. M. Khan, *Expert Opin. Ther. Pat.* **31** (2021) 267 (https://doi.org/10.1080/13543776.2021.1858797)
9. X. Xiao, T. R. Hoye, *Nat. Chem.* **10** (2018) 838 (https://doi.org/10.1038/s41557-018-0075-y)
10. M. H. Cao, N. J. Green, S. Z. Xu, *Org. Biomol. Chem.* **15** (2017) 3105 (https://doi.org/10.1039/C6OB02761J)
11. X. Ji, C. Zhou, K. Ji, R. E. Aghoghovbia, Z. Pan, V. Chittavong, B. Ke, B. Wang, *Angew. Chem. Int. Ed.* **55** (2016) 15846 (https://doi.org/10.1002/anie.201608732)
12. Y. Yamashita, T. Yasukawa, W. J. Yoo, T. Kitanosono, S. Kobayashi, *Chem. Soc. Rev.* **47** (2018) 4388 (https://doi.org/10.1039/C7CS00824D)
13. J. Hu, M. Bian, H. Ding, *Tetrahedron Lett.* **57** (2016) 5519 (https://doi.org/10.1016/j.tetlet.2016.11.007)
14. J. F. Allochio Filho, B. C. Lemos, A. S. de Souza, S. Pinheiro, S. J. Greco, *Tetrahedron* **73** (2017) 6977 (https://doi.org/10.1016/j.tet.2017.10.063)
15. B. L. Oliveira, Z. Guo, G. J. L. Bernardes, *Chem. Soc. Rev.* **46** (2017) 4895 (https://doi.org/10.1039/C7CS00184C)
16. P. L. Wang, S. Y. Ding, Z. C. Zhang, Z. P. Wang, W. Wang, *J. Am. Chem. Soc.* **141** (2019) 18004 (https://doi.org/10.1021/jacs.9b10625)
17. W. Gati, H. Yamamoto, *Acc. Chem. Res.* **49** (2016) 1757 (https://doi.org/10.1021/acs.accounts.6b00243)
18. C. He, J. Hu, Y. Wu, H. Ding, *J. Am. Chem. Soc.* **139** (2017) 6098 (https://doi.org/10.1021/jacs.7b02746)
19. E. Sánchez-Larios, J. M. Holmes, C. L. Daschner, M. Gravel, *Org. Lett.* **12** (2010) 5772 (https://doi.org/10.1021/ol102685u)
20. J. Wang, H. Li, H. Xie, L. Zu, X. Shen, W. Wang, *Angew. Chem*. **119** (2007) 9208 (https://doi.org/10.1002/ange.200703163)
21. B. C. Hong, R. Y. Nimje, A. A. Sadani, J. H. Liao, *Org. Lett.* **10** (2008) 2345 (https://doi.org/10.1021/ol8005369)

22. W. Notz, F. Tanaka, C. F. Barbas, *Acc. Chem. Res.* **37** (2004) 580 (https://doi.org/10.1021/ar0300468)
23. A. Cordova, C. F. Barbas, *Tetrahedron Lett.* **44** (2003) 1923 (https://doi.org/10.1016/S0040-4039(03)00019-4)
24. F. Tanaka, C. F. Barbas III, *J. Syn. Org. Chem. Jpn.* **63** (2005) 709 (https://doi.org/10.5059/yukigoseikyokaishi.63.709)
25. S. Mukherjee, J. W. Yang, S. Hoffmann, B. List, *Chem. Rev.* **107** (2007) 5471 (https://doi.org/10.1021/cr0684016)
26. N. Campillo, J. A. Paez, P. Goya, *Helv. Chim. Acta* **86** (2003) 139 (https://doi.org/10.1002/hlca.200390003)
27. D. B. Ramachary, K. Anebouselvy, N. S. Chowdari, C. F. Barbas, *J. Org. Chem.* **69** (2004) 5838 (https://doi.org/10.1021/jo049581r)
28. R. Thayumanavan, B. Dhevalapally, K. Sakthivel, F. Tanaka, C. F. Barbas III, *Tetrahedron Lett.* **43** (2002) 3817 (https://doi.org/10.1016/S0040-4039(02)00686-X)
29. N. S. Chowdari, C. F. Barbas, *Org. Lett.* **7** (2005) 867 (https://doi.org/10.1021/ol047368b)
30. E. M. Carreira, T. C. Fessard, *Chem. Rev.* **114** (2014) 8257 (https://doi.org/10.1021/cr500127b)
31. L. Hong, R. Wang, *Adv. Synth. Catal*. **355** (2013) 1023 (https://doi.org/10.1002/adsc.201200808)
32. J. Tellenbröker, D. Kuck, *Eur. J. Org. Chem.* **2001** (2001) 1483 (https://doi.org/10.1002/1099-0690(200104)2001:8<1483::AID-EJOC1483>3.0.CO;2-U)
33. A. Boudhar, M. Charpenay, G. Blond, J. Suffert, *Angew. Chem. Int. Ed.* **52** (2013) 12786 (https://doi.org/10.1002/anie.201304555)
34. L. Porcelli, D. Stolfa, A. Stefanachi, R. Di Fonte, M. Garofoli, R. Iacobazzi, N. Silvestris, A. Guarini, S. Cellamare, A. Azzariti, *Cancer Lett.* **445** (2019) 1 (https://doi.org/10.1016/j.canlet.2018.12.013)
35. D. B. Ramachary, C. F. Barbas III, *Chem. Eur. J.* **10** (2004) 5323 (https://doi.org/10.1002/chem.200400597)
36. M. W. Schmidt, K. Baldridge, J. A. Boatz, S. T. Elbert, M. S. Gordon, J. H. Jensen, S. Koseki, N. Matsunaga, K. A. Nguyen, S. Su, T. L. Windus, M. Dupuis, J. A. Montomery, *J. Comput. Chem*. **14** (1993) 1347 (https://doi.org/10.1002/jcc.540141112)
37. Y. Zhao, D. G. Truhlar, *Theor. Chem. Acc*. **120** (2008) 215 (https://doi.org/10.1007/s00214-007-0310-x)
38. A. Castro-Alvarez, H. Carneros, D. Sanchez, J. Vilarrasa, *J. Org. Chem*. **80** (2015) 11977 (https://doi.org/10.1021/acs.joc.5b01814)
39. M. Head-Gordon, J. A. Pople, M. J. Frisch, *J. Chem. Phys. Lett*. **153** (1988) 503 (https://doi.org/10.1016/0009-2614(88)85250-3)
40. Y. Zhao, N. E. Schultz, D. G. Truhlar, *J. Chem. Phys*. **123** (2005) 161103 (https://doi.org/10.1063/1.2126975)
41. S. B. Trickey, *Int. J. Quantum Chem*. **59** (1996) 259 (https://doi.org/10.1002/qua.560590302)
42. M. Attarbashi, N. Zabarjad Shiraz, M. Samadizadeh, *J. Theor. Comput. Chem.* **19** (2020) 2050005 (https://doi.org/10.1142/S0219633620500054)
43. M. Girod, B. Grammaticos, *Nucl. Phys., A* **330** (1979) 40 (https://doi.org/10.1016/0375-9474(79)90535-9).

Journal of the Serbian Chemical Society
JSCS@tmf.bg.ac.rs • www.shd.org.rs/JSCS
J. Serb. Chem. Soc. 86 (11) S380–S419 (2021) *Supplementary material*

SUPPLEMENTARY MATERIAL TO

The evaluation of chemoselectivity in multicomponent domino Knoevenagel/Diels–Alder reaction: A DFT study

MINA ATTARBASHI, NADER ZABARJAD SHIRAZ* and MARJANEH SAMADIZADEH

Department of Chemistry, Central Tehran Branch, Islamic Azad University, Tehran, Iran

J. Serb. Chem. Soc. 86 (11) (2021) 1053–1065

Table S-I. Energy of the relevant optimized transition states, intermediates, and products (**5** and **6**) compared to Gibbs free energy of starting materials in the gas phase

Gas		TS ($\Delta G^{\#}$ / kcal mol^{-1})	Int.	Product	Gas		TS ($\Delta G^{\#}$ / kcal mol^{-1})	Int.	Product
7	**8**	**9**-*SR* (TS) (Endo-y)	**9**-*SR*	**5**-*RS*	**7**	**8**	**9**-*SR* (TS) (Endo-y)	**9**-*SR*	**6**-*RS*
a	a	27.31	-17.16	-23.24	b	b	23.24	-16.61	-24.96
a	b	24.92	-15.44	-23.50	c	c	25.98	-21.05	-23.42
a	c	28.73	-19.84	-25.96					

(a = H, b = OCH_3, c = NO_2)

Table S-II. Optimized geometries (Cartesian coordinates x, y, z (in Å)) of the structures (a=H, b=OCH_3, c=NO_2) at the M062x/6-31+G(d,p) level of theory. Gibbs free energy is presented for compounds in gas phase and methanol.

Atom	*x* / Å	*y* / Å	*z* / Å	Atom	*x* / Å	*y* / Å	*z* / Å
(2a)	*G* = -345.358832 a. u. (Gas phase) *G* = -345.366162 a. u. (In methanol)			**(2b)**	*G* = -459.8130250 a. u. (Gas phase) *G* = -459.8239810 a. u. (In methanol)		
C	1.62532900	-1.21637200	0.00000000	C	-0.83956500	1.03795500	0.00020800
C	0.58745200	-2.14676000	0.00000000	C	-1.29140500	-0.28468200	0.00015800
C	-0.74422300	-1.72166900	0.00000000	C	-0.37274600	-1.34820300	0.00003500
C	-1.04023500	-0.36427000	0.00000000	C	0.98143400	-1.08825500	-0.00004100
C	0.00000000	0.57082400	0.00000000	C	1.44660400	0.23510900	-0.00001500
C	1.32951400	0.14484300	0.00000000	C	0.53099000	1.28275700	0.00013200
C	-0.29941600	2.02300000	0.00000000	C	2.89544000	0.51483400	-0.00008700
H	0.58857800	2.68838300	0.00000000	H	3.16276200	1.59342800	-0.00012300
O	-1.41628900	2.48862600	0.00000000	O	3.75627600	-0.33521000	-0.00011800
H	2.65750200	-1.55083000	0.00000000	H	-1.53564300	1.86777800	0.00041100
H	0.81482800	-3.20826900	0.00000000	H	-0.76328700	2.36015200	0.00001200
H	-1.54607200	-2.45285600	0.00000000	H	1.70950200	-1.89365300	-0.00010600
H	-2.06468900	-0.00457500	0.00000000	H	0.89132600	2.30925900	0.00014900
H	2.12964400	0.88157000	0.00000000	O	-2.59486000	-0.64374100	0.00030000
				C	-3.56315700	0.38464400	-0.00041300
				H	-3.47513300	1.01122300	-0.89557600
				H	-4.53172200	-0.11407200	0.00035300

* Corresponding author. E-mail: zabarjad_sh@yahoo.com

Atom	*x* / Å	*y* / Å	*z* / Å
(3)	*G* = -534.077618 a. u. (Gas phase)		
	G = -534.092167 a. u. (In methanol)		
O	-0.40835700	1.17791500	-0.35373900
C	0.91363100	1.27618000	-0.08696900
C	1.60005600	0.00001100	0.35178400
C	0.91366400	-1.27615300	-0.08703400
O	-0.40833800	-1.17792100	-0.35375100
C	-1.12773700	-0.00001000	0.01664600
C	-2.38585700	-0.00001200	-0.82194900
C	-1.41267300	-0.00001500	1.51133400
O	1.48525100	-2.31979600	-0.22616400
O	1.48521900	2.31980900	-0.22618900
H	2.62030800	0.00002900	-0.03244400
H	1.67468700	-0.00000900	1.44520500
H	-2.11456400	-0.00000800	-1.87883700
H	-2.97332900	-0.89239700	-0.59862700
H	-2.97333800	0.89236600	-0.59862300
H	-1.98863700	-0.89105900	1.76874600
H	-0.49318300	-0.00001100	2.10170800
H	-1.98864800	0.89102000	1.76875300
(3-Enol)	*G* = -534.0617660 a.u. (Gas phase)		
	G = -534.0826691 a.u. (In methanol)		
O	0.46638400	-1.30611300	-0.14223500
C	-0.82691200	-1.22168900	0.04158100
C	-1.57079000	-0.00492600	0.43391700
C	-0.95008300	1.22871900	-0.12032800
O	0.36086700	1.02804000	-0.53131700
C	1.15000100	-0.01491100	0.01455500
C	2.38418900	-0.11922400	-0.84960600
C	1.45347600	0.21702300	1.48383100
O	-1.44780300	2.30444300	-0.26806800
O	-1.67718500	-2.04619700	-0.28327600
H	-2.31801900	-0.82988800	-0.07926300
H	-1.78706700	0.07165700	1.50032500
H	2.08773800	-0.29139100	-1.88538900
H	2.94746300	0.81328600	-0.78575300
H	3.00582600	-0.94796800	-0.50536400
H	1.99009200	1.16207500	1.58834000
H	0.54037500	0.26729600	2.08102600
H	2.07620400	-0.59639800	1.86155600
(7a)	*G* = -786.4733010 a.u. (Gas phase)		
	G = -786.4956164 a.u. (In methanol)		
C	5.02121100	-0.39975400	0.88260200
C	2.73945600	-0.47554500	0.04502300
C	2.99520700	0.69329900	-0.68810300
C	4.23969700	1.30898800	-0.62753800
C	5.25771100	0.76674800	0.15922100
C	1.43541600	-1.15577600	0.03252300
C	0.28908400	-0.66745600	-0.46266200
C	-0.97751100	-1.42839800	-0.48354400
C	-1.01731600	-2.74234700	-0.77636100
N	-2.13380000	-0.65841400	-0.25619000
H	-3.47470600	1.01284600	0.89355200
(3-TS)	*G* = -534.0065840 a. u. (Gas phase)		
	G = -534.0308931 a. u. (In methanol)		
O	0.46638400	-1.30611300	-0.14223500
C	-0.82691200	-1.22168900	0.04158100
C	-1.57079000	-0.00492600	0.43391700
C	-0.95008300	1.22871900	-0.12032800
O	0.36086700	1.02804000	-0.53131700
C	1.15000100	-0.01491100	0.01455500
C	2.38418900	-0.11922400	0.84960600
C	1.45347600	0.21702300	1.48383100
O	-1.44780300	2.30444300	-0.26806800
O	-1.67718500	-2.04619700	-0.28327600
H	-2.31801900	-0.82988800	-0.07926300
H	-1.78706700	0.07165700	1.50032500
H	2.08773800	-0.29139100	-1.88538900
H	2.94746300	0.81328600	-0.78575300
H	3.00582600	-0.94796800	-0.50536400
H	1.99009200	1.16207500	1.58834000
H	0.54037500	0.26729600	2.08102600
H	2.07620400	-0.59639800	1.86155600
O	0.46638400	-1.30611300	-0.14223500
(4)	*G* = -400.8992150 a.u. (Gas phase)		
	G = -400.9067700 a.u. (In methanol)		
C	2.06912700	0.66642200	-0.33707300
C	1.75446600	-0.82653200	-0.36269900
N	0.82812000	-0.95428500	0.76529800
C	-0.08281600	0.17998900	0.70391500
C	0.69120500	1.29226700	-0.06521500
C	-1.38409900	-0.15536400	-0.00467200
O	-1.66181000	-1.22385500	-0.49436400
O	-2.22974400	0.89293000	-0.02227300
H	-3.03736800	0.61144500	-0.47925800
H	2.75545900	0.87808100	0.48771100
H	2.51677700	1.02714200	-1.26591000
H	1.29318200	-1.10093100	-1.32611200
H	2.63371900	-1.45648800	-0.20588900
H	0.31500600	-1.83096900	0.74154400
H	-0.35596400	0.51603500	1.71146100
H	0.18297800	1.52616000	-1.0054620
H	0.74450400	2.21622700	0.51238600
(7b)	*G* = -900.9243880 a.u. (Gas phase)		
	G = -900.9408619 a.u. (In methanol)		
C	4.25486000	-0.82968300	0.62875000
C	2.95904400	-1.34143500	0.62266200
C	1.91530600	-0.70658300	-0.05269600
C	2.21310800	0.47990500	-0.74721100
C	3.49053300	1.00284600	-0.75083300
C	4.52362000	0.35202800	-0.06106000
C	0.57372100	-1.29571400	-0.00808700
C	-0.55783200	-0.75904800	-0.48587500
C	-1.86269300	-1.44774000	-0.44249800
C	-1.98701200	-2.76582500	-0.67111300

Atom	*x* / Å	*y* / Å	*z* / Å
C	-3.42637100	-1.34234000	-0.14127200
C	-4.34426600	-0.27240900	0.44259600
C	-3.41465100	0.43580100	1.43247800
C	-2.08006300	0.48952100	0.66657900
C	-1.95608400	1.81985200	-0.09244200
O	-1.82857300	2.87228200	0.47666400
O	-2.01988700	1.72580500	-1.42664900
H	5.80735500	-0.83190400	1.49367400
H	3.59049700	-1.92417200	1.38886600
H	2.22193100	1.11959000	-1.31974700
H	4.41963300	2.21262300	-1.20127100
H	6.22906000	1.24894600	0.20185100
H	1.41385500	-2.14222800	0.49480800
H	0.25653900	0.34502600	-0.86447200
H	-1.93671500	-3.31362900	-0.78304600
H	-0.10652000	-3.25130000	-1.06318300
H	-3.34611500	-2.19843500	0.54694600
H	-3.74580900	-1.71891200	-1.11786100
H	-4.67161900	0.42020700	-0.34099300
H	-5.23169100	-0.69810200	0.91485900
H	-3.28949700	-0.17663400	2.33067100

Atom	*x* / Å	*y* / Å	*z* / Å
N	-2.96774600	-0.59766000	-0.22887800
C	-4.29708500	-1.19785000	-0.07912500
C	-5.13769800	-0.05764800	0.48692800
C	-4.15665100	0.59604900	1.46398200
C	-2.83146300	0.55459600	0.68402700
C	-2.63801400	1.86818900	-0.09158300
O	-2.49065600	2.92279400	0.46540100
O	-2.66602000	1.74639900	-1.42430500
H	5.03397800	-1.35546400	1.16759700
H	2.75554900	-2.26222700	1.16366500
H	1.43380600	0.99761000	-1.29823100
H	3.72649500	1.91721300	-1.28460900
H	0.50610800	-2.26687300	0.48190900
H	-0.55247400	0.23700900	-0.92776100
H	-2.93649700	-3.28429400	-0.62742500
H	-1.11566400	-3.34159100	-0.95493700
H	-4.26130700	-2.03704900	0.63274300
H	-4.65119400	-1.58254200	-1.04038800
H	-5.41065500	0.64505200	-0.30862100
H	-6.05449200	-0.41042800	0.96339000
H	-4.06797000	-0.01445200	2.36799900
H	-4.41495800	1.61521900	1.75641600
H	-1.96895200	0.44902800	1.34840900
H	-2.83273800	0.79488800	-1.60088800
O	5.74132100	0.94490500	-0.12882100
C	6.80798700	0.32232600	0.55264800
H	7.68387800	0.94679500	0.37877100
H	6.61070500	0.26197300	1.62970800
H	6.99505400	-0.68550100	0.16270200

(7c) *G* = -990.9057230 a.u. (Gas phase)
G = -990.9402728 a.u. (In methanol)

C	3.95199300	-1.12068500	0.71862700
C	2.64374800	-1.58171100	0.67782600
C	1.64510400	-0.87988100	-0.01246200
C	1.99448100	0.30603800	-0.67839100
C	3.29489800	0.78313700	-0.64656000
C	0.27868000	-1.41881100	-0.00689300
C	-0.81592600	-0.80957000	-0.48126600
C	-2.15517400	-1.43210900	-0.48570100
C	-2.33234300	-2.73288700	-0.77043300
N	-3.21828400	-0.53634400	-0.26325600
C	-4.58071200	-1.07129000	-0.17125600
C	-5.37636000	0.09456500	0.40700200
C	-4.39379900	0.66408300	1.43412900
C	-3.04547500	0.57124400	0.69808300
C	-2.74093600	1.89785600	-0.01694600
O	-2.52481500	2.91261600	0.58806100
O	-2.75099600	1.83538600	-1.35481800
H	4.73235300	-1.65200100	1.24922000
H	2.38565300	-2.50251800	1.19274800
H	1.24643400	0.86033800	-1.23527200
H	3.58065000	1.69608700	-1.15429300
H	0.16295800	-2.40183100	0.44707600
H	-0.75477900	0.20128300	-0.88349900

(8a) *G* = -803.0435920 a.u. (Gas phase)
G = -803.0671536 a.u. (In methanol)

O	2.79130600	0.97553600	-0.25201500
C	1.52373200	1.42133500	-0.41872700
C	0.44975500	0.37589700	-0.36985900
C	0.44975500	0.37589700	-0.36985900
C	0.87410000	-1.03842300	-0.52685300
O	2.18975600	-1.28124600	-0.31245900
C	2.99015100	-0.30205900	0.34594400
C	-0.80939200	0.86028600	-0.22103300
H	-0.80605100	1.94921500	-0.16823100
C	-2.15318500	0.30746300	-0.06317800
C	-3.15066400	1.25994000	0.23043100
C	-4.47213500	0.88453800	0.43119300
C	-4.82719500	-0.46042300	0.33771200
C	-3.85504400	-1.41533200	0.04043400
C	-2.52993800	-1.04518100	-0.16231200
C	2.65926100	-0.25455000	1.83122500
C	4.42789800	-0.67911000	0.07059700
O	1.32732900	2.59056700	-0.62305100
O	0.17277500	-1.94994800	-0.88482300
H	-2.87482900	2.30838100	0.30357300
H	-5.22105800	1.63626900	0.65725000
H	-5.85862200	-0.76288500	0.49011200
H	-4.13116200	-2.46152900	-0.04224600

Atom	*x* / Å	*y* / Å	*z* / Å
H	-3.30677200	-3.20479600	-0.77600600
H	-1.48202500	-3.33900900	-1.05499000
H	-4.60941600	-1.93337200	0.51299600
H	-4.92439400	-1.40527100	-1.15490400
H	-5.5825900	0.83468400	-0.37319400
H	-6.32457200	-0.22282500	0.84493200
H	-4.36947000	0.02459400	2.32182300
H	-4.60607900	1.68704500	1.74934800
H	-2.21771500	0.38794500	1.38965800
H	-2.98728700	0.90972200	-1.57913300
N	5.63511700	0.55709100	0.08559800
O	6.45369700	-0.09595100	0.70671600
O	5.87422800	1.59059600	-0.51120400
(8b)	*G* = -917.4706408 a. u. (Gas phase)		
	G = -917.4974766 a. u. (In methanol)		
O	3.60150500	0.95892600	-0.16938400
C	2.33921300	1.43550000	-0.30628200
C	1.25053000	0.40991900	-0.32238800
C	1.64145900	-1.00161300	-0.54365700
O	2.95679500	-1.28127100	-0.35950700
C	3.77513600	-0.35483100	0.34558100
C	-0.00737900	0.91428900	-0.21161100
H	0.01433800	2.00162200	-0.13465500
C	-1.35782900	0.38651200	-0.13416300
C	-2.36979600	1.35261200	0.00794200
C	-3.71070300	1.01546600	0.11745500
C	-4.07131500	-0.33512400	0.09437000
C	-3.07941700	-1.31868400	-0.04101000
C	-1.75042400	-0.97072700	-0.15781700
C	3.45235100	-0.38887600	1.83321700
C	5.20508300	-0.74176800	0.04087300
O	2.16641000	2.61867400	-0.43401300
O	0.91922500	-1.88427000	-0.92949800
H	-2.09340500	2.40329700	0.03398200
H	-4.45373700	1.79654600	0.22150200
H	-3.39050200	-2.35754800	-0.05979900
H	-1.00550700	-1.74300500	-0.28271600
H	2.41155600	-0.10684000	2.01633900
H	3.61495500	-1.39791400	2.21859100
H	4.10301300	0.31026700	2.36320900
H	5.39354200	-1.75811800	0.39260800
H	5.36656900	-0.69625900	-1.03766300
H	5.88692700	-0.04929800	0.53867000
O	-5.33742600	-0.78759500	0.19394500
C	-6.37367600	0.16591900	0.32034900
H	-7.30019800	-0.40375600	0.37919800
H	-6.25230700	0.76288600	1.23140800
H	-6.40670600	0.83084500	-0.55017000
(10a-TS)	*G* = -879.361834 a. u. (Gas phase)		
	G = -879.3959555 a. u. (In methanol)		
O	-2.3554190	-1.12801500	-0.15867200
C	-1.0909470	-1.04577400	-0.63925500
C	-0.4604510	0.24751800	-0.59450900
C	-1.1229270	1.38330200	0.02779600

Atom	*x* / Å	*y* / Å	*z* / Å
H	-1.79201100	-1.79259000	-0.41410000
H	1.61315300	0.01566600	1.99892000
H	2.84216000	-1.23607200	2.27339200
H	3.29496600	0.48706000	2.31930400
H	4.63071200	-1.66966900	0.48191400
H	4.59701900	-0.69270200	-1.00733500
H	5.09232300	0.05330400	0.53278700
(8c)	*G* = -1007.408441 a. u. (Gas phase)		
	G = -100.4483290 a. u. (In methanol)		
O	3.88722600	0.77810500	-0.24977100
C	2.68700600	1.32737500	-0.54357000
C	1.50806300	0.39969600	-0.46385500
C	1.78931600	-1.06207000	-0.44843700
O	3.05245500	-1.40430600	-0.10718900
C	3.91295200	-0.43769800	0.49125500
C	0.30423400	1.01182500	-0.40927500
H	0.39892200	2.09794400	-0.41799900
C	-1.08726600	0.56627200	-0.27353000
C	-1.97082800	1.52900100	0.25107800
C	-3.31354000	1.24760700	0.44444400
C	-3.77251700	-0.00906000	0.07506000
C	-2.94411800	-0.97553300	-0.47573400
C	-1.59601000	-0.68801200	-0.64869300
C	3.50361100	-0.18889600	1.93543400
C	5.31555000	-0.98466600	0.35491800
O	2.61513900	2.47944900	-0.87269700
O	1.01812100	-1.93033800	-0.76007100
H	-1.59044700	2.51053400	0.51796000
H	-4.00107800	1.97416100	0.85879300
H	-3.35803500	-1.93417500	-0.76295900
H	-0.93829500	-1.42736200	-1.08084900
H	2.48283300	0.19971600	1.99612200
H	3.55417300	-1.12566800	2.49459000
H	4.18227300	0.53857000	2.38600800
H	5.39037900	-1.93758700	0.88243500
H	5.54083000	-1.13714800	-0.70208900
H	6.02834400	-0.27444600	0.77858000
N	-5.20102000	-0.32150200	0.26401200
O	-5.90326100	0.54618400	0.74781200
O	-5.58236400	-1.42522700	-0.07473900
(10b-TS)	*G* = -993.812271 a. u. (Gas phase)		
	G = -993.849333 a. u. (In methanol)		
O	-3.0365400	0.93794500	0.54821000
C	-1.7175630	0.86862800	0.85168000
C	-1.0164660	-0.31923200	0.43987500
C	-1.6800290	-1.34593200	-0.34861400

Atom	*x* / Å	*y* / Å	*z* / Å	Atom	*x* / Å	*y* / Å	*z* / Å
O	-2.3710970	1.12578900	0.52529500	O	-2.9963540	-1.10118900	-0.62992700
C	-3.1228840	0.07840100	-0.08265900	C	-3.7282230	-0.28747000	0.28333200
O	-0.5084310	-2.08340100	-0.93260000	O	-1.169687	1.86518200	1.30858100
O	-0.6158790	2.46449000	0.22781000	O	-1.1349450	-2.30497100	-0.84781000
C	-4.2742630	-0.21617400	0.85179300	C	-5.0081320	0.09852600	-0.42270600
C	-3.5756840	0.49378500	-1.47599800	C	-3.9678670	-1.03976600	1.58547900
C	0.91899900	-0.41747700	1.18935600	C	0.07303000	0.84693500	-1.28648800
H	0.51440300	0.32472900	1.87513500	H	-0.3689650	0.24016600	-2.07473400
C	2.20024900	-0.13609500	0.54234700	C	1.44310900	0.54909700	-0.86986500
C	2.61177600	1.20140700	0.43138900	C	1.95070300	-0.73620000	-1.11672100
C	3.82441300	1.50105200	-0.17394700	C	3.24863900	-1.04890600	-0.73687200
C	4.63268100	0.47335500	-0.66744200	C	4.0466010	-0.0853250	-0.11416300
C	4.22565000	-0.85551400	-0.55570200	C	3.54390800	1.19217500	0.12944400
C	3.01067200	-1.16473100	0.04831400	C	2.24321300	1.51366900	-0.24666300
O	0.52373900	-1.64342400	1.45553500	O	-0.4315350	2.05963400	-1.21717900
H	0.37276200	0.43583500	-1.25564900	H	-0.0938060	-0.57109900	0.94194500
H	-3.8814600	-0.50927600	1.82689700	H	-4.7654630	0.63433500	-1.34197300
H	-4.8916130	0.67717000	0.96339100	H	-5.5760510	-0.80121000	-0.66679800
H	-4.8771880	-1.03044000	0.44528100	H	-5.6039970	0.74401100	0.22544000
H	-4.1820550	1.39908800	-1.40402400	H	-4.5189900	-1.95884000	1.37570200
H	-2.7197700	0.69634100	-2.12554600	H	-3.0233430	-1.30081300	2.07051400
H	-4.1697030	-0.30811400	-1.91936000	H	-4.5493220	-0.41359500	2.26539700
H	1.95724900	1.99282800	0.78930700	H	1.30733800	-1.48607900	-1.57127700
H	4.14119500	2.53466300	-0.26461800	H	3.64031600	-2.04337300	-0.92274200
H	5.58163500	0.71007300	-1.13794900	H	4.16622700	1.94017200	0.60922800
H	4.85634400	-1.65226700	-0.93567800	H	1.86146500	2.51394900	-0.06672500
H	2.70491600	-2.20198300	0.14470600	H	-0.3406960	2.43478200	-0.31079800
H	0.54628600	-2.21048300	0.65027100	O	5.38451200	-0.40967100	0.27273800
				C	5.37379800	-1.01059800	1.57030200
				H	4.83248900	-1.93277100	1.53182600
				H	6.37910900	-1.19995400	1.88397800
				H	4.90177800	-0.34871200	2.26600600

(10c-TS)	*G* = -1083.781166 a. u. (Gas phase) *G* = -1083.834224 a. u. (In methanol)			**(11a-TS)**	*G* = -879.389220 a. u. (Gas phase) *G* = -879.422796 a. u. (In methanol)		
C	1.94624000	1.38501700	-0.14274200	O	-2.75586700	0.85649500	0.10262600
O	3.31947000	-1.00079700	0.38890500	C	-1.52970400	1.27075800	-0.09974000
C	2.00774500	-0.97786000	0.72870400	C	-0.38050600	0.29434600	-0.08007300
C	2.00774500	-0.97786000	0.72870400	C	-0.83625200	-1.06521100	-0.57553500
C	1.29918200	0.25524400	0.50615900	O	-2.16009300	-1.35623500	-0.40657000
O	3.25556700	1.18528300	-0.48554400	C	-2.98833600	-0.54781000	0.40295100
C	4.00668600	0.25113300	0.28581700	O	-1.34085500	2.46963300	-0.31513600
O	1.46892700	-2.03034900	1.05117700	O	-0.13621100	-1.85084400	-1.13943700
O	1.39137200	2.40437200	-0.48786300	C	-4.41166100	-0.81647000	-0.02753600
C	5.26985900	-0.02798300	-0.49657400	C	-2.75425600	-0.79637100	1.88351100
C	4.27658900	0.81072000	1.67613400	C	0.87822900	0.89922200	-0.85065500
C	0.16953400	-0.65514200	-1.34380600	H	0.76396200	0.59296600	-1.90714900
H	0.59451200	0.05853700	-2.04730800	C	2.15000800	0.26633700	-0.30068500
C	-1.19041800	-0.42222700	-0.85833800	C	2.72540100	-0.86667300	-0.87694800
C	-1.70168200	0.88418300	-0.90812400	C	3.88652700	-1.41822400	-0.33633500
C	-2.99031600	1.13718600	-0.45854700	C	4.48218900	-0.83984700	0.78307700
C	-3.77538100	0.09325300	0.03831600	C	3.91841900	0.30171200	1.35302300
C	-3.26907900	1.20498700	0.08610800	C	2.76138700	0.85525100	0.80919900
C	-1.97761400	-1.46721600	-0.36107900	O	0.87257000	2.26219300	-0.67669900
O	0.67387600	-1.86441000	-1.45930100	H	-0.07530700	0.19570800	0.97198800

Atom	*x* / Å	*y* / Å	*z* / Å
H	0.38839500	0.43131600	1.05958300
H	5.00584000	-0.42783600	-1.47710600
H	5.83337100	0.89839900	-0.62270500
H	5.87927300	-0.75810400	0.03946500
H	4.82410700	1.75132400	1.58709000
H	3.34357300	0.99826300	2.21450000
H	4.87233800	0.09516300	2.24668800
H	-1.06768300	1.69235500	-1.26556000
H	-3.38471800	2.14726100	-0.49201600
H	-3.88146700	-2.01485000	0.46830500
H	-1.59328000	-2.48221700	-0.33408500
H	0.60293800	-2.36500800	-0.61379300
N	-5.14096500	0.36406900	0.51026900
O	-5.79097700	-0.55169100	0.93132400
O	-5.55054700	1.48996500	0.45541400

(11b-TS) *G* = -993.8632130 a. u. (Gas phase)
G = -993.9000156 a. u. (In methanol)

O	-3.50017200	0.70297600	0.26798300
C	-2.32087500	1.22365800	0.03519600
C	-1.10647900	0.33840200	-0.09125600
C	-1.49420900	-1.00696000	-0.67542000
O	-2.78149300	-1.40982400	-0.46001400
C	-3.61419400	-0.73459900	0.45952000
O	-2.23061900	2.44688300	-0.08701400
O	-0.77587600	-1.68914600	-1.34166400
C	-5.03844700	-1.07408800	0.08589000
C	-3.27381800	-1.08413400	1.89847900
C	0.05733500	1.09710200	-0.87483500
H	-0.09883600	0.86986100	-1.94581600
C	1.40165000	0.51946500	-0.45105900
C	2.01967400	-0.51636200	-1.15246900
C	3.24750200	-1.02075800	-0.72502500
C	3.86756300	-0.49184700	0.40554700
C	3.26012400	0.55386700	1.10076900
C	2.03603700	1.06080800	0.67007800
O	-0.03406600	2.43712800	-0.58508100
H	-0.73186300	0.17801400	0.93033400
H	-5.22216400	-0.78356700	-0.94962100
H	-5.18821700	-2.14998700	0.19037700
H	-5.72905700	-0.5424400	0.74294100
H	-3.41327200	-2.1578720	2.03800700
H	-2.24153800	-0.8356110	2.15182900
H	-3.94137400	-0.5440450	2.57258900
H	1.53525500	-0.93397800	-2.02948900
H	3.72129800	-1.82498700	-1.27962200
H	3.74843600	0.98500900	1.96968500
H	1.57134500	1.90580000	1.16965300
H	-1.16877000	2.61352200	-0.34867300
O	5.12850900	-1.00750100	0.84030600
C	6.18518300	-0.26312800	0.22854800
H	6.12337900	0.76057400	0.53369500
H	7.12824400	-0.66886700	0.53006300
H	6.09458400	-0.32411300	-0.83586400

Atom	*x* / Å	*y* / Å	*z* / Å
H	-4.51620800	-0.60317900	-1.09243700
H	-4.64768000	-1.86623400	0.15466300
H	-5.09495900	-0.18319100	0.54111900
H	-2.98175100	-1.84172400	2.10102000
H	-1.72151100	-0.60069000	2.17795900
H	-3.41489300	-0.15487500	2.46984900
H	2.25937100	-1.32237400	-1.74492400
H	4.32779500	-2.29833500	-0.79408100
H	5.38788900	-1.26842300	1.20129400
H	4.38978700	0.76988900	2.21207400
H	2.33525800	1.77053200	1.20945000
H	-0.25677800	2.53786900	-0.52460800

(11c-TS) *G* = -1083.733342 a. u. (Gas phase)
G = -1083.787786 a. u. (In methanol)

O	-3.72206200	0.56085700	0.37985200
C	-2.59169300	1.16578300	0.11083000
C	-1.33053200	0.36741200	-0.10481000
C	-1.65918500	-0.98049900	-0.71857400
O	-2.90563100	-1.47448900	-0.45753100
C	-3.73365000	-0.88667600	0.52416300
O	-2.58656100	2.39568000	0.02905300
O	-0.93219500	-1.59122100	-1.44229100
C	-5.14979500	-1.30696300	0.20597300
C	-3.30079900	-1.26052900	1.93182300
C	-0.25813500	1.22696600	-0.91426400
H	-0.45206200	1.02558100	-1.98424900
C	1.13988400	0.72569100	-0.57559200
C	1.78793700	-0.24316700	-1.34254100
C	3.06531700	-0.67922200	-0.99205500
C	3.70511500	-0.14831100	0.12651900
C	3.06667000	0.83131100	0.88715100
C	1.79269400	1.27026000	0.53334000
O	-0.42123300	2.54766200	-0.57200200
H	-0.89635400	0.19830700	0.89148400
H	-5.40277200	-0.99500300	-0.80848200
H	-5.22460900	-2.39328300	0.27822100
H	-5.83991000	-0.84422800	0.91373300
H	-3.36374100	-2.34517400	2.03864100
H	-2.27541700	-0.95287200	2.14511000
H	-3.96763800	-0.78841800	2.65583100
H	1.28869000	-0.66253900	-2.21035900
H	3.56195200	-1.43152200	-1.59723400
H	3.56852400	1.26469900	1.74718800
H	1.29978800	2.06564000	1.08464800
H	-1.55187500	2.64072900	-0.27612600
N	5.05327500	-0.60610500	0.49229100
O	5.58049100	-0.11766500	1.45244100
O	5.57213300	-1.44976300	-0.18405000

Atom	*x* / Å	*y* / Å	*z* / Å
(11a-Int)	*G* = -879.410214 a. u. (Gas phase)		
	G = -879.443057 a. u. (In methanol)		
O	2.12096300	-0.83853300	-0.74734700
C	0.86833400	-1.00111400	-0.14989200
C	0.29671700	0.28653500	0.43313700
C	1.17898300	1.51053000	0.38510300
O	2.47121300	1.32795200	0.05176800
C	3.01250200	-0.00912800	-0.02802900
O	0.84514000	-2.08208400	0.70336800
H	1.13428500	-2.86098500	0.20645900
O	0.74514900	2.61622400	0.57128000
C	4.25996100	0.10716600	-0.87494600
C	3.29755500	-0.50682500	1.38343300
C	-0.7091410	0.18110800	-0.75075800
H	-0.5458290	0.95091300	-1.51220000
C	-2.1624870	0.07570700	-0.39396800
C	-2.9601800	1.22123000	-0.42988100
C	-4.2969800	1.15443800	-0.04452800
C	-4.8434750	-0.05977700	0.36961500
C	-4.0482360	-1.20460500	0.40169200
C	-2.7083450	-1.13870400	0.02469800
O	-0.1140180	-1.07408400	-1.15513000
H	-0.1674890	0.17693000	1.41388600
H	3.98819800	0.46874600	-1.86792800
H	4.95555600	0.80861300	-0.41090200
H	4.73329400	-0.87284000	-0.96303100
H	4.02796100	0.15765800	1.84960400
H	2.39558100	-0.52792800	1.99909200
H	3.70258900	-1.52034300	1.34079000
H	-2.5304860	2.16618100	-0.75319400
H	-4.9125240	2.04788900	-0.07338800
H	-5.8870210	-0.11396300	0.66333700
H	-4.4724650	-2.15187100	0.71965000
H	-2.0804270	-2.02416000	0.04226700

Atom	*x* / Å	*y* / Å	*z* / Å
(11b-Int)	*G* = -993.878406 a. u. (Gas phase)		
	G = -993.913121 a. u. (In methanol)		
O	2.88989300	-0.76751700	-0.75440600
C	1.59981800	-0.94376300	-0.25109400
C	1.00996100	0.30026300	0.40056100
C	1.89997100	1.51968600	0.44761700
O	3.21505700	1.33319700	0.21384000
C	3.73758700	-0.00339700	0.07777500
O	1.50630100	-2.08436000	0.51728200
H	1.82651700	-2.82052600	-0.02333700
O	1.46255600	2.62243000	0.62907900
C	5.04177100	0.14686100	-0.67364400
C	3.92033200	-0.60497200	1.46535900
C	0.03425800	0.27526900	-0.81100800
H	0.18639600	1.11953800	-1.49132900
C	-1.4197600	0.07919000	-0.51213500
C	-2.3222630	1.12039100	-0.68650200
C	-3.6707400	0.96818500	-0.36363400
C	-4.1185700	-0.25473800	0.13559300
C	-3.2150210	-1.31135600	0.31114000
C	-1.8800980	-1.14316500	-0.00738800
O	0.68104600	-0.92016300	-1.31445400
H	0.52716200	0.12858300	1.36308300
H	4.83988100	0.57935300	-1.65435500
H	5.71393900	0.80308900	-0.11884400
H	5.50720600	-0.83243800	-0.79859700
H	4.63025400	0.00624100	2.02563300
H	2.97866800	-0.64817000	2.01609300
H	4.30784600	-1.62188200	1.37670300
H	-1.9740860	2.07333000	-1.07617000
H	-4.3513790	1.79745600	0.51077000
H	-3.5944680	-2.25103300	0.69718500
H	-1.1750820	-1.95901700	0.12470300
O	-5.4057860	-0.51996000	0.47655800
C	-6.3489590	0.51658500	0.31530000
H	-7.3058400	0.11072300	0.64139900
H	-6.0946330	1.38744900	0.93109600
H	-6.4246500	0.82804900	-0.73331600

Atom	*x* / Å	*y* / Å	*z* / Å
(11c-Int)	*G* = -1083.786748 a. u. (Gas phase)		
	G = -1083.840682 a. u. (In methanol)		
O	3.10100700	-0.95626600	-0.53196300
C	1.80700900	-1.01745900	-0.01502600
C	1.22288900	0.34898200	0.32462500
C	2.12310200	1.54424300	0.12540100
O	3.43588400	1.30651800	-0.04012700
C	3.94879700	-0.03384000	0.12426700
O	1.69229800	-1.95057700	0.98363800
H	2.05717700	-2.78256700	0.64995000
O	1.68085900	2.65867600	0.05203000
C	5.26013400	-0.05894200	-0.62818800
C	4.11113100	-0.31692700	1.61157400
C	0.29689000	0.06764600	-0.88593500
H	0.49939200	0.72688000	-1.73757000
C	-1.1737030	0.02413300	-0.58863000

Atom	*x* / Å	*y* / Å	*z* / Å
(11a)	*G* = -879.4310770 a. u. (Gas phase)		
	G = -879.4598882 a. u. (In methanol)		
O	2.15989300	-1.33705300	0.15353300
C	0.88760400	-1.11211400	-0.24378000
C	0.39222600	0.32707600	-0.18075800
C	1.51078500	1.32994800	-0.47693600
O	2.76880900	0.94015200	-0.13267900
C	3.00502600	-0.26140100	0.62034400
O	0.21783100	-2.04127100	-0.63621500
O	1.33763800	2.41397900	-0.97041700
C	4.42728700	-0.68504600	0.29523600
C	2.78092000	-0.01983300	2.11173800
C	-0.8811700	0.57954500	-1.05785300
H	-0.8738910	1.64994300	-1.27637500
C	-2.1667920	0.26563300	-0.29160300
C	-2.6137070	1.18237900	0.67273600

Atom	*x* / Å	*y* / Å	*z* / Å	Atom	*x* / Å	*y* / Å	*z* / Å
C	-1.8337250	1.23161200	-0.33897500	C	-3.7791670	0.94502400	1.40436900
C	-3.1883100	1.23621000	-0.04237300	C	-4.5235370	-0.21566300	1.17371500
C	-3.8568120	0.01754100	-0.00513800	C	-4.0936290	-1.12657200	0.2061990
C	-3.2244530	-1.19300500	-0.24483500	C	-2.9242160	-0.88727200	-0.52198000
C	-1.8640730	-1.18397700	-0.53616800	O	-0.7737210	-0.04686200	-2.32025800
O	0.89985300	-1.22503000	-1.07892300	H	0.11165300	0.50577800	0.86802400
H	0.70494300	0.39904800	1.28277500	H	4.52889000	-0.84315300	-0.78158400
H	5.07135300	0.14992400	-1.68187800	H	5.12633200	0.09514400	0.60917500
H	5.93237500	0.69847300	-0.22263200	H	4.66586600	-1.61576900	0.81762200
H	5.71856600	-1.04453700	-0.53074300	H	3.45343600	0.77062400	2.45743600
H	4.81942700	0.39896300	2.03232400	H	1.75342000	0.28206700	2.33318800
H	3.16356000	-0.23379100	2.14756300	H	2.99550800	-0.93770400	2.66678500
H	4.49325300	-1.32985600	1.75319600	H	-2.0545890	2.10220900	0.84163200
H	-1.2731510	2.16298600	-0.36610500	H	-4.1117580	1.67137800	2.14181600
H	-3.7317400	2.15072100	0.15860900	H	-5.4345420	-0.40266500	1.73635500
H	-3.7962910	-2.11124800	-0.19863400	H	-4.6691510	-2.02843300	0.01334400
H	-1.3278960	-2.10716800	-0.72237700	H	-2.6116260	-1.60515400	-1.27325700
N	-5.2952540	0.01246400	0.30635800	H	-0.6929100	-1.00604700	-2.17441600
O	-5.8292890	1.08646600	0.51287100				
O	-5.8602910	-1.06508300	0.33840100				

(11b) *G* = -993.8798972 a. u. (Gas phase)
G = -993.9112178 a. u. (In methanol)

Atom	x / Å	y / Å	z / Å
O	-2.7275400	-0.95844100	1.01604600
C	-1.5087000	-0.39024300	1.01485500
C	-1.1152240	0.37806600	-0.23465000
C	-2.3158300	1.05878800	-0.88188900
O	-3.5117730	0.45301800	-0.69449200
C	-3.5862110	-0.85165800	-0.12513300
O	-0.8030460	-0.48953800	1.98473800
O	-2.2470760	2.06534700	-1.52587600
C	-4.9954280	-0.99351700	0.40668900
C	-3.2402840	-1.91600000	-1.15610000
C	0.03913500	1.37771600	0.03702100
H	0.01177900	2.09425600	-0.78882600
C	1.39031100	0.67626200	0.01497500
C	1.87231300	0.18864200	-1.20404200
C	3.10168300	-0.45973200	-1.27754000
C	3.87060400	-0.62319600	-0.12538300
C	3.40221600	-0.12863400	1.08904900
C	2.16915700	0.51939300	1.15918800
O	-0.2108290	2.13156200	1.19338500
H	-0.7603540	-0.36675500	-0.96007800
H	-5.1854610	-0.20621800	1.13781300
H	-5.7064310	-0.90281900	-0.41648200
H	-5.1091890	-1.96812200	0.88485100
H	-3.9329130	-1.83740800	-1.99638000
H	-2.2221110	-1.81001000	-1.53573300
H	-3.3373250	-2.90285700	-0.69926300
H	1.28760400	0.33487000	-2.11139300
H	3.46366200	-0.82668400	-2.23289000
H	3.99735000	-0.24536100	1.98928000
H	1.82262500	0.90545400	2.11186700
H	-0.2099800	1.53121700	1.95230200

(11c) *G* = -1083.862149 a. u. (Gas phase)
G = -1083.910219 a. u. (In methanol)

Atom	x / Å	y / Å	z / Å
O	-2.8406500	-0.79661700	1.23144300
C	-1.6714500	-0.15006300	1.07855500
C	-1.3462880	0.35100200	-0.31772100
C	-2.60045000	0.77659800	-1.07250500
O	-3.7430180	0.13647300	-0.73025300
C	-3.7099200	-1.01172300	0.11380800
O	-0.9560280	0.02258200	2.03083500
O	-2.6155580	1.61803300	-1.92360100
C	-5.1009180	-1.14120700	0.69450400
C	-3.2838780	-2.24763200	-0.66490900
C	-0.2749070	1.47234300	-0.29806500
H	-0.3632600	1.98416800	-1.26057700
C	1.12818800	-0.19471600	0.89024100
C	1.64270300	-1.28674700	0.18395000
C	2.91990300	-0.36736800	-1.24259600
C	3.70431700	-0.21189100	-0.09981600
C	3.20279500	0.50118900	0.98591700
C	1.92193200	1.05114100	0.93864700
O	-0.5798050	2.44156900	0.66918900
H	-0.9357360	-0.50601700	-0.86899500
H	-5.3505590	-0.22886100	1.23837700
H	-5.8203690	-1.29017800	-0.11269000
H	-5.1339390	-1.99173800	1.37783400
H	-3.9841130	-2.41073100	-1.48652500
H	-2.2791290	-2.14965900	-1.08073700
H	-3.2993370	-3.11349500	-0.00004500
H	1.04431800	-2.19102000	0.08013300
H	3.30619100	-0.90733800	-2.10142600
H	3.80917000	0.63292000	1.87652500
H	1.54949300	1.61029400	1.79032900
H	-0.5274980	2.02584900	1.54143300

Atom	*x* / Å	*y* / Å	*z* / Å
O	5.13653200	-1.28477400	-0.19350600
C	6.16844600	-0.31940100	-0.41283900
H	6.19877100	0.36353200	0.41031400
H	7.11131400	-0.81814700	-0.49741100
H	5.96738500	0.21875200	-1.31553800
(12a-TS)	*G* = -879.3373010 a. u. (Gas phase)		
	G = -879.3705264 a. u. (In methanol)		
O	-2.05520300	-1.16297100	0.60886600
C	-0.74576200	-0.90452000	0.46456400
C	-0.40583200	0.33187600	-0.31175900
C	-1.50288500	1.33439900	-0.54504300
O	-2.75396500	0.91971200	-0.28586400
C	-3.07952200	-0.45211300	-0.08698200
O	0.06521600	-1.62533800	0.97982400
O	-1.29328200	2.45661700	-0.90876800
C	-4.28074900	-0.46079400	0.83336300
C	-3.34554400	-1.11919600	-1.42601600
C	0.90833500	0.93376200	-0.22371400
H	0.88294500	2.00277600	-0.41535700
C	2.20565700	0.30406800	-0.18846100
C	2.42882600	-1.04244200	-0.52258900
C	3.72158300	-1.54495600	-0.52653800
C	4.79589100	-0.72453300	-0.18320400
C	4.58657500	0.61487400	0.14582500
C	3.30087600	1.13063200	0.12524800
O	-0.01186200	1.25861300	1.86211900
H	-0.36824200	-0.48902100	-2.13360000
H	-4.01469700	0.03275900	1.76904300
H	-5.10603500	0.07447100	0.36116000
H	-4.57920800	-1.49064300	1.03568800
H	-4.15739800	-0.59610700	-1.93425400
H	-2.45469500	-1.08948900	-2.05666500
H	-3.63042300	-2.15986600	-1.26159300
H	1.59232200	-1.67646400	-0.78565800
H	3.89416500	-2.58148700	-0.79419000
H	5.80301000	-1.12924800	-0.18006400
H	5.42467900	1.25166100	0.40617900
H	3.11899300	2.17187500	0.37436000
H	0.46266200	0.49938200	2.23736800

Atom	*x* / Å	*y* / Å	*z* / Å
N	5.05581700	-0.78769200	-0.04687500
O	5.70580000	-0.62658600	0.94810500
O	5.45449900	-1.39557800	-1.00078000
(12b-TS)	*G* = -993.7954150 a. u. (Gas phase)		
	G = -993.8315324 a. u. (In methanol)		
O	-2.73778500	-1.20307800	0.59498400
C	-1.43919700	-0.87434200	0.50634500
C	-1.12991200	0.35509400	-0.29348900
C	-2.26800900	1.28524800	-0.61371700
O	-3.50550500	0.80749600	-0.40230100
C	-3.76357500	-0.57401000	-0.17363900
O	-0.61641500	-1.53116500	1.08459200
O	-2.10324600	2.40594400	-1.00422500
C	-5.00761300	-0.62342500	0.68658500
C	-3.92358300	-1.29613900	-1.50093200
C	0.14240200	1.03395100	-0.16149200
H	0.06708000	2.09333800	-0.38993600
C	1.46941800	0.48125600	-0.04166300
C	1.78415400	-0.85983500	-0.31906600
C	3.10150100	-1.28708900	-0.24286400
C	4.10946900	-0.39609900	0.12489500
C	3.80920300	0.93854400	0.39812400
C	2.49939800	1.37866500	0.29734000
O	-0.89921400	1.36935000	1.86471900
H	-0.95406800	-0.51791400	-2.08271400
H	-4.81740200	-0.08685800	1.61706300
H	-5.83648000	-0.15125900	0.15684900
H	-5.25794600	-1.66201900	0.90852700
H	-4.73654600	-0.83645900	-2.06557200
H	-3.00491900	-1.23467700	-2.08786700
H	-4.15784600	-2.34591600	-1.31579700
H	0.99882000	-1.54868300	-0.60132100
H	3.34509800	-2.31972400	-0.46679200
H	4.59611500	1.63015900	0.67765500
H	2.24720500	2.41489700	0.50214700
H	-0.40267100	0.65054900	2.28802500
O	5.46213300	-0.85177000	0.21186900
C	6.24716500	-0.21212900	-0.79782600
H	6.42375800	0.80613300	-0.52059400
H	7.18261200	-0.72174100	-0.89849600
H	5.72252600	-0.24216600	-1.72989500

(12c-TS)	*G* = -1083.750730 a. u. (Gas phase)		
	G = -1083.803421 a. u. (In methanol)c		
O	-2.88167500	-1.23652000	0.66499400
C	-1.60529700	-0.84821500	0.51554900
C	-1.38884200	0.37535500	-0.32285800
C	-2.58293600	1.24215900	-0.61575900
O	-3.78612600	0.71087600	-0.34297300
C	-3.96708000	-0.67560200	-0.07393900
O	-0.72881400	-1.45106300	1.07332200
O	-2.48890700	2.35990800	-1.03694600
C	-5.17153200	-0.76413000	0.83793500

(13a-TS)	*G* = -879.3465120 a. u. (Gas phase)		
	G = -879.3809645 a. u. (In methanol)		
O	2.09159800	-1.29495300	0.31129600
C	1.03845600	-0.89762400	1.05326800
C	0.44119000	0.41796600	0.70667800
C	0.90987900	1.11512400	-0.51469700
O	1.96490900	0.57185200	-1.14809600
C	2.81888500	-0.40084000	-0.53450800
O	0.57374500	-1.62623600	1.89255300
O	0.35988800	2.08475700	0.98036900
C	3.35924100	-1.24749100	-1.66561600

Atom	*x* / Å	*y* / Å	*z* / Å	Atom	*x* / Å	*y* / Å	*z* / Å
C	-4.14505900	-1.43574000	-1.37750800	C	3.90831300	0.29684100	0.26027200
C	-0.14686600	1.11724100	-0.25840500	C	-0.89189900	0.71211400	1.28395500
H	-0.28291700	2.16611400	-0.50643500	H	-0.95746100	0.35116200	2.30659600
C	1.20927800	0.63165900	-0.18168700	C	-1.98781500	0.14556100	0.41139000
C	1.57760800	-0.69902000	-0.44276300	C	-2.45445100	-1.14044200	0.70632300
C	2.91622600	-1.06083300	-0.41194200	C	-3.44750400	0.07984100	-1.71982800
C	3.89354500	-0.11419000	-0.10563400	C	-3.97726200	-1.16182100	-1.01941900
C	3.53980200	1.21064400	0.15081300	C	-3.51078400	-1.45632900	0.26184300
C	2.20709300	1.58508600	0.09484600	C	-2.51355600	-0.67945700	0.84405200
O	-1.12106200	1.45023200	1.80146100	O	-1.07607800	2.39272800	1.48698200
H	-1.24290800	-0.53030000	-2.09849400	H	1.90606600	1.85778100	2.29846000
H	-4.97035800	-0.19722600	1.74789300	H	2.52998700	-2.19597100	-1.7188320
H	-6.04312500	-0.34482000	0.33287400	H	3.92034100	-2.35694200	-0.61614600
H	-5.36176000	-1.80797300	1.09250500	H	4.01538400	-1.25954300	-2.0194720
H	-5.00157800	-1.91782400	-1.02896300	H	4.47707500	0.40606800	-0.9481950
H	-3.25489800	-1.34428900	-2.00317800	H	3.48475200	0.89800900	1.06724100
H	-4.32018700	-2.49085200	-1.16012800	H	4.57283500	-0.45475100	0.69076300
H	0.81606600	-1.43113500	-0.67726100	H	-2.03454200	1.54920200	-1.6826160
H	3.20067100	-0.62333800	2.08563600	H	-3.80936400	-2.71486700	0.15810700
H	4.3026740	1.94553400	0.38246400	H	-4.75434900	-1.46831400	-1.77237800
H	1.9131220	2.61261700	0.28742100	H	-3.92617800	-2.29374200	0.8131400
H	-0.57338900	0.76622300	2.21931600	H	-2.15727400	-0.90633100	1.8420660
N	5.30770900	0.06376100	-0.51329600	H	-0.73592800	0.64397800	2.73232900
O	6.12876900	0.32234200	0.19312200				
O	5.58393700	-1.65861400	-0.28815300				
(13b-TS)	*G* = -993.7834441 a. u. (Gas phase) *G* = -993.8201192 a. u. (In methanol)			**(13c-TS)**	*G* = -1083.756620 a. u. (Gas phase) *G* = -1083.804768 a. u. (In methanol)		
O	2.61487800	-1.28001000	0.67626200	O	2.70661300	-1.29641900	0.78297900
C	1.71127700	-0.49266500	1.29359000	C	1.90520400	-0.36187100	1.33240200
C	1.22513500	0.68499000	0.52911500	C	1.48082000	0.75252300	0.44603100
C	1.61447200	0.82204500	-0.89464400	C	1.80645900	0.67943300	-0.99829300
O	2.51713100	-0.06135800	-1.35749500	O	2.60682800	-0.33113900	-1.38245700
C	3.32716100	-0.86534700	-0.49184600	C	3.39007300	-1.09285200	-0.45605800
O	1.27546000	-0.79587400	2.37495900	O	1.50174900	-0.49062200	2.46017800
O	1.12207500	1.63111900	-1.64462600	O	1.34568700	1.43182000	-1.82360000
C	3.62755100	-2.13027800	-1.26510100	C	3.54311900	-2.46445200	-1.07532800
C	4.57636800	-0.09904000	-0.09492800	C	4.71791200	-0.39889300	-0.20998900
C	0.01380000	1.35972700	1.05284600	C	0.35890900	1.59191800	0.92938400
H	0.03481800	1.40206000	2.13827000	H	0.43925700	1.76428600	1.99906300
C	-1.23685900	0.68750100	0.53578700	C	-0.96867200	0.97643100	0.55243600
C	-1.80306300	-0.32398200	1.31991300	C	-1.57657900	0.12299000	1.48013500
C	-2.94308100	-0.99237600	0.88002000	C	-2.78976200	-0.48921000	1.17469200
C	-3.52098400	-0.65483300	-0.34226900	C	-3.39948300	-0.25287400	-0.05587000
C	-2.95540700	0.35245300	-1.12423200	C	-2.79244100	0.59673900	-0.98087100
C	-1.81210100	1.01951200	-0.69429600	C	-1.57661000	1.20611000	-0.68526300
O	0.04292900	3.00933400	0.63147500	O	0.50453600	3.16850800	0.30267600
H	3.02457400	2.36498900	1.36117400	H	3.45524500	2.35342300	0.98590600
H	2.69244400	-2.63183600	-1.52027900	H	2.55735400	1.22703800	-2.90756800
H	4.16584600	-1.87814100	-2.18053800	H	4.05281600	2.03636500	-2.37512600
H	4.23917700	-2.79408500	-0.65138500	H	4.12770800	-3.10055300	-0.40824000
H	5.12750100	0.17934500	-0.99521400	H	5.24336600	-0.28292300	-1.15983700
H	4.32421300	0.80639300	0.46060300	H	4.57151100	0.58647000	0.23681300
H	5.20151100	-0.73655700	0.53322100	H	5.31890100	-1.00845700	0.46754200
H	-1.34536600	-0.58481400	2.27028200	H	-1.09404700	2.43639300	-0.05991800

Atom	*x* / Å	*y* / Å	*z* / Å
H	-3.38077400	-1.77140500	1.49581500
H	-3.40697200	2.07325500	0.62298400
H	-1.37822000	-1.30053000	1.80606700
H	0.31242400	2.97090300	-0.29996600
O	-4.69486800	0.79231000	-1.33627100
C	-5.85649300	-0.32425300	-0.64601600
H	-5.85523500	-0.70572000	0.35367400
H	-6.73455100	0.66220900	-1.15562300
H	-5.84887800	-0.61961600	0.74539400
(14a-TS1) *G* = -879.3471230 a. u. (Gas phase) *G* = -879.3837326 a. u. (In methanol)			
O	2.66940800	0.87745300	-0.62247300
C	1.40416800	1.28847600	-0.73474900
C	0.32251300	0.23740900	-0.68614000
C	0.71093900	-1.02371500	0.04582500
O	2.02154000	-1.31494000	0.03624500
C	3.06491300	-0.34383500	0.01105700
O	1.15445800	2.43502400	-0.99100700
O	-0.08035800	-1.85394500	0.40373700
C	3.51001100	-0.04005600	1.42752000
C	4.15822300	-0.92964900	-0.85985300
C	-2.22659400	0.33684700	-0.10756700
C	-2.57121300	-0.92218000	-0.65160200
C	-3.88906900	-1.34417100	-0.62898400
C	-4.87481300	-0.53611300	-0.05785500
C	-4.55359400	0.71054400	0.48479600
C	3.24293400	1.14851900	0.45164000
C	-0.91740900	0.87829700	-0.14656300
H	0.15294500	-0.06971500	-1.73484300
H	2.65591400	0.34970100	1.98959100
H	3.87165300	-0.96241300	1.88788700
H	4.32191600	0.68969800	1.39607800
H	4.50394900	-1.86901100	-0.42550200
H	3.77239100	-1.11620400	-1.86404200
H	4.99173200	-0.22777100	-0.91763400
H	-1.79885000	-1.55443300	-1.06904300
H	-4.15489600	-2.30738800	-1.04951600
H	-5.90430700	-0.87984100	-0.03873000
H	-5.32700700	1.33090900	0.92317100
H	-2.97200700	2.11534600	0.86486200
H	0.10087100	1.92774300	0.79763600
O	0.63364600	0.5965200	1.95774000
H	0.12380500	0.11033600	2.37775700
(14b-TS1) *G* = -993.8198403 a. u. (Gas phase) *G* = -993.8612962 a. u. (In methanol)			
O	3.40159200	0.83249300	-0.67844700
C	2.14627600	1.28246600	-0.74235900
C	1.03546500	0.26438100	-0.66060400
C	1.41133700	-1.01295100	0.04948400
O	2.71122600	-1.34372100	-0.00933200
C	3.78219900	-0.40456000	-0.06675400
O	1.92263500	2.43779600	-0.98275800
O	0.60847200	-1.82124100	0.43107200
C	4.28721100	-0.12417400	1.33435600

Atom	*x* / Å	*y* / Å	*z* / Å
H	-3.25895500	1.90102600	-1.14492400
H	-3.26798700	1.93726500	0.78884900
H	-1.11008700	1.40291300	1.87077200
H	0.72154600	0.62668000	2.99274800
N	-4.68290700	0.37709100	-0.89360600
O	-5.17862600	0.43967600	-1.61857000
O	-5.18303400	1.44310600	-0.66580200
(14a-TS2) *G* = -879.3093445 a. u. (Gas phase) *G* = -879.3407527 a. u. (In methanol)			
O	-2.15291900	-0.21440300	-1.20539900
C	-1.72514600	1.04788600	-0.94859500
C	-0.56019700	0.94768300	0.03609900
C	-0.86130400	0.11860900	1.26253500
O	-1.68054600	-0.90998600	1.07288900
C	-2.38349300	-1.20344000	-0.18526900
O	-2.06975300	2.01369600	-1.54700500
O	-0.43511400	0.46836400	2.32865000
C	-1.87216100	-2.52917800	-0.68029800
C	-3.84836200	-1.12312100	0.19159500
C	1.87190700	0.13741600	-0.38920100
C	1.95713500	-0.88297000	0.61151600
C	3.14966400	-1.54021600	0.80870800
C	4.27459600	-1.20356700	0.03528600
C	4.21699400	-0.21797000	-0.95929500
C	3.02769900	0.44126800	-1.17786100
H	-0.22326100	2.14083000	0.88041700
H	-0.79184100	0.84045700	-2.48274200
H	-2.09887500	-3.30173500	0.05583000
H	-2.36354800	1.62399600	-2.76942700
H	-4.00336800	-1.45490900	1.21504300
H	-4.00896100	-0.06584200	0.01716000
H	-4.47308300	0.50578600	-1.68210900
H	1.09293500	-1.14415600	1.21149400
H	3.22320100	-2.31671300	1.56133700
H	5.21062200	-1.72584200	0.20969700
H	5.09485700	0.01928600	-1.54904900
H	2.95524800	1.20061300	-1.95160000
C	0.71861200	0.85896500	-0.67345500
H	0.76687400	1.54922700	-1.52015500
O	0.24157000	3.55596200	1.21621000
H	0.59762400	3.61626100	0.32672100
(14b-TS2) *G* = -993.7698883 a. u. (Gas phase) *G* = -993.8092053 a. u. (In methanol)			
O	-2.83441800	-0.36470500	-1.16249400
C	-2.54108000	0.93293400	-0.89342600
C	-1.33874800	0.94684800	0.05048700
C	-1.50300300	0.06838900	1.26847900
O	-2.20881100	-1.04201200	1.08415700
C	-2.91798500	-1.39067000	-0.15629500
O	-3.01155500	1.86423300	-1.45997000
O	-1.08162900	0.44531100	2.32722400
C	-2.27982600	-2.64218700	-0.69532700

Atom	*x* / Å	*y* / Å	*z* / Å	Atom	*x* / Å	*y* / Å	*z* / Å
C	4.82494700	-1.01725900	-0.98013500	C	-4.36872900	-1.48123800	0.26968300
C	-1.48686600	0.43710700	0.01065600	C	1.15216800	0.42121800	-0.47066000
C	-1.88921300	-0.80711500	-0.52778100	C	1.38506500	-0.60022600	0.50519700
C	-3.21767400	-1.18908500	-0.45979300	C	2.64943200	-1.1219000	0.64965400
C	-4.15700500	-0.35544900	0.15139000	C	3.70240400	-0.6957400	-0.15279400
C	-3.77846000	0.87712800	0.68922100	C	3.50102800	0.4029000	-1.12414800
C	-2.45707900	1.27536600	0.61105600	C	2.23891000	0.86596100	-1.29002600
C	-0.16400700	0.93885400	-0.07269400	H	-1.10754600	0.90814100	2.15555500
H	0.81884800	-0.03023600	-1.70422000	H	-1.21759200	-0.8895800	-2.4724220
H	3.46626900	0.28743300	1.92929300	H	-2.39349900	0.03148300	-3.44776400
H	4.63687800	-1.06022100	1.77595900	H	-2.77388700	-1.6273340	-2.91970000
H	5.11937400	0.58081700	1.27768800	H	-4.45024800	-1.8457800	1.29047700
H	5.15725700	-1.96964200	-0.56405100	H	-4.65191200	-0.4457350	0.12271500
H	4.39759900	-1.18511200	-1.97072300	H	-4.95120700	-2.0945820	-0.41851100
H	5.67688700	-0.34060500	-1.06406900	H	0.57663300	-0.96671600	1.12741600
H	-1.15210400	0.97662100	-1.45961600	H	2.83497500	-1.89936800	1.38309000
H	-3.52782000	0.87596100	-2.14088000	H	4.32604700	0.68435800	-1.73709600
H	-4.51622600	1.51763500	1.15895100	H	2.05562100	-2.04495000	-1.48123800
H	-2.14199300	2.23066400	1.01975400	C	-0.08340700	1.01395400	-0.70204700
H	-0.00336500	1.98245700	0.17629000	H	-0.14165200	1.71969200	-1.53525400
O	1.45266000	0.59576100	1.97227500	O	-0.79166500	3.60784700	1.25812700
H	0.93694600	-0.09825100	2.40642500	H	-0.47561500	3.72284500	0.35896700
O	-5.52460000	-0.76707200	0.22316400	O	5.01104000	-1.19890200	0.02216800
C	-6.31918500	0.06680400	-0.62429400	C	5.93730600	-0.14590000	0.30166200
H	-7.28608900	-0.75246600	-0.37316000	H	6.83705900	-0.56035100	0.70610700
H	-6.42353700	1.03332800	-0.17725800	H	6.16204000	0.60226600	0.38070100
H	-5.84247700	0.16419200	-1.57727200	H	5.50589900	0.52986000	1.01027800
(14c-TS1)	*G* = -1083.746565 a. u. (Gas phase) *G* = -1083.802252 a. u. (In methanol)			**(14c-TS2)**	*G* = -1083.719218 a. u. (Gas phase) *G* = -1083.773376 a. u. (In methanol)		
O	3.69667600	0.69014100	-0.67321000	O	-2.98398100	-0.44627500	-1.20996300
C	2.46969800	1.19513800	-0.82113200	C	-2.82031600	0.85475800	-0.85947800
C	1.30481700	0.24320800	-0.70297100	C	-1.63353600	0.92681000	0.10131900
C	1.58813700	-0.98989400	0.11938600	C	-1.72275800	-0.03596200	1.26204500
O	2.87013600	-1.38830400	0.13742400	O	-2.31585300	-1.19584900	1.00121500
C	3.99026900	-0.51101300	0.04815100	C	-2.97668700	-1.53491900	-0.26825000
O	2.31551700	2.33703500	-1.16009200	O	-3.37378900	1.76922400	-1.37625400
O	0.73113800	-1.72409600	0.53173800	O	-1.34946300	0.31455300	2.34756600
C	4.46010700	-0.14416400	1.44150400	C	-2.21533000	-2.68400300	-0.87160500
C	5.03065800	-1.24611400	-0.77295000	C	-4.41557700	-1.79051700	0.12997400
C	-1.22685700	0.59411100	-0.14612600	C	0.90120100	0.67615900	-0.41329200
C	-1.67491200	-0.66793700	-0.60040100	C	1.22328900	-0.37567800	0.50310500
C	-3.02314900	-0.97692500	-0.55441300	C	2.53106700	-0.78232000	0.63478900
C	-3.93819000	-0.05131500	-0.04767700	C	3.54030900	-0.12219500	-0.16152000
C	-3.51448000	1.20027200	0.40598200	C	3.25261500	0.86170300	-1.03551600
C	-2.17210000	1.52498600	0.34830300	C	1.94700500	1.27255600	-1.18838600
C	0.12261100	1.02138200	-0.21704600	H	-1.52837800	2.09764100	1.03303600
H	1.10958000	-0.12333000	-1.72785500	H	-1.17286700	-2.40124600	-1.03958100
H	3.64164000	0.35413400	1.96982900	H	-2.25686300	-3.53956700	-0.19602100
H	4.74455100	-1.05781200	1.96857400	H	-2.67174800	-2.95047800	-1.82576500
H	5.32958900	0.51189400	1.36208000	H	-4.47052800	-2.22273700	1.12582700
H	5.29781300	-2.17721800	-0.27069300	H	-4.79652700	-0.78006300	0.04098700
H	4.62991100	-1.47175000	-1.76318000	H	-4.92961000	-2.41400500	-0.60222500
H	5.91934200	-0.62143900	-0.87653900	H	0.44865400	-0.85552500	1.09023500
H	-0.95785000	-1.39014500	-0.96752900	H	2.78441600	-1.58027500	1.32318400

Atom	*x* / Å	*y* / Å	*z* / Å	Atom	*x* / Å	*y* / Å	*z* / Å
H	-3.36810600	-1.94258400	-0.90627400	H	4.04584900	-1.61448700	1.32030600
H	-4.23355600	1.91225200	0.79483600	H	1.69769800	-1.89918500	2.05558700
H	-1.82176800	2.49328700	0.69264100	C	-0.38390900	0.62714300	1.16018700
H	0.32901200	2.07239200	-0.04476100	H	-0.50283700	-1.41744100	1.90649600
O	1.64671300	0.76428300	1.90997900	O	-1.35800500	3.54955900	1.47386600
H	1.08045800	0.13385300	2.37689600	H	-1.04652800	3.74902600	0.58797800
N	-5.36602400	-0.39698500	0.00430300	N	4.93230600	-0.60399100	0.04352700
O	-6.13390300	0.41496900	0.43963200	O	5.16240700	-1.48064800	0.82898600
O	-5.70604100	-1.47715800	-0.39069700	O	5.78229600	0.61334600	-0.07065900
(14a-Int)	*G* = -879.3931200 a. u. (Gas phase) *G* = -879.4303725 a. u. (In methanol)			**(14b-Int)**	*G* = -993.8458079 a. u. (Gas phase) *G* = -993.8865184 a. u. (In methanol)		
O	-2.69833100	1.11303500	0.15859700	O	-3.46209200	1.01452700	0.21995200
C	-1.44997500	1.48582700	0.43341600	C	-2.22828900	1.45364100	0.46037200
C	-0.38206100	0.43434500	0.25728000	C	-1.11024400	0.46346000	0.24451600
C	-0.71613300	-0.55875800	-0.82864100	C	-1.42203800	-0.53994200	-0.83855900
O	-2.01524600	-0.71296300	-1.05575200	O	-2.71701900	-0.76387700	-1.02811200
C	-3.01659600	-0.23764700	-0.20366200	C	-3.71675800	-0.34939000	-0.14300900
O	-1.17927700	2.58984100	0.81149000	O	-2.00712700	2.56856100	0.83866800
O	0.12270400	-1.16568000	-1.42742800	O	-0.56966900	-1.09628000	-1.46665300
C	-4.26898600	-0.16361200	-1.04225300	C	-4.99600600	-0.33919200	-0.94339500
C	-3.12209400	-1.11483500	1.03081800	C	-3.73689300	-1.23845300	1.08731300
C	2.17183700	0.49458100	0.02300000	C	1.42832000	0.66523900	-0.06513800
C	2.37325300	-0.88351700	0.29990800	C	1.71306700	-0.70136000	0.19510300
C	3.63936500	-1.41350600	0.23284100	C	3.00368000	-1.16061800	0.08636100
C	4.72257800	-0.10383100	-0.58056200	C	4.02907800	-0.26744600	-0.27598900
C	4.55959000	0.37068700	0.78909800	C	3.78344800	-0.52739000	1.09277800
C	3.29914000	-0.30569500	1.33493700	C	2.49755600	-0.42077000	1.56818600
H	-0.34433800	1.18837200	-0.17479800	H	-1.01123600	1.16938500	-0.14827900
H	-4.09596400	-1.91666800	0.46689600	H	-4.88414200	-1.81771800	0.30511000
H	-4.55337200	-1.37782600	-1.16294500	H	-5.23527500	-1.27800100	-1.35059700
H	-5.08672000	-0.45693900	0.25716500	H	-5.81753700	-0.33082000	0.03252400
H	-3.38637000	0.74196600	-2.13442500	H	-3.95357700	0.79865300	-2.26926100
H	-2.16657400	1.56036200	-1.13155600	H	-2.76637800	1.58806500	-1.20586700
H	-3.89027900	1.70051300	-0.72517100	H	-4.50472900	1.78251800	-0.89558900
H	1.53075000	-1.51678500	0.55402500	H	0.91450100	0.46930700	-1.38144800
H	3.80109500	0.42931700	-2.46718100	H	3.22865000	0.26987100	-2.20498600
H	5.71738500	-0.16687100	-1.01343600	H	4.59371100	-0.80887900	1.75480700
H	5.41299200	-0.63162400	1.40363800	H	2.28889100	-0.59320700	2.62003100
H	3.15376400	-0.49065800	2.39527100	C	0.15697500	-0.01959700	1.19371100
C	0.93063500	0.02706000	1.09214000	H	0.06919600	-0.2070810	2.27405500
H	0.90792100	-0.16947300	2.17420200	O	-0.96911500	-1.57634600	1.64658500
O	-0.39490100	1.67520000	-1.59933700	H	-0.68191200	-2.19830100	1.00001600
H	-0.12318100	-2.24100100	1.04132300	O	5.36421800	-0.76380700	-0.40218900
				C	6.18046100	-0.20615200	0.63109200
				H	7.09723700	-0.75404300	0.69618100
				H	6.39228400	0.81794000	0.40467100
				H	5.66261600	-0.26508700	1.56557800
(14c-Int)	*G* = -1083.789539 a. u. (Gas phase) *G* = -1083.845576 a. u. (In methanol)			**(15a)**	*G* = -918.5995480 a. u. (Gas phase) *G* = -918.6267384 a. u. (In methanol)		
O	-3.73723100	0.93165400	0.13743700	O	-2.80628400	-1.18477300	-0.20227400
C	-2.53737500	1.42541300	0.43650100	C	-1.59458600	-1.70550400	-0.49851100
C	-1.36631200	0.48834200	0.27040400	C	-0.42577600	-0.77187200	-0.41239200
C	-1.58103300	-0.52290400	-0.82885000	C	-0.66816400	0.73404200	-0.62915700
O	-2.85416200	-0.80475100	-1.07936400	O	-2.08906700	1.02707400	-0.35314100

Atom	*x* / Å	*y* / Å	*z* / Å	Atom	*x* / Å	*y* / Å	*z* / Å
C	-3.91197800	-0.44066100	-0.24082400	C	-2.86221400	0.12503000	0.38182300
O	-2.38537100	2.54738800	0.82782000	O	-1.50468300	-2.86962600	-0.79452700
O	-0.67574700	-1.03668200	-1.41794800	O	-0.28074600	1.24787900	-1.70530600
C	-5.15167800	-0.48490200	-1.10011500	C	-2.44885200	0.02227600	1.85710900
C	-3.94865700	-1.33575300	0.98473600	C	-4.30349500	0.57280100	0.24200500
C	1.17201200	0.80724500	0.08034200	C	0.77106900	1.35096100	-0.20321800
C	1.50662100	-0.54620300	0.34981300	H	0.74095100	2.43532400	-0.09529000
C	2.82057800	-0.94556300	0.30025700	C	2.1091550	-0.75170700	-0.06229500
C	3.81975400	-0.01127000	-0.00477000	C	3.01908200	-1.38932000	0.79556300
C	3.52405900	-0.27009900	1.34405100	C	4.30121000	0.98115000	-0.88153500
C	2.21417300	-0.22239600	1.75976900	C	4.70377200	0.28448900	0.25728700
H	-1.28257600	1.19718700	-0.12278100	C	3.81911900	-0.59852100	0.87718600
H	-5.02883800	-1.96645700	0.16812300	C	2.52884700	-0.77435600	0.38351300
H	-5.32852700	-1.44835200	-1.50451300	O	-0.02100600	0.46371600	1.36691700
H	-6.01701300	-0.52559000	-0.15406700	C	0.12000900	0.37217300	2.82537200
H	-4.10422000	0.68339600	-2.37394100	H	-1.46681000	1.98135100	-0.45159100
H	-3.00503200	1.53040600	-0.52290400	H	-2.45477800	2.31194800	1.01944400
H	-4.76293900	1.64423000	-1.03169600	H	-3.16243300	2.39930400	-0.60190100
H	0.72813800	0.58448900	-1.26335500	H	-4.42930700	0.69892500	1.55706700
H	3.08435200	0.49118200	-1.97946900	H	-4.54676800	-0.81949300	0.63605700
H	4.31538100	-0.51155400	2.04373100	H	-4.96825300	0.72713600	-0.14503800
H	1.96581000	-0.40147800	2.80183400	H	2.71133500	1.32237400	-2.28912700
C	-0.12294400	0.0678600	1.27693500	H	4.98885200	1.65629000	-1.38097300
H	-0.25128400	2.35305800	-0.12052000	H	5.70801300	0.41514900	0.64842800
O	-1.19736600	-1.54976800	1.67186300	H	4.14068000	-1.16655000	1.74501300
H	-0.85217200	-2.15478700	1.03770300	H	1.84132400	-1.47691600	0.84629400
N	5.21872200	-0.07810300	-0.45122500				
O	5.46053600	0.14452400	-1.60464700				
O	6.06240700	-0.35259000	0.35578300				
(15b)	*G* = -1033.048469 a. u. (Gas phase)			**(15c)**	*G* = -1123.009546 a. u. (Gas phase)		
	G = -1033.082918 a. u. (In methanol)				*G* = -1123.057317 a. u. (In methanol)		
O	3.39856300	1.46310300	-0.04220600	H	-0.37523400	1.32954600	1.09130400
C	2.14506400	1.97186700	0.07977300	H	0.66859600	1.26324100	3.12244800
C	1.03591300	1.01004400	-0.18330400	H	0.67985900	-0.54059300	2.99874600
C	1.37332200	-0.23876700	-0.91067300	H	-0.87679200	3.25973200	0.31066300
O	2.67924000	-0.60956300	-0.86087500	O	3.77677500	1.01149500	-0.14578000
C	3.55970000	0.05114200	0.04206400	C	2.62733700	1.62414700	-0.49689600
O	1.99970900	3.13454300	0.34935100	C	1.37812400	0.79222900	-0.43394500
O	0.61834900	-0.87064400	-1.60150600	C	1.50084100	-0.73465400	-0.60829200
C	3.32965700	-0.41562300	1.47244600	O	2.88054100	-1.13543700	-0.28670200
C	4.95832100	-0.24152500	-0.45522000	C	3.70305500	-0.28788100	0.46161900
C	-0.21059100	1.44088000	0.12551900	O	2.64033500	2.78249600	-0.82377900
H	-0.22468600	2.46651400	0.49608200	O	1.10057700	-1.22950500	-1.68906900
C	-1.51718800	0.80701600	0.07388600	C	3.24929800	-0.12143400	1.91855100
C	-2.63282200	1.65472900	0.10184500	C	5.10465700	-0.85738400	0.37859900
C	-3.93150200	1.16310200	0.06193300	C	0.22944200	1.47664500	-0.29729700
C	-4.12859400	-0.21990700	0.03329800	H	0.34097200	2.55813000	-0.22099000
C	-3.02363600	-1.08517300	0.05153200	C	-1.15688500	0.98372400	-0.20400200
C	-1.73830200	-0.58591500	0.06453600	C	-2.04394600	1.69092500	0.62406300
O	0.95487200	-2.33556700	0.92358500	C	-3.36536700	1.28851900	0.76775300
C	1.54196600	-3.33533700	0.10501200	C	-3.79318000	0.18091400	0.04640800
H	2.30589200	-0.20829300	1.79163900	C	-2.95671100	-0.51932400	-0.81453600
H	3.49758400	-1.49322100	1.53564600	C	-1.63198400	-0.11548900	-0.93849100
H	4.02912500	0.10248900	2.13278400	O	0.77059700	-1.29152000	0.47353800

Atom	*x* / Å	*y* / Å	*z* / Å	Atom	*x* / Å	*y* / Å	*z* / Å
H	5.13300200	-1.31965100	-0.44184700	C	0.50368800	-2.73636200	0.38522300
H	5.06091900	0.12828300	-1.47703600	H	2.30479100	0.43182900	2.00050700
H	5.68929200	0.25576500	0.18559300	H	3.16104000	-1.10558600	2.39282900
H	-2.47848600	2.72998100	0.14241300	H	3.99169700	0.45559400	2.47393600
H	-4.76699600	1.85229600	0.06630000	H	5.13153700	-1.84026200	0.85438500
H	-3.21235000	-2.15327800	0.05347500	H	5.37741900	-0.95977300	-0.67259000
H	-0.89790400	-1.26902200	0.09575400	H	5.81074400	-0.18919400	0.87588500
H	1.00623800	-2.62427600	1.84457700	H	1.68902500	2.56316400	1.16534500
H	1.04929900	-4.30628800	0.23688500	H	-4.05923400	1.81435900	1.41207600
H	1.41359600	-3.00201800	-0.92459600	H	-3.34906700	-1.35702000	-1.37880900
H	2.61603800	-3.44774600	0.30588200	H	-0.95382200	-0.62980900	-1.61357100
O	-5.34053800	-0.81695600	0.00443900	H	1.14198000	-1.05261100	1.34361300
C	-6.48346600	0.01270400	-0.02013100	H	-0.05420100	-2.98420600	1.28548100
H	-7.34153500	-0.65766100	-0.05535500	H	-0.08206700	-2.86455500	-0.51832400
H	-6.54186500	0.63409300	0.88111200	H	1.45975300	-3.25211800	0.31077100
H	-6.48577400	0.65728000	-0.90669900	N	-5.19240800	-0.25895600	0.19138800
				O	-5.91129300	0.38474800	0.93511700
(16a)	*G* = -918.6116490 a. u. (Gas phase) *G* = -918.6401859 a. u. (In methanol)			**(16b)**	*G* = -1033.060570 a. u. (Gas phase) *G* = -1033.093537 a. u. (In methanol)		
O	-2.4878550	0.12888600	-0.92568100	O	-5.54201700	-1.24261600	-0.43617600
C	-1.3153520	0.79170900	-1.02428100	O	-3.3660070	0.15566300	-0.97732200
C	-0.1645580	0.18593800	-0.28965000	C	-2.1519600	0.70371300	-1.20850700
C	-0.5245640	-0.67208100	0.87029600	C	-1.0218450	0.14592500	-0.40578100
O	-1.7181890	-1.29299100	0.78814400	C	-1.3930740	-0.48539800	0.88048500
C	-2.4968390	-1.19889700	-0.40409900	O	-2.6474640	-0.98357900	0.94966400
O	-1.2598490	1.81359200	-1.66005400	C	-3.4457700	-1.05023100	-0.23173300
O	0.13738500	-0.79826600	1.86989800	O	-2.0403080	1.59213200	-2.01181900
C	-1.9748390	-2.17584100	-1.44791500	O	-0.7056690	-0.51757900	1.87239700
C	-3.9243910	-1.46790800	0.01513900	C	-3.0104780	-2.23200900	-1.08701400
C	1.06708500	0.56334300	-0.69401900	C	-4.8778280	-1.14923400	0.24467700
H	1.03333300	1.28809500	-1.50790300	C	0.22124000	0.43017800	-0.86011200
C	2.42984500	0.19531600	-0.30366200	H	0.19326400	1.02912400	-1.77095400
C	3.45831700	0.97109200	-0.86760800	C	1.57432800	0.10549800	-0.43415000
C	4.79472600	0.70736400	-0.59012000	C	2.60833600	0.70237900	-1.17198400
C	5.12824500	-0.35915700	0.24208400	C	3.94888600	0.47289500	-0.89224700
C	4.11950200	-1.15171400	0.79183900	C	4.28253700	-0.39770100	0.14827400
C	2.78180100	-0.87957600	0.53031300	C	3.26573200	-1.01973400	0.88893300
O	-2.0510950	1.52653000	1.56982700	C	1.93820300	-0.77198700	0.60983400
H	-1.4711990	1.68764700	2.32247000	O	-2.4957530	1.89902200	1.43368400
C	-2.5918490	2.75473000	1.10394000	H	-2.4445660	1.40815800	2.26675800
H	-0.9409430	-1.94537300	-1.71972500	C	-1.3652100	2.75048700	1.36031100
H	-2.0142610	-3.19034700	-1.04559200	H	-1.9698130	-2.12126700	-1.40479400
H	-2.5957460	-2.11607000	-2.34430700	H	-3.1062410	-3.15560600	-0.51156900
H	-3.9977420	-2.46886500	0.44463600	H	-3.6438320	-2.29149800	-1.97495900
H	-4.2136410	-0.72802900	0.76384700	H	-5.0035910	-2.04575800	0.85532800
H	-4.5823840	-1.39120000	-0.85265800	H	-5.1109320	-0.26393400	0.83955300
H	3.19792300	1.79283200	-1.52940500	H	-5.5488530	-1.19417700	-0.61554500
H	5.57149200	1.32568400	-1.02790900	H	2.35246700	1.37007400	-1.99048700
H	6.16955500	-0.57593100	0.45914600	H	4.71188300	0.96273800	-1.48468800
H	4.37630800	-1.98630500	1.43614400	H	3.55538200	-1.69332000	1.68816300
H	2.01431500	-1.49165600	0.98332100	H	1.17399500	-1.24879600	1.20711200
H	-3.2034760	3.24027000	1.87270000	H	-1.4364700	2.07171500	3.58261500
H	-3.2227460	2.51070400	0.24746900	H	-1.3445270	0.34540400	3.15425400
H	-1.8067440	3.44062200	0.76715300	H	-0.4322680	1.54021400	2.20034500

Atom	*x* / Å	*y* / Å	*z* / Å	Atom	*x* / Å	*y* / Å	*z* / Å
				O	5.54566400	-0.70487700	0.51197400
				C	6.60397700	0.20194500	-0.09871500
				H	7.52299500	0.24801500	-0.47226800
				H	6.57629900	-1.26195200	-0.37625100
				H	6.56864100	-0.11019200	0.99291700
(16c)	*G* = -1123.021641 a. u. (Gas phase) *G* = -1123.066911 a. u. (In methanol)			**(17a)**	*G* = -918.6749400 a. u. (Gas phase) *G* = -918.7031981 a. u. (In methanol)		
O	-3.4034050	0.01791400	-0.99758400	C	-2.89666500	0.03701200	0.33707100
C	-2.5360370	1.05565600	-0.48159800	O	-1.32461400	-2.94580100	-0.57631700
C	-1.2294300	0.40004800	0.06330600	O	-0.29188700	1.26978900	-1.67510500
C	-1.4603350	-0.73213100	0.99046300	C	-2.52415900	0.13277900	1.81240000
O	-2.6722520	-1.33495500	0.78057200	C	-4.34585300	0.39152300	0.08123900
C	-3.2048190	-1.30672500	-0.57533000	C	0.85897700	-1.27065300	-0.17266300
O	-2.4302160	2.08102500	-1.16517200	H	0.87042000	0.07417100	-2.35586200
O	-0.8053880	-1.06243600	1.94490800	C	2.18660200	0.05883300	-0.65386900
C	-2.2718760	-2.06290100	-1.51148600	C	3.17614600	0.57266900	-1.42542100
C	-4.5676120	-1.96139600	-0.47240800	C	4.46807500	-0.9393680	0.74368700
C	-0.0757810	0.92269700	-0.37951200	C	4.80123200	0.32266200	0.25649800
H	-0.2528050	1.74778600	-1.07275700	C	3.83665800	-0.40124000	1.08690300
C	1.33621800	0.55846700	-0.19815900	C	2.53951300	-0.55762400	0.61052400
C	2.22152800	1.01433300	-1.19091300	O	-0.13104600	1.38769300	0.57085200
C	3.57567300	0.72217900	-1.13919000	C	-0.26671300	2.80521300	0.53400900
C	4.04146600	-0.01999700	-0.06257100	H	-1.49720800	-0.18803300	1.99562200
C	3.20619400	-0.46920200	0.95048900	H	-2.62422500	1.16868800	2.14610600
C	1.85003000	-0.17753500	0.88168000	H	-3.20456000	-0.49978800	2.38666700
O	-3.3217100	1.36418000	0.74394900	H	-4.53658200	1.41459700	0.41212200
H	-3.5475410	0.56134900	1.26134300	H	-4.55541500	0.30963800	-0.98670900
C	-2.8420680	2.46932000	1.55327800	H	-4.99334900	-0.29559500	0.62900800
H	-1.2988290	-1.57232600	-1.58487000	H	2.91981300	2.41567300	0.93991200
H	-2.1346930	-3.08856700	-1.15997800	H	5.21346300	-1.54757400	1.24583100
H	-2.7188630	-2.07909000	-2.50795400	H	5.81012000	0.70480700	0.37728600
H	-4.4706490	-2.99608000	-0.13643300	H	4.09865600	0.80090800	2.06159600
H	-5.1891560	-1.40714500	0.23549600	H	1.80738800	-1.08836000	1.20444700
H	-5.0496470	-1.93750800	-1.45182100	H	0.06407500	1.51062100	3.15792600
H	1.83222400	1.59911400	-2.01894100	H	0.36164200	-0.25065800	3.23459900
H	4.26694400	1.05866500	-1.90170700	H	-1.30924200	3.09181900	0.36623200
H	3.62296800	-1.03270400	1.77612800	H	-0.91527700	1.01759900	-2.36802000
H	1.18826400	-0.50782800	1.67086500				
H	-3.6671460	2.78598400	2.18771200				
H	-2.5775290	3.22951100	0.82161000				
H	-1.9745700	2.15150300	2.13468200				
N	5.47860700	-0.33113700	0.01207000				
O	6.18814700	0.07534400	-0.88937300				
O	5.86506200	-0.97502100	0.96943000				
(17b	*G* = -1033.123861 a. u. (Gas phase) *G* = -1033.154788 a. u. (In methanol)			**(17c)**	*G* = -1123.08494 a. u. (Gas phase) *G* = -1123.13303 a. u. (In methanol)		
O	3.45073200	1.29287000	-0.03238500	O	3.73770300	1.11700000	-0.05980600
C	2.20650000	1.77248300	-0.26997100	C	2.55851300	1.68861100	-0.38718800
C	1.09187500	0.77642200	-0.31810700	C	1.35206300	0.79455000	-0.38883000
C	1.42836100	-0.69650900	-0.47150300	C	1.56069800	-0.71132200	-0.47022600
O	2.82727300	-0.89010200	-0.48873900	O	2.93370800	-1.02784900	-0.40045300
C	3.58966200	-0.07247000	0.37076800	C	3.73150500	-0.22512500	0.44290700
O	2.05923000	2.95709200	-0.43160500	O	2.51860000	2.86080000	-0.65312600
O	0.98367300	-1.23885400	-1.67873100	O	1.14041500	-1.24999800	-1.68808400

Atom	*x* / Å	*y* / Å	*z* / Å	Atom	*x* / Å	*y* / Å	*z* / Å
C	3.20507700	-0.21466900	1.83926500	C	3.26694600	-0.23045800	1.89412700
C	5.03779300	-0.43340300	0.11428200	C	5.14940800	-0.73044900	0.28421900
C	-0.1478100	1.29613800	-0.20347000	C	0.16930100	1.42397500	-0.28901200
H	-0.1435360	2.37965400	-0.08686900	H	0.24957300	2.50839600	-0.22132900
C	-1.4877400	0.71519900	-0.17131600	C	-1.2081500	0.91539800	-0.20561300
C	-2.5121470	1.54766300	0.29821000	C	-2.1381960	1.73713900	0.45030300
C	-3.8313510	1.12012500	0.39735100	C	-3.4632450	1.35259800	0.59650600
C	-4.1535820	-0.17677300	-0.00564800	C	-3.8529130	0.13931000	0.04883400
C	-3.1495980	-1.01803300	-0.50620000	C	-2.9720440	-0.68702800	-0.63689000
C	-1.8415530	-0.58488400	-0.58595900	C	-1.6465300	-0.29685000	-0.76122300
O	0.81965700	-1.38765800	0.55800400	O	0.83170100	-1.29250900	0.54468400
C	0.95991000	-2.80161000	0.49463300	C	0.82083200	-2.71630600	0.53709900
H	2.18114700	0.11652600	2.02208300	O	3.73770300	1.11700000	-0.05980600
H	3.28673700	-1.26246300	2.14030000	C	2.55851300	1.68861100	-0.38718800
H	3.88857700	0.38798600	2.44214000	C	1.35206300	0.79455000	-0.38883000
H	5.21691100	-1.46963300	0.40980300	C	1.56069800	-0.71132200	-0.47022600
H	5.25426800	-0.31739200	-0.94940200	O	2.93370800	-1.02784900	-0.40045300
H	5.69000900	0.22743100	0.68872200	C	3.73150500	-0.22512500	0.44290700
H	-2.2668580	2.56104500	0.60526200	O	2.51860000	2.86080000	-0.65312600
H	-4.5869270	1.79768400	0.77598600	O	1.14041500	-1.24999800	-1.68808400
H	-3.4337350	-2.01270200	-0.83294100	C	3.26694600	-0.23045800	1.89412700
H	-1.0905020	-1.24284500	-1.00097600	C	5.14940800	-0.73044900	0.28421900
H	0.66119700	-3.17395900	1.47488200	C	0.16930100	1.42397500	-0.28901200
H	0.31113000	-3.22502200	-0.27699200	H	0.24957300	2.50839600	-0.22132900
H	1.99765200	-3.08065200	0.29003700	C	-1.2081500	0.91539800	-0.20561300
H	1.54646300	-0.88084400	-2.38141500	C	-2.1381960	1.73713900	0.45030300
O	-5.3985370	-0.70565200	0.03628800	C	-3.4632450	1.35259800	0.59650600
C	-6.4415940	0.11156000	0.52364600	C	-3.8529130	0.13931000	0.04883400
H	-7.3462840	-0.49382700	0.47705100	C	-2.9720440	-0.68702800	-0.63689000
H	-6.2570950	0.41391000	1.56120500	C	-1.6465300	-0.29685000	-0.76122300
H	-6.5681910	-0.09740600	1.00612100	O	0.83170100	-1.29250900	0.54468400
				C	0.82083200	-2.71630600	0.53709900
(18a)	*G* = -918.6689090 a. u. (Gas phase) *G* = -918.6979001 a. u. (In methanol)			**(18b)**	*G* = -1033.117830 a. u. (Gas phase) *G* = -1033.149873 a. u. (In methanol)		
O	1.45490500	1.91889800	0.09204100	O	-2.26460300	-1.89860200	0.12179900
C	0.33118400	1.42744000	-0.47430100	C	-1.13525000	-1.45638500	-0.47619900
C	0.21397200	-0.06041200	-0.46498600	C	-0.95433200	0.02167600	-0.48254400
C	1.52968300	-0.82008200	-0.63507800	C	-2.24048900	0.84169200	-0.58735800
O	2.63638700	-0.02214900	-0.33622800	O	-3.37234400	0.09452100	-0.25761800
C	2.43775800	1.00453100	0.60832300	C	-3.18271600	-0.94372400	0.67268100
O	-0.4828410	2.19365400	-0.92281600	O	-0.37211800	-2.26558300	-0.93796700
O	1.74531100	-1.16100100	-1.97334500	O	-2.49254900	1.21898700	-1.90747400
C	2.01359300	0.49159900	1.98018200	C	-2.68537400	-0.45631400	2.02923900
C	3.73361000	1.78515300	0.65767200	C	-4.51035500	-1.66526300	0.76939200
C	-0.9199090	-0.75887900	-0.27048000	C	0.21568200	0.68404500	-0.37620900
O	1.48713800	-1.95645300	0.17422300	O	-2.11110300	1.95866800	0.24100000
C	2.67722500	-2.73927500	0.15570300	C	-3.25338600	2.80380000	0.25937200
H	0.95323500	-1.60924200	-2.29638400	H	-1.68399600	1.63883400	-2.23752200
H	1.06349300	-0.04356600	1.94325500	H	-1.71311100	0.03350300	1.95519100
H	2.77909300	-0.19021300	2.35934500	H	-3.40231900	0.25967400	2.43986300
H	1.91887100	1.33998400	2.66143800	H	-2.60430600	-1.30994300	2.70638000
H	4.53180000	1.14466900	1.03883200	H	-5.26560700	-0.99093800	1.17936200
H	3.98749700	2.12224900	-0.34846000	H	-4.81469600	-1.98707300	-0.22800200
H	3.61598100	2.65058300	1.31245600	H	-4.41020000	-2.53791400	1.41793500

Atom	*x* / Å	*y* / Å	*z* / Å
H	2.45399100	-3.63535600	0.73411600
H	2.95038600	-3.01032600	-0.86734400
H	3.50400600	-2.19337400	0.61923300
C	-2.3270090	-0.37158100	-0.07073000
C	-2.9667640	0.71704800	-0.68226700
C	-3.08266400	-1.21559800	0.76269600
C	-4.31521900	0.96307600	-0.43305200
H	-2.41007900	1.36049000	-1.34907300
C	-4.42225500	-0.95511900	1.02327200
H	-2.60315700	-2.07844500	1.21815600
C	-5.04342600	0.14046600	0.42357900
H	-4.79821800	1.80629100	-0.91640000
H	-4.98281000	-1.60993300	1.68271300
H	-6.09243800	0.34396100	0.61485600
H	-0.75750600	-1.83157700	-0.16093700

Atom	*x* / Å	*y* / Å	*z* / Å
H	-2.97393700	3.67563100	0.85140000
H	-3.52954700	3.11023800	-0.75295600
H	-4.10339700	2.29650900	0.72537500
C	1.62448700	0.29388300	-0.27150700
C	2.19795400	-0.91338700	-0.71756300
C	2.47939900	1.24742100	0.30008000
C	3.55123000	-1.14774500	-0.56340000
H	1.57481000	-1.65609600	-1.19498600
C	3.83848800	1.01778000	0.47308300
H	2.06516500	2.19601400	0.63264100
C	4.38106100	-0.19423800	0.03927000
H	4.00149100	-2.07158400	-0.91052600
H	4.45631900	1.78064100	0.93117400
H	0.08329800	1.76203500	-0.27733400
O	5.68825000	-0.52893000	0.14486200
C	6.55955800	0.40850500	0.74001800
H	6.26522000	0.62390800	1.77400700
H	7.54771300	-0.05044400	0.73222000
H	6.58708600	1.34404800	0.16883100

(18c) *G* = -1123.078909 a. u. (Gas phase)
G = -1123.124370 a. u. (In methanol)

O	-2.26238200	-1.93824800	0.19395800
C	-1.19743600	-1.40995400	-0.44227100
C	-1.16935500	0.08390700	-0.49400000
C	-2.53311900	0.76239300	-0.62875200
O	-3.57505400	-0.08402300	-0.25177900
C	-3.27356600	-1.05995300	0.71727000
O	-0.35780500	-2.14105700	-0.89768800
O	-2.82127200	1.03347400	-1.96579200
C	-2.81969500	-0.46959000	2.04709900
C	-4.51744600	-1.91121800	0.85482100
C	-0.06908900	0.84559000	-0.38373100
O	-2.51070700	1.92735600	0.13542800
C	-3.74177900	2.64147900	0.14338300
H	-2.10381500	1.59209900	-2.30192700
H	-1.90747300	0.12043700	1.94351500
H	-3.60694400	0.17939700	2.43960000
H	-2.63974600	-1.28172800	2.75525600
H	-5.33626100	-1.30314400	1.24567500
H	-4.79257100	-2.30266700	-0.12596400
H	-4.32279200	-2.74181400	1.53616900
H	-3.54049800	3.58254200	0.65504400
H	-4.08790100	2.83379700	-0.87537900
H	-4.50920300	2.08085300	0.68461600
C	1.36117200	0.51072700	-0.24939800
C	2.00653200	-0.52736700	-0.93591800
C	2.11908100	1.35346900	0.58165500
C	3.37051100	-0.73596900	-0.76845200
H	1.43875900	-1.16811500	-1.59523400
C	3.47606800	1.14598800	0.77049000
H	1.62875700	2.17605600	1.09435700
C	4.07626900	0.09697400	0.08665100
H	3.88940500	-1.52998000	-1.29103900
H	4.07096200	1.77673600	1.41909200

(19a) *G* = -1014.342830 a. u. (Gas phase)
G = -1014.376818 a. u. (In methanol)

O	-0.47186600	2.17040000	0.01805000
C	-0.42307800	1.20073000	0.80681300
C	-0.25865100	-0.17191700	0.10990900
C	1.13800700	-0.61061900	-0.10081300
O	1.72619700	0.75150800	-1.14042600
C	1.81502500	1.94670800	-0.79100200
O	-0.41367200	1.19142700	2.05074200
O	1.34593700	-1.61293100	-0.90735100
C	2.26591000	2.40808900	0.56270200
C	1.65370500	2.98581000	-1.85390400
C	-1.24020000	-0.96353900	-0.34962100
O	2.03040700	-0.48844800	0.91772300
C	1.58208000	-1.09246900	2.15160700
H	2.33935400	-1.81095900	-0.93076100
N	4.05057300	-1.76400400	-0.91566400
H	4.51083600	-2.10426900	-1.75464100
C	4.61374400	-2.39175300	0.28480200
H	1.80200500	1.85458300	1.37749200
H	3.35201300	2.25739400	0.60523200
H	2.04584500	3.46885600	0.67546800
H	2.52890000	3.64141400	-1.88088000
H	1.48253200	2.52023000	-2.82291000
H	0.78109100	3.57718900	-1.56216200
H	2.40554200	-0.95097800	2.85146600
H	0.68409300	-0.58156800	2.50599700
H	1.40877600	-2.16210400	1.99501400
H	4.09793700	-1.98492300	1.15600800
H	4.42792400	-3.46676600	0.24817700
H	5.69032000	-2.22810300	0.40408900
H	4.19249000	-0.75729000	-0.88220300
H	-0.95131300	-1.86823900	-0.88241800
C	-2.68647700	-0.73993100	-0.23383100
C	-3.53111800	-1.42953600	-1.11474500

Atom	*x* / Å	*y* / Å	*z* / Å
H	-0.26987400	1.91381100	-0.30075900
N	5.52022900	-0.12676900	0.26571100
O	6.11442400	0.62223100	1.01934500
O	6.02763300	-1.04470100	-0.35048400

(19b)	*G* = -1128.792180 a. u. (Gas phase) *G* = -1128.833428 a. u. (In methanol)		
O	1.70529000	2.10528800	0.32881400
C	0.54390300	1.49580900	0.66938200
C	0.41400900	0.08611600	0.22953100
C	1.77467400	-0.54350900	-0.01280500
O	2.46458200	0.24649000	-0.95786000
C	2.60425700	1.62878900	-0.67768600
O	-0.2409210	2.11367800	1.34455100
O	1.67508600	-1.80619600	-0.49684100
C	4.00017300	1.91087000	-0.14766800
C	2.29123000	2.36499000	-1.97004000
C	-0.7074890	-0.62675400	0.01274000
O	2.57078900	-0.48585500	1.16068200
C	2.07491100	-1.26713000	2.23387500
H	2.61778400	-2.10473400	-0.68921400
N	4.31973300	-2.12149000	-1.00768800
H	4.66788000	-2.72347400	-1.74982200
C	5.15920100	-2.22619200	0.18998500
H	4.14944500	1.35080700	0.77670000
H	4.74000800	1.59961900	-0.89109000
H	4.11948800	2.97937600	0.04733900
H	2.97475400	2.03813300	-2.75775600
H	1.26676400	2.13641300	-2.27536500
H	2.39426800	3.44226500	-1.82251000
H	2.80323100	-1.17701200	3.04113000
H	1.10304500	-0.89672000	2.58069700
H	1.97504600	-2.31673700	1.93937300
H	4.76467800	-1.53453100	0.93681900
H	5.08838700	-3.24079400	0.58963200
H	6.21714900	-1.99608200	0.01219800
H	4.33044200	-1.16512200	-1.35980300
H	-0.4911000	-1.63647800	-0.33299300
C	-2.1453750	-0.34905400	0.06045900
C	-2.9669850	-1.29551700	-0.56835000
C	-2.7745370	0.75157300	0.67608000
C	-4.3492580	-1.16259600	-0.62426700
H	-2.5075540	-2.16094300	-1.03902400
C	-4.1487850	0.89164100	0.63358400
H	-2.1765100	1.48441100	1.19953400
C	-4.9474890	-0.05566700	-0.01909100
H	-4.9394930	-1.91778800	-1.12924800
H	-4.6401260	1.73339000	1.11007200
O	-6.2814870	0.18085700	-0.00174300
C	-7.1198570	-0.75556600	-0.64261000

Atom	*x* / Å	*y* / Å	*z* / Å
C	-3.25730400	0.11308800	0.72262000
C	-4.90784100	-1.24918100	-1.07249500
H	-3.09412500	-2.10416600	-1.84641400
C	-4.63592200	0.28468700	0.76619400
H	-2.62524600	0.61391800	1.44805000
C	-5.46399300	-0.38655700	-0.13107300
H	-5.54610700	-1.78308900	-1.76924800
H	-5.06676600	0.94497000	1.51188400
H	-6.53946000	-0.24537500	-0.09047600

(19c)	*G* = -1218.735900 a. u. (Gas phase) *G* = -1218.789775 a. u. (In methanol)		
O	1.71536900	1.99618500	0.67393100
C	0.58560000	1.26382000	0.78130200
C	0.61617300	-0.06725500	0.11136100
C	2.03265000	-0.57250200	-0.08213700
O	2.74306200	0.41705700	-0.79351700
C	2.77890500	72648300	-0.25111200
O	-0.3252460	1.68407100	1.44529900
O	2.06071600	-1.72669300	-0.78807300
C	4.06765600	1.94875900	0.52229100
C	2.61639900	2.67679400	-1.42566600
C	-0.4397640	-0.81162600	-0.24047700
O	2.69212200	-0.67973300	1.16637400
C	2.16612000	-1.68266200	2.01947900
H	3.03061600	-1.90969100	-1.01027100
N	4.69253200	-1.77957800	-1.36475800
H	5.09987200	-2.39142200	-2.06771800
C	5.50570700	-1.76965600	-0.14279400
H	4.10415000	1.26180900	1.36842700
H	4.92029400	1.76499200	-0.13785800
H	4.11213300	2.97861900	0.88468400
H	3.42641900	2.52105200	-2.14267700
H	1.66316200	2.47823100	-1.92242700
H	2.63534700	3.71108200	-1.07593000
H	2.81428600	-1.70893700	2.89602000
H	1.14365200	-1.44186900	2.33419700
H	2.17169400	-2.65778500	1.52322900
H	5.02556300	-1.10500200	0.57819800
H	5.51899700	-2.77594200	0.28277000
H	6.54106600	-1.44558900	-0.30349400
H	4.65162900	-0.84263300	-1.76200200
H	-0.1849690	-1.79292700	-0.63791600
C	-1.8859890	-0.53316600	-0.18985900
C	-2.7417800	-1.63964400	-0.08693600
C	-2.4463410	0.74663500	-0.30692700
C	-4.1204060	-1.48477600	-0.05675700
H	-2.3147920	-2.63629300	-0.02372800
C	-3.8222060	0.91841800	-0.29490100
H	-1.8059880	1.61327400	-0.40392000
C	-4.6343330	-0.20084900	-0.16200200
H	-4.7926500	-2.32862300	0.03487000
H	-4.2733610	1.89854500	-0.38599000
N	-6.0938480	-0.02041700	-0.14628700
O	-6.7824200	-1.01717800	-0.02421900

Atom	*x* / Å	*y* / Å	*z* / Å
H	-7.0334460	-1.74723800	-0.18262700
H	-8.1372350	-0.38555400	-0.51825900
H	-6.8872660	-0.83169900	-1.71151100
(20a-TS)	*G* = -1014.339900 a. u. (Gas phase)		
	G = -1014.374887 a. u. (In methanol)		
O	-2.35625400	-1.80987300	0.39362000
C	-1.08283700	-2.08582600	0.70420200
C	-0.05299600	-1.07449200	0.34327300
C	-0.65991400	0.27484700	0.00252000
O	-1.68362000	-0.95154600	0.02845800
C	-2.74496200	-0.85084600	-0.62379400
O	-0.85005000	-3.11577100	1.31151500
O	0.21984000	-0.56135900	1.13122100
C	-3.94507000	-0.10755700	-0.07151300
C	-3.05954000	-1.63531800	-1.88183300
C	1.22067700	-1.50259300	0.30193900
H	1.34361600	-2.57251100	0.47293300
C	2.48826700	-0.79985900	0.03670400
C	3.45372100	-1.47790300	-0.72367700
C	4.68868400	-0.89167700	-0.98994000
C	4.99082000	0.36414000	-0.46256500
C	4.05252000	1.02743300	0.33035900
C	2.80782200	0.45365800	0.57593700
O	-1.32374200	0.82669400	1.12230400
C	-0.47340100	1.21308000	2.19763500
H	-0.29283400	-0.78599000	2.0223500
N	-1.07902200	-1.06561100	3.32710900
H	-0.62801600	-1.79326200	3.87887000
C	-1.21877700	4.13150900	0.15830300
H	-3.68748500	0.40820800	0.85417100
H	-4.27742200	-0.81411500	0.62266500
H	-4.75861400	-0.81309200	0.11603800
H	-3.35377700	-0.94455400	-2.67626700
H	-2.17237500	-2.19064400	-2.19940800
H	-3.87908500	-2.33217400	-1.69231800
H	3.22583100	-2.46646900	-1.11445100
H	5.41835000	-1.42063400	-1.59562700
H	5.95795900	-0.65644100	0.81864700
H	4.29181100	1.99496800	0.76153200
H	2.08722100	0.97004400	1.19889500
H	-1.13109100	1.56341600	2.99433900
H	0.11295700	0.36220800	2.56437000
H	0.19732500	2.02521100	1.89947800
H	-1.73444200	3.54086500	0.91918800
H	-0.22553200	4.38826500	0.53401800
H	-1.78044600	-0.00504700	5.05710100
H	-2.00026700	-1.42434000	3.08010400
(20c-TS)	*G* = -1218.733800 a. u. (Gas phase)		
	G = -1218.786246 a. u. (In methanol)		
O	-3.23953500	-1.71765500	0.20973700

Atom	*x* / Å	*y* / Å	*z* / Å
O	-6.5221350	1.11334700	-0.25733800
(20b-TS)	*G* = -1128.792990 a. u. (Gas phase)		
	G = -1128.833689 a. u. (In methanol)		
O	-2.87120300	-1.91330400	0.27355400
C	-1.54906300	-2.19397500	0.37400700
C	-0.59940600	-1.05774600	0.16014200
C	-1.28991600	0.28248900	0.03544500
O	-2.40043000	0.12968100	-0.82437100
C	-3.38743700	-0.82897500	-0.49735700
O	-1.22001800	-3.31025800	0.68519300
O	-0.49115900	1.23630700	-0.50089300
C	-4.51345800	-0.21462200	0.31951000
C	-3.87061300	-1.39391500	-1.82422100
C	0.70308800	-1.40196500	0.13820800
H	0.83263000	-2.48127700	0.22136500
C	1.98706800	-0.70072500	0.04316300
C	3.09957400	-1.50628700	-0.23560000
C	4.38895900	-0.99406500	-0.32798100
C	4.59260600	0.36886800	-0.10892800
C	3.49989100	1.19031900	0.19770600
C	2.22272700	0.66931000	0.26968300
O	-1.83657300	0.66911500	1.28662300
C	-0.87016900	1.03534800	2.25254100
H	-1.08032100	2.02962100	-0.70738400
N	-2.38976800	3.08181400	-1.07338300
H	-2.25938000	3.87111300	-1.70112700
C	-3.10301000	3.48786400	0.14262100
H	-4.12554900	0.13626200	1.27545100
H	-4.94360200	0.62606400	-0.23333200
H	-5.29266700	-0.96125100	0.49225200
H	-4.29390000	-0.59417500	-2.43791800
H	-3.02616800	-1.83939400	-2.35572600
H	-4.63163700	-2.15711900	-1.64875300
H	2.95057400	-2.57176100	-0.39020800
H	5.21333200	-1.65881900	-0.55624500
H	3.68744300	2.24395900	0.37576900
H	1.39364300	1.32490900	0.49279400
H	-1.40461100	1.15273700	3.19625400
H	-0.10430800	0.25787500	2.36635600
H	-0.38515500	1.98089800	1.98598100
H	-3.20177900	2.61040300	0.78551100
H	-2.50428900	4.23161500	0.67426200
H	-4.09665200	3.91292500	-0.04638100
H	-2.92841600	2.37660700	-1.57316400
O	5.79880300	0.98366500	-0.16079700
C	6.92443700	0.18838700	-0.46421700
H	6.82780200	-0.27669000	-1.45244900
H	7.78048100	0.86263100	-0.46246100
H	7.07388200	-0.59334700	0.29003700
(21)	*G* = -193.014512 a. u. (Gas phase)		
	G = -193.021701 a. u. (In methanol)		
C	0.0000000	0.18648300	0.00000100

Atom	*x* / Å	*y* / Å	*z* / Å
C	-1.98919400	-2.13008300	0.51019400
C	-0.89073600	-1.12685500	0.32062500
C	-3.52109000	-0.62435100	-0.67045400
O	-1.82100600	-3.23811200	0.94732800
O	-0.44695900	1.13827200	-0.28605600
C	-4.68546100	0.13163400	-0.05238000
C	-3.85429300	-1.20603800	-2.03467300
C	0.35601700	-1.62036100	0.31206600
H	0.39232900	-2.70557900	0.41030000
C	1.68440500	-0.99758300	0.16579000
C	2.66496300	-1.75884800	-0.48887800
C	3.95717700	-1.28201200	-0.65498600
C	4.26689300	-0.03908200	-0.12221100
C	3.33578700	0.72997300	0.56321600
C	2.04320000	0.24621800	0.70270900
O	-2.07643600	0.71732900	1.29595900
C	-1.22239900	0.99268800	2.38924300
H	-0.91254900	1.98780600	-0.58465200
N	-2.00081500	3.16880700	-1.12692100
H	-1.66198900	3.93936600	-1.69769800
C	-2.83047700	3.65881400	-0.01977700
H	-4.40667900	0.48889700	0.93880000
H	-4.94267700	0.98168500	-0.69118700
H	-5.55304100	-0.52797000	0.02733000
H	-4.09855700	-0.40071000	-2.73225400
H	-2.98892000	-1.75380600	-2.41600000
H	-4.70551100	-1.88495900	-1.95257000
H	2.40259800	-2.73714500	-0.88075400
H	4.71884400	-1.85229200	-1.17180100
H	3.63310600	1.68659600	0.97442000
H	1.30444700	0.83767200	1.22517200
H	-1.86941200	1.20300600	3.24159400
H	-0.58662000	0.13007700	2.62739200
H	-0.59043900	1.86391600	2.18499400
H	-3.14923800	2.79814500	0.57234300
H	-2.22298200	4.30329400	0.62019500
H	-3.71290900	4.22326000	-0.34431400
H	-2.54952200	2.55887100	-1.73027300
N	5.63523800	0.47671000	-0.27764100
O	6.43295000	-0.21702100	-0.88121100
O	5.88479100	1.56574700	0.20601600

(21-TS) *G* = -192.9250900 a. u. (Gas phase)
G = -192.9441254 a. u. (In methanol)

C	-0.0385780	0.05179900	0.00002300
O	0.38345800	1.21434100	-0.00004100
C	1.22100600	-0.75247100	-0.00008800
C	-1.4807920	-0.32291400	0.00003900
H	1.46200500	0.45050300	-0.00051800
H	1.37789600	-1.34934900	0.90122800
H	1.37738100	-1.35128600	-0.90017800
H	-2.1184440	0.56075900	0.00032400
H	-1.6881770	-0.94160300	-0.87830100
H	-1.6881410	-0.94223300	0.87793200

Atom	*x* / Å	*y* / Å	*z* / Å
O	-0.0000000	1.39562400	0.00000000
C	-1.2875800	-0.61340900	0.00000300
C	1.28758400	-0.61340800	-0.00000300
H	-2.1415110	0.06424800	0.00016500
H	-1.3297200	-1.26273700	-0.88099000
H	-1.3295790	-1.26300900	0.88080100
H	2.14151200	0.06424900	-0.00017200
H	1.32972400	-1.26273000	0.88099400
H	1.32957600	-1.26301300	-0.88079700

(21-Enol) *G* = -192.9953020 a. u. (Gas phase)
G = -193.0120207 a. u. (In methanol)

C	1.39916500	0.24153400	0.00000900
C	-0.0842000	0.04961200	-0.00002100
C	-0.993549	1.02815200	-0.00000500
O	-0.3951570	-1.27990500	-0.00001900
H	1.65415000	1.30155700	-0.00028300
H	1.83576500	-0.23477700	0.88276200
H	1.83585500	-0.23529000	-0.88241900
H	-2.0592250	0.82018500	0.00001300
H	-0.6805100	2.06375100	0.00002200
H	-1.3532840	-1.39197100	0.00016300

Atom	*x* / Å	*y* / Å	*z* / Å	Atom	*x* / Å	*y* / Å	*z* / Å
(22a-E)	*G* = -821.4560600 a. u. (Gas phase) *G* = -821.4812002 a. u. (In methanol)			**(22b-E)**	*G* = -935.9049820 a. u. (Gas phase) *G* = -935.9404095 a. u. (In methanol)		
C	1.16636600	0.21661300	-0.06285300	C	-1.7303900	-0.47993500	-0.03095400
C	0.49909700	1.38008100	-0.06395900	C	-0.7196580	-1.36195500	-0.07283700
C	2.65099400	0.15365000	-0.02230400	C	3.15147000	-0.90493000	0.00926600
C	0.51027200	-1.13985500	-0.05686800	C	-1.5455590	1.01357900	0.01898900
O	3.27070000	-0.87588400	0.11534200	O	-4.0741010	-0.14667800	0.19160100
O	0.03240200	-1.47562800	1.12233600	O	-1.0352720	1.42622400	1.16146200
O	0.43577600	-1.82911200	-1.05747000	O	-1.8276730	1.73661000	-0.91730600
C	-0.9605900	1.56348200	-0.08264100	C	0.71413600	-1.06141200	-0.12468700
C	-1.4989180	2.69997900	0.53677300	C	1.62139900	-1.99062100	0.38829200
C	-2.8738480	2.91060100	0.56710400	C	2.99294800	-1.75260900	0.39034500
C	-3.7313290	1.99692300	-0.04431800	C	3.47956800	-0.56393300	-0.15639000
C	-3.2043120	0.87895900	-0.69057000	C	2.58658600	0.36392100	-0.70923700
C	-1.8301680	0.66178700	-0.71338400	C	1.22787000	0.11747100	-0.69382600
O	3.23835900	1.35713400	-0.13701400	O	-3.3114950	-2.23133800	-0.15823400
C	4.66550000	1.33824700	-0.07145600	C	-4.6638820	-2.67544000	-0.08638200
H	1.09500200	2.28943900	-0.02443100	H	-0.9855230	-2.41696200	-0.05837600
H	-0.8295030	3.41404500	1.00916100	H	1.24665400	-2.91887800	0.81180900
H	-3.2755600	3.78909300	1.06192000	H	3.66300300	-2.49333700	0.80981600
H	-4.8040040	2.16221500	-0.02902800	H	2.99350600	1.26479300	-1.15647900
H	-3.8663490	0.17815300	-1.18999900	H	-5.2633550	-2.19508500	-0.86260100
H	-1.4269130	-0.19095700	-1.25051300	N	-0.8578730	4.02103800	0.62435700
H	4.97787400	2.37523800	-0.17991000	C	0.29388400	4.10254000	-0.28084400
H	4.99486900	0.93197600	0.88709900	H	-0.8621880	4.79046900	1.28894900
H	5.07201100	0.72458600	-0.87781000	H	-0.9452440	2.44483500	1.10567200
N	-1.0159680	-3.82756300	0.58587700	H	-1.7184340	4.06261200	0.08092500
C	-2.2462320	-3.49475200	-0.14607500	H	1.21214400	3.93045300	0.28591200
H	-1.1758390	-4.56350000	1.26696900	H	0.37590700	5.06221700	-0.80418100
H	-0.3777390	-2.41649400	1.04422300	H	0.18703500	3.30869600	-1.02323900
H	-2.6910240	-4.35085100	-0.66431500	O	4.79108500	-0.22599300	-0.21487000
H	-2.0005300	-2.72744700	-0.88373800	C	5.72550400	-1.13979200	0.31709600
				H	6.70612600	-0.68624100	0.17563500
				H	5.55205600	-1.30856700	1.38659000
				H	5.68794500	-2.09992100	-0.21127600
(22a-z)	*G* = -821.4491640 a. u. (Gas phase) *G* = -821.4738072 a. u. (In methanol)			**(22b-z)**	*G* = -935.8980820 a. u. (Gas phase) *G* = -935.9350404 a. u. (In methanol)		
C	0.73967700	-0.61428600	-0.52753200	C	1.47208000	-0.63299200	-0.48153900
C	-0.3663110	-1.29790500	-0.19582800	C	0.34308900	-1.32121300	-0.24659000
C	0.74191000	0.87358400	-0.68298700	C	1.47216900	0.85160200	-0.65105500
C	1.99731100	-1.40428400	-0.83779100	C	2.75051000	-1.41864200	-0.68945000
O	1.38040800	1.65736500	-0.01121000	O	2.03351200	1.65507800	0.06321400
O	1.90699200	-2.50535200	-1.33125300	O	2.69892700	-2.56896600	-1.05619900
O	3.15821900	-0.83163300	-0.57917900	O	3.89618200	-0.78424200	-0.50003100
O	-0.0644880	1.25434900	-1.67497700	O	0.74524100	1.21189000	-1.71229800
C	-0.2000320	2.66660900	-1.85314200	C	0.59926800	2.61881300	-1.89843900
H	-0.8680790	2.79019100	-2.70272600	H	0.01392500	2.73560800	-2.80842200
H	-0.6317380	3.11444100	-0.95424100	H	0.07343600	3.05663800	-1.04537200
H	0.77310600	3.11922600	-2.05161900	H	1.57627100	3.09498300	-1.99978000
N	3.42867300	0.62584900	1.57919800	N	4.11586700	0.75176100	1.64178000
H	3.18948100	-0.16449800	0.20586500	H	3.89522200	-0.06186700	0.22252600
C	2.51346300	0.06475800	2.58082600	C	3.22059400	0.08929900	2.59434700
H	4.39061000	0.59318000	1.90339500	H	5.07194700	0.76540200	1.98755900
H	3.18363700	1.59019700	1.37488300	H	3.81145600	1.70708000	1.47911700

Atom	*x* / Å	*y* / Å	*z* / Å
H	2.57389000	0.55978200	3.55608500
H	2.73211100	-0.99790500	2.71022300
H	1.49167500	0.15774000	2.20471500
H	-0.2684850	-2.38285300	-0.20103600
C	-1.6861600	-0.75879600	0.16533500
C	-2.8204520	-1.53573200	-0.10640900
C	-1.8557850	0.48501500	0.79163500
C	-4.0947780	-1.06440000	0.19452600
H	-2.6962020	-2.50965300	-0.57186900
C	-3.1291440	0.95078800	1.10287500
H	-0.9884270	1.07918300	1.06731400
C	-4.2526770	0.18235200	0.79764000
H	-4.9635140	-1.67304900	-0.03494000
H	-5.2449420	0.54801400	1.04184800

Atom	*x* / Å	*y* / Å	*z* / Å
H	3.23706700	0.52814900	3.59898200
H	3.49525900	-0.96618000	2.66726100
H	2.20251100	0.15088600	2.20226400
C	-2.10057700	-1.61826500	-0.28505000
C	-1.25696000	0.47744400	0.52974700
C	-3.40935900	-1.18122400	-0.10250700
H	-1.92689000	-2.61784900	-0.67446200
C	-2.54943300	0.92254700	0.72726500
H	-0.43047000	1.11703000	0.82796100
C	-3.63708500	0.10025800	0.40191900
H	-4.23192100	-1.84232400	-0.34724800
H	-2.75385400	1.90137600	1.14784400
O	-4.86286100	0.63044000	0.62786600
C	-5.98681000	-0.16916800	0.32696700
H	-6.86050500	0.43304100	0.57416700
H	-6.01349500	-0.43239000	-0.73708600
H	-5.99374300	-1.08658100	0.92739600

(22c-z) *G* = -1025.859164 a. u. (Gas phase)
G = -1025.910223 a. u. (In methanol)

C	-1.69496400	0.71925000	-0.34464000
C	-0.61662700	1.42676900	0.01820600
C	-1.59616600	-0.71026800	-0.77703300
C	-3.03071200	1.44282600	-0.41005000
O	-2.07473600	-1.65863000	-0.19372500
O	-3.04775400	2.64270200	-0.54592300
O	-4.12513500	0.70822000	-0.36446100
O	-0.88516100	-0.82396000	-1.89846400
C	-0.66022500	-2.16335900	-2.34363100
H	-0.10185200	-2.07334300	-3.27303600
H	-0.07987400	-2.71140500	-1.59666700
H	-1.61049400	-2.67450600	-2.50710100
H	-4.09230600	-0.14631200	0.20937400
C	-3.49530700	-0.69679700	2.51398400
H	-5.26131600	-1.35720600	1.67736200
H	-3.91493900	-2.10986600	1.08424100
H	-2.45800200	-0.61671900	2.17982300
H	-0.79160600	2.48021500	0.23122000
C	0.76884800	0.94612400	0.13083600
C	1.81070300	1.85108700	-0.11498700
C	1.08442800	-0.37199600	0.49500000
C	3.13722300	1.44910600	-0.04689600
H	1.57230400	2.87745900	-0.37697400
C	2.40530000	-0.78804400	0.57471600
H	0.29288000	-1.07155400	0.74704300
C	3.40770800	0.13105600	0.29361600
H	3.95489400	2.13065100	-0.24623300
H	2.67104100	-1.79869000	0.85923600
N	4.80999500	-0.30632600	0.37521400
O	5.67057800	0.52013000	0.13721200
O	5.01897100	-1.46769400	0.67382200

(23b-TS) *G* = -652.7395150 a. u. (Gas phase)
G = -652.7622322 a. u. (In methanol)

C	-1.45736700	-0.35054400	-1.25760900
C	-0.10307600	-0.65746200	-1.13027800
C	0.40927500	-1.06076000	0.10618700
C	-0.45012100	-1.16474200	1.20767000
C	-1.79960400	-0.85842000	1.07758100
C	-2.30644500	-0.44566800	-0.15747000
C	1.85552600	-1.33098800	0.27720500
O	2.63083700	-1.44255400	-0.81607600
H	2.76874100	-0.54735900	-1.21350000
C	2.63853400	0.42561400	1.23722000
C	2.23702000	1.29880800	0.14696200
O	2.77814000	1.21778100	-0.96434200
C	1.05305200	2.21099200	0.35852200
H	-1.84843100	-0.03809300	-2.22066800
H	0.55653600	-0.59267300	-1.98975500
H	-0.05088400	-1.47838000	2.16970000
H	-2.45898700	-0.94275100	1.93562600
H	2.11614600	-2.05164200	1.05093100
H	2.14654500	0.54481400	2.19878100
H	2.14654500	0.54481400	2.19878100
H	3.67877700	0.11399000	1.25229300
H	0.20712700	1.63926200	0.75784300
H	1.30677800	2.98166600	1.09400600
H	0.77337400	2.67759700	-0.58631100
O	-3.69475700	-0.13047900	-0.29217900
C	-3.91196800	1.23478300	0.07357800
H	-4.94011000	1.48663100	-0.08261700
H	-3.66409200	1.37135200	1.10547200
H	-3.29423000	1.86792600	-0.52844400

(23a-TS) *G* = -538.2956440 a. u. (Gas phase)
G = -538.3204576 a. u. (In methanol)

C	-2.10395500	0.37329300	-1.32304300
C	-0.89269800	-0.29810800	-1.15997100

(23c-TS) *G* = -742.7326040 a. u. (Gas phase)
G = -742.7693119 a. u. (In methanol)

C	-1.24401500	0.15361100	-1.15622500
C	0.08731800	-0.26012000	-1.18610700

Atom	*x* / Å	*y* / Å	*z* / Å	Atom	*x* / Å	*y* / Å	*z* / Å
C	-0.54147900	-0.81289900	0.09128200	C	0.61267700	-1.00304900	-0.12495100
C	-1.42022600	-0.65880800	1.17142000	C	-0.21153800	-1.33648400	0.95769800
C	-2.62697300	0.01064300	1.00571500	C	-1.53822500	-0.92291000	0.98450400
C	-2.97029200	0.53298900	-0.24404100	C	-2.05733700	-0.17158600	-0.07315400
C	0.76732200	-1.47421400	0.30012400	C	2.03997800	-1.39858300	-0.10824300
O	1.50491300	-1.81166100	-0.77268000	O	2.76461000	-1.26967500	-1.23390300
H	1.89649800	-0.99570000	-1.17168700	H	2.95442600	-0.31229700	-1.39432600
C	1.98841300	0.00564200	1.26932200	C	2.98623000	-0.00557300	1.22761400
C	1.87166500	0.94245800	0.16429300	C	2.61170100	1.14499800	0.42246900
O	2.39340900	0.69952800	-0.93258500	O	3.10457500	1.32269900	-0.69997000
C	0.98549000	2.15165900	0.34077600	C	1.50757600	2.04283500	0.92587300
H	-2.37030400	0.77041600	-2.29741000	H	0.71829700	-0.01500500	-2.03450000
H	-0.22211600	-0.43097500	-2.00297400	H	0.19782900	-1.91441500	1.78333400
H	-3.91245100	1.05570300	-0.37408300	H	-2.17048600	-1.18649200	1.82647100
H	0.79859800	-2.22919600	1.08430500	H	2.27399500	-2.31086400	0.43847000
H	1.52786900	0.26961500	2.21752000	H	2.53973200	-0.11054500	2.21274500
H	2.89943800	-0.58395700	1.31231500	H	4.00017400	-0.37489900	1.10531000
H	0.00469600	1.84407100	0.72202800	H	0.63639100	1.44095100	1.20994100
H	1.42795100	2.82995400	1.07792900	H	1.84463800	2.57769400	1.82005700
H	0.86874400	2.66589900	-0.61346600	H	1.22939600	2.75616000	0.14970700
				N	-3.46040300	0.26607700	-0.04566000
				O	-3.87733100	0.90323500	-0.97227800
				O	-4.13215300	-0.03148700	0.90229300
(24a)	*G* = -538.3707080 a. u. (Gas phase)			**(24a-TS)**	*G* = -538.3192300 a. u. (Gas phase)		
	G = -538.3947567 a. u. (In methanol)				*G* = -538.3461142 a. u. (In methanol)		
C	-2.14836500	0.10183200	-1.39051300	C	-2.23300600	-0.04497200	-1.37207300
C	-0.92796500	-0.50536300	-1.09131000	C	-1.00711600	-0.62020600	-1.03129000
C	-0.54959400	-0.70810700	0.23558200	C	-0.59238900	-0.65709600	0.29969200
C	-1.41551400	-0.30856700	1.25848800	C	-1.42838900	-0.12639400	1.28808100
C	-2.63407100	0.29662800	0.96232600	C	-2.65228300	0.44650000	0.95127400
C	-3.00147200	0.50850200	-0.36720800	C	-3.05545000	0.49369900	-0.38487600
C	0.81596700	-1.28060800	0.58945800	C	0.78288000	-1.22959700	0.65023800
O	1.40608500	-1.99788000	-0.46501700	O	1.42967500	-1.82136200	-0.37624400
H	1.90610800	-1.37920100	-1.02048900	H	2.10612500	-0.81262900	-0.87767700
C	1.88797800	0.89341400	-0.02394200	C	1.55285200	2.21728500	-0.15574800
O	2.40743200	0.58017000	-1.08136000	H	-2.54881100	-0.02493900	-2.41094700
C	1.30431800	2.26055900	0.20413400	H	-0.36025400	-1.06676500	-1.78039900
H	-2.43242700	0.25393800	-2.42721400	H	-1.12356700	-0.17176900	2.33267600
H	-0.26950100	-0.83426500	-1.88878800	H	-3.29498400	0.84964400	1.72827100
H	-1.13546400	-0.47794200	2.29673200	H	-4.00990000	0.93777900	-0.65003600
H	-3.29903300	0.59718800	1.76617100	H	0.68301100	-1.87398000	1.54039600
H	-3.95102900	0.97891300	-0.60189700	H	1.25082200	0.58404600	1.98707900
H	0.69337600	-1.98836700	1.41736400	H	2.62620800	-0.48406700	1.52404200
H	1.34102100	0.30630800	1.98881100	H	0.45378800	2.23386900	-0.10763400
H	0.22438600	2.15041600	0.36628000	H	1.92607700	2.80509600	0.68585100
H	1.72590700	2.70664900	1.11059300	H	1.88382700	2.62999200	-1.10799200
H	1.49004200	2.89945600	-0.65885600				
(24b)	*G* = -652.8196292 a. u. (Gas phase)			**(24b-TS)**	*G* = -652.7953800 a. u. (Gas phase)		
	G = -652.8375199 a. u. (In methanol)				*G* = -652.8192584 a. u. (In methanol)		
C	-1.49074900	0.00752800	-1.17434500	C	-1.55181200	-0.06451800	-1.17483000
C	-0.21548600	-0.53500000	-1.01017300	C	-0.27501200	-0.59844300	-0.98898300
C	0.27922000	-0.79534600	0.26748000	C	0.23938100	-0.76224100	0.29687900
C	-0.52518800	-0.51933800	1.37767500	C	-0.54748700	-0.40101300	1.39588200
C	-1.79825300	0.02112900	1.21625400	C	-1.82187800	0.13025900	1.21356000

Atom	*x* / Å	*y* / Å	*z* / Å	Atom	*x* / Å	*y* / Å	*z* / Å
C	-2.28281400	0.29146100	-0.06423700	C	-2.32569400	0.30558300	-0.07698200
C	1.70114400	-1.29713800	0.47742900	C	1.66551400	-1.28537400	0.48256800
O	2.24808700	-1.90585600	-0.66491600	O	2.26437800	-1.71442900	-0.64856800
H	2.66338300	-1.22162100	-1.21326600	H	2.84682000	-0.61506300	-1.07131800
C	2.59626000	-0.13229300	0.97025200	C	2.55916400	-0.07190300	1.09777000
C	2.58566000	0.97751300	-0.06610400	C	2.66979300	0.86908800	-0.02377100
O	3.03732100	0.76662800	-1.17858600	O	3.02962400	0.39012200	-1.13083300
C	1.93942900	2.28584500	0.29778600	C	2.18856000	2.27208300	0.04167500
H	-1.86537600	0.20543100	-2.17387800	H	-1.94497700	0.05513200	-2.18006600
H	0.39617300	-0.76862400	-1.87563100	H	0.33691600	-0.91536200	-1.82810000
H	-0.15337200	-0.73480200	2.37787300	H	-0.16348300	-0.54712200	2.40451800
H	-2.41413300	0.22569800	2.08661000	H	-2.42526800	0.40118800	2.07485700
H	1.68855200	-2.06219600	1.26222700	H	1.66687600	-2.03259300	1.29450800
H	2.23797200	0.22984200	1.93767500	H	2.13484400	0.38819700	1.99064600
H	3.61937600	-0.50606200	1.08146400	H	3.52668000	-0.53293300	1.31148200
H	0.88464900	2.09431000	0.53322200	H	1.09684300	2.21529400	0.16601600
H	2.40386500	2.70095500	1.19799900	H	2.59181100	2.78127800	0.91986500
H	2.01625200	2.98872700	-0.53136500	H	2.42502200	2.81096300	-0.87502200
O	-3.59015500	0.84511500	-0.23519000	O	-3.63488800	0.84820500	-0.2679610
C	-4.56092600	-0.20440100	-0.20326500	C	-4.60472200	-0.19763700	-0.16532200
H	-4.56789400	-0.65439600	0.76748600	H	-4.59348600	-0.59837300	0.82673900
H	-5.52894000	0.19852500	-0.41656800	H	-5.57661700	0.19483200	-0.38046700
H	-4.31232400	-0.94263500	-0.93682300	H	-4.36974300	-0.97192500	-0.86543800
(24c)	*G* = -742.7809581 a. u. (Gas phase)			**(24c-TS)**	*G* = -742.699640 a. u. (Gas phase)		
	G = -742.8153712 a. u. (In methanol)				*G* = -742.737974 a. u. (In methanol)		
C	-1.28143200	-0.14124900	-1.16903700	C	-1.33978000	-0.14163500	-1.17354600
C	0.05611300	-0.53131000	-1.08897000	C	-0.00269100	-0.53827200	-1.10495000
C	0.59955500	-0.93476600	0.13037600	C	0.55560400	-0.92439500	0.11328200
C	-0.21743300	-0.95677800	1.26520300	C	-0.24636700	-0.92533000	1.25970900
C	-1.55248800	-0.56890300	1.18751800	C	-1.58066000	-0.53175300	1.19395600
C	-2.08722100	-0.15388200	-0.03287300	C	-2.13000100	-0.13210100	-0.02611400
C	2.07784200	-1.27342700	0.26349400	C	2.03947800	-1.29172300	0.18533600
O	2.68262300	-1.60493300	-0.96083400	O	2.66272000	-1.37268900	-1.00932300
H	2.99669800	-0.78995200	-1.38332500	H	3.09437200	-0.14142700	-1.16499100
C	2.82021700	-0.10026800	0.95164500	C	2.78790800	-0.14744900	1.06856200
C	2.64920400	1.15634100	0.11647700	C	2.75627100	1.03052100	0.19281000
O	3.10796300	1.19602300	-1.01226200	O	3.14913700	0.86570400	-0.99165800
C	1.84295500	2.28880700	0.69027800	C	2.10543000	2.30943100	0.57367400
H	-1.69354000	0.17037200	-2.12383300	H	-1.76629000	0.15324100	-2.12776300
H	0.68012600	-0.53421400	-1.97684500	H	0.62580400	-0.57584600	-1.98959200
H	0.19419400	-1.28603700	2.21768300	H	0.17442700	-1.24768300	2.21111500
H	-2.17681400	-0.59576300	2.07530800	H	-2.19447700	-0.54255700	2.08973900
H	2.17705200	-2.15409000	0.90845200	H	2.15140500	-2.19794200	0.80487100
H	2.43208600	0.04440200	1.96349700	H	2.32882200	0.03980400	2.03971800
H	3.88495600	-0.34969000	1.00600600	H	3.80971000	-0.51910200	1.17858400
H	0.82588800	1.92364600	0.88239500	H	1.03223000	2.08844600	0.67336800
H	2.26247100	2.60458200	1.65084800	H	2.46083300	2.65191200	1.54809800
H	1.81488700	3.12458900	-0.00837400	H	2.25313500	3.06839200	-0.19366100
N	-3.49646900	0.25510100	-0.12037200	N	-3.53875100	0.28126000	-0.09997500
O	-4.16018500	0.23164000	0.87830200	O	-4.18803200	0.27682600	0.90840600
O	-3.92622500	0.59590300	-1.18694200	O	-3.98255700	0.60643200	-1.16567100
(24a-Int)	*G* = -538.3420010 a. u. (Gas phase)			**(24b-Int)**	*G* = -652.8139348 a. u. (Gas phase)		
	G = -538.3678514 a. u. (In methanol)				*G* = -652.8345424 a. u. (In methanol)		
C	2.20124200	-0.02412700	1.21336300	C	-1.30367400	-0.80129200	-1.23155800

Atom	*x* / Å	*y* / Å	*z* / Å
C	1.12504700	-0.86292200	0.94012200
C	0.59376800	-0.91095800	-0.35250200
C	1.13873200	-0.12223400	-1.36571600
C	2.22154900	0.71278300	-1.09423400
C	2.75012900	0.76199400	0.19534400
C	-0.5578300	-1.80563900	-0.65149700
O	-1.0428100	-2.56424600	0.15446800
H	-1.1692100	0.56479800	1.88289000
C	-2.6681650	0.62848000	-0.85341200
C	-1.8868380	1.01836900	0.15753100
O	-1.9264750	0.32763800	1.33493000
C	0.95715900	2.19402700	0.13322600
H	2.62094600	0.01532600	2.21376300
H	0.68217200	-1.49534400	1.70487400
H	0.70626500	-0.15975900	-2.36315200
H	2.64893900	1.32542300	-1.88150700
H	3.59233700	1.41264000	0.40978100
H	-0.9469700	-1.74231400	-1.68725600
H	-2.6816330	1.18925900	-1.77920300
H	-3.3146860	-0.23496400	-0.74594300
H	0.0652790	1.87783800	0.37800800
H	-0.9423450	2.66067500	-0.85269200
H	-1.2695930	2.94065000	0.87191300

Atom	*x* / Å	*y* / Å	*z* / Å
C	-0.02945900	-1.23927100	-0.92654600
C	0.45835200	-1.13715600	0.38389800
C	-0.35100000	-0.59441100	1.37451300
C	-1.64383200	-0.15841900	1.08791500
C	-2.12044800	-0.26272000	-0.22178300
C	1.83417800	-1.58905400	0.69716300
O	2.57018300	-2.10534400	-0.10969100
H	1.44255500	0.77837500	-1.81010000
C	3.05692500	1.32916700	0.78467000
C	2.13542400	1.46867200	-0.16868000
O	2.29484600	0.82329000	-1.36056600
C	0.90557200	2.31915600	-0.06287300
H	-1.71208200	-0.87110600	-2.23396300
H	0.62006500	-1.67217100	-1.68211100
H	0.03398100	-0.50329400	2.38758500
H	-2.25920900	0.25788300	1.87561400
H	2.15120700	-1.42556900	1.74814700
H	2.97183800	1.87811900	1.71315400
H	3.91441300	0.68683400	0.62466100
H	0.01077200	1.71365100	-0.25673400
H	0.81269600	2.75864200	0.93065700
H	0.93507300	3.12372100	-0.80532900
O	-3.35319900	0.12806500	-0.61905000
C	-4.21745000	0.67416700	0.35614200
H	0.81269600	2.75864200	0.93065700
C	-4.21745000	0.67416700	0.35614200
H	-5.14417400	0.91569300	-0.16224300
H	-4.42313000	-0.04844500	1.15401700
H	-3.79616400	1.58654400	0.79393900

(24c-Int) *G* = -742.7429060 a. u. (Gas phase)
G = -742.7801902 a. u. (In methanol)

C	-1.1941900	-0.73810400	-1.05090000
C	0.11280100	-1.17483600	-0.88412100
C	0.70421600	-1.13811800	0.38131600
C	-0.0028230	-0.65964900	1.48308800
C	-1.3144600	-0.22176900	1.33553900
C	-1.8787350	-0.27288100	0.06795500
C	2.11142200	-1.61154200	0.54092900
O	2.75237600	-2.07935100	-0.36626700
H	1.61810500	1.09600600	-1.93276700
C	3.24050000	1.24156400	0.73326800
C	2.29953600	1.47354300	-0.18362100
O	2.40583800	0.89641000	-1.41516000
C	1.08685400	2.32883600	0.02462400
H	-1.6941620	-0.75421300	-2.01138900
H	0.69979600	-1.55356600	-1.71469400
H	0.47816300	-0.62477800	2.45688300
H	-1.8987950	0.15423900	2.16577100
H	2.52714400	-1.51555400	1.56348600
H	3.18022000	1.70791700	1.70756200
H	4.09214600	0.61487500	0.49734700
H	0.17715500	1.74573000	-0.16789700
H	1.04202300	2.71094500	1.04445000
H	1.09370800	3.17863300	-0.66672000

(25b-TS) *G* = -652.7322860 a. u. (Gas phase)
G = -652.7560296 a. u. (In methanol)

C	-2.1104640	-1.20787800	0.15887800
C	-0.7515170	-1.04239700	-0.04676900
C	-0.2002170	0.25148800	-0.11411800
C	-1.0466680	1.36692300	0.02683400
C	-2.4064790	1.19658000	0.23489900
C	-2.9375310	-0.09091300	0.30102700
C	1.19518700	0.48077200	-0.34077500
O	2.44328800	0.09385900	1.91304400
H	2.79591300	0.99437400	1.96973800
C	3.62245700	0.00296900	-0.49705100
H	5.64853500	-0.56388200	-0.12853300
O	-4.3398080	-0.27058500	0.51605300
C	-5.0314190	-0.16448300	-0.73107000
H	-6.0672060	-0.38952200	-0.58477200
H	-4.9328400	0.83131100	-1.10998600
H	-4.6117100	-0.85584600	-1.43161400

Atom	*x* / Å	*y* / Å	*z* / Å
N	-3.2671050	0.19471400	-0.10175100
O	-3.8522190	0.58531200	0.89053800
O	-3.7355470	0.16194200	-1.22389100

(25a-TS) *G* = -538.2746699 a. u. (Gas phase)
G = -538.3008859 a. u. (In methanol)

C	2.93496100	1.35158300	-0.06919500
C	1.57492700	1.13169600	-0.20472400
C	1.06842800	-0.18209500	-0.20035900
C	1.96035100	-1.26160500	-0.06009900
C	3.32118200	-1.03674200	0.07763200
C	3.80764400	0.26991900	0.07322600
C	-0.32664800	-0.46774100	-0.35289500
O	-1.48353000	-0.04125600	1.94207500
H	-1.80028900	-0.95072400	2.04704000
C	-1.38121600	0.48541900	-0.60081500
C	-2.77426100	-0.08031100	-0.41159100
O	-2.98953700	-1.25009900	-0.63327400
C	-3.81455700	0.89068800	0.06885300
H	3.32307100	2.36417500	-0.07057100
H	0.89695600	1.97101500	-0.31181800
H	1.56655500	-2.27361800	-0.05568600
H	4.00316400	-1.87235300	0.18896600
H	4.87258400	0.44895600	0.18126300
H	-0.63631000	-1.50863300	-0.42800500
H	-1.22738200	1.50406300	-0.26253200
H	-1.30250200	0.67427900	-2.28333300
H	-3.53767800	1.13151100	1.09941400
H	-3.79791300	1.80798100	-0.52693200
H	-4.80058500	0.42932000	0.03158500

(25c-TS) *G* = -742.6650760 a. u. (Gas phase)
G = -742.7014658 a. u. (In methanol)

C	-1.85904200	-1.13782900	-0.17128900
C	-0.48650400	-0.98917100	-0.27352800
C	0.08800900	0.29611700	-0.24946900
C	-0.74910300	1.42038900	-0.12379200
C	-2.12275000	1.26679300	-0.01940000
C	-2.67688400	-0.01242800	-0.04298700
C	1.49938600	0.50867800	-0.36749600
O	2.57741300	0.01114900	1.95144200
H	2.93888800	0.90218800	2.06921500
C	2.50806400	-0.49747300	-0.59623100
C	3.92399200	-0.00671600	-0.37098400
O	4.20558000	1.15115300	-0.58060200
C	4.90017400	-1.03334900	0.12799000
H	-2.29962400	-2.12858000	-0.18779200
H	0.14883100	-1.86248600	-0.36964800
H	-0.30294700	2.41024900	-0.10412300
H	-2.76238500	2.13659800	0.08084300
H	1.86495400	1.53217700	-0.42913200
H	2.29297800	-1.50818900	-0.26770800
H	2.45955800	-0.67403200	-2.28122500
H	4.58662000	-1.26410400	1.15031600
H	4.84957000	-1.94568900	-0.47345600
H	5.90966600	-0.62432900	0.11663200
N	-4.13315000	-0.17938600	0.06798400
O	-4.81310000	0.80253500	0.17715800
O	-4.58315700	-1.29085800	0.04491600

(26a-TS) *G* = -538.2952901 a. u. (Gas phase)
G = -538.3226096 a. u. (In methanol)

C	-3.25334600	0.85813000	-0.14077500
C	-1.88476900	1.05089600	-0.28395600
C	-0.99997500	-0.02967800	-0.18428200
C	-1.51598800	-1.31020800	0.03468800
C	-2.88689900	-1.50193800	0.17362800
C	-3.75843200	-0.41956400	0.09143400
C	0.45150500	0.20813900	-0.36026600
O	0.73375300	2.05698500	0.58216300
H	0.68609200	1.82282400	1.51765000
C	1.44428400	-0.63235100	0.00288300
C	2.84727000	-0.28695900	-0.09413900
O	3.16788900	0.88607300	-0.30499800
C	3.89028900	-1.35783600	0.10148700
H	-3.92754700	1.70549500	-0.21208900
H	-1.48155200	2.04461500	-0.45000800
H	-0.83940200	-2.15625500	0.07130300
H	-3.27532200	-2.50192100	0.33766900
H	-4.82764000	-0.57154500	0.19904800
H	0.71813600	0.91586700	-1.14342500
H	1.23709200	-1.46979600	0.66599600
H	2.07838500	2.07097300	0.26762900

(26b-TS) *G* = -652.7496665 a. u. (Gas phase)
G = -652.7734978 a. u. (In methanol)

C	2.33778200	1.10493100	-0.01989400
C	0.96805600	1.21077200	0.18821600
C	0.14510100	0.08183700	0.09501200
C	0.72551500	-1.15881200	-0.18406200
C	2.09769900	-1.26359300	-0.38800600
C	2.90653500	-0.13319100	-0.31162900
C	-1.30848300	0.22673800	0.34081500
O	-1.74176200	2.07997000	-0.53318200
H	-1.72258300	1.87448900	-1.47639400
C	-2.26520200	-0.66203600	-0.00368600
C	-3.68034800	-0.40473300	0.16435200
O	-4.05992000	0.74067100	0.42365300
C	-4.66599100	-1.53095100	-0.01751600
H	2.96323600	1.98921900	0.04720800
H	0.51469500	2.17348000	0.40103500
H	0.09917000	-2.04286700	-0.21637000
H	2.53676800	-2.23349900	-0.59836200
H	-1.58089500	0.89564600	1.15547000
H	-2.03898100	-1.46721000	-0.69973200
H	-3.06931200	2.00423800	-0.16030300
H	-4.36118600	-2.40236700	0.56682000

Atom	*x* / Å	*y* / Å	*z* / Å
H	3.66430700	-2.22801900	-0.51934500
H	4.87443600	-0.95766200	-0.13954700
H	3.87623600	-1.69081500	1.14358900

(26c-TS)	*G* = -742.6836662 a. u. (Gas phase) *G* = -742.7191789 a. u. (In methanol)		
C	-2.05171000	1.13908300	-0.21413700
C	-0.67036700	1.24494400	-0.32066200
C	0.13910700	0.10578700	-0.23401900
C	-0.46480100	-1.14358300	-0.06566100
C	-1.84830100	-1.24813500	0.03660500
C	-2.64485500	-0.10856300	-0.03221800
C	1.60689900	0.25204400	-0.37009500
O	1.98649300	2.05024000	0.63412900
H	1.90081200	1.79288100	1.56077100
C	2.53338500	-0.66239200	-0.01045300
C	3.95791800	-0.40790800	-0.06544600
O	4.35967500	0.74693500	-0.23334600
C	4.92352600	-1.55062500	0.12092400
H	-2.66706200	2.03089100	-0.27479600
H	-0.19904300	2.21418700	-0.44737800
H	0.15386300	-2.03323500	-0.03958200
H	-2.30522800	-2.22454600	0.16145300
H	1.93829900	0.96286100	-1.12522600
H	2.25571600	-1.50306000	0.62211200
H	3.33642600	1.98431200	0.35040900
H	4.65627700	-2.38570000	-0.53095600
H	5.93733900	-1.20964700	-0.08571000
H	4.86230300	-1.91184000	1.15185800
N	-4.10654500	-0.22228400	0.07469900
O	-4.58394300	-1.31137000	0.23090700
O	-4.76331100	0.77856600	0.00145000

(27b-TS)	*G* = -652.724610 a. u. (Gas phase) *G* = -652.746241 a. u. (In methanol)		
C	-2.19966400	0.99442000	0.15793000
C	-0.88840600	1.40750600	-0.05949600
C	0.10587800	0.51634800	-0.46733200
C	-0.24477300	-0.82575600	-0.65333900
C	-1.54701300	-1.25202200	-0.44125200
C	-2.53261700	-0.34760800	-0.03786800
C	1.49667400	1.07909500	-0.70387400
O	1.88401800	1.92692400	0.37364400
H	1.50605300	1.55372100	1.18013100
C	2.59992300	0.04584500	-1.01182200
C	2.97085600	-0.83706800	0.17117100
O	2.47016700	-1.92864400	0.33553400
C	4.01719100	-0.29102300	1.11580300
H	-2.94249700	1.71776700	0.47138600
H	-0.62901000	2.45204400	0.09077400
H	0.50653200	-1.55623100	-0.93025300
H	-1.82659100	-2.29135100	-0.57333200

Atom	*x* / Å	*y* / Å	*z* / Å
H	-5.66020000	-1.19759100	0.27778100
H	-4.67929300	-1.83418100	-1.06866900
O	4.31687100	-0.24410900	-0.52032000
C	4.97968100	-0.34673300	0.74263300
H	6.02265800	-0.52592300	0.58454900
H	4.85304700	0.56565400	1.28707200
H	4.55928800	-1.15672000	1.30128400

(27a-TS)	*G* = -538.2661451 a. u. (Gas phase) *G* = -538.2944759 a. u. (In methanol)		
C	3.20128600	0.87795600	-0.32551400
C	1.96969800	1.31569000	0.12461000
C	0.95036200	0.38497900	0.44789800
C	1.22102100	-1.00047600	0.35314800
C	2.46394400	-1.42970500	-0.08485700
C	3.44444700	-0.49665500	-0.43153700
C	-0.2966870	0.90417300	0.87617300
O	-2.4108830	1.84066800	-0.88264500
H	-1.9493890	2.10798500	-1.68718000
C	-1.5568410	0.21790500	1.04534800
C	-2.0823900	-0.72592100	-0.04511600
O	-1.3429260	-1.37890700	-0.74217600
C	-3.5815770	-0.77475800	-0.13017600
H	3.97339300	1.59112800	-0.59188500
H	1.75717000	2.37774500	0.20764900
H	0.45734400	-1.71323700	0.63518900
H	2.67472200	-2.49079900	-0.15782200
H	4.41372500	-0.84266300	-0.77791600
H	-0.3345690	1.96997700	1.09426500
H	-1.2416560	-0.87957100	2.29580700
H	-2.3352500	0.85158100	1.45477000
H	-4.0118510	-0.93990100	0.86314500
H	-3.8934690	0.20595000	-0.50572900
H	-3.8792710	-1.57141600	-0.81159800

(27c-TS)	*G* = -742.6553701 a. u. (Gas phase) *G* = -742.6924335 a. u. (In methanol)		
C	2.07798700	-1.30874700	-0.11996300
C	0.73839600	-1.66683800	-0.21499000
C	-0.27065300	-0.69933900	-0.19821800
C	0.07417400	0.65207800	-0.08497700
C	1.40856800	1.02827500	0.00763200
C	2.38310800	0.03915500	-0.00909300
C	-1.71481400	-1.17055600	-0.23299800
O	-2.24816700	-1.26006500	1.08213800
H	-1.60199200	-1.70382900	1.64384500
C	-2.68103600	-0.28059800	-1.03760800
C	-3.33463500	0.81105500	-0.18507100
O	-2.81346900	1.89347000	-0.03115600
C	-4.67119700	0.47243000	0.42513500
H	2.87582900	-2.04036400	-0.13611900
H	0.47399000	-2.71655100	-0.31386000
H	-0.70349900	1.40940600	-0.08096300
H	1.70421900	2.06660800	0.09117600

Atom	*x* / Å	*y* / Å	*z* / Å
H	1.45036100	1.74291600	-1.57610700
H	2.28926100	-0.58962300	-1.84512900
H	3.48361500	0.61473300	-1.31775500
H	4.99332000	-0.33551800	0.61982300
H	3.81734400	0.76046300	1.33539600
H	4.04944900	-0.89220800	2.02408700
O	-3.77566400	-0.86469400	0.14165800
C	-4.79534300	0.01858100	0.55253900
H	-5.70086600	-0.58087700	0.63894400
H	-4.56534800	0.47075700	1.52476200
H	-4.95602100	0.81479700	-0.18416800
(28a-TS)	*G* = -538.2698250 a. u. (Gas phase) *G* = -538.2963781 a. u. (In methanol)		
C	-3.12558100	0.42929800	0.16091200
C	-1.94791500	1.04619200	-0.22992100
C	-0.79809400	0.28096200	-0.48189700
C	-0.85206200	-1.10952400	-0.32347000
C	-2.03894100	-1.72561900	0.05638500
C	-3.17514500	-0.95903700	0.29947500
C	0.40837900	0.96293200	-0.93870300
O	0.75302400	2.49590500	0.74808100
H	0.82404700	1.76234200	1.37965100
C	1.72198300	0.29056200	-1.00011100
C	2.23886200	-0.41810500	0.22362700
O	1.72941200	-0.27122900	1.31189700
C	3.42702700	-1.32796300	0.00581300
H	-4.00657300	1.02777900	0.36728300
H	-1.87013600	2.12662800	-0.29616000
H	0.02881400	-1.71525100	-0.51604300
H	-2.07524800	-2.80410100	0.16759700
H	-4.09854000	-1.44116800	0.60363900
H	0.26498200	1.79698700	-1.61605400
H	1.93294000	-0.22514300	-1.94099800
H	2.86033500	1.54248000	-1.09803600
H	3.09182400	-2.24154800	-0.49761300
H	4.17423500	-0.85299400	-0.63420600
H	3.86276400	-1.59160400	0.96845000
(28c-TS)	*G* = -742.6577320 a. u. (Gas phase) *G* = -742.6971179 a. u. (In methanol)		
C	-1.92974800	1.25969100	-0.09333300
C	-0.61431200	1.61959800	-0.33889800
C	0.35700900	0.63347500	-0.57396100
C	-0.01611700	-0.71615300	-0.54670300
C	-1.33931200	-1.07240400	-0.31264500
C	-2.29629400	-0.08742100	-0.08528300
C	1.72081800	1.05479000	-0.87702700
O	2.23775300	2.34418900	0.96260800
H	2.08708900	1.57020500	1.52854900
C	2.85409400	0.10797900	-0.90235400
C	3.08738100	-0.78560100	0.28676400

Atom	*x* / Å	*y* / Å	*z* / Å
H	-1.71290600	-2.16703000	-0.69908600
H	-2.14941600	0.19132000	-1.86730000
H	-3.47050900	-0.91587100	-1.44912100
H	-5.40632000	0.30310700	-0.36873300
H	-4.57581900	-0.45401300	0.99723300
H	-5.00196200	1.28937200	1.06527100
N	3.79829000	0.43494700	0.08752800
O	4.63195900	-0.45200500	0.06927900
O	4.04479800	1.62256600	0.18047200
(28b-TS)	*G* = -652.7251860 a. u. (Gas phase) *G* = -652.7482817 a. u. (In methanol)		
C	2.20312700	1.08206000	-0.16946100
C	0.93526100	1.48452200	0.21879900
C	-0.06025700	0.53028500	0.4824920
C	0.23925600	-0.83022200	0.33835700
C	1.51606200	-1.23014600	-0.03896400
C	2.49795100	-0.27689700	-0.29374100
C	-1.36792400	0.99239400	0.93613900
O	-1.98133400	2.42161400	-0.76535500
H	-1.92200000	1.68029600	-1.38902600
C	-2.54136200	0.09843300	1.00884700
C	-2.92605000	-0.70385800	-0.20575200
O	-2.45223600	-0.48074500	-1.29715700
C	-3.93370000	-1.80759100	0.02541100
H	2.96371600	1.82502000	-0.38493500
H	0.66717800	2.53469200	0.27405400
H	-0.51995300	-1.58044200	0.54010900
H	1.74292200	-2.28623400	-0.13907300
H	-1.37379200	1.84593600	1.60430600
H	-2.65620300	-0.43630100	1.95573300
H	-3.88357200	1.12962100	1.09748400
H	-3.44107800	-2.64175200	0.53720700
H	-4.75241500	-1.46576400	0.66290500
H	-4.31710200	-2.15472200	-0.93299700
O	3.80758900	-0.69066700	-0.69191600
C	4.71623000	-0.51318400	0.39793400
H	5.63912400	-1.00749400	0.17697300
H	4.89723500	0.53109800	0.54494600
H	4.29222200	-0.93035300	1.28736400
(29a-z)	*G* = -461.9555980 a. u. (Gas phase) *G* = -461.9714807 a. u. (In methanol)		
C	-2.11707700	-1.48598200	-0.00006600
C	-0.86856400	-0.87423500	-0.00022800
C	-0.77017800	0.52666600	-0.00013500
C	-1.95941300	1.27750200	0.00011600
C	-3.20345400	0.66272800	0.00028600
C	-3.28504200	-0.72747100	0.00019100
C	0.47415400	1.30632000	-0.00030600
C	1.79600100	1.03178600	-0.00031300
C	2.54759300	-0.24706200	-0.00002100
O	2.04949600	-1.35696100	-0.00021400
C	4.05585100	-0.08545300	0.00051300

Atom	*x* / Å	*y* / Å	*z* / Å	Atom	*x* / Å	*y* / Å	*z* / Å
O	2.52481700	-0.60552700	1.34342700	H	-2.17610300	-2.56964100	-0.00014100
C	4.06095200	-1.92335200	0.07533300	H	0.03405200	-1.46865600	-0.00042800
H	-2.67252000	2.02611400	0.10109100	H	-1.89933300	2.36269000	0.00018700
H	-0.29481100	2.65606300	-0.30096900	H	-4.10572800	1.26538500	0.00048400
H	0.72367800	-1.49057900	-0.72808900	H	-4.25403900	-1.21654000	0.00030600
H	-1.62224900	-2.11961800	-0.30268100	H	0.26517300	2.37667100	-0.00044200
H	1.82753800	1.94609500	-1.48464600	H	2.44547500	1.90467000	-0.00041900
H	3.03202000	-0.37315100	-1.86805500	H	4.37524300	0.48014000	-0.88042800
H	4.24420000	1.07251600	-0.80231300	H	4.37461100	0.48006400	0.88173300
H	3.58063200	-2.69838100	-0.53217000	H	4.52546600	-1.06789000	0.00064200
H	4.95005400	-1.58566000	-0.46225500				
H	4.33745200	-2.34751900	1.03952900				
N	-3.69271000	-0.46740400	0.17266100				
O	-3.97590100	-1.63283200	0.17291700				
O	-4.49303700	0.40318700	0.37255100				
(29b-z)	*G* = -576.4117420 a. u. (Gas phase) *G* = -576.4240607 a. u. (In methanol)			**(29c-z)**	*G* = -666.3984870 a. u. (Gas phase) *G* = -666.4241604 a. u. (In methanol)		
C	1.39953700	-1.09852300	-0.29034500	C	-1.19166300	-0.95682500	-0.00021800
C	0.09107200	-0.64283300	-0.17507400	C	0.13951600	-0.55559800	-0.00032100
C	-0.16983200	0.73364300	-0.07789000	C	0.46373300	0.81081600	-0.00018700
C	0.92094800	1.62117100	-0.10082800	C	-0.58803100	1.74453200	0.00004400
C	2.22533400	1.16194300	-0.21603500	C	-1.91528800	1.33959300	0.00015400
C	2.46834600	-0.20595300	-0.31150700	C	-2.22119400	-0.01898400	0.00001900
C	-1.49373900	1.35623700	0.04808800	C	1.81800900	1.37840600	-0.00029400
C	-2.77149600	0.92476100	0.10983000	C	3.07785500	0.89318800	-0.00026300
C	-3.36707400	-0.43323600	0.07143000	C	3.61215900	-0.49059700	0.00002000
O	-2.74404500	-1.47312400	-0.03076100	O	2.94070000	-1.50505300	-0.00022000
C	-4.88045300	-0.45493000	0.17230500	C	5.12666300	-0.57566600	0.00061000
H	1.58443400	-2.16534900	-0.36449000	H	-1.42560500	-2.01657600	-0.00032400
H	-0.73395400	-1.34078300	-0.15925600	H	0.93381300	-1.28849900	-0.00050500
H	0.73482800	2.68938500	-0.02651600	H	-0.35280100	2.80562100	0.00014900
H	3.04906100	1.86801300	-0.23129400	H	-2.70791200	2.08056500	0.00033800
H	-1.41150900	2.44218200	0.10542800	H	1.78533300	2.46847800	-0.00040900
H	-3.51685400	1.71148800	0.20598400	H	3.86026000	1.64922200	-0.00032300
H	-5.20337800	0.01634500	1.10589100	H	5.53356400	-0.06932200	-0.88030500
H	-5.32181300	0.11782000	-0.64935500	H	5.53286100	-0.06933100	0.88185600
H	-5.23119200	-1.48517900	0.13640700	H	5.43077800	-1.62124400	0.00072900
O	3.80845500	-0.69054400	-0.43058600	N	-3.62354300	-0.45979900	0.00011200
C	4.49813200	-0.49598300	0.80690800	O	-3.85122300	-1.63733100	-0.00000900
H	5.40967000	-1.05628500	0.79913300	O	-4.48398400	0.37569400	0.00030500
H	4.71938600	0.54335000	0.93234300				
H	3.88139200	-0.82943300	1.61520400				
(29a-E)	*G* = -461.9762840 a. u. (Gas phase) *G* = -461.9902225 a. u. (In methanol)			**(29b-E)**	*G* = -576.419620 a. u. (Gas phase) *G* = -576.445673 a. u. (In methanol)		
C	-3.12546100	1.09443200	0.00018200	C	2.16129400	1.21602400	-0.25405500
C	-1.74466200	1.27340900	0.00013400	C	0.77897300	1.35561400	-0.16272500
C	-0.87402700	0.17528900	0.00000400	C	-0.05974000	0.23337800	-0.13079000
C	-1.42454700	-1.11572800	-0.00007500	C	0.52450600	-1.04121200	-0.19304000
C	-2.80208000	-1.29584700	-0.00002800	C	1.90360000	-1.18203600	-0.28418600
C	-3.65818900	-0.19232600	0.00010100	C	2.72767500	-0.05481500	-0.31508500
C	0.57424300	0.42770300	-0.00005300	C	-1.51136200	0.44444100	-0.03361500
C	1.54787500	-0.49638000	-0.00019800	C	-2.45754700	-0.50679200	0.00856100
C	3.00407800	-0.21847300	-0.00013100	C	-3.91778300	-0.27047300	0.10665700
O	3.78267900	-1.15603000	0.00009400	O	-4.66906500	-1.22961700	0.13582100

Atom	*x* / Å	*y* / Å	*z* / Å
C	3.54547800	1.19814300	-0.00009800
H	-3.78280800	1.95797300	0.00028200
H	-1.33050200	2.27847300	0.00019700
H	-0.77464800	-1.98472800	-0.00017100
H	-3.21233600	-2.30067100	-0.00008900
H	-4.73368400	-0.33787200	0.00013900
H	0.84463700	1.48164000	0.00007100
H	1.32409500	-1.56011600	-0.00026700
H	2.78602600	1.97846100	-0.00251800
H	4.17871500	1.31765300	0.88234300
H	4.18282700	1.31609700	-0.87976000

(29c-E) *G* = -666.405564 a. u. (Gas phase)
G = -66.4307275 a. u. (In methanol)

C	-1.85622200	1.26879800	0.01200600
C	-0.46932200	1.39186900	0.01301500
C	0.35626100	0.25954000	0.00235000
C	-0.24594000	-1.00814000	-0.00943500
C	-1.62962300	-1.13248400	-0.01045600
C	-2.44047400	0.00465500	0.00025200
C	1.81354200	0.45326100	0.00400100
C	2.74906700	-0.50934000	-0.00511400
C	4.21530400	-0.29046900	-0.00310700
O	4.95541200	-1.25866100	-0.01189100
C	4.81346400	1.10307100	0.00979600
H	-2.47816400	2.15813800	0.02038000
H	-0.01491700	2.37934800	0.02219700
H	0.36834000	-1.90263400	-0.01785100
H	-2.08011800	-2.11988000	-0.01963800
H	2.12627300	1.49537400	0.01375700
H	2.48251600	-1.56312600	-0.01492500
H	4.08614000	1.91340600	0.01492300
H	5.45106200	1.18873800	0.89303000
H	5.45500400	1.20333500	-0.86901300
N	-3.90396800	-0.13349500	-0.00089100
O	-4.57077000	0.86219500	-0.04981500
O	-4.37272900	-1.23638400	0.04714600

(30a-TS1) G = -538.2876030 a. u. (Gas phase)
G = -538.3162953 a. u. (In methanol)

C	2.92492000	1.34301600	0.02504900
C	1.56970700	1.15290500	-0.18192400
C	1.04148000	-0.15240300	-0.26878000
C	1.91528600	-1.25301200	-0.14101200
C	3.26964700	-1.05657300	0.06787500
C	3.77492200	0.24162500	0.15111400
C	-0.33970000	-0.40447200	-0.50823700
C	-1.38177100	0.61006800	-0.78114400
C	-2.75796700	0.00674700	-0.44598500
O	-3.02457800	-1.10353100	-0.84228600
C	-3.69212300	0.86256800	0.35818600

Atom	*x* / Å	*y* / Å	*z* / Å
C	-4.49633700	1.12989900	0.17104600
H	2.79360400	2.09775300	-0.27743600
H	0.33852300	2.34830000	-0.11517800
H	-0.10022600	-1.92818500	-0.17025100
H	2.34014900	-2.17459300	-0.33148300
H	-1.80972400	1.49006200	0.00580300
H	-2.20542400	-1.56353000	-0.02816700
H	-3.75974900	1.93131000	0.14194100
H	-5.18769500	1.24852600	-0.66676400
H	-5.07912300	1.21250500	1.09162700
O	4.14653900	-0.20616100	-0.40898800
C	4.72216500	-0.13072600	0.89786500
H	5.77117900	-0.33285600	0.83775200
H	4.57024400	0.84975500	1.29846000
H	4.25578700	-0.85263100	1.53523600

(30a-TS2) *G* = -538.2819840 a. u. (Gas phase)
G = -538.3119145 a. u. (In methanol)

C	3.03137000	-1.37297100	-0.11985700
C	1.66068400	-1.36597200	0.07634900
C	0.98504200	-0.14035500	0.23786500
C	1.69667300	1.07676100	0.16219000
C	3.06643700	1.05387200	-0.05315400
C	3.73273200	-0.16501600	-0.18627200
C	-0.42541800	-0.05397700	0.47786300
C	-1.39606300	-1.01519900	0.09749800
C	-2.85243000	-0.62545100	-0.09815100
O	-3.52280800	-1.35762700	-0.78955200
C	-3.33416500	0.65197500	0.52057600
H	3.56087000	-2.31447500	-0.22118300
H	1.11494500	-2.30222800	0.15333200
H	1.11169100	1.99831800	0.18914100
H	3.61742700	1.98532600	-0.13034800
H	4.80589800	-0.17811100	-0.35073800
H	-0.78414900	0.88530000	0.89879200
H	-1.10479700	-1.92046300	-0.43006200
H	-1.51091000	-1.68092900	1.95868400
H	-3.17511500	0.63282100	1.60461800
H	-2.74623500	1.50019200	0.11836300
H	-4.39631300	0.76668300	0.30516400
O	-1.04284500	2.60004800	-0.39077500
H	-0.95726500	2.42619200	-1.34259000

(30b-TS2) *G* = -652.754632 a. u. (Gas phase)
G = -652.776669 a. u. (In methanol)

C	2.18481000	-1.31870400	-0.24582800
C	0.82106500	-1.33089700	-0.00629300
C	0.13396900	-0.11491100	0.17808200
C	0.82591700	1.11202900	0.08143100
C	2.18835400	1.10833700	-0.17722300
C	2.86691500	-0.10107400	-0.33291000
C	-1.26923800	-0.04832100	0.46274600
C	-2.23804200	-1.02261700	0.11211300
C	-3.70513700	-0.65296800	-0.03681600
O	-4.38688300	-1.39381700	-0.70755300
C	-4.18467000	0.61714100	0.59846300

Atom	*x* / Å	*y* / Å	*z* / Å
H	3.32673700	2.34790000	0.09390700
H	0.91003300	2.00858800	-0.27240800
H	1.50678500	-2.25724400	-0.20127400
H	3.93427600	-1.90734600	0.16908100
H	4.83610800	0.39733100	0.31662600
H	-0.65415600	-1.43513400	-0.66086500
H	-1.20330700	1.53278200	-0.22782600
H	-1.39155800	0.84225800	-1.85959700
H	-3.26734000	0.85001500	1.36864000
H	-3.71212700	1.89053400	-0.01475700
H	-4.69206200	0.42958000	0.34873600
O	-1.44502000	-0.34074300	2.00669000
H	-1.78302300	-1.24789100	1.97364300

(30b-TS1) *G* = -652.7705461 a. u. (Gas phase)
G = -652.7911382 a. u. (In methanol)

C	-2.09729300	-1.20853700	0.19077200
C	-0.74456000	-1.06990600	-0.06705900
C	-0.17729100	0.21399800	-0.20915900
C	-1.00973400	1.34648300	-0.08379100
C	-2.36175700	1.20155400	0.17610500
C	-2.90599300	-0.07611800	0.31361500
C	1.20228100	0.41275700	-0.50209800
C	2.20059200	-0.64341200	-0.78060100
C	3.60652800	-0.07768200	-0.50942600
O	3.89540700	1.01162200	-0.94625600
C	4.53947300	-0.94187900	0.28715700
H	-2.52910300	-2.19705100	0.30199400
H	-0.11671600	-1.94946500	-0.15502400
H	-0.57097200	2.33435900	-0.18663200
H	-2.99434000	2.07667100	0.27509000
H	1.54477400	1.42764700	-0.69481200
H	2.01131800	-1.54395300	-0.19527100
H	2.16549300	-0.90552200	-1.85164500
H	4.15051900	-0.88712000	1.31054900
H	4.51297700	-1.97985300	-0.05651500
H	5.55209900	-0.54319300	0.23161800
O	2.39122400	0.38143500	1.97501300
H	2.75733800	1.27544100	1.90452600
O	-4.30187100	-0.22803800	0.58443600
C	-5.03616700	-0.15821200	-0.64064900
H	-6.06847100	-0.36537000	-0.45003500
H	-4.94036900	0.82215000	-1.05851600
H	-4.64909900	-0.87916900	-1.33006900

(30c-TS1) *G* = -742.65137601 a. u. (Gas phase)
G = -742.69025191 a. u. (In methanol)

C	-1.85003100	-1.14859100	-0.18024300
C	-0.48011300	-1.01685600	-0.32705100
C	0.11181700	0.26367000	-0.34342600
C	-0.71389400	1.39988600	-0.20772800
C	-2.08333600	1.26172400	-0.05921700

Atom	*x* / Å	*y* / Å	*z* / Å
H	2.72382300	-2.25268300	-0.36505700
H	0.29106100	-2.27470300	0.08676300
H	0.22937400	2.02535300	0.12805500
H	2.72366500	2.04741400	-0.27066300
H	-1.62742600	0.88554100	0.89600600
H	-1.95113000	-1.92331900	-0.42554500
H	-2.28461600	-1.69139500	1.97516600
H	-3.99109600	0.59931300	1.67689800
H	-3.62158800	1.47376700	0.17889300
H	-5.25459800	0.71726600	0.41694800
O	-1.95058700	2.59758300	-0.38256600
H	-1.89281300	2.42570800	-1.33683200
O	4.27283800	-0.09851800	-0.59420100
C	4.98816700	-0.04473200	0.64285700
H	6.03906400	-0.10225800	0.44997200
H	4.76715400	0.87502300	1.14296200
H	4.69352600	-0.86671400	1.26126700

(30c-TS2) *G* = -742.7359950 a. u. (Gas phase)
G = -742.7759255 a. u. (In methanol)

C	1.93350900	-1.29783600	0.06725100
C	0.55580500	-1.31628900	0.20478900
C	-0.14963400	-0.10301300	0.32740500
C	0.54098300	1.12724000	0.27225600
C	1.91889100	1.12964900	0.11568800
C	2.61364800	-0.07687500	0.02099000
C	-1.57047200	-0.04256600	0.50635400
C	-2.50524400	-1.02538400	0.09277500
C	-3.95915300	-0.66570700	-0.16793200
O	-4.58510000	-1.41590600	-0.88131400
C	-4.49145400	0.60650100	0.41931000
H	2.48491400	-2.22948900	-0.00376700
H	0.02542600	-2.26248200	0.26603600
H	-0.06227700	2.03732000	0.26676700
H	2.45461600	2.07114200	0.05449300
H	-1.96492400	0.89253800	0.90397200
H	-2.17427700	-1.92858100	-0.41452500
H	-2.68674100	-1.67966000	1.95271600
H	-4.37858000	0.59836800	1.50926600
H	-3.90332200	1.46313100	0.03565200
H	-5.54543000	0.69878500	0.15789500
O	-2.20123600	2.59244200	-0.40932600
H	-2.07168400	2.41336700	-1.35518500
N	4.07484500	-0.06773000	-0.13939000
O	4.63696200	0.99074100	-0.18502100
O	4.64651000	-1.11910800	-0.21820300

(31a-TS2) *G* = -538.2862110 a. u. (Gas phase)
G = -538.3158315 a. u. (In methanol)

C	2.13306800	-1.32358600	-0.73985300
C	0.89475000	-0.78181500	-0.39252300
C	0.82397000	0.43886200	0.32951500
C	2.02217600	1.15037000	0.60238900
C	3.25403600	0.65556900	0.18221400

Atom	*x* / Å	*y* / Å	*z* / Å
C	-2.65187900	-0.01268300	-0.04529100
C	1.51187600	0.45717200	-0.51929600
C	2.51545400	-0.59600200	-0.79010100
C	3.90368400	-0.07250700	-0.37898600
O	4.23791800	1.03723100	-0.72194900
C	4.76328100	-1.00112900	0.42756300
H	-2.30098100	-2.13470300	-0.16545900
H	0.14184800	-1.89959200	-0.42447700
H	-0.25665400	2.38471200	-0.21369400
H	-2.71090800	2.13941000	0.04853500
H	1.88024000	1.47628100	-0.62013200
H	2.27161800	-1.52848100	-0.27976900
H	2.55810800	-0.78909500	-1.87544200
H	4.29889200	-1.00473300	1.42051100
H	4.75019000	-2.01464400	0.01669100
H	5.78197800	-0.61694900	0.47347200
O	2.51000800	0.24881800	2.03236400
H	2.89123000	1.13915900	2.04712900
N	-4.10551300	-0.16182800	0.11472600
O	-4.77138700	0.82916100	0.22862100
O	-4.56755200	-1.26854500	0.12499100

(31a-TS1) *G* = -538.291147 a. u. (Gas phase)
G = -538.320535 a. u. (In methanol)

C	-2.03907500	-1.65391200	0.17160000
C	-0.83533500	-1.15603000	-0.30613100
C	-0.70049400	0.22233300	-0.56284300
C	-1.77823100	1.09002400	-0.29705500
C	-2.96864200	0.58531200	0.19639700
C	-3.10260500	-0.78682400	0.42228100
C	0.50939000	0.77367200	-1.10008600
C	1.80445600	0.05132500	-1.14119300
C	2.21145600	-0.72491200	0.12777000
O	2.68124400	-1.83304300	0.00246500
C	2.02568400	-0.04467700	1.45600300
H	-2.14936800	-2.71728600	0.35357100
H	-0.00882900	-1.83276500	-0.50414200
H	-1.61307000	2.15660700	-0.41347600
H	-3.79140300	1.25553800	0.41982200
H	-4.03813800	-1.18081800	0.80630300
H	0.41520000	1.68003500	-1.68843800
H	1.78901000	-0.67699500	-1.96487900
H	2.60103100	0.76999000	-1.35923100
H	2.00881500	1.04707200	1.36590900
H	1.03440400	-0.32376200	1.83430000
H	2.77380800	-0.42304500	2.15328100
O	0.90672600	2.69741400	0.63843800
H	1.51515600	3.19259600	0.06930000

(31b-TS1) *G* = -652.7731890 a. u. (Gas phase)
G = -652.7942097 a. u. (In methanol)

C	-1.50255700	-1.22165100	0.05763100

(31b-TS2) *G* = -652.7569190 a. u. (Gas phase)
G = -652.7781957 a. u. (In methanol)

C	-1.52353000	-1.06677700	0.30651300
C	-0.20629800	-0.63586000	0.14282100
C	0.06763700	0.60944500	-0.48214200
C	-1.01532900	1.45368400	-0.84386800
C	-2.33064300	1.06470900	-0.60407300
C	-2.58215500	-0.27849200	-0.13873200
C	1.49562200	1.05911700	-0.75854000
C	2.55122900	0.03544000	-1.24716500
C	2.78635300	-0.98890000	-0.16433400
O	1.95807900	-1.86209300	0.02953100
C	4.05633200	-0.90041400	0.63634600
H	-1.72093400	-2.01749300	0.79205100
H	0.61857100	-1.25332700	0.48347800
H	0.81440000	2.41082900	-1.32195400
H	-3.11770900	1.81148900	-0.56503000
H	1.80333800	1.67357100	-1.47231000
H	1.95523900	-0.79523500	-2.86050800
H	3.38870100	0.51389700	-1.42071300
H	4.90466000	-1.00194400	-0.05264500
H	4.13797300	0.08277000	1.11077700
H	4.08623200	-1.69074500	1.38595700
O	2.48053900	2.24142200	1.65220500
H	3.43007700	2.04225000	1.64570400
O	-3.91707800	-0.79101800	-0.12463000
C	-4.67472000	-0.12167700	0.88673600
H	-4.95674700	0.84944800	0.53705400
H	-5.55371700	-0.69000900	1.10868900
H	-4.08060400	-0.02363400	1.77122100

(31b-TS1) *G* = -652.7731890 a. u. (Gas phase)
G = -652.7942097 a. u. (In methanol)

C	-1.33594000	-0.86099600	0.41484800

Atom	*x* / Å	*y* / Å	*z* / Å	Atom	*x* / Å	*y* / Å	*z* / Å
C	-0.22120200	-0.91908600	-0.38019000	C	-0.00042500	-0.51791900	0.19971200
C	0.14612000	0.42353700	-0.59560800	C	0.33445300	0.74768500	-0.35029300
C	-0.77989200	1.45138600	-0.32900700	C	-0.69759600	1.69523400	-0.58143000
C	-2.04963800	1.13950300	0.12462200	C	-2.02352800	1.38790300	-0.28765200
C	-2.41427200	-0.19639300	0.30942300	C	-2.35296900	0.03549000	0.09502200
C	1.44389800	0.77920100	-1.09129000	C	1.77520100	1.10979200	-0.68326100
C	2.60241400	-0.14675600	-1.12465700	C	2.71706500	0.05083100	-1.30973600
C	2.84275500	-1.00974400	0.13071100	C	2.93251800	-1.06788200	-0.32022000
O	3.12603200	-2.17714400	-0.01519600	O	2.05051400	-1.88935900	-0.13765000
C	2.73782800	-0.33994600	1.47302000	C	4.24938600	-1.13545600	0.40300600
H	-1.79170100	-2.25603100	0.20762000	H	-1.57944300	-1.82872400	0.84238200
H	0.48692900	-1.71862400	-0.57914200	H	0.79141600	-1.21919800	0.44244100
H	-0.43780800	2.47826800	-0.41222100	H	-0.44965100	2.66852300	-1.00130800
H	-2.75580600	1.93139700	0.34887200	H	-2.74576000	2.18593800	-0.14552100
H	1.51595100	1.70238400	-1.65614900	H	2.08889100	1.75241300	-1.36907900
H	2.48802700	-0.84260100	-1.96837600	H	1.96583700	-0.60755300	-2.93770700
H	3.51214000	0.43481900	-1.30554600	H	3.57828500	0.47758400	-1.50099500
H	2.90392700	0.74131000	1.41291400	H	5.04611700	-1.24680900	-0.34364900
H	1.70465600	-0.45967900	1.82209400	H	4.43534700	-0.20019000	0.94068300
H	3.39494800	-0.85365600	2.17540600	H	4.25990200	-1.98078200	1.09057400
O	2.10879800	2.56843800	0.70806100	O	2.98698700	2.02797200	1.73915800
H	2.80513300	2.96925800	0.16605400	H	3.91593500	1.75986600	1.65847300
O	-3.72835600	-0.51577400	0.77426700	N	-3.75937800	-0.38749700	0.15823000
C	-4.66757200	-0.33618800	-0.28899400	O	-4.00120400	-1.51744600	0.47940500
H	-5.60802100	-0.76361900	-0.01014200	O	-4.60882400	0.41424800	-0.11389900
H	-4.79363700	0.70890300	-0.48080700				
H	-4.30382700	-0.81947300	-1.17161800				
(31c-TS1)	*G* = -742.656059 a. u. (Gas phase)			**(32b-Int)**	*G* = -652.8139270 a. u. (Gas phase)		
	G = -742.695454 a. u. (In methanol)				*G* = -652.8403562 a. u. (In methanol)		
C	-1.32639300	-1.08961200	-0.30077200	C	-1.97741900	-1.22546400	0.04307800
C	0.00507300	-0.82618600	-0.58871100	C	-0.64232800	-1.05920100	-0.24356400
C	0.44768700	0.50672200	-0.69556900	C	-0.09031300	0.25823200	-0.31513800
C	-0.45819600	1.56248700	-0.47244200	C	-0.93752000	1.38754100	-0.08503900
C	-1.78016400	1.28848000	-0.16809200	C	-2.27377400	1.20690800	0.20429800
C	-2.21662600	-0.03639300	-0.09102600	C	-2.78660000	-0.09577700	0.26710800
C	1.80370500	0.82510500	-1.03655400	C	1.24438700	0.50527500	-0.61064200
C	2.92038800	-0.15073800	-0.99888600	C	2.31753200	-0.45767900	-0.86379000
C	2.99242300	-1.08222100	0.22814700	C	3.67276200	0.07201100	-0.28623600
O	3.24128800	-2.25325900	0.05181900	O	3.84257000	1.25799400	-0.19047100
C	2.77515500	-0.47243000	1.58549100	C	4.68037400	-0.97882500	0.07337400
H	-1.67183200	-2.11546800	-0.23494500	H	-2.40974300	-2.21839400	0.09780100
H	0.69674100	-1.64727400	-0.75515100	H	-0.01291400	-1.92500400	-0.42089500
H	-0.06744900	2.57526400	-0.46689800	H	-0.51206200	2.38538300	-0.14115500
H	-2.47284200	2.10065600	0.02328300	H	-2.92182400	2.05712700	0.38081300
H	1.97228600	1.76962100	-1.54251300	H	1.56786000	1.54741100	-0.65221500
H	2.86648300	-0.79994000	-1.88476400	H	2.09822500	-1.48386600	-0.56359400
H	3.86713600	0.39611100	-1.05524000	H	2.49411000	-0.46131300	-1.95533300
H	2.99084400	0.60163700	1.59876700	H	4.31591300	-1.55852300	0.92825000
H	1.70708600	-0.56068800	1.82016800	H	4.81709800	-1.67517300	-0.76070000
H	3.33352700	-1.04852300	2.32399300	H	5.62648800	-0.50322500	0.32829800
O	2.34947100	2.49476900	0.91164600	O	1.50199700	-0.14157300	1.90074600
H	3.11455900	2.88816300	0.46533700	H	1.36655400	0.78353400	2.01561600
N	-3.62238300	-0.32419400	0.22821900	O	-4.17188800	-0.28581700	0.56670900
O	-3.97051300	-1.47033500	0.28809300	C	-4.94194900	-0.15231300	-0.63082300

Atom	*x* / Å	*y* / Å	*z* / Å
O	-4.36501800	0.59863800	0.41605800

Atom	*x* / Å	*y* / Å	*z* / Å
H	-5.96508400	-0.38851100	-0.42514200
H	-4.87315100	0.85367300	-0.98881600
H	-4.56381000	-0.82220600	-1.37456600

(32a-Int) *G* = -538.341999 a. u. (Gas phase)
G = -538.373973 a. u. (In methanol)

C	-2.77360200	-1.36859300	-0.10328400
C	-1.43673600	-1.14767400	-0.34047500
C	-0.93323800	0.19056400	-0.37334400
C	-1.83033700	1.28338900	-0.15657000
C	-3.16790900	1.04802600	0.08306300
C	-3.63253000	-0.27386300	0.10876300
C	0.40046100	0.49232200	-0.61822000
C	1.51764800	-0.42542000	-0.84766800
C	2.83096600	0.14558000	-0.21525700
O	2.95200600	1.33543100	-0.09623300
C	3.86493100	-0.87222000	0.16402600
H	-3.16936400	-0.07830400	-2.3778290
H	-0.76901300	-1.98624800	-0.50829500
H	-1.44157100	2.29729700	-0.18311100
H	-3.85362100	1.87034100	0.24918500
H	-4.68583900	-0.46132700	0.29718600
H	0.68518600	1.54641900	-0.63315500
H	1.32742600	-1.46379200	-0.57041100
H	1.73176700	-0.40498000	-1.93228500
H	3.49359000	-1.47879300	0.99701400
H	4.05679600	-1.54952600	-0.67485300
H	4.78286100	-0.36550100	0.45890400
O	0.59581300	-0.18439700	1.89091000
H	0.42129900	0.73300900	2.01450100

(34a-TS) *G* = -862.788880 a. u. (Gas phase)
G = -62.8236322 a. u. (In methanol)

C	-5.03696800	-0.61053300	-0.55732900
C	-3.77429900	-1.19342100	-0.48185900
C	-2.65037700	-0.43777200	-0.12413800
C	-2.82002800	0.93164400	0.13058500
C	-4.08092800	1.51442700	0.05591600
C	-5.19562800	0.74661400	-0.28449200
C	-1.32961000	-1.09360700	-0.04818500
C	-0.27911700	-0.62778200	0.63638700
C	1.09814100	-1.28379700	0.82786200
O	1.49008300	-1.16189200	2.09975800
C	1.03870000	-2.76464800	0.37300000
N	2.09053600	-0.55594200	0.08388000
H	2.64986200	-0.27817800	0.91714100
C	3.03550100	-1.26343000	-0.84427000
C	3.87978200	-0.12554700	-1.39122400
C	2.83508400	0.95912100	-1.68512500
C	1.71260600	0.71815400	-0.64414300
H	-3.65452500	-2.25346300	-0.69174800
H	-1.95678300	1.54700100	0.37004900
H	-4.19308500	2.57586200	0.25498300
H	-1.25119900	-2.03911600	-0.58384500
H	-0.38532100	0.27810700	1.23418100
H	1.98618800	-3.25325500	0.61041600
H	0.79343400	-2.92572300	-0.68461300
H	0.26974200	-3.23609200	0.98502800
H	3.58528100	-2.01427000	-0.27862300
H	2.44583700	-1.74806400	-1.62645300
H	4.44694600	-0.41808400	-2.27668600
H	4.58601300	0.21516200	-0.62722300
H	3.24665600	1.96797800	-1.61594700
H	2.42014100	0.83407500	-2.68785700
H	0.73750700	0.57469700	-1.10563400
H	2.56831300	2.64261900	1.77246200
H	-6.17750400	1.20547300	-0.34431900

(32c-Int) *G* = -742.7429120 a. u. (Gas phase)
G = -742.7852963 a. u. (In methanol)

C	-1.73684200	-1.14672300	-0.28148600
C	-0.38098100	-0.99892800	-0.46057300
C	0.19834600	0.30862700	-0.44834300
C	-0.64366100	1.44738600	-0.24760300
C	-2.00114400	1.28517300	-0.06637200
C	-2.54047000	-0.00817300	-0.08389800
C	1.55593900	0.53742400	-0.63373600
C	2.62792200	-0.43896300	-0.83503800
C	3.94425800	0.04553500	-0.13983300
O	4.12741000	1.22441100	0.00600600
C	4.90247300	-1.03584100	0.26179600
H	-2.18976000	-2.13190400	-0.29116300
H	0.24458000	-1.87154100	-0.61691900

(34c-TS) *G* = -1067.241665 a. u. (Gas phase)
G = -1067.285873 a. u. (In methanol)

C	-4.27813500	-1.17576200	-0.61389100
C	-2.96054600	-1.52744800	-0.35522800
C	-2.08774500	-0.64620200	0.29799700
C	-2.56492600	0.61851800	0.67632500
C	-3.87664800	0.98790800	0.42550600
C	-4.71200100	0.07996500	-0.21504100
C	-0.70597900	-1.07745900	0.55429700
C	0.17531000	-0.46428500	1.35305700
C	1.56389800	-0.94078700	1.59551900
O	2.25065800	-0.36094600	2.41648300
C	2.06848600	-2.15562200	0.84942800
N	2.59033900	0.67972400	-0.43726900
H	2.48711700	0.75588000	-1.44987200

Atom	*x* / Å	*y* / Å	*z* / Å
H	-0.19739400	2.43765600	-0.23968000
H	-2.64550000	2.14261400	0.08725200
H	1.90021500	1.57358400	-0.61765800
H	2.36799400	-1.46909400	-0.58495900
H	2.88737500	-0.41323100	-1.90959900
H	4.46339500	-1.63357900	1.06778200
H	5.09012400	-1.70932800	-0.58110100
H	5.83466600	-0.58738500	0.60270300
O	1.60911300	-0.18998600	1.86824100
H	1.48183400	0.73378400	2.00170200
N	-3.98715500	-0.18388600	0.10878700
O	-4.43382400	-1.29680900	0.09123200
O	-4.66300900	0.79270000	0.27585100

(34b-TS) *G* = -977.2255453 a. u. (Gas phase)
G = -977.2550138 a. u. (In methanol)

C	4.40064700	1.40591300	-0.72823200
C	3.09648600	1.59270600	-0.30811500
C	2.39584700	0.58953700	0.38088200
C	3.06401800	0.63378600	-0.61278600
C	4.37465900	-0.81873500	0.22026000
C	5.05066200	0.19512500	-0.46633800
C	1.01503800	0.84291600	0.80042400
C	0.19167500	-0.00643700	1.43179100
C	-1.20400000	0.31299800	1.81022400
O	-1.90723500	-0.55780500	2.29524500
C	-1.72331000	1.71942600	1.59853500
N	-2.42430800	-0.37166600	-0.75198200
H	-2.44204800	-0.12296300	-1.73744200
C	-2.05705500	-1.80186300	-0.61749000
C	-3.29754300	-2.52716300	-0.05614700
C	-4.45651400	-1.59876300	-0.42615600
C	-3.78652100	-0.22765200	-0.22138600
C	-4.54454600	0.90275800	-0.86922100
O	-5.26701900	1.67929000	-0.29989900
O	-4.36049700	0.93839800	-2.21040600
H	4.94398300	2.17870100	-1.26113700
H	2.60010500	2.53716900	-0.51626100
H	2.55706500	-1.41100100	1.16710700
H	4.85741200	-1.76421600	0.43668200
H	0.64013800	1.83545500	0.55207100

Atom	*x* / Å	*y* / Å	*z* / Å
C	2.40161100	2.00181400	0.17172800
C	3.71320000	2.79559000	-0.05352900
C	4.77040300	1.70879800	-0.36432700
C	3.99436400	0.38254800	-0.14787600
C	4.52926000	-0.74770800	-0.98957000
O	5.26401700	-1.62235400	-0.60988700
O	4.11426900	-0.65642400	-2.27382100
H	-4.96532500	-1.84745800	-1.11331000
H	-2.59910900	-2.50561800	-0.65887500
H	-1.89957600	1.32612600	1.15934600
H	-4.26163800	1.95991200	0.70820100
H	-0.40571800	-1.99024800	0.04197900
H	-0.08060500	0.43078700	1.91554400
H	3.12879500	-2.29228400	1.06811300
H	1.92886000	-2.02356500	-0.22717700
H	1.52047100	-3.05073500	1.16410100
H	1.51649900	2.48732700	-0.24651000
H	2.23453700	1.84460000	1.24333500
H	3.97931200	3.38474300	0.82726300
H	3.61520200	3.48816500	-0.89370100
H	5.10063100	1.77554700	-1.40586000
H	5.65426200	1.76992800	0.27381800
H	4.06731800	0.07182000	0.89980900
H	4.52372100	-1.39953900	-2.75046100
N	-6.10362000	0.46793600	-0.48698000
O	-6.81323400	-0.34417400	-1.05132700
O	-6.45759700	1.57662100	-0.13049400

(36b-TS) *G* = -977.2232340 a. u. (Gas phase)
G = -977.2542333 a. u. (In methanol)

C	4.27058100	-1.10280400	0.85450500
C	2.88208700	-1.14174700	0.76463800
C	2.17449700	-0.11296400	0.12900200
C	2.89064400	0.97268500	-0.39804100
C	4.27641500	1.01276300	-0.30592600
C	4.97167300	-0.02584300	0.31657600
C	0.71128400	-0.20104800	0.04803300
C	-0.07758600	0.52986300	-0.75627900
C	-1.52515200	0.36094900	-0.85203200
O	-2.12684700	2.64202500	-0.59431400
C	-2.14537100	0.58719400	-2.15355100
N	-2.24931000	0.03525700	0.21365500
C	-1.86247300	0.49536000	1.57696800
C	-3.16714100	1.05492800	2.13292200
C	-4.21684100	0.11598100	1.54431700
C	-3.72366600	-0.03288800	0.09864800
C	-4.23302400	-1.32452800	-0.52652800
O	-5.35692200	-1.42679100	-0.93556500
O	-3.38294600	-2.36757700	-0.53901800
H	4.80361300	-1.91101300	1.34511300
H	2.33601600	-1.98313700	1.18380700
H	2.35995900	1.79843900	-0.86215700
H	4.81778800	1.86103400	-0.71253600
H	0.25325300	-0.95430500	0.68931500
H	0.32862700	1.24238700	-1.46695500

Atom	*x* / Å	*y* / Å	*z* / Å	Atom	*x* / Å	*y* / Å	*z* / Å
H	0.49643400	-1.01575800	1.69848900	H	-1.99768600	3.58406000	-0.44333700
H	-2.73186300	1.79288500	2.00751300	H	-3.06514300	0.04422600	-2.36027400
H	-1.75095600	1.93358500	0.52597100	H	-2.35981100	1.71550900	-1.90266600
H	-1.07835600	2.45659400	2.08659700	H	-1.43722000	0.50414100	-2.97554500
H	-1.76472000	-2.20258700	-1.59382800	H	-1.49171300	-0.34716700	2.17068800
H	-1.20392400	-1.91056800	0.05817200	H	-1.09307600	1.26013500	1.46435500
H	-3.21730300	-2.59181500	1.03311700	H	-3.29776800	2.06278400	1.72742800
H	-3.41176600	-3.53781700	-0.45594400	H	-3.17239800	1.08136100	3.22462500
H	-4.73582700	-1.71639900	-1.48021200	H	-4.20833300	-0.85518100	2.05497200
H	-5.34539800	-1.73670900	0.19405900	H	-5.23411100	0.50794900	1.56499300
H	-3.74412600	-0.01168400	0.85029200	H	-4.06680900	0.81934700	-0.49558000
H	-4.90199700	1.67566600	-2.54182700	H	-2.51703000	-2.08720800	-0.20694600
O	6.32627700	0.09909700	-0.91338000	O	6.39780100	0.02170300	0.41037500
C	7.01872600	-1.10570800	-0.66603000	C	6.97252400	-0.68281100	-0.69337100
H	8.01055000	-0.97801700	-1.09868100	H	8.03913900	-0.61320900	-0.64450100
H	7.11176000	-1.29736400	0.40952900	H	6.67990900	-1.71116800	-0.65143500
				H	6.62856100	-0.25120900	-1.61005500
(36a-TS)	*G* = -862.7869580 a. u. (Gas phase)			**(36c-TS)**	*G* = -1067.239282 a. u. (Gas phase)		
	G = -862.8228895 a. u. (In methanol)				*G* = -1067.283682 a. u. (In methanol)		
C	5.01272400	-1.44161200	0.48955600	C	4.00851700	-1.33981800	0.31116300
C	3.62191400	-1.41591800	0.43960400	C	2.61705400	-1.34121700	0.27461300
C	2.94068600	-0.28078400	-0.01921100	C	1.90677500	-0.18564600	-0.07648800
C	3.68670200	0.84237600	-0.40811600	C	2.62428100	0.98404500	-0.37023000
C	5.07489900	0.81758000	-0.35569100	C	4.01313600	0.98606000	-0.33111600
C	5.74305800	-0.32491700	0.08912200	C	4.71037300	-0.17590100	0.00548800
C	1.47346100	-0.30220800	-0.06499900	C	0.43998700	-0.23605900	-0.11246300
C	0.69434300	0.56571200	-0.73069700	C	-0.36436300	0.66948600	-0.69252700
C	-0.76096900	0.46591500	-0.80318100	C	-1.81779600	0.54365500	-0.76212800
O	-1.26131900	2.70657000	-0.20245000	O	-2.36093200	2.71058100	0.03862000
C	-1.40553100	0.90031400	-2.03835200	C	-2.48377600	1.07085400	-1.94886500
N	-1.46949900	0.01681400	0.22757700	N	-2.50621000	-0.01066700	0.23033400
C	-1.02818000	0.26080400	1.62959900	C	-2.05656100	0.11836100	1.64494600
C	-2.29358400	0.78205900	2.30146500	C	-3.32636300	0.54949600	2.37026300
C	-3.39619900	-0.02275400	1.61848300	C	-4.41783300	-0.21649500	1.62736400
C	-2.94793400	0.02042800	0.15133000	C	-3.98505100	-0.03370700	0.16632600
C	-3.52632400	-1.14780700	-0.63563500	C	-4.54554800	-1.14058000	-0.71645300
O	-4.66389200	-1.14843800	-1.01885200	O	-5.68654200	-1.13302200	-1.08927000
O	-2.72049100	-2.20879100	-0.82454600	O	-3.71867900	-2.16225200	-1.00492400
H	5.52484100	-2.33126500	0.84208200	H	4.54333900	-2.24535600	0.57946800
H	3.05296600	-2.28825400	0.75131200	H	2.07034200	-2.25030900	0.51228900
H	3.17835000	1.74547000	-0.73200000	H	2.09321100	1.90052200	-0.60884500
H	5.63976900	1.69508200	-0.65384000	H	4.55579200	1.89900700	-0.55479700
H	6.82750300	-0.33944700	0.13000400	H	-0.00820100	-1.11159800	0.35763300
H	1.00194100	-1.12269100	0.47621100	H	0.02847800	1.52197700	-1.23722500
H	1.11059800	1.35784100	-1.34472000	H	-2.20621300	3.59091500	0.39636400
H	-1.08958000	3.61154900	0.07759400	H	-3.42214300	0.60064900	-2.23505300
H	-2.35199700	0.42717000	-2.29106900	H	-2.66448500	2.11331400	-1.43637700
H	-1.56668000	1.98776000	-1.62180100	H	-1.81035400	1.17147400	-2.79764600
H	-0.72336100	0.91065800	-2.88604800	H	-1.68051900	-0.84249300	2.01260200
H	-0.67682700	-0.67167400	2.08441200	H	-1.27631000	0.87970500	1.67810500
H	-0.23122400	1.00490700	1.60300500	H	-3.45164900	1.62509800	2.21327500
H	-2.39331800	1.84200200	2.04880800	H	-3.28818200	0.32362600	3.43800300
H	-2.26890300	0.65087400	3.38531200	H	-4.40964400	-1.27924700	1.90028800
H	-3.41415000	-1.05708000	1.98433100	H	-5.42506100	0.17168600	1.78134900

Atom	*x* / Å	*y* / Å	*z* / Å
H	-4.39558500	0.39939800	1.72765600
H	-3.27131700	-0.30348100	0.96156000
H	-1.83530500	-2.01141500	-0.48369700

Atom	*x* / Å	*y* / Å	*z* / Å
H	-4.33331900	0.93639600	-0.20078200
H	-2.83469900	-1.97583800	-0.65489800
N	6.17975100	-0.16723100	0.04735700
O	6.74971700	0.87001600	-0.14674500
O	6.74991500	-1.19775400	0.27394900

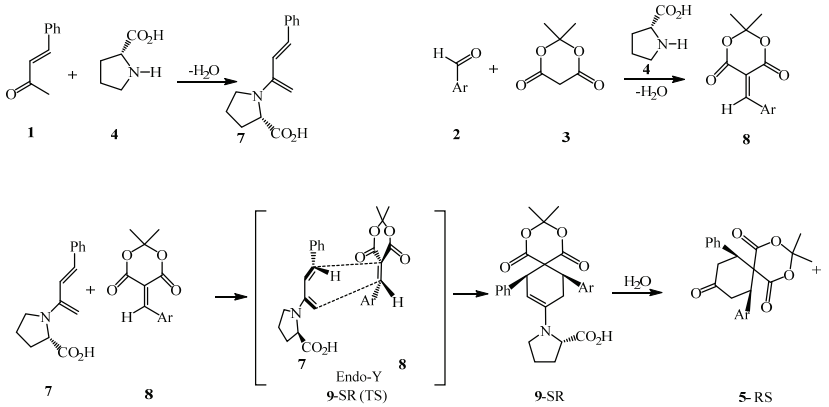

Scheme S-1. Mechanism of multicomponent domino Knoevenagel/Diels–Alder reaction.

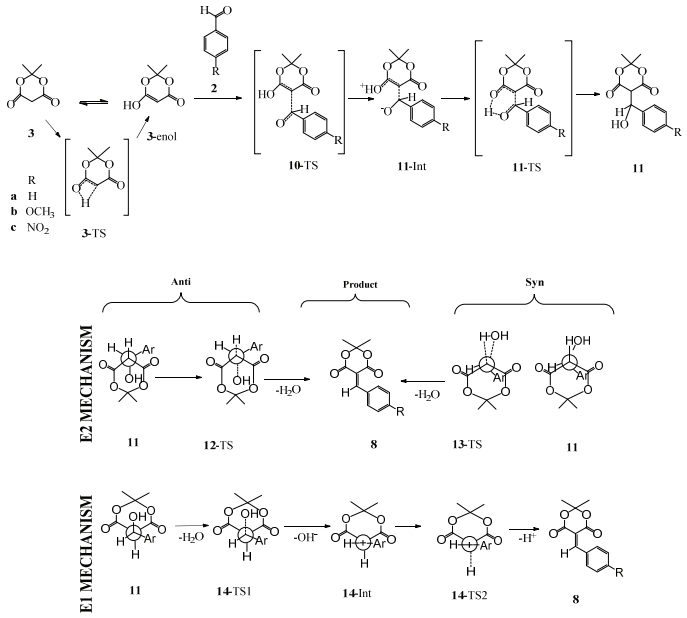

Scheme S-2. Mechanism of knoevenagel reaction to produce dienophile **8**.

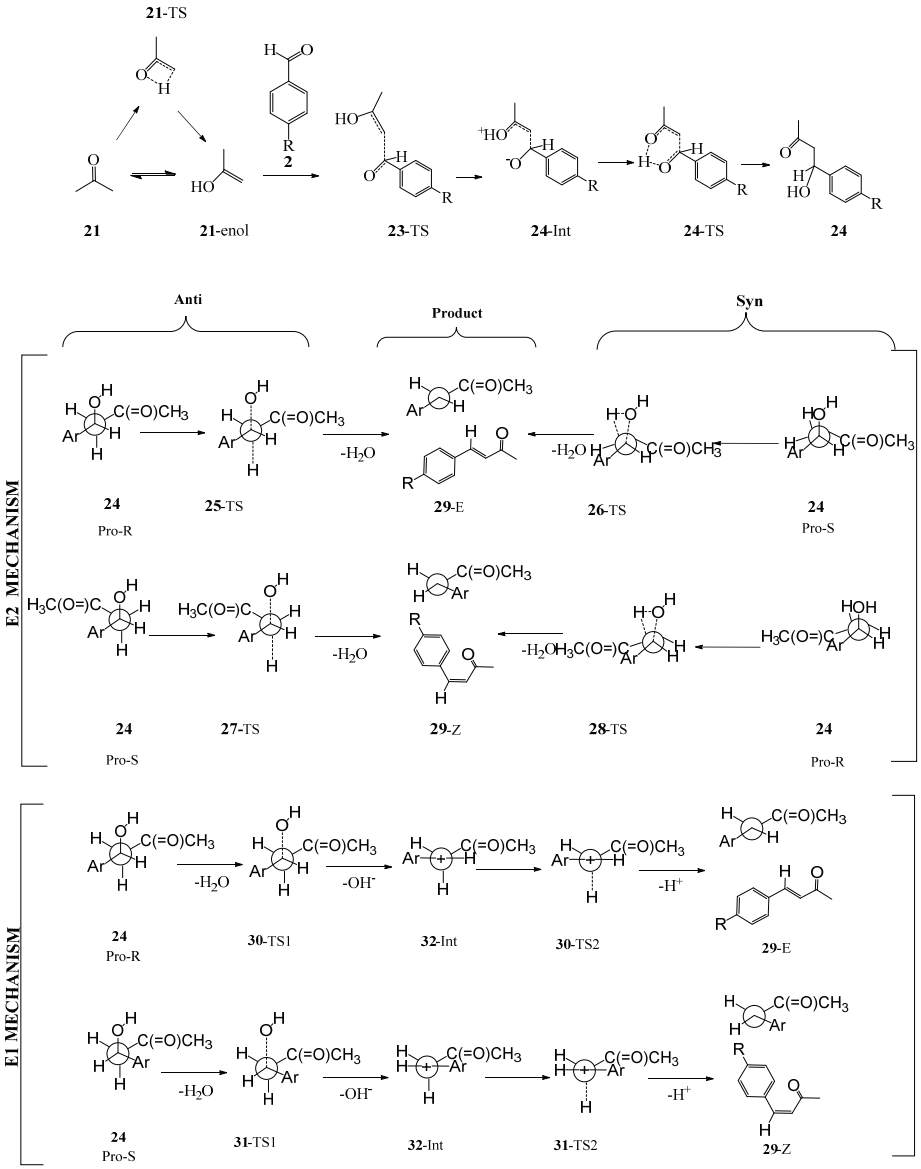

Scheme S-3. Mechanism of aldol reaction to produce compound **22**.

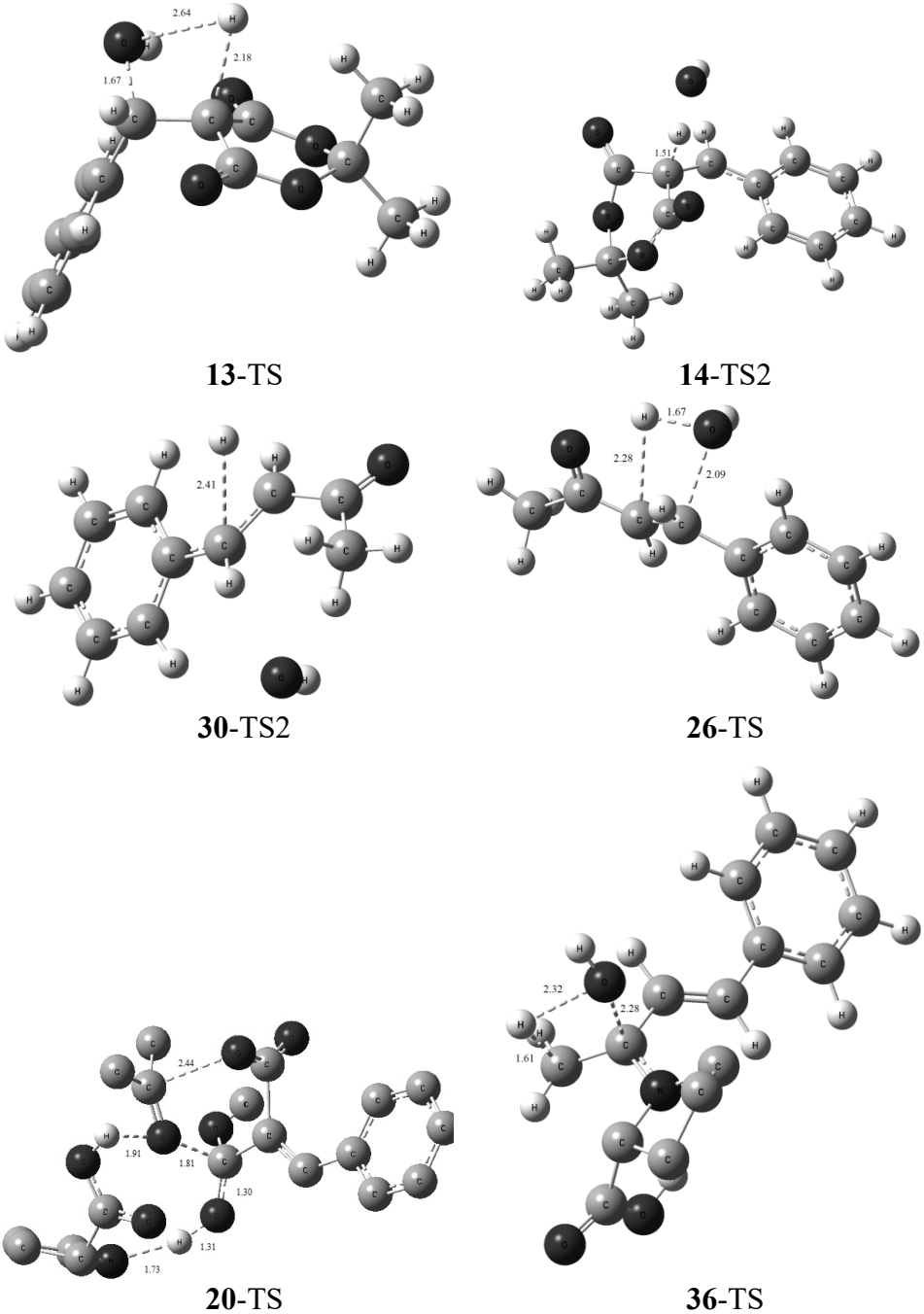

Fig. S-1. Optimized structures of selected transition states involved in Knoevenagel step of reaction (Bond lengths in Å).

Journal of the Serbian Chemical Society
JSCS-info@shd.org.rs • www.shd.org.rs/JSCS
J. Serb. Chem. Soc. *86* (11) 1067–1074 (2021)
JSCS–5483
Original scientific paper
Published 14 September 2021

IR detection of the methane halides fluid-like state at ambient conditions

IOSIF GRINVALD* and ROSTISLAV KAPUSTIN

Nizhny Novgorod State Technical University n.a. R.E. Alekseev Minin str. 24, 603950 Nizhniy Novgorod, Russia

(Received 26 April, revised 24 June, accepted 28 June 2021)

Abstract: The paper presents the IR-study of the fluid-like state, generated at ambient conditions, for methane halides (iodomethane, tetrachloromethane, trichloromethane and dichloromethane). It was shown that at vapor compression-extension procedure realized in variable thickness spectral cell (VTOC), the dual phase state exhibiting both gas and liquid properties arises. A reversible transition from a gas-like to a liquid-like shape, independent on the thermodynamic characteristics of the studied methane halides, was revealed.

Keywords: dual phase state; phases transition.

INTRODUCTION

Fluid is a unique phase state of matter generating under supercritical conditions and combining the properties of gas and liquid. It is conventional to divide fluid state into gas-like and liquid-like shapes, depending on which properties prevail in them. However, this definition is ambiguous due to the continuous nature of the transition between these two states.[1,2]

Supercritical fluids have many applications in industry, largely due to their tunable density, for example, they are used as environmentally friendly solvents for hazardous waste cleanup. However, the same properties that make fluids useful also make their generation quite difficult. Besides the high pressures and temperatures required, chemically active fluids can corrode many components of the experimental apparatus. Therefore, the formation of supercritical fluids is generally limited to the simplest compounds – water and carbon dioxide.[3,4]

One of the most perspective methods of fluid study seems to be IR-spectroscopy since it clearly shows the transition of gaseous properties to liquid ones, with all accompanying transformations. However, IR study of fluids behavior and their liquid-like to gas-like state transitions are presented only in a few works

* Corresponding author. E-mail: grinwald@mts-nn.ru
https://doi.org/10.2298/JSC210426048G

to date.[5,6] Nevertheless, what has already been published is thought-provoking. For example, in supercritical water the broad band of stretching O–H vibrations typical for liquid water or the bands with rotational structure of gaseous state are not observed at all. Instead, the P-, Q-, R-branches appear (for dilute gas-like fluid state) and then transform into non-broadened bands (for dense liquid-like fluid state).[7]

This effect is similar to the transformation in IR spectra of some organic species at liquid–gas transition observed at ambient conditions.[7] For example, in the gas phase spectrum of benzene the band of C–H bond out-of-plane bending vibrations has the P-, Q-, R-branches. In the spectrum recorded for liquid benzene in thin layer between optical windows three unresolved components resembling the mentioned branches are observed.[8] The gaseous spectrum of iodomethane manifests two band shapes for each vibration with the C–H bond participation. The first of them has a gas-like rotational structure, and the second one has a single counter like in liquid.[8] The analogous picture was revealed for the C–Cl stretching in the gaseous spectrum of tetrachloromethane.[9]

The presented data indicate on the fact that the organic substances can demonstrate, at ambient conditions, a combination of gas and liquid properties. Therefore, it was reasonable to formulate the aim of this work, to generate at ambient conditions and to study by IR method the phase state that has fluid features, which could be defined by the term “fluid-like state”. According to this problem we have obtained and analyzed IR spectral data relating to fluid-like state of iodomethane, tetrachloromethane, trichloromethane and dichloromethane.

EXPERIMENTAL

For the fluid-like phase generation, the variable thickness IR optical cell was applied (here we use the abbreviation VTOC). In Fig. 1 the projection on the left side shows the optical design of the cell, and the projection on the right side shows the design for controlling the thickness of the cell. The cotton balls, soaked in liquid, were put inside two stainless steel

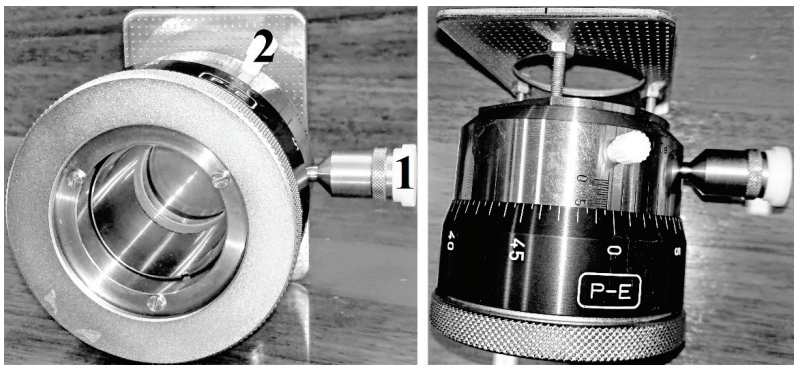

Fig. 1. The VTOC for the fluid-like state generation and detection. 1 – stainless steel funnel; 2 – Luer plug.

funnels with the plastic lids (Fig.1, (1)) to initiate the evaporation process. After the vapor inside the cell reached the required concentration, which was monitored by IR spectroscopy, the funnels were replaced with the Luer plugs (Fig.1, (2)).

The formation of the dual gas-liquid state occurred under the compression-extension procedure of the cell inter-window distance from 6 to 1 mm and in reverse. The optimal evaporation time required for the fluid-like state formation highly depends on the compound type and varies from 2 to 70 h. Experimental data for the selected samples is listed in the Table I, as well as their boiling temperatures.[10] For the spectral detection of the generated state, IR spectra recorded in VTOC were compared with those obtained in a gas cell (for gas phase) and between optical KBr windows (for liquid state) at 23 °C.

TABLE I. The optimal time for the fluid-like state formation and the boiling point of the selected compounds

Parameter	CH_3I	CCl_4	$CHCl_3$	CH_2Cl_2
t / h	70	2	12	26
T / oC	42.5	76.7	71.3	39.8

IR-spectra were recorded by IR-Fourier spectrometer FSM 1202 (InfraSpec Co.) in 4000–500 cm^{-1} range with 2 cm^{-1} resolution by 60 scans. The spectra fragments in the figures are given with the wavenumber's axis extension accordingly to original recording of the spectral device. The VTOC used with KBr windows was manufactured by Perkin-Elmer Co. The purity of halides was not less than 99 % as it was confirmed by chromato-mass spectrometry data obtained by GCMS-QP2010 Plus spectrometer (Shimadzu Co. Inc.).

RESULTS AND DISCUSSION

Iodomethane

In the spectrum region of iodomethane bending (H–C–H) vibrations, recorded at 6 mm thickness (Fig. 2, spectrum 1), the gas-like phase bands at 1263, 1241 cm^{-1} (Fig. 2, band A, B) as well as a broad band with rotational structure at 1426 cm^{-1} (Fig. 2, band C), were observed. Since the IR spectra of regular gases cannot be observed at such distance between optical windows, the appearance of two band types, with rotational structure and without it, corresponding to the same vibration, can occur owing to the formation of two differently built systems in gas-like state. Taking this conception, the band with the rotational structure assigns to bonded molecules with flatter geometry of (CH_3)-fragment, arising due to the iodine atom shift in the cluster. In this shape, it is not the molecule as a whole that rotates, but the (CH_3)-group, because the iodine atom is bound under the intermolecular binding. Two single bands in gas-like state can be referred to the unbonded shape, in which the initial geometry of the molecule remains.

In the spectrum 2 (Fig. 2), recorded after the compression of inter-window distance to 1 mm, the band C with rotational structure and band A at 1260 cm^{-1}, which coincides in its position with the liquid phase band (Fig. 2, spectrum 3), remain. The rotational structure of the band C unambiguously indicates the formation of state with gaseous properties in the thin layer. After the extension of

the inter-window distance up to 6 mm, the spectrum has transformed instantly to the shape of spectrum 1 and returned to the spectrum 2 after the compression of the inter-window distance to 1 mm. Similar reversible transitions from a gas-like to a liquid-like state and back is typical for supercritical fluids when their density varies.

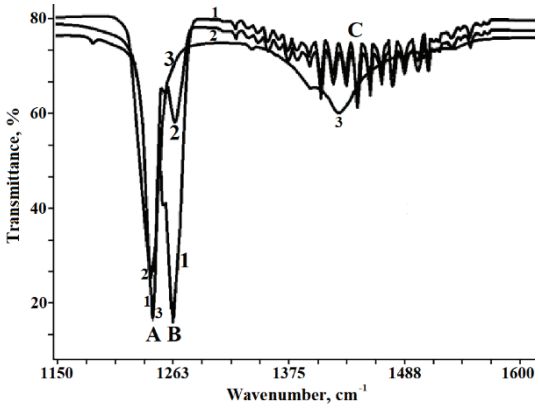

Fig. 2. Fragment of iodomethane spectra in H–C–H bending region. 1 – spectrum at 6 mm VTOC thickness; 2 – spectrum at 1 mm VTOC thickness; 3 – spectrum of liquid between KBr windows; A – band assigning to gas and liquid phases; B – band assigning to gas phase; C – band assigning to gas (with rotational structure) and liquid phases.

Tetrachloromethane

The gas-like state bands at 795 and 779 cm^{-1} (Fig. 3, bands A, D), assigning to the C–Cl bond stretching vibrations of tetrachloromethane, are observed in spectrum 1 (at the 6 mm optical distance). These bands have a different counter view: band A consists of several non-resolved components, and band D is a single band.

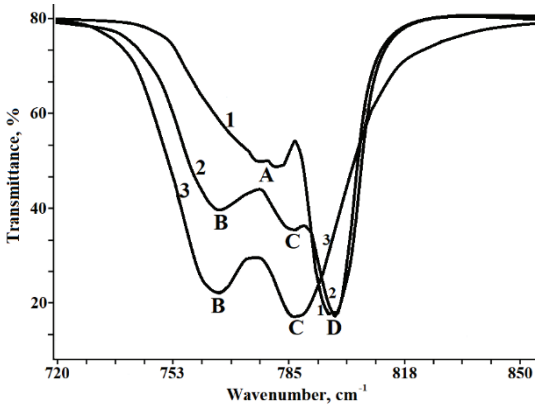

Fig. 3. Fragment of tetrachloromethane spectra in C–Cl stretching region. 1 – spectrum at 6 mm VTOC thickness; 2 – spectrum at 1 mm VTOC thickness; 3 – spectrum of liquid between KBr windows; A – band assigning to gas phase; B, C – bands assigning to liquid phase; D – band assigning to gas phase.

The arising of two C–Cl stretching bands instead of one band in accordance with selection rules (T_d symmetry point group) can be explained assuming the formation of different molecular structures in gas-like state as in the previous

case. The single band can be assigned to unbonded molecules, and the multi-component one – to the cluster shape, forming with chlorine atom shift under intermolecular binding, in which (CCl_3)-group rotates.

In spectrum 2 (Fig. 3) recorded at optical distance 1 mm, the gas-like state band D at 797 cm^{-1} and the liquid-like state bands C, B at 784 and 761 cm^{-1}, respectively, are observed. This spectrum changes negligibly after opening the cell ports. The spectrum recorded in a thin liquid layer between KBr windows (Fig. 3, spectrum 3) exhibits bands C and B at 788 and 765 cm^{-1}, respectively. The following optical distance extension up to 6 mm leads to the rapid reversible transition of the spectrum 2 into the gas-like spectrum 1 as it was observed for iodomethane. Since the boiling point of tetrachloromethane is relatively high, while the inter-window space available for evaporation is too small, the observed transformation of spectra cannot be caused by subsequent evaporation and condensation of the substance. Also taking into account that the small thickness of the cell excludes the IR manifestation of a regular gas spectra, this state can also be defined as fluid-like.

Dichloromethane

In the spectra of dichloromethane at the 6 mm optical distance, the gas-like state bands C, B **(**Fig. 4, spectrum 1) at 764 and 750 cm^{-1}, assigning to C–Cl bond stretching vibrations, are revealed. In the spectrum recorded at 1 mm VTOC thickness (Fig. 4, spectrum 2), the gas-like state band at 764 cm^{-1}, and the non-resolved liquid-like state band at 748 cm^{-1} were observed. The spectrum changes negligibly after opening the cell ports. The clearly manifested band A at 742 cm^{-1} is shown in spectrum 3 recorded in the thin layer of liquid between optical windows at ambient conditions.

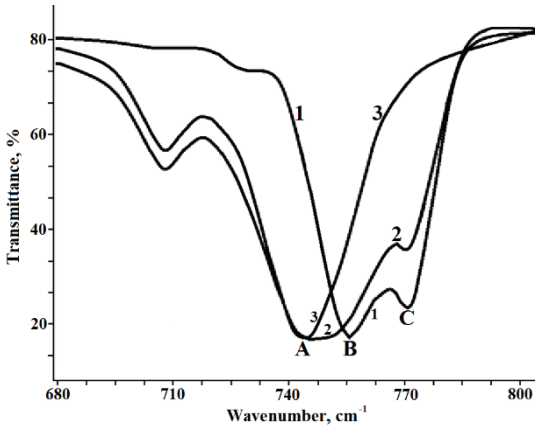

Fig. 4. Fragment of dichloromethane spectra in C-Cl stretching region. 1 – spectrum at 6 mm VTOC thickness; 2 – spectrum at 1 mm VTOC thickness; 3 – spectrum of liquid between KBr windows; A – band assigning to liquid phase; B, C – bands assigning to gas phase.

After the optical distance extension up to 6 mm, the gas-like state bands reappear, while the liquid-like state band is absent. Since, as already discussed,

the synchronous condensation-evaporation mechanism is less possible here, the presented IR data justify the fluid-like state formation.

Trichloromethane

The generation of the similar fluid-like state was spectrally confirmed under the VTOC compression-extension procedure for both trichloromethane (Fig. 5) and trichloromethane-d (Fig. 6). However, this pair of substances has some differences from other samples.

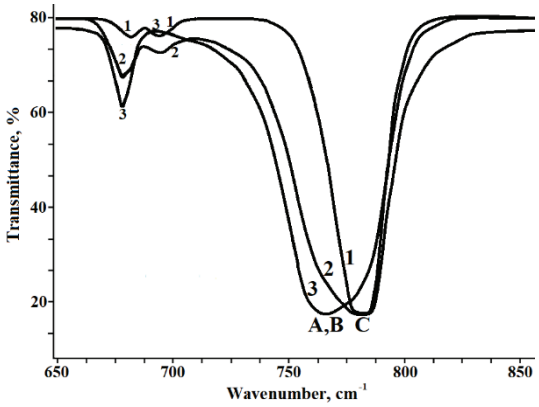

Fig. 5. Fragment of trichloromethane spectrum in C–Cl stretching region. 1 – spectrum at 6 mm VTOC thickness; 2 – spectrum at 1 mm VTOC thickness; 3 – spectrum of liquid between KBr windows; A, B – bands assigning to liquid phase; C – band assigning to gas phase.

A single gas-like state band C was detected in the spectrum recorded at 6 mm of VTOC thickness (Figs. 5 and 6, spectrum 1). The non-resolved liquid-like state bands A, B and the gas-like state band C assigning to C–Cl bond stretching vibrations were detected at 1 mm (Figs. 5 and 6, spectrum 2). The spectrum of liquid trichloromethane between KBr windows is presented as well (Fig. 5, spectrum 3).

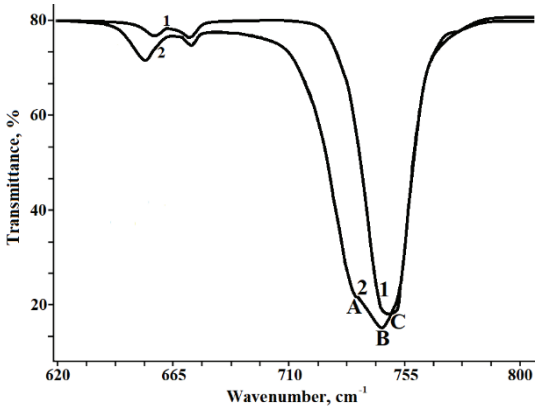

Fig. 6**.** Fragment of trichloromethane-d spectra in C-Cl stretching region. 1 – spectrum at 6 mm VTOC thickness; 2 – spectrum at 1 mm VTOC thickness; A – band assigning to liquid phase; B – band assigning to liquid phase; C – band assigning to gas phase.

The overlapping shape of the C–Cl stretching liquid bands' components can be caused by the formation of intermolecular hydrogen bond leading to the hydrogen atom shift,[11] unlike the molecular transformations with the participation of halogen atoms, causing stronger separation of C–Cl stretching bands in other systems.

CONCLUSION

The obtained data obviously indicate a phase state formation having a lot of similarities with the supercritical fluids; therefore, it can be defined as a "fluid-like state". There are at least three main reasons for this conclusion. First, the spectrum of a true gas cannot be recorded at such a small thickness of the optical cell, as it was confirmed by many data of spectral practice. Second, there seems to be no dependence of the fluid-like state formation rate on the compound boiling point. Third, the gas–liquid state transition occurs rapidly and reversibly at compression–extension procedure, like in known fluid systems. Besides, this state remains inside the cell even without any tightness (when the plugs are removed), what would be impossible for regular gas.

It can be assumed that two different types of molecular structure – with unbonded molecules and a cluster shape, arising in the near-surface area (near optical window), are involved in the generation of the fluid-like state. Cluster shapes of molecules combine to form a dense layer, and unbonded molecules, being located around, maintain the required pressure, preventing the layer from disintegrating.

Thus, the obtained results confirm that the state with dual gas–liquid properties, or fluid-like state in other words, can be generated at ambient conditions not only for simple inorganic species, but also for organic systems.

ИЗВОД

ДЕТЕКЦИЈА ХАЛИДА МЕТАНА У СТАЊУ СЛИЧНОМ ТЕЧНОМ, ПРИ АМБИЈЕНТАЛНИМ УСЛОВИМА, ИНФРАЦРВЕНОМ СПЕКТРОСКОПИЈОМ

IOSIF GRINVALD и ROSTISLAV KAPUSTIN

Nizhny Novgorod State Technical University n.a. R.E. Alekseev Minin str. 24, 603950 Nizhniy Novgorod, Russia

У овом раду представљено је испитивање стања сличног течном, генерисаног при амбијенталним условима, за халиде метана (јодометан, тетрахлорометан, трихлорометан и дихлорометан) IC спектроскопијом. Показано је да при процедури компресије––ширења паре у спектралној ћелији променљиве дебљине, долази до формирања стања дуалне фазе које показује особине и гасова и течности. Утврђен је реверзибилни прелаз из облика сличног гасу у облик сличан течности, независно од термодинамичких карактеристика испитиваних халида метана.

(Примљено 26. априла, ревидирано 24. јуна, прихваћено 28. јуна 2021)

REFERENCES

1. E. S. Alekseev, A. Yu. Alentiev, A. S. Belova, V. I. Bogdan, T. V. Bogdan, A. V. Bystrova, E. R. Gafarova, E. N. Golubeva, E. A. Grebenik, O. I. Gromov, V. A. Davankov, S. G. Zlotin, M. G. Kiselev, A. E. Koklin, Y. N. Kononevich, A. E. Lazhko, V. V. Lunin, S. E. Lyubimov, O. N. Martyanov, I. I. Mishanin, A. M. Muzafarov, N. S. Nesterov, A. Yu. Nikolaev, R. D. Oparin, O. O. Parenago, O. P. Parenago, Y. A. Pokusaeva, I. A. Ronova, A. B. Solovieva, M. N. Temnikov, P. S. Timashev, O. V. Turova, E. V. Filatova, A. A. Philippov, A. M. Chibiryaev, A. S. Shalygin, *Russ. Chem. Rev.* **89** (2020) 1337 (http://doi.org/10.1070/rcr4932)
2. K. Tutek, A. Masek, A. Kosmalska, S. Cichosz, *Polymers* **13** (2021) 729 (http://doi.org/10.3390/polym13050729)
3. F. Maxim, K. Karalis, P. Boillat, D. T. Banuti, J. I. Marquez Damian, B. Niceno, C. Ludwig, *Adv. Sci.* **8** (2021) 2002312 (http://doi.org/10.1002/advs.202002312)
4. T. Wu, B. Han, in *Green Chemistry and Chemical Engineering. Encyclopedia of Sustainability Science and Technology Series*, B. Han, T. Wu, Eds., Springer, New York, 2019, p.173 (http://doi.org/10.1007/978-1-4939-9060-3_391)
5. G. N. Pack, M .C. Rotondaro, P. P. Shah, A. Mandal, S. Erramilli, L. D. Ziegler, *Phys. Chem. Chem. Phys.* **21** (2019) 21249 (http://doi.org/10.1039/c9cp04101j)
6. N. J. Hestand, S. E. Strong, L. Shi, J. L. Skinner, *J. Chem. Phys.* **150** (2019) 054505 (http://doi.org/10.1063/1.5079232)
7. B. K. Smith, *Infrared Spectral interpretation, a systematical approach*, CRC Press, Boca Raton, FL, 1999, p. 266 (http://www.doi.org/10.1201/9780203750841)
8. I. I. Grinvald, I. Yu. Kalagaev, A. N. Petukhov, R. V. Kapustin, *Rus. J. Phys. Chem*., *A* **93** (2019) 69 (http://doi.org/10.1134/S0036024419130107)
9. I. Grinvald, I. Kalagaev, A. Petukhov, A. Vorotyntsev, R. Kapustin, *Struct. Chem*. **30** (2019) 1659 (http://doi.org/10.1007/s11224-019-01349-2)
10. R. M. Stephenson, S. Malanowski, *Handbook of the Thermodynamics of Organic Compounds*, Springer, Dordrecht, 1987, p. 552 (http://doi.org/10.1007/978-94-009-3173-2)
11. I. I. Grinvald, I. Yu. Kalagaev, A. N. Petukhov, A. I. Grushevskaya, R. V. Kapustin, I. V. Vorotyntsev, *J. Struct. Chem.* **59** (2018) (http://doi.org/10.1134/S0022476618020087).

Journal of the Serbian Chemical Society
JSCS-info@shd.org.rs • www.shd.org.rs/JSCS
J. Serb. Chem. Soc. *86* (11) 1075–1087 (2021)
JSCS–5484
Original scientific paper
Published 14 September 2021

Electrodeposition of aluminum-doped thin silicon films from a KF–KCl–KI–K_2SiF_6–AlF_3 melt

MICHAEL V. LAPTEV, ANASTASIA O. KHUDOROZHKOVA, ANDREY V. ISAKOV*, OLGA V. GRISHENKOVA, SERGEY I. ZHUK and YURII P. ZAIKOV

Ural Branch of the Russian Academy of Sciences, Institute of High Temperature Electrochemistry, 20 Academicheskaya St., 620137 Ekaterinburg, Russian Federation

(Received 17 September 2020, revised 16 August, accepted 17 August 2021)

Abstract: The regularities of silicon and aluminum co-deposition on glassy carbon from KF–KCl (2:1)–75 mol % KI–0.15 mol % K_2SiF_6–(up to 0.15 mol %) AlF_3 melts at 998 K were studied by cyclic voltammetry, chronoamperometry, scanning electron microscopy, atomic force microscopy and Raman spectroscopy. The cyclic voltammograms demonstrated the presence of only one cathodic peak (or nucleation loop at a low reverse potential) and the corresponding anodic peak. The cathodic peak shifted in the cathodic direction with decreasing concentration of aluminum ions in the melt or with increasing scan rate. The Scharifker–Hills model was used to analyze potentiostatic current density transients and estimate the values of the apparent diffusion coefficient and the number density of nuclei. The morphology and elemental analysis of the samples obtained during potentiostatic and galvanostatic deposition for 30–60 s were studied. Continuous thin silicon films doped with aluminum were obtained under galvanostatic conditions.

Keywords: molten salts; co-deposition; kinetics; 3D nucleation/growth.

INTRODUCTION

Silicon is the dominant source material for the production of electronic devices, solar cells and anode materials for Li-ion batteries (LIBs) because it is an intrinsic semiconductor and has excellent physicochemical properties and stability.[1,2] The use of thin Si films improves the characteristics of photovoltaic devices and advanced LIBs. In particular, thin-film silicon solar cells compensate for many of the disadvantages of conventional ones and expand the range of applications.[2,3] Thin Si films improve cycle stability and rate capabilities of the batteries and retain the structural integrity of the anodes during operation.[4]

* Corresponding author. E-mail: ihte_uran@mail.ru
https://doi.org/10.2298/JSC200917065L

There are various ways for producing thin Si films, *e.g*. plasma-enhanced chemical vapor deposition (PECVD) and liquid phase crystallization (LPC) are widespread.[5–8] Electrodeposition from molten salts is a promising method for producing thin silicon films due to the simplicity of the process, and the low capital and operating costs.[9–19] In addition, high deposition rates of continuous silicon layers and the ability to control the structure and morphology of films are the advantages of this technique.

Suitable process media are silicon-containing melts based on alkali metal halides. In particular, the molten KF–KCl–K_2SiF_6 mixture is a good electrolyte for obtaining continuous Si films.[10,14–18] Stability in the silicon concentration, relatively low operating temperatures (from 923 K), solubility in water, and less aggressiveness in comparison with pure fluoride melts are important advantages of this electrolyte. Partial replacement of KF–KCl with potassium iodide contributes to an additional decrease in the aggressiveness of the melt and the liquidus temperature. In addition, a decrease in the electrical conductivity of melts with KI provides for the formation of more compact deposits.[20–22] Thin (≈600 nm for 1-2 min) continuous silicon films with good adhesion are formed on glassy carbon and tungsten substrates during electrodeposition from a KF–KCl (2:1)––75 mol % KI–0.5 mol % K_2SiF_6 melt.[23]

Electrolytes based on KF–KCl–K_2SiF_6 and KF–KCl–KI–K_2SiF_6 can also be used to obtain doped silicon films by co-deposition of silicon with a selected dopant (*e.g*., P, B, Al). Apparently, this approach can be useful for the manufacture of silicon films (n-type, p-type and p–n junction) with various thicknesses and surface morphologies, which is important for the simplified production of photovoltaic and optoelectronic devices. For example, high-quality tin-doped silicon films with n-type semiconductor behavior (a photocurrent up to 44 % that of a commercial n-type Si wafer) from the KCl–KF–1 mol % K_2SiF_6 melt containing 0.020–0.035 wt. % Sn were electrodeposited.[18] Doping of silicon films with aluminum can facilitate the production of p-type silicon materials[19] that are promising for a number of applications in solar cells.[24,25]

To date, there are no published data on the co-deposition of silicon and aluminum from KF–KCl–K_2SiF_6 and KF–KCl–KI–K_2SiF_6 melts. Only information is available on the production of Al–Si alloys by electrolysis of cryolite melts with SiO_2 additives[26,27] and aluminum-doped silicon films (p-type) from a CaO––$CaCl_2$–SiO_2–Al_2O_3 melt.[19]

The aim of this work was to determine the regularities of the electrochemical co-deposition of silicon with aluminum on glassy carbon from KF–KCl (2:1)–75 mol % KI–K_2SiF_6–AlF_3 melts with different mole ratios of the depositing ions as well as to study the effect of electrodeposition conditions on the morphology and elemental composition of thin films.

EXPERIMENTAL

The starting materials for the preparation of the electrolyte were KF·HF (99.95 wt. %, Chimreaktivsnab, RF), KCl (99.98 wt. %, Chimreaktivsnab), K_2SiF_6 (99.92 wt. %, Vekton, RF), KI (99.9 wt. %, Vekton, RF) and AlF_3 (99.9 wt.%, Vekton, RF).

The electrolyte components were pretreated. A mixture of KF·HF and KCl powders was placed in a glassy carbon crucible and heated with the stepwise increase in temperature (2 h at 373 K, 3 h at 573 K) for thermal decomposition of KF·HF and removal of HF. Then the salts were melted and exposed at 1023 K for 2 h. Potassium iodide was purified from oxygen-containing impurities by heating a mixture of KI with an excess of crystalline iodine in the same way as in:[28]

$$2K_2O + 2I_2 \rightarrow 4KI + O_2\uparrow \quad (1)$$

The process was carried out at 723 K until evaporation of the iodine. Then KI was remelted and kept at 1073 K for 1 h. Potassium hexafluorosilicate was mixed with 2 wt. % NH_4F in a glassy carbon crucible and exposed to 673 K for 6 h to remove the oxygen-containing impurities:[29]

$$4NH_4F + SiO_2 \rightarrow 4NH_3\uparrow + SiF_4\uparrow + 2H_2O\uparrow. \quad (2)$$

A similar procedure was used to purify AlF_3. The prepared salts were stored in a dry box.

In this work, we used KF–KCl (2:1)–75 mol % KI–K_2SiF_6–AlF_3 melts with concentrations c_{Si} = 0.15 mol% and c_{Al} from 0.015 to 0.15 mol % were used. Before the experiment, the salts were mixed in the required amounts in a glassy carbon crucible, heated to 998 K, and held for 1 h. This melt was subjected to galvanostatic purification electrolysis at cathode current densities of 0.05 and 0.1 A·cm^{-2} (for 1 h and 20 min, respectively). The chemical composition of the electrolyte (before and after testing) was monitored by the atomic emission spectroscopy with inductively coupled plasma using iCAP 6300 Duo (Termo Scientific, USA).

The experiments were carried out in a three-electrode quartz cell (Fig. 1) in an atmosphere of high-purity dehydrated argon at 998 K. A nickel shield (2) protected the cell walls from interaction with sublimates.

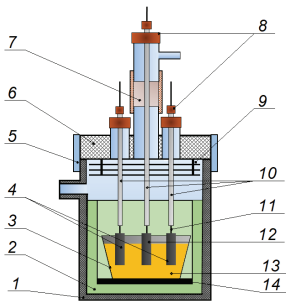

Fig. 1. Scheme of the experimental cell: 1 – quartz cell; 2 – Ni shield; 3 – glassy carbon crucible; 4 – Si electrodes; 5 – vacuum-rubber cuff; 6 – fluoroplastic cover; 7 – vacuum-rubber sluice device; 8 – rubber seals; 9 – Ni shields; 10 – quartz covers for current leads; 11 – tungsten current leads; 12 – working glassy carbon electrode; 13 – melt; 14 – graphite support.

A glassy carbon crucible (3) placed on a graphite support (14) served as a container for the electrolyte. Monocrystalline silicon plates (99.9999 wt. %) were used as a reference electrode and an auxiliary electrode (4), when performing electrochemical measurements) The working glassy carbon electrode (12) (SU-2000, Uralmetalgraphit, RF) was washed with distilled water, degreased with ethanol, and dried under vacuum. Tungsten rods (11) protected by quartz covers (10) served as current leads. A sluice device (7) was provided for replacing the working electrode during the experiment.

Cyclic voltammetry, chronoamperometry, and scanning electron microscopy with energy-dispersive X-ray spectroscopy (SEM-EDS) were used to study cathodic processes and the initial stages of electrocrystallization. The electrochemical measurements were performed using an Autolab PGStat302N with Nova 2.1.2 software. The resistance of the circuit was determined by the FRA method before each series of measurements and compensated using Autolab.

Al-doped thin Si films were obtained under galvanostatic and potentiostatic conditions. The samples were washed in boiling distilled water for 10–15 min to remove electrolyte residues. A Tescan Mira 3 LMU scanning electron microscope (Tescan, CR) equipped with an energy-dispersive X-ray spectrometer. Oxford instruments INCA Energy 350/X-max 80 was used to study the morphology and elemental analysis of deposits. A number of samples were additionally examined using a Bruker Dimension FastScan atomic force microscope (Bruker, Germany) with the ScanAsyst system.

The Raman spectra of samples were recorded using a Raman microscope-spectrometer Renishaw U1000 (Renishaw, UK) with confocal Leica DML microscope (50×, 100× objective, a notch filter, and a cooled charge-coupled device (CCD) detector) at the excitation of spectra by argon laser (the wave length 514.5 cm^{-1}, power of 20 mV) in the range of 50-1900 cm^{-1} and exposure time of 30–120 s. The spectral resolution was ±2 cm^{-1}, and wave number accuracy was about ±1 cm^{-1}; the laser beam had a focal-spot ≈1 μm in diameter.

RESULTS AND DISCUSSION

A typical series of cyclic voltammograms (CVs) obtained in the KF–KCl (2:1)–75 mol % KI–0.15 mol % K_2SiF_6–0.03 mol % AlF_3 melt (mole ratio $\gamma = c_{Si}/c_{Al} = 5$) at scan rates ($\nu$) from 0.1 to 1.5 $V \cdot s^{-1}$ are presented in Fig. 2a. It can be seen that the CVs are characterized by the presence of a single cathodic peak and the corresponding anodic peak. It should be noted that the shape of CVs is similar to that observed in the KF-KCl (2:1)–75 mol % KI–K_2SiF_6 melt, which does not contain aluminum ions.[23] Apparently, the presence of only one cathodic peak indicates a single-stage discharge of Si (IV) and Al (III) (*i.e.*, Si(IV) + 4*e* = Si and Al(III) + 3*e* = Al) and similar values of their electroreduction potentials under these conditions. The nucleation loop characteristic of the stage of nucleateon/growth on a foreign substrate[30–32] was detected in the cathode region when the reversal point was lower than the potential corresponding to the cathodic peak, $|E_\lambda| < |E_p|$ (Fig. 2b).

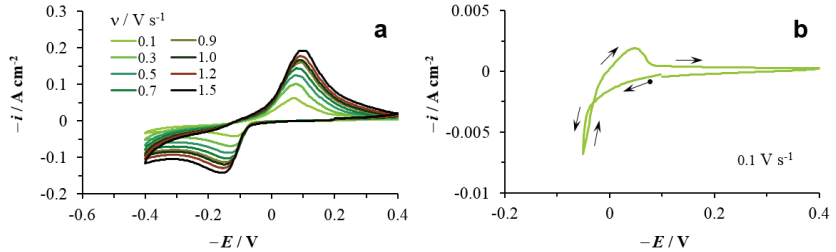

Fig. 2. Typical series of cyclic voltammograms (a) and a nucleation loop (b) obtained in the KF–KCl (2:1)–75 mol % KI–0.15 mol % K_2SiF_6–0.03 mol % AlF_3 melt ($\gamma = c_{Si}/c_{Al} = 5$) on glassy carbon at 998 K. The scan rate values are given in the figure. In this work, cathode currents and potentials were considered to have positive values (for convenience of calculations and discussion).

The same regularities were observed in melts with mole ratio $\gamma = 10$ and $\gamma = 1$ (Fig. 3). A comparison of CVs in melts with different concentrations of aluminum ions shows that E_p shifts in the anodic direction with increasing c_{Al} (Fig. 3a, c). In all cases, the cathodic peaks shifted in the cathodic direction with increasing scan rate, which indicates the quasi-reversibility or irreversibility of the process under these conditions. Figs. 3b, c demonstrate that at $\nu > 0.9$ V·s^{-1}, the electroreduction mechanism can be characterized as irreversible.

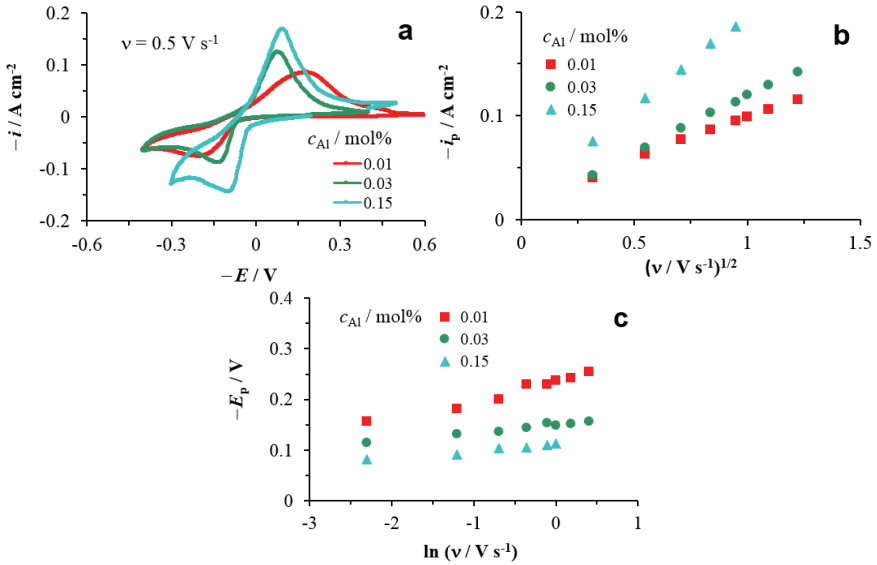

Fig. 3. Comparison of CVs (a), dependences of the cathode current density peak on the square root of the scan rate (b), and the dependences of the cathode peak potential on the logarithm of the scan rate (c) in KF–KCl (2:1)–75 mol % KI–0.15 mol % K_2SiF_6–AlF_3 melts with different concentrations of aluminum ions.

Typical families of potentiostatic current density transients, $i(t)$, obtained at co-deposition of silicon and aluminum from the melts with $\gamma = 1$ and $\gamma = 5$, respectively, are shown Figs. 4a and 5a. The form of these dependencies does not differ from the usual appearance for the electrocrystallization of silicon on glassy carbon.[14,20,23] Therefore, they could be qualitatively analyzed within the framework of the Scharifker–Hills model (SH model).[33,34] Fig. 4b demonstrates a comparison of experimental dependencies in the form of $(i/i_m)^2$ *vs.* (t/t_m) with dimensionless theoretical dependencies of the SH model for instantaneous and progressive nucleation with diffusion-controlled growth, respectively:

$$\left(\frac{i}{i_m}\right)^2 = \frac{1.9542}{t/t_m}\left\{1-\exp\left[-1.2564\left(t/t_m\right)\right]\right\}^2 \quad (3)$$

$$\left(\frac{i}{i_{\mathrm{m}}}\right)^2 = \frac{1.2254}{t/t_{\mathrm{m}}}\left\{1-\exp\left[-2.3367\left(t/t_{\mathrm{m}}\right)^2\right]\right\}^2 \quad (4)$$

where t_{m}, i_{m} are the coordinates of the maximum of $i(t)$.

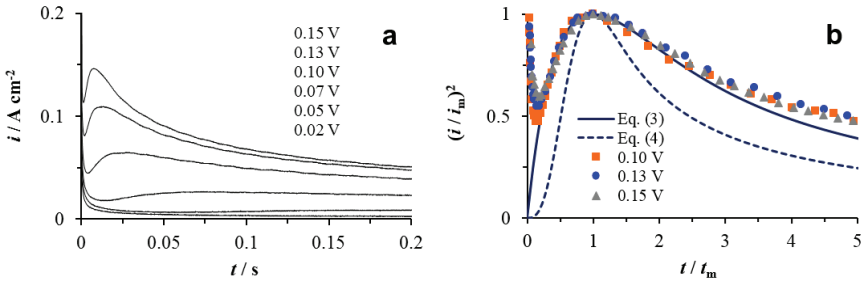

Fig. 4. Typical family of potentiostatic current density transients for co-deposition of silicon and aluminum from the KF–KCl (2:1)–75 mol % KI–0.15 mol % K_2SiF_6–0.15 mol % AlF_3 melt (a) and comparison of the experimental and theoretical (SH model) dimensionless dependences (b).

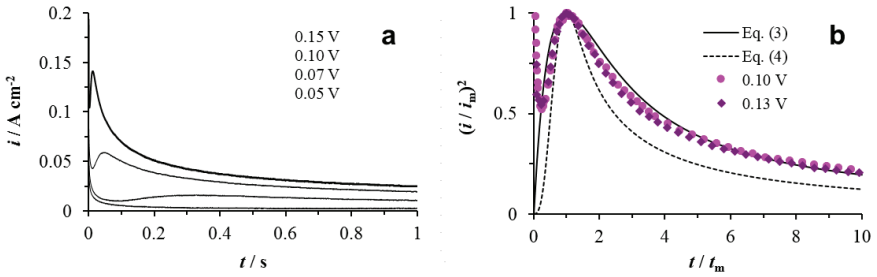

Fig. 5. Typical family of potentiostatic current density transients for the co-deposition of silicon and aluminum from the KF–KCl (2:1)–75 mol % KI–0.15 mol % K_2SiF_6–0.03 mol % AlF_3 melt (a) and comparison of experimental and theoretical (SH model) dimensionless dependences (b).

It can be seen that at $t/t_{\mathrm{m}} < 3$, the experimental dependences agree with the theoretical curve for instantaneous nucleation.

An approximate quantitative analysis is possible in this case under certain assumptions.[35,36] It was shown[36] that the equations of the SH model with modified values of the parameters can be used to estimate the apparent diffusion coefficient ($\tilde{D}$) and the number density of active centers (or nuclei in the case of instantaneous nucleation) on the electrode surface (N_0). Considering the total flux of two types of depositing ions in the electrolyte bulk and averaging the concentration profile with allowance for the mole ratio of the components (γ), gives for instantaneous nucleation:

$$t_{\mathrm{m}} = 1.2564/\pi\tilde{k}N_0\tilde{D} \quad (5)$$

$$i_{\mathrm{m}}{}^2 t_{\mathrm{m}} = 0.1629(\tilde{z}ec_0)^2\tilde{D} \quad (6)$$

$$\tilde{k} = (8\pi c_0 \tilde{\upsilon})^{1/2}\,,\ \tilde{\upsilon} = (\gamma \upsilon_{Si} + \upsilon_{Al})/(\gamma+1)\,,\ \tilde{z} = (\gamma z_{Si} + z_{Al})/(\gamma+1)$$

where c_0 is the bulk concentration of silicon ions, υ_{Si} and υ_{Al} are the volumes of Si and Al atoms, respectively (the volume of the new phase is the sum of the volumes of the individual components taking into account γ), z_{Si} and z_{Al} are the valances of the Si and Al ions, respectively.

Calculation with $\upsilon_{Si} = 2.01\times10^{-23}$ cm^3, $\upsilon_{Al} = 1.66\times10^{-23}$ cm^3, $z_{Si} = 4$, $z_{Al} = 3$, and $\gamma = 1$ gives $\tilde{z} = 3.5$, $\tilde{\upsilon} = 1.84\times10^{-23}$ cm^3, and $\tilde{k} = 8.31\times10^{-2}$. Substituting these values and $c_0 = 1.50\times10^{19}$ cm^{-3} into Eqs. (5) and (6), $\tilde{D}$ = = 1.43×10^{-5} cm^2 s^{-1} and $N_0 = 4.44\times10^7$ cm^{-2} were obtained for the curve at E = = 0.15 V.

Discrepancies with the theoretical dependence at $t/t_m > 3$ (Fig. 4b) should disappear at a lower concentration of deposited ions. In fact, this behavior can be observed in a melt with $\gamma = 5$ (Fig. 5b). In this case, the last portions of the current density transients coincide with the curve described by the Cottrell equation:

$$i = \tilde{z} e c_0 (\tilde{D}/\pi t)^{1/2} \qquad (7)$$

The $\tilde{D}$ value found from Eq. (7) was 1.38×10^{-5} cm^2 s^{-1}. This value is less than the diffusion coefficient of silicon ions in the KF–KCl (2:1)–75 mol % KI––0.5 mol % K_2SiF_6 melt, $D_{Si} \approx 1.95\times10^{-5}$ cm^2 s^{-1}.[23] This fact is consistent with more explicit diffusion limitations in melts with a higher concentration of aluminum ions (see Fig. 3a, c). The reasons may be the lower mobility of aluminum ionic complexes in comparison with silicon ones and a change in the structure of the complexes.

It was also noted that a more complex time dependence of the number density of nuclei is observed for a melt with $\gamma = 5$ in the potential range from 0.10 to 0.13 V, $N = N_0[1–\exp(–At)]$, where A is the nucleation rate constant. This is evidenced by the deviations of the experimental dimensionless curves at $t/t_m <$ < 5 from the theoretical one described by Eq. (3) (Fig. 5b), as well as the SEM and AFM images of nuclei (Fig. 6). Elemental analysis (Table I) demonstrates the presence of silicon and aluminum in the deposit composition; the availability of other components is due to the existence of electrolyte residues and oxidation of the surface of the deposit in air.

The morphology of the deposit obtained in the melt with the same concentration of depositing ions at the cathodic potential of 0.45 V for 60 s and the SEM-EDS maps for Si and Al are shown in Fig. 7.

It can be seen that the distribution of aluminum is quite uniform, but the surface of the deposit is not smooth but porous. More compact deposits can be produced at a cathodic potential of 0.2 V (Fig. 8). Continuous aluminum-doped silicon films were obtained under galvanostatic conditions at cathode current

densities from 0.025 to 0.1 A·cm^{-2} for $t \geq 30$ s from aq. melt containing 0.015 mol % AlF_3 (Fig. 9, Table I).

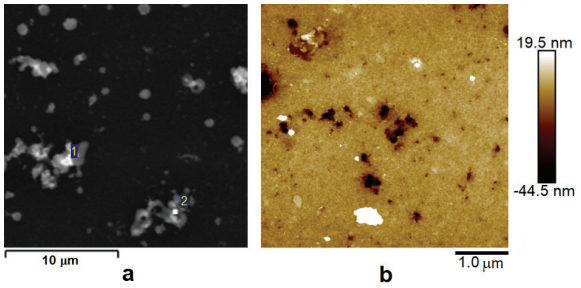

Fig. 6. SEM (a) and AFM (b) images of new-phase nuclei on glassy carbon during the co-deposition of silicon and aluminum from the KF–KCl (2:1)–75 mol % KI–0.15 mol % K_2SiF_6–0.03 mol % AlF_3 melt under potentiostatic conditions (E = 0.11 V, t = 0.04 s).

TABLE I. SEM-EDS data

Figure	Spectrum	Content, at. %						
		Si	Al	K	F	Cl	I	O
6a	1	13.61	0.90	11.28	0.49	1.17	7.04	65.51
	2	18.53	1.15	6.10	0.48	0.48	0.68	72.60
9d	1	85.42	0.34	2.59	0.56	–	–	11.09
	2	75.93	0.43	3.76	0.65	0.47	0.98	17.78
	3	87.09	0.44	2.97	0.61	–	–	8.890

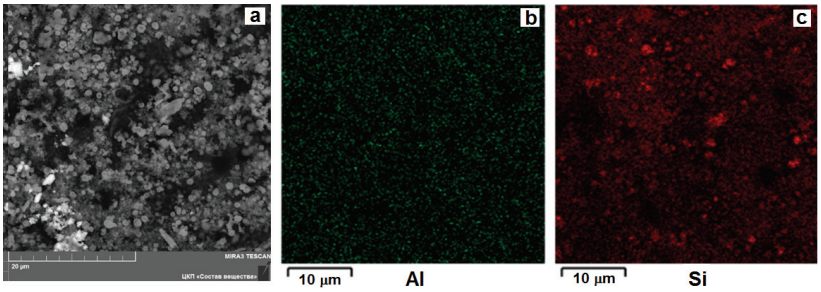

Fig. 7. SEM image of deposit (a) and maps of Al (b) and Si (c) after their co-deposition from the KF–KCl (2:1)–75 mol % KI–0.15 mol % K_2SiF_6–0.03 mol% AlF_3 melt under potentiostatic conditions (E = 0.45 V, t = 60 s).

A typical Raman spectrum of the Al-doped Si film on glassy carbon is shown in Fig. 10. The strong first-order Raman peak with a maximum at 511 cm^{-1} and two second-order bands at 300 and 940–1000 cm^{-1} can be attributed to the silicon vibrations.[17,37] In the high-frequency range, the spectrum contains two characteristic peaks at about 1330 and 1580 cm^{-1}, which correspond to the main carbon bands.[38] In general, this pattern is similar to the Raman spectrum of a continuous Si coating on C obtained in an earlier work.[17] The main differences are in

the shift of the strong band from the typical value for bulk crystalline Si (519 cm^{-1}) to 511 cm^{-1} and the expansion of its left flank towards the value typical for amorphous Si (480 cm^{-1}).[39] The same was observed in the Raman spectra of the Al-doped Si films obtained by radio-frequency magnetron sputtering, which did not have a well-crystallized structure.[39] Due to the fact that the atomic weights of Al and Si differ from each other by less than 4 %, the local mode produced by the additional Al atoms is very close to the strong Raman peak of Si and is difficult to identify even at a high Al concentrations.[40]

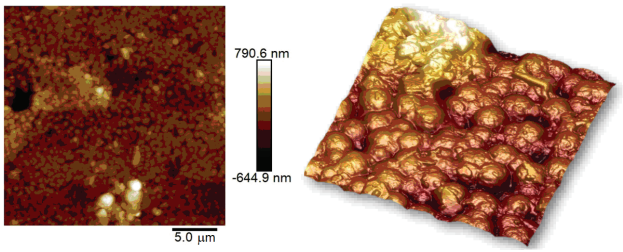

Fig. 8. AFM images of the deposit obtained from a KF–KCl (2:1)–75 mol % KI–0.15 mol % K_2SiF_6–0.03 mol% AlF_3 melt under potentiostatic conditions (E = 0.2 V, t = 30 s).

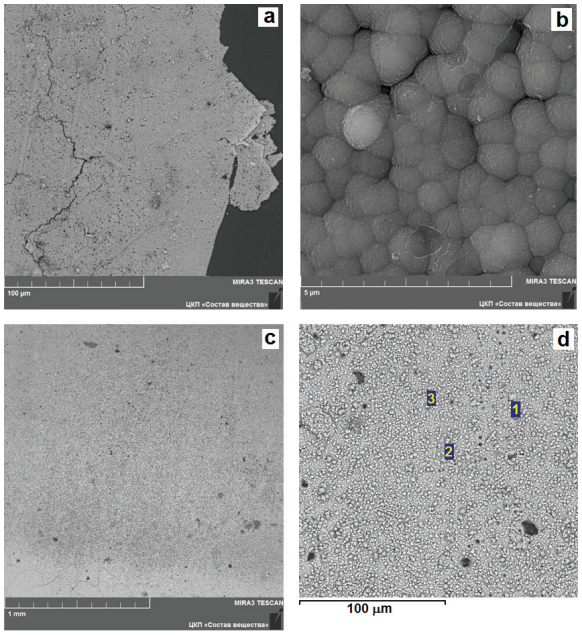

Fig. 9. SEM images of deposits obtained by co-deposition of silicon and aluminum from the KF–KCl (2:1)–75 mol% KI–0.15 mol % K_2SiF_6–0.015 mol % AlF_3 melt under galvanostatic conditions at 0.025 $A \cdot cm^{-2}$ (a, b) and 0.1 $A \cdot cm^{-2}$ (c, d) for 30 s. SEM-EDS data for Fig. 9d are given in Table I.

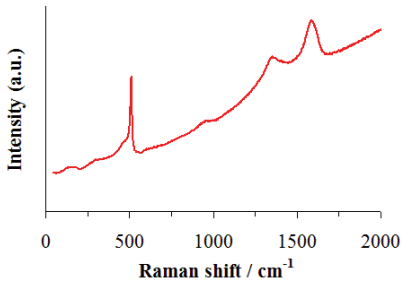

Fig. 10. Raman spectrum of an Al-doped Si film on glassy carbon. The electrodeposition conditions are the same as for Fig. 8.

CONCLUSIONS

The co-deposition of silicon and aluminum on glassy carbon from melts based on KF–KCl (2:1)–75 mol % KI containing 0.15 mol. % K_2SiF_6 and 0.015, 0.03, or 0.15 mol % AlF_3 at 998 K was studied. Analysis of cyclic voltammograms showed that: *i*) discharge of Si (IV) and Al (III) is a one-stage process; *ii*) the cathodic process can be characterized as quasi-reversible at scan rates from 0.1 to 0.9 $V \cdot s^{-1}$; *iii*) the share of diffusion limitations increases with increasing concentration of aluminum ions in the melt. The nucleation loop in the cyclic voltammograms at low reverse potentials and the shape of the potentiostatic current density transients indicate the presence of a 3D nucleation/growth stage. A comparison of dimensionless experimental and theoretical (the Scharifker–Hills model) dependencies demonstrated that instantaneous nucleation with the diffusion-controlled growth occurs in the melt with a mole ratio of Si and Al ion concentrations $\gamma = 1$. The nuclei appear gradually during electrodeposition from the melt with $\gamma = 5$. The apparent diffusion coefficient was estimated from the maximum of the current density transient (at $\gamma = 1$) and by the Cottrell equation (at $\gamma = 5$); its value was $\approx 1.4 \times 10^{-5}$ cm^2 s^{-1}. Analysis of the SEM-EDS and AFM data showed that continuous thin films of aluminum-doped silicon can be obtained under galvanostatic conditions at cathode current densities from 0.025 to 0.1 A cm^{-2}. Raman spectroscopy data indicate the formation of an amorphous phase.

Acknowledgements. The study is supported by the Russian Science Foundation Grant (project No. 16-13-00061). This work has been (partly) realized using the facilities of the shared access centers “Composition of compounds” (IHTE, UB RAS). The authors are grateful to ZEISS Russia & CIS (Moscow) for the demonstration measurements performed with a Bruker Dimension FastScan atomic force microscope.

ИЗВОД

ЕЛЕКТРОХЕМИЈСКО ТАЛОЖЕЊЕ ТАНКИХ ФИЛМОВА СИЛИЦИЈУМА ДОПИРАНИХ АЛУМИНИЈУМОМ ИЗ РАСТОПА KF–KCl–KI–K_2SiF_6–ALF_3

MICHAEL V. LAPTEV, ANASTASIA O. KHUDOROZHKOVA, ANDREY V. ISAKOV, OLGA V. GRISHENKOVA, SERGEY I. ZHUK и YURII P. ZAIKOV

Ural Branch of the Russian Academy of Sciences, Institute of High Temperature Electrochemistry, 20 Academicheskaya St., 620137 Ekaterinburg, Russian Federation

Законитости истовременог таложења силицијума и алуминијума из растопа KF–KCl (2:1)–75 mol % KI–0,15 mol % K_2SiF_6–(до 0,15 mol %) AlF_3 на подлогу од стакластог угљеника испитиване су коришћењем цикличне волтаметрије, хроноамперометрије, скенирајуће електронске микроскопије, микроскопије атомских сила и Раманове спектроскопије. Циклични волтамограми су показали присуство само једног катодног пика (или петље нуклеације при ниском повратном потенцијалу) и одговарајућег анодног пика. Катодни пик се померао у катодном смеру при смањењу конентрације јона алуминијума у растопу, као и при повећању брзине линеарне промене потенцијала. Шарифкер-Хилсов модел је коришћен за анализу потенциостатских струјних транзијената и процену вредности привидних коефицијената дифузије и густине нуклеуса. Испитавани су и морфологија и елементални састав узорака таложених под потенциостатским и галваностатским условима током 30–60 s. Континуални танки филмови силицијума допирани алуминијумом су добијени под галваностатским условима.

(Примљено 17. септембра 2020, ревидирано 16 августа, прихваћено 17. августа 2021)

REFERENCES

1. Y. Sakanaka, T. Goto, *Electrochim. Acta* **164** (2015) 139 (http://dx.doi.org/10.1016/j.electacta.2014.12.159)
2. S. C. Bhatia, *Advanced Renewable Energy Systems*, Woodhead Publishing India Pvt. Ltd., New Delhi, 2014 (ISBN-13: 978-9380308432, ISBN-10: 9380308434)
3. S. G. Dorofeev, N. N. Kononov, V. M. Zverolovlev, K. V. Zinoviev, V. N. Sukhanov, N. M. Sukhanov, B. G. Gribov, *Semiconductors* **48** (2014) 360 (https://doi.org/10.1134/S1063782614030105)
4. D. Ma, Z. Cao, A. Hu, *Nano-Micro Lett*. **6** (2014) 347 (https://doi.org/10.1007/s40820-014-0008-2)
5. M. Rohde, M. Zelt, O. Gabriel, S. Neubert, S. Kirner, D. Severin, T. Stolley, B. Rau, B. Stannowski, R. Schlatmann, *Thin Solid Films* **558** (2014) 337 (https://doi.org/10.1016/j.tsf.2014.03.008)
6. E. Yu. Gusev, J. Y. Jityaeva, O. A. Ageev, *Mater. Phys. Mech.* **37** (2018) 67 (http://dx.doi.org/10.18720/MPM.3712018_9)
7. D. Amkreutz, J. Haschke, T. Häring, F. Ruske, B. Rech, *Sol. Energy Mater. Sol. Cells* **123** (2014) 13 (http://dx.doi.org/10.1016/j.solmat.2013.12.021)
8. J. Haschke, D. Amkreutz, L. Korte, F. Ruske, B. Rech, *Sol. Energy Mater. Sol. Cells* **128** (2014) 190 (http://dx.doi.org/10.1016/j.solmat.2014.04.035)
9. R. Boen, J. Bouteillon, *J. Appl. Electrochem*. **13** (1983) 277 (https://doi.org/10.1007/BF00941599)
10. D. B. Frolenko, Z. S. Martem'yanova, A. N. Baraboshkin, S. V. Plaksin, *Rasplavy* No.5 (1993) 42 (in Russian) (https://www.elibrary.ru/item.asp?id=12739574)

11. S. I. Zhuk, V. A. Isaev, O. V. Grishenkova, A. V. Isakov, A. P. Apisarov, Yu. P. Zaykov, *J. Serb. Chem. Soc*. **82** (2017) 51 (https://doi.org/10.2298/JSC160712109Z)
12. J. T. Moore, T. H. Wang, M. J. Heben, K. Douglas, T. F. Ciszek, in *Conference Record of the 26th IEEE Photovoltaic Specialists Conference*, 1997, Anaheim, CA, USA, IEEE, Anaheim, 1997, p. 775 (http://dx.doi.org/10.1109/PVSC.1997.654204)
13. O. Chemezov, A. Apisarov, A. Isakov, Yu. Zaikov, *EPD Congress 2012*, in *Proceedings of the TMS 2012 Annual Meeting & Exhibition*, 2012, Orlando, FL, USA, *Proceedings TMS 2012*, L. Zhang, J.A. Pomykala, A. Ciftja, Eds., Wiley, New York, 2012, p. 493 (https://doi.org/10.1002/9781118359341.ch58)
14. Yu. P. Zaykov, S. I. Zhuk, A. V. Isakov, O. V. Grishenkova, V. A. Isaev, *J. Solid State Electrochem*. **19** (2015) 1341 (https://doi.org/10.1007/s10008-014-2729-z)
15. K. Yasuda, K. Maeda, T. Nohira, R. Hagiwara, T. Homma, *J. Electrochem. Soc*. **163** (2016) D95 (https://doi.org/10.1149/2.0791603jes)
16. K. Maeda, K. Yasuda, T. Nohira, R. Hagiwara, T. Homma, *J. Electrochem. Soc*. **162** (2015) D444 (https://doi.org/10.1149/2.0441509jes)
17. S. I. Zhuk, A. V. Isakov, A. P. Apisarov, O. V. Grishenkova, V. A. Isaev, E. G. Vovkotrub, Yu. P. Zaykov, *J. Electrochem. Soc*. **164** (2017) H5135 (https://doi.org/10.1149/2.0171708jes)
18. J. Peng, H. Yin, J. Zhao, X. Yang, A. J. Bard, D. R. Sadoway, *Adv. Funct. Mater*. **28** (2017) 1703551 (https://doi.org/10.1002/adfm.201703551)
19. X. Zou, L. Ji, J. Ge, D. R. Sadoway, E. T. Yu, A. J. Bard, *Nat. Commun*. **10** (2019) 5772 (https://doi.org/10.1038/s41467-019-13065-w)
20. Yu. P. Zaykov, S. I. Zhuk, A. V. Isakov, O. V. Grishenkova, V. A. Isaev, *Rasplavy* No.5 (2016) 441 (in Russian) (https://www.elibrary.ru/item.asp?id=36286045)
21. A. P. Apisarov, A. A. Redkin, Yu. P. Zaikov, O. V. Chemezov, A. V. Isakov, *J. Chem. Eng. Data* **56** (2011) 4733 (https://doi.org/10.1021/je200717n)
22. A. Khudorozhkova, A. Isakov, A. Apisarov, A. Redkin, Y. Zaikov, *J. Chem. Eng. Data* **65** (2020) 2505 (https://doi.org/10.1021/acs.jced.9b01161)
23. M. V. Laptev, A. V. Isakov, O. V. Grishenkova, A. S. Vorob'ev, A. O. Khudorozhkova, L. A. Akashev, Yu. P. Zaikov, *J. Electrochem. Soc.* **167** (2020) 042506 (https://doi.org/10.1149/1945-7111/ab7aec)
24. M. Rüdiger, M. Rauer, C. Schmiga, M. Hermle, S. W. Glunz, *Energy Procedia* **8** (2011) 527 (https://doi.org/10.1016/j.egypro.2011.06.177)
25. C. Gong, S. Singh, J. Robbelein, N. Posthuma, E. Van Kerschaver, J. Poortmans, R. Mertens, *Prog. Photovoltaics* **19** (2010) 781 (https://doi.org/10.1002/pip.1035)
26. P. S. Pershin, A. V. Suzdaltsev, Y. P. Zaikov, *J. Electrochem. Soc*. **163** (2016) D167 (https://doi.org/10.1149/2.0521605jes)
27. A. Liu, Z. Shi, X. Hu, B. Gao, Z. Wang, *J. Electrochem. Soc*. **164** (2017) H126 (https://doi.org/10.1149/2.1381702jes)
28. A. O. Khudorozhkova, A. V. Isakov, A. A. Kataev, A. A. Redkin, Yu. P. Zaykov, *Russ. Metallurgy (Metally)* **2020** (2020) 918 (https://doi.org/10.1134/S0036029520080078)
29. Yu. P. Zaikov, A. A. Redkin, A. P. Apisarov, I. V. Korzun, N. P. Kulik, A. V. Isakov, A. A. Kataev, O. V. Chemezov, *J. Chem. Eng. Data* **58** (2013) 932 (https://doi.org/10.1021/je301195x)
30. S. Fletcher, C. S. Halliday, D. Gates, M. Westcott, T. Lwin, G. Nelson, *J. Electroanal. Chem.* **159** (1983) 267 (https://doi.org/10.1016/S0022-0728(83)80627-5)

31. D. Pletcher, R. Greff, R. Peat, L. M. Peter, J. Robinson, in *Instrumental Methods in Electrochemistry*, Woodhead, New Delhi, 2010, p. 210 (ISBN: 9781782420545).
32. V. A. Isaev, O. V. Grishenkova, A. V. Kosov, O. L. Semerikova, Y. P. Zaykov, *J. Solid State Electrochem*. **22** (2018) 2775 (https://doi.org/10.1007/s10008-018-3989-9)
33. B. R. Scharifker, G. J. Hills, *Electrochim. Acta* **28** (1983) 879 (https://doi.org/10.1016/0013-4686(83)85163-9)
34. V. A. Isaev, Yu. P. Zaykov, O. V. Grishenkova, A. V. Kosov, O. L. Semerikova, *J. Electrochem. Soc*. **166** (2019) D851 (https://doi.org/10.1149/2.1061915jes)
35. O. Díaz-Morales, J. Mostany, C. Borrás, B. R. Scharifker, *J. Solid State Electrochem*. **17** (2013) 345 (https://doi.org/10.1007/s10008-012-1881-6)
36. O. V. Grishenkova, A. V. Kosov, Yu. P. Zaikov, V. A. Isaev, *Russ. Metallurgy (Metally)* **2020** (2020) 914 (https://doi.org/10.1134/S0036029520080042)
37. I. G. Aksyanov, M. E. Kompan, I. V. Kul'kova, *Phys. Solid State* **52** (2010) 1850 (https://doi.org/10.1134/S1063783410090106)
38. N. A. Solopova, N. Dubrovinskaia, L. Dubrovinsky, *Appl. Phys. Lett.* **102** (2013) 121909 (http://dx.doi.org/10.1063/1.4798660)
39. Y.-J. Kim, M.-H. Kim, J.-H. Yang, J.-W. Park, *J. Korean Phys. Soc*. **49** (2006) 1196 (https://www.jkps.or.kr/journal/view.html?uid=7876&vmd=Full)
40. M. Becker, U. Gösele, A. Hofmann, S. Christiansen, *J. Appl. Phys*. **106** (2009) 074515 (https://doi.org/10.1063/1.3236571).

Journal of the Serbian Chemical Society
JSCS@tmf.bg.ac.rs • www.shd.org.rs/JSCS
J. Serb. Chem. Soc. *86* (11) 1089–1102 (2021)
JSCS–5485
Original scientific paper
Published 8 September 2021

LabVIEW virtual instrument for zone penetration studies in flow-based analytical systems

ALEKSANDRA KULJANIN and NATAŠA GROS*

University of Ljubljana, Faculty of Chemistry and Chemical technology, Večna pot 113, 1000 Ljubljana, Slovenia

(Received 9 July, revised 30 July, accepted 4 August 2021)

Abstract: In the flow method development, zone penetration studies are usually conducted as a part of the initial screening phase. A lack of an appropriate tool can keep these studies on the level of rough estimations. The developed LabVIEW virtual instrument (VI) which processes peak signals and calculates the overlapping area and fundamental peak-related parameters was used for the calculations in experiments that are modelling sample and reagent plug interaction within liquid conduits. The reliability of the predictions was initially confirmed on the artificial data set based on thirty-six files covering all the different types of cases that can be foreseen. To continue, the volumes of model solutions, propelling flow rate, and the coil length in the sequential injection analysis system, were varied by following the Box–Behnken response surface design. In three examples, it is demonstrated how the VI can help the planning of further experiments in the range which ensures the efficient zone overlapping, the economic exploitation of reagent plug and the adequate dispersion. The application of the VI is not limited just to the flow-based chemistry, it can also be used in spectroscopy and chromatography. In order to use the graphical user interface, it is not necessary to have the LabVIEW program installed.

Keywords: peak processing; peak overlapping area; open-code program; sequential injection analysis; dispersion coefficient.

INTRODUCTION

The processing and the analysis of peak signals are inevitable in many scientific disciplines. Different methods for peak evaluation have been developed and applied so far, depending on the problem which has to be solved.[1–8] The extracting information about the individual chemical component from the overlapped peak signals is still challenging in chromatographic analysis. Power functions were tested for the modulation of peak shape, noise decreasing[1,2] and for

* Corresponding author. E-mail: Natasa.Gros@fkkt.uni-lj.si
https://doi.org/10.2298/JSC210709058K

resolving partially overlapped peaks.[3] Deconvolution in gas chromatography was done by using an exponentially modified Gaussian model,[4] while multivariate curve resolution was employed for the resolving of overlapped HPLC peaks.[5] Methods founded on Gaussian model were used for the resolving of overlapped peaks in UV–Vis spectrum[6] and the deconvolution of peaks in chiral chromatography.[7] The flow analysis methods, as flow injection analysis (FIA), sequential injection analysis (SIA) and lab-on-a-valve (LOV), provide information about the analyte in the form of peak signal, too.[9] Unlike the aforementioned examples, where the peak overlapping was considered to be the unwanted phenomena, the investigation of zone penetration in flow systems means the evaluation of peak overlapping areas. Overlapping of the zones influences the reaction yield and the sensitivity of the method. The most common approach is to simulate a sample plug with a defined volume of a non-reactive dye, while the reagent plug is simulated with water or an adequate buffer, and *vice versa.* The overlapping area of recorded peaks gives information about the zone penetration and merging. Ružička and Hansen have reported that it is rather complex to create a general model for the prediction of peak profiles based on variations of different factors within the FIA system.[10] This is in agreement with the reported data dealing with the topic, where it was also underlined that the results obtained from the examinations of FIA systems cannot be extrapolated to other flow systems.[9] It was stated that the zone penetration and the dispersion are the key parameters for the successful performance of SIA systems.[11,12] The zone penetration studies were used for the investigation of the effects of a single bead string reactor on dispersion and mixing of the zones in the SIA system.[13] This type of studies was also conducted by Jakmunee and co-workers, in order to define optimal volumes and aspiration sequence for the examination of fruit juices acidity.[14] In the flow method development, the zone penetration is usually employed in the initial screening phase, and the changes in the overlapping area are judged by appearance.[15–17] Even if the numerical values were given, it was not exposed which approach was employed for zone penetration evaluation. Most common approach used in development of sequential injection and flow analysis methods is still univariate optimization.[18–20] More detailed study of the zone penetration and other parameters of importance could decrease the number of experiments in later phases. When programs of wider scope are used, it is necessary to adapt their functions to a specific application, which can be time-consuming and demanding. Also, the creation of automation scripts for general-purpose programs requires programming skills. The processes within Origin can be automatized by using LabTalk, scripting language native to Origin, or Origin C, high level programming language. Origin C provides the access to the import and export of data, processing, and analysis.[21] In Excel, the automation is usually done by employing Visual Basic.[22,23] National Instruments Laboratory Virtual Instrument Engineering

Workbench (NI LabVIEW) is a highly modular graphical programming language that disposes of large libraries of different functions, enables building adaptable instrumental platforms and convenient user interfaces.[24,25] The use of the LabVIEW VI for the processing and the chemometric analysis of spectroscopic data was demonstrated for modelling of the diffuse reflectance spectra in the visible, NIR and mid-IR spectra for the predictions of the mineral-organic composition of soil mixes.[26] The program was also utilized for creation of flexible platforms which facilitate employing and testing of different temperature and pressure sensors.[27,28] LabVIEW VIs were also applied for the precise control and the monitoring of hardware components of automated SIA systems.[29–31] However, to the best of our knowledge, the open code LabVIEW software for the zone penetration studies was not yet reported. Our main objective was to develop LabVIEW VI that would not only provide the user with the most fundamental peak-related parameters but it would also support the zone penetration studies in flow-based analytical systems, by the evaluation of the peak overlapping areas. To use the developed VI and its graphical user interface one does not have to be familiar with LabVIEW and it is not necessary to have the program installed. A further objective was to test the reliability of the predictions using artificial and experimental data sets and to demonstrate the usability of the VI for more comprehensive zone penetration studies of SIA system.

EXPERIMENTAL

Algorithm of the developed program

The algorithm of the developed program is presented in Fig. 1.

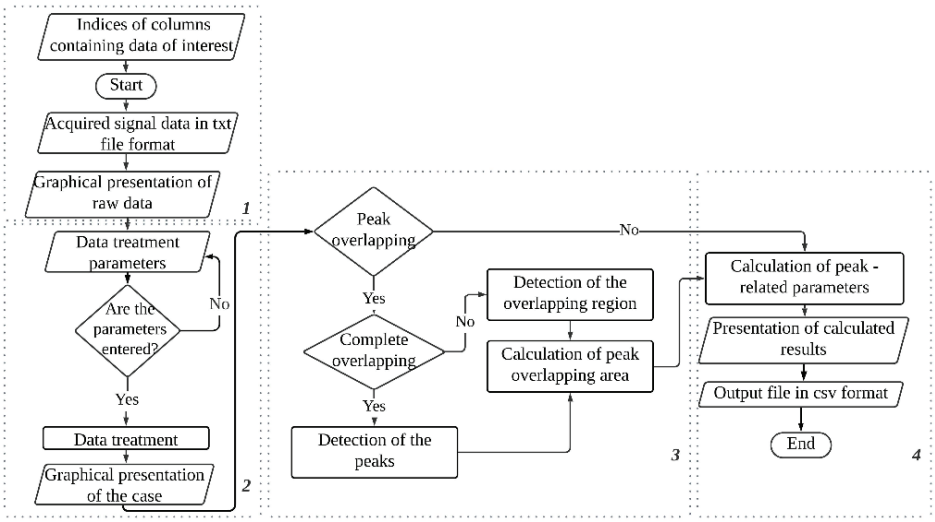

Fig. 1. Algorithm of the processes executed within four main sequence structures of the developed VI.

The program comprises four main sequence structures, and each of them executes a set of different operations. The graphical user interface is presented in Fig. 2.

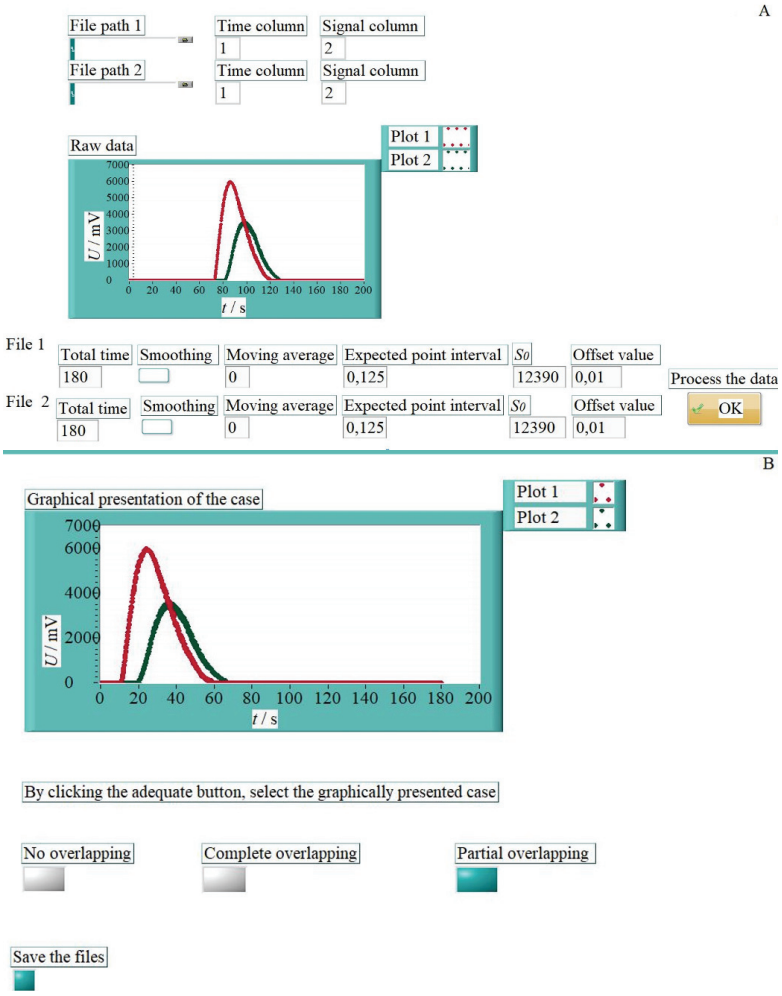

Fig. 2. The graphical user interface of the VI. Required input parameters and raw data presentation (A); graphical presentation of the processed data and choice of the case (B).

The numerical controls called the Time column and Signal column define which columns will be extracted from the raw data file, and it is necessary to fill them in before the program is started. After the program has been run, the user is offered to upload two text files of interest. The input data for the program has to be in the form of a text file with string headers on top and numerical data placed in columns. The number of columns is not limited, but at least one of them must have the header “Time” where the time is written. The read delimited spreadsheet VI has been used for file reading. A combination of functions and

subVIs from the Array and String palette has been used for data extraction. The last operation, executed within the first structure, is a graphical presentation of the raw data sets.

The next step is to define the following input parameters by filling in control fields: the total time interval, the expected point-to-point interval, the offset value, and the parameter S_0. If it is necessary, the user can also request the curve smoothing via moving an average function, by defining the number of points that will be used for the mean calculation. This structure is based on the do/while loop, and it operates until the value of the control button "Process the data" is set to true. The program waits for the input on the parameter values and does not execute other processes until it is done. From the moment when the data acquisition ended, the start of the relevant data acquisition is calculated based on the total time interval parameter. It is useful when data acquisition has been started in advance since it eliminates the initial part of the sequence of no value for further analysis. After that, the time axis is transferred to a relative. During the data acquisition, some points could have been missed due to computer's multitasking, especially if the point intervals are narrow. The problem was observed within the experimental data sets with 0.125 s data collection interval. The value of the expected point-to-point interval presents the input for the Interpolate 1 D VI, which was applied for the interpolation. In our case, the linear interpolation was satisfying since the number of points which defined the shape of the peak was high, and the signal interval was narrow.

The last parameter (S_0) presents the signal recorded when the detection cell is filled with undiluted solution, and it is used for the calculation of the dispersion coefficient. The demonstration of the effect of the processing tool on the acquired data sets is given in Fig. 3.

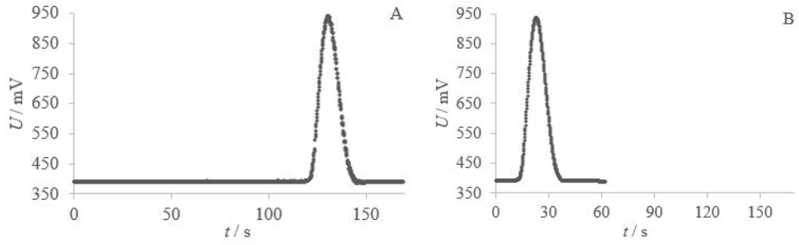

Fig. 3. Graphical presentation of the acquired data before (A) and after (B) the application of the processing tool.

The numerical detection of the intersection point is based on the minimal difference between two signals from different arrays, so it is necessary to have arrays of the same length. If not, the shorter array is recognized, and it is prolonged with its last element. The last process executed within the second sequence structure is the data presentation.

The presented sample and the reagent peaks give insight into what is happening within the liquid conduits. In general, it is possible to have three different situations. The graphical presentation of the cases is given in Fig. 4.

The third sequence structure contains an event structure. Based on the visualized data, the user decides between three possible events by choosing one of the options on the graphical interface: no overlapping (1), complete overlapping (2) or partial overlapping (3). Within all the events, the first step is the elimination of the signals below the offset value.

Event 1. Since the peaks do not overlap, this event just transfers the information that the overlapping area is zero to the next sequence structure.

Event 2. The program detects the narrower peak. The area of the smaller and narrower peak presents the overlapping area.

Event 3. The program detects the start and the end of the peaks. Later on, the signal columns from both arrays are extracted, subtracted, and the new 1D array is formed. The sign change within the 1D array indicates that the curves intersected. Depending on the number of the intersection points, one or two, the overlapping area is the sum of two or three sections.

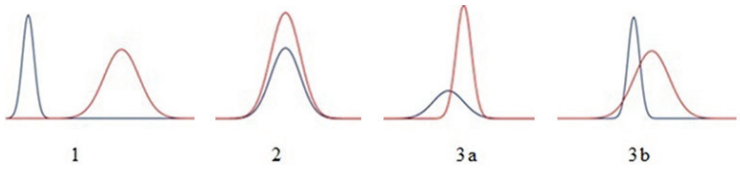

Fig. 4. Graphical presentation of the foreseen cases used as the basis for creation of simulation files (1 – no overlapping; 2 – total overlapping; 3a – partial overlapping with curves intersecting at one point; 3b – partial overlapping with curves intersecting at two points).

The user can also activate the control button "Save the files". The value of the local variable for the control is sent to the fourth structure.

The fourth structure employs the functions from Array, Comparison and Mathematical palette, and executes the calculation of individual peak areas, and the zone overlapping expressed as a fraction of total peaks area. Also, the other important peak-related parameters as dispersion coefficient, residence time, peak width, and peak height are calculated. If the value of the "Save the files" button was changed, the output CSV file composed of the processed data sets is exported. Afterward, the value of all control buttons is reset to false, and the program is prepared for the next run. Reliability of the software predictions was tested by weighing method. The results obtained by weighing correlate with VI predictions at a high level (R^2 = 0.9993). More details can be found in the Supplementary material to this paper.

Chemicals

Potassium chloride *p.a.* (Honeywell – Fluka, Germany) and milliQ water (Millipore SA, France) were used in the zone penetration studies. We have simulated the plug of the reagent with 0.15 mol L^{-1} potassium chloride, while the sample plug was simulated with milliQ water, and *vice versa*.

SIA system

A schematic presentation of the used SIA system is given in Fig. 5.

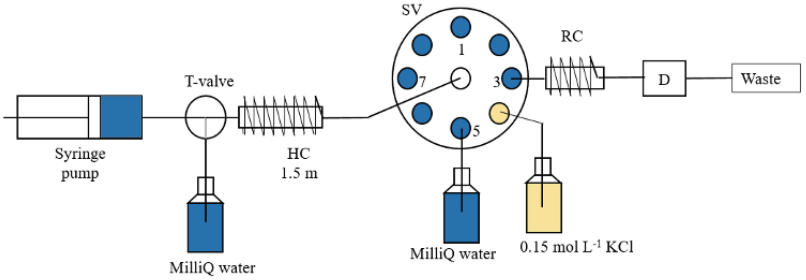

Fig. 5. Schematic presentation of the SIA system used for the experiments.

The system consisted of a Harvard Apparatus 11-Elite syringe pump, solenoid T-valve (Neptune Research, Inc., West Caldwell, NJ, USA), eight to one port selector valve (Vici Valco, Schenkon, Switzerland). Polytetrafluoroethylene tubings (internal diameter, i.d., 0.75 mm) obtained from Vici Valco, Switzerland, were used for the creation of holding coil (HC) and reaction coils (RC). A laboratory-made conductivity meter with stainless steel flow-through cell was used as a detector (D).

Zone penetration experiments

It is recognized that sample volume, reagent volume, propelling flow rate, and coil length are the factors which influence the yield of reactions performed within the flow systems. The important factors in the SIA system were varied in order to examine how they affect the most important parameter in sequential injection systems, the zone penetration. Box-Behnken response surface design in 12 blocks was used. The experimental matrix consisted of 27 experiments. Every measurement was conducted in four replicates. Four factors were varied at three levels, by respecting the rules of Box Behnken design, which is presented in Table I.

TABLE I. Experimental factors and factor levels chosen for the Box Behnken response surface design

Experimental factor	Level –1	Level 0	Level +1
Sample volume, μL	30	75	120
Reagent volume, μL	30	75	120
Propelling flow rate, $mL \cdot min^{-1}$	0.5	1	1.5
Coil length, cm	20	40	60

The reagent plug was simulated with 0.15 mol L^{-1} potassium chloride, while the sample plug was simulated with milliQ water, and *vice versa*. The sample plug was aspirated first, and subsequently the reagent plug. The aspiration flow rate was kept at constant 0.25 mL min^{-1} while the flow rate used for syringe refill was always 1 mL min^{-1}. The operating sequences of the SIA methods are presented in Table II. The obtained peaks were further processed and analyzed by the developed VI.

TABLE II. Operating sequences of used SIA methods

Step	Time, s	Pump	T-valve	Selector valve	Description
1	2	Stop	On	4	Switching the valve
2	7.2, 18 or 28.8	Reverse	On	4	Aspiration of KCl solution
3	2	Stop	On	5	Switching the valve
4	7.2; 18 or 28.8	Reverse	On	5	Aspiration of milliQ water
5	2	Stop	On	3	Switching the valve
6	45, 60 or 120	Forward	On	3	Propelling the plugs to the detector
7	2	Stop	Off	3	Switching T-valve
8	60	Reverse	Off	3	Filling in the syringe with milliQ water

The response surface graphs which present the influence of varied factors on the chosen responses were created. The chosen responses were: zone overlapping, dispersion coefficient of sample plug, dispersion coefficient of reagent plug and overlapped fraction of the reagent peak.

Software packages

The hardware control and the data acquisition were done *via* LabVIEW 2015 SP1 software, National Instruments, USA. For the design of the experiments and graphical presentation of the results in the form of response surface graphs, the Statgraphics Centurion (Statgraphics Technologies, Inc, USA) was used. For the creation of the scheme of developed VI, the Lucidchart application was applied.

RESULTS AND DISCUSSION

Benefits of more comprehensive studies of zone penetration in association with other peak-related parameters supported by the developed VI

As aforementioned, the zone penetration studies are usually a brief introductory step in flow method development. The geometry of every SIA system has specific characteristics, and it is profitable to explore how the change of important factors affects the response. A deeper understanding of the behaviour of liquid conduits can reduce the number of later experiments and contribute to greener analytical chemistry. A lack of an appropriate tool can keep these studies on the level of rough estimations, based on the judgments of peak overlapping by appearance. It is demonstrated here how the designed VI supports more comprehensive studies of zone penetration in association with other peak-related parameters. The conclusions in the continuation are derived from the three-level Box–Behnken design and presented as response surface graphs.

Zone penetration studies

For the introductory understanding of the behaviour of liquid conduits in the SIA system the overlapping area relatively expressed as a fraction of the total area of the two peaks, called the zone overlapping was used. The zone overlapping as a function of the sample and reagent volume for the flow rate 1 mL min^{-1} and 40 cm coil is presented in Fig. 6.

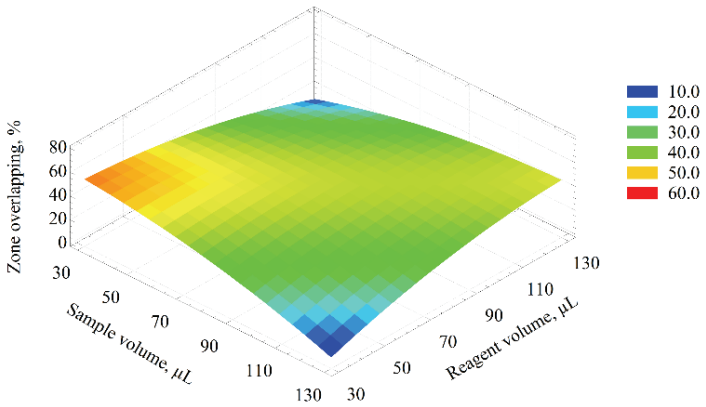

Fig. 6. The effect of sample and reagent volumes on zone overlapping at 1 mL min^{-1} flow rate and 40 cm coil length.

The combination of very low sample and reagent volumes (30–50 μL) resulted in the most efficient overlapping and zone penetration. In contrary to this, the lowest value of zone overlapping was obtained when low reagent volumes were combined with high sample volumes and *vice versa*. Low volume plugs overlap very efficiently, but it can be expected that they will be dispersed to a higher extent on their way to the detector. Low sample and reagent volumes can be considered for the development of analytical methods based on fast one-step reactions in combination with a detector of appropriate sensitivity. In that case, a manifold can employ a short reaction coil, and the effect of dispersion will consequently be less expressed.

Dispersion

The dispersion coefficients for reagent (D_r) and sample plug (D_s) were calculated as the VI's output parameters by dividing the signal recorded for 0.15 mol L^{-1} potassium chloride (S_0) by peak height. The obtained values were used for the creation of response surface graphs presented in Fig. 7.

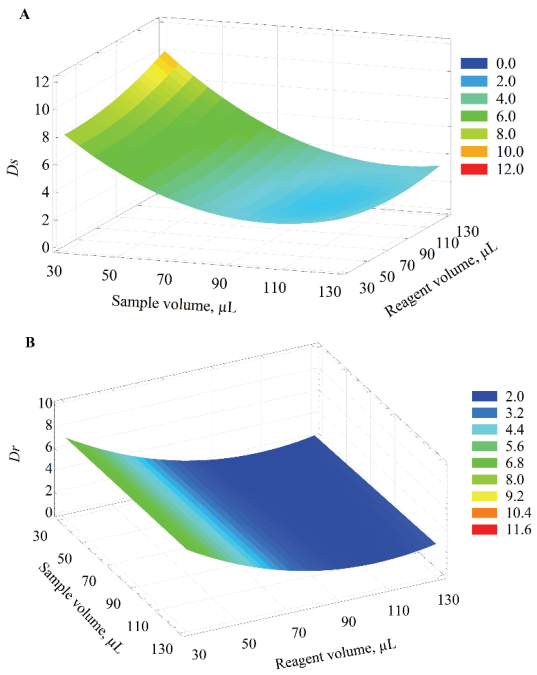

Fig. 7. The effect of sample and reagent volumes on sample dispersion coefficient (A) and reagent dispersion coefficient (B) at 1 mL min^{-1} flow rate and 40 cm coil length.

SIA systems employ bi-directional pumps for the manipulation of liquid plugs back and forth. The unique characteristic of SIA is that flow reversals are favouring the mutual interdispersion of reagent and sample, the reactants. The previous studies have shown that the first flow reversal is increasing the mixing of the zones significantly, while later cycles less affect the zone interpenetration.[11]

We confirmed that sample dispersion coefficients are higher compared to reagent dispersion coefficients. Since the sample plug is aspirated first, its dispersion is additionally affected as the sample plug is displaced and partially penetrated by the reagent plug. The flow reversal enhances interpenetration in the opposite direction. The sample dispersion coefficient varies between 2 and 10, over the tested range. The reagent dispersion coefficient exceeded value 3 only when low reagent volumes were used. It varies less over the tested range as the traveling path is shorter, and the sample volume has no effect on it. Even though the medium dispersion of a sample and a reagent plug is the most common, the model indicates that over the whole examined range dispersion coefficients are convenient and adaptable to the specific needs, considering the sample and reagent characteristics and the reaction type.

From the presented results, we can observe how the single flow reversal increased the dispersion of sample plug. In order to better evaluate the flow reversal effect on plug dispersion, the cell can be placed between the selector valve and the holding coil.

Zone penetration and reagent economy

In the very wide range of conducted experiments excluding the above mentioned combinations, the zone overlapping values were around 40 % (Fig. 7). Similar zone overlapping expressed relatively, corresponds to different overlapping areas, if presented in the units of measurement. Consequently, in the case of a definite reaction, a higher or lower quantity of a product would have been formed, respectively. By choosing the appropriate conditions one can adapt the signal to the sensitivity and the linear range of the detector. But, here an another aspect, the reagent economy was targeted, and it also cannot be judged based on the zone overlapping, since it considers the entire area of the two peaks. This is enabled by the VI which also provides the overlapped fraction of the reagent peak. The area of similar zone penetration profiles in the range of different volumes of sample and reagent plug was further explored, by considering under which combination of experimental conditions the reagent could have been more economically used, while keeping the zone overlapping value constant. Graph of the created contour plots in which the zone overlapping and the overlapped fraction of the reagent peak were used as responses and superimposed is presented in Fig. 8.

The scaling of the axis was the same for both graphs, and they were of the same size. The overlapped fraction of the reagent peak varied from 10 (pale blue area) to 100 % (dark blue area) over a range of different experimental values. When the overlapped fraction of the reagent peak reaches 100 %, the reagent peak is completely overlapped, and every part of the plug will participate in a chemical reaction. The other contour plot, describing the distribution of zone

overlapping values, was presented with grey lines with numbers adjoined. The zone overlapping, as a parameter, gives information concerning both plugs. By the overlaying of two response variables, an insight in the reagent economy, which is a very important aspect of SIA optimization was obtained. It was demonstrated on three examples how the VI can support more detailed zone penetration studies that help us plan the experiments in the range which ensures efficient zone overlapping, adequate dispersion, and high reagent exploitation. Some additional considerations are still possible.

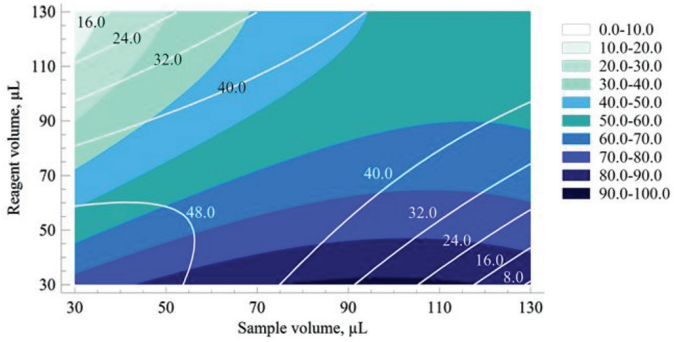

Fig. 8. Contour plots obtained when zone overlapping (grey lines) and overlapped fraction of the reagent peak (graded blue colour areas) were used as responses at 1 mL min^{-1} flow rate and 40 cm coil length.

CONCLUSION

The applicability of the created virtual instrument for the data pre-treatment, calculation of peak overlapping area, and the most important peak-related parameters was confirmed. The virtual instrument was applied to characterize the behaviour of the sample and reagent plug in a system with 0.75 mm i.d. tubes, 1 m holding coil, and 40 cm reaction coil at 1 mL·min^{-1} propelling flow rate. A general model was based on potassium chloride and conductometric detection. More detailed zone penetration studies, supported by the developed VI, enabled the general characterization of the behaviour of the SIA system. The presented studies supported with the experimental design techniques have also proven useful for the more specific goals. It was possible to detect the volume range of interest for two very important aspects in SIA method optimization, the reagent economy and the employment of detectors of different sensitivity. Even though the VI was developed for the processing of peak signals obtained within the flow system, its use is not only limited to this type of chemical analysis. The VI has the potential to be applied in other areas, *e. g.*, spectroscopy or chromatography. The examinations of the Stokes shift in fluorescence,[32,33] or the development of an expert system for simultaneous ion-chromatographic determination of ions in wide concentration range as found in highly mineralized waters,[34] are the

examples of studies that can also potentially profit from the VI. The developed software is available upon request from the authors. For the access to the graphical user interface of the created VI, it is not necessary to have the LabVIEW program installed. NI Run-Time engine 2015 SP1 which is required for running the executables created within the LabVIEW program, can be downloaded for free.[35] The more experienced users, already using the LabVIEW program, can further modify the code and adapt it to their specific needs.

SUPPLEMENTARY MATERIAL

Additional data and information are available electronically at the pages of journal website: https://www.shd-pub.org.rs/index.php/JSCS/article/view/10940, or from the corresponding author on request.

Acknowledgement. The financial support is gratefully acknowledged from the Slovenian Research Agency (ARRS) through program P1-0153.

ИЗВОД

LABVIEW ВИРТУЕЛНИ ИНСТРУМЕНТ ЗА СТУДИЈЕ ПРЕКЛАПАЊА ЗОНА У ПРОТОЧНИМ АНАЛИТИЧКИМ СИСТЕМИМА

ALEKSANDRA KULJANIN и NATAŠA GROS

University of Ljubljana, Faculty of Chemistry and Chemical technology, Večna pot 113, 1000 Ljubljana, Slovenia

Један од основних корака у развоју проточних метода је испитивање ефикасности преклапања зоне узорка и реагенса. Иако студије имају далеко већи потенцијал, евалуација параметара од значаја није довољно детаљна и користи се искључиво у почетним фазама истраживања. Креирани виртуални инструмент у LabVIEW програмском пакету омогућава обраду сигнала у форми пика, израчунавање површине преклапања зона као и осталих параметара у експериментима који моделују интеракцију зоне узорка и реагенса. Поузданост инструмента најпре је потврђена на сету од 36 фајлова који је креиран тако да обухвата све потенцијалне могућности за интеракцију зона у проточном систему. У наставку, поштујући правила Box–Behnken дизајна, вариране су запремине узорка и реагенса, брзина протока и дужина петље за мешање у секвенцијалном инјекционом систему. На три примера демонстрирано је како развијени виртуелни инструмент може бити користан при планирању експеримената у опсегу који ће омогућити ефикасно преклапање зона, економичну употребу реагенса и адекватну дисперзију зона. Употреба виртуелног инструмента није ограничена само на проточне системе, може наћи своју примену и у спектроскопији и хроматографији. Приступ графичком интефејсу могућ је и без претходне инсталације LabVIEW програма.

(Примљено 9. јула, ревидирано 30. јула, прихваћено 4. августа 2021)

REFERENCES

1. P. K. Dasgupta, Y. Chen, C.A. Serrano, G. Guiochon, H. Liu, J.N. Fairchild, R.A. Shalliker, *Anal. Chem.* **82** (2010) 10143 (https://doi.org/10.1021/ac102242t)
2. I. A. Haidar Ahmad, A. Blasko, J. Tam, N. Variankaval, H. M. Halsey, R. Hartman, E. L. Regalado, *J. Chromatogr., A* **1603** (2019) 1 (https://doi.org/10.1016/j.chroma.2019.04.017)

3. M. F. Wahab, A. Berthod, D. W. Armstrong, *J. Sep. Sci.* **42** (2019) 3604 (https://doi.org/10.1002/jssc.201900799)
4. H. Kong, F. Ye, X. Lu, L. Guo, J. Tian, G. Xu, *J. Chromatogr., A* **1086** (2005) 160 (https://doi.org/10.1016/j.chroma.2005.05.103)
5. M. J. Rodríguez-Cuesta, R. Boqué, F. X. Rius, J. L. Martínez Vidal, A. Garrido Frenich, *Chemometr. Intell. Lab. Systems* **77** (2005) 251 (https://doi.org/10.1016/j.chemolab.2004.09.010)
6. Y. Hu, J. Liu, W. Li, *Anal. Chim. Acta* **538** (2005) 383 (https://doi.org/10.1016/j.aca.2005.02.024
7. M. Perez-Baeza, L. Escuder-Gilabert, M. J. Medina-Hernandez, J. J. Baeza-Baeza, M. C. Garcia-Alvarez-Coque, *J. Chromatogr., A* **1625** (2020) 461273 (https://doi.org/10.1016/j.chroma.2020.461273)
8. M. Karakaplan, F. M. Avcu, *J. Chemom.* **34** (2020) 3229 (https://doi.org/10.1002/cem.3229)
9. V. Cerdà, L. Ferrer, J. Avivar, A. Cerdà, *Evolution and Description of the Principal Flow Techniques In Flow Analysis*, Elsevier, Boston, MA, 2014, pp. 1–42 (https://doi.org/10.1016/B978-0-444-59596-6.00001-2)
10. J. Ruzicka, E. H. Hansen, *Flow injection analysis*, John Wiley and Cons, New York, 1988, pp. 365–371 (ISBN: 978-0-471-81355-2)
11. T. Gubeli, G. D. Christian, J. Ruzicka, *Anal. Chem.* **63** (1991) 2407 (https://doi.org/10.1021/ac00021a005)
12. R. E. Taljaard, J. F. van Staden, *Lab. Rob. Autom.* **10** (1998) 325 (https://doi.org/10.1002/(SICI)1098-2728(1998)10:6<325::AID-LRA3>3.0.CO;2-L)
13. J. F. van Staden, T. McCormack, *Instrum. Sci. Technol.* **27** (1999) 167 (https://doi.org/10.1080/10739149908085847)
14. J. Jakmunee, T. Rujiralai, K. Grudpan, *Anal. Sci.* **22** (2006) 157 (https://doi.org/10.2116/analsci.22.157)
15. C. X. Galhardo, J. C. Masini, *Anal. Chim. Acta* **417** (2000) 191 (https://doi.org/10.1016/S0003-2670(00)00933-8)
16. W. Khongpet, S. Pencharee, C. Puangpila, S. Kradtap Hartwell, S. Lapanantnoppakhun, J. Jakmunee, *Talanta* **177** (2018) 77 (https://doi.org/10.1016/j.talanta.2017.09.018)
17. A. R. Araujo, M. L. Saraiva, J. L. Lima, *Talanta* **74** (2008) 1511 (https://doi.org/10.1016/j.talanta.2007.09.028)
18. L. D. Chen, J. Xu, T. Wang, Y. M. Huang, D. X. Yuan, Z. B. Gong, *Talanta* **232** (2021) 122404 (https://doi.org/10.1016/j.talanta.2021.122404)
19. S. Liawruangrath, K. Prasertboonyai, *Anal. Lett.* **54** (2021) 364 (https://doi.org/10.1080/00032719.2020.1764970)
20. T. J. Trinklein, M. Thapa, L. A. Lanphere, J. A. Frost, S. M. Koresch, J. H. Aldstadt, *Talanta* **231** (2021) 122355 (https://doi.org/10.1016/j.talanta.2021.122355)
21. *OriginLab*, https://www.originlab.com/index.aspx?go=PRODUCTS/Origin (accessed 31. 5. 2021)
22. J. Walkenbach, *Excel® 2010 Power Programming with VBA,* Wiley Publishing, Indianapolis, IN, 2010, pp. 1–10 (ISBN: 978-0-470-47535-5)
23. T. Mikhailova, S. M. Mustafina, V. Mikhailov, S. Mustafina, *Entomol. Appl. Sci. Lett.* **5** (2018) 21 (https://easletters.com/article/brwa-automation-of-controls-process-of-macro-of-microsoft-excel-file-for-data-processing-of-chemical-experiments)
24. L. Liu, J. Li, L. Deng, *Adv. Mat. Res.* **569** (2012) 808 (https://doi.org/10.4028/www.scientific.net/AMR.569.808)

25. *National Instruments*, http://www.ni.com (accessed 31.5.2021)
26. R. A. Viscarra Rossel, *Chemom. Intell. Lab. Systems* **90** (2008) 72 (https://doi.org/10.1016/j.chemolab.2007.06.006)
27. W.B. Wang, J. Li, Q. J. Wu, *J. Automat. Chem.* **2007** (2007) 68143 (https://doi.org/10.1155/2007/68143)
28. M. R. Liu, Y. Liu, Y, L. M. Zhou, *Micromachines* **12** (2021) 602 (https://doi.org/10.3390/mi12060602)
29. J. Ma, P. Li, Z. Chen, K. Lin, N. Chen, Y. Jiang, J. Chen, B. Huang, D. Yuan, *Anal. Chem.* **90** (2018) 6431 (https://doi.org/10.1021/acs.analchem.8b01490)
30. C. Lenehan, N. Barnett, S. Lewis, *J. Autom. Chem.* **24** (2002) 99 (10.1080/14639240210136747)
31. Y. Deng, P. C. Li, T. Y. Fang, Y. Y. Jiang, J. X. Chen, N. W. Chen, D. X. Yuan, J. Ma, *Anal. Chem.* **92** (2020) 4379 (10.1021/acs.analchem.9b05252)
32. X. L. Ronghui Zhou, Q. Yang, P. Wu, *Chin. Chem. Lett.* **30** (2019) 1843 (https://doi.org/10.1016/j.cclet.2019.07.062)
33. A. Bavali, P. Parvin, M. Tavassoli, M. R. Mohebbifar, *Appl. Opt.* **57** (2018) B32 (https://doi.org/10.1364/AO.57.000B32)
34. N. Gros, B. Gorenc, *J. Chromatogr., A* **697** (1995) 31 (https://doi.org/10.1016/0021-9673(95)92840-K)
35. *National Instruments LabVIEW*, https://www.ni.com/sl-si/support/downloads/software-products/download.labview-runtime.html#369481 (accessed 31. 5. 2021).

Journal of the Serbian Chemical Society
JSCS@tmf.bg.ac.rs • www.shd.org.rs/JSCS
J. Serb. Chem. Soc. 86 (11) S420–S421 (2021) *Supplementary material*

SUPPLEMENTARY MATERIAL TO

LabVIEW virtual instrument for zone penetration studies in flow-based analytical systems

ALEKSANDRA KULJANIN and NATAŠA GROS*

University of Ljubljana, Faculty of Chemistry and Chemical technology, Večna pot 113, 1000 Ljubljana, Slovenia

J. Serb. Chem. Soc. 86 (11) (2021) 1089–1102

EVALUATION OF THE RELIABILITY OF PREDICTED PEAK OVERLAPPING AREAS BY WEIGHING METHOD

We created an auxiliary LabVIEW VI (TwoPeaks simul XY Graph.VI) to generate artificial sets of data. A while loop comprises the Continuous PDF VIs that create the normal probability density functions (Owning Palette: Probability VIs). Noise is optionally added by employing the Random Number Functions (Owing Palette: Numeric Functions). To ensure independence, someone who prepared the testing set of data was a different person from the one who used them in the evaluation. Thirty-six text files each comprising two sets of artificial Gaussian peaks data points included all the different types of cases that can be foreseen. Graphs that represented chosen thirty-six cases were printed on paper in A3 format. All graphs were of the same size with equal scales. Printed graphs were left in the room at controlled temperature, where the weighing was later performed. After achieving stable paper mass, one peak which extended over the whole overlapping area was cut out and weighed. After that, the overlapping area was also cut out of it and weighed. Paper manipulation was done with the gloves. For the measurements, we were using XPR micro-balance with the readability of 0.5 μg (Mettler Toledo, Australia).

Graphical presentation of the predictions tested by weighing method on the artificial sets of Gaussian peaks is given in Fig. S-1. The calculated overlapping area was expressed relatively against the area of the first peak. The results obtained by weighing correlate with VI predictions at high level (R^2 = 0.9993).

* Corresponding author. E-mail: Natasa.Gros@fkkt.uni-lj.si

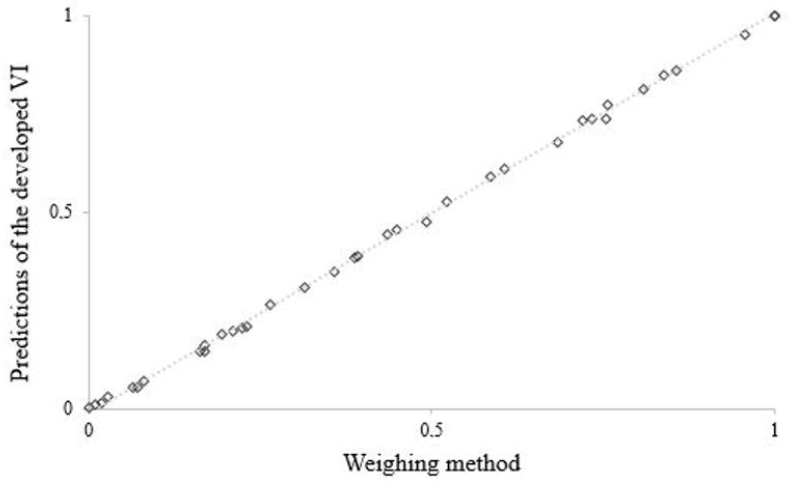

Fig. S-1. Correlation of the VI predictions of overlapping area with values obtained by weighing method, all expressed relatively as the fraction of overlapping areas against the area of the first peak.

HARDWARE CONTROL AND DATA ACQUISITION MODULES

Hardware control and data acquisition were done *via* LabVIEW 2015 software through NI cRIO 9066 controller integrating NI 9025 16-Bit Analog Input module, NI-USB-9472 Digital Output device, and NI-9870 4-Port, RS232 Serial Module. NI 9870 serial module was used for the control of the syringe pump, while data acquisition was done via NI 9025 AI module. The frequency of signal collection within the LabVIEW software was 8 signals per second.

Journal of the Serbian Chemical Society
JSCS-info@shd.org.rs • www.shd.org.rs/JSCS
J. Serb. Chem. Soc. *86* (11) 1103–1112 (2021)
JSCS–5486
Original scientific paper
Published 24 September 2021

Hydroxyapatite/nifuroxazide conjugate: Characterization, drug release and antimicrobial activity

ŽELJKO RADOVANOVIĆ[1]*, KATARINA MIHAJLOVSKI[2], LIDIJA RADOVANOVIĆ[1#], ĐORĐE JANAĆKOVIĆ[2] and RADA PETROVIĆ[2]

[1]*Innovation Centre of the Faculty of Technology and Metallurgy, University of Belgrade, Karnegijeva 4, 11000 Belgrade, Serbia and* [2]*Faculty of Technology and Metallurgy, University of Belgrade, Karnegijeva 4, 11000 Belgrade, Serbia*

(Received 20 April, revised 25 May, accepted 26 May 2021)

Abstract: Synthetic hydroxyapatite ($Ca_{10}(PO_4)_6(OH)_2$, HAp) is very similar to the inorganic part of the bones and teeth of mammals. It is a well-known biomaterial with good biocompatibility, osteoconductivity and bioactivity. Nifuroxazide ($C_{12}H_9N_3O_5$, NFX) is a broad-spectrum antibacterial drug and poorly soluble in water. In order to increase the solubility of NFX, nano-sized HAp powder and raw NFX drug were mixed giving, as a result, a HAp/NFX conjugate. Characterization of the raw materials and the obtained conjugate confirmed the integration of NFX on the HAp surface. An *in vitro* study of drug release in simulated stomach acid and intestinal fluid showed a much faster release of NFX from HAp surface than those of the raw drug. The HAp/NFX conjugate showed excellent inhibitory effects against Gram-positive bacterium *Staphylococcus aureus*, Gram-negative bacterium *Escherichia coli* and yeast *Candida albicans*, proving the nano-sized HAp powder as a promising drug carrier.

Keywords: biomaterials; nanomaterials; drug delivery; antimicrobial properties.

INTRODUCTION

Hydroxyapatite ($Ca_{10}(PO_4)_6(OH)_2$, HAp) as a nano-sized and calcium-deficient material is the main inorganic component of the bones and teeth of mammals.[1] Due to its excellent bioactivity, biocompatibility, osteoconduction and osteoinduction, the broad spectrum of applications of HAp is known so far: in bone tissue engineering, implant osteointegration[1] together with being a gene, protein and drug carrier.[2–6] Drug carriers based on HAp have been of particular

* Corresponding author. E-mail: zradovanovic@tmf.bg.ac.rs
# Serbian Chemical Society member.
https://doi.org/10.2298/JSC210420040R

interest during the last decades, especially for the promising treatment of bone infections, arthritis, cancer and cardiovascular diseases.[7–9]

Nifuroxazide ($C_{12}H_9N_3O_5$, NFX), a poorly water-soluble drug that belongs to the class of nitrofuran derivatives, shows significant antibacterial activity against Gram-positive bacteria, such as *Staphylococcus aureus* and *Streptococcus spp*., and Gram-negative bacteria, such as *Escherichia coli* and *Pseudomonas aeruginosa*. Due to the presence of a nitro group in its structure, NFX is efficient in the treatment of infections in the gastrointestinal and urogenital tracts, and is known to have a bacteriostatic effect in small doses as well as a bactericidal effect in high doses.[10] Furthermore, there are studies that proved NFX as a promising drug in the treatment of different types of cancer.[10–12] Nevertheless, NFX, which was frequently used for treatment of colitis and diarrhoea, showed low effect against those diseases due to poor absorption from the digestive tract (low burst effect) that resulted in fast removal from the body without being metabolized.[13] Some studies showed that improvement of the efficiency (faster dissolution rate and higher solubility) of low soluble drugs such as carvedilol, ibuprofen and silybin, can be achieved by integration with HAp.[5,6,14] It is assumed that the connection between HAp and drugs occurred mainly through establishment of hydrogen bonds between OH groups at the HAp surface and some of the functional groups of the drug.[5,6]

In the current study, HAp nanoparticles were prepared by the hydrothermal method, while HAp/NFX conjugate was obtained by impregnation under vacuum. The structure, morphology, specific surface area, spectral and thermal properties of HAp, raw NFX and HAp/NFX conjugate were investigated by X-ray powder diffraction (XRPD), Field emission scanning electron microscopy (FESEM), the Brunauer, Emmett and Teller method (BET), attenuated total reflectance-Fourier transform infrared spectroscopy (ATR-FTIR) and thermal analysis. *In vitro* drug release tests in simulated gastric and intestinal fluids were performed for NFX and HAp/NFX, while all materials were studied *in vitro* for their antimicrobial activities.

EXPERIMENTAL

Materials and measurements

For the synthesis of HAp powder, calcium nitrate tetrahydrate (≥ 98 %, Carl Roth, Germany), sodium dihydrogen phosphate dihydrate (99.8 %, VWR), and ammonium hydroxide (*p.a.,* Zorka Pharma, Šabac, Serbia) were used. Nifuroxazide (5-nitro-2-furaldehyde *p*-hydroxybenzoylhydrazone) was purchased from Sigma–Aldrich.

XRPD measurements were performed on a Rigaku SmartLab diffractometer using CuKα radiation, at 40 kV and 30 mA, in Bragg–Brentano geometry. Diffraction data for HAp and HAP/NFX were collected in the range $5° < 2\theta < 70°$ (scan speed: 0.12° min^{-1}, step width: $2\theta = 0.01°$), whereas diffraction data for NIF were collected in the range $5° < 2\theta < 50°$ (scan speed: 0.06° min^{-1}, step width: $2\theta = 0.01°$) at room temperature. ATR-FTIR spectra of the samples were recorded in absorbance mode using a Nicolet™ iS™ 10 FTIR spectrometer

(Thermo Fisher Scientific) with Smart iTR™ ATR sampling accessories, within the range of 4000–400 cm^{-1}, at a resolution of 4 cm^{-1} and in 20 scan mode. Thermal properties were examined from room temperature up to 1200 °C for HAp and HAp/NFX and up to 800 °C for NFX in platinum sample cups using an SDT Q600 instrument (TA Instruments). The heating rate was 20 °C min^{-1} and the furnace atmosphere consisted of air at a flow rate of 100 mL min^{-1} (weight accuracy is ±1 %). FESEM Tescan Mira 3 XMU was used for the morphological characterization of the samples. Before analysis, the samples were coated with Au. The specific surface areas (*SSA*) of HAp, NFX and HAp/NFX were calculated according to the Brunauer, Emmett and Teller (BET) method from the linear part of the nitrogen adsorption isotherm at 77 K on a Micrometrics ASAP 2020 instrument. Before the measurements, the samples were out-gassed at 150 °C for 10 h under vacuum. The total pore volume (V_{tot}) was given at p/p_0 = 0.998. The volume of the mesopores was calculated according to the Barrett, Joyner and Halenda (BJH) method from the desorption branch of the isotherm.

Synthesis of nano-sized HAp and HAp/NFX conjugate

Nano-HAp was obtained as reported earlier.[15] Briefly, appropriate amounts of $Ca(NO_3)_2 \cdot 4H_2O$, $NaH_2PO_4 \cdot 2H_2O$ and NH_4OH were dissolved in 2 L of distilled water. The obtained solution with Ca/P ratio 1.67 and pH 10.10 was placed in an autoclave for 3 h at 160 °C. After slow cooling, the obtained powder was filtered and dried.

The HAp/NFX conjugate was prepared according to the following procedure: commercial drug NFX (0.14 g) was dissolved in 1 M NaOH (5 mL) under vigorous magnetic stirring. Next, HAp (0.60 g) was added to the solution and stirred for 30 min. The obtained mixture was transferred into round bottom flask (100 mL) and stirred in a rotavapor at 60 °C for 45 min until most of the solvent has evaporated. Then, the prepared sample was dried in an oven at 100 °C for 1 h and spontaneously cooled to the room temperature.

In vitro *drug release study*

In vitro drug release tests for NFX and HAp/NFX were performed in two types of fluids: aqueous solution of HCl (pH 1.2) and phosphate buffer solution (pH 6.8), which simulated stomach acid and intestinal fluid, respectively. 450 mL of each fluid was used for analysis, at 37 °C under continuous stirring rate of 100 rpm. Then 1 mg of NFX as well as 5.28 mg of HAP/NFX, containing 1 mg of NFX, was added to each fluid. At predetermined time intervals, an aliquot of 2.5 mL was taken for analysis and 2.5 mL of fresh fluid was added immediately, to maintain a constant volume. The aliquot was filtered and then analysed by UV–Vis spectrophotometry (UV-1800, Shimadzu, Japan) at a wavelength of 255 nm. The reported results were an average value of two measurements.

Antimicrobial test

Quantitative tests of the antimicrobial activity of HAp, NFX and HAp/NFX samples against Gram-positive (G^+) bacterium *Staphylococcus aureus* (*S. aureus*, ATCC 25923), Gram-negative (G^-) bacterium *Escherichia coli* (*E. coli*, ATCC 25922) and yeast *Candida albicans* (*C. albicans*, ATCC 10259) were performed according to the liquid challenge method in sterile normal saline solution. A mass of 0.01 g of each sample was suspended in a tube containing 0.9 mL of sterile normal saline and inoculated with 0.9 mL microorganism suspension to achieve the appropriate concentrations (in CFU cm^{-1}). The tubes were then incubated at 37 °C for 1 h. After incubation, 9 mL of sterile normal saline was added. Subsequently, 1 mL aliquots were taken as samples for determination of the viable cell. Sterile normal saline solution was used for dilution of the number of colonies and 0.1 mL of the appropriately diluted solution was placed in a Petri dish and overlaid with TSAY (Tripton soy

agar with 0.6 % yeast extract). The Petri dishes were incubated at 37 °C for 24 h. As a control, a blank sterile normal saline solution without sample was used. The degree of reduction, R / %, was calculated according to Eq. (1):

$$R = 100(CFU_{cont} - CFU_M)/CFU_{cont} \quad (1)$$

where CFU_{cont} is the number of microorganism colonies in the control tube and CFU_M is the number of microorganism colonies in the tubes with the samples.

RESULTS AND DISCUSSION

The XRPD patterns of HAp nanoparticles, NFX, and the HAp/NFX conjugate are shown in Fig. 1. The details about the crystal structure and Rietveld refinement analysis of the prepared nanosized HAp can be found in a previous study.[15] As could be observed from the patterns, HAp and NFX are highly crystalline, whereas HAp/NFX conjugate does not show the reflections characteristic for NFX but shows only broad reflections of a HAp phase, probably due to formation of highly dispersed and/or amorphous thin layer of NFX, which was similarly found in previous studies for other drugs.[5,6]

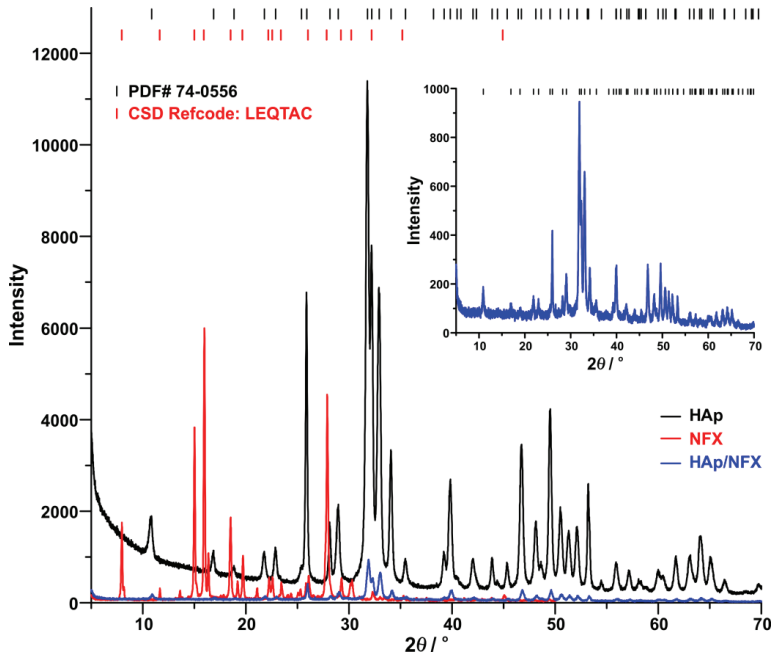

Fig. 1. XRPD patterns of HAp, NFX and HAp/NFX. The XRPD pattern of HAp is compared with the standard PDF# 74-0556 card. The XRPD pattern of NFX is compared with the pattern obtained from single crystal data (Cambridge Structural Database, CSD Refcode: LEQTAC).[16] An enlarged diffractogram of HAp/NFX is shown as the inset.

The FTIR spectra of HAp, NFX and HAP/NFX are presented in Fig. 2a. The characteristic bands corresponding to the presence of the OH^- and PO_4^{3-} groups

on the surface of the HAp are found at 3572 cm^{-1} as well as at 1088, 1020 and 560 cm^{-1}. These groups can, according to Zhao *et al.*,[5] improve the water solubility of insoluble drugs. In the spectrum of NFX, the band found at 1254 cm^{-1} can be assigned to the deformation of the furan ring, while the bands observed at 1465 and 851 cm^{-1} correspond to ν(C–C) and ν(C–H) vibrations of the phenyl ring, respectively. The presence of the N–H and C=O bonds is confirmed by the band at 3363 cm^{-1} for the former and at 1667 cm^{-1} for the later, while the vibration at 1606 cm^{-1} is ascribed to the C=N bond. In addition, the asymmetric (ν_{as}) and symmetric (ν_s) vibrations at 1507 and 1360 cm^{-1}, respectively, are ascribed to the existence of the resonant NO_2 group.[17] In the FTIR spectrum of HAp/NFX the characteristic group of bands of NFX, which are observed in the 1700–1200 cm^{-1} region, are slightly shifted towards lower wavelengths relative to the position of the same bands in the spectrum of raw NFX. In addition, the broad band centred at 3220 cm^{-1} indicates that there could be the connection of NFX with the HAp surface, probably through the formation of hydrogen bonds between NO_2 or C=O groups from NFX and OH^- group from HAp.[18]

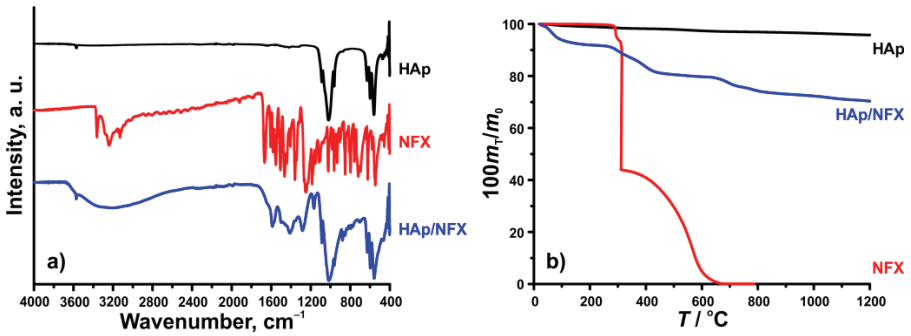

Fig. 2. FTIR spectra (a) and TGA curves (b) of HAp, NFX and HAp/NFX.

In order to determine the amount of drug in HAp/NFX,[5] the TGA analysis was performed in an air atmosphere and the results are presented in Fig. 2b. The TGA curve for HAp revealed a negligible mass loss of 4.3 %. In the temperature range investigated, the TGA curve of NFX shows stability up to ≈280 °C after which the combustion reaction of NFX occurs rapidly with a total mass loss of 100 % up to ≈650 °C. In the TGA curve of HAp/NFX, the observed mass loss of 6.1 % up to 100 °C was ascribed to the loss of adsorbed moisture, whereas the total mass loss up to final temperature of the analysis was 29.8 %.[19] According to the obtained data, it was found that the prepared HAp/NFX had a drug loading efficiency up to 19.4 %, which is close to theoretical value of 18.9 %. The difference between found and theoretical value of drug loading is in accordance with the weight accuracy of the instrument.

The FESEM micrographs of HAp, NFX and the HAp/NFX conjugate are presented in Fig. 3. As it has been shown earlier,[15] HAp consists of rod-like nanoparticles with an average size of 87 nm, which further form the agglomerates with sizes in the range 2–5 μm. The NFX drug is comprised of plate-like particles with wide particle size distributions (length in the range 0.3–10 μm, and width in the range 0.1–8 μm). The analysis of morphology of HAp/NFX shows that particles of HAp were overlaid by drug, with a thicker coating of the drug in some segments. The damage of the sample caused by the electron beam was not detected, which indicates that a thin layer of drug was formed on the surface of HAp.[6] In addition, the agglomeration of HAp/NFX conjugate is more pronounced than those of raw HAp and NFX, and HAP/NFX agglomerates are more compact.

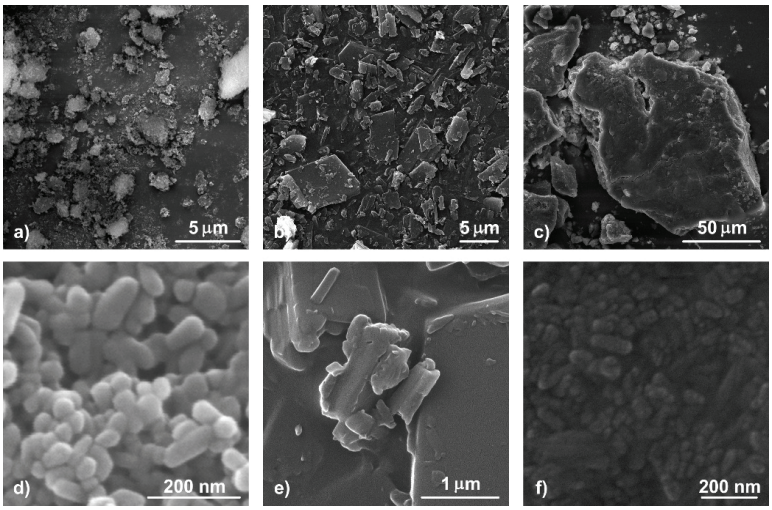

Fig. 3. FESEM images of HAp (a), NFX (b), HAp/NFX (c), HAp (d), NFX, (e) and HAp/NFX (f).

The morphology analysis of the samples is in accordance with the results of the BET analysis (Fig. 4, Table I). The value of *SSA* for the HAp/NFX conjugate was significantly smaller (0.24 m^2 g^{-1}) in comparison to values for HAp and NFX (47.8 and 3.51 m^2 g^{-1}, respectively), indicating a very good integration of the starting materials into HAp/NFX. The pores present in HAp sizes 20–30 nm were due to the voids between the nanoparticles. During the formation of a homogeneous mixture of HAp and NFX, these pores closed quite easily resulting in a low total porosity of the HAp/NFX conjugate.

The cumulative release profiles of raw NFX and NFX from the HAp/NFX conjugate in simulated stomach acid (pH 1.2) and intestinal fluid (pH 6.8) are shown in Fig. 5.

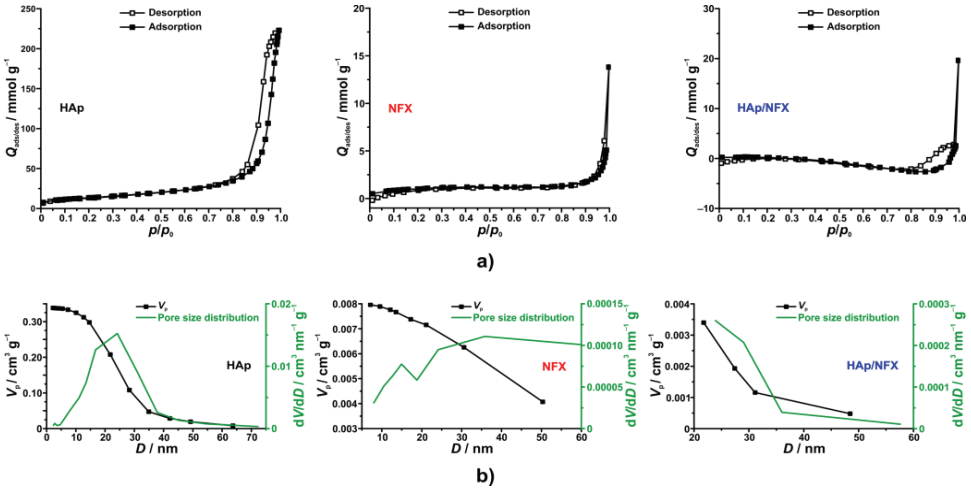

Fig. 4. Adsorption-desorption curves (a) and pore volume and pore size distribution (b) for HAp, NFX and HAp/NFX.

TABLE I. The results of BET analysis of HAp, NFX and HAp/NFX

Sample	*SSA* / m^2 g^{-1}	V_{tot}[a] / mL g^{-1}	V_{meso}[b] / mL g^{-1}	V_{micro}[c] / mL g^{-1}	D_{sr}[d] / nm	D_{max}[e] / nm
HAp	47.8	0.3395	0.3384	0.0142	20.2	24
NFX	3.51	0.0094	0.0080	0.0013	35.1	36
HAp/NFX	0.24	0.0044	0.0034	0.0007	29.5	–[f]

[a]V_{tot} – total pore volume; [b]V_{meso} – mesopore volume; [c]V_{micro} – micropore volume; [d]D_{sr} – average pore diameter; [e]D_{max} – the diameter of the pores that occupy the largest part of the volume. [f]Due to the low value of *SSA*, there was not enough data to determine D_{max} and there are negative values on the adsorption-desorption curves (Fig. 4)

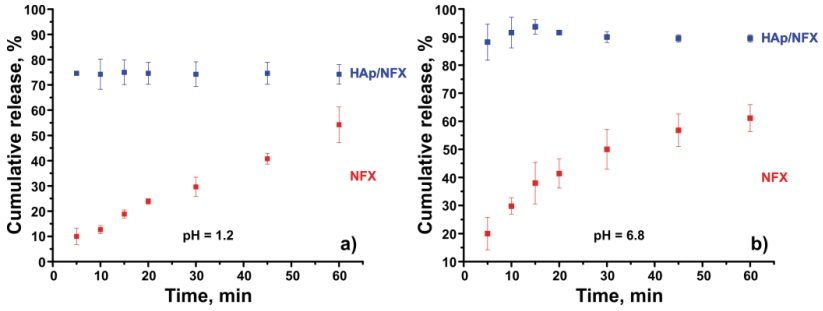

Fig. 5. *In vitro* drug release profiles of NFX and HAp/NFX at pH 1.2 (a) and 6.8 (b).

The release profile of raw NFX exhibited a slow, constant increase with time in both simulated fluids. After 60 min, 54 % of raw NFX in the stomach acid and 61 % in intestinal fluid had been excreted. Nevertheless, the HAp/NFX conjugate showed an initial fast release of NFX (burst effect) in both fluids, which could be associated with the integration of the drug with the surface of HAp.[20] A very high cumulative release of NFX from HAp/NFX was observed in the simulated

intestinal fluid with the value of 90 %. Such a releasing profile is more favourable from the point of its application proving that a combination of NFX with HAp leads to significantly better and faster utilization of the drug.

The *in vitro* antimicrobial activities of HAp, NFX and HAp/NFX were screened against *S. aureus* (as a G^+ bacterium), *E. coli* (as a G^- bacterium) and yeast *C. albicans* and the obtained results are presented in Table II. The HAp/NFX conjugate was found to be the most active, showing a high inhibitory effect against all examined bacteria (99.0 % for *S. aureus* and 94.0 % for *E. coli*) and moderate activity against *C. albicans* (Table II). In contrast to HAp/NFX, pure HAp and pure NFX were less effective, with the latter showing a high activity only against *S. aureus* (94.3 %). Such results are in agreement with the NFX release from HAp/NFX conjugate. Furthermore, it must be taken into account that excellent antimicrobial activity of HAp/NFX is achieved with about five times smaller mass of drug than that of pure NFX, which makes these results even more convincing.

TABLE II. The data of the antimicrobial test of HAp, NFX and HAp/NFX

Sample	*S. aureus*		*E. coli*		*C. albicans*	
	Number of colonies	$R \pm SD$ / %	Number of colonies	$R \pm SD$ / %	Number of colonies	$R \pm SD$ / %
Control	4.0×10^5	–	1.0×10^5	–	1.9×10^7	–
HAp	5.8×10^5	n. a.[a]	2.7×10^5	n. a.	8.0×10^6	57.9±1.4
NFX	2.3×10^4	94.3±1.1	5.2×10^4	48.0±1.7	7.9×10^6	58.4±0.6
HAp/NFX	4.0×10^3	99.0±0.7	6.0×10^3	94.0±1.2	7.1×10^6	62.6±1.0

[a]Not active

CONCLUSIONS

The low crystalline HAp/NFX conjugate was prepared successfully by impregnation of nanosized HAp with NFX under vacuum. The FTIR analysis showed the presence of hydrogen bonding between NFX and HAp, while the TGA analysis revealed a maximum drug loading efficiency. The *in vitro* release tests showed that HAp nanoparticles demonstrated immediate burst effect during NFX release, compared to that of raw NFX in simulated gastric and intestinal fluid. According to the *in vitro* antimicrobial study, the HAp/NFX conjugate showed the highest inhibitory activity, reaching more than 94 % inhibition against *S. aureus* and *E. coli*. The results of this study demonstrate that nanosized HAp is a suitable carrier for a poorly water-soluble drug. This could improve the release rate as well as antibacterial and antifungal activity of the drug.

Acknowledgement. This work was supported by the Ministry of Education, Science and Technological Development of the Republic of Serbia (Contract No. 451-03-68/2021-14/ /200287 and Contract No. 451-03-68/2021-14/200135).

ИЗВОД

ХИДРОКСИАПАТИТ/НИФУРОКСАЗИД КОЊУГАТ: КАРАКТЕРИЗАЦИЈА, ОТПУШТАЊЕ ЛЕКА И АНТИМИКРОБНА АКТИВНОСТ

ЖЕЉКО РАДОВАНОВИЋ[1], КАТАРИНА МИХАЈЛОВСКИ[2], ЛИДИЈА РАДОВАНОВИЋ[1], ЂОРЂЕ ЈАНАЋКОВИЋ[2] и РАДА ПЕТРОВИЋ[2]

[1]Иновациони центар Технолошко–металуршког факултета, Универзитет у Београду, Карнегијева 4, 11000 Београд и [2]Технолошко–металуршки факултет, Универзитет у Београду, Карнегијева 4, 11000 Београд

Синтетисани хидроксиапатит ($Ca_{10}(PO_4)_6(OH)_2$, HAp) веома је сличан неорганском делу кости и зуба сисара. То је познат биоматеријал са добром биокомпатибилношћу, остеокондуктивношћу и биоактивношћу. Нифуроксазид ($C_{12}H_9N_3O_5$, NFX) је антибиотски лек широког спектра и слабо растворан у води. Како би се повећала растворљивост лека NFX, припремљен је HAp/NFX коњугат мешањем HAp наночестичног праха и лека NFX. Карактеризацијом почетних материјала и добијеног коњугата потврђено је повезивање лека са површином HAp праха. Испитивање отпуштања лека *in vitro* у симулираној стомачној киселини и симулираној цревној течности показало је знатно брже отпуштање NFX са површине HAp у односу на отпуштање чистога лека. HAp/NFX коњугат показао је одличан инхибиторски ефекат на Грам-позитивну бактерију *Staphylococcus aureus*, Грам-негативну бактерију *Escherichia coli* и гљивицу *Candida albicans*, чиме је доказано да је наночестични HAp обећавајући носач лека.

(Примљено 20. априла, ревидирано 25. маја, прихваћено 26.маја 2021)

REFERENCES

1. S. V. Dorozhkin, *Hydroxyapatite and Other Calcium Orthophosphates*, Nova Publisher, New York, 2017 (ISBN: 978-1-53611-897-1)
2. J. Klesing, S. Chernousova, M. Epple, *J. Mater. Chem.* **22** (2012) 199 (https://dx.doi.org/10.1039/C1JM13502C)
3. T. Matsumoto, M. Okazaki, M. Inoue, S. Yamaguchi, T. Kusunose, T. Toyonaga, Y. Hamada, J. Takahashi, *Biomaterials* **25** (2004) 3807 (https://dx.doi.org/10.1016/j.biomaterials.2003.10.081)
4. T. S. P. Cellet, G. M. Pereira, E. C. Muniz, R. Silva, A. F. Rubira, *J. Mater. Chem., B* **3** (2015) 6837 (https://dx.doi.org/10.1039/c5tb00856e)
5. Q. Zhao, T. Wang, J. Wang, L. Zheng, T. Jiang, G. Cheng, S. Wang, *Appl. Surf. Sci.* **257** (2011) 10126 (https://dx.doi.org/10.1016/j.apsusc.2011.06.161)
6. Y. Ryabenkova, N. Jadav, M. Conte, M. F. A. Hippler, N. Reeves-McLaren, P. D. Coates, P. Twigg, A. Paradkar, *Langmuir* **33** (2017) 2965 (https://dx.doi.org/10.1021/acs.langmuir.6b04510)
7. A. L. C. Maia, C. de Aguiar Ferreira, A. L. B. deBarros, A. T. M. e Silva, G. A. Ramaldes, A. da Silva Cunha Júnior, D. C. de Pádua Oliveira, C. Fernandes, D. C. F. Soares, *J. Drug Target.* **26** (2018) 592 (https://dx.doi.org/10.1080/1061186X.2017.1401078)
8. D. Loca, J. Locs, A. Dubnika, V. Zalite, L. Berzina-Cimdina, in H*ydroxyapatite (HAp) for Biomedical Applications*, M. Mucalo, Ed., 1st ed., Woodhead Publishing, Cambridge, 2015, pp.189–209 (Hardcover ISBN: 9781782420330)
9. Z. Yang, W. Xu, M. Ji, A. Xie, Y. Shen, M. Zhu, *Eur. J. Inorg. Chem.* (2017) 5621 (https://dx.doi.org/10.1002/ejic.201701081)

10. C. Bailly, *Drug Discov. Today* **24** (2019) 1930 (https://dx.doi.org/10.1016/j.drudis.2019.06.017)
11. L. Luo, F. Xu, H. Peng, Y. Luo, X. Tian, G. Battaglia, H. Zhang, Q. Gong, Z. Gu, K. Luo, *J. Control. Release* **318** (2020) 124 (https://dx.doi.org/10.1016/j.jconrel.2019.12.017)
12. R. T. Peterson, *Cell Chem. Biol.* **25** (2018) 1439 (https://dx.doi.org/10.1016/j.chembiol.2018.12.005)
13. N. H. Zuma, J. Aucamp, D. D. N'Da, *Eur. J. Pharm. Sci.* **140** (2019) 105092 (https://dx.doi.org/10.1016/j.ejps.2019.105092)
14. L. Chen, H. Zhu, S. Yang, B. Zhou, F. You, X. Yan, *Mater. Lett.* **143** (2015) 252 (https://dx.doi.org/10.1016/j.matlet.2014.12.118)
15. Ž. Radovanović, A. M. Kazuz, P. Vulić, L. Radovanović, Đ. Veljović, R. Petrović, Đ. Janaćković; in *Proceedings of 6th International Conference on Electrical, Electronic and Computing Engineering (Ic)ETRAN* (2019), Silver Lake, Serbia, *Proceedings_IcETRAN_ETRAN_2019*, ETRAN Society, Belgrade, Academic Mind, Belgrade, 2019, p. 676 (https://etran.rs/2019/Proceedings_IcETRAN_ETRAN_2019.pdf)
16. C. R. Groom, I. J. Bruno, M. P. Lightfoot, S. C. Ward, *Acta Crystallogr., B* **72** (2016) 171 (https://dx.doi.org/10.1107/S2052520616003954)
17. M. I. Toral, M. Paine, P. Leyton, P. Richter, *J. AOAC Int.* **87** (2004) 1323 (https://dx.doi.org/10.1093/jaoac/87.6.1323)
18. N. S. Sambudi, S. Cho, K. Cho, *RSC Adv.* **6** (2016) 43041 (https://dx.doi.org/10.1039/C6RA03147A)
19. T. Bera, A. N. Vivek, S. K. Saraf, P. Ramachandrarao, *Biomed. Mat.* **3** (2008) 025001 (https://dx.doi.org/10.1088/1748-6041/3/2/025001)
20. M. Ponjavić, M. S. Nikolić, J. Nikodinović-Runić, T. Ilić-Tomić, J. Djonlagić, *Int. J. Polym. Mater.* **68** (2019) 308 (https://dx.doi.org/10.1080/00914037.2018.1445631).

Journal of the Serbian Chemical Society
JSCS@tmf.bg.ac.rs • www.shd.org.rs/JSCS
J. Serb. Chem. Soc. *86* (11) 1113–1126 (2021)
JSCS–5487
Original scientific paper
Published 24 August 2021

Deashing and desulfurization of subbituminous coal from the East field (Bogovina Basin, Serbia) – Insights from chemical leaching

KATARINA PANTOVIĆ SPAJIĆ[1], BRANISLAV MARKOVIĆ[1], MIROSLAV M. PAVLOVIĆ[2,3*#], MIROSLAV SOKIĆ[1], SNEŽANA ZILDŽOVIĆ[1], NATAŠA ĐORĐEVIĆ[1] and KSENIJA STOJANOVIĆ[4]

[1]Institute for Technology of Nuclear and Other Mineral Raw Materials, Belgrade, Serbia, [2]University of Belgrade, Institute of Chemistry, Technology and Metallurgy, National Institute of the Republic of Serbia, Department of Electrochemistry, Belgrade, Serbia, [3]University of Belgrade, Institute of Chemistry, Technology and Metallurgy, National Institute of the Republic of Serbia, Center of Excellence in Environmental Chemistry and Engineering, Belgrade, Serbia and [4]University of Belgrade, Faculty of Chemistry, Belgrade, Serbia

(Received 19 July, revised 12 August, accepted 14 August 2021)

Abstract: The study is focused on the determination of the most effective chemical leaching process for the simultaneous demineralization/deashing and desulfurization of subbituminous coal from the Bogovina Basin. Coal was treated for 30 min, at different temperatures, using variable concentrations of hydrochloric, nitric, acetic and citric acids; hydrogen peroxide, mixture of hydrogen peroxide and nitric acid (pH 2), as well as by the stepwise leaching process (nitric acid + mixture of hydrogen peroxide and nitric acid, pH 2). The changes in mineral composition, caused by the chemical leaching, are followed using X-ray diffraction, whereas alterations of coal organic matter are tracked by Fourier-transform infrared spectroscopy and the content of fixed carbon. Inorganic acid leaching, regardless of the temperature and acid concentration, enabled the successful deashing of coal, whereas the percent of desulfurization was insufficient. The organic acid leaching was not satisfactory for both, deashing and desulfurization. Leaching by H_2O_2 and H_2O_2/HNO_3 mixture (pH 2) resulted in moderate desulfurization, but the ash reduction was low. The most suitable method for the simultaneous effective ash (78 wt.%) and the sulfur (66 wt. %) removal from Bogovina coal is the two-step leaching, combining 10 vol. % HNO_3 and mixture of 35 vol. % H_2O_2/10 vol. % HNO_3 of pH 2 at 60 °C.

Keywords: Bogovina coal; stepwise leaching; acidic leaching; oxidizing agents leaching; ash removal; sulfur removal.

* Corresponding author. E-mail: mpavlovic@tmf.bg.ac.rs
# Serbian Chemical Society member.
https://doi.org/10.2298/JSC210719061P

INTRODUCTION

Coal is fossil fuel and an important source of power generation all over the world.[1] However, the coal combustion is associated with the release of a large quantity of pollutants that have negative impact on ecosystem and human health, agricultural products and also causes corrosion of metal in stokeholes.[2–4] The major coal components that cause problems with combustion are sulfur/its compounds and mineral matter (MM), which is transformed into ash.[4] Sulfur in coal is present in the elemental form, as well as in inorganic compounds and organic matter (OM). The latter includes "free" sulfur compounds in bitumen, but are also part of sulfur bounded in kerogen. The inorganic sulfur forms comprise sulfides (*e.g.*, pyrite, marcasite) and sulfates (gypsum, barite, *etc*).[4] The organic sulfur compounds in bitumen are represented by: thiols, sulfides, disulfides, thiophenes, benzothiophenes, dibenzothiophenes, benzo[*b*]naphtho[*d*]thiophenes, *etc*. In the addition to ash formation by combustion, MM in coal decreases the calorific value and increases transport costs.[1]

Therefore, the processes of demineralization/deashing and desulfurization of coal may prevent the serious environmental problems caused by the coal combustion.[1] Methods for deashing and desulfurization can be conducted using chemical treatments, physical processing and microbial treatments.[1,5–7] Some of physical methods like dry fluidization, jigging, dense media/heavy media separation, hydrocyclone washing, magnetic separation, oil agglomeration, float and sink, air dense medium separation *etc.* can remove ash to a limited extent.[8] The combination of physical and chemical methods (*e.g.*, flotation and leaching with potassium hydroxide/methanol) applied on Mezino coal is shown to achieve the reduction of ash content of up to 83 wt. % and total sulfur up to 82 wt. %.[9] Treatment of Mezino coal by froth flotation and nitric/hydrochloric acid leaching process resulted in ash reduction of 54.7 wt. %, whereas sulfur reduction was 74.1 wt. %.[10]

Numerous chemical leaching processes, single acid leaching,[11,12] stepwise acid leaching,[13–15] leaching with oxidizing and chelating agents,[16–19] alkali treatments[20] and combined alkali-acid leaching[3,21] was applied to decrease the ash and the sulfur content in coal, with relatively high efficiency. The percentage of ash reduction was between 38.9 and 90.0 wt. %, whereas the degree of desulfurization ranged from 52.7 to 89.7 wt. % for different alkali–acid leaching of diverse coal under variable conditions.[1,21]

The microbial treatment of coal under mild conditions (25–75 °C) is also reported in literature,[1,7] but this process is time consuming, with long incubation period. The biodesulfurization study of Colombian coal sample, using the native mixture of microorganisms showed 30–50 wt. % of total sulfur removal. Out of the total sulfur removed, 85–96 wt. % was pyritic sulfur.[22]

Concerning that coals have very different and complex chemical composition, depending on biomass sources, depositional and post-depositional factors

and maturity,[4] there is no single and unique reagent for the efficient demineralization/deashing and desulfurization.[1] Furthermore, since the calorific value of coal depends on content of organic matter (primarily on the amount of fixed carbon, C_{fix}),[4] it is important that the applied of demineralization/desulfurization process does not alter coal OM.

Considering the above-mentioned problems regarding pollution, and the significance of coal as the main source for energy production in Serbia,[23] designing of cheap and efficient methods for removal of MM and sulfur from coal is of essential importance. Hence, the manuscript is focused on the determination of the cost and time effective chemical leaching process for simultaneous demineralization/deashing and desulfurization of subbituminous coal from the Bogovina Basin (Eastern Serbia). For that purpose, the coal was treated by: hydrochloric acid, nitric acid, acetic acid, citric acid, hydrogen peroxide, mixture of hydrogen peroxide and nitric acid (pH 2), as well as by the stepwise leaching process (nitric acid + mixture of hydrogen peroxide and nitric acid, pH 2). Variable concentrations of mentioned reagents were used (with exception of hydrogen peroxide, 35 vol. %) and the leaching experiments were performed at different temperatures. The changes in mineral composition and alterations in structure of coal OM, caused by chemical leaching, were followed using X-ray diffraction (XRD) analysis and Fourier-transform infrared spectroscopy (FTIR), respectively. Furthermore, C_{fix} was determined in solid residues obtained by chemical leaching, since the coal calorific value mostly depends on this parameter.

EXPERIMENTAL

Coal sample, proximate analysis and determination of sulfur content

The subbituminous coal sample was collected from the Bogovina East field (Lower Miocene ≈ 20–16 million years ago) of the Bogovina Basin (Eastern Serbia). According to an average huminite reflectance, R_r, which equals 0.42±0.04 %,[24] the coal from this deposit belongs to bright brown coal group (Low-Rank A).[4] The sample was selected based on the previous studies of Bogovina East Field,[24,25] which indicated the high amount of sulfur, the relatively high percent of mineral matter and the considerable amount of liptinites for humic coal, that represent the most reactive maceral group.[4,25] Therefore, it serves as good substrate for checking the efficiency of demineralization and desulfurization, as well as the influence of applied chemical leaching treatments on OM structure.

The air-dried sample was crushed using Fritsch mortar grinder pulverisette 2 and sieved through a 200 μm sieve. Proximate analysis (determination of analytical moisture, volatile matter, ash and fixed carbon) of the coal was performed according to the ASTM D3172 standard,[26] whereas total sulfur content was determined by the Eschka method.[27] Bogovina coal sample, used in this study, contains 16.82 wt. % moisture, 38.44 wt. % of volatile matter, 17.52 wt. % of ash, 27.22 wt. % of fixed carbon and 6.03 wt. % of total sulfur.

Leaching procedure

Chemical leaching of coal was conducted with inorganic acids (hydrochloric and nitric), organic acids (acetic and citric), oxidizing agent (hydrogen peroxide), and the combination of

acid/oxidizing agent (nitric acid/hydrogen peroxide) in a single and two-step process. The acid-leaching treatment was chosen concerning the geological settings which are such that the coal from the Bogovina East field was formed in a slightly alkaline depositional environment generated by bentonite from the basement of the Main coal seam.[24] It was further confirmed by our preliminary leaching experiments using diverse concentrations of sodium hydroxide solution at different temperatures, which showed low efficiency of both deashing and desulfurization, attaining maximally 11.94 and 8.95 wt. %, respectively.

For each test, 600 cm^3 of leaching reagent was added to 30 g of coal sample and the mixture was heated and shaken on magnetic stirrer for 30 minutes at the constant mixing speed of 250 rpm. After the leaching, the hot leached residue was cooled, filtered by vacuum pump and rinsed with hot distilled water until the neutral reaction (pH 7) of filtrate. Finally, the leached residue was dried in the oven (Memmert UNE 400 drying oven) at 105 °C to the constant mass. The ash and sulfur contents, as well as of C_{fix}, in the obtained leached residues were determined using the same methods as the in initial coal sample.[26,27] For determining the optimal temperature of leaching treatment, the first set of experiments (I) was performed at temperatures 30, 60 and 90 °C using the 10 vol. % water solution of inorganic acids (hydrochloric and nitric), whereas treatment with organic acids (acetic and citric) of the same concentration (10 vol. %), hydrogen peroxide (35 vol. %), mixture of 35 vol. % hydrogen peroxide/10 vol. % nitric acid (pH 2), as well as 10 vol. % nitric acid + 35 vol. % hydrogen peroxide/10 vol. % nitric acid mixture at pH 2 (two-step leaching process) was carried out at 20, 40 and 60 °C. For establishing the influence of acids concentration on deashing and desulfurization, the second set of experiments (II) was conducted in the same way as previous one using the following concentrations of acids: 5, 10 and 15 vol. % at optimal temperature, which was determined in the first set of experiments. This range of concentrations was selected based on the data from literature, since it was shown that higher concentrations of acids (*e.g.*, 30 vol. % HNO_3) could alter the coal structure.[1] Considering literature data[5] which states that the desulfurization of coal by 20 vol. % hydrogen peroxide is unsuitable for removing organic sulfur and that 30 vol. % H_2O_2 could remove it up to 36 wt. % of sulfur from coal having similar content of total sulfur (5.8 wt. %) as here studied Bogovina coal sample, all experiments were done using 35 vol. % H_2O_2 and mixture of 35 vol. % hydrogen peroxide/10 vol. % nitric acid (pH 2). The performed leaching experiments are summarized in Table I. All experiments were repeated three times and mean values are reported here with standard deviation less than 0.5 %.

RESULTS AND DISCUSSION

Coal leaching with inorganic acids

The treatment with 10 vol. % HCl at all temperatures (30, 60 and 90 °C) resulted in ash reduction from 17.52 wt. % in the initial coal to about 3.65 wt. % in leached samples (Table I), indicating the deashing efficiency of about 79 wt. % (Table II). The sulfur reduction was also very similar at all temperatures, however, slightly better results were obtained at 60 and 90 °C (8.62 and 8.29 wt. %, respectively) than at 30 °C (7.46 wt. %; Table II). Independently of temperature, the amount of C_{fix} increases uniformly from 27.22 wt. % in initial coal to ~39.5 wt. % in all samples treated by HCl (Table I), due to the considerable removal of MM. This has a positive impact on calorific value. Although, the data from

Tables I and II clearly show that temperature plays insignificant role in coal treatment by 10 vol. % HCl, but the best results are obtained at 60 °C. Therefore, this temperature was chosen as optimal leaching temperature.

TABLE I. Summary of the performed experiments and contents of ash, total sulfur and fixed carbon (C_{fix}) in initial coal sample and solid residues obtained by chemical leaching

Exp. set	Leaching reagent	t / °C	Leaching reagent concentration, vol. %	Reaction time, min	Amount, wt.%		
					Ash	Sulfur	C_{fix}
Initial coal sample					17.52	6.03	27.22
I	HCl	30	10	30	3.65	5.58	39.57
		60			3.62	5.51	39.64
		90			3.68	5.53	39.34
	HNO_3	30	10	30	3.62	5.64	41.17
		60			3.16	4.9	38.25
		90			3.29	4.77	35.76
	CH_3COOH	20	10	30	6.78	5.37	38.17
		40			6.21	5.33	39.11
		60			5.80	5.32	38.92
	Citric acid	20	10	30	11.26	5.56	32.08
		40			9.59	5.39	35.87
		60			8.93	5.37	35.93
	H_2O_2	20	35	30	11.01	4.90	33.00
		40			8.60	4.14	34.24
		60			13.08	4.94	35.80
	H_2O_2/HNO_3 pH 2	20	35 (H_2O_2)/10 (HNO_3)	30	13.73	5.40	31.70
		40			8.81	4.64	35.25
		60			7.12	4.04	36.57
	HNO_3 followed by H_2O_2/HNO_3, pH 2 (two-step process)	20	10 (HNO_3) followed by 35 (H_2O_2)/10 (HNO_3)	15 followed by 15	4.09	5.05	40.96
		40			4.08	4.25	38.82
		60			3.86	2.03	37.59
II	HCl	60	5	30	3.35	5.69	40.84
		60	10		3.62	5.51	39.64
		60	15		3.33	5.49	43.45
	HNO_3	60	5	30	3.47	5.13	36.02
		60	10		3.16	4.90	38.25
		60	15		3.41	4.45	34.99
	CH_3COOH	40	5	30	8.51	5.50	36.28
		40	10		6.21	5.33	39.11
		40	15		7.04	5.47	37.44
	CH_3COOH	60	5	30	5.79	4.72	39.45
		60	10		5.80	5.32	38.92
		60	15		5.27	5.22	39.12
	Citric acid	60	5	30	8.08	5.35	35.95
		60	10		8.93	5.37	35.93
		60	15		10.18	5.38	34.85

TABLE II. Ash and sulfur reduction in solid residues obtained by chemical leaching; the results for optimal concentrations and temperatures are marked by bolded text

Exp. set	Leaching reagent	*t* / °C	Leaching reagent concentration; vol.%;	Reaction time, min	Amount reduction, %	
					Ash[a]	Sulfur[b]
I	HCl	30	10	30	79.17	7.46
		60			79.34	8.62
		90			79.00	8.29
	HNO_3	30	10	30	79.34	6.47
		60			81.96	18.74
		90			81.22	20.90
	CH_3COOH	20	10	30	61.30	10.95
		40			64.55	11.61
		60			66.89	11.77
	Citric acid	20	10	30	35.73	7.79
		40			45.26	10.61
		60			49.03	10.95
	H_2O_2	20	35	30	37.16	18.74
		40			**50.91**	**31.34**
		60			25.34	18.08
	H_2O_2/HNO_3 pH 2	20	35 (H_2O_2)/10 (HNO_3)	30	21.63	10.45
		40			49.71	23.05
		60			**59.36**	**33.00**
	HNO_3 followed by H_2O_2/HNO_3, pH 2 (two-step process)	20	10 (HNO_3) followed by 35 (H_2O_2)/10 (HNO_3)	15 followed by 15	76.66	16.25
		40			76.71	29.52
		60			77.97	66.33
II	HCl	60	5	30	80.88	5.64
		60	10		79.34	8.62
		60	**15**		**80.99**	**8.96**
	HNO_3	60	5	30	80.19	14.93
		60	10		81.96	18.74
		60	**15**		**80.54**	**26.20**
	CH_3COOH	40	5	30	51.43	8.79
		40	**10**		**64.55**	**11.61**
		40	15		59.82	9.29
	CH_3COOH	**60**	**5**	30	**66.95**	**21.72**
		60	10		66.89	11.77
		60	15		69.92	13.43
	Citric acid	**60**	**5**	30	**53.88**	**11.28**
		60	10		49.03	10.95
		60	15		41.89	10.78

[a]Ash reduction = 100(Ash content in initial coal – Ash content in leached coal)/Ash content in initial coal; [b]bulfur reduction = 100(Sulfur content in initial coal – Sulfur content in leached coal)/Sulfur content in initial coa

The results from Table II indicate that the HCl concentration (5–15 vol. %) does not considerably affect deashing of Bogovina coal (being in range from

79.34 to 80.99 wt. %), whereas the influence on desulfurization is obvious. The percentage of desulfurization increases from 5.64 wt. % for 5 vol. % HCl to 8.62 wt. % for 10 vol. % HCl, being similar to 15 vol. % HCl (8.96 wt. %). The contents of C_{fix} in leached residues are also comparable for all studied concentrations of HCl (39.64–43.45 wt. %), however the highest abundance is observed for 15 vol. % HCl. Considering all data related to HCl treatment, it can be noted that the best results are achieved using 15 vol. % acid concentration at 60 °C.

Leaching with 10 vol. % HNO_3 at 30 °C resulted in almost identical deashing efficiency as leaching with 10 vol. % HCl at all temperatures (the ash content in leached residue was 3.62 wt. %; the ash reduction was 79.34 %; Tables I and II). At 60 and 90 °C slightly greater ash reduction is achieved using 10 vol. % HNO_3 (81.96 and 81.22 wt. %, respectively) than by 10 vol. % HCl (Table II). In difference to deashing, the influence of temperature on desulfurization by leaching with 10 vol. % HNO_3 is more evident.

The percent of sulfur reduction was 6.47 wt. % at 30 °C, 18.74 wt. % at 60 °C and 20.90 wt. % at 90 °C. The contents of C_{fix} in residues after leaching by 10 vol. % HNO_3 are higher than in the initial coal (Table I), as expected. However, the continuous decrease of C_{fix} content from 41.17 to 35.76 wt. % with the temperature rise was observed (Table I). This can be attributed to the oxidizing effect of HNO_3, which becomes more pronounced with the increase of temperature. The aforementioned data indicate the diverse efficiency of leaching by 10 vol. % HNO_3 depending on temperature. Since the highest efficiency for deashing by 10 vol. % HNO_3 is observed at 60 °C and considering that heating of HNO_3 from 60 to 90 °C reduces the sulfur content for 0.13 wt. %, only, but also decreases C_{fix} for 2.5 % (Table I), as well as, the energy consumption (that is lower at 60 °C than at 90 °C), the temperature of 60 °C was chosen as optimal.

The results from Table II indicate that HNO_3 concentration (5–15 vol. %) does not considerably affect the deashing of Bogovina coal (80.19–81.96 wt. %), with the highest ash reduction for 10 vol. % HNO_3 treatment. Different from the deashing efficiency, the increase of HNO_3 concentration showed significant impact on desulfurization and C_{fix} content. The percentage of desulfurization increased from 14.93 wt. % for 5 vol. % HNO_3 to 18.74 wt. % for 10 vol. % HNO_3, being the highest for 15 vol. % HNO_3 (26.20 wt. %). C_{fix} rose in leached residues from 36.02 wt. % for leaching by 5 vol. % HNO_3 to 38.25 wt. % for treatment with 10 vol. % HNO_3 and then decreased to 34.99 wt. % by leaching with 15 vol. % HNO_3. The results of leaching experiments with HNO_3 indicated that the highest efficiency of deashing and desulfurization can be obtained using the concentration of 15 vol.% at 60 °C. However, for coal utilization processes where C_{fix} content plays a more significant role than content of sulfur, leaching by 10 vol. % HNO_3 at 60 °C can be also considered.

The results from Tables I and II show that deashing has rather high and almost constant values for both HCl and HNO_3, regardless of temperature and acid concentration, while desulfurization process is more influenced by these leaching parameters, particularly for HNO_3. Comparing the results obtained by leaching with 5 vol. % acids at 60 °C, and 10 vol. % acids at 30 °C it can be noticed that desulfurization efficiency of HCl depends more on concentration, whereas in the case of HNO_3 temperature has a more pronounced impact. The optimal chemical leaching of Bogovina coal with both acids can be obtained using the concentration of 15 vol. % at 60 °C. However, it is evident that both single acid leaching treatments enable successful deashing of Bogovina coal, whereas percent of desulfurization is insufficient. The better efficiency of HNO_3 than HCl in desulfurization can be attributed to the fact that nitric acid in difference to hydrochloric acid has oxidizing properties. On the other hand, similar efficiency of both acids in deashing indicates that mineral part of Bogovina coal is relatively resistant to oxidizing agents. This suggests a low amount of sulfides (*e.g.*, pyrite), pointing out that sulfur in Bogovina coal is mostly present in OM as well as the inorganic sulfates (anhydrite), which is also documented by XRD data. The changes in qualitative composition of MM, caused by chemical leaching, are followed by XRD after subjecting the initial coal and the leached solid residues to the LTA process (Fig. S-1 of the Supplementary material to this paper), as explained in more detail in Supplementary material.

Since the content of OM, particularly C_{fix} controls heating value of coal, C_{fix} is determined (Table I) and the FTIR spectra of the initial and the leached coal are recorded (Fig. S-2). The FTIR spectra were done for all experiments, however, due to their great congruence for the same reagent they were done independently on concentration and temperature; those corresponding to the optimal conditions are explained in more detail in Supplementary material and shown in Fig. S-2.

Coal leaching with organic acids

The possibility of Bogovina coal deashing and desulfurization using organic acids (acetic and citric), that are generally less hazardous than HCl and HNO_3, was investigated as well.

Deashing by leaching with 10 vol.% acetic acid increases from 61.30 to 64.55 wt. % with temperature rise from 20 to 40 °C, being the highest (66.89 wt. %) at 60 °C. In difference to inorganic acid treatments, the temperature showed less impact on desulfurization ranged between 10.95 wt. % at 20 °C and 11.77 wt. % at 60 °C. The same is related to C_{fix} content, which slightly increases from 38.17 wt. % at 20 °C to 39.11 wt. % at 40 °C, being similar at 60 °C (38.92 wt. %). Since the results at 40 and 60 °C were rather uniform and considering lower energy con-

sumption at 40 °C, the influence of acetic acid concentration on leaching efficiency was tested at both temperatures.

The obtained data indicate greater impact of CH_3COOH concentration on coal deashing at 40 °C than at 60 °C, where results are similar. The sulfur reduction generally diminishes with the increase of acid concentration at both temperatures. Contents of C_{fix} are uniform; the highest values are detected for CH_3COOH concentration of 10 and 5 vol. % CH_3COOH at 40 and 60 °C, respectively. The greatest efficiency at 40 °C is recorded for 10 vol. % acid concentration, whereas at 60 °C it is achieved with 5 vol. %. Comparison of the data from the experiments with 10 vol. % acid at 40 °C and 5 vol. % acid at 60 °C, clearly shows better efficiency of the latter, that can be considered as optimal for leaching with CH_3COOH (Tables I and II). This also led to the conclusion that temperature plays more important role in the leaching treatment than acid concentration.

The leaching with citric acid demonstrated a steady increase of deashing (35.73–49.03 wt. %) and desulfurization (7.79–10.95 wt. %) with the temperature rise from 20 to 60 °C. The content of C_{fix} also increases from 20 to 40 °C (32.08–35.87 wt. %), being almost identical to the latter (35.93 wt. %) at 60 °C. Therefore, it is evident that optimal temperature for citric acid leaching is 60 °C (Tables I and II). The coal leaching using different concentrations of citric acid at 60 °C showed greater influence on ash removal, ranged from 41.89 to 53.88 wt. %., in comparison with percent of desulfurization (10.78–11.27 wt. %) and C_{fix} (34.85–35.95 wt. %). The data from Table II clearly indicate that the highest efficiency by leaching with citric acid could be obtained using 5 vol. % concentration at 60 °C.

The most efficient leaching with both tested organic acids is achieved using the concentration of 5 vol. % at 60 °C. Better efficiency of acetic than citric acid is obvious (Tables I and II). This can be attributed to the more pronounced interactions of citric acid with coal OM and complexation with metal ions from MM, since it contains three carboxylic groups, in difference to monocarboxylic CH_3COOH that favours incorporation (capturing) of the former into coal structure. These interactions are most probably responsible for the decreasing of leaching efficiency with the increasing of acids concentration, the exception being deashing by CH_3COOH, which is slightly greater using 15 vol. % in comparison to 5 vol. %. However, it is obvious that the single step organic acid leaching is not satisfactory method for both, deashing and desulfurization (up to 67 and 22 wt. %, respectively) of Bogovina coal (Table II).

The results of inorganic and organic acids treatments under optimal conditions (concentration and temperature) clearly indicate that organic acids are much less effective in deashing, whereas leaching by both, CH_3COOH and citric acid enabled greater sulfur reduction than those by HCl. However, the leaching by organic acids cannot compete to the treatment with HNO_3 (Table II).

Coal leaching with oxidizing reagents

It was shown that oxidizing reagents (*e.g.*, hydrogen peroxide) are able to decrease the content of sulfur in coal, oxidizing both organic and pyritic sulfur to sulfonic acids and sulfates.[16,18] Therefore, some oxidizing agents were also tested on Bogovina coal.

The results from Tables I and II indicate that temperature plays significant role in deashing and desulfurization of Bogovina coal by leaching with 35 vol. % H_2O_2, due to the partial thermal decomposition of hydrogen peroxide at temperatures > 40 °C. Deashing increases from 37.16 wt. % at 20 °C to 50.91 wt. % at 40 °C, and falls back to 25.34 wt. % at 60 °C. The same stands for desulfurization, having maximum value of 31.34 wt. % at 40 °C, whereas at 20 and 60 °C sulfur the removal was very similar ~18 wt. %. The content of C_{fix} was uniform (33.00––35.80 wt. %); however the highest percent is recorded at 60 °C, consistent with partial thermal decomposition of hydrogen peroxide at > 40 °C. Since the coal leaching with 35 vol. % H_2O_2 resulted in the highest degree of desulfurization among the tested reagents (31.34 wt. %), whereas deashing was low (up to 50.91 wt. %; Table II), in order to improve the latter, as well as thermal stability, H_2O_2 was mixed with 10 vol. % HNO_3 at pH 2. 10 vol. % HNO_3 was chosen, since it showed the greatest deashing efficiency among the tested reagents (Table II).

Leaching of coal with this mixture resulted in deashing varied from 21.63 wt. % at 20 °C to 59.36 wt. % at 60 °C, whereas desulfurization raised from 10.45 to 33.00 wt. % in the same temperature range, indicating considerable impact of temperature. Percent of C_{fix} was higher in leached residues obtained by acidified H_2O_2 than H_2O_2 treatment at 40 and 60 °C, resulting from more effective deashing. The sulfur reduction by leaching with acidified H_2O_2 was apparently lower in comparison to treatment with pure H_2O_2 at 40 °C (23.05 *vs.* 31.34 wt. %), whereas at 60 °C application of H_2O_2/HNO_3 mixture resulted in greater desulfurization efficiency of 33.00 wt. % (Table II). This signifies that H_2O_2 plays a major role in desulfurization process and confirms improved thermal performances of acidified reagent. On the other hand, H_2O_2/HNO_3 mixture (pH 2) demonstrated more effective deashing (59.36 wt. %) than H_2O_2 solely (50.91 wt. %), implying that HNO_3 has dominant role in ash reducing, however at higher temperature (60 *vs.* 40 °C). Data from Table II clearly indicate that optimal temperatures for H_2O_2 and H_2O_2/HNO_3 mixture (pH 2) leaching are 40 and 60 °C respectively. Although, treatment with H_2O_2/HNO_3 mixture (pH 2) resulted in the most effective desulfurization (33 wt. %) comparing with all previous leaching treatments, the ash reduction was low, attaining maximally 59.36 wt. % (Table II). Therefore, Bogovina coal was further treated firstly by 10 vol. % HNO_3 (15 min) and then by H_2O_2/HNO_3 mixture (pH 2, 15 min) in the two-step process, maintaining the total leaching time of 30 min, as in all previous experiments (Table I).

Temperature does not have significant impact on the deashing efficiency in the two-step leaching process ranged from 76.66 wt. % at 20 °C to 77.97 wt. % at 60 °C. The result is in accordance with those of leaching by inorganic acids. The two--step process showed slightly lower deashing efficiency (77.97 wt. %) than the treatment with 10 vol. % HNO_3 solely (81.96 wt. %, Table II). Since, former experiments indicated that 10 vol. % HNO_3 plays the dominant role in deashing in comparison to H_2O_2/HNO_3 mixture (pH 2) and this result can be attributed to shorter duration of the acidic leaching in the two-step process than by pure HNO_3 (15 *vs*. 30 min). On the other hand, desulfurization by the two-step process considerably increases from 20 °C (16.25 wt. %) to 60 °C (66.33 wt. %) which is evidently the most efficient result among all performed leaching experiments (Table II). Furthermore, greater percent of desulfurization of 66.33 wt. % by the two-step leaching process at 60 °C that exceeds the sum of desulfurization percents by each treatment alone (18.74 wt. % for 10 vol. % HNO_3 + 33.00 wt. % for H_2O_2/HNO_3 mixture of pH 2, 51.74 %), under the same temperature, indicates certain synergetic effect resulted from combining of above mentioned reagents. The percent of C_{fix} after the two-step leaching process at 60 °C was 37.59 wt. % which is higher than after treatment with 35 vol. % H_2O_2/10 vol. % HNO_3 mixture (pH 2, 36.57 wt.%) and insignificantly lower than after 10 vol. % HNO_3 treatment (38.25 wt. %).

Taking into consideration results of all the performed experiments it can be concluded that the two-step leaching process combining 10 vol. % HNO_3 and mixture of 35 vol. % H_2O_2/10 vol. % HNO_3 of pH 2 is the most suitable single method for the simultaneous effective ash (~78 wt. %) and sulfur (~ 66 wt. %) removal from Bogovina coal, increasing in the same time C_{fix} from 27 wt. % in the initial sample to 38 wt. % in leached residue (Tables I and II). The obtained results are comparable or even better than those of deashing and desulfurization by chemical leaching reported in literature.[1,28]

Our further research would be addressed to the investigation of possible reuse of HNO_3 after adjusting the concentration to 10 vol. % and cost effective recovering of accumulated metals from filtrates, aimed to prevent the negative environmental impact of applied leaching reagent.

CONCLUSIONS

The study is aimed to determine the most effective chemical leaching process for the simultaneous demineralization/deashing and desulfurization of subbituminous coal from the Bogovina Basin. The sample is selected based on the high amount of sulfur, the relatively high percent of MM and the considerable amount of liptinites for humic coal, which represent the most reactive OM maceral group.

The leaching with HCl or HNO_3, regardless of temperature and acid concentration, enabled the successful deashing of coal (~80 wt. %), confirmed also by XRD, whereas the percent of desulfurization (up to 26 wt. %) was insufficient. The best results for both the inorganic acids are observed for the concentration of 15 vol. % at 60 °C. Nitric acid demonstrated better efficiency than hydrochloric acid, particularly for the sulfur removal, due to the oxidation properties.

The single step organic acid leaching was not satisfactory for both, deashing and desulfurization (up to 67 and 22 wt. %, respectively) of Bogovina coal. The most efficient leaching with organic acids is achieved using the concentration of 5 vol. % at 60 °C. Acetic acid showed greater efficiency than citric acid. The comparison of inorganic and organic acids treatments under optimal conditions indicated that organic acids are less effective in deashing, whereas the leaching by both, CH_3COOH and citric acid enabled greater sulfur reduction than those by HCl. However, the leaching by organic acids cannot compete to the treatment with HNO_3.

The leaching of coal by oxidizing reagents 35 % H_2O_2, and the mixture of 35 vol. % H_2O_2 and 10 vol. % HNO_3 (pH 2) resulted in better desulfurization (31–33 wt. %) than single step acidic treatments, whereas the percent of deashing was low (up to 60 wt. %). The optimal temperatures for H_2O_2 and H_2O_2/HNO_3 mixture (pH 2) leaching were 40 and 60 °C, respectively.

The most suitable method for simultaneous effective ash (78 wt. %) and sulfur (66 wt. %) removal from Bogovina coal is the two-step leaching, combining 10 vol. % HNO_3 and mixture of 35 vol. % H_2O_2/10 vol. % HNO_3 of pH 2 at 60 °C. XRD data showed the removal of all minerals with the exception of quartz and olivine, the content of C_{fix} increased for 11 wt. % in relation to initial coal, whereas FTIR implied no significant alteration in the structure of coal OM by the treatment. Furthermore, greater percent of desulfurization by the two-step leaching process which exceeds the sum of desulfurization percents by each the treatment alone (10 vol. % HNO_3 and H_2O_2/HNO_3 mixture of pH 2), indicates the synergetic effect resulted from the combination of above-mentioned reagents.

SUPPLEMENTARY MATERIAL

Additional data and information are available electronically at the pages of journal website: https://www.shd-pub.org.rs/index.php/JSCS/article/view/10983, or from the corresponding author on request.

Acknowledgement. This study was financed by the Ministry of Education, Science and Technological Development of the Republic of Serbia (Contract numbers: 451-03-9/2021-14/ /200026, 451-03-9/2021-14/200023 and 451-03-9/2021-14/200168).

ИЗВОД

ОТПЕПЕЉАВАЊЕ И ОДСУМПОРАВАЊЕ МРКОГ УГЉА ИЗ ИСТОЧНОГ ПОЉА БАСЕНА БОГОВИНА (СРБИЈА) ХЕМИЈСКИМ ТРЕТМАНОМ

КАТАРИНА ПАНТОВИЋ СПАЈИЋ[1], БРАНИСЛАВ МАРКОВИЋ[1], МИРОСЛАВ ПАВЛОВИЋ[2,3], МИРОСЛАВ СОКИЋ[1], СНЕЖАНА ЗИЛЈОВИЋ[1], НАТАША ЂОРЂЕВИЋ[1] и КСЕНИЈА СТОЈАНОВИЋ[4]

[1]Институт за технологију нуклеарних и других минералних сировина, Булевар Франше д'Епереа 86, 11000 Београд, [2]Универзитет у Београду, Институт за хемију, технологију и металургију; Центар за електрохемију, Његошева 12, 11000 Београд, [3]Универзитет у Београду, Институт за хемију, технологију и металургију, Центар изузетних вредности за хемију и инжењеринг животне средине, Његошева 12, 11000 Београд и [4]Универзитет у Београду, Хемијски факултет, Студентски трг 12–16, 11000 Београд

Циљ рада је одређивање најефикаснијег хемијског третмана за истовремену деминерализацију/отпепељавање и одсумпоравање мрког угља из басена Боговина. Угаљ је третиран 30 min, на различитим температурама, користећи различите концентрације хлороводоничне, азотне, сирћетне и лимунске киселине; водоник-пероксид, смешу водоник-пероксида и азотне киселине (pH 2), као и двостепено испирање (азотна киселина + смеша водоник-пероксида и азотне киселине, pH 2). Промене у минералном саставу, проузроковане хемијским третманом, праћене су дифракцијом рендгентских зрака, док су промене органске супстанце угља праћене помоћу инфрацрвене спектроскопије са Фуријеовом трансформацијом и садржаја фиксног угљеника. Третман неорганским киселинама, независно од температуре и концентрације реагенса, омогућио је успешно отпепељавање угља, док је проценат одсумпоравања био недовољан. Третман органским киселинама није био задовољавајући, ни за отпепељавање, ни за одсумпоравање. Третман угља са H_2O_2 и смешом H_2O_2/HNO_3 (pH 2) резултовао је умереним одсумпоравањем, али је смањење садржаја пепела било мало. Најприкладнија метода за истовремено ефикасно уклањање пепела (78 мас. %) и сумпора (66 мас. %) из боговинског угља је двостепено испирање, комбинацијом 10 запр. % HNO_3 и смеше 35 запр. % H_2O_2/10 запр. % HNO_3 (pH 2) на 60 °C.

(Примљено 19. јула, ревидирано 12. августа; прихваћено 14. августа 2021)

REFERENCES

1. H. Dhawan, D. K. Sharma, *Int. J. Coal Sci. Technol.* **6** (2019) 169 (https://doi.org/10.1007/s40789-019-0253-6)
2. K. Goto, K. Yogo, T. Higashii, *Appl. Energy* **111** (2013) 710 (https://doi.org/10.1016/j.apenergy.2013.05.020)
3. F. Rubiera, A. Arenillas, B. Arias, J. J. Pis, I. Suárez-Ruiz, K. M. Steel, J. W. Patrick, *Fuel* **82** (2003) 2145 (https://doi.org/10.1016/S0016-2361(03)00181-9)
4. D. Životić, *Coal Geology*, University of Belgrade, Faculty of Mining and Geology, Belgrade, 2018 (in Serbian) (https://rgf.bg.ac.rs/Dokumenta/Publikacije/Biblioteka/Promocija_izdanja_katalog_2019.pdf)
5. A. Ali, S. K. Srivastava, R. Haque, *Fuel* **71** (1992) 835 (https://doi.org/10.1016/0016-2361(92)90139-F)
6. P. Meshram, B. K. Purohit, M. K. Sinha, S. K. Sahu, B. D. Pandey, *Renew. Sustain. Energy Rev.* **41** (2015) 745 (http://doi.org/10.1016/j.rser.2014.08.072)
7. D. K. Sharma, G. Wadhwa, *World J. Microbiol. Biotechnol*. **13** (1997) 29 (https://doi.org/10.1007/BF02770804)

8. M. Rahman, D. Pudasainee, R. Gupta, *Fuel Process. Technol.* **158** (2017) 35 (http://doi.org/10.1016/j.fuproc.2016.12.010)
9. M. Abdollahy, A. Z. Moghaddam, K. Rami, *Fuel* **85** (2006) 1117 (https://doi.org/10.1016/j.fuel.2005.10.011)
10. H. G. Alam, A. Z. Moghaddam, M. R. Omidkhah, *Fuel Process. Technol.* **90** (2009) 1 (http://doi.org/10.1016/j.fuproc.2008.06.009)
11. J. M. Andrés, A. C. Ferrando, L. Membrado, *Energy Fuels* **10** (1996) 425 (https://doi.org/10.1021/ef9501612)
12. K. M. Steel, J. Besida, T. A. O'Donnell, D. G. Wood, *Fuel Process. Technol*. **70** (2001) 193 (https://doi.org/10.1016/S0378-3820(01)00173-4)
13. K. M. Steel, J. W. Patrick, *Fuel* **82** (2003) 1917 (https://doi.org/10.1016/S0016-2361(03)00149-2)
14. E. Jorjani, H. G. Chapi, M. T. Khorami, *Fuel Process. Technol*. **92** (2011) 1898 (http://doi.org/10.1016/j.fuproc.2011.05.008)
15. K. M. Steel, J. Besida, T. A. O'Donnell, D.G. Wood, *Fuel Process. Technol.* **70** (2001) 171 (https://doi.org/10.1016/S0378-3820(01)00171-0)
16. S. Mukherjee, S. K. Srivastava, *Energy Fuels* **18** (2004) 1764 (https://doi.org/10.1021/ef0499731)
17. W. Li, E.H. Cho, *Energy Fuels* **19** (2005) 499 (https://doi.org/10.1021/ef0400767)
18. H. Karaca, K. Ceylan, *Fuel Process. Technol.* **50** (1997) 19 (https://doi.org/10.1016/S0378-3820(96)01042-9)
19. A. A. Yahya, N. Ali, N. L. Mohd Kamal, S. Shahidan, S. Beddu, M. F. Nuruddin, N. Shafiq, *MATEC Web Conf.* **103** (2017) 01004 (https://doi.org/10.1051/matecconf/201710301004)
20. J. Wang, A. Tomita, *Ind. Eng. Chem. Res*. **36** (1997) 1464 (https://doi.org/10.1021/ie960516k)
21. S. Mukherjee, P. C. Borthakur, *Fuel* **80** (2001) 2037 (https://doi.org/10.1016/S0016-2361(01)00094-1)
22. I. C. Cardona, M. A. Márquez, *Fuel Process. Technol*. **90** (2009) 1099 (https://doi.org/10.1016/j.fuproc.2009.04.022)
23. *Energy Resources of the Republic of Serbia*, http://www.smeits.rs/include/data/docs0066.doc (last accessed July 19, 2021) (in Serbian)
24. D. Životić, B. Jovančićević, J. Schwarzbauer, O. Cvetković, I. Gržetić, M. Ercegovac, K. Stojanović, A. Šajnović, *Int. J. Coal Geol.* **81** (2010) 227 (https://doi.org/10.1016/j.coal.2009.07.012)
25. N. Vuković, D. Životić, J. G. Mendonça Filho, T. Kravić-Stevović, M. Hámor-Vidó, J. O. Mendonça, K. Stojanović, *Int. J. Coal Geol.* **154-155** (2016) 213 (http://doi.org/10.1016/j.coal.2016.01.007)
26. *ASTM D3172: Standard Practice for Proximate Analysis of Coal and Coke* , 2013
27. *ISO 334: Solid mineral fuels – Determination of total sulfur – Eschka method*, 2013
28. S. K. Behera, S. Chakraborty, B. C. Meikap, *Int. J. Coal Sci. Technol.* **5** (2018) 142 (https://doi.org/10.1007/s40789-018-0208-3).

Journal of the Serbian Chemical Society
JSCS@tmf.bg.ac.rs • www.shd.org.rs/JSCS
J. Serb. Chem. Soc. 86 (11) S422–S427 (2021) *Supplementary material*

SUPPLEMENTARY MATERIAL TO

Deashing and desulfurization of subbituminous coal from the East field (Bogovina Basin, Serbia) – Insights from chemical leaching

KATARINA PANTOVIĆ SPAJIĆ[1], BRANISLAV MARKOVIĆ[1], MIROSLAV M. PAVLOVIĆ[2,3]*, MIROSLAV SOKIĆ[1], SNEŽANA ZILDŽOVIĆ[1], NATAŠA ĐORĐEVIĆ[1] and KSENIJA STOJANOVIĆ[4]

[1]*Institute for Technology of Nuclear and Other Mineral Raw Materials, Belgrade, Serbia,* [2]*University of Belgrade, Institute of Chemistry, Technology and Metallurgy, National Institute of the Republic of Serbia, Department of Electrochemistry, Belgrade, Serbia,* [3]*University of Belgrade, Institute of Chemistry, Technology and Metallurgy, National Institute of the Republic of Serbia, Center of Excellence in Environmental Chemistry and Engineering, Belgrade, Serbia and* [4]*University of Belgrade, Faculty of Chemistry, Belgrade, Serbia*

J. Serb. Chem. Soc. 86 (11) (2021) 1113–1126

Low temperature ashing (LTA) process and X-ray diffraction (XRD) analysis

X-ray diffraction (XRD) analysis was used for determination of the qualitative composition of the minerals in the samples' ashes before and after the leaching treatments. Prior to XRD, all samples were subjected to low temperature ashing (LTA) process.[1] The method is favorable for isolating the MM from coal, as unaltered, as possible. Dried and weighted initial coal sample and solid residues obtained by chemical leaching (~3 g) were burnt at 370 °C in the air atmosphere for 3 h using the Nabertherm L3/11/B 410 pre-heating furnace. The samples were gradually heated to 200 °C with the heating rate of 3 °C min^{-1} followed by the heating rate of 10 °C min^{-1} up to the final temperature of 370 °C.

The XRD analysis was performed using a "Philips" X-ray diffractometer, type PW-1710, with graphite monochromator and a scintillation counter. The intensities of diffracted CuKα X-ray radiation (λ = 1.54178 Å) were measured at room temperature. Samples were recorded in 2θ range from 4 to 65° in 0.02° intervals for duration of 1 s. The working voltage was 40 kV and working current was 30 mA. The slits for directing the primary and diffracted beam were fixed at 1° and 0.1 mm.

* Corresponding author. E-mail: mpavlovic@tmf.bg.ac.rs

Fourier-transform infrared spectroscopy (FTIR)

Fourier-transform infrared (FTIR) analysis of initial and treated coal samples was performed on a Thermo Fisher Scientific Nicolet IS-50. Recording was done by ATR (Attenuated Total Reflectance) technique in the range from 4000 to 450 cm^{-1}, and 32 scans at resolution 4.

XRD results

XRD has been done on all samples, however due to their congruence for same reagent independently on concentration and temperature, those corresponding to optimal leaching conditions, marked by bolded text in Table II, are shown here). LTA of Bogovina coal dominates by amorphous matter, whereas other constituents are quartz (Q), olivine (O), calcite (C) anhydrite (A), mica (M) and unidentified phase (U) (Fig. S-1). Amorphous matter also dominates in LTA of HCl and HNO_3 leached solid residues. As expected, treatment with both inorganic acids resulted in removal of calcite, anhydrite and mica,[2] as well as unidentified phase (Fig. S-1). Scarce distribution of minerals in leached solid residues, represented mostly by resistant quartz, is consistent with efficient deashing (~ 80 %; Table II). In addition to quartz, the solid residues obtained by HCl treatment contain low amount of olivine (Fig. S-1), which is also relatively prone to acidic dissolution resulted from ion-exchange reaction between Mg^{2+}/Fe^{2+} and H^+.[3] The solid residue obtained by HNO_3 treatment does not contain even olivine, probably due to the possible oxidation of Fe^{2+} from fayalite to Fe^{3+}, associated with common dissolution by ion-exchange reaction mentioned above. The very low amount of plagioclase (P) in this solid residue can be attributed to the presence of this mineral in initial coal sample rather than its formation during chemical leaching (Fig. S-1). However, due to the extremely low content of plagioclase in comparison to other minerals it is not identified in other samples, with exception of HNO_3 leaching residue from which other minerals were almost fully removed. The presence of plagioclase in leached solid residue after leaching with HNO_3 can be attributed to greater resistance of feldspar mineral groups against acidic treatment than other silicates with exception of quartz.[2,4]

FTIR results

The main changes in FTIR spectra of coal OM after treatment with 15 vol.% HCl at 60 °C or 15 vol.% HNO_3 at the same temperature are expressed by decrease of amount of unsaturated comparing to saturated hydrocarbons moieties that is reflected by lowering of intensity of C=C stretching (around 1600 cm^{-1}) in relation to peaks around 2900 cm^{-1}, representing C–H stretching in saturated aliphatic chains. Acid treated samples contain less O–H bending peaks around 1400 cm^{-1}, whereas C–O stretching peaks and aliphatic C–H bending vibrations about 1050 cm^{-1} become more prominent in leached solid residues (Fig. S-2). In

the case of HNO_3 treatment, the increase of peak abundance in the latter area in partly can be attributed to the S=O stretching resulted from oxidation of organic bounded sulfur.

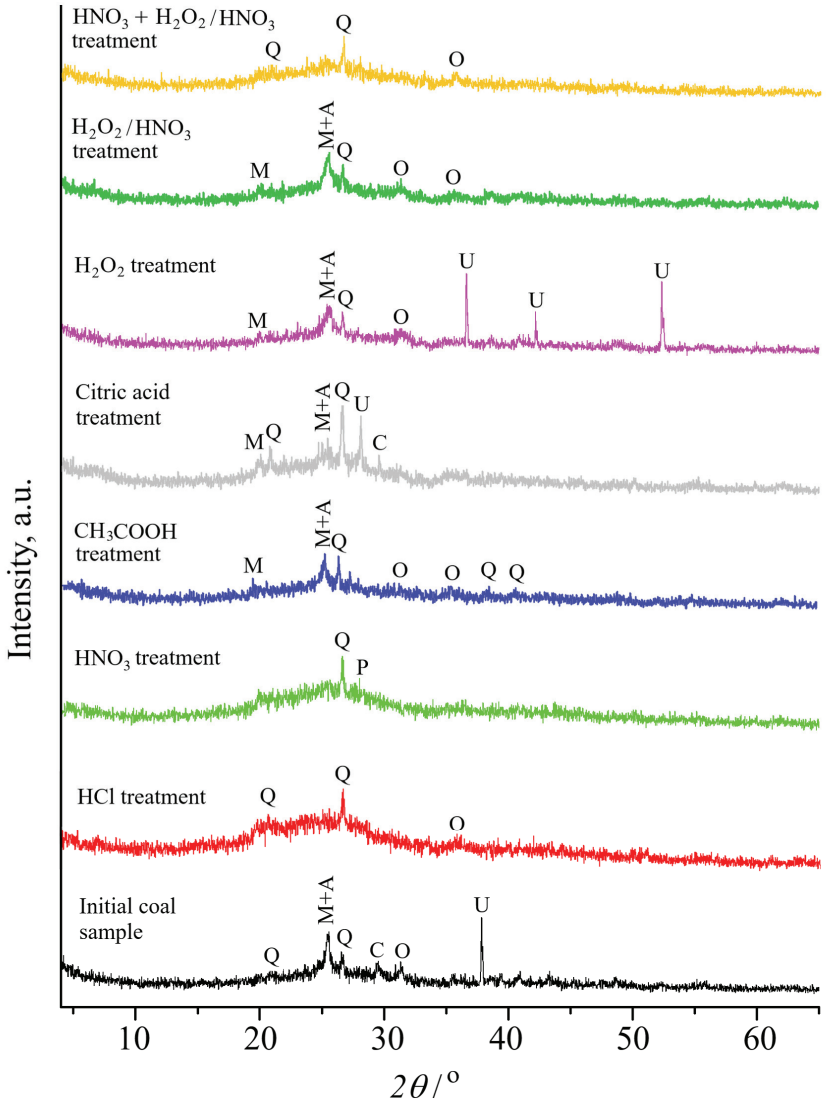

Fig. S-1. XRD spectra of LTA of initial coal sample and solid residues obtained by chemical leaching with: HCl, HNO_3, CH_3COOH, citric acid, H_2O_2, H_2O_2/HNO_3 mixture, pH 2 and HNO_3, followed by H_2O_2/HNO_3 mixture, pH 2 in two-step leaching process; legend: Q – quartz; O – olivine; C – calcite; A – anhydrite; M – mica; U – unidentified phase; P – plagioclase; note: the results for optimal concentrations and temperatures (marked by bolded text in Table II) are provided.

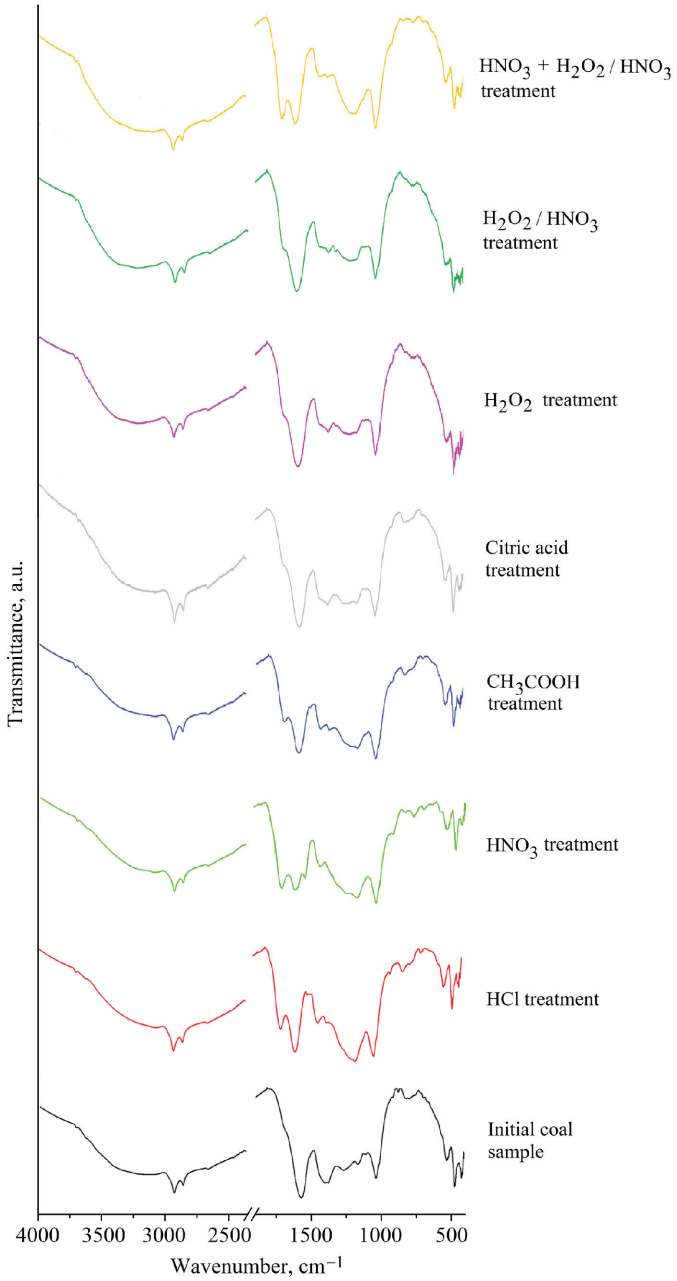

Fig. S-2. FTIR spectra of initial coal sample and solid residues obtained by chemical leaching with: HCl, HNO_3, CH_3COOH, citric acid, H_2O_2, H_2O_2/HNO_3 mixture, pH 2 and HNO_3, followed by H_2O_2/HNO_3 mixture, pH 2 in two-step leaching process; note: results for optimal concentrations and temperatures (bolded text in Table II) are provided.

Both acid leached residues have more intense peak at about 1720 cm^{-1} corresponding to C=O stretching (in carbonyl compounds and acids) in relation to C=C stretching (around 1600 cm^{-1}) than initial coal. This is particularly visible for HNO_3 leaching due to its oxidation properties. Interaction of HCl with coal OM is recorded by C–Cl stretching peak at around 820 cm^{-1}. Decrease in intensity of bands in area from 450 to 600 cm^{-1} that corresponds to mineral part of the coal is consistent with its partial removal. Despite mentioned changes, the FTIR spectra (Fig. S-2) show that there are not significant alterations of coal OM structure caused by inorganic acids treatments. The result is expected since kerogen is generally insoluble in conventional acids and bases water solutions and in accordance with literature data.[5] Furthermore, kerogen is usually in close connection with MM[6] that is primarily degraded/dissolved, protecting the significant alteration of the OM structure.

Coal leaching with organic acids

XRD diagrams in Fig. S-1 are consistent with low deashing efficiency of organic acids. They dominate by amorphous matter and indicate that only calcite and unidentified mineral phase are removed from the coal sample. Furthermore, it is obvious that after treatment with citric acid new unidentified mineral phase is formed, confirming the incorporation of this acid into coal MM.

The FTIR spectra of residues obtained by leaching with organic acids are almost identical to FTIR spectrum of initial coal, indicating that alterations of structure of coal OM by treatment with organic acids are less pronounced in comparison to inorganic acids leaching (Fig. S-2). The solely difference is noticed in the FTIR spectrum of CH_3COOH leached residue, that is reflected through a more intense peak at about 1720 cm^{-1} corresponding to C=O stretching (in carbonyl compounds and acids) in relation to C=C stretching (around 1600 cm^{-1}) than in initial coal.

Coal leaching with oxidizing reagents

Low efficiency of 35 vol.% H_2O_2 and 35 vol.% H_2O_2/10 vol.% HNO_3 mixture (pH 2) in deashing (51–59 wt.% at optimal temperature, Table II) is also confirmed by XRD data that indicate prevalence amorphous matter and successful calcite removal, only, using aforementioned reagents. Furthermore it is obvious that 35 vol.% H_2O_2 treatment resulted in formation of new unidentified mineral phases (Fig. S-1). On the other hand, XRD diffractogram of the solid residue after the two-step leaching process is very similar to those obtained by 10 vol.% inorganic acids treatment, indicating the presence of amorphous matter (dominating), quartz and olivine (Fig. S-1).

The FTIR spectra of solid residues obtained by treatment with 35 vol.% H_2O_2 at 40 °C and H_2O_2/HNO_3 mixture (pH 2) at 60 °C are almost identical and generally similar to those of initial coal sample. The main difference is reflected

through a more intense peak at about 1720 cm^{-1} (representing C=O stretching in carbonyl compounds and acids), associated with less pronounced C=C stretching peak at 1600 cm^{-1} in relation to initial coal, resulting from oxidation properties of aforementioned reagents (Fig. S-2). The two-step leached solid residue (10 vol.% HNO_3 + H_2O_2/HNO_3 mixture at pH 2) has almost identical FTIR spectrum as residue obtained by 10 vol.% HNO_3, indicating greater impact of HNO_3 on structure of coal OM in comparison to H_2O_2 (Fig. S-2).

REFERENCES

1. R. N. Miller, R. F. Yarzab, P. H. Given, *Fuel* **58** (1979) 4 (https://doi.org/10.1016/0016-2361(79)90044-9)
2. T. H. N. G. Amaraweera, H. M. T. G. A. Pitawala, G. W. A. R. Fernando, in *Proceeding of the 2nd Earth Resource Engineering Conference*, 2007, Colombo, Sri Lanka, *Proceeding of ERE 2007*, University of Moratuwa, Faculty of Engineering, Moratuwa, 2007, p. 25 (https://www.researchgate.net/publication/237102401_Stability_of_Mica_KFeldspar_and_Apatite_in_Water_Organic_Matters_and_Citric_Acid)
3. V. Prigiobbe, M. Mazzotti, *Chem. Eng. Sci.* **66** (2011) 6544 (https://doi.org/10.1016/j.ces.2011.09.032)
4. R. Oxburgh, J. I. Drever, Y-T. Sun, *Geochim. Cosmochim. Acta* **58** (1994) 661 (https://doi.org/10.1016/0016-7037(94)90496-0)
5. S. K. Behera, S. Chakraborty, B. C. Meikap, *Int. J. Coal Sci. Technol.* **5** (2018) 142 (https://doi.org/10.1007/s40789-018-0208-3)
6. D. Životić, *Coal Geology*, University of Belgrade, Faculty of Mining and Geology, Belgrade, 2018 (in Serbian) (https://rgf.bg.ac.rs/Dokumenta/Publikacije/Biblioteka/Promocija_izdanja_katalog_2019.pdf).

Journal of the Serbian Chemical Society
JSCS@tmf.bg.ac.rs • www.shd.org.rs/JSCS
J. Serb. Chem. Soc. 86 (11) 1127–1130 (2021)
EuCheMS news

DIVISION OF ANALYTICAL CHEMISTRY
EUROPEAN CHEMICAL SOCIETY

EUCHEMS NEWS

European Analytical Column No. 49•

SLAVICA RAŽIĆ[1*#], MARTIN VOGEL[2**] and MARCELA A. SEGUNDO[3***]

[1]*Department of Analytical Chemistry, Faculty of Pharmacy, University of Belgrade, Vojvode Stepe 450, 11222 Belgrade, Serbia,* [2]*Institute for Inorganic and Analytical Chemistry, University of Münster, Münster, Corrensstraße, 28, 48149 Münster, Germany and* [3]*Department of Chemical Sciences, Faculty of Pharmacy, University of Porto, R Jorge Viterbo Ferreira, 228, 4050-313 Porto, Portugal*

The European Analytical Column is the voice of the Division of Analytical Chemistry (DAC) as a Professional Network of chemical societies and their members working in all fields of analytical sciences within the European Chemical Society (EuChemS). The strategy for 2021–2023 comprehends the promotion of Analytical Chemistry to a wider community, co-operation with other professional networks and to support members' activities, particularly through study groups and task forces. This year we will focus on how our community has managed to adapt to teaching analytical chemistry during the pandemic. Please feel free to share your own experience through our social media and networks!

1. DAC-EUCHEMS ACTIVITIES

One of the main activities of DAC-EuChemS is the promotion of organization of Euroanalysis conference. Every two-years, one of the participating scientific chemical societies will host Euroanalysis, with active involvement of local scientists in the organization. Euroanalysis XXI was scheduled for August 2021, but the pandemic prevented us to meet in person as an Analytical Community this year. Instead, we have met online last September for the webinar dedicated to our Awardees Prof. Aldo Roda (DAC-EuChemS Award) and Prof.

* Correspondence E-mails: (*)slavica.razic@pharmacy.bg.ac.rs; (**)martin.vogel@uni-muenster.de; (***)msegundo@ff.up.pt
# Serbian Chemical Society member.
• Reprint from *Analytical and Bioanalytical Chemistry*, https://doi.org/10.1007/s00216-021-03760-3, with permission from Springer.

Karen Faulds (Rober Kellner Lecture Award), who gifted us with two wonderful lectures that can be seen at https://youtu.be/I2runlAeq5A, which were sponsored by Springer. Euroanalysis XXI is now rescheduled to 2023 and it will take place in Geneva, Switzerland, under the auspices of the Swiss Chemical Society (https://www.euroanalysis2023.ch/), organized by Prof. Eric Bakker (University of Geneva), Dr. Marc Suter (EAWAG), Dr. Franka Kalman (HES Sion) and Dr. Bodo Hattendorf (ETH Zurich).

The Study Groups are also responsible for several ongoing activities of DAC-EuChemS. The topics addressed include “Bioanalytics”, “Chemometrics”, “Education”, “Electroanalytical Chemistry”, “History”, “Nanoanalytics”, “Quality Assurance” and “Sample Preparation”. Please visit the DAC-EuChemS website for updated reports (https://www.euchems.eu/divisions/analytical-chemistry/) and contact the Heads of the Study Groups in order to have more information or to participate in their activities.

Lastly, one of DAC-EuChemS objectives is to support its delegates on the organization of local events open to the international community through dissemination of the event within the Professional Network, including online events. The Steering Committee of DAC-EuChemS will be happy to receive input for additional activities. Feel free to contact one of the following persons: Slavica Ražić, University of Belgrade, Serbia (Chair), Marcela Segundo, University of Porto, Portugal (Secretary), Jiří Barek, Charles University, Czech Republic (Treasurer), Charlotta Turner, Lund University, Sweden, Sibel A. Özkan, Ankara University, Turkey, Lutgarde Buydens, Radboud University, the Netherlands, and Martin Vogel, University of Münster, Germany.

2. TEACHING ANALYTICAL CHEMISTRY DURING THE PANDEMIC: AN ENDURING ENDEAVOUR – BUT NOT IN VAIN!

When the corona pandemic first hit many parts of the world in spring 2020, surely only few of us had imagined that its influence on our everyday live became that drastic, and, even worse, that enduring. It would be idle to enumerate once again what has been changing over the last 15 months or so. However, it is surely worth to have a closer look onto the dramatic changes in teaching (not only) analytical chemistry with which instructors all over the world have been faced since 2020.

As social distancing had early been recognized as a key measure to interrupt the spread of Covid-19, remote teaching was rapidly introduced wherever and whenever possible. This was – and still is – an endeavour for all of us teaching a subject such as analytical chemistry that is fundamentally dependent on experimental practice in the laboratory. While many instructors were thrown in at the deep end in early 2020, many of them rapidly developed innovative and smart approaches to cope with the new challenges. The many experiences made, the

many lessons learned and the many conclusions drawn by instructors are worth to be shared with the analytical community as a whole.

In January 2021, "ABCs of Education and Professional Development in Analytical Science" column started a series of articles featuring the teaching of analytical chemistry during the pandemic. The idea of this series is to support instructors all over the world in preparing their courses. Several articles on different aspects of remote teaching have been published up to now and will surely be inspiring for many readers and hopefully activate some of them to share their experiences and ideas by publishing also an article for the column.

For example, Emily Niemeyer and co-authors contributed with a paper describing some hands-on laboratory experiments that students can complete while studying off the campus.[1] In their paper, easy remote laboratory experiments are described that are based on carbonate chemistry and that are used to deal with gravimetry and titrimetry, just to mention one example. Supplemental material is provided, allowing readers to implement the experiments described also into their courses.

Another paper published in this special series by Elise Heiss and Susan Oxley describes the implementation of a flipped classroom approach for two different analytical chemistry courses.[2] While presenting their experiences with different aspects of flipped classrooms, personal reflections and also recommendations of best practices, the article may serve as an inspiration for readers when thinking about the different forms of remote learning (asynchronous, synchronous, as well as assessment).

All of us having taught remotely during the last months have surely been faced with the question of how to enhance student engagement in their courses. Jill Venton and Rebecca Pompano provide many good ideas and answers on this question while discussing active learning as a strategy.[3] The article is a valuable source of practical tips for student engagement and provides many answers to didactic questions rising from the current Zoom world.

Another paper dealing also with the question of student interaction and student engagement has been contributed by Anna Cavinato and co-authors.[4] Based on their experiences, four instructors describe their view on engaging students in an online environment. The article will surely inspire readers through the authors' profound description of their experiences in different remote setting and their conclusions drawn hereof.

An aspect that has turned out to be even more crucial during the pandemic under normal times is the different access to technical infrastructure and financial resources. Vilmalí López-Mejías and co-authors from the University of Puerto Rico therefore describe their way and their experiences of remote teaching of analytical chemistry at an institution that, prior to the pandemic, had already been hit by, e.g., hurricanes and earthquakes.[5] The article is a good combination of

showing different didactic approaches for remote learning in a synchronous as well in an asynchronous mode and of presenting remote laboratory experiences to the readers. Supplemental material allows having a deeper look into the functioning of the courses.

All these articles presented show that teaching during the pandemic has been – and still is – a challenge, and to serve our students in the best way has even more become an endeavour. However, the experiences made and the concepts developed will surely be not in vain, as many of them can be integrated into regular courses. Moreover, I am sure, we shall return to a normal life – with many lessons learned from the pandemic.

I hope that this small survey on articles recently published in "ABCs of Education and Professional Development in Analytical Science" supports many readers while preparing and carrying out their course and stimulates them to share their experiences and concepts developed with colleagues in the field.

REFERENCES

1. J. F. Destino, E. M. Gross, E. D. Niemeyer, S. C. Petrovic, *Anal. Bioanal. Chem*. **413** (2021) 1237
2. E. M. Heiss, S. P. Oxley, *Anal. Bioanal. Chem*. **413** (2021)1245
3. B. J. Venton, R. R. Pompano. *Anal. Bioanal. Chem*. **413** (2021):1507
4. A. G. Cavinato, R. A. Hunter, L. S. Ott, J. K. Robinson, *Anal. Bioanal. Chem*. **413** (2021):1513
5. A. L. Morales-Cruz, B. M. Ortiz-Andrade, J. del Pilar-Albaladejo, L. M. Díaz-Vázquez, U. Rivera-González, V. López-Mejías, *Anal. Bioanal. Chem.* **413** (2021):2845.